Interlocked halogen bonding host systems for anion recognition

Sean W. Robinson

St John's College, University of Oxford



A thesis submitted for the degree of Doctor of Philosophy

Inorganic Chemistry Laboratory

University of Oxford

Hilary Term 2016

INTERLOCKED HALOGEN BONDING HOST SYSTEMS FOR ANION RECOGNITION

Sean Wade Robinson, St John's College, University of Oxford

Abstract of thesis submitted for the degree of D. Phil., Hilary Term 2016

This thesis describes the synthesis and anion recognition properties of acyclic and mechanically interlocked anion receptors containing either the 3,5-bis-iodotriazole pyridinium or pyridine-*N*-oxide motifs.

Chapter One introduces the field of supramolecular chemistry, highlighting areas of particular relevance to this thesis, *viz.* anion coordination, recognition, templation, halogen bonding and synthesis of interlocked structural frameworks.

Chapter Two describes the synthesis of acyclic, [2]catenane and water-soluble [2]rotaxane anion receptors containing the novel 3,5-bis-iodotriazole pyridinium motif and details their anion recognition properties. X-ray crystal structures of the [2]catenane bearing this motif are provided in support of the anion binding results. X-ray Absorption Spectroscopy is used to probe the nature, and quantify the degree of covalency, of halogen-bonding interactions.

Chapter Three details further work incorporating the 3,5-bis-iodotriazole pyridinium motif into elaborate symmetric and asymmetric [2]rotaxane anion hosts designed for nitrate binding in competitive aqueous solvent media. Moreover, the synthesis of an analogous water-soluble [2]rotaxane is presented and its anion recognition properties investigated.

Chapter Four focuses on the synthesis of acyclic and asymmetric interlocked anion receptors bearing the novel neutral 3,5-bis-iodotriazole pyridine-*N*-oxide motif. The anion recognition properties of these hosts are presented with an emphasis on [2]rotaxane species capable of binding chloride and nitrate in competitive aqueous solvent media.

Chapter Five provides a summary of the major conclusions of this thesis.

Chapter Six furnishes procedures pertaining to chemicals, instrumentation, data handling and analytical protocols, as well as detailing synthetic methods and characterisation of novel compounds.

Chapter Seven provides the references cited within Chapters One to Six.

Full crystallographic information and details of molecular modeling experiments are provided in Digital Appendices on an enclosed DVD.

Acknowledgements

There are many people who deserve a tremendous amount of thanks for their individual contributions that have brought me to this point in my life. Firstly, I would like to thank Prof. Paul D. Beer for seeing my potential and giving me the life-changing opportunity to work, learn and grow in his group. I am truly grateful for his personal approach to supervision, unwavering support, encouragement, and for his guidance and wisdom both in and out of the laboratory.

For expert advice, knowledge and practical help, I must thank Dr Asha Brown for many discussions and for always making time to share her unparalleled synthetic genius, Dr Michal Rezanka for demystifying cyclodextrin synthesis and Dr Vicente Martí-Centelles for endless synthetic guidance and help. Dr Nick White has my continual gratitude for convincing me to join the Group, introducing me to the lab and sharing his crystallographic expertise. I would also like to thank Drs Lydia Gilday and Ben Mullaney for patiently answering all my unceasing questions and for being true friends: always providing a listening ear when things in life were not quite going according to my best-laid plans.

I was fortunate to supervise a wonderful Masters student, Ju Won Cha, who unfortunately had some tricky synthesis—and a rather critical supervisor—to contend with but excelled against the odds! She was a pleasure to work with in those times that I managed to transfer her attention from the Spotify playlist to the fumehood!

I owe a great deal of thanks to my various local and international collaborators: Dr Amber Thompson for developing my crystallographic skills, making time to help me with structures far beyond my ability and giving me the opportunity to work at the Diamond Synchrotron on many occasions; Dr Nick Rees and Dr James Wickens for their help with NMR spectroscopy and Mass Spectrometry, respectively, Dr Matthew Langton for his work on the cyclodextrin-appended rotaxanes; and Prof. Pierre Kennepohl and Ms Chantal Mustoe for their remarkable XAS work—I am truly grateful for their tireless efforts!

My time in the Group would never have been as enjoyable without the wonderful friends I have been fortunate enough to get to know and work with during my time in the lab. I could not have imagined better friends than Tim Barendt, Stuart Cornes, Tom Mole and Remi Tirfoin who introduced me to so much more music than I was aware existed and made the last three and a half years genuinely entertaining both in and out of the lab. I sincerely appreciate all of your synthetic advice over the years, and all those pub trips which somehow kept me sane! Thanks must also be made to many Group members during my time in Oxford: Jim Mercurio, Rich Knighton, Alex Hess, Jason Lim, Hena Bagha, Valentine Bunchuay, Sam Sutton, Grace Turner, Harry Klein, George Li, Dave Blyghton, Alastair Hope-Morley, Ben Partridge,

Greg Carton, Dan Lucy, Will Arter and Andrew Docker; all of whom contributed towards making our labs a wonderful work environment over the years. Special mentions go to my superb proof-readers, Asha, Tom, Grace, Hena and, of course, Paul, who graciously read it all... repeatedly!

Outside the lab, my deepest appreciation goes to my friends in St John's College; they are all too many to name and I am indebted to each for welcoming me to the UK and providing wonderful distractions from my work. To my friends in the St John's College Chapel Choir and the Arcadian Singers, many thanks for allowing me to sing and create beautiful music with you all—you have been a home away from home for me.

I would never have made it this far if it weren't for the tremendous efforts of some people back in South Africa. My utmost thanks to Mr Barry Lane who introduced me to science and chemistry in primary school, and has been a life-long inspiration for my study in this area—I still remember growing crystals of copper sulfate and learning to purify compounds by distillation! Also worthy of thanks are my lecturers at the University of Stellenbosch, in particular, my Masters supervisors Prof. Delia Haynes and Dr Gareth Arnott whose excellent teaching and stalwart support have allowed me to achieve more than I could have dreamed. For their friendship and encouragement, I must thank the members of The Company: Laura, Kate, Chandré, Daniella, Heleen and Luke, as well as Helene, Leigh, Storm and Malcolm, and my all-time best friend, Jamie.

For financially supporting my studies, I am indebted to the generosity of the Clarendon Fund, St John's College and the SCG Fund. I would also like to acknowledge the Diamond and the Stanford Synchrotron Lightsources for awards of beamtime, and the invaluable data they provided.

Finally, none of this would be possible without the love, support, encouragement and prayers of my parents, Kay and Ashley, my Aunty Charmaine and my dearest Grandma. Words cannot express the depths of my gratitude for every call, email, text and parcel, and how much I love each of you!

This thesis is dedicated to the loving memory of my dearest grandmother:

Always my greatest supporter, mentor, provider, carer and prayer-warrior

I miss you every day and wish I could have shared this with you

Drevin Torrente née English (1929–2015)

"Trust in the Lord with all thine heart; and lean not unto thine own understanding.

In all thy ways acknowledge Him, and he shall direct thy paths."

– Proverbs 3:5–6 (KJV)

Previously Published Work

Publications arising from this thesis

- **Robinson, S. W.**, Mustoe, C. L., White, N. G., Brown, A., Thompson, A. L., Kennepohl, P., Beer, P. D., *Evidence for halogen bond covalency in acyclic and interlocked halogen-bonding receptor anion recognition.*, *J. Am. Chem. Soc.*, **2015**, 137, 499–507.

- Langton, M. J., **Robinson, S. W.**, Marques, I., Félix, V., Beer, P. D., *Halogen bonding in water results in enhanced anion recognition in acyclic and rotaxane hosts.*, *Nature Chem.*, **2014**, 6, 1039–1043.

Publications arising during the course of this work

- Gilday, L. C., **Robinson, S. W.**, Barendt, T. A., Langton, M. L., Mullaney, B. R., Beer, P. D., *Halogen Bonding in Supramolecular Chemistry.*, *Chem. Rev.*, **2015**, 115, 7118–7195.

- Langton, M. J., Marques, I., **Robinson, S. W.**, Félix, V., Beer, P. D., *Iodide Recognition and Sensing in Water by a Halogen-Bonding Ruthenium(II)-Based Rotaxane*, *Chem. Eur. J.*, **2016**, 22, 185–192.

Abbreviations

$\Delta\delta$	change in chemical shift relative to free host
μ	micro
Å	Angstrom
A	hydrogen or halogen bond acceptor
app.	apparent
aq.	aqueous
ATP	adenosine triphosphate
BAr_4^{F-}	tetrakis[3,5-bis(trifluoromethyl)phenyl]borate anion
Bn	benzyl
br.	broad
calc.	calculated
cf.	*confer*
c	centi
°C	degrees Celsius
conc.	concentrated
COSY	homonuclear correlation spectroscopy
CuAAC	copper(I)-catalysed azide alkyne cycloaddition
d	doublet
dd	doublet of doublets
D	hydrogen bond donor
DCM	dichloromethane
DIPEA	*N,N′*-diisopropylethylamine
DMF	*N,N′*-dimethylformamide
DMSO	dimethylsulfoxide
DNA	deoxyribonucleic acid
DVD	digital versatile disc
e.g.	*exempli gratia*
EI	electron ionisation
en	ethylenediamine
equiv.	equivalent
ESI	electrospray ionisation
Et	ethyl
F^2	square of the structure factor
g	gram
G	Gibbs free energy
Grubbs' II	Grubbs' second generation catalyst
H	enthalpy
HRESI-MS	high resolution electrospray ionisation mass spectrometry

Hz	Hertz
i.e.	*id est*
IPA	isopropyl alcohol
ITC	isothermal calorimetry
IUPAC	International Union of Pure and Applied Chemistry
J	joule
J	coupling constant
K	Kelvin
K_a	association constant
L	litre
LRESI-MS	low resolution electrospray ionisation mass spectrometry
m	*meta*
m	metre, milli, multiplet
M	mega
M	moles per litre
MD	molecular dynamics
Me	methyl
MIM	mechanically interlocked molecule
MM	molecular mechanics
mol	mole
n	nano
neg.	negative
NMR	nuclear magnetic resonance
OAc^-	acetate anion
OTf^-	triflate anion
p	*para*
Ph	phenyl
pH	$-log_{10}[H^+]$
pK_a	$-log_{10}K_a$
pos.	positive
Pr	propyl
q	quartet
QM	quantum mechanics
quin	quintet
R	chemical substituent
RCM	ring-closing metathesis
ROESY	rotating-frame nuclear Overhauser effect correlation spectroscopy
s	singlet
S	entropy

syn	synperiplanar
t	triplet
TBA	tetrabutylammonium cation
TBTA	tris[1-benzyl-1,2,3-triazol-4-yl)methyl]amine
^{t}Bu	*tert*-butyl
THF	tetrahydrofuran
TLC	thin layer chromatography
TIPS	triisopropylsilyl
TMS	trimethylsilyl
tosyl	4-toluenesulfonyl
Ts	4-toluenesulfonyl
TTF	tetrathiafulvalene
UV	ultraviolet

Contents

1 Introduction **1**

1.1 Supramolecular chemistry . . . 2

1.1.1 Host–guest chemistry . . . 3

1.1.2 Non-covalent interactions . . . 5

1.2 Anion binding . . . 10

1.2.1 The importance of anions . . . 10

1.2.2 Intrinsic properties of anions . . . 11

1.2.3 Biological receptors . . . 14

1.2.4 Synthetic receptors . . . 14

1.3 Halogen bonding . . . 29

1.3.1 Halogen bonding with anions . . . 30

1.4 Self-assembly and templation . . . 32

1.5 Interpenetrated and interlocked structures . . . 35

1.5.1 Synthetic approaches . . . 36

1.5.2 Applications of interlocked structures . . . 44

1.6 Project Aims . . . 47

2 The 3,5-bis-iodotriazole pyridinium motif **49**

2.1 Introduction . . . 50

2.1.1 Triazole and iodotriazole receptors for anions . . . 50

2.1.2 Chapter aims . . . 52

2.2 Acyclic receptors . . . 52

2.2.1 Synthesis . . . 53

2.2.2 Crystal structures . . . 55

2.2.3 ^{1}H NMR anion binding studies . . . 56

2.3 A monocationic [2]catenane . . . 58

2.3.1 Synthesis . . . 58

2.3.2 ^{1}H NMR anion binding studies . . . 62

2.3.3 Crystal structures . . . 64
2.3.4 X-ray absorption spectroscopy (XAS) . . . 67
2.4 A dicationic [2]catenane . . . 75
2.4.1 Synthesis . . . 76
2.4.2 ^{1}H NMR anion binding studies . . . 78
2.5 Integration of the 3,5-bis-iodotriazole pyridinium motif into further higher-order architectures . . . 80
2.5.1 Synthesis of an axle . . . 80
2.5.2 Synthesis of a macrocycle . . . 83
2.5.3 Attempted synthesis of all-halogen-bonding [2]catenanes . . . 84
2.5.4 Attempted synthesis of all-halogen-bonding [2]rotaxanes . . . 85
2.6 Water-soluble rotaxanes . . . 85
2.6.1 Towards water-soluble receptors . . . 86
2.6.2 β-Cyclodextrin synthesis . . . 88
2.6.3 Rotaxane syntheses . . . 89
2.6.4 ^{1}H NMR anion binding studies . . . 93
2.6.5 Thermodynamics of binding . . . 96
2.6.6 Molecular dynamics simulations . . . 97
2.6.7 Attempted synthesis of a water-soluble all-halogen-bonding [2]rotaxane . . . 99
2.7 Conclusion and future work . . . 100

3 Halogen-bonding [2]rotaxanes for nitrate recognition 102

3.1 Introduction . . . 103
3.1.1 Halogen bonding receptor design . . . 105
3.1.2 Chapter aims . . . 106
3.2 Axle synthesis *via* asymmetric methods . . . 106
3.2.1 Initial synthetic attempts . . . 106
3.2.2 Alternative synthetic strategies . . . 109
3.3 Axle synthesis *via* statistical methods . . . 115
3.4 Monocationic and dicationic halogen-bonding [2]rotaxanes . . . 118
3.4.1 Synthesis . . . 118
3.4.2 ^{1}H NMR anion binding studies . . . 121
3.5 A water-soluble rotaxane . . . 123
3.5.1 Synthesis . . . 123
3.5.2 ^{1}H NMR anion binding studies . . . 125
3.6 Conclusion and future work . . . 127

4 The 3,5-bis-iodotriazole pyridine-*N*-oxide motif **129**

4.1 Introduction . . . 130

4.1.1 Chapter aims . . . 133

4.2 Acyclic receptors . . . 133

4.2.1 Synthesis . . . 133

4.2.2 ^{1}H NMR anion binding studies . . . 133

4.3 [2]Rotaxane host systems . . . 135

4.3.1 Synthesis of axle precursors . . . 135

4.3.2 Synthesis of macrocyclic components . . . 135

4.3.3 [2]Rotaxane synthesis . . . 137

4.3.4 ^{1}H NMR anion binding studies . . . 140

4.4 Attempted syntheses towards water-soluble neutral [2]rotaxanes . . . 142

4.4.1 Terphenyl-stoppered axle . . . 142

4.4.2 Permethyl-β-cyclodextrin-stoppered axle . . . 143

4.5 Conclusion and future work . . . 145

5 Conclusions **147**

6 Experimental **150**

6.1 General considerations . . . 151

6.1.1 Chemicals and solvents . . . 151

6.1.2 Instrumentation . . . 151

6.1.3 Titration protocols . . . 152

6.1.4 X-ray Crystallography . . . 153

6.1.5 X-ray Absorption Spectroscopy . . . 154

6.2 Synthesis . . . 156

6.2.1 Compounds from Chapter 2 . . . 156

6.2.2 Compounds from Chapter 3 . . . 206

6.2.3 Compounds from Chapter 4 . . . 231

7 References **247**

8 Appendix **258**

8.1 Crystallographic Data Tables . . . 259

List of Figures

1.1.1 Examples of synthetic receptors: (a) Lehn's three-dimensional cryptand, (b) Cram's spherands and (c) Park and Simmons' macrobicyclic anion receptors. 2

1.1.2 Crystal structures of (a) Stoddart's Borromean rings (each of the macrocycles are coloured in blue, red and green for simple visualisation), and (b) Leigh's pentameric Fe^{II} chloride-templated knot. . 3

1.1.3 Models of host–guest binding: (a) Fischer's 'lock and key' hypothesis, and (b) Koshland's 'induced-fit' model. 4

1.1.4 The three classes of Coulombic forces: (a) ion–ion, (b) ion–dipole, and (c) dipole–dipole interactions. 5

1.1.5 Hydrogen bonding: (a) cartoon representation of Donor–H···Acceptor hydrogen bonds, and (b) pairing of DNA base pairs *via* hydrogen bonds. 6

1.1.6 Halogen bonding: (a) electrostatic potential diagram of CF_3I showing the σ-hole as the region of positive potential (red) in Hartrees, at the 0.001 electrons $Bohr^3$ iso-density surface, and (b) cartoon representation of a halogen bond with a Lewis base (R = halogen, aryl, alkyl, etc.; X = Cl, Br, I; B = N, O, S, Se, Cl, Br, I, F^-, Cl^-, Br^-, I^-, etc.). 7

1.1.7 Aromatic π–π donor–acceptor interactions: (a) face-to-face, and (b) face-to-edge. 7

1.1.8 Examples of ion–π interactions: (a) cation–π interaction, (b) anion–π interaction, and (c) one of Matile's anion–π slides for transmembrane transport. 9

1.1.9 Example of a supramolecular $M_{24}L_{48}$ cage structure assembled *via* metal–ligand coordinate bonds between simple starting components. 10

1.2.1 Selected examples of different geometries adopted by anions. 12

1.2.2 Two dimensional projection of binding cavities of truncated biological protein structures: (a) phosphate binding protein (PBP), and (b) sulfate binding protein (SBP). 14

1.2.3 Common hydrogen-bonding motifs used in anion receptors for neutral anion recognition. 15

1.2.4 Examples of amide-based receptors: (a) Pascal's seminal cryptand, (b) Crabtree's acyclic isophthalamide receptor, and (c) Jurczak's macrocyclic host. 16

1.2.5 Examples of amide-based receptors: (a) Anslyn's bicyclic cyclophane, (b) crystal structure of Bowman-James' cryptate receptor, and (c) Kubik's 'molecular oyster'. 17

1.2.6 Further examples of amide-based receptors: (a) Jurczak's acyclic pyrrole-based amide and thioamide receptors, (b) Hughes and Smith's boronate-appended receptor, (c) Reinhoudt's tripodal sulfonamide-containing receptor and (d) Crabtree's sulfonamide-functionalised receptor. 18

1.2.7 Examples of urea- and thiourea-based receptors: (a) Gale's bis-urea host, (b) crystal structure of Das and Ganguly's host with sulfate, (c) crystal structure of Böhmer's tetrameric macrocycle, and (d) Reinhoudt's tetra-thiourea-functionalised cavitand. 19

1.2.8 Examples of pyrrole receptors: (a) crystal structure of Gale and Sessler's calix[4]pyrrole receptor with fluoride, and (b) crystal structure of Sessler's bis-indole receptor with dihydrogen phosphate. 20

1.2.9 Examples of anion receptors which operate *via* C–H hydrogen bonds: (a) crystal structure of Farnham and Dixon's fluorinated macrocyclic ether binding fluoride, (b) crystal structure of a truncated derivative of Craig's foldamer binding chloride with supplementary hydrogen bonds from water, and (c) Flood's cyanostar macrocycle which binds large anions. 21

1.2.10 Examples of anion–π receptors: (a) anion–π interactions can be seen in Kochi's crystal structure of tetrakis(tetracyanopyrazine) with chloride, and (b) crystal structure of Ballester's aryl-appended calix[4]pyrrole with chloride. 22

1.2.11 Common cationic motifs used in anion receptors. 22

1.2.12 Examples of protonated ammonium-based receptors: (a) crystal structure of Lehn's azide-binding cryptand, and (b) Lehn's fluoride-binding cryptand. 23

1.2.13 Examples of quaternary ammonium and pyridinium-based receptors: (a) Schmidtchen's tetrahedral cages, (b) crystal structure of Steed's tripodal host that binds bromide in acetonitrile, and (c) Shinoda's tetra-pyridinium macrocycle. 23

1.2.14 Examples of guanidinium-based receptors: (a) crystal structure of Anslyn's tris-guanidyl receptor with tricarballylate, and (b) crystal structure of Schmidtchen's bicyclic guanidinium receptor with acetate. 24

1.2.15 Examples of imidazolium-based receptors: (a) Sato's tripodal imidazolium receptor, (b) crystal structure of Alcade's macrocyclic host with chloride, and (c) crystal structure of Sessler's tetracationic macrocycle with mono-terephthalate. 25

1.2.16 Examples of triazolium-based receptors: (a) Schubert's bis-triazolium benzene receptor, and (b) Beer's tetra-triazolium macrocycle. 26

1.2.17 Examples of Lewis acidic receptors: (a) crystal structure of Gabbaï's B···F$^-$···Hg receptor and (b) Jollife's pyrophosphate selective bis-Zn^{II} bipodal host. 26

1.2.18 Cartoon representation of the different anion sensor mechanisms: (a) binding causes a response in an attached reporter group, (b) release of a dye upon anion binding results in a response, and (c) a chemodosimeter which affords a response upon reaction with the target anion. 27

1.2.19 Examples of electrochemical anion sensors: (a) Beer's cobaltocenium macrocycle, (b) crystal structure of Sessler's bis-indole–tetrathiafulvalene receptor with dihydrogen phosphate, and (c) Becher's tetrathiafulvalene-appended calix[4]pyrrole. 28

1.2.20 Examples of optical sensors: (a) Czarnik's hydrogen phosphate-binding fluorescent receptor, (b) Sessler's hydroxyanthraquinone-appended calix[4]pyrrole, and (c) crystal structure of Aldridge's boron-appended receptor with cyanide. 28

1.2.21 Examples of anion host systems in transport, catalysis and gelation: (a) crystal structure of Gale's fluorinated thiourea host with chloride, (b) Lehn's ATP-binding polyammonium azacrown macrocycle, and (c) one of Steed's anion-responsive gelators. 29

1.3.1 Examples of acyclic halogen-bonding receptors: (a) crystal structure of Resnati and Metrangolo's heteroditopic NaI receptor, (b) structure of Taylor's halogen-bonding tripodal receptor, (c) structure of Taylor's bipodal mixed hydrogen–halogen-bonding receptor, (d) crystal structure of Huber's bis-iodoimidazolium receptor with convergent halogen bonds to bromide, and (e) crystal structure of Resnati and Metrangolo's dihydrogen phosphate-selective iodoimidazolium receptor. 31

1.3.2 Examples of cyclic and more recent halogen-bonding receptors: (a) structure of Beer's bromoimidazolium-containing catenane, (b) crystal structure of Beer's bromoimidazoliophane macrocycle with convergent halogen bonds to bromide, (c) crystal structure of Beer's iodoimidazoliophane receptor which forms a 2:2 complex in the solid state, and (d) crystal structure of Schubert's bis-iodotriazolium receptor with convergent halogen bonds to sulfate. 32

1.4.1 Examples of biological self-assembly: (a) structure of haemoglobin with separate protein domains depicted in red and blue and the haem cofactors shown as a space-filling models, (b) the double helix structure of B-DNA, and (c) a representation of the phospholipid bilayer which makes up the cell membrane. 33

1.4.2 Examples of cation-templated supramolecular structures: (a) Nitschke's Fe^{II}-templated cage, and (b) Anderson's 12 Zn^{II}-porphyrin templated nanoring. 33

1.4.3 Examples of anion-templated supramolecular structures: (a) Lehn's pentanuclear Fe^{II} helicate, (b) Dunbar's BF_4^--templated molecular square, (c) Dunbar's SbF_6^--templated molecular pentagon, and (d) Böhmer's chloride-templated macrocycle. 34

1.4.4 Anion-templated structures: (a) Amouri's cage, and (b) Fujita's nanotube. 35

1.5.1 Cartoon representations of (a) [2]rotaxane, (b) [2]catenane, and (c) [2]pseudorotaxane. 36

1.5.2 Cartoon representation of the different synthetic approaches to forming [2]rotaxanes. 36

1.5.3 Cartoon representation of the different synthetic approaches to forming [2]catenanes. 37

1.5.4 Selected examples of Sauvage's cation-templated interlocked structures: (a) Cu^{I}-templated bis-phenanthroline catenane, (b) Cu^{I}-templated trefoil knot, and (c) crystal structure Cu^{I}-templated [4]rotaxane. 38

1.5.5 Cationic templation *via* different metal geometries: (a) Goldup's linear Au^{I}-templated catenane, (b) Leigh's square planar Pd^{II}-templated rotaxane, and (c) Sauvage's octahedral Ru^{II}-templated catenane. 39

1.5.6 Selected examples of interlocked molecules templated by organic cation motifs: (a) Stoddart's suit[2]ane structure with adjacent crystal structure, and (b) Takata's *N*-alkylated rotaxane which displays shuttling of the macrocycle under acid–base control. 40

1.5.7 Interlocked and interpenetrated systems templated by charge-assisted donor–acceptor interactions: (a) structure of Stoddart's bipyridinium–hydroquinone catenane with adjacent crystal structure, (b) crystal structure of Stoddart's bipyridinium–TTF/dihydroxynaphthalene catenane, and (c) crystal structure of Stoddart's bipyridinium–dihydroxynaphthalene pseudorotaxane. 41

1.5.8 Selected examples of neutral amide hydrogen-bond templated interlocked structures: (a) Hunter's [2]catenane, (b) Leigh's [2]rotaxane, and (c) Smith's squaraine-containing [2]rotaxane. 42

1.5.9 Neutral interlocked systems templated by π–π donor–acceptor interactions: (a) Sanders' napthalene diimide–dihydroxynaphthalene [2]catenane, (b) Sanders' naphthalene diimide trefoil knot, and (c) Anderson's [2]rotaxane containing γ-cyclodextrin. 42

1.5.10 Early examples of anion-templated interlocked structures: (a) proposed reaction mechanism to form Vögtle's [2]rotaxane using a kinetic anion template, and (b) Ghosh and Schalley's phenoxide-templated [2]rotaxane. 43

1.5.11 Selected examples of discrete anion templation of interlocked and interpenetrated structures: (a) crystal structure of Beer's chloride-templated orthogonal complex, forming a [2]pseudorotaxane, (b) crystal structure of Beer's [2]rotaxane using the same templating method, (c) crystal structure of Beer's handcuff catenane, and (d) crystal structure of Beer's [3]rotaxane. 44

1.5.12 Selected examples of molecular machines: (a) cartoon representation of molecular motion available to catenanes and rotaxanes, and (b) Stoddart's seminal molecular shuttle. 45

1.5.13 Selected examples of molecular machines: (a) Sauvage's metal-responsive "molecular muscles", and (b) cartoon representation of Leigh's oligopeptide-synthesising [2]rotaxane. 45

1.5.14 Applications of interlocked molecules as receptors and sensors for anions: (a) Beer's triazolium-containing [2]rotaxane that is selective for bromide, and (b) crystal structure of Beer's ferrocene-appended electrochemical [2]catenane. 46

2.1.1 Structures of C–H hydrogen-bonding triazole-containing receptors: (a) Flood's foldamer, and (b) Sessler's pyrophosphate-binding triazolophane. 50

2.1.2 Structure of Beer's asymmetric C–H hydrogen-bonding triazolium [2]rotaxane (left) with the 1:1 bromide:host crystal structure (right). 51

2.1.3 Structures of 3,5-bis-triazole pyridinium anion receptors: (a) a hexyl-appended acyclic derivative, (b) a [2]catenane, and (c) a [2]rotaxane. 51

2.1.4 Structures of (a) the *N*-propyl carbazole bis-iodotriazolium [2]rotaxane, and (b) the all-halogen-bonding *N*-propyl carbazole bis-iodotriazolium axle–Re^{I}-bipyridyl bis-iodotriazole macrocycle [2]rotaxane. 52

2.2.1 Crystal structure of **11**·Cl: (a) Perspective view of the receptor drawn as capped sticks and halides as spheres, showing the planar iodotriazole-pyridinium-iodotriazole heterocyclic motif (hydrogen atoms omitted for clarity), and (b) space-filling representation of the receptor showing the host–guest close contacts. Triazole–I···Cl^- halogen bonds (3.121(2)–3.195(2) Å) are indicated as red dashed lines. 56

2.2.2 Crystal structure of **12**·I: (a) Perspective view of the receptor drawn as capped sticks and halides as spheres, showing the planar iodotriazole-pyridinium-iodotriazole heterocyclic motif and (b) thermal ellipsoid representation of the receptor drawn at the 90% confidence level. Triazole–I···I halogen bonds (3.404(1)–3.533(1) Å) are indicated as red dashed lines. Hydrogen atoms and dichloromethane molecules are omitted for clarity. 56

2.2.3 Truncated ^{1}H NMR spectra showing the shift of the pyridinium peak *c* upon addition of 1.0 equivalent of chloride to **13**·PF_6. 57

2.2.4 Anion binding titrations with **13**·PF_6 following proton *c* in DMSO-d_6: experimental titration data (circles) with WinEQNMR2 fitted binding isotherms indicated as lines (298 K). 57

2.3.1 Comparison of truncated ^{1}H NMR spectra of catenane precursors **21** and **27** with catenane **28**·Cl indicating proton shifts due to catenane formation ($CDCl_3$, 500 MHz, 298 K). 61

2.3.2 Truncated 2D ROESY NMR spectrum of **28**·Cl showing selected through-space ^{1}H–^{1}H correlations indicative of an interlocked assembly ($CDCl_3$, 500 MHz, 298 K). 62

2.3.3 Anion binding titrations with **28**·PF_6 following isophthalamide proton *3* in the aqueous solvent mixture 45:45:10 $CDCl_3$:CD_3OD:D_2O: experimental titration data (circles) with WinEQNMR2 fitted binding isotherms indicated as lines (298 K). 63

2.3.4 Crystal structure of **28**·Cl: (a) Perspective view of the receptor drawn as capped sticks and halides as spheres, showing Cl^- bound within the cavity which adopts an "open" conformation in the solid-state (hydrogen atoms (except amide) omitted for clarity), and (b) space-filling representation of the receptor showing the host–guest close contacts. Triazole–I···Cl^- halogen bonds (3.110(2)–3.300(3) Å) are indicated as red dashed lines and amide N–H···Cl^- hydrogen bonds are indicated as orange dashed lines. 64

2.3.5 Crystal structures of **28**$^+$ with (a) chloride (b) bromide, and (c) iodide bound within the cavity, and showing the structural similarity between the host–halide complexes. Hydrogen atoms and the positional disorder in the bromide structure are omitted for clarity. 65

2.3.6 Crystal structure of $\mathbf{28}_2 \cdot SO_4$ showing the 2:1 catenane–anion complex with the anion (SO_4^{2-}) positioned between the two catenane hosts rather than penetrating the binding cavity. Halogen-bonding and hydrogen-bonding interactions are shown as red and orange dashed lines, respectively. Hydrogen atoms (except amide), and the SO_4^{2-} positional disorder on the inversion centre, are omitted for clarity. 66

2.3.7 Crystal structure of$\mathbf{28}\cdot H_2PO_4$ showing the 2:1 catenane–anion complex with the anion ($H_2PO_4^-$) positioned between the two catenane hosts rather than penetrating the binding cavity. Halogen- and hydrogen-bonding interactions are shown as red and orange dashed lines, respectively. Hydrogen atoms (except amide), and the $H_2PO_4^-$ positional disorder on the inversion centre, are omitted for clarity. 67

2.3.8 A simple generic X-ray absorption spectrum showing the various regions that can be used to extract data. 68

2.3.9 Schematic molecular orbital diagram of the contributions to the pre-edge transition energy for $CuCl_4^{2-}$. The pre-edge energy is dependent on shifts both in the Cl_{1s} core energy and in the energy of the highest occupied molecular orbital (HOMO) of the complex. The HOMO energy is determined by overall shifts in the *d*-manifold which correlate to coordination number and charge on the metal as well as the specific repulsive interaction of the HOMO determined by the ligand field of the complex. 69

2.3.10 Systematic series: Molecular structures of the four samples synthesised for study by XAS. 70

2.3.11 Normalised and background subtracted: (a) Cl K- and (b) Br K-edge XAS data for **32**·Cl, **11**·Cl, **30**·Cl and **28**·Cl. 72

2.3.12 Visual representation of the important $\sigma^*_{AX\leftarrow X^-}$ Kohn-Sham acceptor orbitals for $\mathbf{32}^+$, $\mathbf{11}^+$ and $\mathbf{28}^+$. Surface volumes for each orbital are plotted for $\pm$ 0.05 e/Å^3. 74

2.3.13 TDDFT simulated (a) Cl K-edge and (b) Br K-edge XAS spectra for selected halogen-bonding adducts. A constant linear shift was applied to the calculated energies to better match experimental K-edge energies. 75

2.4.1 Truncated ^{1}H NMR spectra of a) bis-amide pyridinium macrocycle $\mathbf{34}\cdot PF_6$, and b) dicationic [2]catenane $\mathbf{35}\cdot(NO_3)_2$ in 1:1 D_2O:CD_3OD (500 MHz, 298 K). 77

2.4.2 Truncated 2D ROESY NMR spectrum for the dicationic catenane $\mathbf{35}\cdot(NO_3)_2$ in 1:1 D_2O:CD_3OD (500 MHz, 298 K). 78

2.4.3 Truncated ^{1}H NMR spectra for the titration of catenane $\mathbf{35}\cdot(NO_3)_2$ with NaCl in 1:1 D_2O:CD_3OD (500 MHz, 298 K) showing spectra for 0.0, 1.0 and 10.0 equivalents of anion, with dotted lines indicating notable shifts. 79

2.4.4 Chemical shifts (ppm) of bis-iodotriazole pyridinium proton *c* on addition of Cl^-, Br^-, I^- and SO_4^{2-} as sodium salts to a solution of $\mathbf{35}\cdot(NO_3)_2$ in 1:1 D_2O:CD_3OD (500 MHz, 298 K). Solid symbols represent experimental data points; continuous lines represent theoretical binding isotherms. . . . 80

2.6.1 Figure showing a) β-cyclodextrin, b) the crystal structure of β-cyclodextrin with cavity dimensions, and c) cartoon representation of the truncated-cone shape of β-cyclodextrin. 86

2.6.2 Figure showing a) the numbering scheme for the carbohydrate units and b) the distribution of 1° and 2° alcohol moieties on the narrow and wide rims, respectively, of the β-cyclodextrin cone. . . 87

2.6.3 2D ROESY spectra for (a) the monocationic [2]rotaxane **71**·Cl and (b) the dicationic [2]rotaxane **73**·$(NO_3)_2$. 91

2.6.4 2D ROESY spectra for (a) the monocationic [2]rotaxane **77**·Cl and (b) the dicationic [2]rotaxane **78**·I · Cl. 93

2.6.5 Plots of change in chemical shift against increasing anion concentration for pCD-appended halogen- and hydrogen-bonding anion receptors in D_2O (298 K). Experimental titration data (circles) with WinEQNMR2 fitted binding isotherms indicated as lines. 94

2.6.6 van 't Hoff analysis of iodide binding for (a) XB-rotaxane **73**·$(NO_3)_2$, (b) HB-triazole rotaxane **72**·$(NO_3)_2$ and HB-amide rotaxane **78**·$(NO_3)_2$ in D_2O. The determined enthalpy and entropy values, and the linear correlation coefficient are shown in each case. 96

2.6.7 MD simulation of **73**·$(NO_3)_2$ with I^-. Representative snapshot showing the iodide binding through two halogen- and hydrogen-bonding interactions, surrounded by four water molecules. The N–H···I^- and C–I···I^- bonding interactions are drawn as purple and yellow dashed lines, respectively. The cyclodextrin stoppers are depicted by a space filling representation. Carbon atoms are shown in cyan in the axle and in orange in the macrocycle, while oxygen, nitrogen and iodine atoms are respectively shown in red, blue, and purple. Selected hydrogen atoms are shown in white. 98

2.6.8 Histogram built with the positions occupied by the iodide along the 50 ns of MD simulation with **73**·$(NO_3)_2$. Colour scheme as in Figure 2.6.7. 98

3.1.1 Examples of hydrogen-bonding nitrate receptors: (a) Singh's fluorescent nitrate sensor, (b) Johnson and Haley's tripodal urea receptor (c) Hamilton's tri-amide macrocycle, (d) Anslyn's bicyclic cyclophane, and (e) Romański's heteroditopic receptor. 104

3.1.2 Figure showing the hydrogen-bonding nitrate-binding [2]rotaxane. 104

3.1.3 Figure showing the hydrogen-bonding nitrate-binding [2]catenane. 105

3.1.4 Cartoon representation of the design of the target halogen-bonding [2]rotaxane for nitrate binding. 106

3.4.1 2D ROESY NMR spectrum of **112**·Cl showing selected through-space ^1H–^1H correlations indicative of an interlocked assembly. 119

3.4.2 Anion binding titrations: (a) **112**·PF_6 following pyridinium proton *j* (1:1 $CDCl_3$:CD_3OD), and (b) **113**·2 PF_6 following the external pyridinium protons *j,k* in the aqueous solvent mixture 45:45:10 $CDCl_3$:CD_3OD:D_2O. Experimental titration data (circles) with WinEQNMR2 fitted binding isotherms indicated as lines (298 K). 122

3.5.1 Anion binding titration data for **121**·$(OTf)_3$ following pyridinium proton *j*. Experimental titration data (circles) with WinEQNMR2 fitted binding isotherms indicated as lines (9:1 D_2O:acetone-d_6, 298 K). 126

4.1.1 Figure showing Schmidtchen's zwitterionic anion host systems. 130
4.1.2 Figure showing Ballester's pyridine-*N*-oxide-containing [2]pseudorotaxane templated by cyanate. 130
4.1.3 Jiang's pseudorotaxane assembly with pH-switchable threading capability between a pyridine-*N*-oxide threading species and an isophthalamide macrocycle. 131
4.1.4 The formation of an interpenetrated assembly with a pyridine-*N*-oxide thread and an isophthalamide macrocycle, with dethreading induced by chloride. 131
4.1.5 Figure showing *N*-oxide-containing [2]rotaxanes: a) alkali metal-templated [2]rotaxane displaying cation-induced pirouetting molecular motion, and b) lanthanide-containing [2]rotaxane. 132
4.1.6 Figure showing *N*-oxide-containing neutral and cationic [2]rotaxanes for anion recognition. . . . 132
4.2.1 Anion binding titrations with **124** following the internal pyridine-*N*-oxide proton *i* in the solvent mixture 9:1 $CDCl_3$:CD_3OD: experimental titration data (circles) with WinEQNMR2 fitted binding isotherms indicated as lines (298 K). 134
4.3.1 2D ROESY NMR spectrum of **138** showing (a) selected through-space ^1H–^1H correlations indicative of an interlocked assembly, and (b) an enlargement of the aromatic region of the spectrum showing selected cross-couplings which reveal the preferred co-conformation of the axle and macrocycle components. 139
4.3.2 Anion binding titrations: (a) **138** following the internal pyridine proton *o* (1:1 $CDCl_3$:CD_3OD), and (b) **140**·2 PF_6 following the internal pyridine-*N*-oxide proton *i* (45:45:10 $CDCl_3$:CD_3OD:D_2O): experimental titration data (circles) with WinEQNMR2 fitted binding isotherms indicated as lines (298 K). 141
4.5.1 Proposed structure of a terphenyl-stoppered 3,5-bis-iodotriazole pyridine-*N*-oxide-containing [2]rotaxane. 146

8.1.1 Thermal ellipsoid plot showing the asymmetric unit for the single-crystal structure of compound **11**·Cl. Atomic displacement ellipsoids drawn at the 50% probability level. Hydrogen atoms have been omitted. 259
8.1.2 Thermal ellipsoid plot showing the asymmetric unit for the single-crystal structure of compound **12**·I. Atomic displacement ellipsoids drawn at the 90% probability level. Hydrogen atoms have been omitted. 260
8.1.3 Thermal ellipsoid plot showing the asymmetric unit for the single-crystal structure of compound **28**·Cl. Atomic displacement ellipsoids drawn at the 50% probability level. Hydrogen atoms have been omitted. 261

8.1.4 Thermal ellipsoid plot showing the asymmetric unit for the single-crystal structure of compound **28**·Br. Atomic displacement ellipsoids drawn at the 50% probability level. Hydrogen atoms have been omitted. 262

8.1.5 Thermal ellipsoid plot showing the asymmetric unit for the single-crystal structure of compound **28**·I. Atomic displacement ellipsoids drawn at the 50% probability level. Hydrogen atoms have been omitted. 263

8.1.6 Thermal ellipsoid plot showing the asymmetric unit for the single-crystal structure of compound $\mathbf{28}_2 \cdot SO_4$. Atomic displacement ellipsoids drawn at the 50% probability level. Hydrogen atoms have been omitted. 264

8.1.7 Thermal ellipsoid plot showing the asymmetric unit for the single-crystal structure of compound **28**·H_2PO_4. Atomic displacement ellipsoids drawn at the 50% probability level. Hydrogen atoms have been omitted. 265

List of Tables

1.2.1 Effective ionic radii of isoelectronic cations and anions. 12

1.2.2 Hydration energies of isoelectronic cations and anions. 13

2.2.1 Results of CuAAC click reactions to synthesise the 3,5-bis-iodotriazole pyridine precursors. . . . 55

2.2.2 Association constants (K_a) determined for various TBA·anions with **13**$^+$ compared with the prototriazole analogue. 58

2.3.1 Association constants for **28**·PF_6 with various anions compared with the prototriazole analogue. . 63

2.3.2 Crystallographically determined halogen-bond lengths and percentage shortening of the sum of the van der Waals' radii (%VdW). 65

2.3.3 Experimentally obtained pre-edge intensities and the corresponding % charge donation of chloride donor complexes. 72

2.3.4 DFT-calculated parameters obtained for halide adducts. All calculated values are for fully optimised structures at the B3LYP/def2-TZVP+ZORA level of theory. 74

2.4.1 Association constants for **35**·$(NO_3)_2$ with various anions in 1:1 D_2O:CD_3OD (500 MHz, 298 K). . 80

2.6.1 Anion association constants K_a (M^{-1}) in water. 95

2.6.2 Thermodynamic parameters (kJ mol^{-1}) for I^- in D_2O. 97

2.6.3 Halogen- and hydrogen-bond distances (Å)[a], and the average number of water molecules within the first solvation shell of each bound halide anion (3.5 Å cut-off) for 100 ns of sampling of MD simulations of **73**·$(NO_3)_2$ with halides. 99

2.6.4 $\Delta\Delta G$ (kJ mol^{-1}) for halide complexes of **73**·$(NO_3)_2$. 99

3.2.1 Synthetic conditions for the deprotection of **81**. 109

3.2.2 Synthetic conditions for the preparation of **94**. 112

3.2.3 Attempted reaction conditions for the synthesis of **94**. 112

3.4.1 Association constants $(K_a)^{[a]}$ determined for **112**·PF_6 and **113**·2 PF_6 with various TBA·anions. . 122

3.5.1 Association constants $(K_a)^{[a]}$ determined for **121**·$(OTf)_3$ with various Na·anions. 126

4.2.1 Association constants $(K_a)^{[a]}$ determined for various TBA·anions with acyclic 3,5-bis-iodotriazole pyridine-*N*-oxide receptor **124**. 134

4.3.1 Association constants $(K_a)^{[a]}$ determined for various TBA·anions with neutral asymmetric [2]rotaxane **138** and dicationic asymmetric [2]rotaxane **140**·2 PF_6 141

8.1.1 Crystal data and structure refinement for **11**·Cl 259
8.1.2 Crystal data and structure refinement for **12**·I 260
8.1.3 Crystal data and structure refinement for **28**·Cl 261
8.1.4 Crystal data and structure refinement for **28**·Br 262
8.1.5 Crystal data and structure refinement for **28**·I 263
8.1.6 Crystal data and structure refinement for $\mathbf{28}_2 \cdot SO_4$ 264
8.1.7 Crystal data and structure refinement for **28**·H_2PO_4 265

List of Schemes

1.2.1 The Hofmeister Series. 13

1.5.1 The use of "*active metal templation*" in the synthesis of interlocked molecules: Leigh's proposed mechanism for the metal-templated CuAAC reaction to form a [2]rotaxane. 39

1.5.2 Schematic mechanism for the β-galactosidase enzyme-mediated release of Met-enkephalin from Leigh's [2]rotaxane. 47

2.2.1 Synthetic scheme to prepare **1** and **2**. 53

2.2.2 Synthetic scheme to prepare azides: **3**, **4**, **5** and **6**. 54

2.2.3 Synthetic scheme to prepare the 3,5-bis-iodotriazole pyridine precursors: a) using the one-pot method and b) the two-pot method. 54

2.2.4 Synthesis of cationic acyclic receptors $\mathbf{11}^+$, $\mathbf{12}^+$, $\mathbf{13}^+$ and $\mathbf{14}^+$. 55

2.3.1 Synthesis of the vinyl-appended azide **19**. 59

2.3.2 Synthetic route to prepare the vinyl-appended 3,5-bis-iodotriazole pyridinium-containing macrocycle precursor **21**·Cl *via* the one-pot click methodology, and subsequent methylation and anion exchange. 59

2.3.3 Synthesis of the isophthalamide macrocycle **27**. 60

2.3.4 Synthetic route to prepare catenane **28**·PF_6 *via* clipping using Grubbs' II ring-closing metathesis catalyst. 60

2.3.5 Synthesis of **30**·X: CuAAC click reaction to form 3,5-bis-triazole pyridine precursor **30**, followed by methylation and anion exchange to afford the 3,5-bis-triazole pyridinium receptor samples. . . 70

2.3.6 Synthesis of **32**·X: one-pot CuAAC iodo-click reaction to form the bis-octyl-appended iodotriazole precursor **31**, followed by methylation and anion exchange to afford the bis-octyl-appended iodotriazolium receptor samples. 71

2.4.1 Synthetic scheme to prepare monocationic pyridinium bis-acid macrocycle **34**·PF_6 for use in catenane formation. 76

2.4.2 Synthetic scheme to prepare dicationic catenane **35**·$(NO_3)_2$ *via* a clipping method using Grubbs' II ring-closing metathesis catalyst. 77

2.5.1 Synthesis of the aryl-azide stopper **38**, the propyl-azide stopper **41** and the alkynyl stopper **42**. . . 81

2.5.2 Attempted synthesis of axle components bearing the 3,5-bis-iodotriazole pyridinium motif. 82

2.5.3 Attempted synthesis of the bis-azide-appended 3,5-bis-iodotriazole pyridine synthon **51**. 82
2.5.4 Synthesis of the halogen-bonding macrocycle **53**. 83
2.5.5 Attempted synthesis of a macrocycle from the Grubbs' II ring-closing metathesis reaction with vinyl-appended macrocycle precursor **21**·Cl. 84
2.5.6 Attempted synthesis of a homocatenane of vinyl-appended bis-iodotriazole pyridinium macrocycle precursor *via* chloride-templated double cyclisation methodology. 84
2.5.7 Attempted synthesis of [2]rotaxane hosts comprised of a proto- or iodo-triazolium axle with a macrocyclic component containing the 3,5-bis-iodotriazole pyridinium motif. 85
2.6.1 Initial synthetic scheme to form mono-functionalised azido-permethylated β-cyclodextrin **65**. . . 88
2.6.2 Synthetic scheme to form mono-functionalised azide-permethylated-β-cyclodextrin **65**. 89
2.6.3 Synthesis of water-soluble permethyl-β-cyclodextrin-appended hydrogen- and halogen-bonding [2]rotaxanes **72**·$(NO_3)_2$ and **73**·$(NO_3)_2$. 90
2.6.4 Synthesis of water-soluble permethyl-β-cyclodextrin-appended amide hydrogen-bonding [2]rotaxane **78**·$(NO_3)_2$. 92
2.6.5 Attempted synthesis of an all-halogen-bonding [2]rotaxane **79**·Cl. 100
3.2.1 Synthetic scheme to prepare an asymmetric halogen-bonding axle. 107
3.2.2 Scheme for the attempted synthesis of **90**. 109
3.2.3 Synthetic scheme to deprotect **81** with TBAF to facilitate asymmetric synthesis *via* a different route. 109
3.2.4 Alternative attempts at TBDMS-alkyne deprotection using intermediates in the synthetic route and different deprotection agents. 110
3.2.6 Synthetic scheme to prepare TMS-protected asymmetric diyne **94**. 110
3.2.5 Synthetic scheme to prepare an asymmetric halogen-bonding axle. 111
3.2.7 Alternative synthetic scheme to prepare TMS-protected asymmetric diyne **94**. 112
3.2.8 Synthetic scheme for the deprotection of **94** to form **91** and the subsequent attempt at iodination of the alkyne to form **96**. 113
3.2.9 Attempted syntheses to append suitable stopper units to **91** *via* the one-pot click methodology with azides **65**, **38** and **41**. 114
3.2.10 Attempted syntheses to form the axle component from the inside out by joining two equivalents of precursor alkynes with bis-azide **50**. 115
3.3.1 Initial test reactions of the one-pot click methodology for the formation of mono-substituted alkynes. 115
3.3.2 Attempted mono-click of di-iodoethynyl pyridine **2** and azido propanol **46** to form monosubstituted pyridine **105**. 115
3.3.3 Synthesis of the key intermediate in the preparation of an asymmetric axle component: mono-stoppered iodoalkyne pyridine **106**. 116
3.3.4 Synthesis of asymmetric stoppered 3,5-bis-iodotriazole mesylate **108** and subsequent stoppered 3,5-bis-iodotriazole azide **109**. 116

3.3.5 Synthesis of cationic asymmetric axle precursor **110**·BF_4. 117
3.3.6 Synthesis of the asymmetric axle *via* a two-pot click reaction between **110**·BF_4 and **106**. 117
3.4.1 Synthetic scheme for the two-pot click reaction to form the monocationic asymmetric [2]rotaxane **112**·PF_6. 118
3.4.2 Methylation of monocationic asymmetric [2]rotaxane **112**·PF_6 to form the dicationic symmetric [2]rotaxane **113**·2 PF_6. 120
3.4.3 Synthetic scheme for the two-pot click reaction to form the dicationic asymmetric [2]rotaxane **114**·2 PF_6. 121
3.5.1 Synthetic route towards the preparation of a cyclodextrin-appended asymmetric axle precursor *via* the monosubstituted pyridine-iodoalkyne **115** and the permethyl-β-cyclodextrin-appended bis-iodotriazole pyridine mesylate **116**. 123
3.5.2 Synthesis of the asymmetric cyclodextrin-appended bis-iodotriazole azide **117**, and subsequent methylation and anion exchange to **118**·Cl. 124
3.5.3 Two-pot synthetic scheme to prepare the monosubstituted cyclodextrin-appended iodo-ethynyl pyridine **119**. 124
3.5.4 Synthesis of the permethyl-β-cyclodextrin-appended asymmetric monocationic and symmetric dicationic [2]rotaxanes, **120**·Cl and **121**·$(OTf)_3$, respectively. 125
4.2.1 Synthesis of acyclic bis-proto- and iodo-triazole pyridine-*N*-oxide receptors. 133
4.3.1 Synthesis of the 3,5-bis-iodotriazole pyridine-*N*-oxide half-axle **126**. 135
4.3.2 Synthetic scheme to prepare the bis-azide ditopic macrocycle precursor **130**. 136
4.3.3 Synthesis of the halogen-bonding ditopic macrocycle, **132**. 136
4.3.4 Synthesis of hydrogen-bonding ditopic macrocycles **134** and **135**. 137
4.3.5 Synthesis of the neutral asymmetric [2]rotaxane **138**, and the attempted synthesis of **136** and **137**. 138
4.3.6 Test reaction to determine whether CH_3I could methylate the pyridine-*N*-oxide using **124** as the test compound. 139
4.3.7 Synthesis of the dicationic asymmetric *N*-oxide [2]rotaxane **140**·2 PF_6. 140
4.4.1 Attempted synthesis of a neutral terphenyl-stoppered [2]rotaxane **142**. 143
4.4.2 Attempted synthesis of a neutral water-soluble permethyl-β-cyclodextrin-appended all-halogen-bonding [2]rotaxane **144** *via* chloride-templated double CuAAC click reaction. 144
4.4.3 Attempted synthesis of a neutral water-soluble permethyl-β-cyclodextrin-appended [2]rotaxane **146** *via* chloride-templated amide condensation. 144

Chapter 1

Introduction

1.1 Supramolecular chemistry

The field of supramolecular chemistry has experienced rapid growth over the last few decades, encompassing an extensive and interdisciplinary approach to the fundamental understanding of non-covalent interactions, and their application in the design and assembly of discrete supermolecules, complex molecular architectures and functional systems. The concept of the supramolecular synthon was introduced by Desiraju[1] and is analogous to Corey's organic synthon:[2] supermolecules can be assembled through non-covalent intermolecular bonds in the same way that molecules are built up *via* covalent bonds. Lehn described supramolecular chemistry as:

> *"the chemistry of the intermolecular bond, covering the structures and functions of the entities formed by the association of two or more chemical species."*[3]

In addition, supramolecular chemistry encompasses the subordinate fields of host–guest chemistry and self-assembly. Host–guest chemistry refers to the association of a substrate molecule with a larger receptor molecule *via* intermolecular interactions. Pedersen's seminal reports in 1967 on the ability of crown ethers to complex alkali metal cations stimulated research into synthetic molecular recognition through the design and synthesis of complex host architectures capable of selective guest binding in addition to many other desirable properties.[4] Indeed, the field developed with the reports of selective Group I metal cation recognition in both Lehn's three-dimensional cryptands (Figure 1.1.1a)[5] and Cram's rigid spherands (Figure 1.1.1b)[6], resulting in the 1987 Nobel Prize in Chemistry being awarded to Lehn,[3] Cram[7,8] and Pedersen[9] *"for their development and use of molecules with structure-specific interactions of high selectivity."* The first abiotic anion receptors were reported soon after Pedersen's crown ethers; Park and Simmons' protonated macrobicyclic amine derivatives were shown to encapsulate halide anions in aqueous TFA solution (Figure 1.1.1c).[10] Despite this early example, the field of anion supramolecular chemistry was, for the most part, neglected in comparison to the more popular field of cation coordination chemistry until the late 1970s. Nonetheless, the surge in interest in the last few decades has established the rapidly advancing field of anion supramolecular chemistry as a significant area of research.[11]

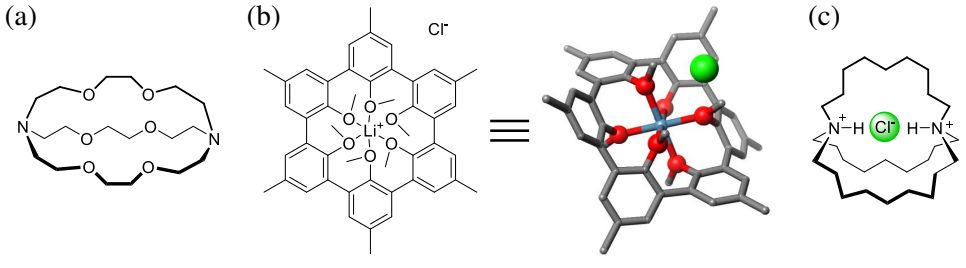


Figure 1.1.1: Figure showing (a) Lehn's three-dimensional cryptands,[5] (b) Cram's spherands[6,7] and (c) Park and Simmons' macrobicyclic anion receptors.[10]

Self-assembly, on the other hand, refers to the spontaneous, autonomous arrangement of multiple specially-designed molecules in the construction of higher-order, complex architectures. Using these principles, impressive structures such as Stoddart's Borromean rings (Figure 1.1.2a)[12] and Leigh's pentameric chloride-templated knot (Figure 1.1.2b)[13,14] can be prepared.

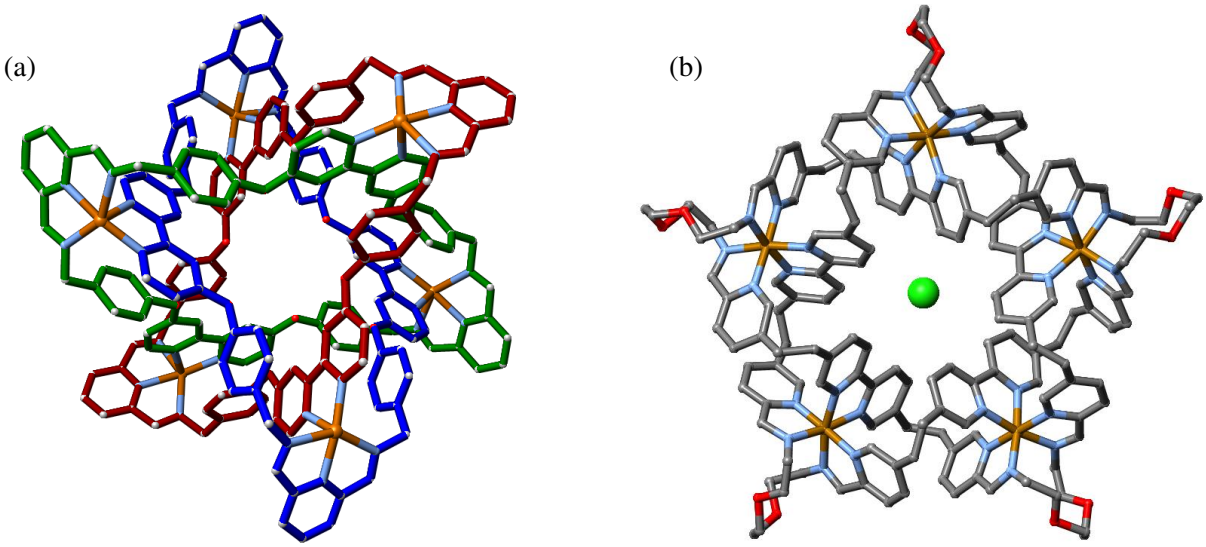


Figure 1.1.2: Crystal structures of (a) Stoddart's Borromean rings[12] (each of the macrocycles are coloured in blue, red and green for simple visualisation), and (b) Leigh's pentameric Fe^{II} chloride-templated knot.[13,14]

Of course, Nature's ability to recognise molecular substrates in biological processes is unparalleled, as exemplified by the highly-selective binding of substrates to enzymes. Certainly, enzymes themselves are multimolecular superstructures formed by the aggregation of uniquely-devised molecular units into which the substrate binding site is encoded. Furthermore, the folding of polypeptides into highly ordered architectures, cellular recognition and the transcription, translation and replication of nucleic acids, all represent remarkable examples of Nature's ability to use intermolecular interactions in fundamental biological processes.[11]

This chapter will introduce the field of supramolecular chemistry, particularly emphasising the areas relevant to the theme of this thesis: specifically anion receptor chemistry and recognition, and the assembly of interpenetrated and interlocked structures.

1.1.1 Host–guest chemistry

The field of supramolecular host–guest chemistry is inspired by Nature and molecular recognition in biochemical processes: the binding of a substrate to a host molecule, such as a protein or enzyme. Towards the end of the 19^{th} Century, Fischer proposed the 'lock and key' hypothesis, describing the specific binding of a substrate, the key, to the active site in an enzyme, the lock (Figure 1.1.3a).[15] This

analogy was expounded by Koshland in the 1950s to consider the ability of a substrate molecule to induce a conformational change in the enzyme host, with a concomitant, observable enhancement in recognition and selectivity: known as the 'induced-fit' model (Figure 1.1.3b).[16,17] Since then, research in this area has elucidated some general principles for the design of supramolecular architectures for synthetic molecular recognition.

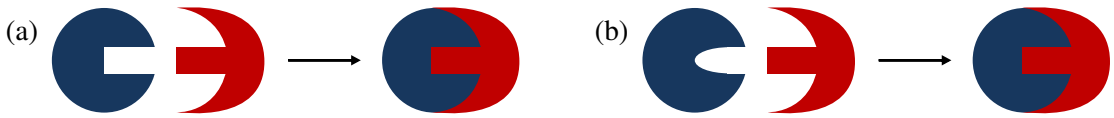


Figure 1.1.3: Models of host–guest binding: (a) Fischer's 'lock and key' hypothesis,[15] and (b) Koshland's 'induced-fit' model.[16,17]

1.1.1.1 Fundamental aspects and design principles

Complementarity: The concepts of the 'lock and key' and 'induced-fit' mechanisms are now more generally encompassed by the term *complementarity*, which states that the cumulative effect of weak, non-covalent interactions is maximised between two or more interacting molecular species when they are geometrically complementary to one another. Consequently, the design of suitable hosts for target guest molecules typically considers the geometric and electronic properties of the guest, matching the *size* and *shape* of the synthetic receptor's cavity. Moreover, in order to maximise the strength of association, the inclusion of appropriate non-covalent interactions further aids selective binding of the guest over mismatched guests of incorrect size/shape.

Preorganisation and the chelate/macrocyclic effects: Cram introduced the concept of *preorganisation* in the 1980s,[8] describing the enhanced binding strength observed when the host exists in a favourable conformation prior to guest association:

> *"the more highly hosts and guests are organized for binding and low solvation prior to their complexation, the more stable will be their complexes."*[8]

The chelate effect pertains to the enhanced stability of complexes containing chelate rings when compared to those analogous complexes that contain no such rings,[18,19] where the entropy of desolvation is more favourable for multidentate ligands than monodentate ligands.

Similarly, the macrocyclic effect refers to ligand donors which have been incorporated into cyclic structural frameworks, which results in improved complex stability when compared with acyclic analogues.[20–22] This is due to several factors: enhanced kinetic stability of the host–guest complex due to

size complementarity which lowers the enthalpy, the relatively lower solvation of macrocycles, resulting in a lower enthalpic penalty from desolvation prior to guest binding, and a favourable entropic term arising from the more rigid preorganised macrocyclic structure, losing fewer degrees of freedom upon host–guest complexation.

1.1.2 Non-covalent interactions

The term "supramolecular" literally means "*beyond the molecule*" and consequently, supramolecular chemistry is concerned with the interactions between molecules, which govern the processes of host–guest association and self-assembly. Non-covalent interactions, with the exception of the electrostatic attraction between opposite charges, tend to be remarkably weaker than traditional covalent bonds: non-covalent bond enthalpies range up to $\sim$ 200 kJ mol^{-1} in comparison to 300–500 kJ mol^{-1} for covalent carbon–carbon single bonds.[23] As a result, non-covalent interactions are often reversible and subject to thermodynamic control. However, when used in concert, the cumulative effect of multiple associative intermolecular interactions can facilitate the formation of stable assemblies. The set of intermolecular interactions are discussed below with a special emphasis on those relevant to this thesis.

1.1.2.1 Coulombic forces

These encompass the attractive electrostatic interactions between opposite charges, which are subdivided into *ion–ion*, *ion–dipole* and *dipole–dipole* interactions, the strength of which is dependent on the magnitude of the charges and their separation (Figure 1.1.4). Attractive ion–ion interactions arise between oppositely-charged species and while they are comparable in strength to covalent bonds, facilitating, for example, anion binding in competitive solvent media (polar, protic solvents), they are isotropic requiring more directional interactions to enhance selective binding.[24] Ion–dipole and dipole–dipole interactions, although weaker in magnitude, display enhanced directionality as the strength of interaction is maximised according to the relative orientation of the dipole. For this reason, these interactions have been exploited in supramolecular chemistry as they allow for improved selectivity in molecular recognition.[25]

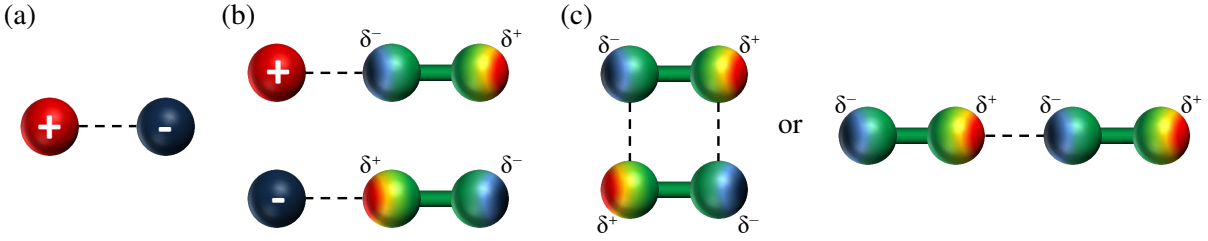


Figure 1.1.4: The three classes of Coulombic forces: (a) ion–ion, (b) ion–dipole, and (c) dipole–dipole interactions.

1.1.2.2 Hydrogen bonding

Hydrogen bonds (HBs) are ubiquitous in Nature; responsible for the stabilisation of the secondary and tertiary structures of proteins and enzymes, as well as DNA base-pair recognition, for example. The hydrogen bond was recently defined by IUPAC as:

> *"[a] hydrogen bond is an attractive interaction between a hydrogen atom from a molecule or a molecular fragment X–H in which X is more electronegative than H, and an atom or a group of atoms in the same or a different molecule, in which there is evidence of bond formation."*[26]

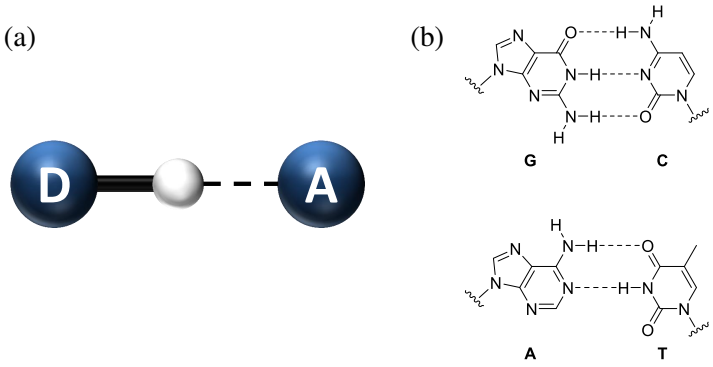


Figure 1.1.5: Hydrogen bonding: (a) cartoon representation of Donor–H···Acceptor hydrogen bonds, and (b) pairing of DNA base pairs *via* hydrogen bonds.

Consequently, the hydrogen bond is a special class of dipole–dipole interactions, or ion–dipole interactions when interacting with an anion *via* the partial positive charge developed by the polarisation of the hydrogen atom. Hydrogen-bonding interactions are primarily electrostatic in nature with energies in the range of 4–170 kJ mol^{-1}.[27] The strength of these interactions is maximised when the donor–H···acceptor angle is near linearity, with weaker interactions deviating greatly from 180°. For these reasons, it is unsurprising that hydrogen bonds have been the most widely-exploited interaction in supramolecular chemistry (Figure 1.1.5).

1.1.2.3 Halogen bonding

The halogen bond (XB) is similar to the hydrogen bond as it also constitutes a special class of dipole–dipole interactions, or ion–dipole interactions. Recently defined by IUPAC, a "halogen bond" is said to occur when:

> *"there is evidence of a net attractive interaction between an electrophilic region on a halogen atom X belonging to a molecule or a molecular fragment RX (where R can be another*

atom, including X, or a group of atoms) and a nucleophilic region of a molecule, or molecular fragment, YZ."[28]

While it may seem counterintuitive for a halogen atom to possess an electrophilic region, when bound to an electron-withdrawing R-group, the halogen atom may become polarised, developing an equatorial belt of partial negative charge and a region of partial positive charge at the terminus of the R–X bond, termed the σ-hole (Figure 1.1.6a).[29] The σ-hole is capable of interacting with electron-rich Lewis bases (both neutral and anionic) *via* electrostatic, charge transfer and dispersion contributions in addition to orbital interactions, making halogen bonds highly anisotropic, and constraining the interaction angles close to linearity (Figure 1.1.6b). The strength of halogen-bonding interactions increases with greater polarisability of the halogen atom in the order F $<<$ Cl $<$ Br $<$ I, with interaction energies spanning 5–180 kJ mol^{-1}.[30] Furthermore, the strength can be maximised by increasing the electron-withdrawing nature of the R-group and/or varying the *sp*-hybridisation of the R-group in the order C(sp^3)–X $<$ C(sp^2)–X $<$ C(sp)–X. An appealing consequence is that this offers tunability and selectivity to the interaction.[31]

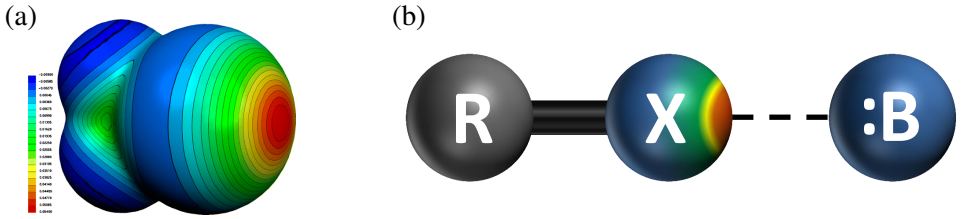


Figure 1.1.6: Halogen bonding: (a) electrostatic potential diagram of CF_3I showing the σ-hole as the region of positive potential (red) in Hartrees, at the 0.001 electrons Bohr^3 iso-density surface,[29] and (b) cartoon representation of a halogen bond with a Lewis base (R = halogen, aryl, alkyl, etc.; X = Cl, Br, I; B = N, O, S, Se, Cl, Br, I, F^-, Cl^-, Br^-, I^-, etc.).

1.1.2.4 π–π, Donor–acceptor and solvophobic interactions

The spontaneous alignment of aromatic rings in an offset parallel *face-to-face* (commonly termed π–π stacking) manner (Figure 1.1.7a) has, for a long time, been considered a notable interaction in supramolecular and biological chemistry,[32,33] with *face-to-edge* (Figure 1.1.7b) and directly stacked geometries also observed. In particular, recent theoretical calculations have shown that the face-to-face interactions arise from a combination of solvation effects, dispersion forces and electrostatics—factors which influence all intermolecular interactions, and thus disprove previous theories of π-orbital overlap.[34–36]

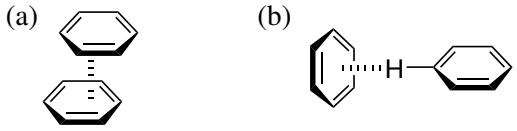


Figure 1.1.7: Aromatic π–π donor–acceptor interactions: (a) face-to-face, and (b) face-to-edge.

Of the non-covalent interactions present between aromatic rings, donor–acceptor and solvophobic effects are commonly used in supramolecular chemistry despite their relatively weak enthalpies. Donor–acceptor aromatic interactions refer to the favourable attractive association of electron-rich and electron-deficient rings, the strength of which can be enhanced by the incorporation of electrostatic charge on one or both rings. Notably, the alignment of these contacts is often significantly influenced by the ring substituents.[37,38]

Solvophobic effects refer to the preferential aggregation of apolar molecules in polar solvents and is termed the hydrophobic effect when aqueous media is used.[39–41] The "classical" hydrophobic effect is characteristically driven by entropy: although favourable dispersion forces are present between the apolar molecules and the polar solvent, desolvation of the molecules due to aggregation results in a gain in entropy, which is only slightly mitigated by the molecular association in solution.[39,42–44] In contrast, the "non-classical" hydrophobic effect is characterised by a dominant enthalpy term owing to the liberation of high-energy water molecules from the hydrophobic cavity of a host, for example, a macrocycle.[45] Within the cavity, these molecules form fewer hydrogen bonds than the bulk water, but upon release may form more cohesive water–water interactions leading to a gain in enthalpy.

1.1.2.5 Cation– and anion–π interactions

The attractive interaction between charged substrates and aromatic π-systems is known in the solid, solution and gas phases, and in biological systems. The well-established cation–π interaction, driven by electrostatics, arises between a cationic species and an electron-rich, partially negative quadrupole of an aromatic π-system (Figure 1.1.8a).[46–49] Conversely, the more recently identified anion–π interactions[50] form between an anionic species and an electron-deficient aromatic system and have been more widely studied in the solid[51] and gas phases[52] than in solution (Figure 1.1.8b). Although anion–π interactions tend to be weak in solution, they are often supplemented by additional non-covalent interactions and employed in aprotic, relatively non-competitive solvents to maximise the strength of interaction.[53–57] It should be noted that the π-electrons do not play any role in this particular case of anion–π interactions and thus, the term "anion–π" is misleading. Indeed, since the anion–π interaction is dominated by electrostatics and anion-induced polarisation of the delocalised electron density, it is more accurate to consider this interaction in terms of the electrostatic, donor–acceptor and solvophobic effects.[36] Nonetheless, Matile has exploited this interaction to great effect in his synthetic membrane transport compounds capable of transporting anions across bilayer membranes (Figure 1.1.8c).[58]

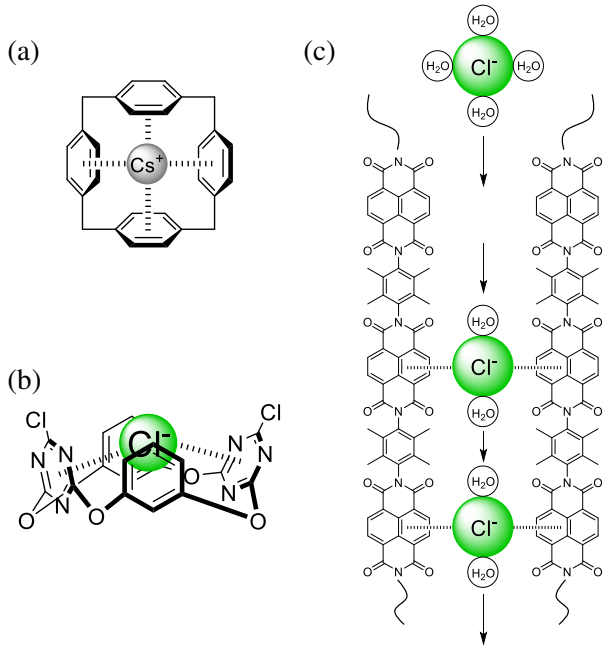


Figure 1.1.8: Examples of ion–π interactions: (a) cation–π interaction,[59] (b) anion–π interaction,[55] and (c) one of Matile's anion–π slides for transmembrane transport.[58]

1.1.2.6 Dispersion (van der Waals') forces

The attractive interaction between random, spontaneous dipoles arises as the result of the polarisation of an electron cloud by proximal adjacent nuclei, and is dependent on the number of electrons in the system. Furthermore, the polarisation of these instantaneous dipoles can be augmented by the presence of dipoles on nearby molecules, known as a dipole–induced dipole interactions. Although, these interactions are weakly attractive, when acting in concert they are known to provide additional stabilisation to the association of molecules. The electrostatic nature of these forces implies less directional constraint than in other intermolecular interactions, and therefore, these are less commonly considered in the design and assembly of supramolecular architectures.[11]

1.1.2.7 Coordinate bond

Lewis acid–base coordination, encompassing metal–ligand coordination, often involves a significant degree of orbital overlap, resulting in the classification of these interactions as molecular rather than supramolecular. However, they possess many of the qualities of supramolecular interactions such as the reversibility observed in these sometimes labile bonds, making them acutely suitable for application in strong host–guest association, self-assembly and the construction of higher-order supramolecular architectures (Figure 1.1.9), particularly when considering the specific geometric requirements of metal ion coordination.[11,60,61]

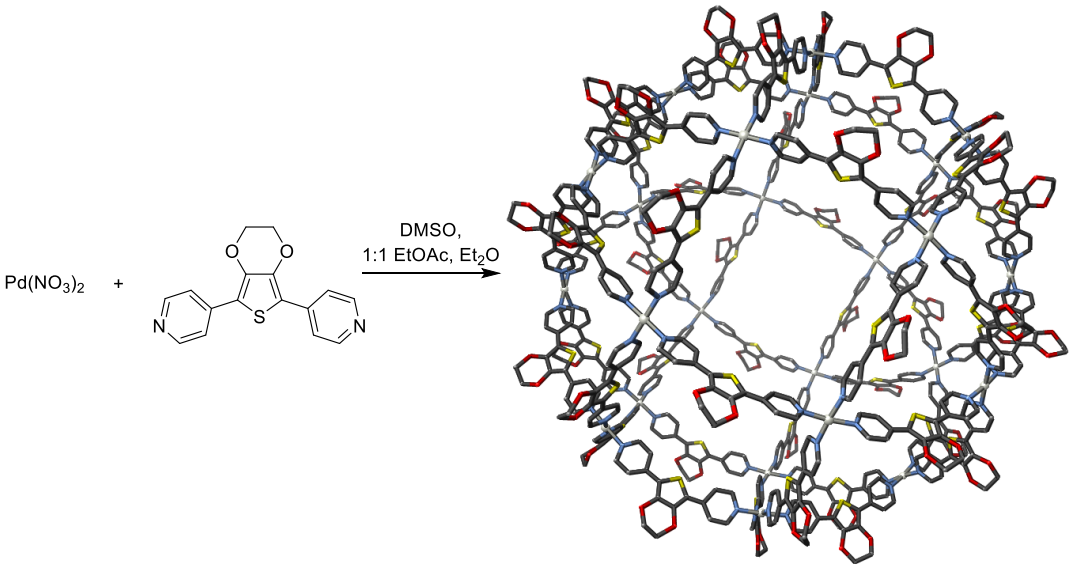


Figure 1.1.9: Example of a supramolecular $M_{24}L_{48}$ cage structure assembled *via* metal–ligand coordinate bonds between simple starting components.[60,61]

1.2 Anion binding

The *leitmotif* of this thesis is the complexation of anions by complementary receptors. This section is intended to provide a brief discussion of the vast field of anion supramolecular chemistry, in particular highlighting relevant biological and synthetic receptor examples from the early, as well as modern literature.

1.2.1 The importance of anions

The critical importance of anions in many chemical, environmental, biological and medical processes is well-known. Chemically, anions can behave as bases, nucleophiles and catalysts, and their efficacy can be tuned by modifying their coordination properties. Regarding the environment, anions such as phosphate and nitrate are necessary in agricultural fertilisers; however, their overuse in arable farming has resulted in the eutrophication and disruption of natural aquatic ecosystems. Anions such as pertechnetate, produced as a radioactive by-product of the nuclear fuels industry, present major pollution hazards, whilst naturally occurring arsenate and cyanide pose significant health risks due to their acute toxicity.[11]

In the context of biology, the familiar DNA and RNA macromolecules, responsible for the storage and dissemination of genetic information within living organisms, are polyanions, comprising phosphate-ester backbone scaffolds to support the sugar-nucleotides.[62] Furthermore, the molecular energy currency,

ATP, is anionic and performs crucial roles in intracellular energy transfer and signal transduction. Indeed, approximately 70% of enzymatic co-factors and substrates are negatively charged.[63]

Many inorganic anions are also involved in biochemical processes: chloride performs a central role in a variety of vital mammalian physiological processes, such as respiration, metabolism, osmotic and blood pressure, neurotransmission, and the acid–base balance within the body.[11,64,65] However, disruptions in cellular transmembrane ion transport can have life-threatening effects, particularly where chloride misregulation is concerned, implicating this halide anion in several diseases such as cystic fibrosis,[66] Best disease[67] and Dent's disease,[68] which cause the severe degeneration of lungs and other vital organs, loss of vision and renal failure, respectively. Of the other halides, iodide is essential in the biosynthesis of hormones in the thyroid gland, and fluoride is found in drinking water and toothpaste to strengthen teeth, although over-exposure to fluoride has been blamed for several health conditions. Furthermore, over-exposure to nitrate has been implicated in diseases such as methemoglobinemia (blue-baby syndrome) in infants.

Considering these examples, it is clear that the design and fabrication of suitable anion sensors and sequestering agents is of great importance, and their application in environmental and medical contexts is cogent.

1.2.2 Intrinsic properties of anions

The field of anion receptor chemistry is relatively underdeveloped when compared to that of cation receptors. While strong and selective binding of cations may be commonly achieved in aqueous media, the same is not true for anions; this section will discuss some of the reasons for this.

Size: Anions are larger than their isoelectronic cations owing to lower effective nuclear charge: a comparison of effective ionic radii is shown in Table 1.2.1. As a result, anions have lower charge densities, which leads to weakened electrostatic interactions between a target anion and positively-charged host, often requiring supplementary interactions for effective recognition. Nonetheless, anions are often more polarisable than their isoelectronic cations, allowing dispersive interactions to contribute more substantially towards stabilising host–anion complexes.

Table 1.2.1: Effective ionic radii of isoelectronic cations and anions.

Cation	Effective ionic radius (Å)	Anion	Effective ionic radius (Å)
Na^+	1.02	F^-	1.31
K^+	1.37	Cl^-	1.81
Rb^+	1.52	Br^-	1.96
Cs^+	1.67	I^-	2.20

Effective ionic radii of 6-coordinate ions as reported by Shannon.[69]

Geometry: Anions adopt a variety of geometries (Figure 1.2.1) including spherical (halides), linear (cyanide, cyanate, azide), trigonal planar (acetate, nitrate), tetrahedral (sulfate, phosphate, tetrafluoroborate), octahedral (hexafluorophosphate,) and more complex structures (ATP, DNA, etc.), contrasting the exclusively spherical shape of metal cations. While this offers potential advantages in selectivity *via* host–guest complementarity, the design and synthesis of such hosts is synthetically challenging.

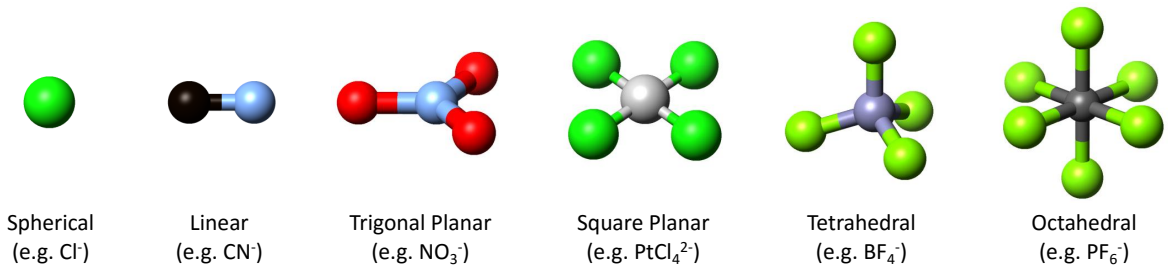


Figure 1.2.1: Selected examples of different geometries adopted by anions.

pH dependence: Many anions are subject to protonation equilibria that result in the loss of negative charge at low pH, impairing the use of electrostatic interactions for anion binding.[70,71] Consequently, receptors containing ammonium or guanidinium groups can only function in low pH environments where they remain protonated. Therefore, in these systems, anion recognition must occur within a limited range or "pH window", wherein both the anion is deprotonated and the host is protonated. The guanidinium functional group having a pK_a value of 13.7 can operate over a relatively wide pH range.[72] Strongly basic anions, such as fluoride or acetate, can also deprotonate acidic sites on the receptor.

Solvation: When compared to their isoelectronic cations, anions have higher free energies of solvation in hydroxylic solvents (Table 1.2.2), due to their ability to form hydrogen bonds with the solvent.[25,73] A receptor will have to compete with the solvation of the anion and its counter cation in order for recognition to occur.

Table 1.2.2: Hydration energies of isoelectronic cations and anions.

Cation	$\Delta\, G_{hyd}$ **(kJ mol^{-1})**	**Anion**	$\Delta\, G_{hyd}$ **(kJ mol^{-1})**
Na^+	-365	F^-	-465
K^+	-295	Cl^-	-340
Rb^+	$-$	Br^-	-315
Cs^+	-250	I^-	-275

Values taken from Steed and Atwood.[25]

The Hofmeister series (Scheme 1.2.1)[74] classifies anions for a given charge according to their hydrophobicity and therefore, indicates the degree of hydration of the anions. Larger anions tend to be more hydrophobic and therefore, less solvated while smaller anions are more hydrophilic and more solvated. Consequently, hydrophobic anions tend to be more strongly bound by a receptor with a hydrophobic cavity than hydrophilic anions in aqueous and aqueous–organic solvent mixtures due to their poorer solvation.

organic anions $> ClO_4^- > SCN^- > I^- >$ salicylate $> NO_3^- > Br^- > Cl^- > HCO_3^- > H_2PO_4^- > F^- > SO_4^{2-} > HPO_4^{2-}$

Scheme 1.2.1: The Hofmeister Series.[74]

1.2.2.1 Solvent effects

The role of solvent is of critical importance in solution phase anion supramolecular chemistry, influencing the strength of the intermolecular interactions associated with anion binding, and therefore, the selectivity of binding.[75,76] The extent of solvation for anions varies considerably with solvent choice: protic solvents tend to form strong hydrogen bonds to anionic species, perturbing host–guest recognition processes in systems which rely on hydrogen-bonding interactions for guest binding. Consequently, the incorporation of positive electrostatic charge is often required for receptors to compete effectively for negatively-charged guests in protic solvents. In contrast, anions are more weakly solvated in less polar aprotic solvents, allowing neutral receptors to function.

The solvation of both host and guest molecules governs the enthalpic and entropic contributions to host–guest binding. Desolvating both the host and guest incurs a severe enthalpic penalty; however, the expulsion of solvent molecules from the host cavity is entropically favourable. The inverse is true

upon guest binding: resolvation of the host–guest complex is enthalpically favoured but entropically disfavoured. Overall, the guest binding event may be driven by a favourable change in the enthalpic and/or entropic term, depending on the system under consideration.

1.2.3 Biological receptors

The unrivalled ability of Nature to selectively bind anions provides the inspiration for preparing synthetic receptors. The phosphate binding protein (PBP) selectively binds HPO_4^{2-} with a remarkably high affinity ($K_d = 0.31 \times 10^{-6}$ M at pH 8.5), employing a combination of electrostatic ion–ion and 12 hydrogen-bonding interactions: eleven of which arise from protein hydrogen donor amino acid residues and one protein hydrogen-bond acceptor aspartate residue, which exclusively interacts with the single *ortho*-phosphate proton (Figure 1.2.2a).[77] The tetrahedral sulfate anion binds at least five orders of magnitude less tightly than phosphate, owing to its lack of hydrogen bond donor groups and destabilisation by unfavourable electrostatic interactions. The binding cavity is also able to accommodate $H_2PO_4^-$ *via* an induced-fit mechanism but with diminished affinity as evidenced by the crystal structure. The sulfate binding protein (SBP), by contrast, employs 7 protein hydrogen bond donors located on neutral amino acid residues to achieve selective binding of the dianionic oxoanion (Figure 1.2.2b).[78] Notably, small molecule pyrrole-based anion receptors also exist in biological systems where they function as transmembrane chloride transporters. It is these simple receptors that serve as the basis for synthetic analogues.[79–81]

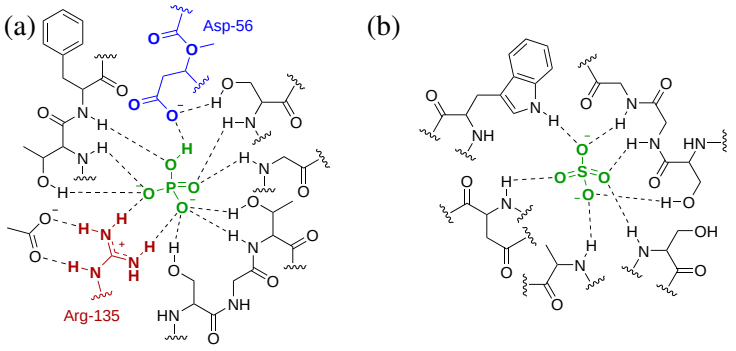


Figure 1.2.2: Two dimensional projection of binding cavities of truncated biological protein structures: (a) phosphate binding protein (PBP),[77] and (b) sulfate binding protein (SBP).[78]

1.2.4 Synthetic receptors

With a view towards recognising anions strongly and selectively in solution using synthetic receptors, a wide variety of hosts have been prepared and can be broadly divided into three general categories: *neutral*, *cationic* and *Lewis acidic*. Neutral anion receptors primarily employ non-covalent interactions

(excluding electrostatic interactions) for anion binding, with the advantage that several of these interactions, such as hydrogen bonding, impose a directionality constraint, which affords the receptor some degree of selectivity. However, since anions are negatively charged, the use of cationic host systems exploits stronger ion–ion interactions for anion binding, but at the loss of selectivity due to the omnidirectionality of electrostatic interactions. The prevailing strategy when designing synthetic anion receptors centres around the incorporation of both positively-charged binding motifs and other more directional non-covalent interactions, which then act in concert to afford receptors with high affinity and selectivity for anions. Lewis acidic anion receptors are able to recognise anions *via* metal-anion or Lewis acid–base coordination.

1.2.4.1 Neutral receptors

Commonly designed to function in aprotic organic solvent media, neutral anion receptors make use of non-covalent interactions (*cf.* Section 1.1.2), the strength of which varies greatly. Whilst these interactions are much weaker than electrostatic interactions, particularly in competitive polar and hydroxylic solvent media, the cumulative effect of multiple interactions acting in concert, can afford the receptor satisfactory binding strength and good selectivity. Of the non-covalent interactions employed in neutral receptors, hydrogen bonding is one of the strongest, and by far, the most widely exploited interaction for anionic guest recognition. While halogen bonding has recently become a strong candidate in anion host systems, competing efficiently with hydrogen bonding, these particular examples will be discussed, in depth, later in this chapter.

Hydrogen bonding Several hydrogen-bonding motifs have become popular for anion binding and include: amide, thioamide, urea, thiourea, pyrrole and triazole functional groups (Figure 1.2.3).

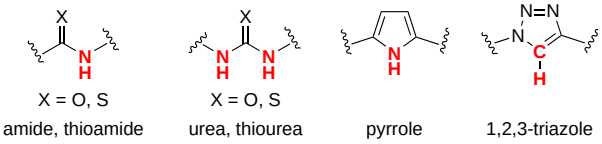


Figure 1.2.3: Common hydrogen-bonding motifs used in anion receptors for neutral anion recognition.

Amide-based receptors

Amides were first incorporated into neutral receptor design by Pascal *et al.* in 1986, whose cryptand, containing three convergent amide hydrogen-bond donors, was able to bind fluoride in DMSO-d_6 (Figure 1.2.4a).[82] However, it was Crabtree's report of the isophthalamide motif in 1997 that inspired the incorporation of this bis-amide motif into a variety of acyclic and macrocyclic anion hosts, as well as those

with higher-order tertiary structures (Figure 1.2.4b).[83] In the absence of a bound anion, the isophthalamide motif adopts a thermodynamically favourable *syn-anti* conformation; however, upon anion binding it adopts a *syn-syn* conformation, binding halides in 1:1 stoichiometry in the preferential order $Cl^- > Br^- > I^-$ in CD_2Cl_2 solution *via* two convergent amide hydrogen bonds. Jurczak's similar pyridine-2,6-bis-amide motif demonstrated the role that preorganisation plays when incorporated into macrocyclic host systems, enhancing chloride binding strength *via* intramolecular hydrogen bonding between the amides and pyridine-nitrogen in the *syn-syn* conformation (Figure 1.2.4c).[84,85] In addition, the macrocycle's selectivity for chloride could be reinforced in DMSO-d_6 by varying the size of the macrocyclic receptors.

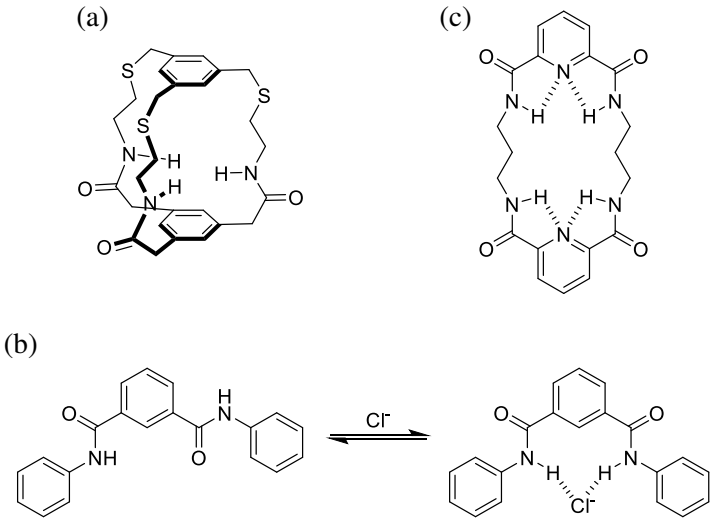


Figure 1.2.4: Examples of amide-based receptors: (a) Pascal's seminal cryptand,[82] (b) Crabtree's acyclic isophthalamide receptor,[83] and (c) Jurczak's macrocyclic host.[84]

Similarly, Anslyn *et al.* reported a bicyclic cyclophane, incorporating three pyridine-2,6-bis-amide moieties in C_3 symmetry, that preferentially binds trigonal acetate and nitrate anions over cyanide, halides, dihydrogen phosphate and hydrogen sulfate in 25% CD_2Cl_2:CD_3CN due to host–guest complementarity (Figure 1.2.5a).[86] Furthermore, Bowman-James *et al.* described an analogous cryptand receptor containing three convergent pyridine-2,6-bis-amide moieties which displays a marked affinity for F^- ($K = 8.1 \times 10^5$ M^{-1} in DMSO-d_6) (Figure 1.2.5b).[87–89] Taking inspiration from amides in Nature, which form the backbone of polypeptide chains and perform crucial roles in protein folding and molecular recognition processes, Kubik *et al.* have prepared a series of bis-cyclopeptides which bind anions in aqueous media *via* multiple convergent amide hydrogen bond interactions.[90] The receptor shown in Figure 1.2.5c showed remarkable binding for SO_4^{2-} ($K = 3.5 \times 10^5$ M^{-1}) in 50% D_2O/MeOD *via* a combination of hydrogen bonding and solvophobic interactions, resulting in the concerted encapsulation of the anion between the two cyclopeptides, comparable to a 'molecular oyster'.

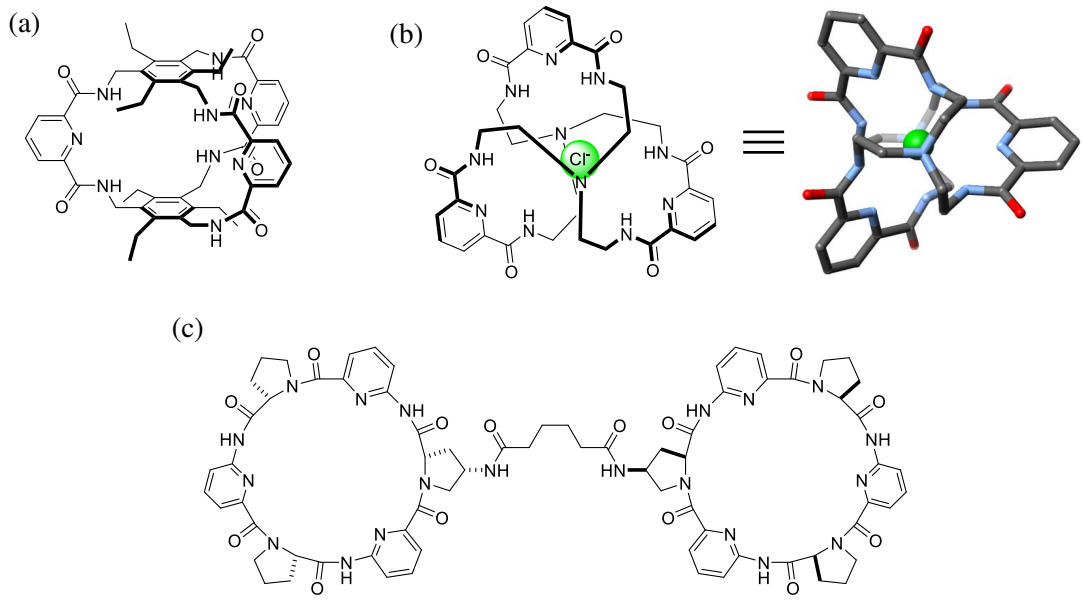


Figure 1.2.5: Examples of amide-based receptors: (a) Anslyn's bicyclic cyclophane,[86] (b) crystal structure of Bowman-James' cryptate receptor,[88] and (c) Kubik's 'molecular oyster'.[90]

Thioamides are known to be stronger acids and weaker hydrogen-bond acceptors than their amide analogues, making them attractive motifs for anion recognition. However, the enhanced acidity of the N–H proton makes the receptor more susceptible to deprotonation by basic anions.[91] Jurczak compared simple acyclic pyrrole-based amide and thioamide receptors, the latter showing two-fold stronger affinity for chloride and benzoate than the amide analogue in DMSO-d_6+ 0.5% H_2O.[92] By appending boronate groups to simple, acyclic isophthalamide receptors, Hughes and Smith were able to enhance carboxylate binding 20-fold due to preorganisation of the host and a cooperative polarisation effect in DMSO-d_6 solution (Figure 1.2.6a).[93] The integration of sulfonamide groups into neutral receptors was first reported by Reinhoudt in 1993 where they were appended to a tris(2-aminoethyl)amine (TREN) tripodal core (Figure 1.2.6b),[94] and bound dihydrogen phosphate selectively over hydrogen sulfate and chloride in acetonitrile. Since then, these groups have been incorporated into a variety of anion hosts[95,96] (Figure 1.2.6c) and transmembrane transporters.[97–101]

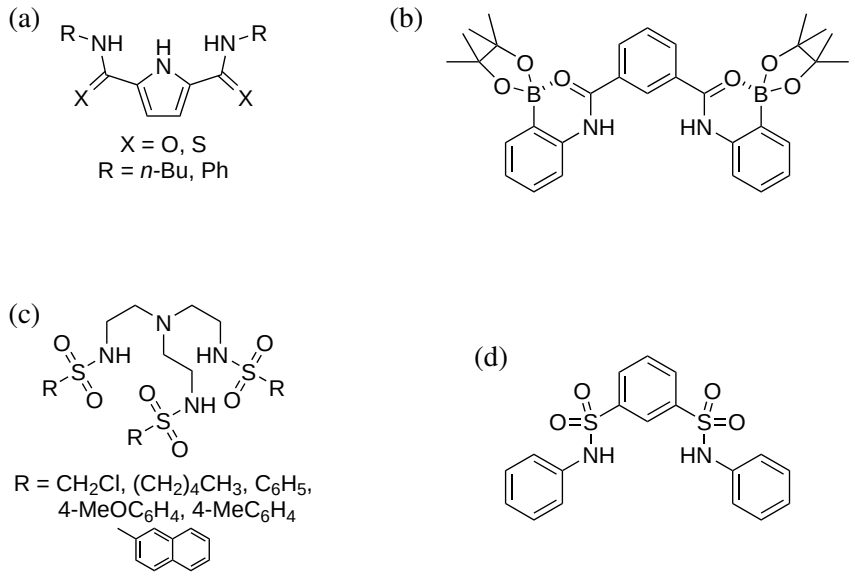


Figure 1.2.6: Further examples of amide-based receptors: (a) Jurczak's acyclic pyrrole-based amide and thioamide receptors,[92] (b) Hughes and Smith's boronate-appended receptor,[93] (c) Reinhoudt's tripodal sulfonamide-containing receptor,[94] and (d) Crabtree's sulfonamide-functionalised receptor.[95]

Urea-based receptors

Ureas and thioureas are potent hydrogen-bond donors and their synthetic accessibility has made these groups popular for anion recognition applications. Moreover, their two parallel N–H hydrogen-bond donors are optimally spaced for interaction with Y-shaped anions such as carboxylates, nitrates and phosphates. Since Wilcox's seminal report in 1992,[102] ureas and thioureas have been incorporated into a variety of host molecules. Fabbrizzi *et al.* studied an acyclic urea-based receptor in acetonitrile solution, showing strong binding for acetate ($logK_a = 6.61$) *via* two cooperative N–H···O hydrogen bonds, which was confirmed by X-ray structural data.[103] Similarly, Gale's acyclic bis-urea host (Figure 1.2.7a) exhibits acetate selectivity in competitive DMSO-d_6 containing 0.5% D_2O.[104] Tripodal receptors containing urea groups have been reported by Ghosh *et al.*,[105] and Das and Ganguly (Figure 1.2.7b)[106] which display selectivity for fluoride and dihydrogen phosphate in DMSO-d_6, and sulfate and dihydrogen phosphate in 5% water:acetonitrile solutions, respectively over other oxoanions in both cases. Böhmer and co-workers have described macrocyclic urea host systems (Figure 1.2.7c) which bind acetate and dihydrogen phosphate anions in 1:1 host–guest stoichiometry in 3:1 THF:MeCN solution with association constants of $logK_a = 5.2$ and 5.8, respectively.[107] Thioureas have been incorporated into cavitand structures such as Figure 1.2.7d which is selective for chloride $K_a = 250\ \text{M}^{-1}$ in 1:1 water:acetonitrile.[108] Similarly to thioamides, thioureas are vulnerable to deprotonation. For example, whereas Wu and co-workers' tris-urea receptor is capable of binding PO_4^{3-} and SO_4^{2-} strongly in 3:1 DMSO:water, the tris-thiourea

analogue undergoes deprotonation in the same solvent mixture by strongly basic anions such as acetate.[109,110]

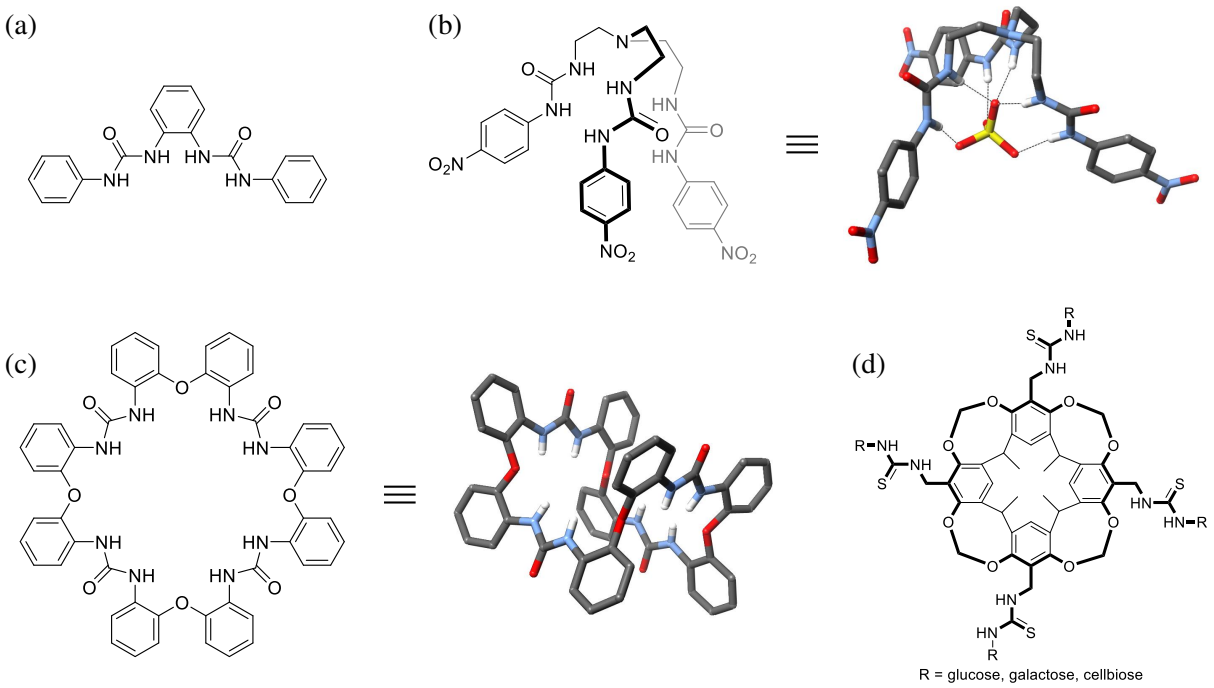


Figure 1.2.7: Examples of urea- and thiourea-based receptors: (a) Gale's bis-urea host,[104] (b) crystal structure of Das and Ganguly's host with sulfate (tetrabutylammonium counterions are omitted for clarity),[106] (c) crystal structure of Böhmer's tetrameric macrocycle,[107] and (d) Reinhoudt's tetra-thiourea-functionalised cavitand.[108]

Pyrrole-based receptors

Pyrrole offers a robust N–H hydrogen-bond donor for anion recognition and it has been incorporated into a wide variety of anion host structures; the most notable of which are the calix[4]pyrroles. Pioneered by Sessler, calix[4]pyrroles are macrocycles containing four pyrrole units arranged with their N–H hydrogen-bond donors pointing towards the central cavity. Upon anion complexation, calix[4]pyrrole adopts a cone conformation with all four pyrroles participating in linear N–H···A^- hydrogen bonds, with preferential binding for fluoride and chloride in a range of polar organic solvents (Figure 1.2.8a).[111,112] Extending this work, Sessler *et al.* showed that the incorporation of a pyrrole-containing "strap" resulted in a near 100-fold enhancement in chloride binding in acetonitrile.[113] Indeed, higher-order calix[n]pyrroles (n $>$ 4) have been developed which preferentially bind larger anionic guests. For example, Eichen *et al.* reported a calix[6]pyrrole with selectivity for iodide—the other halides are simply too small to take advantage of the six convergent pyrrole hydrogen bonds upon complexation.[114] Simpler acyclic pyrrole-containing receptors are also potent anion binding reagents. For example, Gale and co-workers' bis-amidodipyrrolylmethane host, which employs a combination of pyrrole and amide N–H hydrogen bonds to enhance fluoride binding in 1:3 D_2O:DMSO-d_6 ($K_a = 110$ M^{-1}).[115]

Closely related are the indole, carbazole and indolocarbazole groups, in which the pyrrole sub-unit is fused to an aromatic ring, increasing both the rigidity and preorganisation of the motif, as well as the hydrogen-bond donor ability through enhanced acidity. Sessler's bis-indole receptor is selective for dihydrogen phosphate in CD_2Cl_2, manifesting a colorimetric response upon anion complexation (Figure 1.2.8b).[116] Lin's carbazole-based host shows iodide selectivity $K_a = 5 \times 10^4$ M^{-1} in DMF.[117] Jeong and co-workers have successfully incorporated both indoles and indolocarbazoles into neutral, oligomeric foldamer hosts that are capable of binding chloride.[118,119] Moreover, the indolocarbazole-containing receptor binds chloride $K_a = 65$ M^{-1} in pure water. When incorporated into cyclic hosts, indolocarbazole has been shown to bind fluoride[120] and azide,[121] *via* complementary size match.

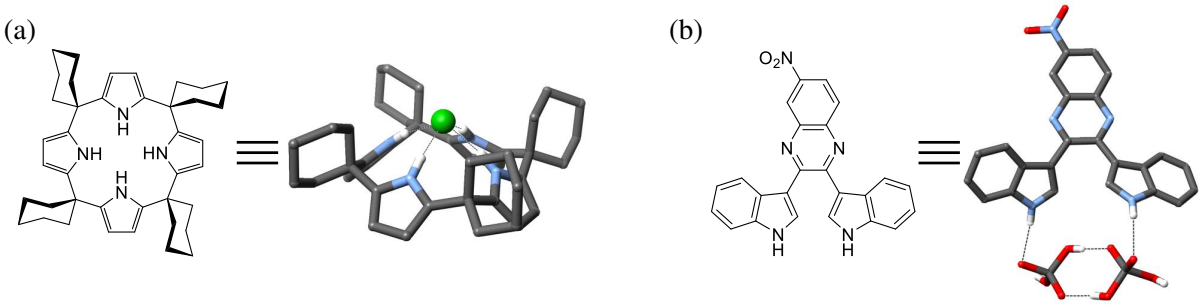


Figure 1.2.8: Examples of pyrrole receptors: (a) crystal structure of Gale and Sessler's calix[4]pyrrole receptor with fluoride (the tetrabutylammonium counterion is omitted for clarity),[111] and (b) crystal structure of Sessler's bis-indole receptor with dihydrogen phosphate (the tetrabutylammonium counterions are omitted for clarity).[116]

C–H-based receptors

The C–H···A$^-$ hydrogen-bonding interaction has recently become a pervasive motif in anion host systems, particularly through the use of 1,2,3-triazole functional groups, despite being weaker than the more acidic N–H···A$^-$ hydrogen bonds. The use of C–H hydrogen-bond donors for anion recognition was reported as early as 1990, with the report of a fluorinated macrocyclic ether which associates with fluoride *via* polarised CH_2 groups incumbent on the anion binding cavity, both in THF-d_8 solution and the solid state (Figure 1.2.9a).[122] The CH_2 group has also found application in resorcinarene and bambus[6]uril derivatives, which bind anions within the central cavity of the macrocycle.[123,124] Indeed, Sindelar described a water-soluble bambus[6]uril derivative that binds anions with high affinity in pure water, and with selectivity for the more hydrophobic anions such as ClO_4^- and I$^-$ ($K_a = 5.5 \times 10^7$ and 1.0×10^7 M^{-1}, respectively).[125] The aforementioned 1,2,3-triazole moiety, however, offers a highly polarised C–H bond due to the electron-withdrawing nature of the sp^2-hybridised carbon and the three, contiguous, heterocyclic nitrogen atoms, resulting in a motif well-suited to anion coordination. Hecht *et al.*[126] and Craig *et al.*[127] have both reported poly-triazole foldamers which exhibit a helix inversion upon

binding of an achiral halide anion in 75% water:acetonitrile, and helical folding from an open conformation in response to chloride in acetone-d_6 (Figure 1.2.9b), respectively. The triazole group has also been incorporated into macrocyclic host systems such as Flood's triazolophane which binds chloride selectively in CD_2Cl_2 over other halides, in part due to size-complementarity, and further displaying sensing properties with an associated change in the host's UV absorption spectrum.[128]

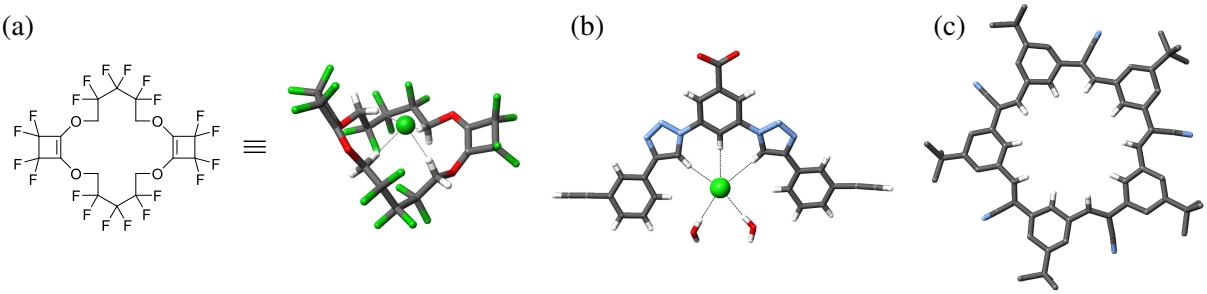


Figure 1.2.9: Examples of anion receptors which operate *via* C–H hydrogen bonds: (a) crystal structure of Farnham and Dixon's fluorinated macrocyclic ether binding fluoride (the tris(dimethylamino)sulfonium counterion is omitted for clarity),[122] (b) crystal structure of a truncated derivative of Craig's foldamer binding chloride with supplementary hydrogen bonds from water (the tetrabutylammonium counterion is omitted for clarity),[127] and (c) crystal structure of Flood's cyanostar macrocycle which binds large anions.[129]

Flood's cyanostilbene 'campestarene' (cyanostar) macrocycle offers a more recent example of anion hosts employing C–H hydrogen-bond donors: specifically five Ar–H protons directed towards the central cavity of the macrocycle, which bind large anions such as BF_4^-, PF_6^- and ClO_4^- in 2:1 complexes in 2:3 CD_3OD:CD_2Cl_2 (Figure 1.2.9c).[129]

Anion–π interactions Although anion–π interactions are much weaker than other non-covalent interactions, they have successfully been employed to form favourable complexes with anions in both solution and the solid state. For example, Kochi *et al.* reported the formation of charge transfer complexes between electron-deficient tetracyanopyrazine (TCP) and halide anions in acetonitrile solution. In the solid state, the anions are encapsulated within the macrocyclic cavity, surrounded by four TCP molecules which stabilise the structure *via* anion–π interactions (Figure 1.2.10a).[53] Nonetheless, anion–π interactions are typically used in concert with other, stronger interactions such as hydrogen bonding, as is exemplified in Ballester's systematic investigation of substituents on aryl-appended calix[4]pyrrole. In these systems, the more electron-withdrawing substituents ($-NO_2$) amplified the stabilising effect of anion-π interactions upon anion complexation, whilst the more electron-donating substituents ($-$OMe) exhibited attenuated anion binding with chloride in acetonitrile solution (Figure 1.2.10b).[54]

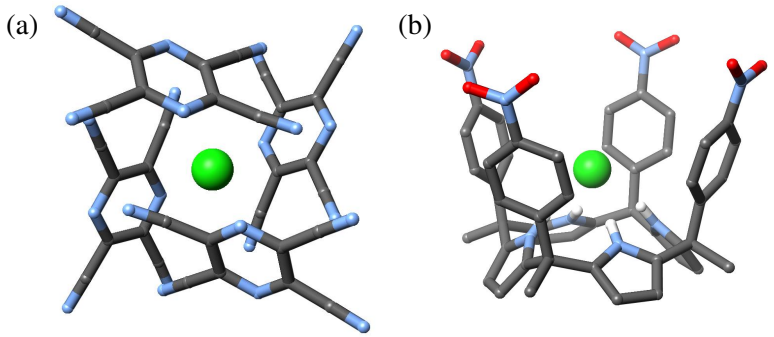


Figure 1.2.10: Examples of anion–π receptors: (a) anion–π interactions can be seen in Kochi's crystal structure of tetrakis(tetracyanopyrazine) with chloride (the tetrabutylammonium counterion is omitted for clarity),[53] and (b) crystal structure of Ballester's aryl-appended calix[4]pyrrole with chloride (the tetrabutylammonium counterion and extraneous hydrogen atoms are omitted for clarity).[54]

1.2.4.2 Positively-charged receptors

Electrostatic ion–ion interactions are the strongest of the non-covalent interactions, making them particularly suited for anion recognition *via* the incorporation of positive charge into the host structure. Advantageously, this allows the design of anion receptors that are functional in highly competitive polar, protic solvent media, including pure water. However, the isotropic nature of these interactions may result in a lack of anion selectivity, and is the reason that they are often supplemented by other non-covalent interactions, in particular hydrogen bonding. A variety of cationic motifs have been incorporated into simple acyclic as well as more complex higher-order host structures for anion recognition, and these include: ammonium, pyridinium, guanidinium, imidazolium, and triazolium (Figure 1.2.11).

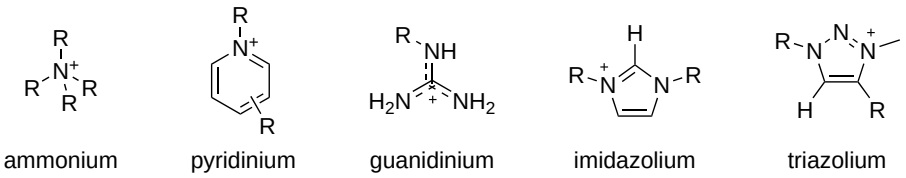


Figure 1.2.11: Common cationic motifs used in anion receptors.

Protonated ammonium-based receptors

Supplementing electrostatics with hydrogen bonding, Park and Simmons' seminal report in 1968 of a series of macrobicyclic receptors, known as katapinands, pioneered modern anion receptor chemistry (Figure 1.1.1c).[10] These receptors, incorporating two protonated tertiary ammonium groups at the diaza-cryptand junctions, bind halides in aqueous trifluoroacetic acid solution. Single crystal X-ray analysis showed that chloride was encapsulated within the cryptand. Lehn and co-workers developed this concept further with a range of macrocyclic and macrobicyclic polyammonium-based receptors[130–133] that

selectively bind azide (Figure 1.2.12a),[134] fluoride (Figure 1.2.12b),[135–137] and dicarboxylate anions,[138] all due to size complementarity of the guest to the host binding cavity.

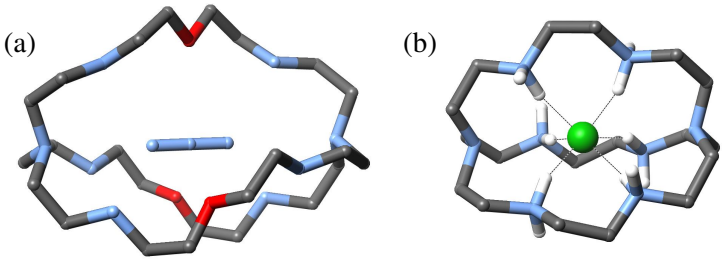


Figure 1.2.12: Examples of protonated ammonium-based receptors: (a) crystal structure of Lehn's azide-binding cryptand,[134] and (b) Lehn's fluoride-binding cryptand.[135]

Whilst these protonated ammonium-based receptors are able to operate in highly competitive aqueous solvent mixtures, their function and efficacy is pH dependent. This led to the construction of cationic pH independent host systems which are discussed in the next section.

Quaternary ammonium and pyridinium-based receptors

Adopting a holistic electrostatic approach to anion binding, Schmidtchen *et al.* developed a series of tetrahedral cage receptors that are able to encapsulate halide anions within a cavity formed by four quaternary ammonium moieties in pure water (Figure 1.2.13a).[139]

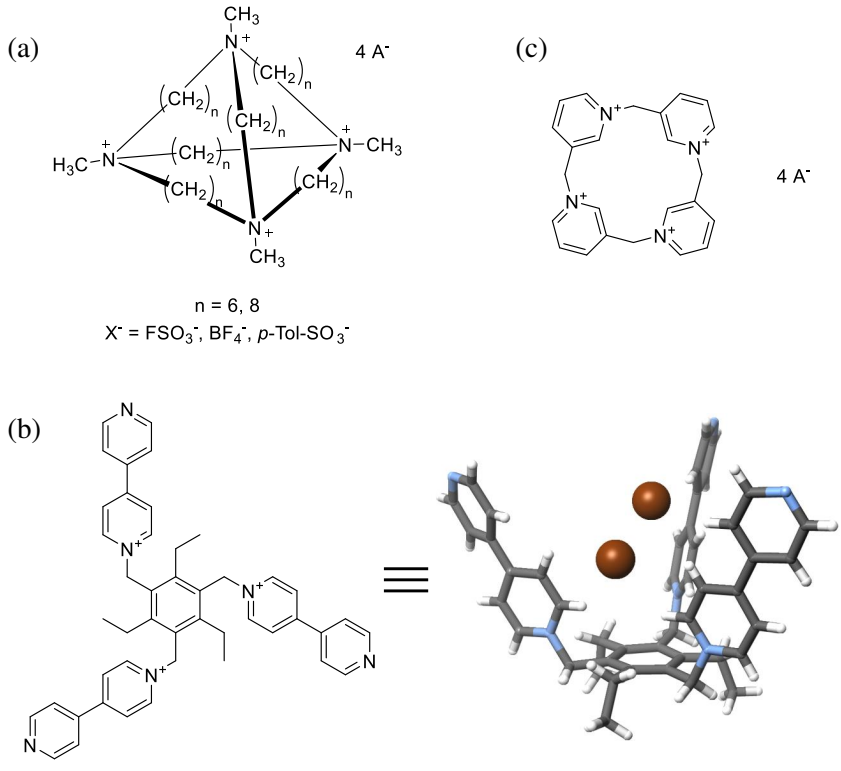


Figure 1.2.13: Examples of quaternary ammonium and pyridinium-based receptors: (a) Schmidtchen's tetrahedral cages,[139] (b) crystal structure of Steed's tripodal host that binds bromide in acetonitrile,[140] and (c) Shinoda's tetra-pyridinium macrocycle.[141]

The use of alkylated pyridine groups in both acyclic and macrocyclic hosts has been reported by Steed *et al.* (Figure 1.2.13b)[140] and Shinoda *et al.* (Figure 1.2.13c).[141] Steed's tripodal tris-pyridinium benzene host binds bromide in acetonitrile, and X-ray structural analysis revealed that the halide anion is bound *via* both electrostatic and C–H···A$^-$ interactions. Shinoda's tetra-pyridinium macrocycle displays strong binding for tricarboxylate anions in pure water. More recently, the use of pyridinium groups for anion recognition has been supplemented with other non-covalent interactions such as hydrogen bonding.[142]

Guanidinium-based receptors

The guanidinium functional group is a naturally occurring anion binding motif which is found in arginine residues within proteins and enzymes, such as carboxypeptidase-A.[143] Its highly basic character (p$K_a \sim 13.5$), which allows it to remain functional over a wide pH range, makes this group well-suited for anion recognition.[144] In particular, the guanidinium moiety forms a planar Y-shaped geometry offering two parallel N–H hydrogen bonds with good complementarity for anions such as carboxylates, sulfates, phosphates and nitrate. It was initially incorporated into anion receptors by Lehn,[145,146] Hamilton[147] and Anslyn (Figure 1.2.14a),[148] who independently showed that its anion binding properties could be enhanced by constraining the motif into cyclic structures with greater rigidity to produce acyclic receptors which bind glutarate in aqueous DMSO, and citrate and tricarballylate in pure water, respectively. In addition, Schmidtchen *et al.* also described a bicyclic guanidinium receptor with a preference for oxoanions (Figure 1.2.14b),[149] as well as a bipodal receptor capable of binding hydrogen phosphate in pure water.[150] Related to the guanidinium motif is the amidinium functional group, which was reported by Gale and co-workers to associate with bis-carboxylate anions in DMSO when distally appended to a calix[4]arene scaffold.[151]

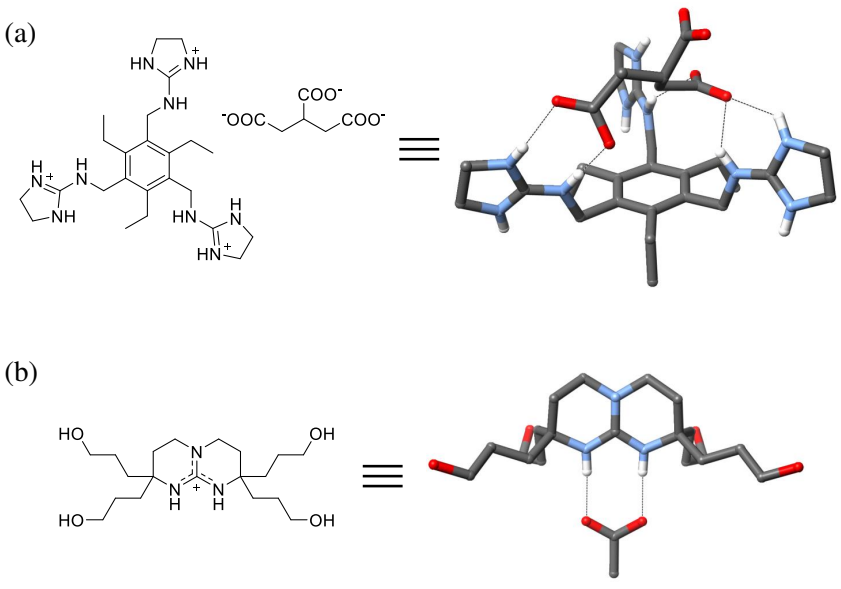


Figure 1.2.14: Examples of guanidinium-based receptors: (a) crystal structure of Anslyn's tris-guanidyl receptor with tricarballylate,[148] and (b) crystal structure of Schmidtchen's bicyclic guanidinium receptor with acetate.[149]

Imidazolium-based receptors

The 1,3-disubstituted imidazolium functional group combines electrostatic and C–H···A^- hydrogen-bonding interactions for anion recognition. Imidazolium was initially shown to form hydrogen bonds with halides in solution in the field of ionic liquids, and since then, has been incorporated into a wide variety of acyclic, macrocyclic and higher-order anion host systems. Seminal reports in 1999 by Sato (Figure 1.2.15a)[152] and Alcade (Figure 1.2.15b)[153] described tripodal and macrocyclic hosts, respectively, for anions. Notably, Sato's receptor displayed a high affinity for halide anions in CD_3CN, and Alcade's 'imidazoliophane' macrocycle binds a variety of anions in the order: $H_2PO_4^- > F^- > CH_3COO^- > CN^- > Cl^-$ in DMSO-d_6. More recently, Sessler described a tetracationic macrocycle, which contains two pyridine bis-imidazolium units, binding mono- and di-terephthalate anions in DMSO-d_6 (Figure 1.2.15c),[154] and Kang *et al.* reported a bis-imidazolium-appended glycouril acyclic host that displays high affinity for acetate in 9:1 CD_3CN/DMSO-d_6.[155]

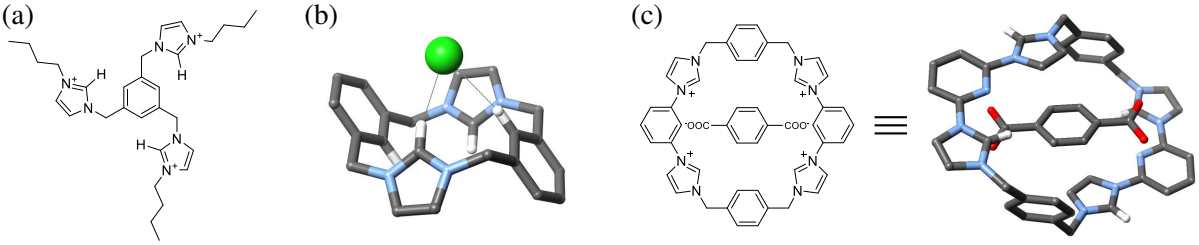


Figure 1.2.15: Examples of imidazolium-based receptors: (a) Sato's tripodal imidazolium receptor,[152] (b) crystal structure of Alcade's macrocyclic host with chloride,[153] and (c) crystal structure of Sessler's tetracationic macrocycle with mono-terephthalate.[154]

Triazolium-based receptors

Following the reports of triazole-based receptors, it was demonstrated that the anion binding properties of the triazole group could be enhanced *via* alkylation to form *triazolium* groups. Pandey's seminal report of a steroid-based bis-triazolium receptor in 2008 showed that dihydrogen phosphate was bound selectively over halides and acetate in $CDCl_3$. However, the analogous macrocycles bound dihydrogen phosphate with lower affinity than the acyclic receptor, which was attributed to diminished flexibility in the macrocycle, preventing it from adopting a complementary geometry for binding the tetrahedral oxoanion.[156] Subsequently, Schubert and co-workers described an acyclic bis-triazolium benzene receptor which forms an orthogonal 2:1 host–guest complex with sulfate (Figure 1.2.16a).[157] More recently, Beer *et al.* reported a tetra-triazolium macrocycle capable of binding anions strongly in the highly-competitive 1:1 DMSO-d_6:D_2O solvent mixture (Figure 1.2.16b).[158]

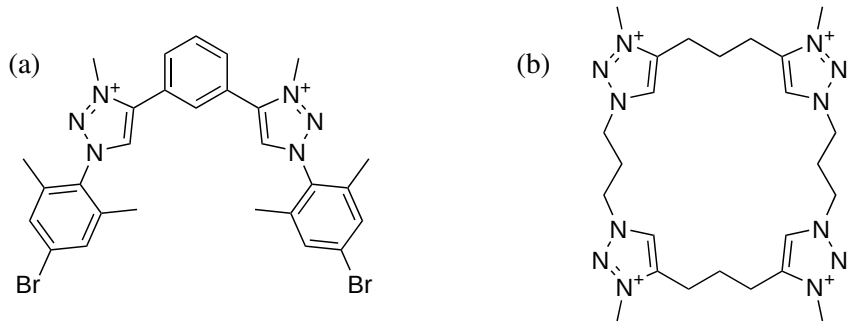


Figure 1.2.16: Examples of triazolium-based receptors: (a) Schubert's bis-triazolium benzene receptor,[157] and (b) Beer's tetra-triazolium macrocycle.[158]

1.2.4.3 Lewis acidic receptors

Lewis acidic elements can facilitate anion binding *via* a number of different mechanisms: (1) the formation of a Lewis acid···A^- dative bond; (2) electrostatic interactions if cationic, and additionally polarise adjacent hydrogen- or halogen-bond donors; (3) preorganise host structures for optimal anion binding, and (4) operate as a non-coordinating optical or electrochemical reporter group. Inspired by Shriver and Biallas' seminal report of the complex formed between methoxide and a bidentate boron derivative, Lewis acidic elements, including three-coordinate boron,[159] tin[160] and transition metals,[161–163] have been incorporated into a variety of anion receptors. Notable examples include Gabbaï's neutral boron and mercury-containing fluoride receptor (Figure 1.2.17a),[164] as well as cationic examples such as Jollife's pyrophosphate selective bis-Zn^{II} bipodal host (Figure 1.2.17b),[165] and Fabbrizzi's azide selective bis-Cu^{II} cryptand.[166]

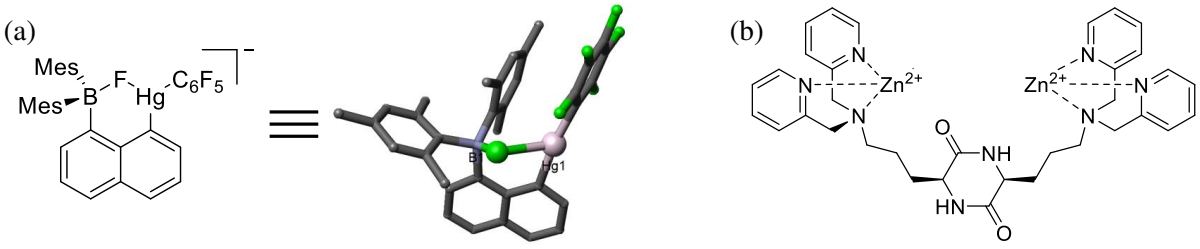


Figure 1.2.17: Examples of Lewis acidic receptors: (a) crystal structure of Gabbaï's B···F^-···Hg receptor[164] and (b) Jollife's pyrophosphate selective bis-Zn^{II} bipodal host.[165]

1.2.4.4 Anion Sensors

The incorporation of reporter groups that manifest a modulation in a macroscopic property (optical or electrochemical) of the host molecule upon anion recognition and binding is an active area of research, which allows the *sensing* of anions. An ideal anion sensor displays both strong, selective binding for a target anion, combined with an optimal response. The reporting of an anion binding event can be

signalled *via* three different mechanisms. Firstly, the binding of an anion alters the photo-physical or electrochemical properties of the reporter group *via* the host, which causes a measurable macroscopic response (Figure 1.2.18a). Secondly, in a displacement assay the host may be designed to carry a dye guest, which is expelled from the cavity by preferential binding of an anion, signalling the event by a concommitant change in the optical properties of the dye (Figure 1.2.18b).[167,168] Finally, chemodosimeters are receptors that undergo a specific chemical reaction with the target anion to induce a change in optical or electrochemical properties of the original host (Figure 1.2.18c).[169–171]

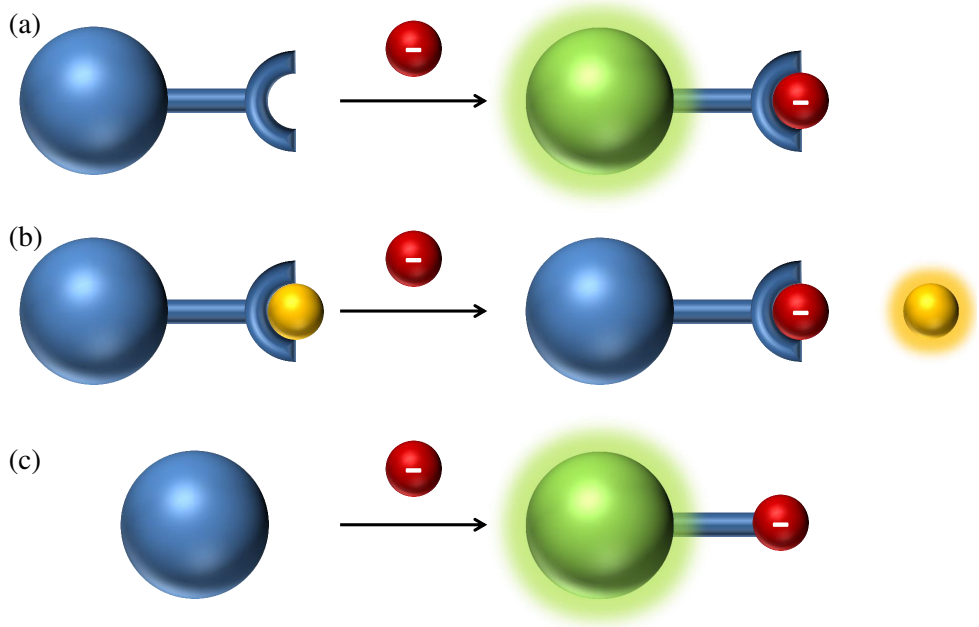


Figure 1.2.18: Cartoon representation of the different anion sensor mechanisms: (a) binding causes a response in an attached reporter group, (b) release of a dye upon anion binding results in a response, and (c) a chemodosimeter which affords a response upon reaction with the target anion.

Electrochemical anion sensors The incorporation of redox-active reporter groups into anion host structural frameworks allows for electrochemical sensing of anions when the reporter group is appended in close proximity to the binding cavity. Beer and co-workers' described cathodic shifts in the metallocene redox couples of cobaltocenium- and ferrocene-based receptors, owing to the stabilising effect of the bound anion (Figure 1.2.19a).[172,173] Since then, a wide variety of redox-active acyclic, macrocyclic and interlocked anion host systems have been reported.[174,175] Other redox-active functional groups such as tetrathiafulvalene (TTF) have also been integrated into anion hosts: for example, Sessler's bis-indole TTF receptor displays a cathodic shift of 112 mV of the first oxidation potential of the appended tetrathiafulvalene subunit, upon binding of dihydrogen phosphate anions in dichloromethane (Figure 1.2.19b).[176] Similarly, Becher reported a TTF-appended calix[4]pyrrole capable of sensing chloride and bromide an-

ions in acetonitrile solution *via* a 460 mV cathodic perturbation of the first TTF oxidation potential for both anions (Figure 1.2.19c).[177]

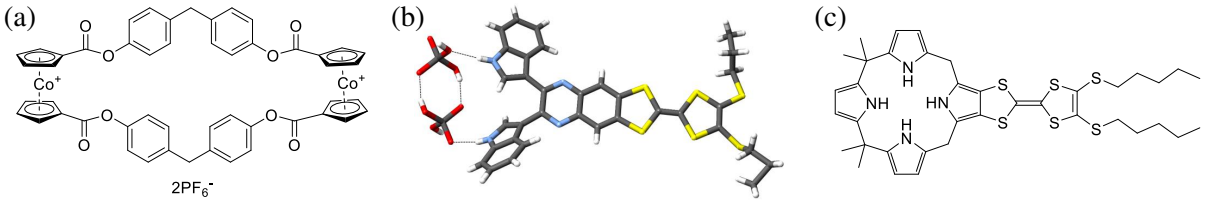


Figure 1.2.19: Examples of electrochemical anion sensors: (a) Beer's cobaltocenium macrocycle,[172] (b) crystal structure of Sessler's bis-indole–tetrathiafulvalene receptor with dihydrogen phosphate,[176] and (c) Becher's tetrathiafulvalene-appended calix[4]pyrrole.[177]

Optical anion sensors Optical anion sensors are typically divided into two classes, *fluorescent* and *colorimetric* sensors. An early example of anion sensing *via* a fluorescent host was reported in 1989 by Czarnik, who described an anthracene-appended polyamine, which exhibited an enhancement in fluorescent emission upon binding of hydrogen phosphate (Figure 1.2.20a).[178] This resulted from quenching of photo-induced electron transfer (PET) upon anion binding.

The appeal of colorimetric anion sensors lies in the fact that the absorbance of the host changes in the visible region upon anion complexation, resulting in a response that is visible to the naked eye. An elegant example is Sessler's series of anthraquinone-appended calix[4]pyrroles; the hydroxyanthraquinone derivative manifests anion-specific colour changes in dichloromethane solution for fluoride (red to blue), chloride (red to purple) and dihydrogen phosphate (red to dark purple) (Figure 1.2.20b).[179] Furthermore, boron-appended hosts represent a class of anion chemodosimeter sensors:[180,181] Aldridge's ferrocene-appended boron host (Figure 1.2.20c) generates a colorimetric response for cyanide or fluoride in the presence of a compatible redox-active dye such as tetrazolium violet acetonitrile:methanol solution.

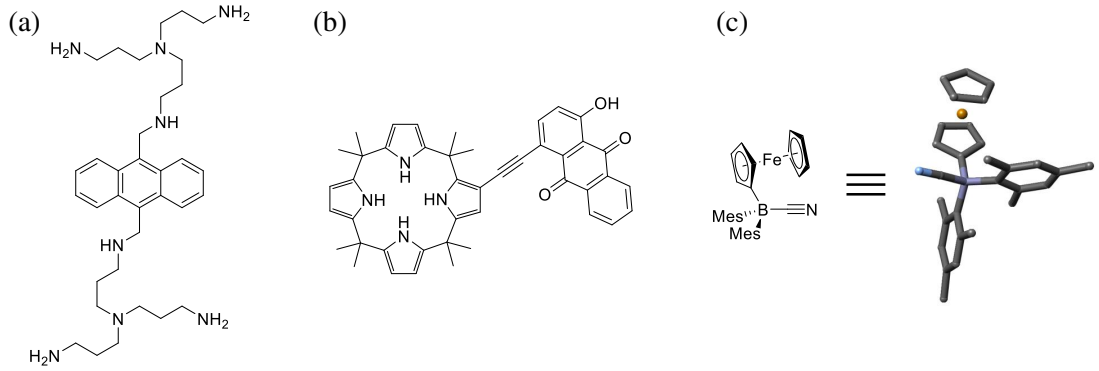


Figure 1.2.20: Examples of optical sensors: (a) Czarnik's hydrogen phosphate-binding fluorescent receptor,[178] (b) Sessler's hydroxyanthraquinone-appended calix[4]pyrrole,[179] and (c) crystal structure of Aldridge's boron-appended receptor with cyanide (the tetrabutylammonium counterion is omitted for clarity).[181]

1.2.4.5 Applications

Stimulated by the objective of treating diseases such as cystic fibrosis, naturally occurring ion carriers and channels which transport anions across the cell membrane in living systems have inspired research into anion transporters. Gale *et al.* have reported promising anticancer activity in several thiourea-containing hosts.[182,183] The most effective of these, which induces apoptosis in target cancer cells, due to enhanced lipophilicity and transport efficiency as a result of fluorination, is shown in Figure 1.2.21a. Matile and Guichard described the anion transport properties (halides, perchlorate, thiocyanate, acetate) of amide/urea-containing macrocycles, which are thought to self-assemble into channel-like structures across the cell membrane, facilitating anion transport *via* a "Jacob's ladder" mechanism.[184] In the field of anion catalysis, Lehn's pioneering work showed that anions could undergo chemical reactions in addition to the binding event: for example, the hydrolysis of ATP by a polyammonium azacrown macrocycle (Figure 1.2.21b).[185] Gels are a colloidal state of matter, comprising a multicomponent system of a fibrous solid-like phase, which contributes about 1% by weight, and immobilises a much larger solvent volume.[25] The use of anions to trigger gel dissolution has been reported by Steed and co-workers[186,187] who showed that larger, more uniform crystals of organic compounds, particularly pharmaceuticals, could be grown within a gel-matrix and then recovered *via* disruption of the gel network (Figure 1.2.21c).

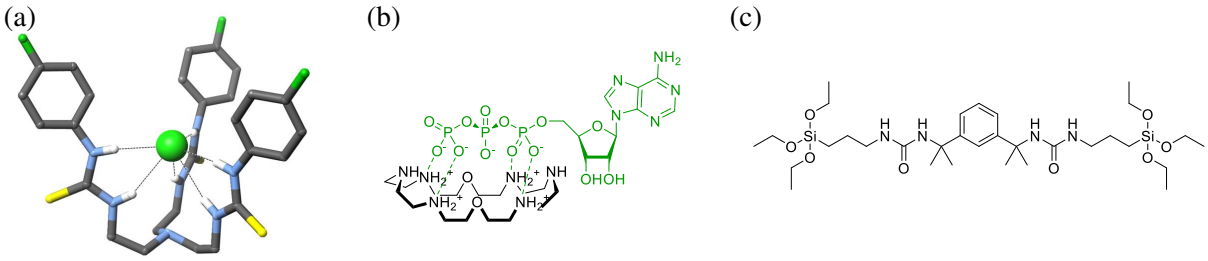


Figure 1.2.21: Examples of anion host systems in transport, catalysis and gelation: (a) crystal structure of Gale's fluorinated thiourea host with chloride,[183] (b) Lehn's ATP-binding polyammonium azacrown macrocycle,[185] and (c) one of Steed's anion-responsive gelators.[187]

1.3 Halogen bonding

To paraphrase the definition briefly outlined in Section 1.1.2, a halogen bond is the attractive interaction between a polarised halogen atom and an electron-rich Lewis base *via* a σ-hole. Halogen bonding has only very recently been incorporated into anion host systems, where it has found striking application as a strongly competitive interaction.[188] The halogen bond dates back to 1814,[189] when adduct formation between molecular iodine and ammonia was observed, and was later identified in 1863 by Guthrie as $NH_3 \cdot I_2$.[190] However, it was not until 1983 when Dumas *et al.* termed such an interaction a 'halogen

bond'.[191] Nonetheless, halogen bonding has been extensively studied in the solid state, particularly in the area of crystal engineering where it has proved to be a robust and potent supramolecular synthon. It was Hassel's pioneering, systematic studies of charge transfer interactions in co-crystals of molecular halogens and Lewis bases in the 1950s and 1960s that gained him the Nobel Prize in Chemistry in 1969, and sparked an interest in the use of halogen bonds in self-assembly.[192,193] Around the same time, Benesi and Hildebrand determined the association constants between arenes and I_2, providing a wealth of thermodynamic data pertaining to the interactions between homo- and heterodiatomic halogens with Lewis bases.[194] Mulliken's quantum mechanical calculations provided insight into the geometry of interactions between arenes and homodiatomic halogens,[195] whilst the use of organic halogen-bond donors (R–X) was pioneered by Laurence *et al.* who studied interactions between iodoacetylenes and Lewis bases.[196] In the 1990s, Legon and co-workers drew parallels between halogen bonding and the better-known hydrogen-bonding interaction in their extensive and systematic studies using matrix isolation and supersonic expansion of gases to examine the rotational spectra of prereactive gas-phase complexes formed between dihalogens and a variety of Lewis bases.[197] More recently, Resnati and Metrangolo have reported the formation of halogen bonds between iodo- and bromo-perfluorocarbons with neutral and anionic halogen-bond acceptors, highlighting their application as potent structure-directing synthons in crystal engineering.[30,31,31,198,199] Since then, halogen bonding has found further application in the design and fabrication of solid-state functional materials[200–202] including liquid crystals,[203–211] conducting and magnetic materials,[212–218] nonlinear optics,[219–223] porous materials,[224,225] gels,[226] surface relief gratings[227,228] and in topochemical synthesis.[229–233] While solution-state applications are still relatively underdeveloped, halogen bonding has also been exploited in catalysis,[234–246] anion binding,[247–249] and interactions with metal complexes,[250–253] as well as for biological functions[254–258] such as drug design[259,260] and protein–ligand complexation.[261]

1.3.1 Halogen bonding with anions

In the solid state, halogen bonding has been exploited with anions, including halides and a host of organic and inorganic oxoanions, to form a wide range of structures, flaunting the versatility of these robust synthons.[262,263] Indeed, the benefits of using halogen bonding for anion recognition include: (1) their strong interaction energies of the same order as hydrogen bonding, (2) a strict directional constraint *via* the σ-hole, which is only slightly affected by dispersion forces, (3) tunability of the halogen-bond donor *via* substitution of the halogen and/or R-group, and (4) pH-independence and general tolerance of strongly basic anions. Moreover, anions are well-suited to act as halogen-bond acceptors since they are

electron rich, and their diffuse, isotropic electron cloud allows them to form mono-, bi- and polydentate interactions with halogen-bond donors.

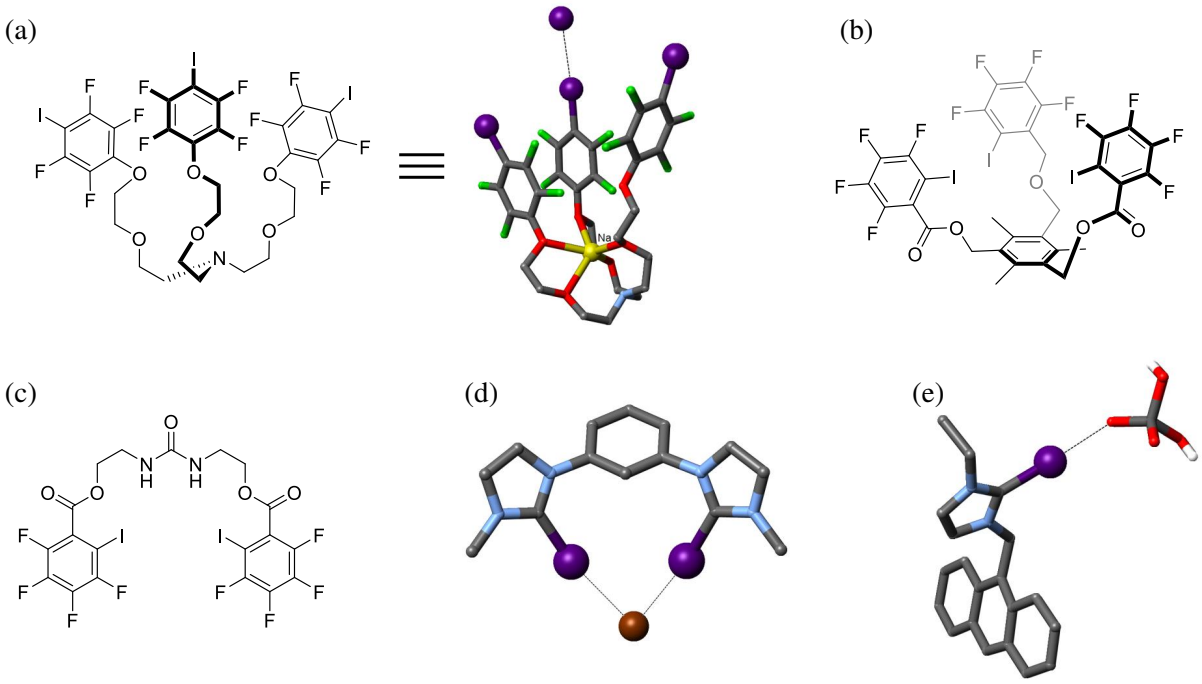


Figure 1.3.1: Examples of halogen-bonding receptors: (a) crystal structure of Resnati and Metrangolo's heteroditopic NaI receptor,[249] (b) structure of Taylor's halogen-bonding tripodal receptor,[264] (c) structure of Taylor's bipodal mixed hydrogen–halogen-bonding receptor,[265] (d) crystal structure of Huber's bis-iodoimidazolium receptor with convergent halogen bonds to bromide,[266] and (e) crystal structure of Resnati and Metrangolo's dihydrogen phosphate-selective iodoimidazolium receptor.[267]

In the solution state, the number of reports of anion host systems incorporating halogen-bond donors has increased since Resnati and Metrangolo's seminal report of a heteroditopic, tripodal receptor for NaI (Figure 1.3.1a).[249] Taylor reported a neutral tripodal iodoperfluoroaryl-appended benzene receptor, which binds Cl^- selectively over the other halides with no binding observed for the oxoanions TsO^-, HSO_4^- and NO_3^- in acetone (Figure 1.3.1b).[264] Furthermore, in conjunction with a urea group, Taylor's neutral bipodal iodoperfluoroaryl receptor was shown to strongly complex benzoate anions in CD_3CN (Figure 1.3.1c).[265] Introducing positive charge into halogen-bonding anion hosts has the potential advantage of further polarising the halogen-bond donor, enabling anion binding in competitive polar organic (Figure 1.3.1d,e)[266–268] and organic–aqueous (Figure 1.3.2a)[269,270] solvent mixtures. Moreover, Beer's haloimidazoliophane macrocycles[270,271] bind halides in 9:1 methanol:water (Figure 1.3.2b,c). More recently, after the commencement of this work, Schubert *et al.* reported a series of anion receptors based on halo-1,2,3-triazolium binding motifs (Figure 1.3.2d).[272]

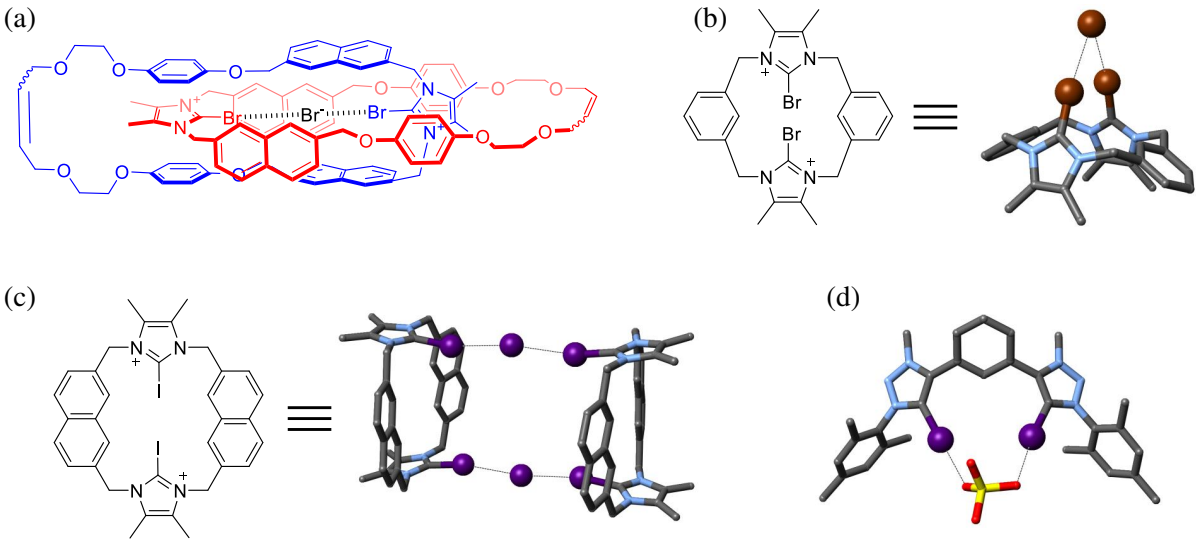


Figure 1.3.2: Examples of halogen-bonding receptors: (a) structure of Beer's bromoimidazolium-containing catenane,[269] (b) crystal structure of Beer's bromoimidazoliophane macrocycle with convergent halogen bonds to bromide,[271] (c) crystal structure of Beer's iodoimidazoliophane receptor which forms a 2:2 complex in the solid state,[270] and (d) crystal structure of Schubert's bis-iodotriazolium receptor with convergent halogen bonds to sulfate.[272]

1.4 Self-assembly and templation

Self-assembly comprises another branch of supramolecular chemistry, and refers to the spontaneous and reversible non-covalent association of multiple complementary substrate molecules to form complex higher-order superstructures. In some cases, the product structure can be controlled by the addition of a *template* species that directs the association of the individual subunits. Nature provides myriad examples of elegantly self-assembled architectures: haemoglobin, the biological oxygen-transporter protein, is a supermolecule comprised of four globular protein subunits, each of which is strongly associated with a non-protein haem cofactor (Figure 1.4.1a);[273] DNA is comprised of two anti-parallel, helical strands that associate strictly *via* complementary hydrogen-bonding nucleotide bases on the partner strand (Figure 1.4.1b);[62] and the cell membrane which is made of a phospholipid bilayer held together by hydrophobic van der Waals' forces (Figure 1.4.1c).[274] Templation is also well-documented in Nature with the processes replication, transcription and translation of DNA providing exceptional examples.[62] Busch defined a chemical template as a species which "*organises an assembly of atoms, with respect to one or more geometric loci, in order to achieve a particular linking of atoms*."[275] Sanders suggested that templates be classified as linear, cyclisation or interweaving in order to reflect the topology of the precursor–template complex arrangement.[276]

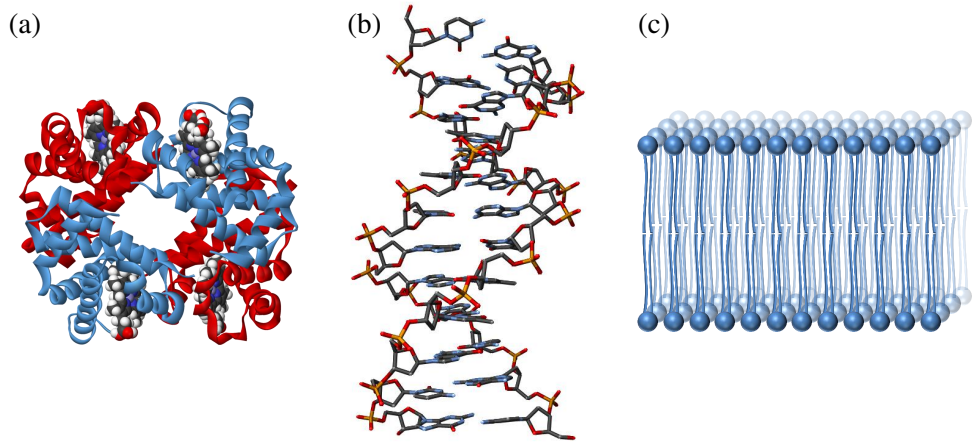


Figure 1.4.1: Examples of biological self-assembly: (a) structure of haemoglobin with separate protein domains depicted in red and blue and the haem cofactors shown as a space-filling models,[273,277] (b) the double helix structure of B-DNA,[278], and (c) a representation of the phospholipid bilayer which makes up the cell membrane.

Templation by cations The construction of extremely large and elaborate supramolecular architectures has been achieved using relatively simple but creatively-shaped polydentate ligands with transition metal cation templates which can influence the overall structure *via* their favoured coordination geometries. Since Busch pioneered the use of metal cations in templation, showing that Ni^{II} ions could influence the product ratio of the reaction between diketones and mercaptoamines,[279–281] their utilisation has led to structures of ever increasing complexity, such as macrocycles,[282,283] 3D metal-organic frameworks (Figure 1.1.9),[284,285] cages (Figure 1.4.2a),[286,287] polyhedra,[60,284,286,287] Borromean rings (Figure 1.1.2a)[12] and nanorings (Figure 1.4.2b).[288–291]

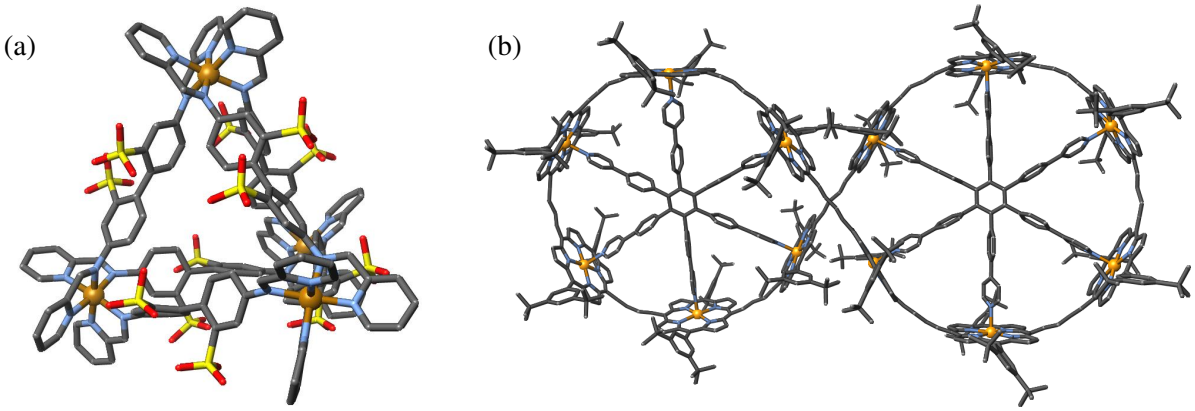


Figure 1.4.2: Examples of cation-templated supramolecular structures: (a) Nitschke's Fe^{II}-templated cage,[287] and (b) Anderson's 12 Zn^{II}-porphyrin templated nanoring.[289]

Templation by anions The use of anions as templating species is much less developed in comparison to cation templation. Indeed, many of the early examples of anion templates arose from serendipitous discoveries. Lehn's chloride-templated pentanuclear Fe^{II} helicate (Figure 1.4.3a) and the hexanuclear

analogue, templated by bromide, sulfate, BF_4^- or SiF_6^{2-}, undoubtedly illustrate the potential of anions as templating species in the fabrication of higher-order structures.[292,293] Dunbar's more recent polymetallic Ni^{II} macrocycles, templated by BF_4^- ([2+2] molecular square, Figure 1.4.3b), NO_3^- (molecular triangle) and SbF_6^- (molecular pentagon, Figure 1.4.3c), elegantly show that the presence of the appropriate anion dictates the type of cyclic structure formed.[294]

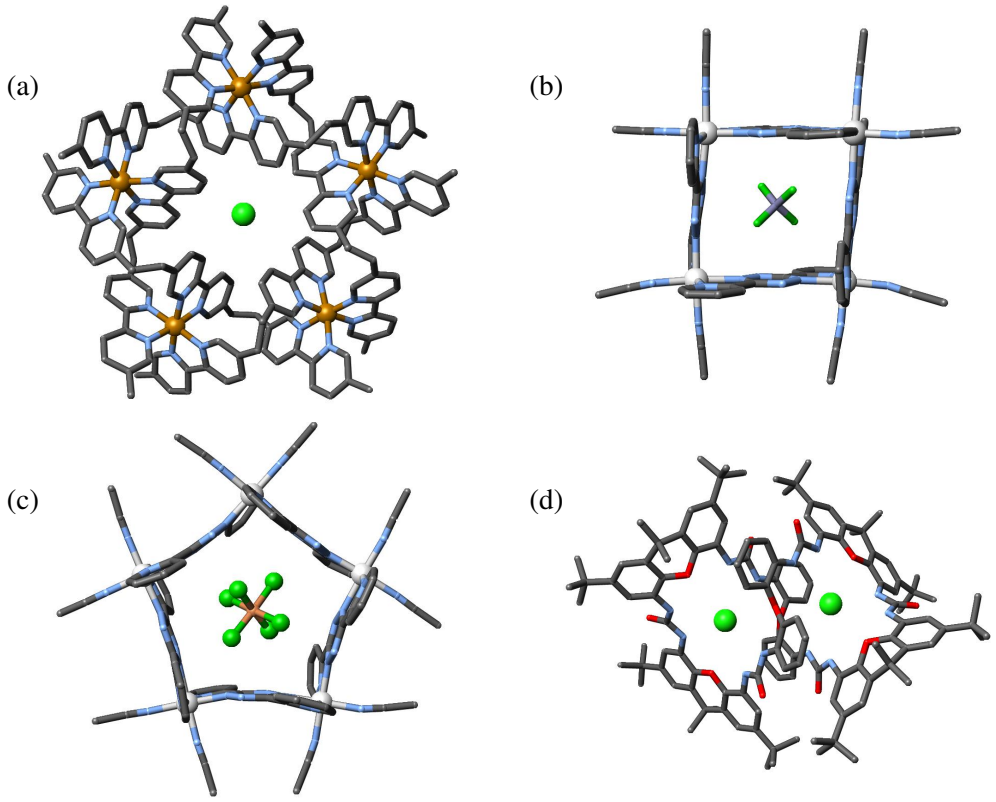


Figure 1.4.3: Examples of anion-templated supramolecular structures: (a) Lehn's pentanuclear Fe^{II} helicate,[293] (b) Dunbar's BF_4^--templated molecular square,[294] (c) Dunbar's SbF_6^--templated molecular pentagon,[294] and (d) Böhmer's chloride-templated macrocycle.[295]

Böhmer *et al.* have reported poly-urea macrocyclic anion host systems formed by the reaction in acetonitrile of diisocyanate- and diamine-appended bis-aryl ethers, which displayed a marked enhancement in yield upon the addition of templating chloride anions (Figure 1.4.3d).[295] Similarly, Sessler and coworkers employed Schiff-base chemistry in the preparation of poly-pyrrolic macrocycles which may be templated by the presence of sulfuric[296] or nitric acid.[297] More recently, Alfonso and Luis demonstrated the use of anions to template pseudopeptidic [2+2] macrocycle formation reactions between a diamine and dialdehyde, reflecting the roots of templation in Busch's work. In the absence of a template, a complex mixture of oligomers was obtained, but in the presence of a terephthalate template, the macrocycle was isolated as the major product in yields of greater than 90%.[298]

Anions have also been used to template a wide variety of other supramolecular architectures such as cages (Figure 1.4.4a),[299–302] and nanotubes (Figure 1.4.4b).[303]

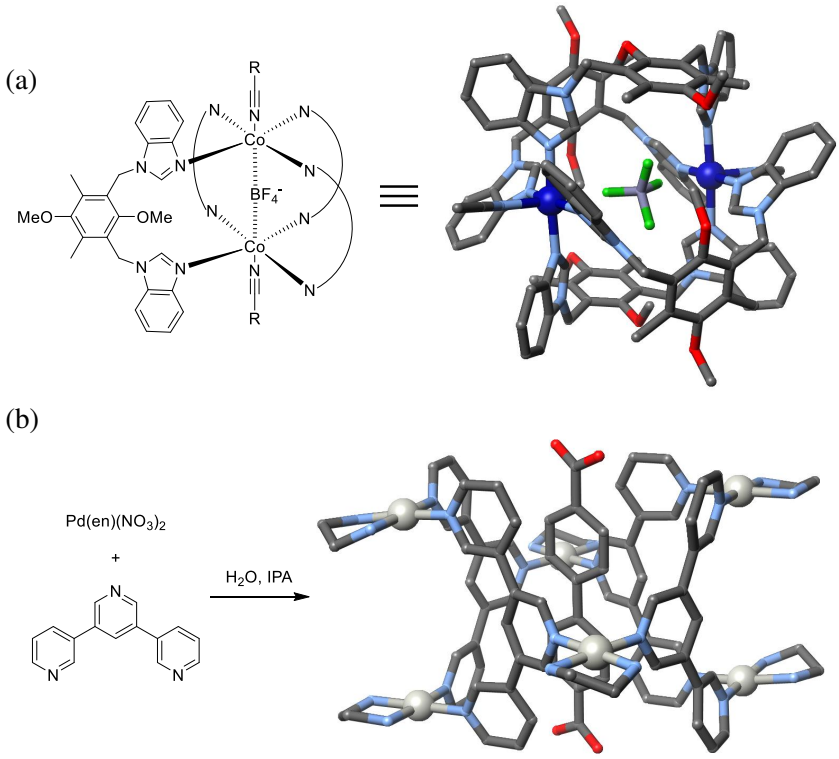


Figure 1.4.4: Anion-templated structures: (a) Amouri's cage,[299] and (b) Fujita's nanotube.[303]

1.5 Interpenetrated and interlocked structures

Interlocked structures are three-dimensional, mechanically bonded systems, consisting of two or more molecular entities that cannot be separated without the cleavage of a chemical bond. Their elaborate molecular topologies have captured the imagination of synthetic chemists for a number of reasons, including their aesthetic appeal and applications in molecular machinery and nanotechnology. The most common of these structures are [*n*]rotaxanes and [*n*]catenanes (Figure 1.5.1a,b), where *n* refers to the number of interlocked constituents. A rotaxane incorporates one or more 'axle' components threaded through one or more macrocyclic rings, which are held in place by large, bulky stopper groups at the termini of the axle to prevent de-threading of the ring(s). Catenanes, however, are composed of two or more interlocked macrocyclic rings. A related class of such structures are [*n*]pseudorotaxanes (Figure 1.5.1c) in which the axle and macrocyclic components form an *interpenetrated* assembly rather than an interlocked one. Pseudorotaxanes exist in equilibrium with the free thread and macrocyclic components in solution, and are often important precursors to rotaxanes or catenanes, following covalent modification

to lock the assembly together. More complex interlocked architectures are also possible such as Solomon knots, Borromean rings (Figure 1.1.2a) and trefoil knots.[304]



Figure 1.5.1: Cartoon representations of (a) [2]rotaxane, (b) [2]catenane, and (c) [2]pseudorotaxane.

1.5.1 Synthetic approaches

Rotaxanes can be prepared *via* a variety of routes: *clipping* or *stoppering* are the two most common strategies, whilst the methods of *slippage*, *snapping*, *swelling* and *shrinkage* are less commonly exploited (Figure 1.5.2). Clipping involves covalently joining the two ends of an acyclic macrocycle precursor around a stoppered axle *via* a ring-closing reaction, and stoppering involves functionalising the axle precursor component of a preformed pseudorotaxane complex with bulky stopper groups.[305] Under thermodynamically forcing conditions, a macrocycle may be coaxed over the bulky stopper groups of the axle component, known as slippage, to form an interlocked assembly which does not dissociate under ambient conditions.[306] Snapping refers to the joining of two half-axle components within a macrocycle, typically by an active metal template which can be removed post-synthetically.[307] Swelling involves the

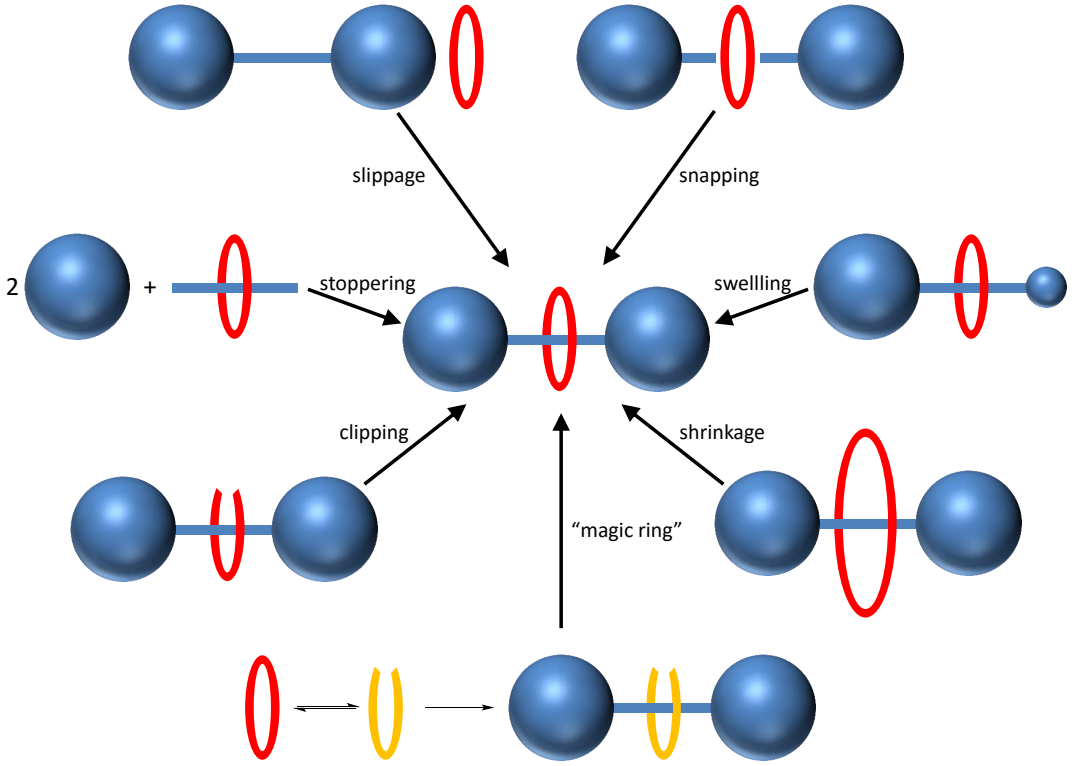


Figure 1.5.2: Cartoon representation of the different synthetic approaches to forming [2]rotaxanes.

formation of a pseudorotaxane assembly between a macrocycle and an axle appended with small stoppers, which can be dilated *via* thermal or photochemical stimuli to become larger, bulky stoppers.[308] Conversely, a macrocycle may undergo shrinkage after slipping onto a stoppered axle.[309,310] There have been reports of mechanical bond formation whereby a closed macrocycle will open and re-close around the axle component, known as "*magic ring*" synthesis,[311] or the axle will subdivide into two components that reconnect within the macrocycle, known as "*magic rod*" synthesis.[312]

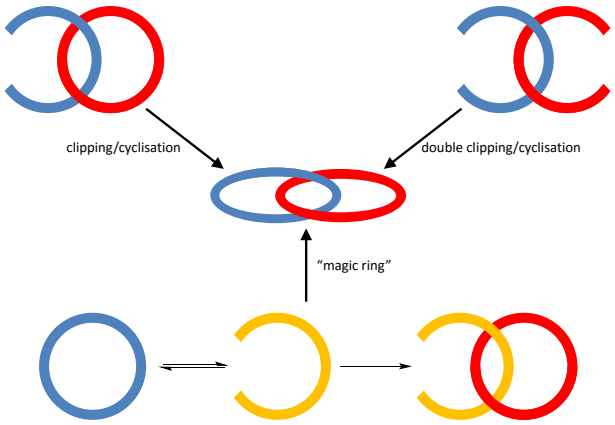


Figure 1.5.3: Cartoon representation of the different synthetic approaches to forming [2]catenanes.

Although fewer routes to catenanes exist, their synthesis similarly involves the *clipping* or *cyclisation* of a macrocyclic precursor around a second macrocyclic component after formation of an interpenetrated assembly.[313] In addition, *double clipping/cyclisation* of an orthogonal complex of macrocyclic precursors offers an alternative method, whilst the use of *magic ring* systems are less common (Figure 1.5.3).[313,314]

1.5.1.1 Templation

Whilst the synthesis of interlocked structures initially relied upon low-yielding statistical strategies, the use of templating species in the assembly of such mechanically bonded systems has proven an efficient tool to improve yields and reliably construct complex architectures.[315–318] Historically, the templated synthesis of rotaxane and catenane systems by cationic[319,320] or neutral[321–324] species is prevalent, however, the strategic use of anionic species as templates for mechanical bond formation has only developed much over the last two decades or so.[325]

Cation templation Sauvage's pioneering report of a Cu^{I}-templated catenane paved the way for the templated synthesis of interlocked structures. The tetrahedral geometric preference of Cu^{I} enabled two bidentate phenanthroline ligands to be orthogonally arranged to allow for catenane formation *via* a clip-

ping or a double clipping methodology (Figure 1.5.4a).[326,327] Furthermore, the copper template could be removed by TBA·CN to afford the 'free' catenane species. The same authors demonstrated the versatility of cation templation by synthesising a [3]catenane,[328,329] [3]rotaxane[330] and the first trefoil knot (Figure 1.5.4b).[331] Indeed, Sauvage and co-workers have used this approach to construct ever more complex structures, reaching a climax with the synthesis of an astounding porphyrin-containing [4]rotaxane in 95% yield (Figure 1.5.4c),[332] which can act as a "molecular clamp" for ditopic guest species.

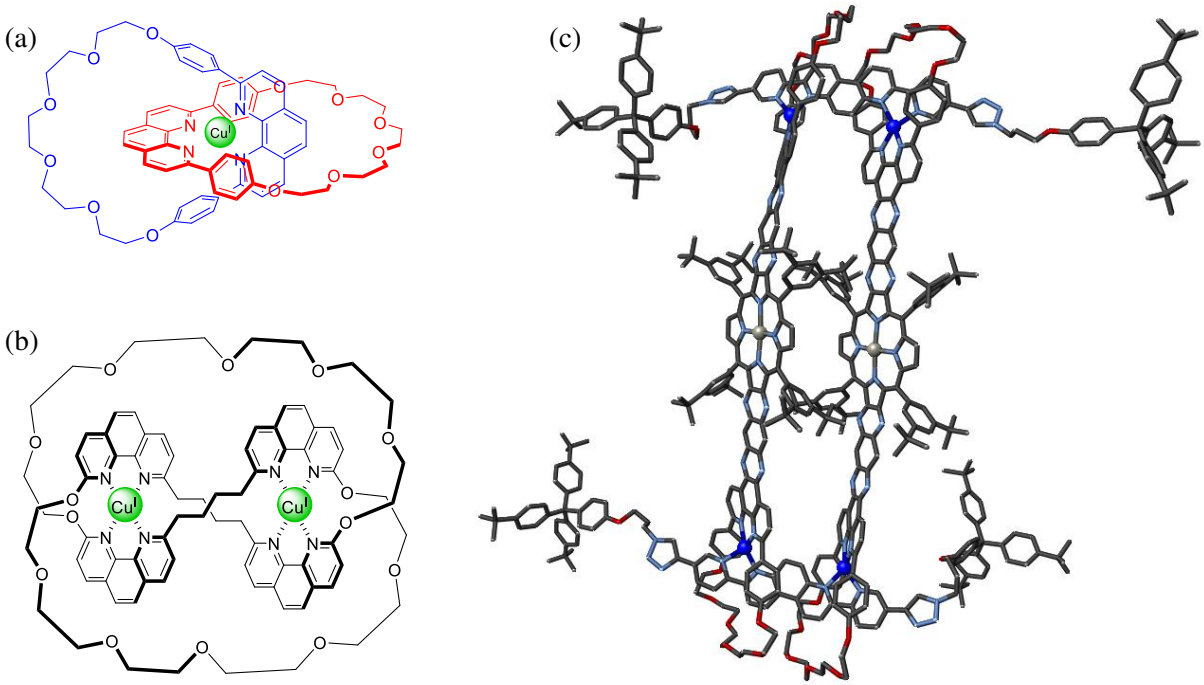


Figure 1.5.4: Selected examples of Sauvage's cation-templated interlocked structures: (a) Cu^{I}-templated bis-phenanthroline catenane,[327] (b) Cu^{I}-templated trefoil knot,[331] and (c) crystal structure Cu^{I}-templated [4]rotaxane.[332]

The strength of metal–ligand coordinate bonds and the stringent geometric preferences of transition metal cations, dictated by their intrinsic electronic configurations, has led to the preparation of a wide variety of interlocked structural frameworks based on linear (Au^{I}) (Figure 1.5.5a),[333] square planar (Pd^{II}) (Figure 1.5.5b),[334] octahedral (Fe^{II}, Co^{III} and Ru^{II}, Figure 1.5.5c)[335–337] and trigonal bipyramidal (Zn^{II})[338] geometries.

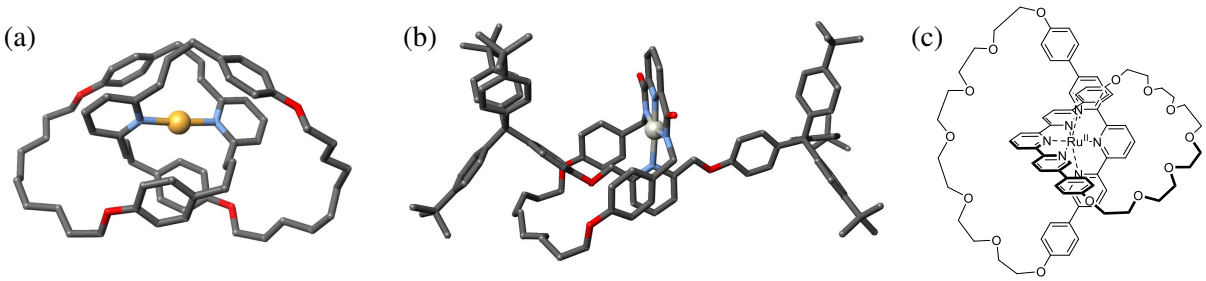
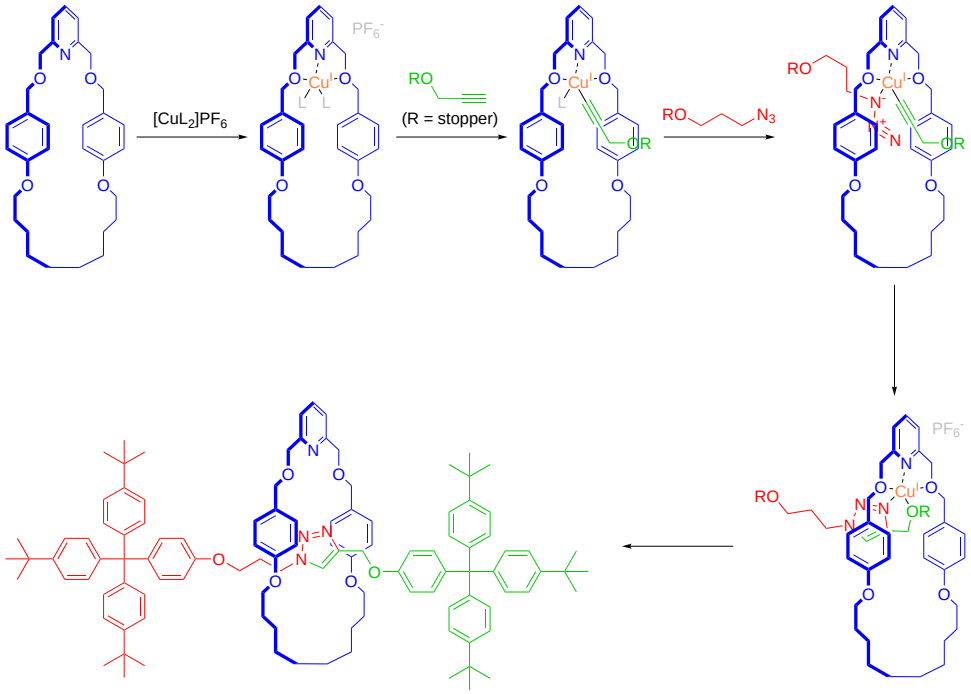


Figure 1.5.5: Cationic templation *via* different metal geometries: (a) Goldup's linear Au^{I}-templated catenane,[333] (b) Leigh's square planar Pd^{II}-templated rotaxane,[334] and (c) Sauvage's octahedral Ru^{II}-templated catenane.[337]

The recent development of "*active metal templation*" by the Leigh group has enabled the synthesis of interlocked structures *via* a catalytically-active metal that spatially orients the precursor components with regards to one another before catalysing the covalent axle-forming or ring-closing reaction to afford the rotaxane or catenane product.[319] The Cu^{I}-catalysed alkyne-azide cycloaddition[339] (CuAAC) reaction was exploited in the snapping synthesis of the first active-metal-templated preparation of a [2]rotaxane by Leigh *et al.* in 2006 (Scheme 1.5.1).[340] Subsequently, a range of metals have been utilised for their unique catalytic activities, including Cu^{I}- and Pd^{II}-catalysed alkyne homocouplings,[341–345] Pd^{II}-catalysed cross-coupling[346] and Michael addition[347] reactions and Ni^{II}-catalysed C(sp^3)–C(sp^3) homocoupling[348,349] and C–C heterocoupling[342] reactions.



Scheme 1.5.1: The use of "*active metal templation*" in the synthesis of interlocked molecules: Leigh's proposed mechanism for the metal-templated CuAAC reaction to form a [2]rotaxane.[340]

Organic cation motifs, such as secondary ammonium functional groups, have been used in conjunction with polyether macrocycles to assemble [*n*]pseudorotaxanes,[350] [*n*]rotaxanes[351,352] and [*n*]catenanes.[314,353,354] Indeed, this interaction has been used to great effect in the preparation of Stoddart's [20]rotaxane[355] and suit[2]ane (Figure 1.5.6a),[356,357] a new category of interlocked molecule. The advantage of the ammonium motif is that once the interlocked structural framework has been formed, it may be deprotonated or alkylated (Figure 1.5.6b),[358,359] affording a reversible or permanent positional displacement of the macrocycle: the basic principle required for molecular machines.[360–362]

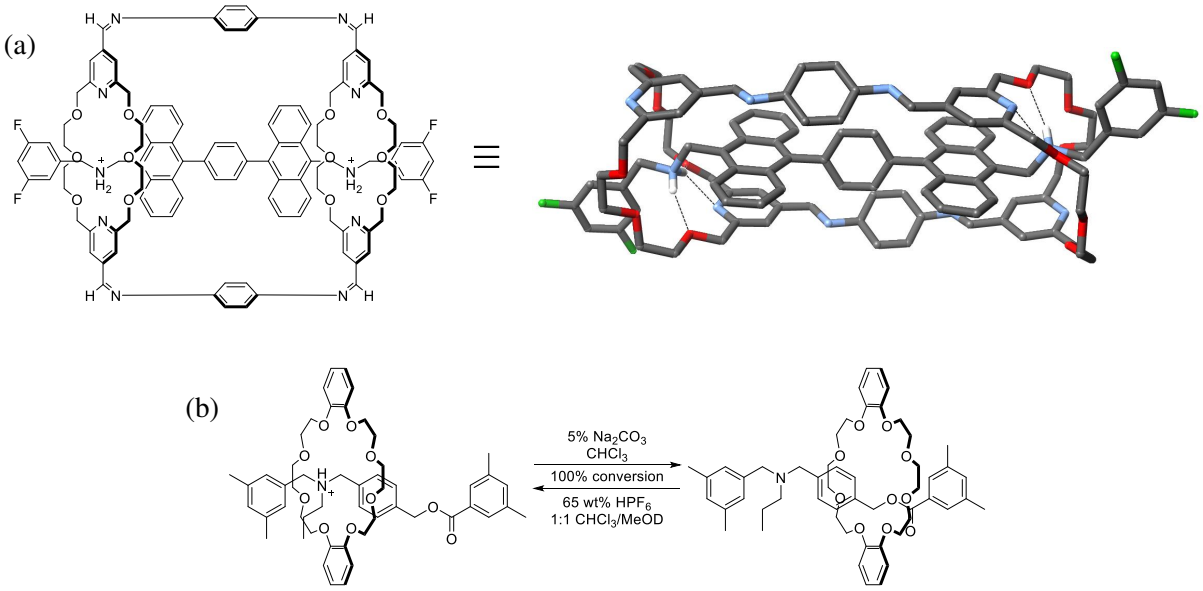


Figure 1.5.6: Selected examples of interlocked molecules templated by organic cation motifs: (a) Stoddart's suit[2]ane structure with adjacent crystal structure,[356] and (b) Takata's *N*-alkylated rotaxane which displays shuttling of the macrocycle under acid–base control.[358]

Charge-assisted aromatic donor–acceptor interactions present another approach to the formation of mechanically bonded structures. For example, Stoddart's bis-viologen-containing macrocycle forms donor–acceptor interactions between its electron deficient 4,4′-bipyridinium groups and electron-rich hydroquinone (Figure 1.5.7a),[363] TTF–dihydroxynaphthalene (Figure 1.5.7b)[364–366] and dihydroxynaphthalene (Figure 1.5.7c)[367] derivatives, which facilitate the synthesis of interlocked systems.

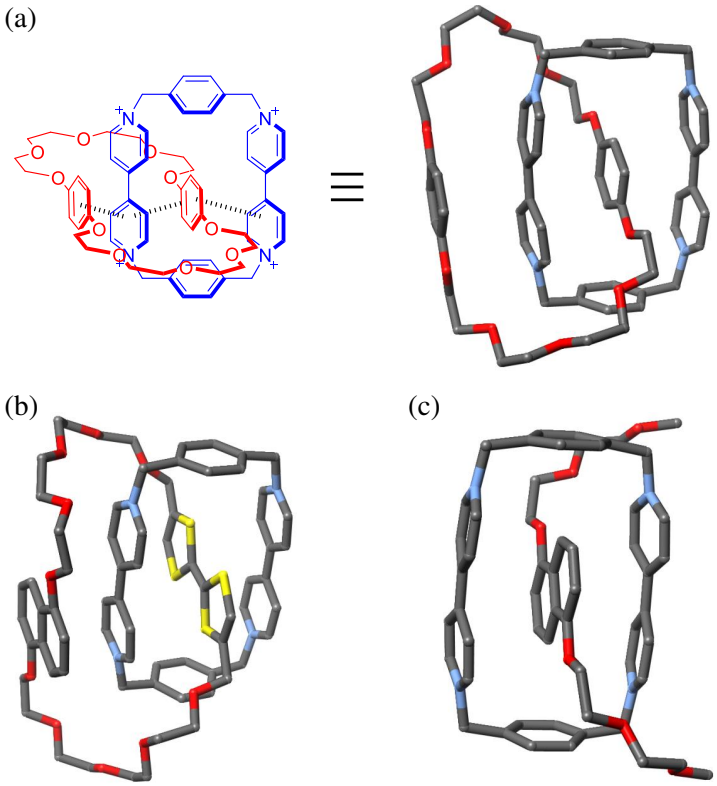


Figure 1.5.7: Interlocked and interpenetrated systems templated by charge-assisted donor–acceptor interactions: (a) structure of Stoddart's bipyridinium–hydroquinone catenane with adjacent crystal structure,[363] (b) crystal structure of Stoddart's bipyridinium–TTF/dihydroxynaphthalene catenane,[364] and (c) crystal structure of Stoddart's bipyridinium–dihydroxynaphthalene pseudorotaxane.[367]

Neutral templation The first instances of the neutral-templated synthesis of catenanes were reported in 1992 by Hunter (Figure 1.5.8a)[323] and Vögtle,[368] both of whom coincidentally employed intermolecular amide–amide hydrogen bonds to prepare [2]catenane species. Hunter's [2]catenane, which can be formed in 34% yield, is self-templated after initial acid chloride–amine condensation reactions form amides which then facilitate catenane formation *via* hydrogen bonds. Subsequently, this approach has been exploited by Leigh *et al.* who used the reaction between isophthaloyl dichloride and a selection of diamines in the synthesis of related rotaxanes and catenanes (Figure 1.5.8b).[369–371] Inspired by this work, N–H···O hydrogen bonds have been used to template the formation of interpenetrated structures with pyridine-*N*-oxide (Figure 4.1.3)[372] and squaraine (Figure 1.5.10c)[373] functional groups *via* stoppering methodologies.

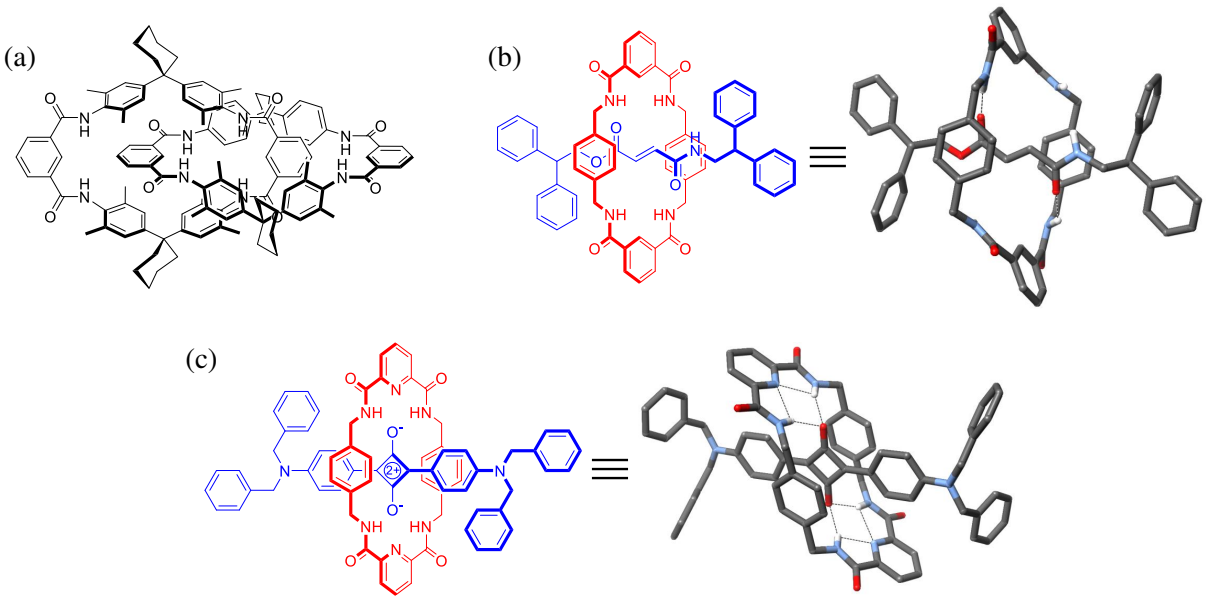


Figure 1.5.8: Selected examples of neutral amide hydrogen-bond templated interlocked structures: (a) Hunter's [2]catenane,[323] (b) Leigh's [2]rotaxane,[369] and (c) Smith's squaraine-containing [2]rotaxane.[373]

Neutral aromatic donor–acceptor interactions have been put to good use by Sanders *et al.* who used the association between naphthalene diimide and dihydroxynaphthalene components to drive the formation of a [2]catenane from a combinatorial library (Figure 1.5.9a),[374] as well as the hydrophobic effect to form a trefoil knot using naphthalene diimide units (Figure 1.5.9b).[375,376] The hydrophobic effect has also been used to template the synthesis of interlocked structures, particularly inclusion complexes with cyclodextrin derivatives in aqueous solution as reported by Anderson (Figure 1.5.9c)[377,378] and Harada.[379,380]

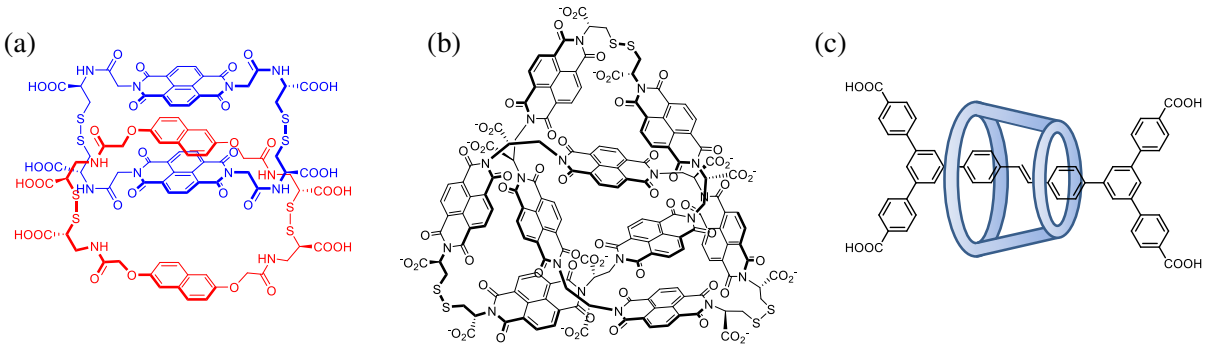


Figure 1.5.9: Neutral interlocked systems templated by π–π donor–acceptor interactions: (a) Sanders' napthalene diimide–dihydroxynaphthalene [2]catenane,[374] (b) Sanders' naphthalene diimide trefoil knot,[376] and (c) Anderson's [2]rotaxane containing γ-cyclodextrin.[378]

Anion templation Mirroring the delayed growth of anion receptor chemistry, the use of anions as templates in the synthesis of interlocked structures was also slow to develop initially. The first anion-templated interlocked structure synthesis was reported in 1999 by Vögtle who used a tetra-amide macro-

cycle to bind a phenolate half-axle within the annulus of the macrocycle *via* hydrogen bonds in dichloromethane before it reacted with a bromo-benzyl half-axle to afford the neutral [2]rotaxane in 95% yield (Figure 1.5.10a).[381] Similarly, Ghosh has used phenoxide to prepare a [2]rotaxane (Figure 1.5.10b)[382]

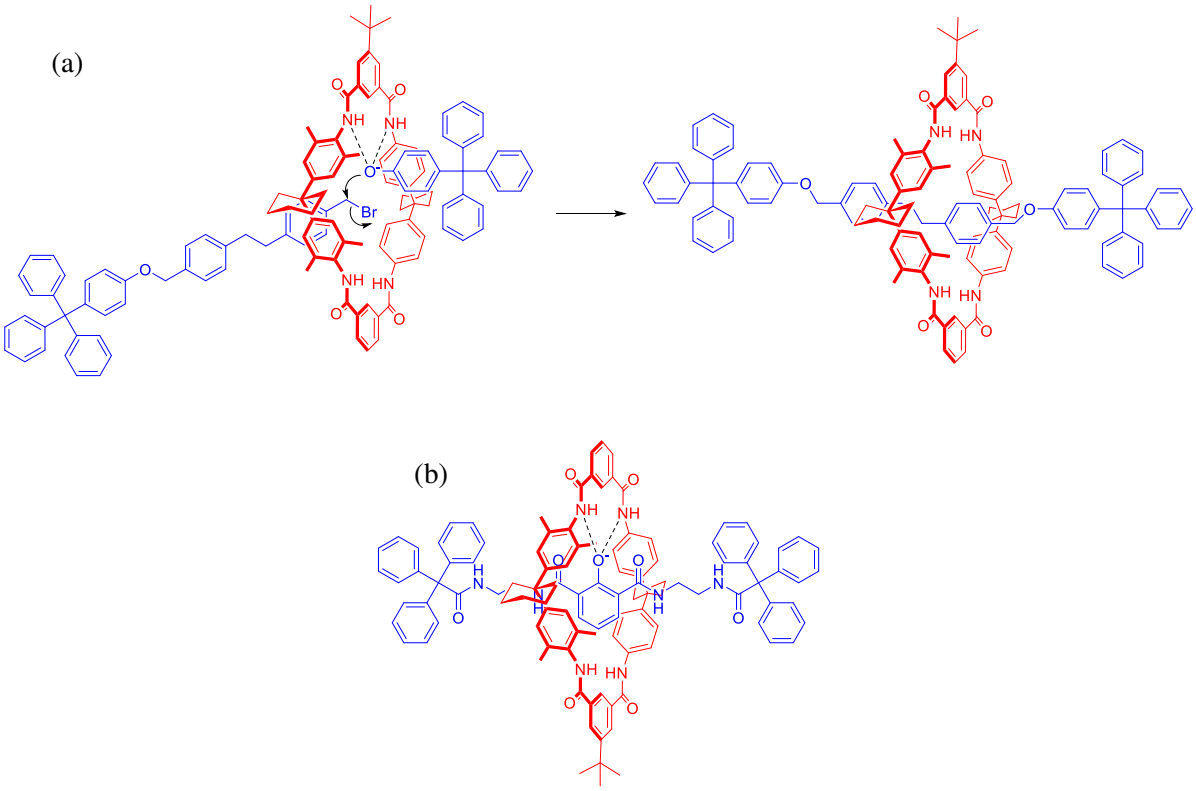


Figure 1.5.10: Early examples of anion-templated interlocked structures: (a) proposed reaction mechanism to form Vögtle's [2]rotaxane using a kinetic anion template,[381] and (b) Ghosh and Schalley's phenoxide-templated [2]rotaxane.[382]

Following their initial discovery that chloride could template the formation of an orthogonal complex between a 3,5-bis-amide pyridinium compound and a neutral isophthalamide derivative,[383] Beer and co-workers have exploited this interaction in the synthesis of interpenetrated (Figure 1.5.11a) and interlocked structures. These assemblies are also stabilised by aromatic donor–acceptor interactions between the two electron-rich hydroquinone groups of the macrocycle and the electron-deficient pyridinium motif. This strategy, known as *discrete anion templation*, has since been exploited by the same authors in the construction of interlocked species where the templating anion is "shared" between the interlocked components (Figure 1.5.11b),[383–386] and which advantageously allows the post-synthetic removal of the template to furnish a three-dimensional cavity capable of selectively binding anions.[325,384,387,388] A variety of anion coordinating groups such as indolocarbazole,[389,390] imidazolium[391] and triazolium,[392] have been integrated into elaborate mechanically-bonded structures such as a sulfate-templated, neutral urea-containing triply-interlocked capsule,[393] a handcuff catenane (Figure 1.5.11c),[394] [3]rotaxanes (Figure

1.5.11d)[395,396] and a Janus [2]rotaxane.[397] Moreover, anions such as Br^-,[269,392] NO_3^-,[398] and NO_2^-[399] have also been used to template interlocked structure synthesis.

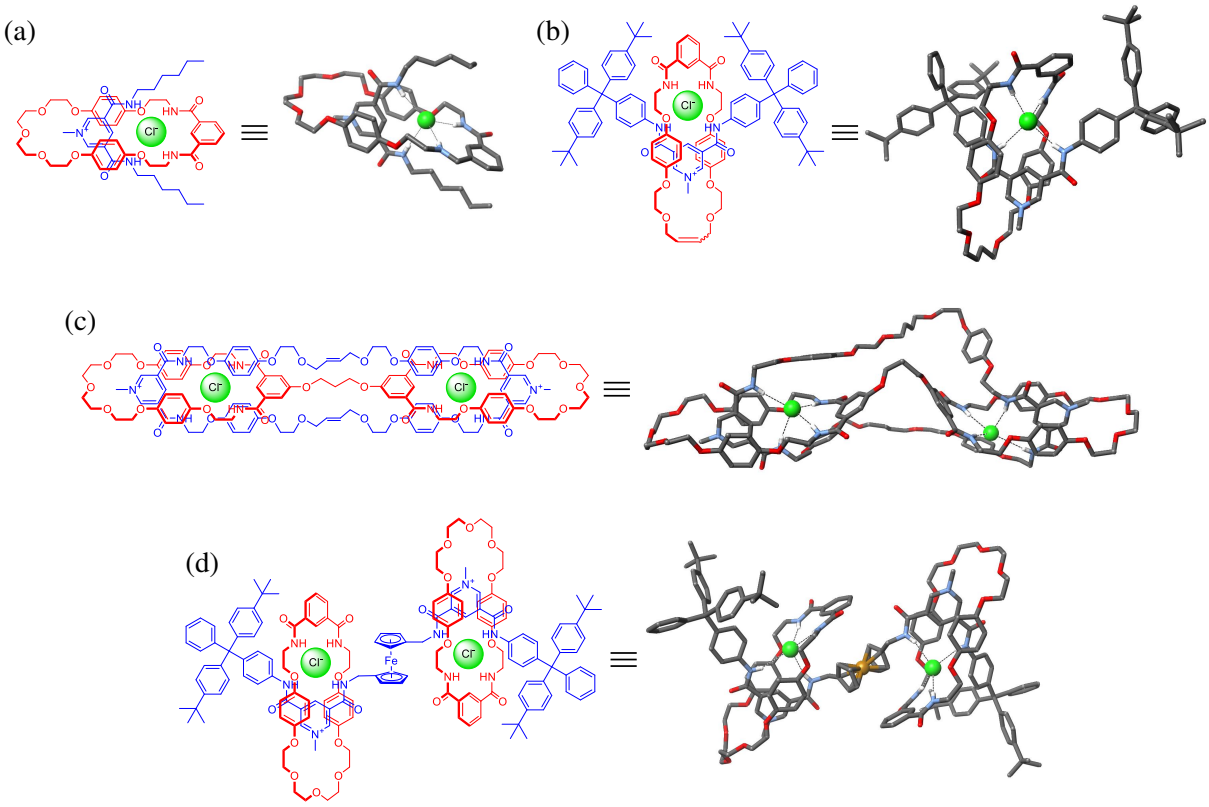
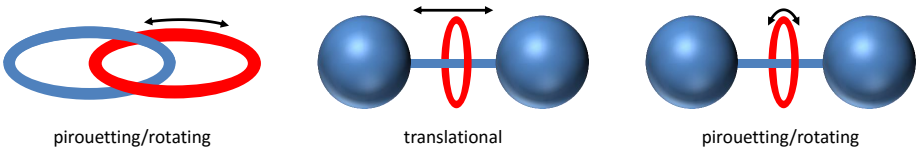


Figure 1.5.11: Selected examples of discrete anion templation of interlocked and interpenetrated structures: (a) crystal structure of Beer's chloride-templated orthogonal complex, forming a [2]pseudorotaxane,[383] (b) crystal structure of Beer's [2]rotaxane using the same templating method,[386] (c) crystal structure of Beer's handcuff catenane,[394] and (d) crystal structure of Beer's [3]rotaxane.[395]

1.5.2 Applications of interlocked structures

Inspired by the intricate molecular machinery of natural systems, the design of molecular devices has long held the imagination of chemists.[400,401] Indeed, catenanes and rotaxanes are capable of certain kinds of translational motion, allowing them to be used as "*molecular machines*" or "*switches*;" in particular, one ring can pirouette or rotate around the other in [2]catenane systems, whilst the macrocycle in a [2]rotaxane can exhibit both pirouetting motion as well as positional displacement or shuttling along the axle (Figure 1.5.12a).[402] Stoddart's seminal molecular shuttle, which displays translational motion of the macrocyclic component between two identical stations (Figure 1.5.12b),[361] has inspired the synthesis of more intricate and sophisticated systems[403,404] that show explicit molecular motion of macrocyclic components from one station to another upon an appropriate acid–base, redox, light-induced isomerisation or molecular stimulus.[352,405] Other noteworthy examples include Stoddart's redox-responsive [2]rotaxane,[406] [3]rotaxane molecular elevator;[407] Sauvage's redox-switchable catenane based on Cu^I/Cu^{II}

(a)



(b)

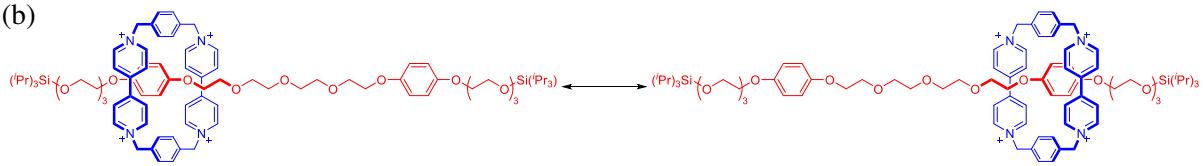
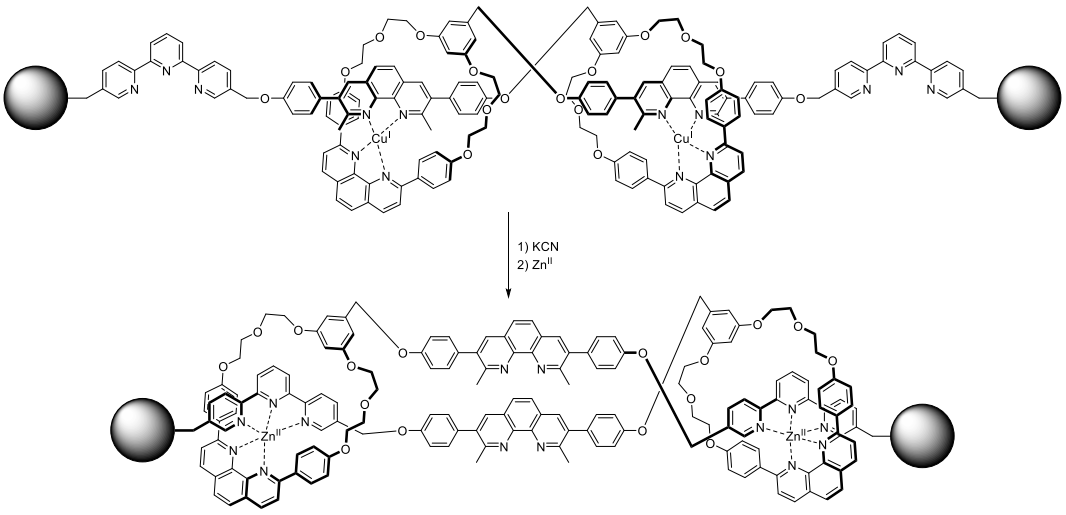


Figure 1.5.12: Selected examples of molecular machines: (a) cartoon representation of molecular motion available to catenanes and rotaxanes,[361] and (b) Stoddart's seminal molecular shuttle.[409]

coordination geometry,[408] "molecular muscles" that respond to stimuli *via* expanding and contracting motions (Figure 1.5.13a);[409] and Leigh's light-responsive [3]catenane,[410] rotaxane-functionalised surface that can propel macroscopic liquids up an incline,[411] pH-responsive [2]rotaxane organocatalyst,[412] and the impressive sequence-specific oligopeptide-synthesising [2]rotaxane (Figure 1.5.13b).[413]

(a)



(b)

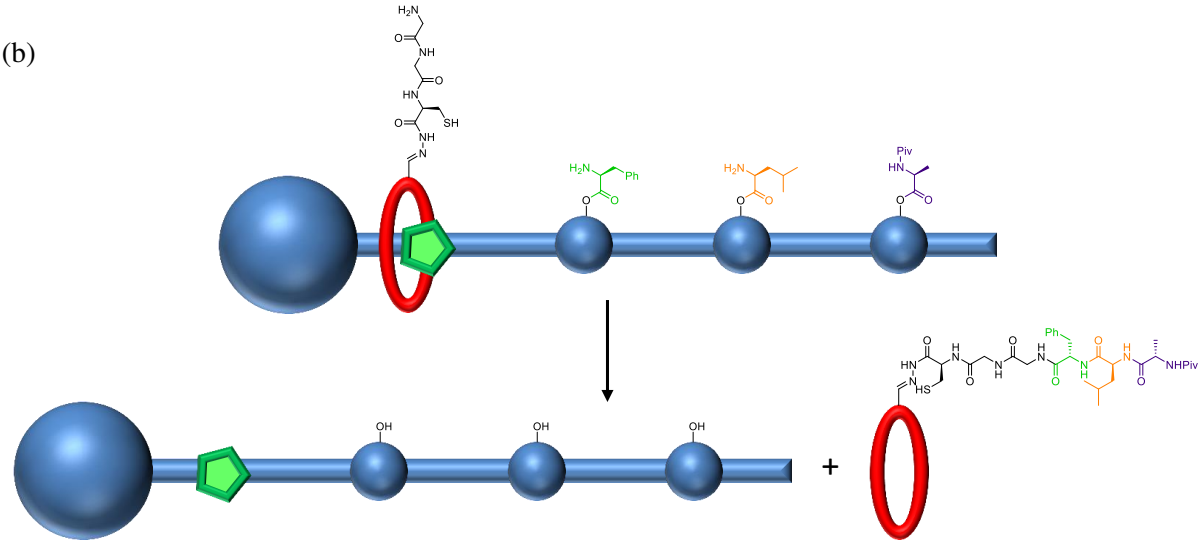


Figure 1.5.13: Selected examples of molecular machines: (a) Sauvage's metal-responsive "molecular muscles",[409] and (b) cartoon representation of Leigh's oligopeptide-synthesising [2]rotaxane.[413]

Owing to the formation of a three-dimensional binding cavity within interlocked systems, rotaxanes and catenanes have demonstrated enhanced binding strength and selectivity for the recognition and sensing of molecular guests, particularly charged species, compared to non-interlocked systems.[414,415] Whilst examples of cation binding and sensing in interlocked hosts are known, such as Hiratani's Cs-sensitive [3]rotaxane[416] and Li's Li/Zn-sensing [2]rotaxane,[417] of particular interest to this thesis are interlocked host systems for anion recognition and sensing. Beer and co-workers have exploited discrete anion templation in the design and preparation of interlocked hosts furnished with three-dimensional cavities for anion binding and, in some cases, appended reporter groups for anion sensing. Indeed, Beer has demonstrated that chloride may be selectively bound ($K_a = 1130$ M^{-1}) over the more basic dihydrogen phosphate ($K_a = 300$ M^{-1}) and acetate ($K_a = 100$ M^{-1}) in 1:1 $CDCl_3$:MeOD employing N–H···Cl^- hydrogen-bonding interactions (Figure 1.5.11b).[386] Furthermore, the triazolium motif has been incorporated into interlocked structural frameworks such as the [2]rotaxane shown in Figure 1.5.14a which binds bromide ($K_a = 970$ M^{-1}) over chloride ($K_a = 90$ M^{-1}) *via* C–H···A^- hydrogen bonds, and it was later shown that the self-assembly of the rotaxane could be enhanced by a templating bromide anion instead of chloride).[392] Beer's ferrocene-appended [2]catenane is a good example of a mechanically-bonded electrochemical sensor, which detects chloride in 1:1 dichloromethane:acetonitrile, exhibiting the maximum cathodic shift after the addition of one equivalent of chloride. This is in contrast to oxoanions which required greater equivalents of anion to obtain a maximum shift perturbation (Figure 1.5.14b).[418] More recently, Beer *et al.* reported a [2]catenane that exhibits a fluorescent response upon anion binding: only chloride ($K_a = 3.71 \times 10^6$ M^{-1}) and bromide ($K_a = 1.48 \times 10^5$ M^{-1}) anions are bound by the bromoimidazolium groups *via* halogen bonds in acetonitrile, with no binding observed for other anions (Figure 1.3.1g).[269]

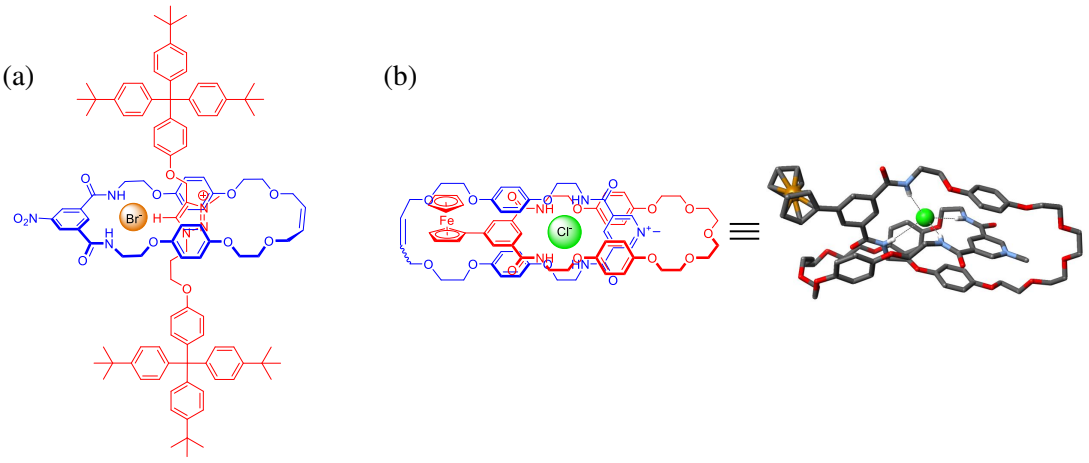
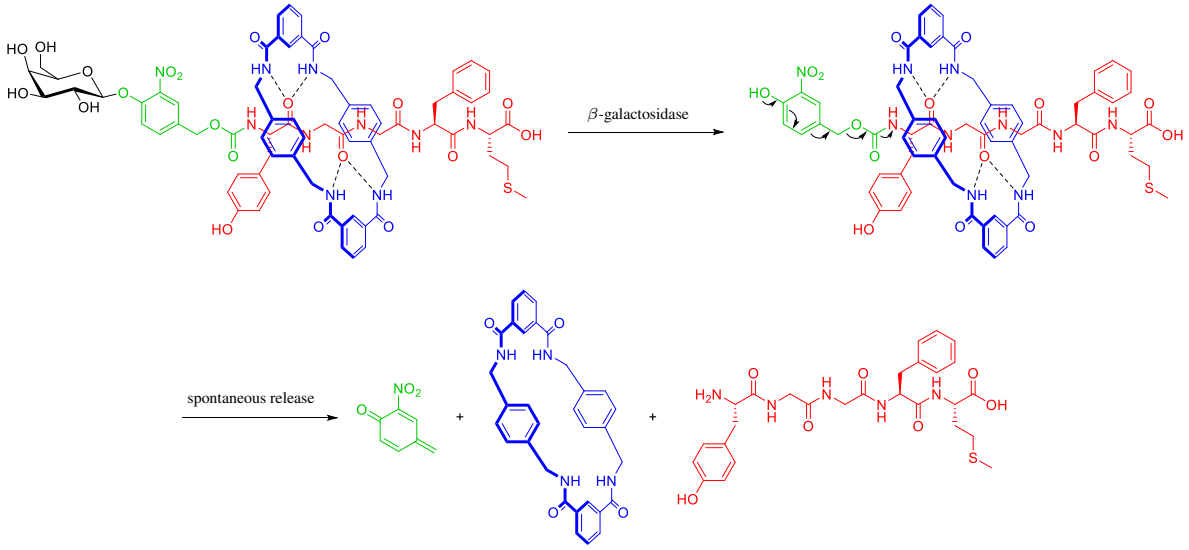


Figure 1.5.14: Applications of interlocked molecules as receptors and sensors for anions: (a) Beer's triazolium-containing [2]rotaxane that is selective for bromide,[392] and (b) crystal structure of Beer's ferrocene-appended electrochemical [2]catenane.[418]

Interlocked structures have also been introduced into medicinal chemistry as a prodrug or drug delivery method since the mechanically-bonded components can display enhanced stability compared to the free components. Leigh *et al.* prepared a monosaccharide-stoppered [2]rotaxane containing a biologically active peptide Met-enkephalin as part of the axle component (Scheme 1.5.2).[419] The peptide is released by β-galactosidase enzyme-mediated hydrolysis, whereafter it may deliver its therapeutic effect to cells.



Scheme 1.5.2: Schematic mechanism for the β-galactosidase enzyme-mediated release of Met-enkephalin from Leigh's [2]rotaxane.[419]

1.6 Project Aims

The predominant aim of this project is to investigate the use of halogen bonding for anion recognition *via* its incorporation into acyclic, macrocyclic, interpenetrated and interlocked structural frameworks. At the inception of this project, a timely report of the simple, one-pot synthesis of the iodotriazole motif was published by Zhu *et al.*.[420] Consequently, a bidentate 3,5-bis-iodotriazole-pyridinium motif was envisaged for use in potent, selective anion host systems.

Chapter Two focuses on systems involving iodotriazole donors. The 3,5-bis-iodotriazole pyridinium motif is introduced: the initial syntheses of a series of acyclic receptors and their anion recognition properties are reported. The incorporation of this motif into interlocked [2]catenane and [2]rotaxane systems is described, and their anion recognition properties are examined, supported by solid-state structures of the [2]catenane structural framework.

Chapter Three extends this work by describing the non-trivial incorporation of the 3,5-bis-iodotriazole pyridinium motif into an asymmetric [2]rotaxane host system with a view towards nitrate-selective binding. The anion recognition properties of the rotaxane hosts are reported.

Chapter Four investigates the use of neutral anion recognition *via* the use of the 3,5-bis-iodotriazole pyridine-*N*-oxide motif. Initial syntheses of acyclic receptor systems is described and their anion recognition properties are expounded. The work of Chapter 3 is expanded *via* the synthesis of an asymmetric, neutral [2]rotaxane host system and its anion recognition properties are investigated.

Chapter 2

The 3,5-bis-iodotriazole pyridinium motif

2.1 Introduction

This chapter introduces triazole- and iodotriazole-based receptors for anion recognition, with a specific focus on the novel 3,5-bis-iodotriazole pyridinium motif. Initially, the synthesis and anion binding properties of acyclic model host systems containing this motif are described, followed by the design and incorporation of this motif into two [2]catenane anion host systems. The anion binding properties of these interlocked receptors are discussed. The results of a collaboration with Prof. Pierre Kennepohl at the University of British Columbia, Canada, whereby the covalent nature of the halogen-bonding interactions with anions was investigated using X-ray absorption spectroscopy, are expounded. Thereafter, the incorporation of the 3,5-bis-iodotriazole motif into a water-soluble [2]rotaxane host system for aqueous anion recognition is described and its anion binding properties are presented.

2.1.1 Triazole and iodotriazole receptors for anions

Due to the synthetic ease with which 1,2,3-triazoles may be prepared,[421,422] there has been increased interest in the incorporation of this motif into anion-coordinating host molecules owing to the acidic C–H bond: notable examples of this include Flood's foldamers (Figure 2.1.1a).[423–425] Recently, Sessler reported a macrocycle which contains triazole C–H hydrogen-bond donors supplemented with pyrrole N–H hydrogen-bond donors (Figure 2.1.1b).[426] These all converge on the macrocyclic cavity which binds the biologically relevant pyrophosphate anion ($K_a = 2.30 \times 10^6$ M^{-1}) in $CDCl_3$ an order of magnitude more strongly than dihydrogen phosphate ($K_a = 2.38 \times 10^5$ M^{-1}). The complementary size match of the macrocycle to pyrophosphate is supported by solid-state evidence.

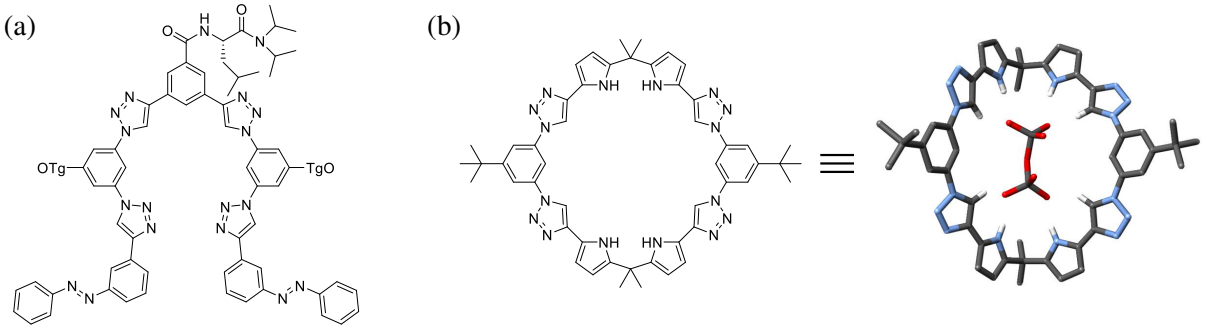


Figure 2.1.1: Structures of C–H hydrogen-bonding triazole-containing receptors: (a) Flood's foldamer,[423] and (b) Sessler's pyrophosphate-binding triazolophane.[426]

As was mentioned in Section 1.2.4.2, when the triazole motif is methylated, the resulting triazolium moiety displays competitive C–H hydrogen-bond capability and has been incorporated into a variety of interlocked host architectures for the application of anion recognition by Beer (see Figure 1.5.14).[392] An

asymmetric [2]rotaxane containing an axle component bearing both a C–H hydrogen-bonding triazolium group and an amide group was prepared, which showed remarkably strong binding for chloride and bromide (K_a = 2035 and 1948 M^{-1}, respectively) in 1:1 $CDCl_3$:CD_3OD and no binding of the strongly basic acetate or dihydrogen phosphate oxoanions (Figure 2.1.2).[427]

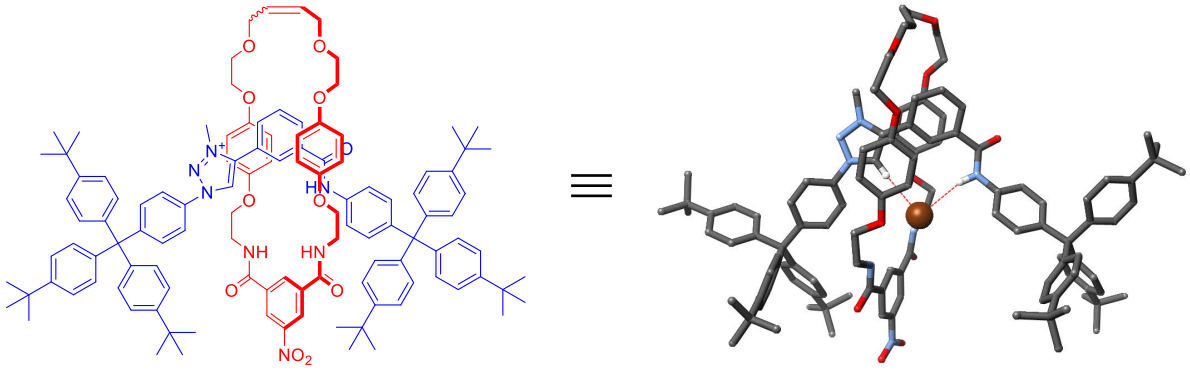


Figure 2.1.2: Structure of Beer's asymmetric C–H hydrogen-bonding triazolium [2]rotaxane (left) with the 1:1 bromide:host crystal structure (right).[427]

The effectiveness of charge-assisted C–H hydrogen bonding using the 1,2,3-triazole moiety is notable when incorporated into a 3,5-bis-triazole pyridinium motif: a series of acyclic, macrocyclic, catenane and rotaxane host systems bearing this motif were prepared by White and Beer.[158,428] The acyclic derivative (Figure 2.1.3a) displayed good affinity for anions, which followed basicity trends in CD_3CN.[429] However, binding for the 3,5-bis-amide pyridinium analogue was much stronger owing to the enhanced N–H hydrogen-bonding ability of the amides. The catenane and rotaxane hosts (Figure 2.1.3b,c) displayed strong binding for halide anions in competitive 1:1 $CDCl_3$:CD_3OD solvent mixture (*vide infra*).[430] This work inspired the design of the analogous halogen-bonding 3,5-bis-iodotriazole pyridinium motif which is investigated in this thesis.

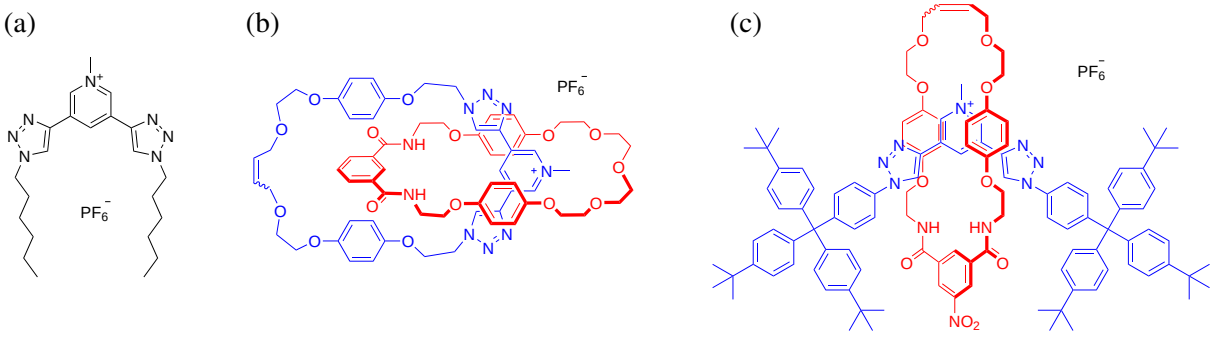


Figure 2.1.3: Structures of 3,5-bis-triazole pyridinium anion receptors: (a) a hexyl-appended acyclic derivative,[429] (b) a [2]catenane,[430] and (c) a [2]rotaxane.[428]

During the course of this study, the iodotriazole moiety, and its methylated iodotriazolium derivative, have been incorporated into a variety of acyclic and interlocked motifs for anion recognition by Beer. In

particular, acyclic and rotaxane host systems containing an *N*-propyl carbazole bis-iodotriazolium motif were reported to bind halide anions with high affinity in aqueous mixtures, with enhanced binding observed for the halogen-bonding derivatives over their hydrogen-bonding triazolium counterparts (Figure 2.1.4a).[431] Moreover, an all-halogen-bonding rotaxane was reported that incorporated an *N*-propyl carbazole bis-iodotriazole motif into an axle component, with a Re^{I}-bipyridyl bis-iodotriazole macrocycle component (Figure 2.1.4b). The rotaxane was able to recognise and sense halide anions over oxoanions *via* quenching of the rhenium MLCT emission in aqueous mixtures containing up to 50% water.[432]

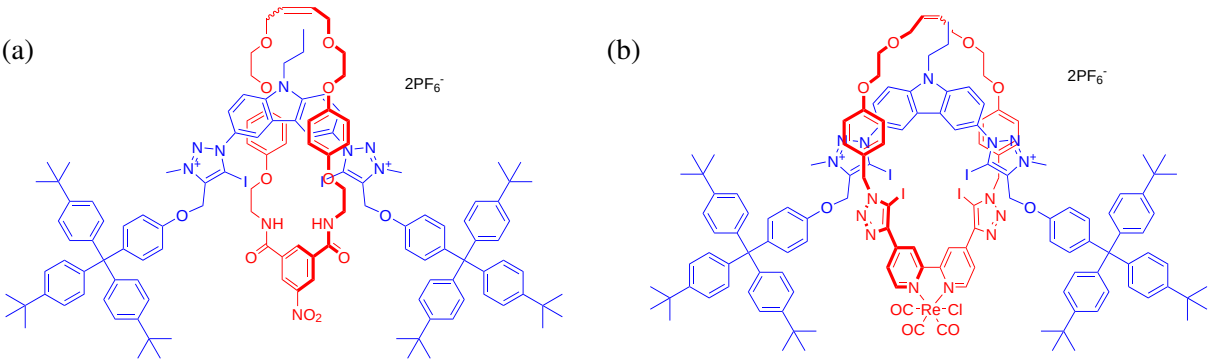


Figure 2.1.4: Structures of (a) the *N*-propyl carbazole bis-iodotriazolium [2]rotaxane,[431] and (b) the all-halogen-bonding *N*-propyl carbazole bis-iodotriazolium axle–Re^{I}-bipyridyl bis-iodotriazole macrocycle [2]rotaxane.[432]

2.1.2 Chapter aims

Considering the facile synthesis of 1,2,3-iodotriazoles, and the promising anion recognition properties of halogen-bonding moieties, this chapter will introduce the 3,5-bis-iodotriazole pyridinium motif through its incorporation into acyclic, macrocyclic and interlocked [2]catenane and [2]rotaxane host structural frameworks. Furthermore, the anion recognition properties of these receptors will be discussed, leading towards anion recognition in aqueous media.

The nature of halogen-bonding–anion interactions will also be investigated: employing X-ray absorption spectroscopic techniques has allowed for the quantification of the degree of halogen-bond covalency.

2.2 Acyclic receptors*

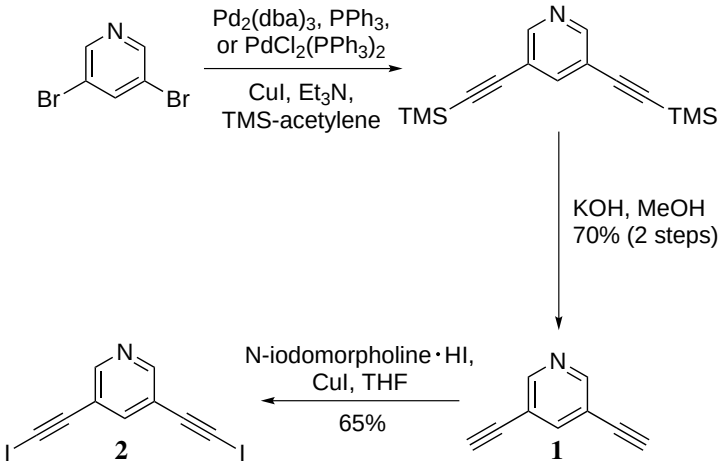
A series of target acyclic anion receptors containing the 3,5-bis-iodotriazole pyridinium motif were initially envisaged. The design of this motif would allow for the binding of anions *via* two convergent C–I···A^- halogen bonds: the synthesis and anion binding studies of these simple acyclic receptors would

*The work in Sections 2.2 and 2.3 was published in the Journal of the American Chemical Society: Robinson, S. W., Mustoe, C. L., White, N. G., Brown, A., Thompson, A. L., Kennepohl, P., Beer, P. D., *Evidence for halogen bond covalency in acyclic and interlocked halogen-bonding receptor anion recognition.*, *J. Am. Chem. Soc.*, 2015, **137**, 499–507.

assess the ability of two *meta*-substituted iodotriazoles to recognise anions convergently despite the close proximity of the voluminous iodine atoms.

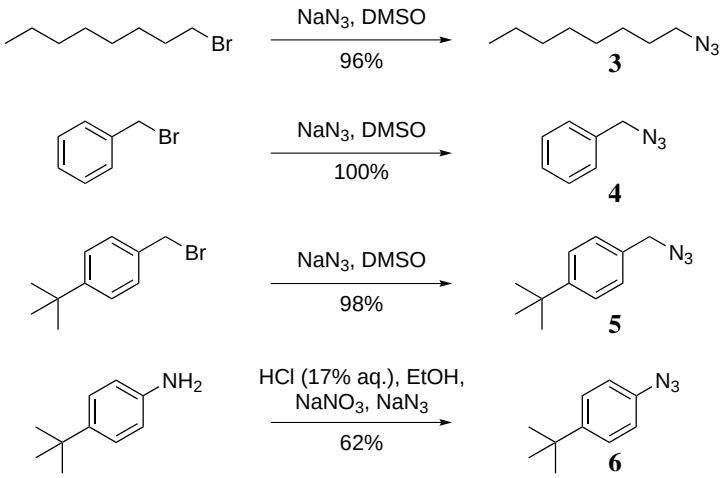
2.2.1 Synthesis

The synthesis of the 3,5-bis-iodotriazole pyridinium receptors required the use of Cu^{I}-catalysed Azide-Alkyne Cycloaddition (CuAAC), so-called 'click', reactions to form the requisite precursors. At the time of this work, two high-yielding routes towards the synthesis of iodotriazoles *via* CuAAC click conditions were available in the literature. The first, more commonly employed method is the cycloaddition reaction between an organic azide and a pre-formed iodoalkyne in the presence of a Cu^{I} catalyst, which was coined the 'two-pot' method.[433] The second was reported by Zhu *et al.* in 2012: the high yielding 'one-pot' cycloaddition of an azide and a terminal alkyne, following the *in situ* generation of a Cu^{I} catalyst and electrophilic triiodide.[420] To that end, 3,5-diethynylpyridine **1**, was synthesised by a modification of literature procedures:[434,435] Sonogashira[436] coupling of commercially available 3,5-dibromopyridine with trimethylsilyl-acetylene afforded the TMS-protected diethynylpyridine intermediate (Scheme 2.2.1). Subsequent deprotection with potassium hydroxide in methanol, and purification by sublimation, afforded **1** as a white crystalline solid in yields up to 70%. The iodo-alkyne derivative, 3,5-di-iodoethynyl pyridine **2** was prepared by the reaction of **1** with *N*-iodomorpholine·HI in the presence of catalytic CuI in yields up to 65% after purification.



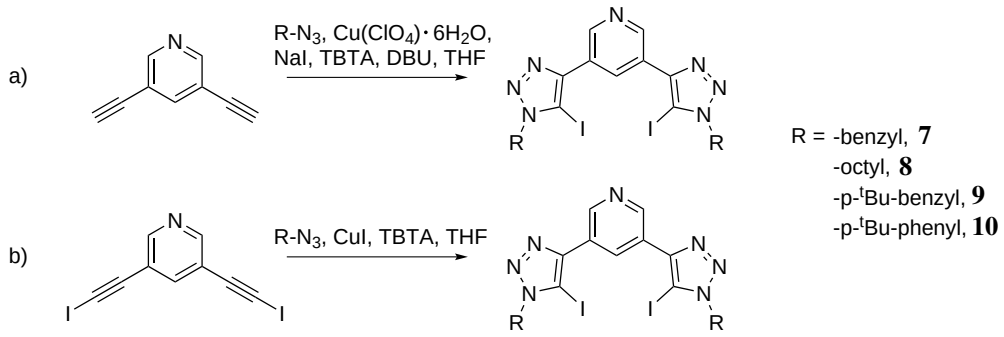
Scheme 2.2.1: Synthetic scheme to prepare **1** and **2**.

A series of suitable azides for CuAAC reaction were prepared by the substitution of a parent alkyl bromide with NaN_3 (**3**, **4** and **5**) or *via* the diazotisation of the parent aniline and substitution with NaN_3 (**6**) (Scheme 2.2.2).



Scheme 2.2.2: Synthetic scheme to prepare azides: **3**, **4**, **5** and **6**.

Initial reactions to form the 3,5-bis-iodotriazole pyridine precursors investigated the use of both the one-pot and two-pot procedures (Scheme 2.2.3) as outlined in Table 2.2.1 below. It quickly became apparent that optimisation of the reaction conditions was necessary: **7** was formed in excellent yields *via* the two-pot method but resulted in a disappointing yield when the one-pot method was used. This was rectified by the addition of catalytic TBTA, a Cu^{I}-stabilising ligand, and standardising the order in which reagents were added such that a 0–79% increase in yield was observed for the synthesis of **8** *via* the one-pot method, whilst the two-pot method similarly afforded **8** in a good yield. The aforementioned modifications to the one-pot method resulted in good yields for **9** and **10**, however, no formation **10** *via* the two-pot method was observed. This is assumed to be due to steric crowding of the dinuclear Cu^{I}-complex[422] in which the large, bulky iodine substituent on the alkyne hinders the cyclisation with an azide directly attached to a phenyl ring. Consequently, the one-pot method was selected as the primary means towards the synthesis of iodotriazoles.



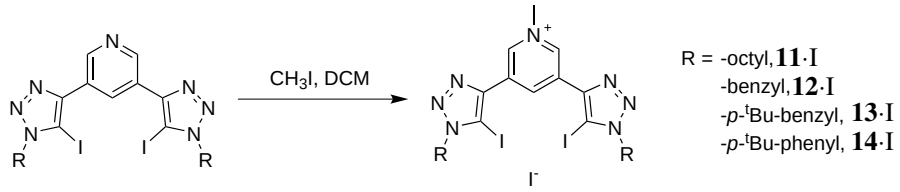
Scheme 2.2.3: Synthetic scheme to prepare the 3,5-bis-iodotriazole pyridine precursors: a) using the one-pot method and b) the two-pot method.

Table 2.2.1: Results of CuAAC click reactions to synthesise the 3,5-bis-iodotriazole pyridine precursors.

Thread	Alkyne	Azide	Method	Yield (%)[a]
7	**1**	**4**	one-pot	0
	2	**4**	two-pot	93 (60)
8	**1**	**3**	one-pot	79
	2	**3**	two-pot	88 (57)
9	**1**	**5**	one-pot	76
10	**1**	**6**	one-pot	85
	2	**6**	two-pot	0

[a] Yields over the two steps (iodination of the alkyne and click reaction) are shown in parenthesis.

The 3,5-bis-iodotriazole pyridine precursors were methylated using excess CH_3I in dry dichloromethane, however in some cases, the iodide salts were poorly soluble in organic solvents, making anion exchange difficult (Scheme 2.2.4). The iodide salt of the octyl-appended receptor was marginally soluble in organic solvents, however, a suspension of **11**·I in $CHCl_3$ could be anion exchanged to the more soluble chloride salt by repeated washing with $NH_4Cl_{(aq.)}$. The benzyl-appended receptor **12**·I, was very insoluble in organic solvents and could not be anion exchanged for use in anion binding studies. The *para-tert*-butylbenzyl-appended receptor **13**·I, displayed better solubility than **11**·I in $CHCl_3$ and was anion exchanged to the non-coordinating hexafluorophosphate (PF_6^-) salt for anion binding studies. The *para-tert*-butylphenyl-appended receptor **14**·I, was poorly soluble in organic solvents, but could be anion exchanged to the BAr_4^{F-} salt by stirring a suspension of **14**·I in $CHCl_3$ with $NaBAr^F_{4(aq.)}$, however, its insolubility with other counter-anions disqualified its use in anion binding studies.



Scheme 2.2.4: Synthesis of cationic acyclic receptors $\mathbf{11}^+$, $\mathbf{12}^+$, $\mathbf{13}^+$ and $\mathbf{14}^+$.

2.2.2 Crystal structures

Crystals suitable for X-ray diffraction structural analysis were obtained from the chloride salt of the octyl-appended acyclic receptor **11**·Cl. The solid-state structure displays convergent iodotriazole–I···Cl halogen bonds (Figure 2.2.1) and planarity across the iodotriazole-pyridinium-iodotriazole heterocyclic motif, despite the large size of the iodine substituents. The asymmetric unit consists solely of one molecule of **11**·Cl. The chelating halogen bonds vary in length from 3.121(2)–3.195(2) Å corresponding

to 84–86% of the sum of the van der Waals' halide radii, which is indicative of strong halogen-bonding interactions to the anion.

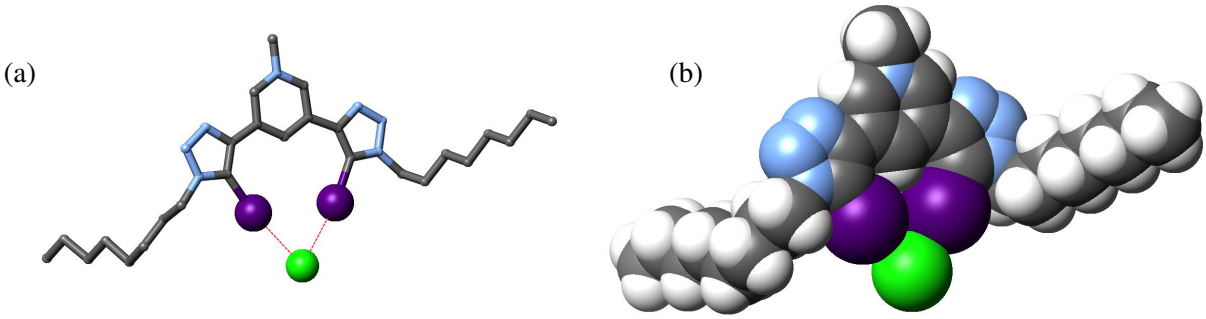


Figure 2.2.1: Crystal structure of **11**·Cl: (a) Perspective view of the receptor drawn as capped sticks and halides as spheres, showing the planar iodotriazole-pyridinium-iodotriazole heterocyclic motif (hydrogen atoms omitted for clarity), and (b) space-filling representation of the receptor showing the host–guest close contacts. Triazole–I···Cl^- halogen bonds (3.121(2)–3.195(2) Å) are indicated as red dashed lines.

Furthermore, crystals were also obtained for **12**·I by vapour diffusion of dichloromethane into a solution of the compound in DMSO-d_6. Once again in this structure, the iodotriazoles are co-planar with the pyridinium ring resulting in perfectly convergent halogen-bond donors which feature iodotriazole–I···I^- close contacts 86–90% shorter than the sum of the van der Waals' radii (3.96 Å) indicating strong interactions (Figure 2.2.2). The asymmetric unit is comprised of two molecules of **12**·I and four dichloromethane molecules.

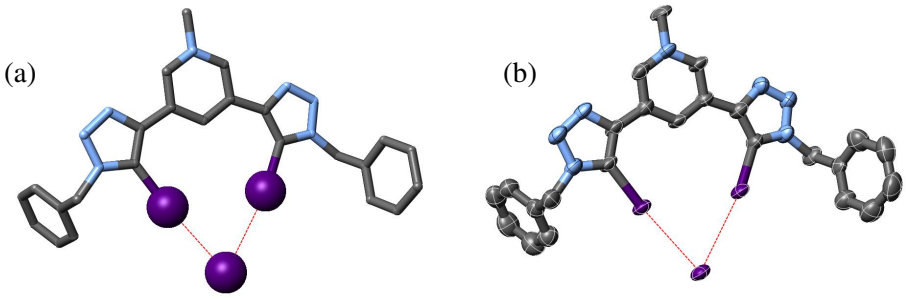


Figure 2.2.2: Crystal structure of **12**·I: (a) Perspective view of the receptor drawn as capped sticks and halides as spheres, showing the planar iodotriazole-pyridinium-iodotriazole heterocyclic motif and (b) thermal ellipsoid representation of the receptor drawn at the 90% confidence level. Triazole–I···I halogen bonds (3.404(1)–3.533(1) Å) are indicated as red dashed lines. Hydrogen atoms and dichloromethane molecules are omitted for clarity.

2.2.3 ^{1}H NMR anion binding studies

The anion binding properties of the acyclic receptor **13**·PF_6 were investigated using ^{1}H NMR anion titration experiments by adding aliquots of anions as their tetrabutylammonium salts to solutions of the receptor. Job plot approximations of initial titrations with TBA·Cl in acetone-d_6 determined 1:1 stoichiometric association constants of $> 10^4$ M^{-1} for both receptors. Consequently, titrations were repeated in the more competitive CD_3CN to allow for comparison with the previously reported prototriazole ana-

logue;[429] however, association constants for the halogen-bonding receptor **13**·PF_6 with chloride were still $> 10^4$ M^{-1}. As a result, titrations were undertaken in the even more competitive solvent DMSO-d_6 indicating the superior anion binding capability of the halogen-bonding receptor. In DMSO-d_6, the pyridinium protons *b* and *c* of **13**·PF_6 are initially co-resonant, however, upon anion binding, the resonances separate with a downfield perturbation of pyridinium proton *c* incumbent on anion binding (Figure 2.2.3), generating the binding isotherms shown in Figure 2.2.4. Similarly, addition of anions to the analogous hydrogen-bonding prototriazole receptor typically caused downfield perturbations of the triazole proton *d*, directly involved in anion coordination.[429]

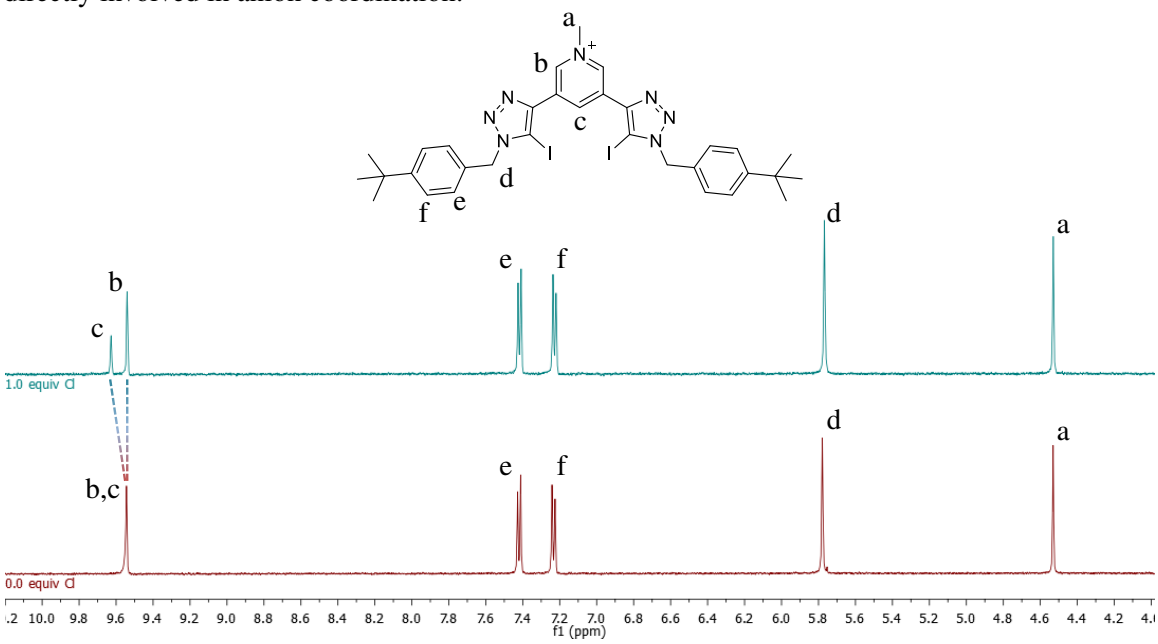


Figure 2.2.3: Truncated ^{1}H NMR spectra showing the shift of the pyridinium peak *c* upon addition of 1.0 equivalent of chloride to **13**·PF_6.

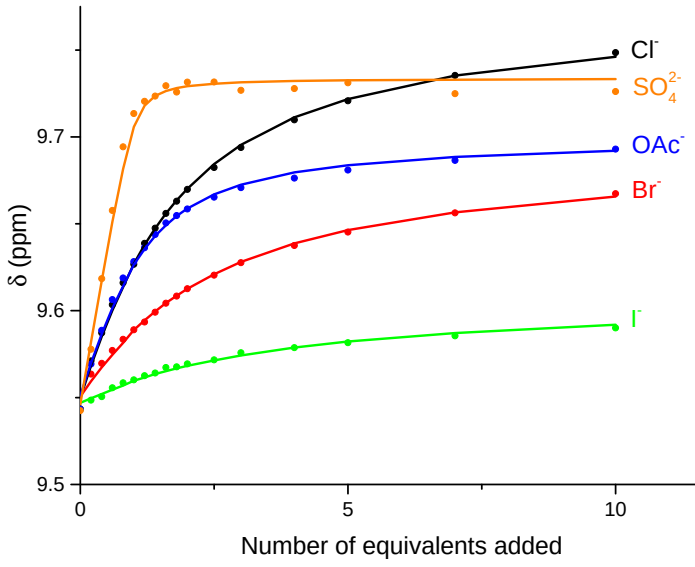
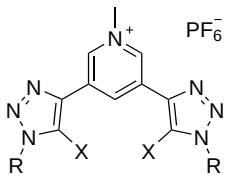


Figure 2.2.4: Anion binding titrations with **13**·PF_6 following proton *c* in DMSO-d_6: experimental titration data (circles) with WinEQNMR2[437] fitted binding isotherms indicated as lines (298 K).

Table 2.2.2: Association constants (K_a) determined for various TBA·anions with **13**$^+$ compared with the prototriazole analogue.



Anion	K_a (M^{-1})[a]	
	13$^+$ X = I R = ^{t}Bu-benzyl (DMSO-d_6)	X = H[429] R = hexyl (CD_3CN)
F^-	NB[b]	–[c]
Cl^-	387(20)	206(11)
Br^-	238(12)	106(3)
I^-	146(3)	59(2)
OAc^-	1025(9)	–
$H_2PO_4^-$	NB[d]	precipitation
NO_3^-	NB	–
SO_4^{2-}	$> 10^4$	–

[a] Anions added as TBA salts, estimated standard errors are given in parentheses. Association constants calculated using WINEQNMR2[437] (DMSO-d_6, 298 K). [b] Degradation of the receptor observed. [c] Anion not titrated. [d] Negligible δ (ppm) shifts observed.

WinEQNMR2[437] analysis and approximations of Job plots of the titration data determined the 1:1 stoichiometric association constants shown in Table 2.2.2. The anion binding selectivity of prototriazole receptor follows anion basicity trends, as would be expected for an anion receptor in an aprotic solvent, with the larger halides complexed more weakly than chloride. Similarly, for the halogen-bonding acyclic receptor **13**·PF_6, selectivity follows anion basicity trends for the halides, with OAc^- being the most strongly associated anion; the association constant, K_a, is 2.5 times larger in magnitude than chloride. Interestingly, no binding was observed for $H_2PO_4^-$ and NO_3^-, while SO_4^{2-} was bound at $> 10^4$ M^{-1}, presumably due to the greater negative charge. To the best of our knowledge, this is only the second example of a halogen-bonding oxoanion-selective anion receptor.[267]

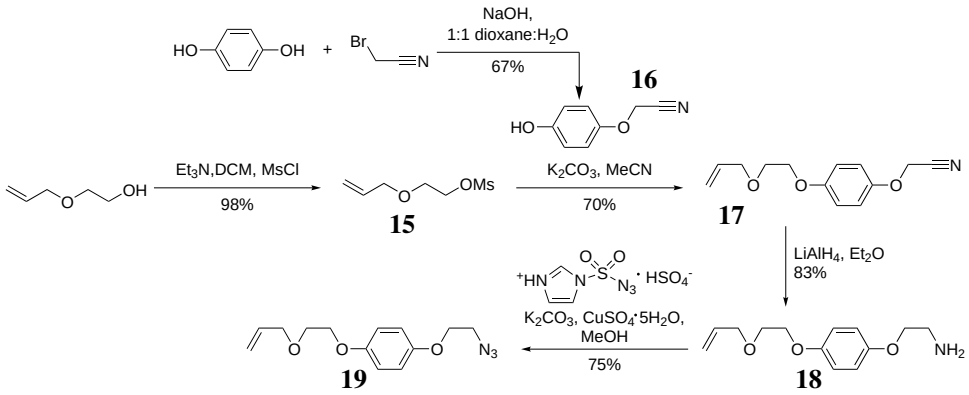
2.3 A monocationic [2]catenane

As a result of the enhanced anion recognition properties of the acyclic halogen-bonding receptor **13**·PF_6, in comparison to the hydrogen-bonding analogue, the integration of the bis-iodotriazole-pyridinium motif into a [2]catenane host structural framework was undertaken *via* a chloride anion-templated clipping synthetic procedure.

2.3.1 Synthesis

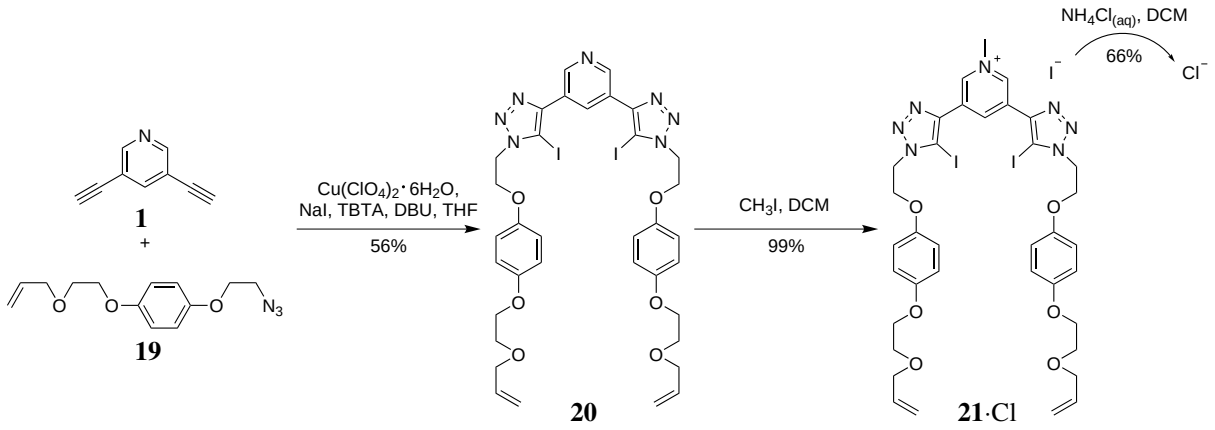
In order to incorporate the 3,5-bis-iodotriazole pyridinium motif into a [2]catenane, a vinyl-appended azide **19** was prepared (Scheme 2.3.1). This was achieved first by mesylation of commercially available allyloxyethanol to form the allyloxyethyl mesylate **15**, which was coupled with nitrile-appended hydro-

quinone **16** to afford the vinyl-appended hydroquinone derivative **17** in 70% yield. Reduction of the nitrile with $LiAlH_4$ afforded the amine **18** which on reaction with azide transfer reagent (1-(azidosulfonyl)-1*H*-imidazol-3-ium hydrogen sulfate) gave the azide **19** in 75% yield.



Scheme 2.3.1: Synthesis of the vinyl-appended azide **19**.

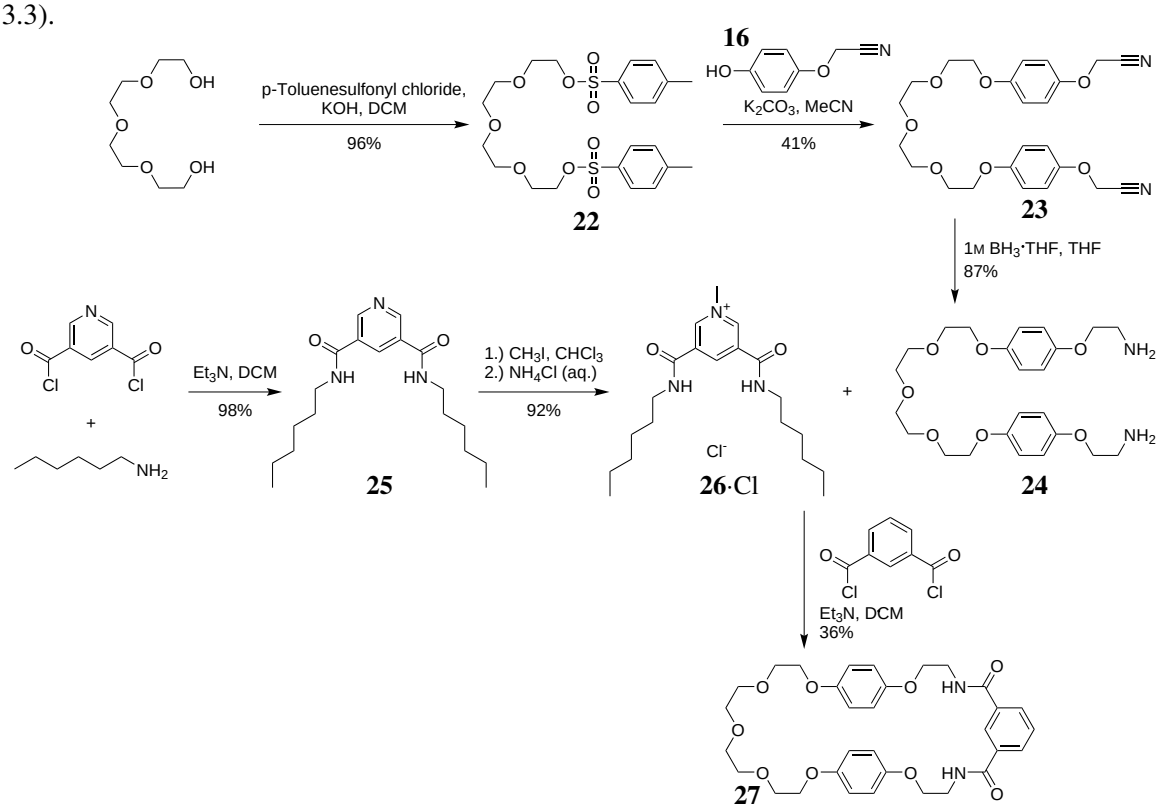
A macrocycle precursor containing the 3,5-bis-iodotriazole pyridinium motif was prepared from the CuAAC reaction between **1** and 2.2 equivalents of azide **19**, using the one-pot click methodology to afford **20** in 56% after purification by silica gel column chromatography (Scheme 2.3.2). Methylation using an excess of CH_3I gave **21**·I, which was anion exchanged to the more soluble chloride salt by repeated washing with $NH_4Cl_{(aq.)}$.



Scheme 2.3.2: Synthetic route to prepare the vinyl-appended 3,5-bis-iodotriazole pyridinium-containing macrocycle precursor **21**·Cl *via* the one-pot click methodology, and subsequent methylation and anion exchange.

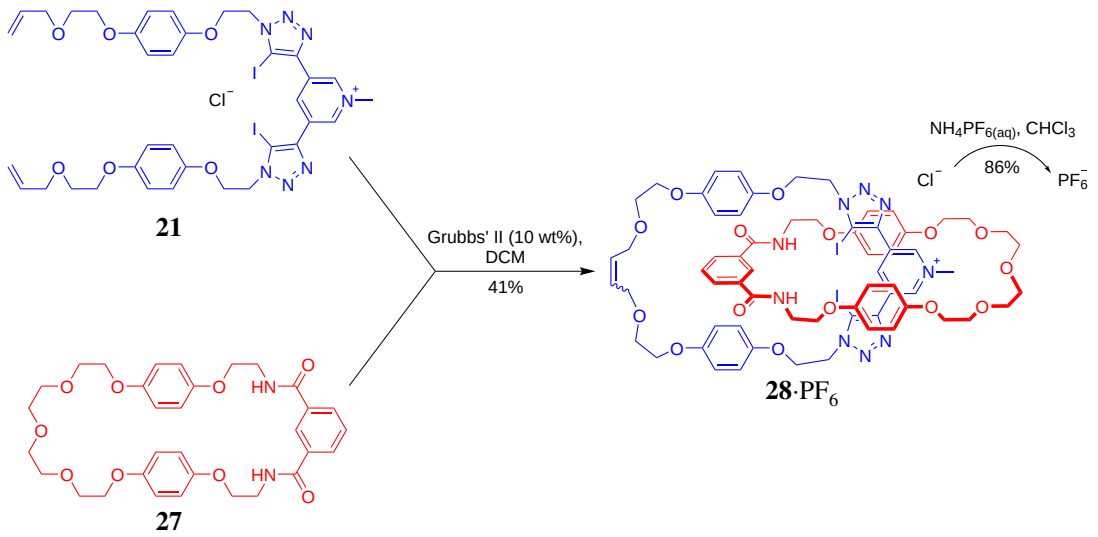
A known isophthalamide-containing macrocycle was prepared for the formation of the [2]catenane.[438] Commercially available tetraethylene glycol was reacted with two equivalents of tosyl chloride to form the bis-tosylate **22**, which was coupled with **16** under basic conditions to produce the bis-nitrile compound **23** (Scheme 2.3.3). Reduction of **23** with BH_3 in THF gave bis-amine macrocycle precursor **24** in 87% yield. A pyridinium bis-amide chloride template **26**·Cl was prepared by the methylation of the pyridine bis-amide precursor **25**, which was prepared by the amide condensation of *n*-hexylamine with

pyridine-3,5-diacid chloride. The isophthalamide macrocycle **27** was obtained in 36% yield from the chloride-anion templated amide condensation reaction between **24** and isophthaloyl dichloride (Scheme 2.3.3).



Scheme 2.3.3: Synthesis of the isophthalamide macrocycle **27**.

Synthesis of the [2]catenane was accomplished using chloride anion templation *via* a ring-closing metathesis strategy. An initial interpenetrated assembly was prepared by mixing equimolar amounts of isophthalamide macrocycle **27** with **21**·Cl in dry dichloromethane (Scheme 2.3.4). Addition of Grubbs' II ring-closing metathesis catalyst afforded the [2]catenane **28**·Cl in 41% yield following purification by preparative thin layer chromatography.



Scheme 2.3.4: Synthetic route to prepare catenane **28**·PF_6 *via* clipping using Grubbs' II ring-closing metathesis catalyst.

Catenane **28**·Cl was characterised by ^{1}H, ^{13}C and 2D COSY NMR experiments and high-resolution mass spectrometry. Notable shifts in the pyridinium and isophthalamide protons *c* and *3*, respectively, were observed, in addition to the splitting and upfield perturbation of the hydroquinone protons *5* and *6* consistent with π–π donor–acceptor interactions between the electron-rich hydroquinone groups and the electron-deficient pyridinium group, which confirms the interlocked nature of the catenane (Figure 2.3.1). Further evidence for the interlocking of the two macrocyclic components was obtained by 2D ROESY NMR which revealed through-space interactions including those between hydroquinone and pyridinium protons of the two macrocycles (Figure 2.3.2).

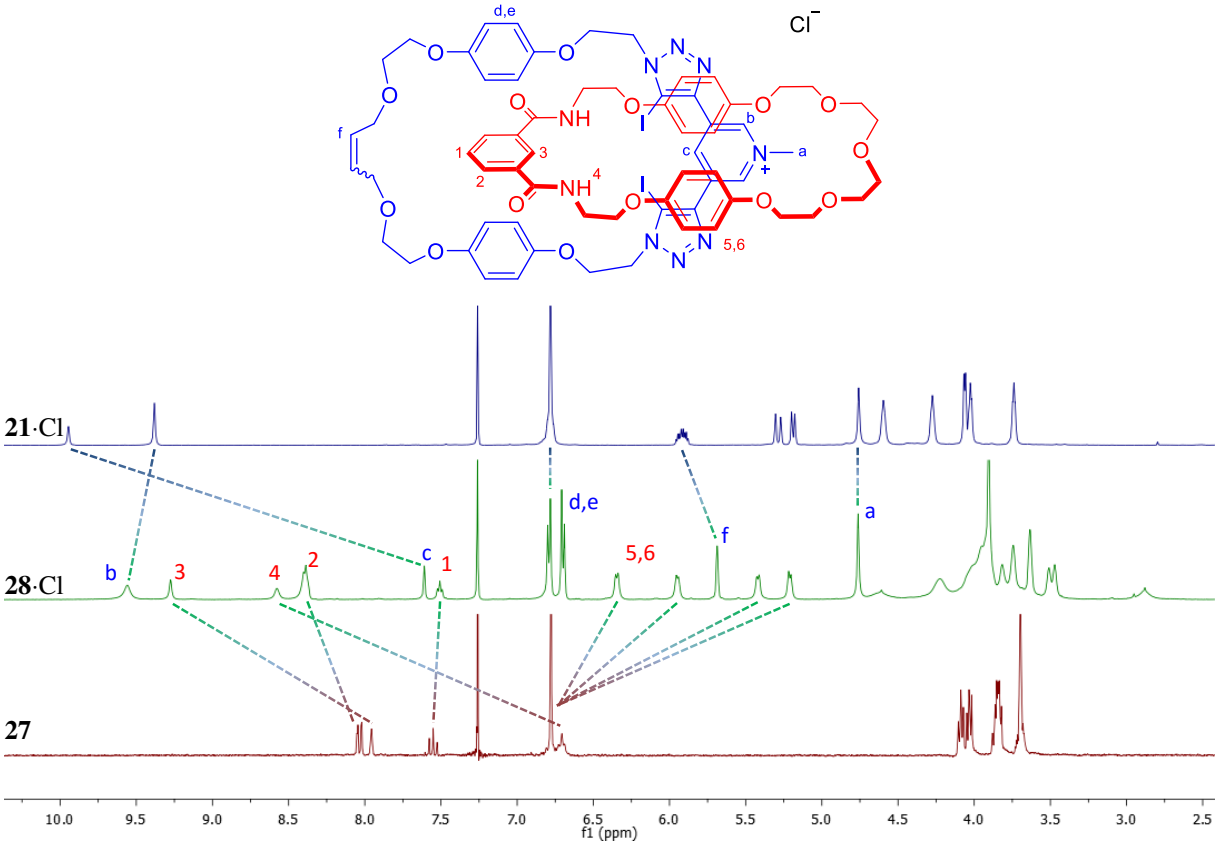


Figure 2.3.1: Comparison of truncated ^{1}H NMR spectra of catenane precursors **21** and **27** with catenane **28**·Cl indicating proton shifts due to catenane formation ($CDCl_3$, 500 MHz, 298 K).

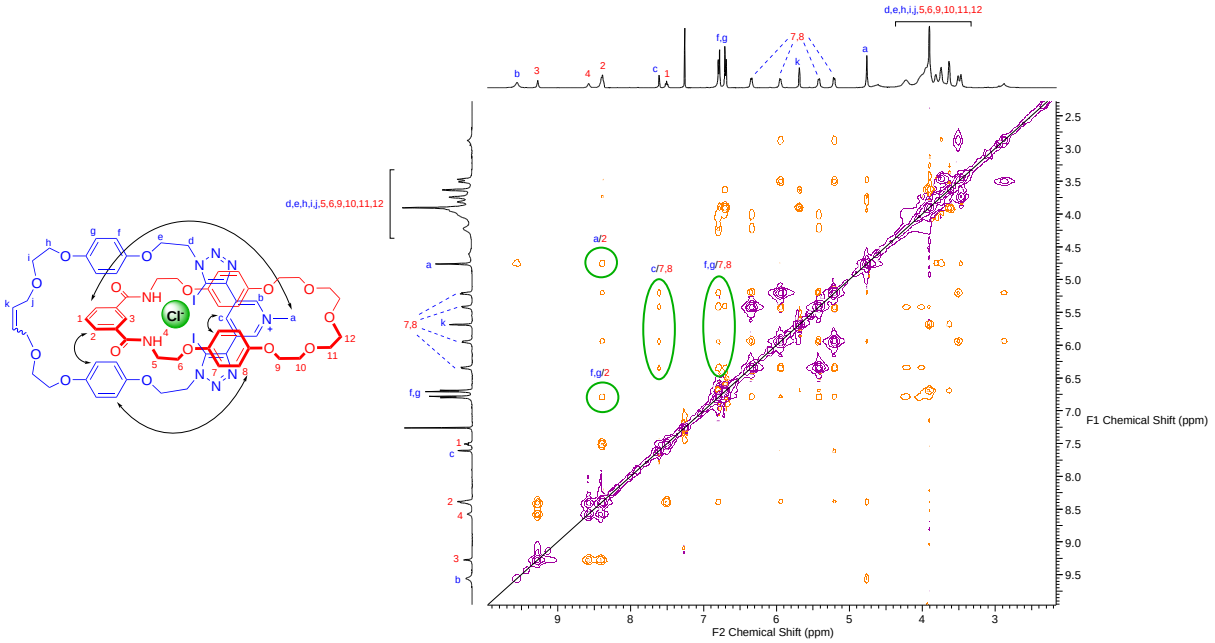


Figure 2.3.2: Truncated 2D ROESY NMR spectrum of **28**·Cl showing selected through-space ^{1}H–^{1}H correlations indicative of an interlocked assembly ($CDCl_3$, 500 MHz, 298 K).

The chloride anion template was removed by repeated washing with $NH_4PF_{6(aq.)}$ to afford **28**·PF_6 for anion recognition studies, and was similarly fully characterised (Scheme 2.3.4).

2.3.2 ^{1}H NMR anion binding studies

Association constants for the formation of 1:1 stoichiometric host–guest complexes of catenane **28**·PF_6 with various anions were determined using ^{1}H NMR titration experiments and approximations of Job plots. The shifts of the internal isophthalamide proton *3* were monitored upon addition of aliquots of anions added as their tetrabutylammonium salts. The internal pyridinium proton *c* could not be followed as shifts caused it to overlap with other resonances as anions were added. A preliminary titration of **28**·PF_6 with TBA·Cl in 1:1 $CDCl_3$:CD_3OD resulted in an association constant $K_a > 10^4$ M^{-1}, much greater than the value obtained for the previously reported analogous prototriazole-containing hydrogen-bonding catenane (Table 2.3.1).[430] Consequently, all subsequent titrations were conducted in the aqueous solvent mixture 45:45:10 $CDCl_3$:CD_3OD:D_2O, which is more competitive (Figure 2.3.3). The association constants shown in Table 2.3.1 were determined by WinEQNMR2[437] analysis of the titration data.

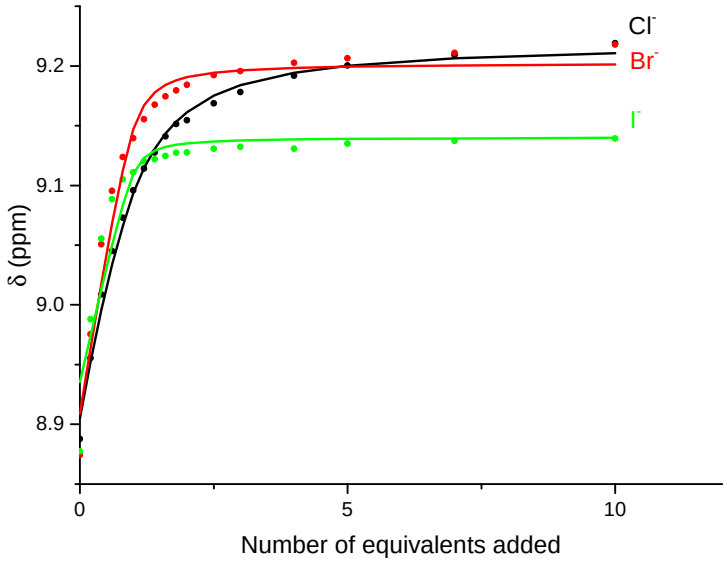
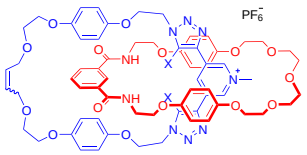


Figure 2.3.3: Anion binding titrations with **28**·PF_6 following isophthalamide proton *3* in the aqueous solvent mixture 45:45:10 $CDCl_3$:CD_3OD:D_2O: experimental titration data (circles) with WinEQNMR2[437] fitted binding isotherms indicated as lines (298 K).

Very strong binding of the halides is observed for **28**·PF_6 in this aqueous solvent mixture. Indeed, association constants determined for Br^- and I^- are both $> 10^4$ M^{-1} which highlights the fact that binding is dramatically enhanced in the halogen-bonding catenane when compared to the hydrogen-bonding catenane analogue. Whilst attempts were made to quantify anion association constants in aqueous solvent mixtures containing greater percentages of D_2O, insolubility did not allow for this. Furthermore, in contrast, the halogen-bonding host demonstrates a preference for the larger halides despite the voluminous iodine halogen-bond donors. Indeed, a reversal in selectivity for the halides is observed for **28**·PF_6 in comparison to the acyclic receptor **13**·PF_6 due the interlocked host's unique three-dimensional binding cavity.

Table 2.3.1: Association constants for **28**·PF_6 with various anions compared with the prototriazole analogue.

Anion	K_a (M^{-1})[a]	
	28$^+$: X = I (45:45:10 $CDCl_3$:CD_3OD:D_2O)	X = H (1:1 $CDCl_3$:CD_3OD)
Cl^-	1850(224)	679(20)
Br^-	$>10^4$	632(45)
I^-	$>10^4$	509(10)
OAc^-	NB[b]	–[c]
$H_2PO_4^-$	NB[b]	49(4)



[a] Anions added as TBA salts, estimated standard errors are given in parentheses. Association constants calculated using WINEQNMR2[437] (45:45:10 $CDCl_3$:CD_3OD:D_2O, 298 K). [b] Negligible δ (ppm) shifts were observed. [c] Anion not titrated.

Despite the OAc^- selectivity observed for the acyclic halogen-bonding receptor **13**·PF_6, no evidence for oxoanion binding was discerned for OAc^- or $H_2PO_4^-$ for the halogen-bonding catenane **28**·PF_6. This

may be attributed to the oxoanions' large size and unfavorable geometry towards binding and encapsulation by the unique interlocked catenane host cavity.

2.3.3 Crystal structures

Crystals suitable for X-ray diffraction structural analysis were obtained for catenane **28**$^+$ with chloride, bromide, iodide, dihydrogen phosphate, and sulfate counter-anions. Crystals were obtained by vapour diffusion of diisopropyl ether into solutions of **28**$^+$ and ten equivalents of TBA·anion in 45:45:10 $CDCl_3$:CD_3OD:D_2O. In all cases, crystals were small and despite the use of synchrotron radiation, diffraction was relatively weak and data were of relatively low quality. Despite this, the structure of the catenane and the location of the anion could be determined unambiguously for each of the anions. All structures crystallise in $P\bar{1}$ with 1:1 complexes obtained for chloride, bromide, and iodide, which are isomorphous, and 2:1 complexes were obtained for dihydrogen phosphate and sulfate, which in turn are isomorphous. In all cases, thermal motion of the polyether parts of the macrocycles was apparent. For some structures, it was possible to model this motion as positional disorder over two sites while in others, the quality of the data did not allow this. For all structures, it was necessary to apply restraints to bond lengths and angles, as well as thermal and vibrational ellipsoid parameters of the affected atoms to ensure a chemically sensible refinement.

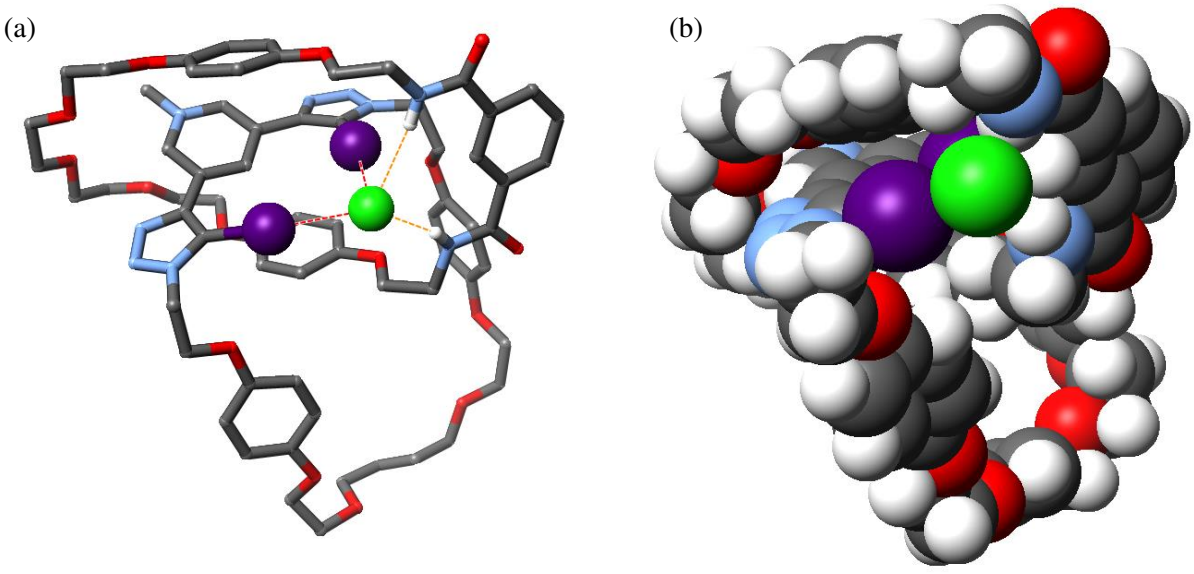


Figure 2.3.4: Crystal structure of **28**·Cl: (a) Perspective view of the receptor drawn as capped sticks and halides as spheres, showing Cl^- bound within the cavity which adopts an "open" conformation in the solid-state (hydrogen atoms (except amide) omitted for clarity), and (b) space-filling representation of the receptor showing the host–guest close contacts. Triazole–I···Cl^- halogen bonds (3.110(2)–3.300(3) Å) are indicated as red dashed lines and amide N–H···Cl^- hydrogen bonds are indicated as orange dashed lines.

While both hydrogen and halogen bonds are observed between the host **28**$^+$ and the anionic guest, the catenane curiously adopts an "open" conformation in the solid state rather than completely encapsulating the anion. Presumably this is due to the sterically-demanding iodo-substituted triazoles, which appear to force the catenane to adopt a reasonably strained geometry, and the most energetically favorable conformation for crystallisation. However, these crystal structures bear a striking resemblance to those of the previously reported protic analogue.[430] This is exemplified in the crystal structure of the chloride salt (Figure 2.3.4) which shows the spherical chloride anion coordinated within the cavity *via* two triazole–I···Cl$^-$ halogen bonds (3.110(2)–3.300(3) Å) and two amide N–H···Cl$^-$ hydrogen bonds (2.597(9)–2.631(11) Å). The space-filling model of **28**·Cl shows the very limited space within the anion binding cavity.

The remarkable structural similarity between the crystal structures of the halides is shown in Figure 2.3.5. In each of the structures, the anion binding site remains conserved, with slight adjustments in the cavity conformation observable in order to accommodate the larger Br$^-$ and I$^-$ anions. The same halogen- and hydrogen-bonding interactions, shorter than the sum of the van der Waals' radii, contribute towards the formation of the catenane–halide complex and their contact distances are summarised in Table 2.3.2.[439]

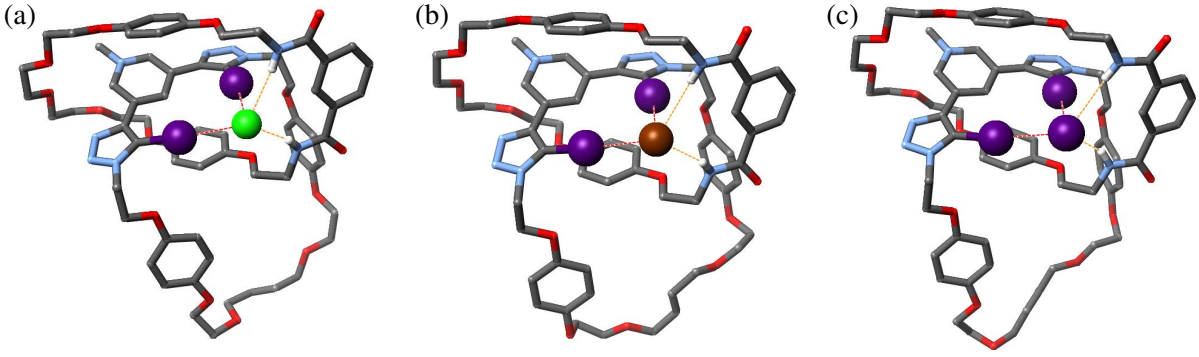


Figure 2.3.5: Crystal structures of **28**$^+$ with (a) chloride (b) bromide, and (c) iodide bound within the cavity, and showing the structural similarity between the host–halide complexes. Hydrogen atoms and the positional disorder in the bromide structure are omitted for clarity.

Table 2.3.2: Crystallographically determined halogen-bond lengths and percentage shortening of the sum of the van der Waals' radii (%VdW).[439]

Anion	Interatomic Distances (I···X$^-$)[a]	%VdW
Cl$^-$	3.110(2)–3.305(3)	83–88%
Br$^-$	3.178(2)–3.359(2)	83–88%
I$^-$	3.324(1)–3.543(1)	84–89%

[a] Calculated errors given in parentheses.

The structure of $\mathbf{28}_2 \cdot SO_4$ (Figure 2.3.6) clearly shows the SO_4^{2-} anion situated between two catenane hosts rather than being encapsulated within the cavity, as it is too large to penetrate the interlocked binding pocket. Furthermore, the anion is situated on the inversion center in the asymmetric unit allowing it to adopt one of two symmetry-related orientations. Two independent S–O···I–C halogen bonds are formed rather than bifurcated halogen bonds from one oxygen to each of the iodine halogen-bond donors. Additionally, amide N–H···O–S hydrogen bonds serve to stabilise the 2:1 catenane–anion complex.

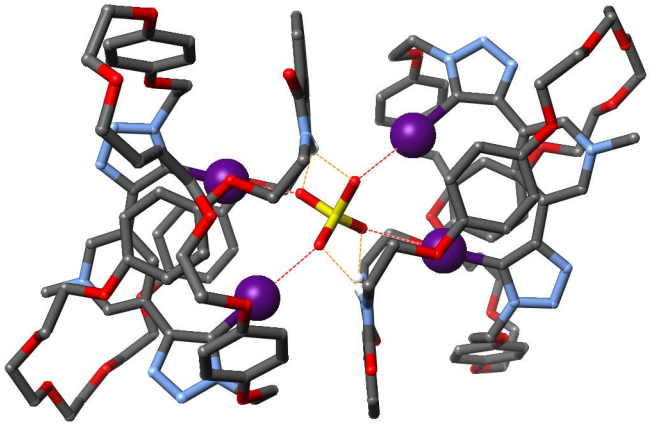


Figure 2.3.6: Crystal structure of $\mathbf{28}_2 \cdot SO_4$ showing the 2:1 catenane–anion complex with the anion (SO_4^{2-}) positioned between the two catenane hosts rather than penetrating the binding cavity. Halogen-bonding and hydrogen-bonding interactions are shown as red and orange dashed lines, respectively. Hydrogen atoms (except amide), and the SO_4^{2-} positional disorder on the inversion centre, are omitted for clarity.

Crystals of $\mathbf{28}{\cdot}H_2PO_4$ were particularly poorly diffracting, resulting in low quality data and challenging crystallography. The dihydrogen phosphate structure (Figure 2.3.7) is isomorphous with the sulfate structure: a 2:1 catenane–anion complex is formed in the solid-state with $H_2PO_4^-$ situated upon the inversion centre between two host molecules. This presents a puzzling situation as there does not appear to be space in the unit cell for a charge-balancing anion. Based on the similarity to the sulfate-containing structure, it appears that deprotonation to form HPO_4^{2-} has occurred, and that this HPO_4^{2-} bridges the two catenanes. Nonetheless, the possibility that this anion is, in fact, $H_2PO_4^-$ cannot be ruled out, with a charge balancing anion (e.g. PF_6^-) that cannot be identified due to the low quality of the data. Due to the weak diffraction data, and the difficulties associated with the anion's position (located on the centre of inversion), it is not possible to deduce the protonation state from the P–O bond lengths. The Fourier difference map did not present any observable peaks corresponding to hydrogen atoms, and there is no obvious chemically-sensible location for these atoms owing to the location of the anion on a special position. Consequently, no hydrogen atoms have been placed on this anion. Despite the difficulties experienced with this structure, the connectivity and general conformation of the binding cavity, and the position of the anion outside the catenane host's cavity, can be clearly determined.

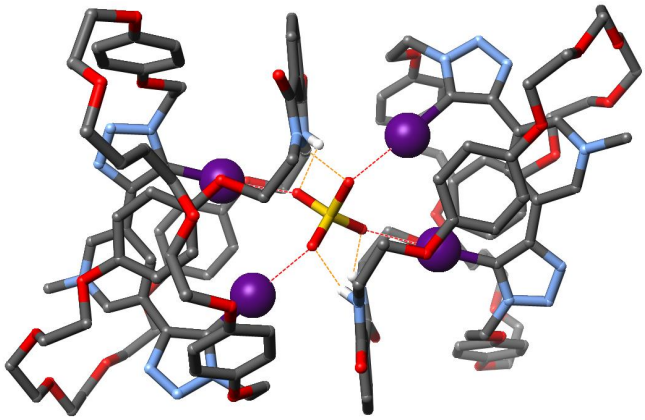


Figure 2.3.7: Crystal structure of **28**·H_2PO_4 showing the 2:1 catenane–anion complex with the anion ($H_2PO_4^-$) positioned between the two catenane hosts rather than penetrating the binding cavity. Halogen- and hydrogen-bonding interactions are shown as red and orange dashed lines, respectively. Hydrogen atoms (except amide), and the $H_2PO_4^-$ positional disorder on the inversion centre, are omitted for clarity.

2.3.4 X-ray absorption spectroscopy (XAS)

In collaboration with Prof. Pierre Kennepohl and his group at the University of British Columbia, Canada, Cl and Br K-edge X-ray Absorption Spectroscopic (XAS) techniques were exploited to establish the nature of the interactions between the halide (Cl^-/Br^-) donor (halogen-bond acceptor) and the iodine acceptor (halogen-bond donor). XAS is a spectroscopic technique capable of probing the coordination sphere of a suitable X-ray absorber *via* the excitation of a core electron into an unoccupied valence orbital by using high-energy synchrotron X-ray radiation of tunable wavelength. These transitions are termed an "edge" as the spectra display a sharp increase in absorption upon excitation. The type of core electron excited is related to the principal quantum numbers, n = 1, 2 and 3, and correspond to the K-, L- and M-edges, respectively. XAS spectra are generally divided into three main regions:

1. The 'absorption' threshold consisting of pre-edge features and determined by the electronic transition to the lowest unoccupied states

2. The X-ray Absorption Near Edge Structure (XANES), also termed the Near Edge X-ray Absorption Fine Structure (NEXAFS), consisting of the 'rising edge' and the beginning of the fine oscillations that correspond to the constructive and destructive interference between the outgoing photoelectron wave and backscattered wave. These photoelectrons experience strong multiple scattering by the first and even higher coordinating shells of the X-ray absorber.

3. The Extended X-ray Absorption Fine Structure (EXAFS) which also represents the scattering of the electron to its neighbouring atoms; however, these possess much greater kinetic energy and undergo single scattering by the nearest neighbours to the X-ray absorber.

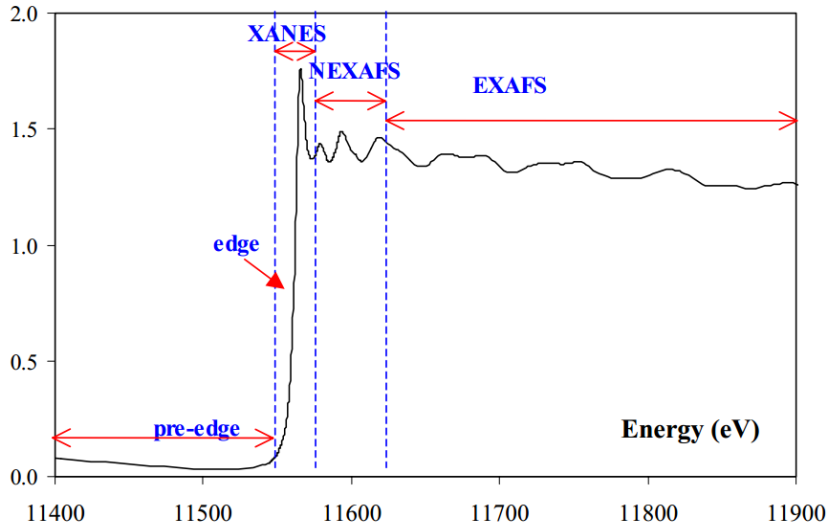


Figure 2.3.8: A simple generic X-ray absorption spectrum showing the various regions that can be used to extract data.[440]

A free halide anion would exhibit a simple XAS spectrum such as in Figure 2.3.8 owing to its closed-shell electronic configuration, however pre-edge features may arise when the halide (X) is bound to a metal, for example, due to the excitation of a X_{1s} electron to empty valence *d*-orbitals on the transition metal acceptor (Figure 2.3.9). It has been clearly established that Cl K-edge XAS can be used to evaluate the degree of delocalisation in chloro–metal bonds.[441–443] In such cases, a pre-edge feature is observed in the spectrum that formally corresponds to excitation of a Cl_{1s} electron to empty valence *d*-orbitals on the transition metal acceptor. The intensity of such transitions is directly proportional to the amount of Cl_{3p} character mixed into these empty metal acceptor orbitals, providing a convenient method of obtaining a quantitative measure of the degree of mixing between the chloro-donor and the metal acceptor. This methodology is equally applicable in cases where non-metal acceptors are under investigation, although to our knowledge it has not been applied for other types of donor–acceptor systems. XAS studies involving halogen bonding are unprecedented in the literature as it is most often studied using single-crystal X-ray diffraction, UV-Vis spectroscopy or IR spectroscopic methods.

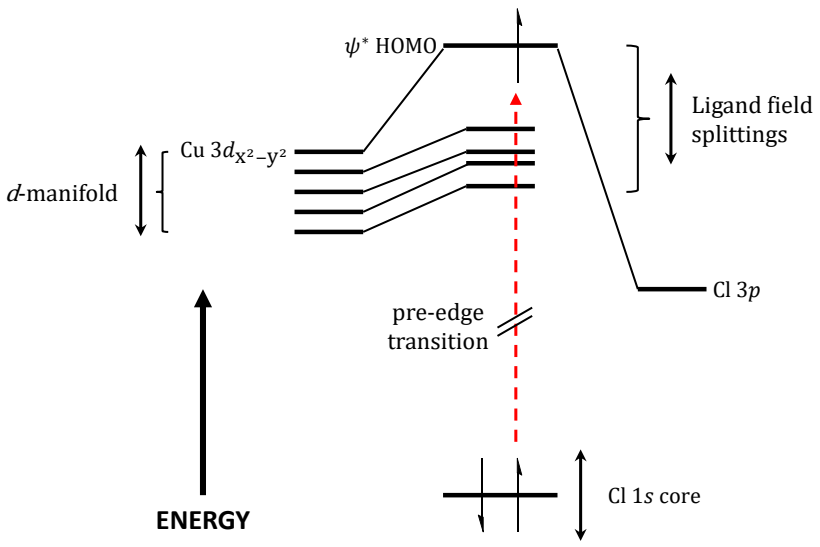


Figure 2.3.9: Schematic molecular orbital diagram of the contributions to the pre-edge transition energy. The pre-edge energy is dependent on shifts both in the Cl_{1s} core energy and in the energy of the highest occupied molecular orbital (HOMO) of the complex. The HOMO energy is determined by overall shifts in the *d*-manifold which correlate to coordination number and charge on the metal as well as the specific repulsive interaction of the HOMO determined by the ligand field of the complex.[442]

Within the context of this work, one would expect a free halide ion (Cl^- and/or Br^-) to exhibit simple K-edge XANES spectra with no pre-edge features owing to their closed-shell electron configuration. Electric-dipole allowed $Cl_{3p} \leftarrow Cl_{1s}$ (or $Br_{4p} \leftarrow Br_{1s}$) transitions would not be observed since these valence *p*-states are filled (ns^2np^6). Covalent delocalisation of the filled Cl_{3p} orbital with an empty acceptor orbital (e.g., *via* hydrogen or halogen bonding) would result in the possibility of a new allowed transition corresponding to charge transfer from the chloride to its bonding partner ($\sigma^*_{AX\leftarrow Cl} \leftarrow Cl_{1s}$). Given that the intensity of such transitions is directly proportional to the amount of Cl_{3p} in the final state wavefunction, $\sigma^*_{AX\leftarrow Cl^-}$, the intensity of any observable pre-edge feature provides a direct measure of the degree of covalency in the halogen bond.

2.3.4.1 Synthesis

The following systematic series of halogen-bonding receptors were synthesised as their Cl^-, Br^- and PF_6^- salts, for study by XAS (Figure 2.3.10).

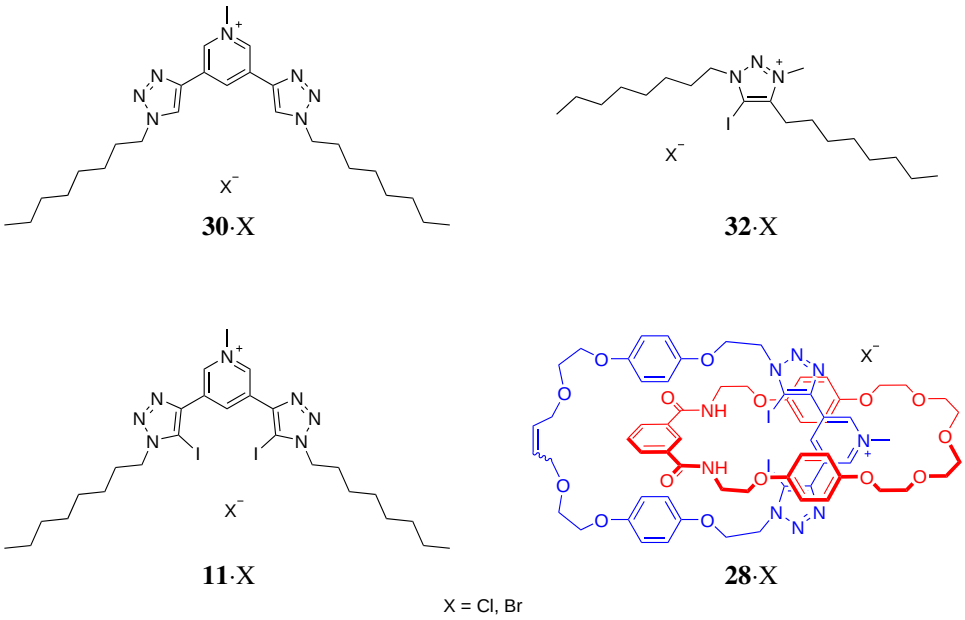
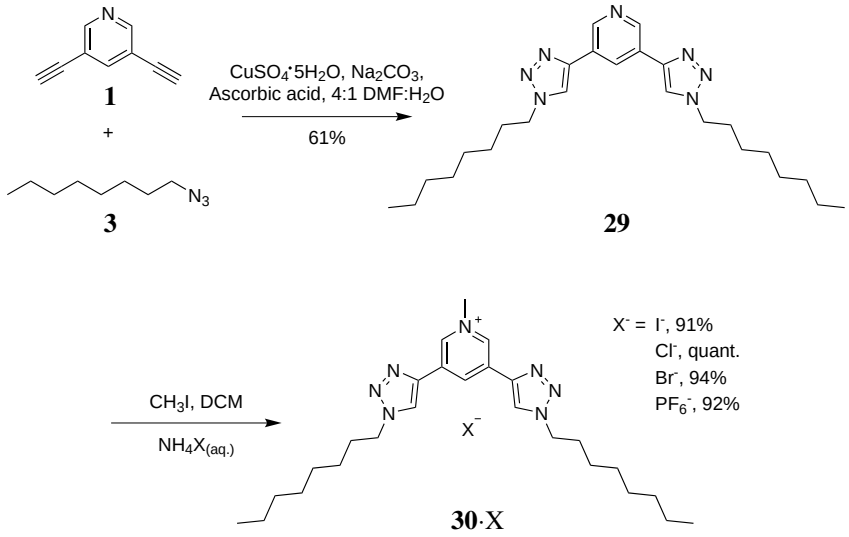


Figure 2.3.10: Systematic series: Molecular structures of the four samples synthesised for study by XAS.

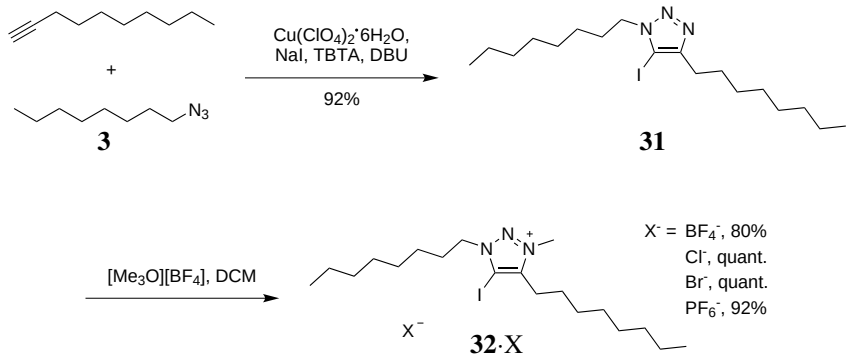
The hydrogen-bonding 3,5-bis-triazole pyridinium receptor **30**·X, was synthesised by the CuAAC click reaction between diethynylpyridine **1** and 2.2 equivalents of octylazide **3** in 4:1 DMF:H_2O, affording the bis-triazole precursor **29** in 61% yield after purification (Scheme 2.3.5). Subsequent methylation by CH_3I in dry dichloromethane gave the iodide salt of the hydrogen-bonding receptor **30**·I (91%), which was then anion exchanged to the chloride, bromide and hexafluorophosphate salts for analysis.



Scheme 2.3.5: Synthesis of **30**·X: CuAAC click reaction to form 3,5-bis-triazole pyridine precursor **30**, followed by methylation and anion exchange to afford the 3,5-bis-triazole pyridinium receptor samples.

The mono-iodotriazolium receptor **32**·X was prepared *via* the one-pot click reaction between octylazide **3** and commercially available 1-decyne, affording the bis-octyl-appended iodotriazole precursor **31** (Scheme 2.3.6). Methylation of the iodotriazole-*N* required a stronger methylating agent: $[Me_3O][BF_4]$

(a derivative of Meerwein's salt) was employed in dry dichloromethane to afford the tetrafluoroborate salt of the mono-iodotriazolium receptor **32**·BF_4 (80%), which was then anion exchanged to the chloride, bromide and hexafluorophosphate salts for analysis.



Scheme 2.3.6: Synthesis of **32**·X: one-pot CuAAC iodo-click reaction to form the bis-octyl-appended iodotriazole precursor **31**, followed by methylation and anion exchange to afford the bis-octyl-appended iodotriazolium receptor samples.

2.3.4.2 XAS spectra

Chlorine K-edge XAS data were obtained for a series of donor–acceptor complexes at beamline 4-3 at the Stanford Synchrotron Radiation Lightsource. The near-edge spectra for **11**·Cl and **28**·Cl (Figure 2.3.11) each exhibit an intense pre-edge feature that is not present in ionic chloride salts. The presence of this intense feature can only result from charge transfer between the chloro-donor and its partners.[441,443] Fitting of the pre-edge and edge features allows experimental quantification of the degree of charge donation in each of these species (Table 2.3.3).[444–446] These results clearly demonstrate charge transfer from the donor *via* halogen bonding in **11**·Cl, and a combination of halogen- and hydrogen-bonding interactions in **28**·Cl. For comparison, data were also collected on the hydrogen-bonding analogue of **11**·Cl (**30**·Cl) as well as a simple halogen-bonded adduct 5-iodo-3-methyl-1,4-dioctyl-1*H*-1,2,3-triazol-3-ium chloride (**32**·Cl) (Figure 2.3.11a). These data provide a measure of the total donation from the chloride anion to all of its bonding partners, and thus the number of interactions must be considered when interpreting these results.

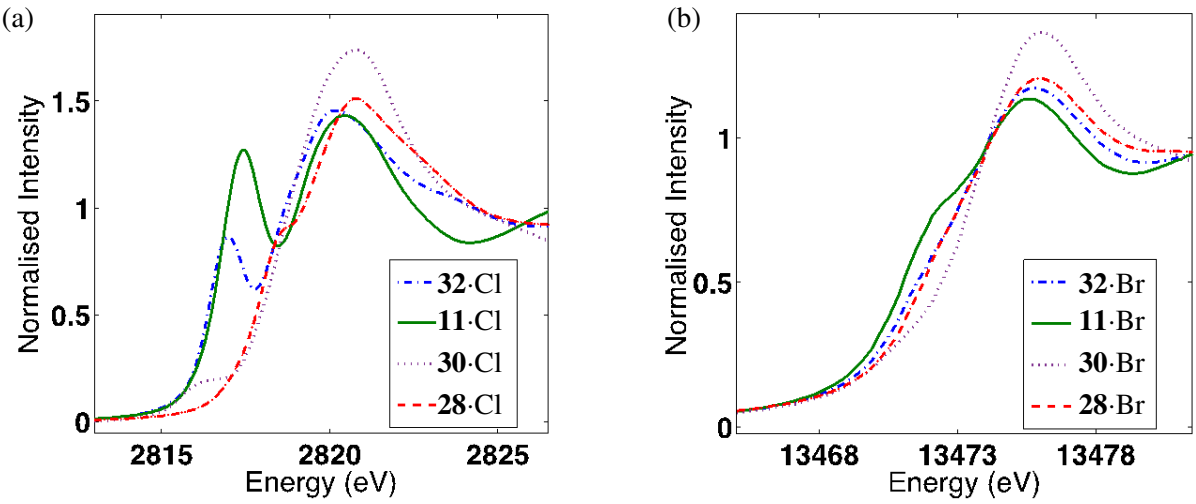


Figure 2.3.11: Normalised and background subtracted: (a) Cl K- and (b) Br K-edge XAS data for **32**·Cl, **11**·Cl, **30**·Cl and **28**·Cl.

Table 2.3.3: Experimentally obtained pre-edge intensities and the corresponding % charge donation of chloride donor complexes.

Compound	Interactions		Pre-edge	Normalised Pre-edge	Total Donation
	$Cl^-\cdots I$	$Cl^-\cdots H$	Energy (eV)	Intensity[a]	(% Cl_{3p})[b]
32·Cl	1	-	2816.9(1)	0.90(5)	6.4(2.1)
11·Cl	2	-	2817.3(1)	1.59(4)	11.3(2.0)
30·Cl	-	2	2816.2(2)	0.13(3)	0.9(1.9)
28·Cl	2	2	2818.4(2)	1.00(6)	7.1(2.3)

[a]Calculated errors (parenthesis) are obtained from statistical distribution of fit results for >50 fits for each data set. [b]Total donation is calculated in comparison with Cl K-edge XAS data on a $CuCl_4^{2-}$ reference, errors include an estimate of the error in charge transfer of this reference compound.

It is apparent that, with a chloride donor, halogen-bonding interactions are significantly more covalent in character than comparable hydrogen-bonding interactions. These data are consistent with previous reports that charge transfer is an important factor in halogen bonds.[447] These XAS data, however, allow us to quantify the degree of covalency in the halogen bond and thus compare the degree of charge transfer in different systems, which to our knowledge is unprecedented. In **32**·Cl, where only a single halogen bonding interaction is possible, the degree of donation is consistent with $\sim$ 6% charge transfer to the iodinated triazole acceptor. The magnitude of charge donation/covalent character in the halogen bond is notable in that it is of a similar magnitude to that which is commonly observed in transition metal complexes, where covalent contributions are considered to be of great importance in defining chemical properties. For example, in simple divalent metal chlorides ($[MCl_4]^{2-}$, where M = Cu, Ni, Co, Fe), bond covalencies have been determined to range from 6% to 9%.[441]

In the bis-triazole **11**·Cl, the total charge donation from the halide ion almost doubles to $\sim$ 11%, which implies that each of the halogen bonds are independent from each other and additive. By contrast,

replacement of the iodine acceptors for protons in the bis-triazole (**30**·Cl) leads to an almost complete loss of intensity in the Cl K-edge XAS pre-edge feature, reflecting very poor charge donation through hydrogen bonding in this system.

Data for the catenane **28**·Cl, where both hydrogen and halogen bonds are present, indicate that charge donation from the chloride anion decreases substantially (as compared to **11**·Cl). This presumably reflects weakened halogen bonding due to competition with amide hydrogen-bonding interactions.

Qualitatively similar data were obtained for the bromide donor complexes **32**·Br, **11**·Br, **30**·Br, and **28**·Br (Figure 2.3.11b). Unfortunately, lifetime broadening at the higher energy Br K-edge, as well as smaller energy separation between features, leads to poorer resolution of the pre-edge features of interest. The data indicate the presence of a low-energy shoulder, indicating a pre-edge feature similar to that observed in the Cl K-edge data. Notably, the pre-edge shoulder is larger for the halogen-bonded systems as compared to the hydrogen-bonded system (**30**·Br). However, quantitative comparisons between the different halogen-bonded systems are inconclusive owing to large errors in the associated fits.

2.3.4.3 Computational results

To further explore the details of the covalent nature of halogen bonding in these systems, a series of density functional calculations, and TDDFT simulations of the XAS data were performed.[448] Optimised geometries (Table 2.3.4) are in good agreement with experimental data. For example, the r_{Cl-I} in **11**·Cl are calculated to be 3.18(3) Å, which compare favorably with that observed crystallographically (3.120(2)–3.195(2) Å). TDDFT simulations of the Cl K- and Br K-edge XAS data reproduce the low energy pre-edge feature assigned to the $\sigma^*_{AX\leftarrow X^-} \leftarrow X_{1s}$ transition in each case. The relevant $\sigma^*_{AX\leftarrow X^-}$ orbitals for **32**·Cl and **11**·Cl are shown in Figure 2.3.12. In each case, these antibonding acceptor orbitals reflect the covalent nature of the $X^-\rightarrow$I bond(s). Two relevant acceptor orbitals are present in **11**·Cl since two $X^-\rightarrow$I interactions are possible; the splitting of these two orbitals in **11**·Cl is small ($\sim$ 0.3 eV), and thus the resulting transitions cannot be resolved experimentally.

Table 2.3.4: DFT-calculated parameters obtained for halide adducts. All calculated values are for fully optimised structures at the B3LYP/def2-TZVP+ZORA level of theory.

	Average Bond Distances (Å)		Total $\%Cl_{3p}$	$10^3 * f_{osc}$ for
	$X^-\cdots I$	$X^-\cdots H$	in $\sigma^*_{AX\leftarrow X^-}$	$\sigma^*_{AX\leftarrow X^-} \leftarrow X_{1s}$
32·Cl	3.00	–	6.9	1.292
11·Cl	3.18	–	7.7	1.862
30·Cl	–	2.54	1.1	0.215
28·Cl	3.21	2.62	6.1	–
32·Br	3.21	–	6.4	0.198
11·Br	3.40	–	8.0	0.286
30·Br	–	2.76	1.7	0.045
28·Br	3.41	2.82	5.6	–

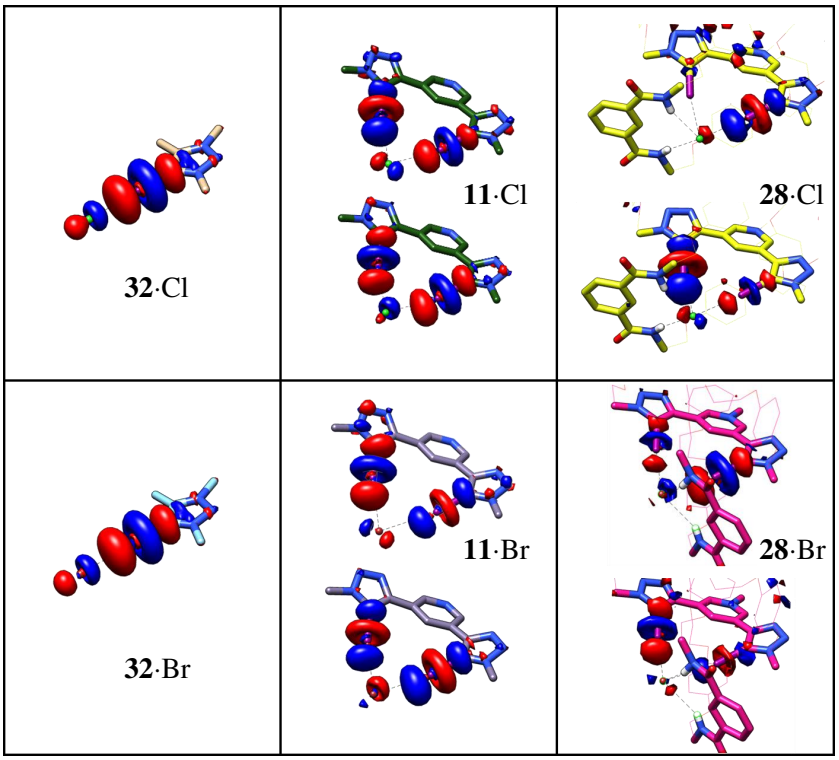


Figure 2.3.12: Visual representation of the important $\sigma^*_{AX\leftarrow X^-}$ Kohn-Sham acceptor orbitals for **32**$^+$, **11**$^+$ and **28**$^+$. Surface volumes for each orbital are plotted for $\pm$ 0.05 e/Å^3.

TDDFT-based simulations of the Cl K- and Br K-edge XAS data are in good qualitative agreement with the experimental data (Figure 2.3.13). As anticipated, the intensities of the $\sigma^*_{AX\leftarrow X^-} \leftarrow X_{1s}$ pre-edge transitions correlate with the degree of charge transfer from the halide to the acceptor. The trends observed in the TDDFT-calculated intensities of the transitions are in reasonable agreement with those observed in the experimental data. However, the calculated pre-edge intensities (and calculated halogen-bond charge donation) are in good agreement with those obtained from the Cl K-edge XAS data. Trends observed in pre-edge transition energies are also reproduced in the DFT results. A small shift to higher energy ($\sim$ 0.4 eV) on going from a single halogen bond donor (**32**·Cl) to two donors (in **11**·Cl) is con-

sistent with a similar shift observed in the experimental data (see Table 2.3.3). This shift correlates with decreased electron density on the chloride, which leads to stabilisation of the Cl_{1s} donor orbital.

The bromide adducts show similar trends as those observed in the chlorides; the TDDFT simulations are also in reasonable agreement with the Br K-edge experimental data. The calculated degree of charge donation is very similar between the two halides, suggesting that the degree of covalent mixing is similar in both cases.

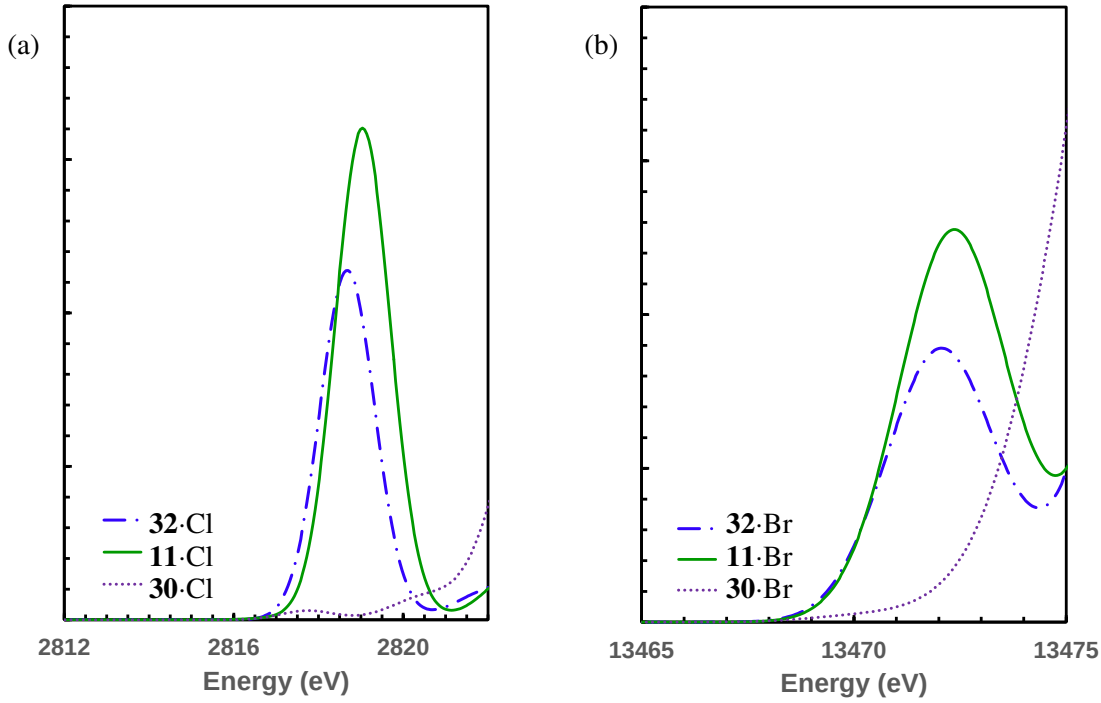


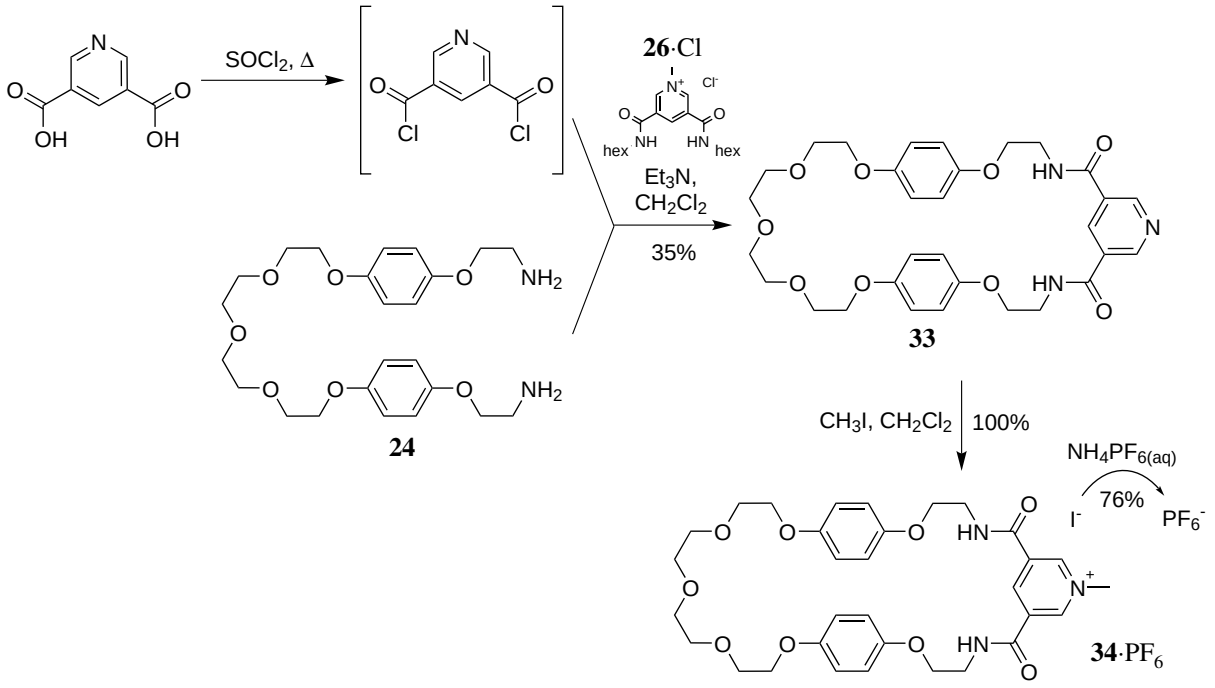
Figure 2.3.13: TDDFT simulated (a) Cl K-edge and (b) Br K-edge XAS spectra for selected halogen-bonding adducts. A constant linear shift [449] was applied to the calculated energies to better match experimental K-edge energies.

2.4 A dicationic [2]catenane

Since the monocationic [2]catenane **28**·PF_6 precipitated in titration experiments involving solvent mixtures with a water content greater than 10%, it was envisaged that a dicationic [2]catenane incorporating the same 3,5-bis-iodotriazole pyridinium and bis-amide motifs would be capable of anion binding in aqueous mixtures containing a higher percentage of water due to the greater charge of the catenane host. This work was undertaken by Ju Won Cha, a final year undergraduate Part II student, under my supervision.

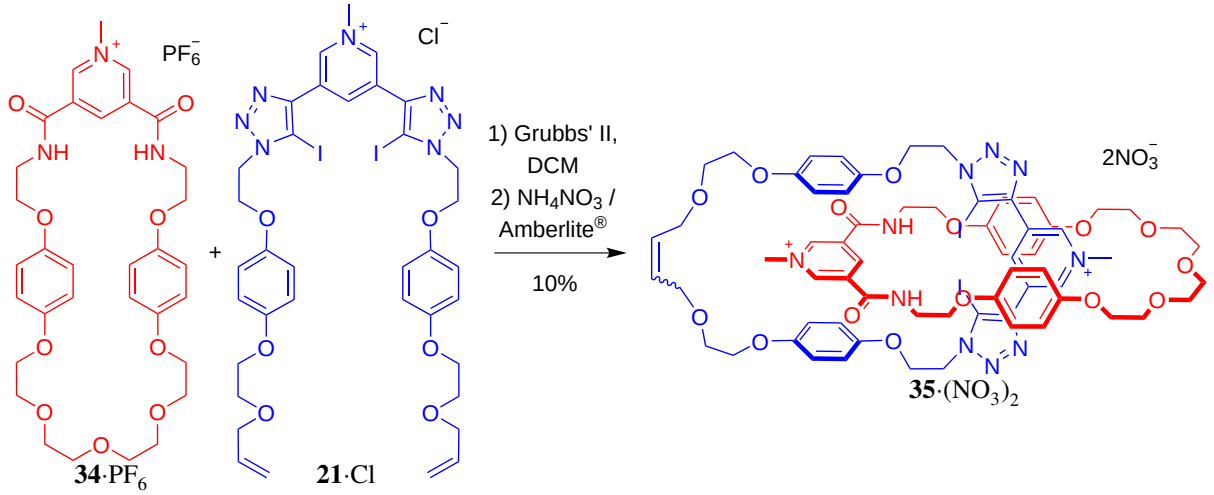
2.4.1 Synthesis

The incorporation of the additional charge into the [2]catenane host structural framework was envisaged through the use of a bis-amide-pyridinium macrocycle **34**·PF_6. Synthesis of the bis-amide-pyridine macrocycle **33** was undertaken *via* the well-established hexyl-appended pyridinium bis-amide chloride anion templation methodology[438] from the amide condensation reaction of pyridine 3,5-diacid chloride with bis-amine **24** in 35% yield (Scheme 2.4.1). Subsequent methylation and anion exchange to the PF_6^- salt afforded **34**·PF_6 in 76% over two steps.



Scheme 2.4.1: Synthetic scheme to prepare monocationic pyridinium bis-acid macrocycle **34**·PF_6 for use in catenane formation.

Synthesis of the target dicationic [2]catenane was accomplished using an analogous procedure to producing **28**·PF_6; chloride templation *via* a ring-closing metathesis strategy. An initial interpenetrated assembly was prepared by mixing a 1:1 stoichiometric ratio of **21**·Cl and **34**·PF_6 in dry dichloromethane. A portion of Grubbs' II catalyst (10 wt%) was added and the reaction was stirred for 7 days under N_2 (Scheme 2.4.2). Catenane **35**·2 X was isolated by preparative thin layer chromatography (silica, 14:2:1 $CH_3OH/CH_2Cl_2/KNO_{3(aq.)}$) and anion exchanged to the NO_3^- salt to afford **35**·$(NO_3)_2$ in 10% overall yield. The increased charge of this [2]catenane resulted in challenging purification and the diminished isolated yield.



Scheme 2.4.2: Synthetic scheme to prepare dicationic catenane **35**·$(NO_3)_2$ *via* a clipping method using Grubbs' II ring-closing metathesis catalyst.

Characterisation by ^{1}H and ^{13}C NMR spectroscopy, and high resolution ESI mass spectrometry confirmed the formation of catenane **35**·$(NO_3)_2$—specifically, a large upfield shift and splitting of the hydroquinone protons of the bis-amide macrocycle is observed in the ^{1}H NMR spectrum, indicative of aromatic donor–acceptor interactions upon formation of an interpenetrated assembly. Additionally, a downfield shift of the bis-amide pyridinium proton, *3*, is observed (Figure 2.4.1).

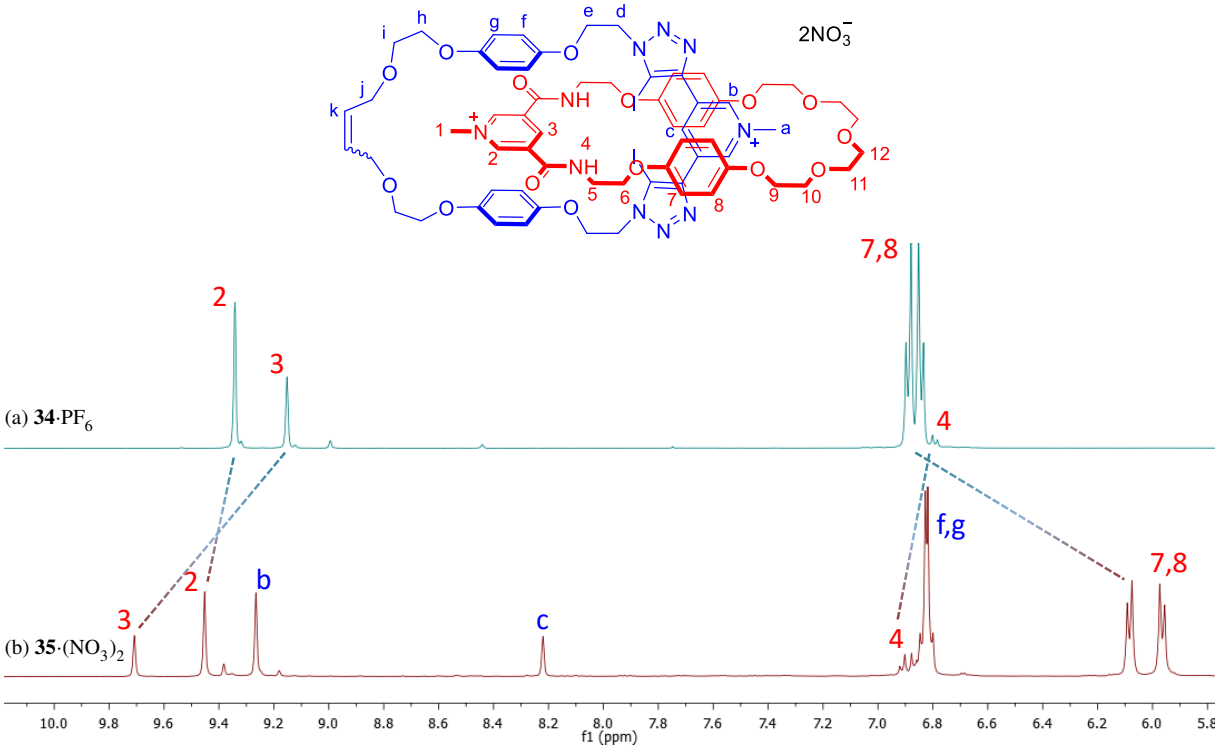


Figure 2.4.1: Truncated ^{1}H NMR spectra of a) bis-amide pyridinium macrocycle **34**·PF_6, and b) dicationic [2]catenane **35**·$(NO_3)_2$ in 1:1 D_2O:CD_3OD (500 MHz, 298 K).

The ^{1}H–^{1}H ROESY NMR spectrum provided further evidence for the formation of an interlocked assembly due to the presence of significant 'through-space' cross-coupling interactions between the mechanically bonded macrocyclic components of the catenane. Noteworthy correlations arise between the pyridinium protons of each macrocycle and the hydroquinone protons of the contiguous macrocycle (Figure 2.4.2).

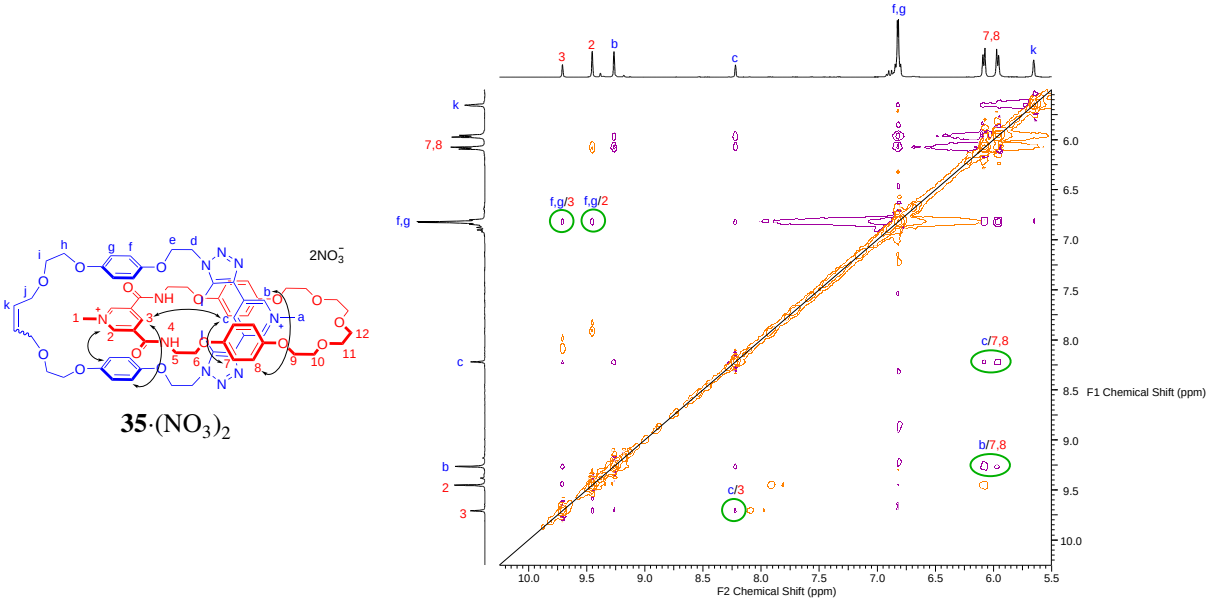


Figure 2.4.2: Truncated 2D ROESY NMR spectrum for the dicationic catenane **35**·$(NO_3)_2$ in 1:1 D_2O:CD_3OD (500 MHz, 298 K).

2.4.2 ^{1}H NMR anion binding studies

The anion recognition properties of **35**·$(NO_3)_2$ were investigated using ^{1}H NMR titrations; aliquots of anions as their sodium salts were added to a solution of the catenane in 1:1 D_2O:CD_3OD. An initial titration with chloride revealed a significant upfield perturbation of the bis-iodotriazole pyridinium proton, *c*, as well as a downfield perturbation of the bis-amide pyridinium proton, *3*. Unsurprisingly, negligible shifts are observed for pyridinium protons *b* and *2* as these are directed away from the binding cavity and thus do not participate in anion coordination (Figure 2.4.3).

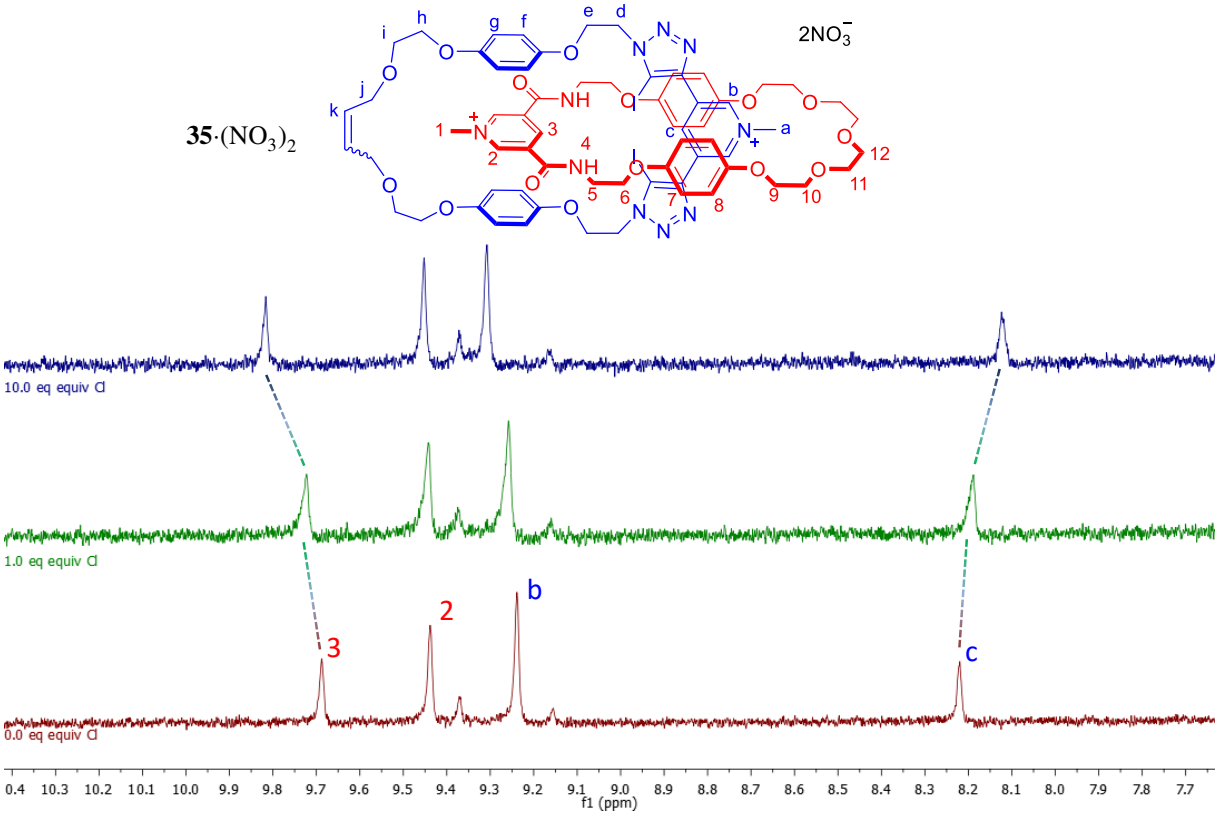


Figure 2.4.3: Truncated ^{1}H NMR spectra for the titration of catenane **35**·$(NO_3)_2$ with NaCl in 1:1 D_2O:CD_3OD (500 MHz, 298 K) showing spectra for 0.0, 1.0 and 10.0 equivalents of anion, with dotted lines indicating notable shifts.

Monitoring the shifts in the bis-iodotriazole pyridinium proton, *c*, as a function of anion concentration (Figure 2.4.4) and a combination of WinEQNMR2[437] and approximate Job plot analysis of the data determined 1:1 stoichiometric association constants, K_a, for Cl^-, Br^-, I^- and SO_4^{2-} (Table 2.4.1). Whilst halides are bound strongly in this competitive solvent mixture containing 50% water, minimal selectivity is observed between the halides. It is possible that the increased charge, combined with some flexibility in the three-dimensional binding cavity, could account for a loss in selectivity between the spherical halide guest species. Furthermore, the increased electrostatic contribution to binding appears to dominate over the soft iodo-halogen-bond donor–soft iodide interaction, and competes with the higher enthalpy of solvation of chloride to result in stronger binding for chloride, and bromide, than expected. Nonetheless, modest selectivity is observed for the halides over the dianionic sulfate anion which is bound more weakly. This is due to the fact that sulfate is too large to penetrate the catenane host's binding cavity, and moreover, the tetrahedral geometry of sulfate is not complementary with the shape of the cavity. Additionally, the higher solvation enthalpy for sulfate contributes towards the weaker binding of this anion.

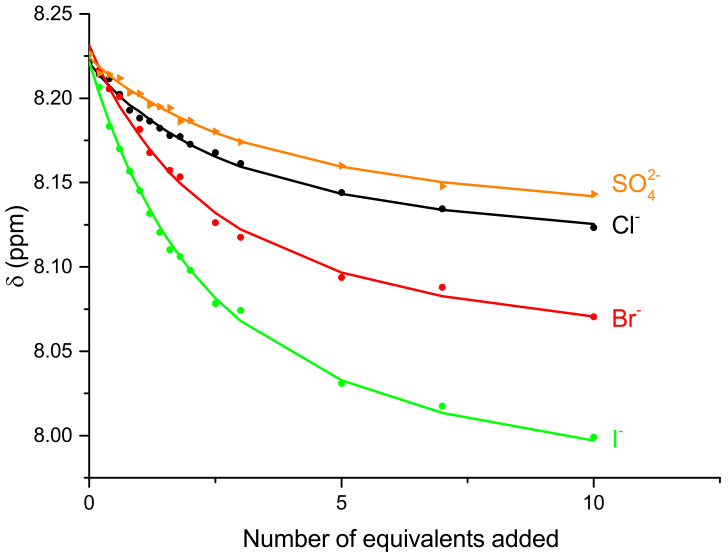


Figure 2.4.4: Chemical shifts (ppm) of bis-iodotriazole pyridinium proton *c* on addition of Cl^-, Br^-, I^- and SO_4^{2-} as sodium salts to a solution of **35**·$(NO_3)_2$ in 1:1 D_2O:CD_3OD (500 MHz, 298 K). Solid symbols represent experimental data points; continuous lines represent theoretical binding isotherms.

Table 2.4.1: Association constants for **35**·$(NO_3)_2$ with various anions in 1:1 D_2O:CD_3OD (500 MHz, 298 K).

Anion[a]	K_a (M^{-1})[b]
Cl^-	205(6)
Br^-	254(34)
I^-	263(8)
SO_4^{2-}	156(23)

[a] Anions added as sodium salts, estimated standard errors are given in parentheses. [b] Association constants calculated using WINEQNMR2[437] monitoring the upfield shift of bis-iodotriazole pyridinium proton *c*.

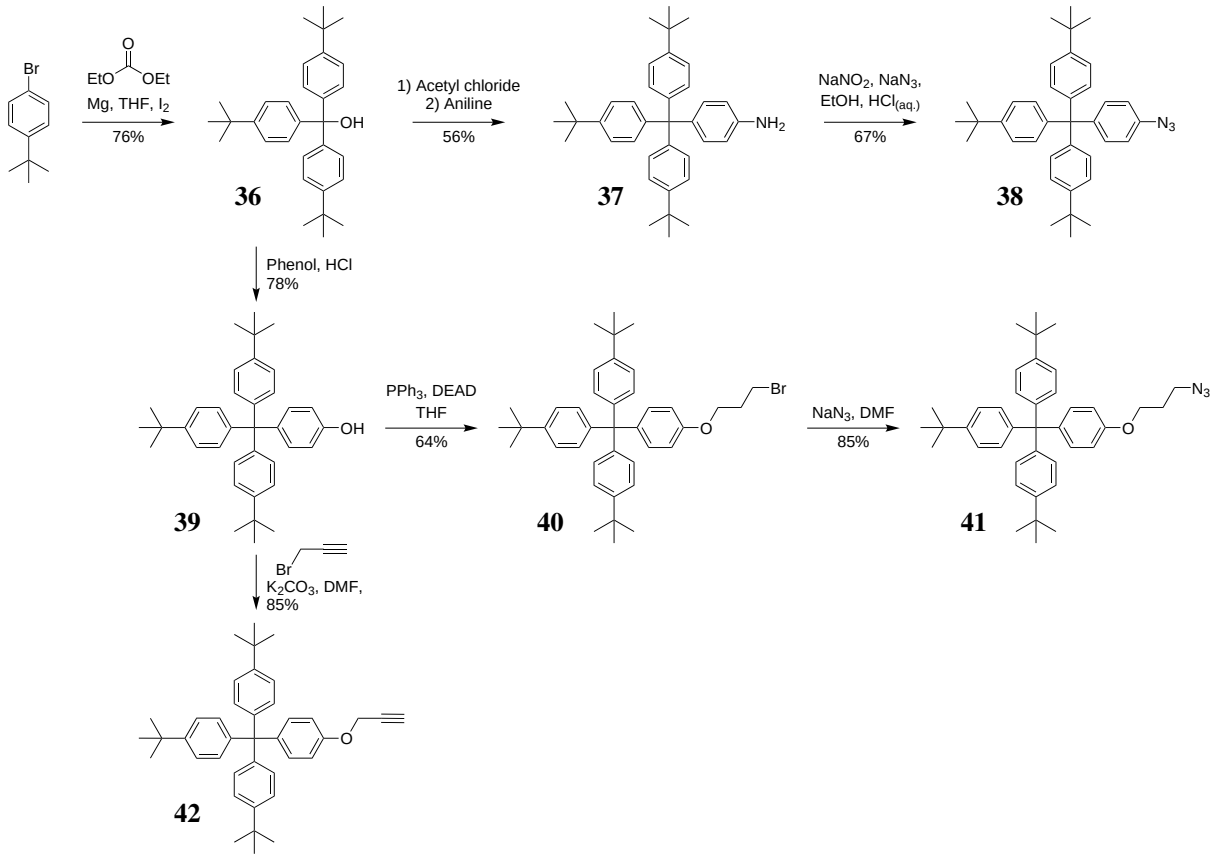
2.5 Integration of the 3,5-bis-iodotriazole pyridinium motif into further higher-order architectures

Following the success of preparing [2]catenane derivatives containing the 3,5-bis-iodotriazole pyridinium group, attempts to incorporate this potent anion binding motif into a variety of structures were investigated, including axle and macrocycle components, as well as interlocked all-halogen-bonding [2]catenanes and [2]rotaxanes.

2.5.1 Synthesis of an axle

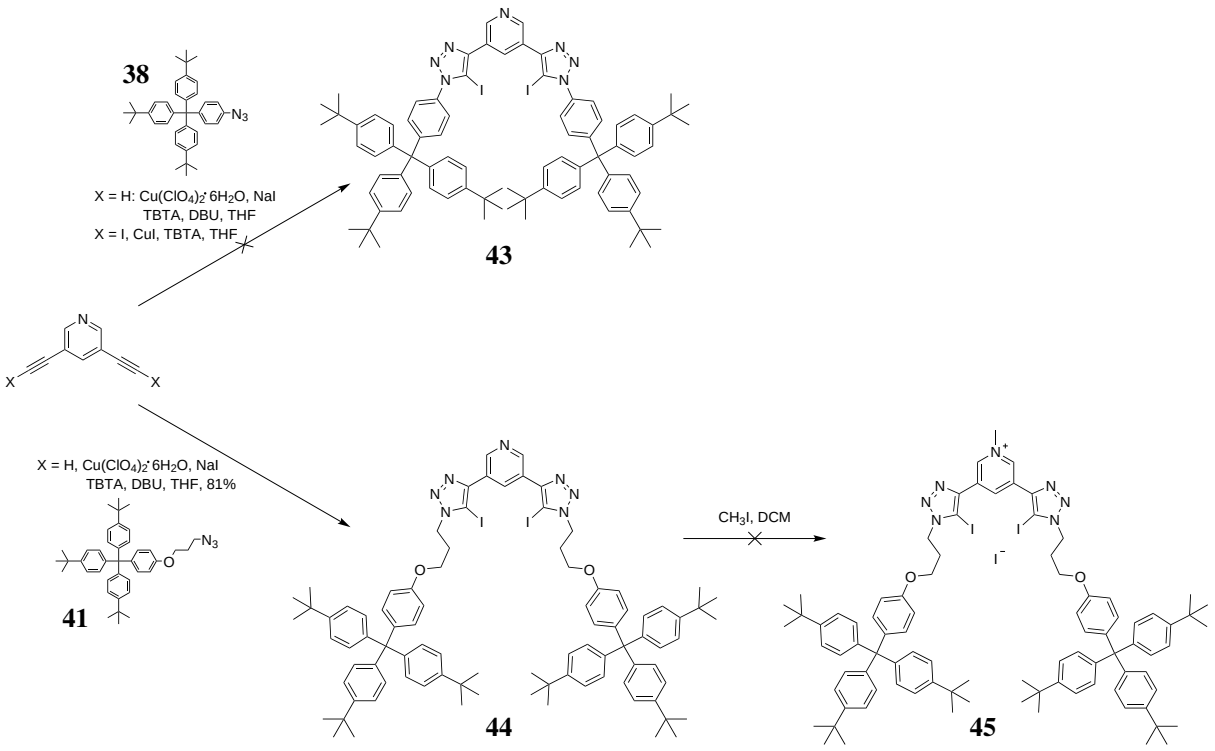
The synthesis of two axle components began with the preparation of suitable stopper-azide synthons which could be appended to diethynylpyridine **1** *via* previously employed CuAAC click reaction methods. The trityl alcohol **36** was prepared by Grignard reaction of *tert*-butyl-bromobenzene and diethylcarbonate in 76% yield (Scheme 2.5.1).[450] For the aryl-azide stopper **38**, the trityl alcohol **36** was reacted

with aniline to form the aniline-stopper **37**, and thereafter the amine was substituted for an azide *via* a Sandmeyer-type reaction: diazotisation of the amine, followed by azide substitution, affording **38** in 67% yield. For the propyl-azide stopper **41**, the trityl alcohol **36** was substituted with phenol *via* an S_N1 reaction to form the stopper-aryl-alcohol **39** in 78% yield. Mitsunobu reaction between 3-bromo-propan-1-ol and **39** afforded the stopper-bromide **40**, and thereafter the propyl-azide stopper **41** was obtained after substitution with NaN_3 in 85% yield. A stopper bearing an alkyne group was also prepared by appending propargyl bromide to terphenyl alcohol **39** in 85% yield (Scheme 2.5.1).



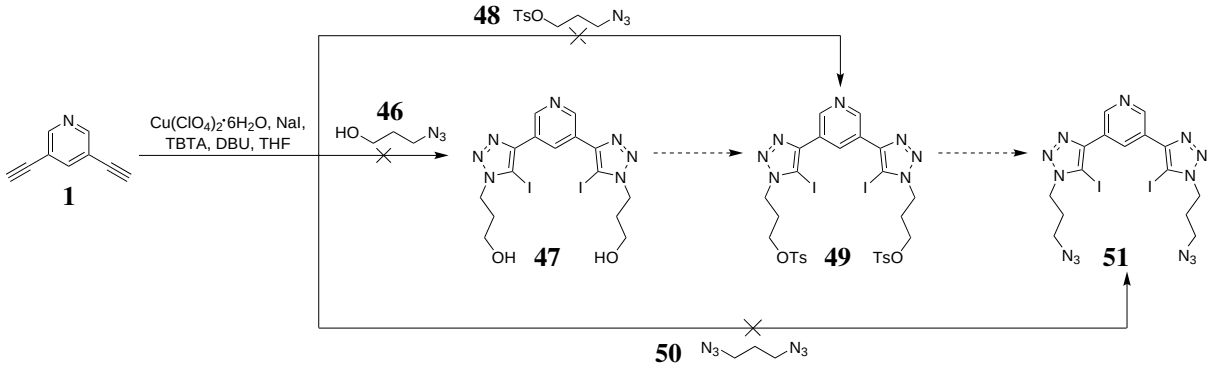
Scheme 2.5.1: Synthesis of the aryl-azide stopper **38**, the propyl-azide stopper **41** and the alkynyl stopper **42**.

The synthesis of two axle components was attempted: both the one- and two-pot methods were unsuccessful in the preparation of **43** *via* the reaction between stopper-aryl-azide **38** and either diethynylpyridine **1** or di-iodoethynyl pyridine **2** (Scheme 2.5.2). However, the one-pot click reaction between diethynylpyridine **1** and stopper-propyl-azide **41** successfully afforded the axle precursor **44** in 81%. Methylation of **44** was undertaken with CH_3I to obtain the 3,5-bis-iodotriazole pyridinium axle **45**·I. However, despite mass spectrometric evidence, the axle component **45**·I could not be isolated using chromatographic techniques due to degradation during purification. Consequently, the target axle components were not obtained and other routes towards analogous axles were investigated.



Scheme 2.5.2: Attempted synthesis of axle components bearing the 3,5-bis-iodotriazole pyridinium motif.

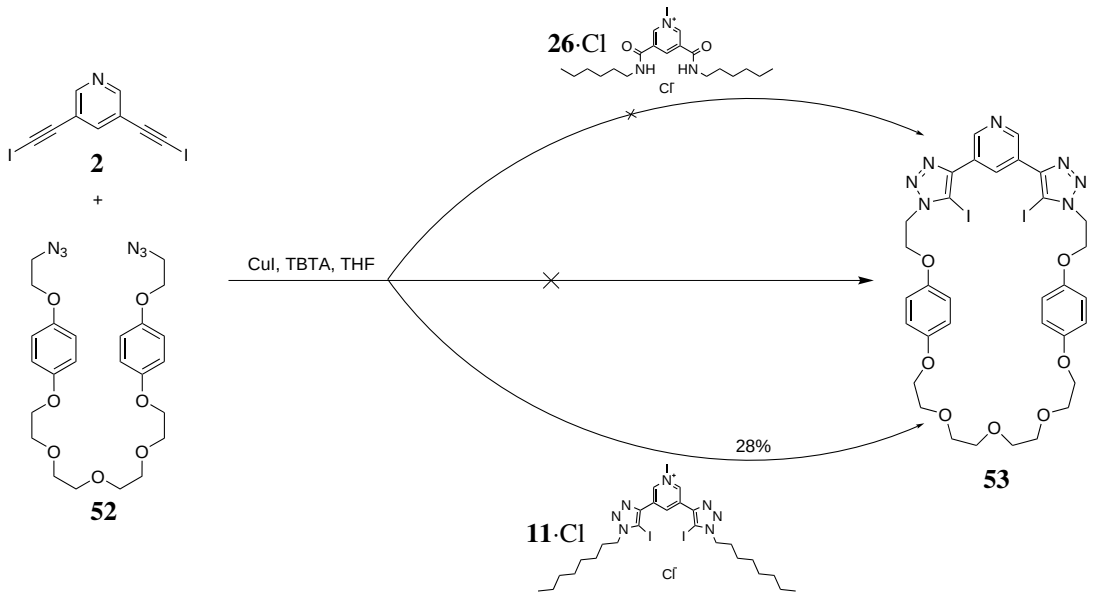
The synthesis of an alternative axle component was investigated using the stopper-alkyne **42**, which required the synthesis of a bis-azide-appended bis-iodotriazole pyridine precursor **51** *via* the route shown in Scheme 2.5.3. The initial approach to the synthesis of this synthon was the one-pot click reaction between diethynylpyridine **1** and azido-propanol **46** to form the bis-hydroxy-appended bis-iodotriazole pyridine **47**, however, this was unsuccessful. Consequently, routes towards intermediates were investigated: the one-pot click reaction between azidopropyl tosylate **48** (prepared by the tosylation of **46**) and diethynylpyridine **1** to form the bis-tosylate-appended precursor **49** afforded a mixture of mono- and di-iodo-substituted impurities. As a final alternative, diazidopropane **50** was prepared by the substitution of commercial dibromopropane with NaN_3, and reacted with diethynylpyridine **1** under one-pot click conditions but did not afford the desired bis-azide **51**.



Scheme 2.5.3: Attempted synthesis of the bis-azide-appended 3,5-bis-iodotriazole pyridine synthon **51**.

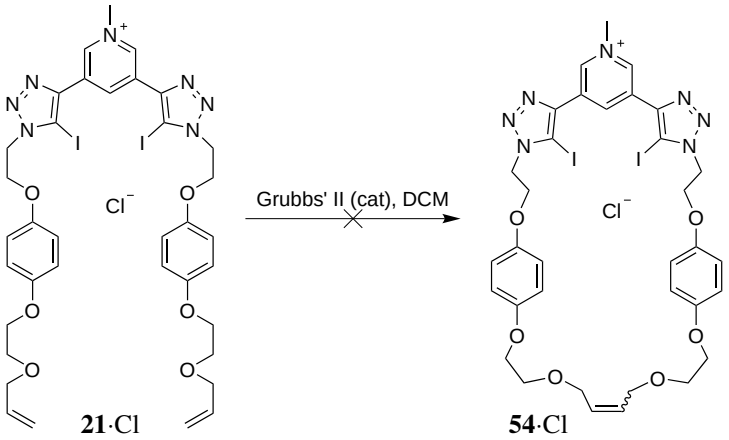
2.5.2 Synthesis of a macrocycle

The 3,5-bis-iodotriazole pyridine motif was incorporated into a 5-*O*-polyether macrocycle *via* a double CuAAC click methodology between di-iodoethynyl pyridine **2** and the bis-azide macrocycle precursor **52** (prepared *via* azide substitution of the bis-amine **24**) as shown in Scheme 2.5.4. In the absence of a templating species, negligible formation of the macrocycle was observed; rather a mono-clicked 'intermediate' was obtained. Similarly, no macrocycle was formed when the bis-amide pyridinium chloride template **26**·Cl was used. However, in the case when the octyl-appended bis-iodotriazole pyridinium chloride **11**·Cl was used as a templating species, the halogen-bonding macrocycle **53** was obtained in 28% yield. Attempts at optimising the reaction revealed that the yield could not be further improved.



Scheme 2.5.4: Synthesis of the halogen-bonding macrocycle **53**.

The synthesis of a macrocycle from the vinyl-appended macrocycle precursor **21**·Cl was also investigated using Grubbs' II ring-closing metathesis catalyst (Scheme 2.5.5). However, only a small portion of the macrocycle **54** formed which unfortunately could not be isolated.

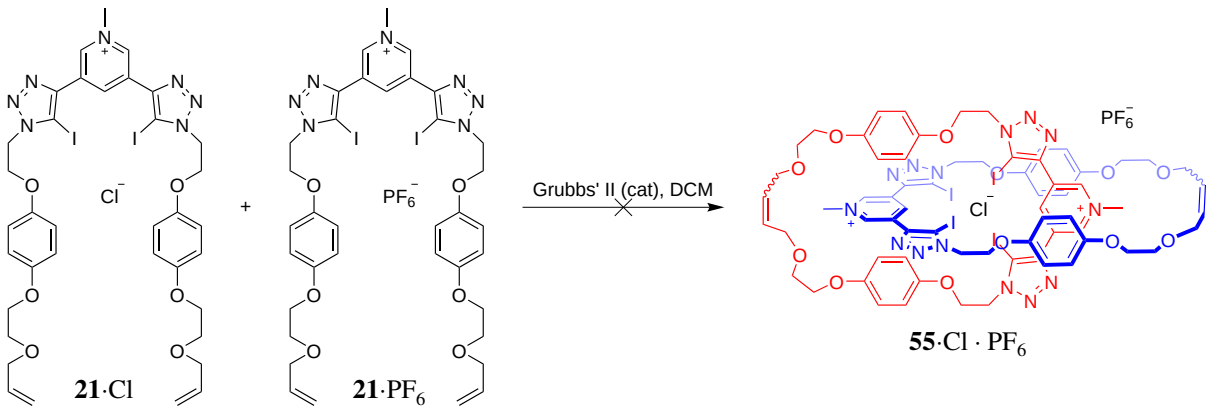


21·Cl **54**·Cl

Scheme 2.5.5: Attempted synthesis of a macrocycle from the Grubbs' II ring-closing metathesis reaction with vinyl-appended macrocycle precursor **21**·Cl.

2.5.3 Attempted synthesis of all-halogen-bonding [2]catenanes

Attempts were made at preparing an all-halogen-bonding [2]catenane *via* a double cyclisation methodology using Grubbs' II ring-closing metathesis catalyst with the vinyl-appended macrocycle precursors **21**·Cl and **21**·PF_6 (Scheme 2.5.6). The difficulty with this method is that the target [2]catenane **55**·Cl weighs precisely double that of the ring-closed macrocycle **54**·Cl but is dicationic, resulting in identical mass spectrometric m/z values; the only difference being the isotope splitting pattern in the spectrum. However, whilst a negligible quantity of macrocycle **54**·X was isolated, no evidence for the formation of the desired homocatenane was observed in the mass spectra or by other techniques. Optimisation of the reaction showed the same result in each case, and it is assumed that the 3,5-bis-iodotriazole pyridinium motif is incapable of forming an orthogonal complex with a templating chloride anion.

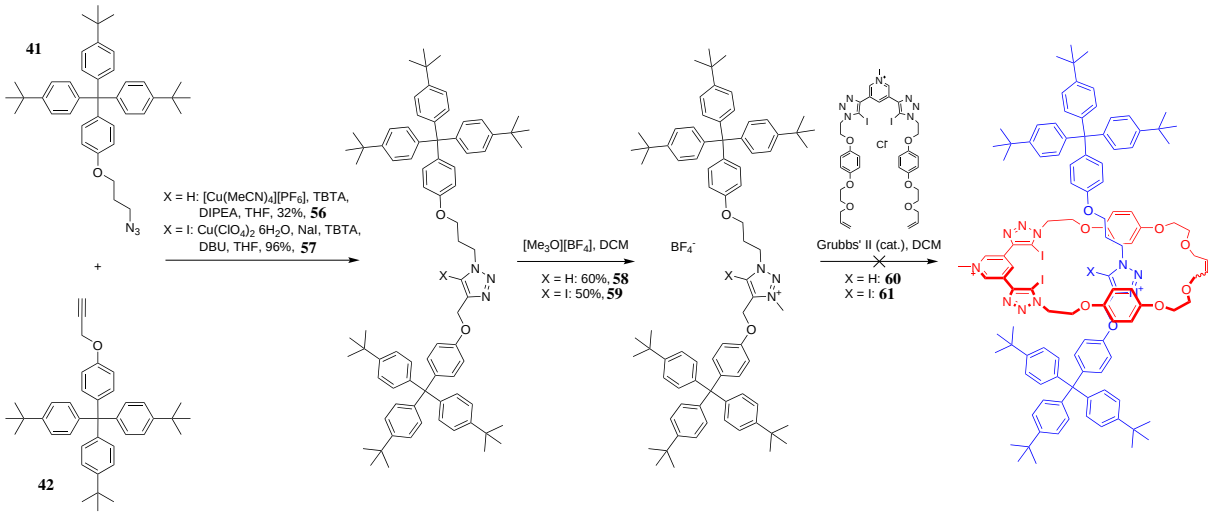


21·Cl **21**·PF_6 **55**·Cl · PF_6

Scheme 2.5.6: Attempted synthesis of a homocatenane of vinyl-appended bis-iodotriazole pyridinium macrocycle precursor *via* chloride-templated double cyclisation methodology.

2.5.4 Attempted synthesis of all-halogen-bonding [2]rotaxanes

Following the discovery that the formation of all-halogen-bonding interlocked structures comprising orthogonally oriented 3,5-bis-iodotriazole pyridinium members was not possible, the design was simplified to the use of triazolium-bearing axles such as those previously employed (see Chapter 1, Figure 1.5.14). Both the proto- and iodo-triazolium axles were prepared *via* initial CuAAC click reactions between stopper-alkyne **42** and stopper-propyl-azide **41** to afford the proto- and iodo-triazole axle precursors **56** (96%) and **57** (32%), respectively (Scheme 2.5.7). The triazoles were methylated using $[Me_3O][BF_4]$ in DCM to afford the proto- and iodotriazole axles **58**·BF_4 (60%) and **59**·BF_4 (50%), respectively. Attempts to prepare the corresponding [2]rotaxanes was undertaken *via* Grubbs' II ring-closing metathesis clipping of the vinyl-appended bis-iodotriazole pyridinium chloride macrocycle precursor **21**·Cl around each of the axles, however, no evidence for the formation of the proto- or all-halogen-bonding iodo-triazolium [2]rotaxanes **60**·Cl · BF_4 or **61**·Cl · BF_4, respectively, was obtained. The formation of a small quantity of the ring-closed macrocycle product **54**·X was detected by mass spectrometry.



Scheme 2.5.7: Attempted synthesis of [2]rotaxane hosts comprised of a proto- or iodo-triazolium axle with a macrocyclic component containing the 3,5-bis-iodotriazole pyridinium motif.

2.6 Water-soluble rotaxanes

Due to the potent anion binding properties of the 3,5-bis-iodotriazole pyridinium motif in competitive solvent mixtures, and motivated by the goal of recognising anions in pure water, the possibility of preparing a water-soluble axle incorporating the halogen-bonding motif was investigated.

2.6.1 Towards water-soluble receptors

Despite many examples of anion receptors which are capable of anion recognition in organic or organic–aqueous solvent mixtures, there are relatively few reports of anion host systems which function in pure water.[76] However, most of these receptors are highly charged in order to compete with the hydration energy of the anions. Moreover, they tend to be pH-sensitive and only operate within a restricted pH range, subject to multiple protonation equilibria. Nonetheless, there remains the need to selectively recognise, sense and sequester anions of biological and environmental importance in aqueous media as outlined in Section 1.2.1.

In this thesis, β-cyclodextrin has been investigated as a means to solubilise the 3,5-bis-iodotriazole pyridinium motif in pure water. Advantageously, these organic synthons are synthetically accessible, can be functionalised with a range of moieties, and they are sufficiently large to prevent de-threading in rotaxane host systems.

Cyclodextrins (CD) are cyclic oligosaccharides produced *via* the enzyme-catalysed degradation of starch by CD transglycosylase obtained from the bacterium *Bacillus macerans*, and most commonly consisting of 6,7 or 8 glucose units: termed α-, β- and γ-cyclodextrin, respectively (Figure 2.6.1). CDs are shaped as truncated cones with a wide and a narrow rim comprised of secondary and primary alcohols, respectively, and a tapered, hydrophobic central cavity capable of including aliphatic and aromatic guest species.[451,452] The inclusion chemistry of CDs has been extensively studied, with that of β-cyclodextrin arguably the most exploited due to the optimum size of its cavity for complexation of a wide range of guest species.

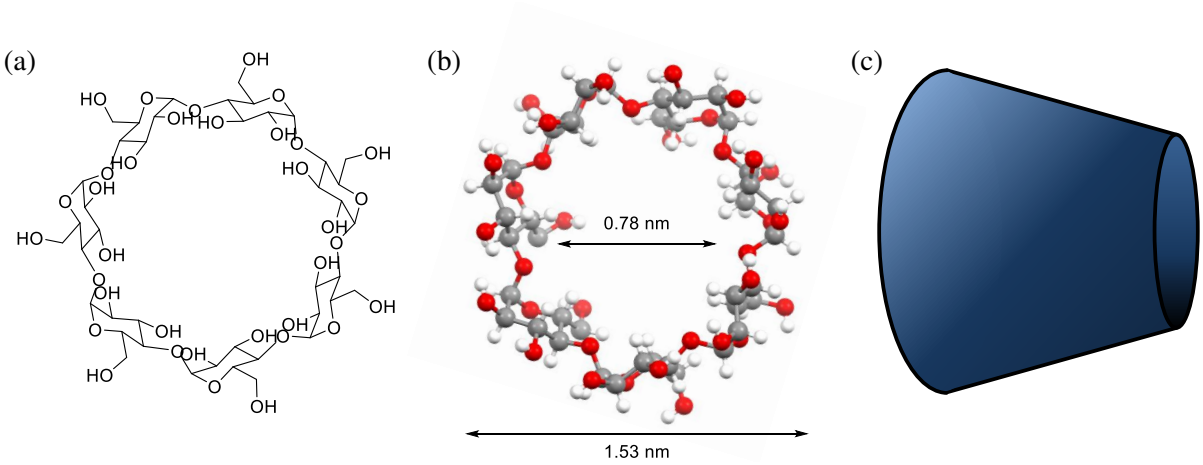


Figure 2.6.1: Figure showing a) β-cyclodextrin, b) the crystal structure of β-cyclodextrin[453] with cavity dimensions[454], and c) cartoon representation of the truncated-cone shape of β-cyclodextrin.

The three most common forms of cyclodextrin are all water soluble to some degree, however, the β-form is significantly less soluble than the α- or γ-forms: 18.5 g/L in comparison to 145 and 232 g/L, respectively.[455] Fortuitously, the aqueous solubility of β-CD can be improved upon substitution of the hydrogen-bonding hydroxyl groups by alkylation to form hydrophobic methoxy moieties: $\sim$ 50 g/L for permethylated β-CD (pCD). Furthermore, permethylation confers solubility in a wide range of polar organic solvents such as $CHCl_3$, CH_2Cl_2, THF, EtOAc, DMF and DMSO, facilitating synthetic manipulation.

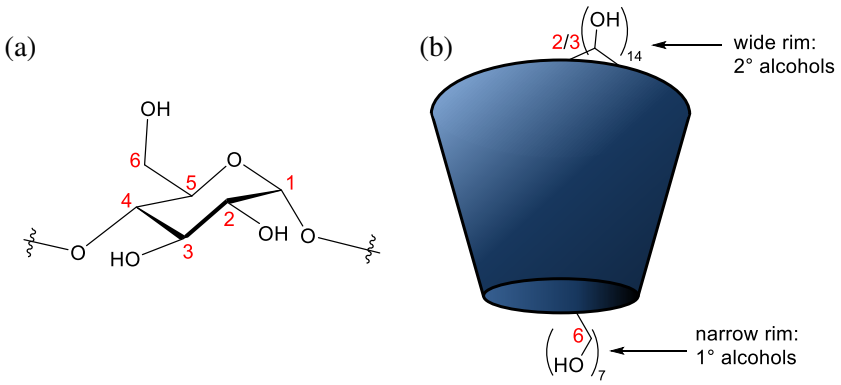
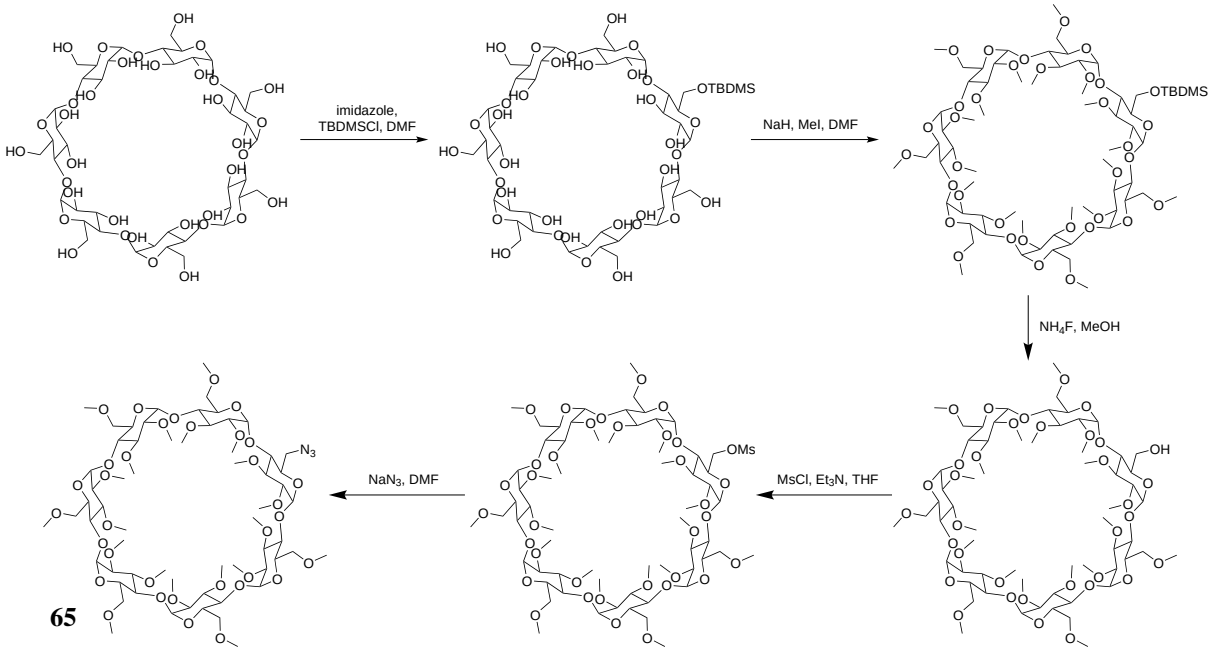


Figure 2.6.2: Figure showing a) the numbering scheme for the carbohydrate units and b) the distribution of 1° and 2° alcohol moieties on the narrow and wide rims, respectively, of the β-cyclodextrin cone.

The selective mono-functionalisation of β-cyclodextrin has been reported in the literature[456] allowing for simple chemical modification and minimal synthetic by-products, advantageous for use as axle stopper components. These procedures exploit the differing nucleophilic and basic properties of the primary and secondary alcohols to allow synthetic discrimination between the two rims of the cone (Figure 2.6.2). The narrow rim can be preferentially alkylated through the reaction with an electrophile, and taking advantage of the more acidic secondary alcohols *via* initial deprotonation allows for the alkylation of the wider rim upon reaction with a suitable electrophile. Nonetheless, selectively functionalising just one of the several identical hydroxy groups invariably results in statistical reactions, necessitating painstaking chromatographic techniques in order to purify the mono-functionalised product from a complex mixture. Since the alkylation of the narrow rim, comprised of primary alcohols, is much easier to achieve than discriminating between the two secondary alcohols on the wider rim, and is more widely studied in the literature, this method was chosen for the mono-functionalisation of β-CD as a stopper unit.

2.6.2 β-Cyclodextrin synthesis

Owing to its solubility in aqueous and organic solvents, the mono-functionalised azido-permethylated β-cyclodextrin (pCD-azide, **65**) was targeted as a synthon for use as a stopper unit *via* CuAAC click reactions. Synthesis of this compound was initially established *via* a modification of literature procedures[456,457] (Scheme 2.6.1). This protocol involves the initial mono-protection of a primary alcohol on the cyclodextrin lower rim using *tert*-butyldimethylsilyl chloride (TBDMSCl) followed by methylation and deprotection to form the mono-hydroxy permethylated cyclodextrin derivative. Thereafter, mesylation of the primary alcohol and subsequent substitution using NaN_3 affords the pCD-azide target (**65**). Unfortunately, this methodology suffers from water sensitivity resulting in irreproducibility, and repeated attempts at preparing **65** *via* this methodology were unsuccessful.

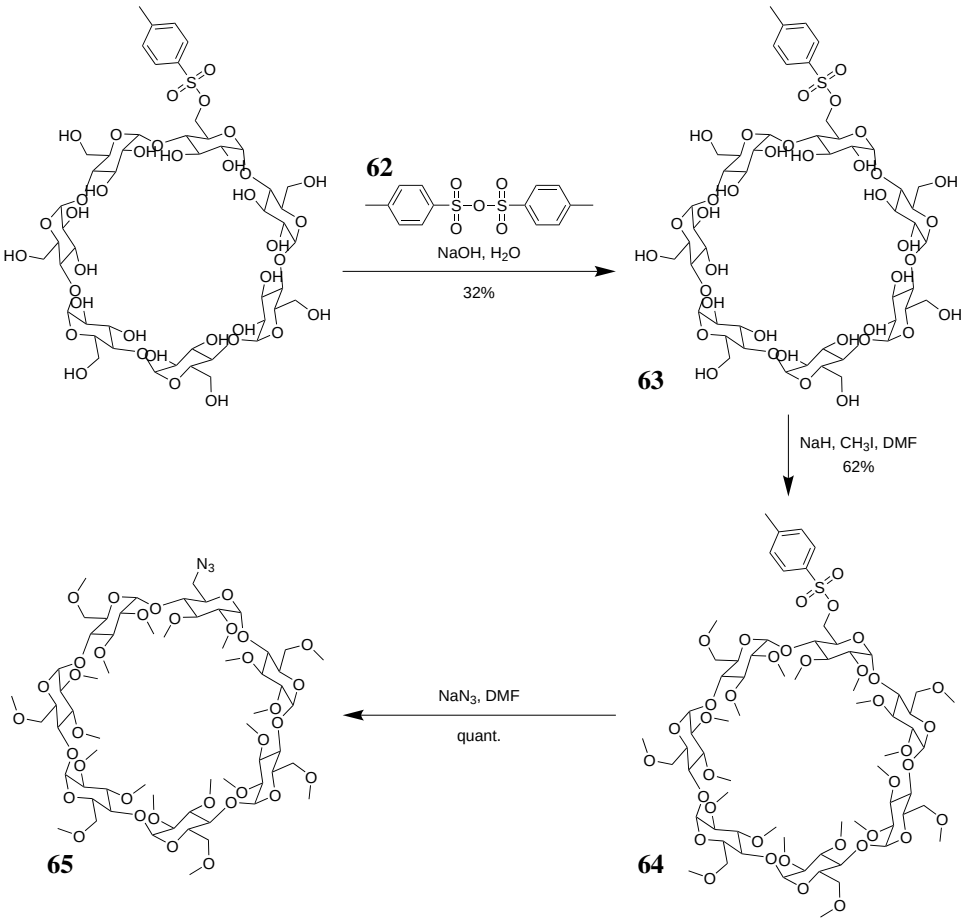


Scheme 2.6.1: Initial synthetic scheme to form mono-functionalised azido-permethylated β-cyclodextrin **65**.

A second route was considered as an alternative, involving the addition of seven equivalents of diisobutylaluminium hydride (DIBAL) to a toluene solution of permethylated cyclodextrin.[458] Rather than employing a statistical reaction for mono-functionalisation before permethylation, this method affords the desired mono-hydroxy intermediate compound, as a minor product in $\sim$ 20% yield *via* a de-*O*-methylation reaction of permethylated cyclodextrin. The major product is the double de-*O*-methylation of permethylated cyclodextrin on the upper rim. However, this particular methodology was not attempted as part of this work.

The synthetic methodology employed reproducibly in this thesis was finally developed in collaboration with Dr Michal Rezanka, a post-doctoral researcher in our group, using modifications of a series of

literature procedures (Scheme 2.6.2).[456,459,460] The key precursor to the synthesis of the desired mono-azide is a mono-functionalised *O*-tosyl β-cyclodextrin **63**, which was prepared by stirring an excess of freshly prepared *p*-toluenesulfonic anhydride **62** with β-cyclodextrin in water for 2 hours.[459] A 2.5 M^{-1} aqueous solution of NaOH was added and the mixture stirred for 10 minutes precisely, affording **63** in 32% yield after purification. Thereafter, **63** was methylated using NaH and CH_3I under strict dilution conditions.[460] The reaction was quenched by careful addition of H_2O to afford the desired product **64** in 62% yield after purification. The tosylate was substituted for the azide by heating a solution of **64** with NaN_3 in DMF at 100 °C under N_2, yielding the desired mono-azide permethyl-β-cyclodextrin **65** quantitatively.[456]



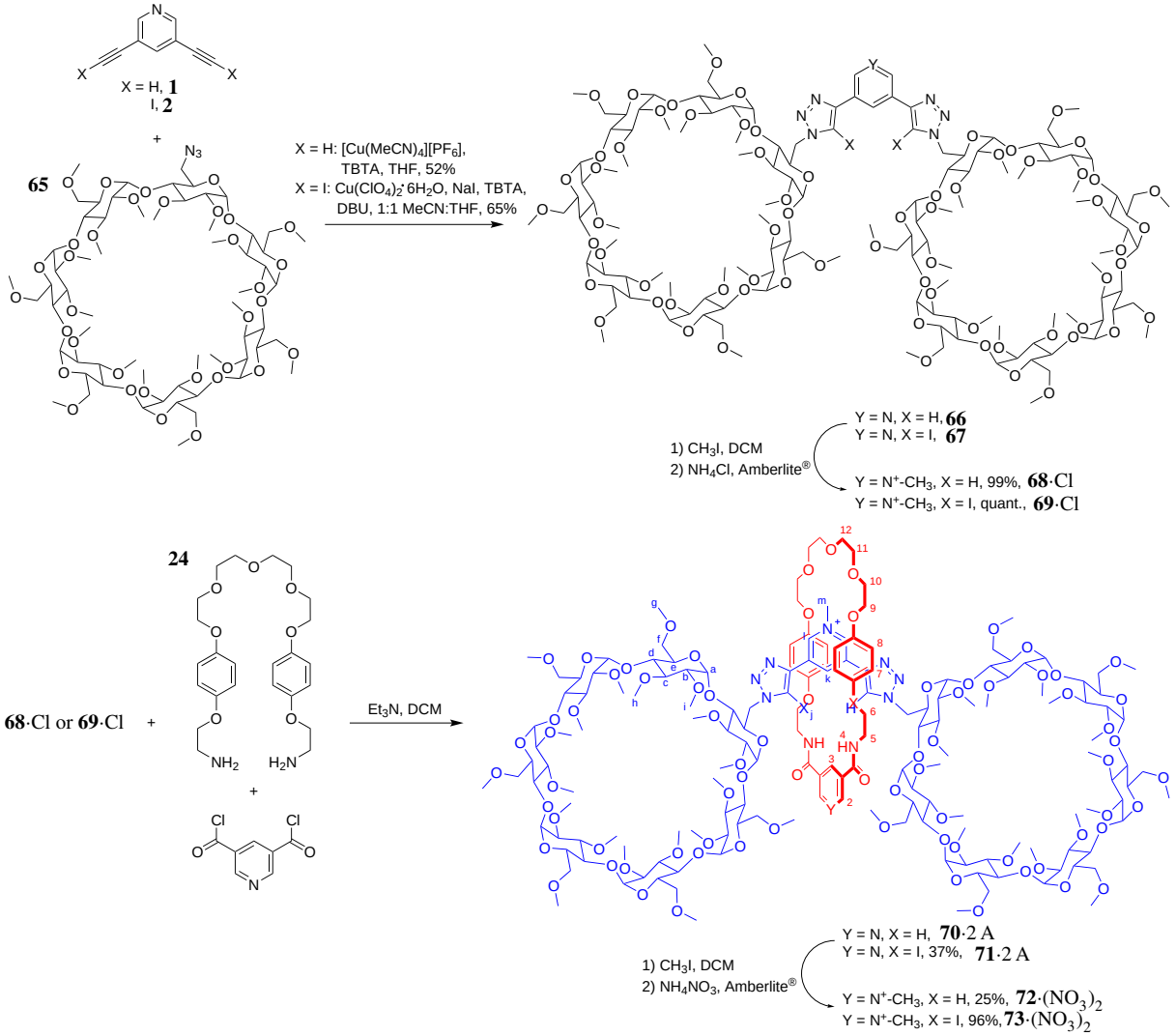
Scheme 2.6.2: Synthetic scheme to form mono-functionalised azide-permethylated-β-cyclodextrin **65**.

2.6.3 Rotaxane syntheses[†]

In collaboration with Matthew J. Langton, a previous member of the Beer group, the 3,5-bis-proto- and 3,5-bis-iodotriazole pyridinium motifs were incorporated into β-cyclodextrin-stoppered rotaxanes.

[†]The work in the following section was published in Nature Chemistry: Langton, M. J.; Robinson, S. W.; Marques, I.; Félix, V.; Beer, P. D., *Halogen bonding in water results in enhanced anion recognition in acyclic and rotaxane hosts*, *Nature Chem.*, 2014, **6**, 1039–1043.

The two permethyl-β-cyclodextrin-appended axles were prepared *via* the CuAAC click reaction between **1** and **65**: the prototriazole-containing axle precursor (**66**) was synthesised using well-established protocols, whilst the iodotriazole-containing axle precursor (**67**) was obtained from the one-pot iodo-click reaction (Scheme 2.6.3). Subsequent, methylation using excess CH_3I, and anion exchange afforded the proto- and iodo-axle components **68**·Cl and **69**·Cl, respectively. The corresponding [2]rotaxanes were prepared using a chloride-templation methodology: the two axle components were each stirred with the 5-*O*-polyether bis-amine macrocycle precursor **24**, 3,5-bis-chlorocarbonyl pyridine and Et_3N in dry dichloromethane. The mono-cationic [2]rotaxanes (proto: **70**·I and iodo: **71**·I) were purified by preparative thin layer silica gel chromatography. Thereafter, they were methylated using an excess of CH_3I, and anion exchanged to their respective nitrate salts by passing through a nitrate-loaded Amberlite® column affording the dicationic proto- and iodo-[2]rotaxanes **72**·$(NO_3)_2$ and **73**·$(NO_3)_2$.



Scheme 2.6.3: Synthesis of water-soluble permethyl-β-cyclodextrin-appended hydrogen- and halogen-bonding [2]rotaxanes **72**·$(NO_3)_2$ and **73**·$(NO_3)_2$.

The interlocked nature of the two [2]rotaxanes was confirmed by 2D ROESY NMR spectra which reveal significant through-space ^{1}H–^{1}H couplings between the macrocyclic component and the axle as shown in Figure 2.6.3.

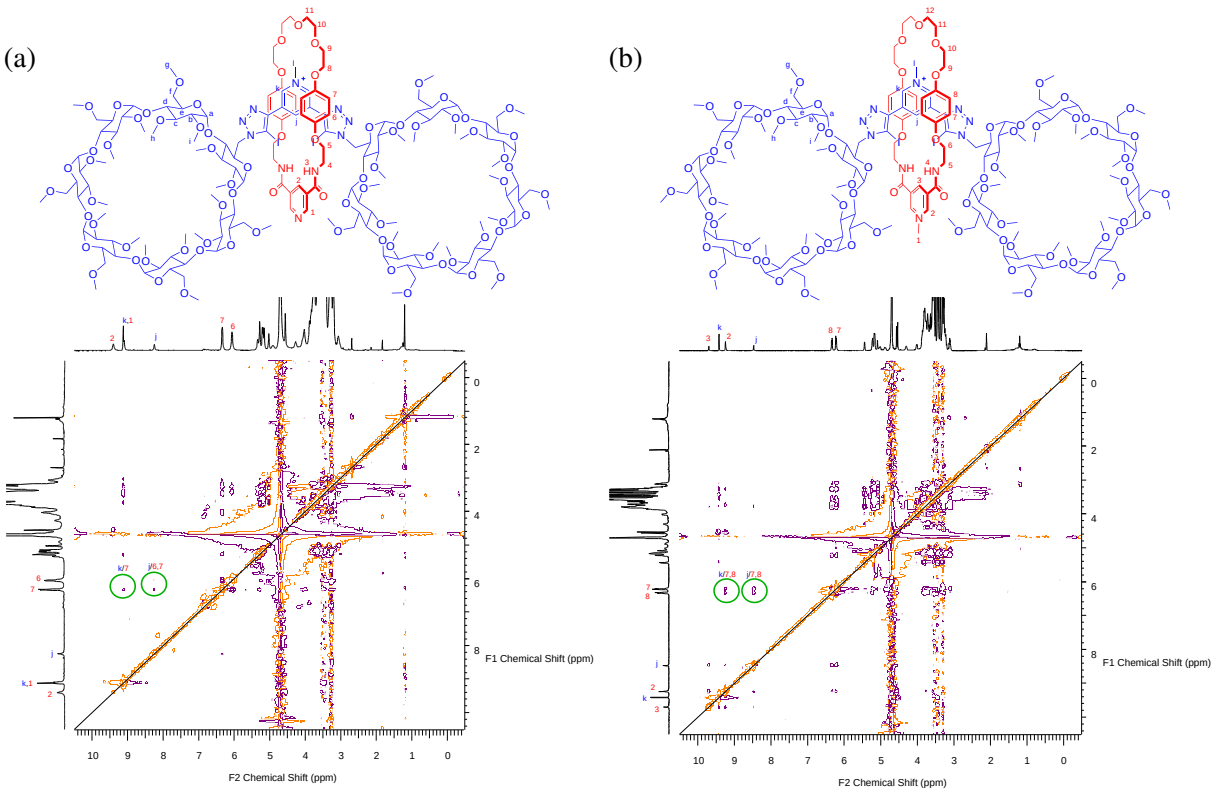
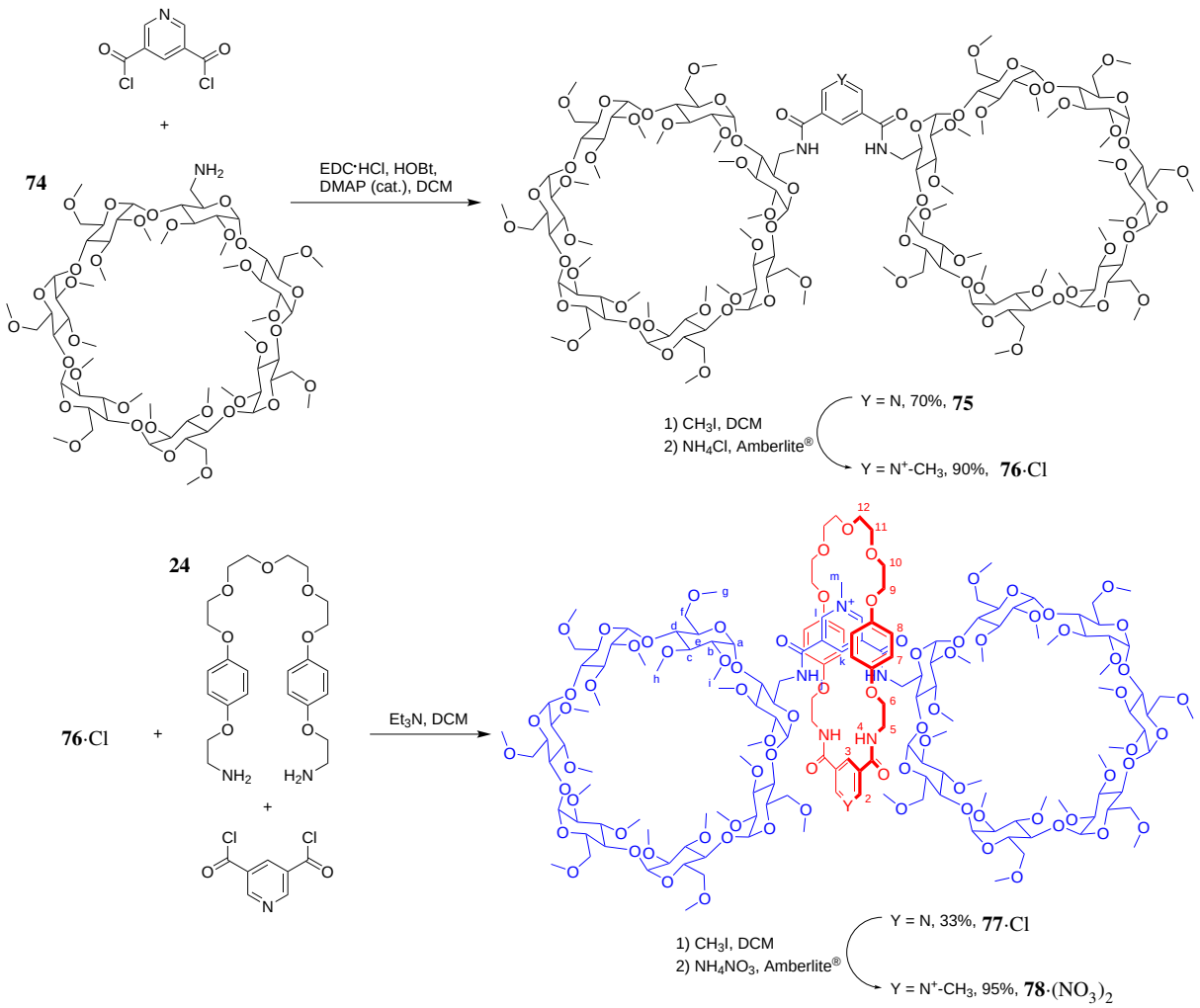


Figure 2.6.3: 2D ROESY spectra for (a) the monocationic [2]rotaxane **71**·Cl and (b) the dicationic [2]rotaxane **73**·$(NO_3)_2$.

An analogous pyridinium bis-amide-axle-containing [2]rotaxane was also synthesised for comparison by Matthew J. Langton. The permethyl-β-cyclodextrin axle precursor **75** was prepared by the amide condensation of mono-amino permethyl-β-cyclodextrin (prepared according to a literature procedure[459]) and 3,5-bis-chlorocarbonyl pyridine (Scheme 2.6.4). Thereafter, methylation with CH_3I and anion exchange to the chloride salt afforded the axle **76**·Cl. Similarly, the [2]rotaxane was prepared using a chloride-templation methodology: the axle stirred with the bis-amine macrocycle precursor **24**, 3,5-bis-chlorocarbonyl pyridine and Et_3N in dry dichloromethane. The mono-cationic [2]rotaxane **77**·Cl was purified by preparative thin layer silica gel chromatography. The dicationic [2]rotaxane **78**·$(NO_3)_2$ was obtained from the methylation reaction of **77**·Cl with CH_3I, and subsequent anion exchange to the nitrate salts by passing through a nitrate-loaded Amberlite® column. Characterisation by 2D ROESY NMR confirmed the interlocked nature of the dicationic [2]rotaxane (Figure 2.6.4).



Scheme 2.6.4: Synthesis of water-soluble permethyl-β-cyclodextrin-appended amide hydrogen-bonding [2]rotaxane **78**·$(NO_3)_2$.

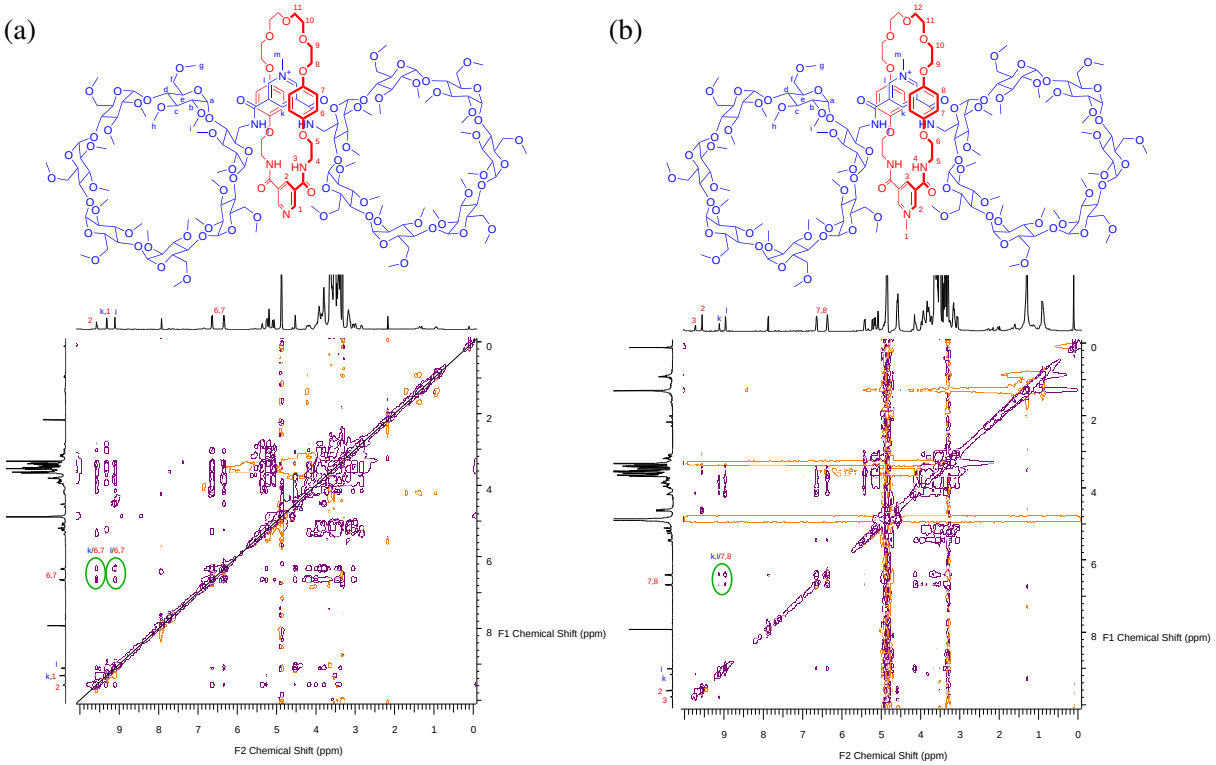


Figure 2.6.4: 2D ROESY spectra for (a) the monocationic [2]rotaxane **77**·Cl and (b) the dicationic [2]rotaxane **78**·I · Cl.

2.6.4 ^{1}H NMR anion binding studies

The anion recognition properties of the acyclic receptors **68**·NO_3, **69**·NO_3 and **76**·NO_3 and their respective [2]rotaxanes **72**·$(NO_3)_2$, **73**·$(NO_3)_2$ and **78**·$(NO_3)_2$, were investigated using ^{1}H NMR anion titration experiments by adding aliquots of anions (Cl^-, Br^-, I^- and SO_4^{2-}) as their sodium salts to solutions of the receptors in D_2O. Perturbations in the chemical shift of the protons incumbent upon the anion binding cavity (*j*, *k*, *3* and *4*) were observed and monitored as a function of anion concentration (Figure 2.6.5). WinEQNMR2[437] and approximate Job plot analysis of the titration data determined the 1:1 stoichiometric association constants shown in Table 2.6.1, which were independent of the proton monitored for a given anion.

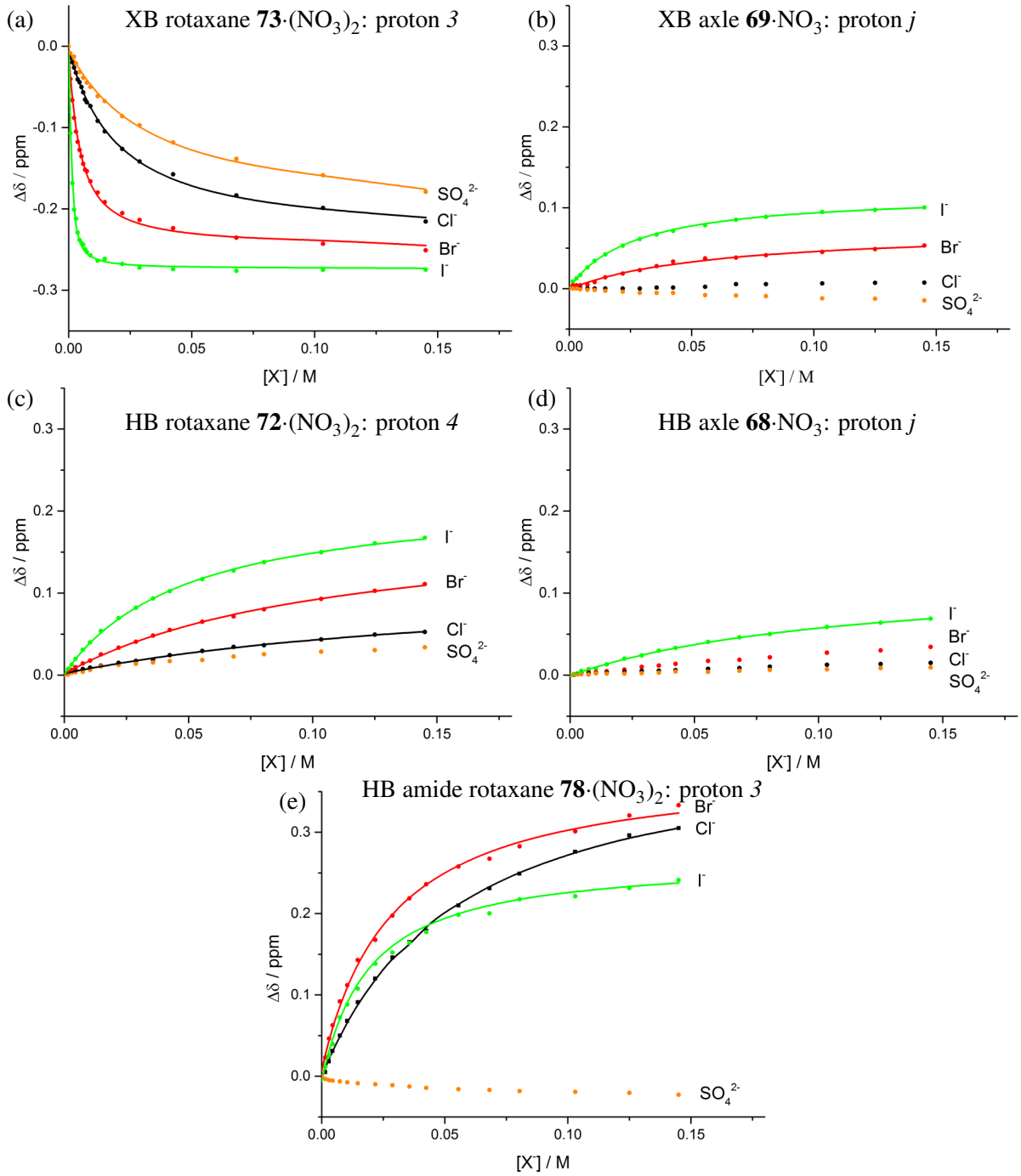


Figure 2.6.5: Plots of change in chemical shift against increasing anion concentration for permethyl-β-cyclodextrin-appended halogen- and hydrogen-bonding anion receptors in D_2O (298 K). Experimental titration data (circles) with WinEQNMR2[437] fitted binding isotherms indicated as lines.

Table 2.6.1: Anion association constants K_a (M^{-1}) in water.

		K_a (M^{-1})			
		Cl^-	Br^-	I^-	SO_4^{2-}
Triazole Receptors					
X = H	Axle, **68**·NO_3	–*	–*	5	–*
	Rotaxane, **72**·$(NO_3)_2$	–*	10	20	–*
X = I	Axle, **69**·NO_3	–*	15	40	–*
	Rotaxane, **73**·$(NO_3)_2$	55	290	2200	30
Amide Receptors					
HB	Axle, **76**·NO_3	–*	–*	–*	–*
	Rotaxane, **78**·$(NO_3)_2$	15	35	50	–*

Association constants were measured by ^{1}H NMR spectroscopy anion binding titrations in D_2O at 298 K. Anions were added as the sodium salts and association constants calculated using WinEQNMR2.[437] Errors were estimated to be <10%. *No binding.

Comparison of the anion binding properties of the acyclic monocationic hosts revealed that the halogen-bonding receptor **69**·NO_3 binds bromide and iodide with significant association constants (K_a = 15 M^{-1} and 40 M^{-1}, respectively) for a singly-charged, acyclic receptor. In contrast, the analogous hydrogen-bonding host **68**·NO_3 associates weakly with iodide with no observable binding of the other anions. While hydrogen-bonding amide-based motifs have previously been shown to bind halide anions strongly in organic–aqueous solvent mixtures,[414] the acyclic pyridinium bis-amide receptor **76**·NO_3 showed no measurable association for anions.

The halogen-bonding rotaxane **73**·$(NO_3)_2$ displayed remarkably strong binding for Cl^-, Br^- and I^- in water. Indeed, iodide was bound with an association constant $K_a = 2200\ \text{M}^{-1}$. Typically, a much higher positive charge on the host is required to achieve this magnitude of binding in water.[76] Weak binding is observed for the sulfate anion owing to its large hydration energy, size and unfavourable geometry, making it unable to penetrate the rotaxane's binding cavity. In contrast, the anion binding strength of rotaxane **72**·$(NO_3)_2$, where the halogen-bonding iodotriazole donors are substituted for C–H hydrogen-bonding prototriazole donors, is dramatically diminished, showing no binding for Cl^- or SO_4^{2-} and only the weak association of Br^- and I^- (K_a = 10 M^{-1} and 20 M^{-1}, respectively). Surprisingly, the binding for **72**·$(NO_3)_2$ is weaker still than the monocationic acyclic halogen-bonding receptor **69**·NO_3. Despite the use of stronger N–H hydrogen-bond donors in rotaxane **78**·$(NO_3)_2$, only a modest enhancement of anion binding is observed over the C–H hydrogen-bonding rotaxane **72**·$(NO_3)_2$.

Consistent with the previously reported effect observed for interlocked receptors that encapsulation of an anion within a three-dimensional binding cavity results in augmented association strength in comparison to the acyclic counterparts in organic–aqueous solvent mixtures, the association constants for the above rotaxane hosts are notably greater in magnitude than their acyclic precursors in all cases.[414]

Moreover, the enhancement of iodide binding by halogen-bonding rotaxane **73**·$(NO_3)_2$ is particularly impressive with over two orders of magnitude greater than the hydrogen-bonding analogues **72**·$(NO_3)_2$ and **78**·$(NO_3)_2$. This impressive enhancement can be attributed to simply replacing two protons in **72**·$(NO_3)_2$ with two iodine atoms, substituting hydrogen-bond donors for halogen-bond donors in the axle component, demonstrating the superiority of this intermolecular interaction for anion recognition in water.

2.6.5 Thermodynamics of binding

A van 't Hoff analysis (Figure 2.6.6) was conducted for the hydrogen-bonding rotaxanes **72**·$(NO_3)_2$ and **78**·$(NO_3)_2$ and the halogen-bonding rotaxane **73**·$(NO_3)_2$ in D_2O, determining the thermodynamic parameters for iodide complexation (Table 2.6.2), in order to investigate the origin of the strong halide anion binding. For the hydrogen-bonding receptors **72**·$(NO_3)_2$ and **78**·$(NO_3)_2$, iodide binding was shown to be enthalpically unfavourable (endothermic) with a strong entropic term contributing entirely towards the binding of the halide. This favourable entropy arises from the expulsion of ordered water molecules from both the host and guest species, and is indicative of anion binding driven by the hydrophobic effect,[76] which has been exploited in the few receptors capable of aqueous anion recognition.[414] However, iodide binding for the halogen-bonding rotaxane **73**·$(NO_3)_2$ is driven by a strong favourable enthalpic (exothermic) contribution, which is counterbalanced by an unfavourable entropic term. Recent halogen-

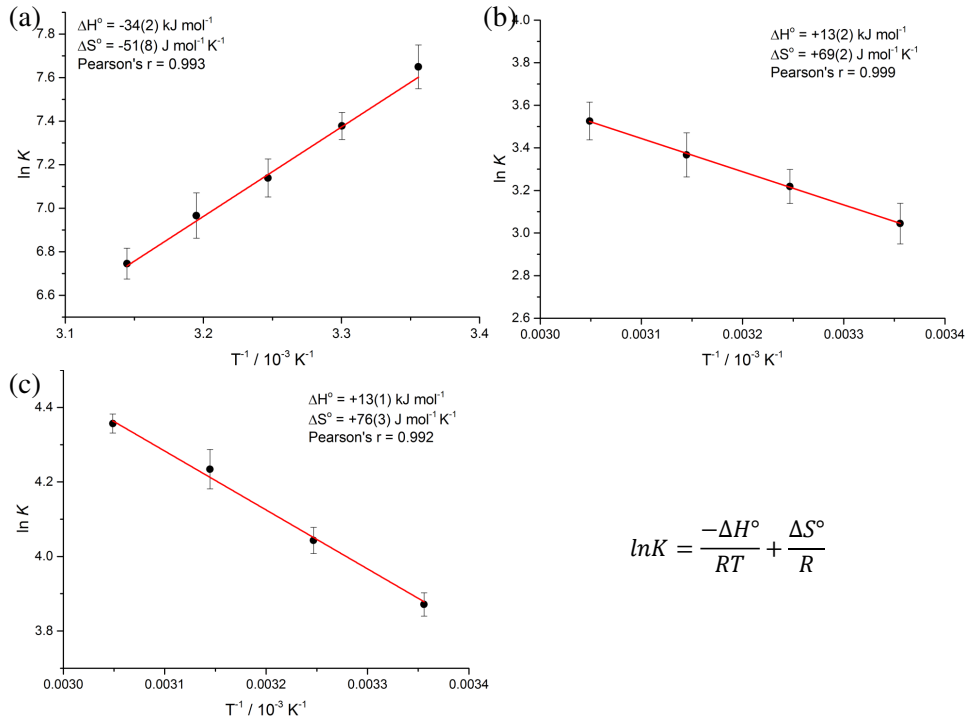


Figure 2.6.6: van 't Hoff analysis of iodide binding for (a) XB-rotaxane **73**·$(NO_3)_2$, (b) HB-triazole rotaxane **72**·$(NO_3)_2$ and HB-amide rotaxane **78**·$(NO_3)_2$ in D_2O. The determined enthalpy and entropy values, and the linear correlation coefficient are shown in each case.

bonding receptor anion binding studies by Huber[266] and Taylor[461] in organic solvents, and investigations into the thermodynamics of halogen-bonding associations between C_6F_5I and metal fluorides[252] and metal hydrides[462] in toluene by Brammer, Hunter and Perutz, show guest binding by halogen-bonding interactions to be driven by enthalpic contributions.

Table 2.6.2: Thermodynamic parameters (kJ mol^{-1}) for I^- in D_2O.

		ΔG	ΔH	$T\Delta S$
HB rotaxanes	Triazole, **72**·$(NO_3)_2$	-7	13	21
	Amide, **78**·$(NO_3)_2$	-10	13	23
XB rotaxanes	Iodotriazole, **73**·$(NO_3)_2$	-19	-34	-15

The dramatic enhancement of iodide binding by the halogen-bonding rotaxane **73**·$(NO_3)_2$ may be attributed to the two iodine atoms located within the binding cavity since one can reasonably assume that the thermodynamic terms, arising from the desolvation of the free iodide anion in solution and the macrocyclic pyridinium bis-amide recognition site, are similar for all three rotaxane host systems. Furthermore, where the hydrogen-bonding rotaxanes **72**·$(NO_3)_2$ and **78**·$(NO_3)_2$ reveal favourable entropy, the halogen-bonding rotaxane **73**·$(NO_3)_2$, in contrast, displays an unfavourable entropic term, which negates the assertion that the iodine atoms simply provide a more lipophilic binding domain leading to stronger iodide binding. If that were the case, this hydrophobic effect would lead to an enhanced entropic contribution, with a possible supplementary enthalpic contribution.[463] Consequently, it appears that the formation of halogen bonds between **73**·$(NO_3)_2$ and I^- is the dominant factor over the hydrophobic effect in controlling the iodide recognition process.

2.6.6 Molecular dynamics simulations

In collaboration with Prof. Vítor Félix at the University of Aveiro, Portugal, the halide-binding properties of **73**·$(NO_3)_2$ in water were further investigated using a combination of molecular mechanics (MM) and molecular dynamics (MD) simulations. The halogen-bonding interactions were described with the σ-hole of each iodine atom represented by a positively charged extra point (EP), with density functional theory (DFT) optimised structures affording the optimal iodine-EP distances.

The three halide complexes (**73**·Cl, **73**·Br and **73**·I) exhibit an orthogonal arrangement of the axle and macrocycle components in the interlocked structure throughout the MD simulations (Figure 2.6.7 for **73**·I). Each halide anion is tightly coordinated within rotaxane $\mathbf{73}^+$ *via* two independent linear halogen-bonding interactions, which are supplemented by two intermittent N–H···X^- hydrogen bonds, which is

illustrated with the confined 3D histogram constructed with the iodide positions for a single 50 ns MD replicate (Figure 2.6.8).

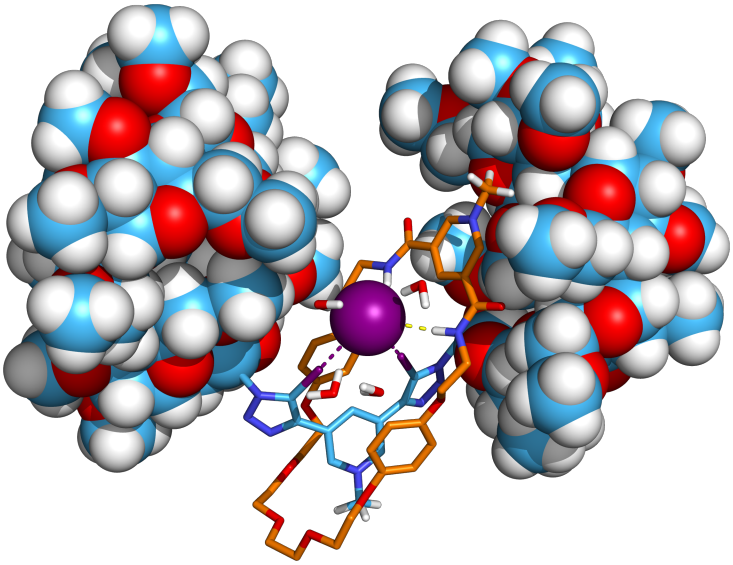


Figure 2.6.7: MD simulation of **73**·$(NO_3)_2$ with I^-. Representative snapshot showing the iodide binding through two halogen- and hydrogen-bonding interactions, surrounded by four water molecules. The N–H···I^- and C–I···I^- bonding interactions are drawn as purple and yellow dashed lines, respectively. The cyclodextrin stoppers are depicted by a space filling representation. Carbon atoms are shown in cyan in the axle and in orange in the macrocycle, while oxygen, nitrogen and iodine atoms are respectively shown in red, blue, and purple. Selected hydrogen atoms are shown in white.

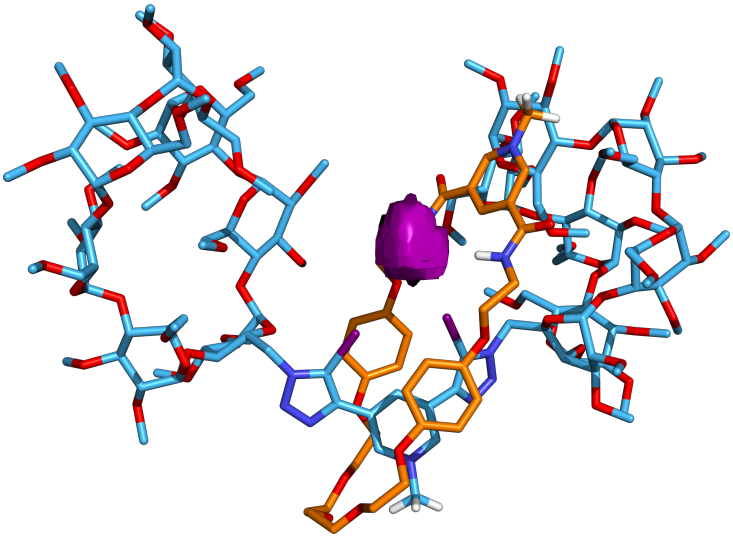


Figure 2.6.8: Histogram built with the positions occupied by the iodide along the 50 ns of MD simulation with **73**·$(NO_3)_2$. Colour scheme as in Figure 2.6.7.

The anions are positioned slightly above the plane of the macrocycle with the I···X^- and N···X^- distances mirroring the increasing size of the halide anion (Table 2.6.3).

Table 2.6.3: Halogen- and hydrogen-bond distances (Å)[a], and the average number of water molecules within the first solvation shell of each bound halide anion (3.5 Å cut-off) for 100 ns of sampling of MD simulations of **73**·$(NO_3)_2$ with halides.

X^-	I···X^-	N···X^-	Number of Water Molecules
Cl^-	3.50(14) 3.55(16)	3.55(24) 3.76(38)	3.58(73)
Br^-	3.69(16) 3.74(19)	3.96(65) 4.13(57)	3.99(80)
I^-	3.94(20) 4.06(24)	4.21(55) 4.37(59)	4.12(85)

[a] Average bond distances with errors given in parentheses.

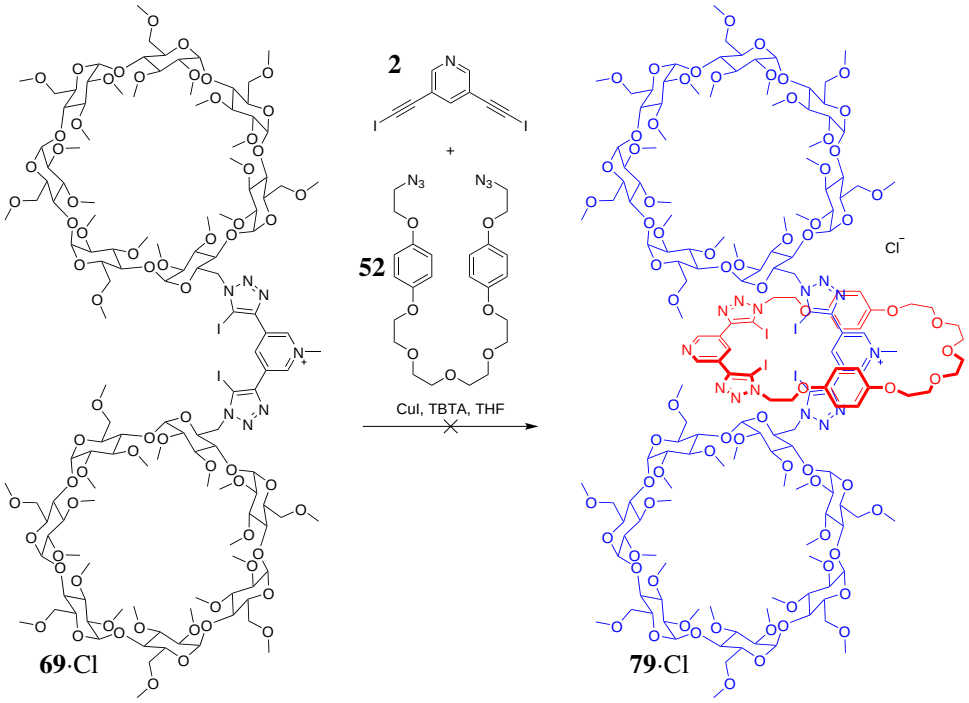
Using the thermodynamic integration method, whereby the relative binding free energies ($\Delta\Delta G$) of a pair of halide anions may be estimated, the selectivity of **73**·X complexes (X = Cl^-, Br^- and I^-) were studied by free energy calculations. Table 2.6.4 shows that the relative free energies of the halide complexes for $\mathbf{73}^{2+}$ correlate well with the experimentally determined selectivity trend: complex stability increases with the size of the halide anion. Consequently, the iodide selectivity arises from both the complementary size and shape of the anion binding cavity of $\mathbf{73}^{2+}$ and the Hofmeister series bias towards larger, less heavily-solvated halides.

Table 2.6.4: $\Delta\Delta G$ (kJ mol^{-1}) for halide complexes of **73**·$(NO_3)_2$.

Mutation	ΔG $\mathbf{73}^+ \cdot$ X	ΔG X^-	$\Delta\Delta G$
$I^- \rightarrow Br^-$	-17.18	-35.61	18.39
$Br^- \rightarrow Cl^-$	-9.15	-27.13	17.97

2.6.7 Attempted synthesis of a water-soluble all-halogen-bonding [2]rotaxane

Considering the remarkably enhanced binding of halide anions in pure water by the halogen-bonding 3,5-bis-iodotriazole pyridinium motif, an all-halogen-bonding water-soluble [2]rotaxane was envisaged (Scheme 2.6.5). The synthesis of this [2]rotaxane was attempted *via* a double CuAAC click ring-formation reaction around the permethyl-β-cyclodextrin-appended axle using the two-pot method: the bis-azide macrocycle precursor **52** and di-iodoethynyl pyridine **2** were mixed with the halogen-bonding axle **69**·Cl in THF with catalytic CuI and TBTA. However, no spectroscopic evidence was obtained for the formation of the target [2]rotaxane **79**·Cl: unfortunately, only starting materials were isolated from the reaction mixture.



Scheme 2.6.5: Attempted synthesis of an all-halogen-bonding [2]rotaxane **79**·Cl.

2.7 Conclusion and future work

Conclusion

In conclusion, the use of the 3,5-bis-iodotriazole pyridinium group as a potent motif for anion recognition has been demonstrated by its initial incorporation in acyclic receptors, and its exploitation in interlocked host structural frameworks: two [2]catenanes and a water-soluble [2]rotaxane.

Strong binding was observed for the acyclic receptor **13**·PF_6 in DMSO-d_6 with unprecedented binding for OAc^-. Thereafter, the monocationic halogen-bonding [2]catenane **28**·PF_6 displayed a remarkable enhancement in anion binding ability over the hydrogen-bonding analogue in the organic aqueous solvent mixture 45:45:10 $CDCl_3$:CD_3OD:D_2O with binding of Br^- and I^- both $> 10^4$ M^{-1}, and no binding for oxoanions. Unfortunately, poor solubility in aqueous mixtures hampered the determination of accurate association constants in more competitive aqueous solvent mixtures. Attempting to improve the solubility *via* the incorporation of additional positive charge with the synthesis of dicationic [2]catenane **35**·$(NO_3)_2$, allowed the determination of association constants in 1:1 D_2O:CD_3OD. Whilst the catenane showed modest selectivity for spherical halides over the tetrahedral sulfate anion, minimal discrimination between the halides was observed primarily due to electrostatic charge domination.

X-ray absorption spectroscopic analysis has presented the first evidence for the quantification of the covalent character of the halogen-bonding–halide anion interaction. A single halogen-bond donor

iodotriazolium receptor **32**·Cl showed $\sim 6\%$ covalent character, which is of the same magnitude as those interactions commonly observed in transition metal complexes. This contribution is nearly doubled in the acyclic 3,5-bis-iodotriazole pyridinium receptor ($\sim 11\%$), indicating that halogen bonds can be considered to be independent and additive in nature. The reduction in charge donation observed for the catenane **28**·Cl ($\sim 7\%$) is attributed to competition with the amide N–H hydrogen-bonding interactions.

The first examples of water-soluble interlocked host structural frameworks for the recognition of anions in pure water have been prepared, exploiting the aqueous solubility of permethylated-β-cyclodextrin stopper units. The incorporation of the 3,5-bis-iodotriazole pyridinium motif into a [2]rotaxane architecture resulted in a dramatic enhancement in halide anion binding in pure water: even the acyclic halogen-bonding derivative exhibited slightly stronger binding than the C–H hydrogen-bonding [2]rotaxane, whilst the halogen-bonding [2]rotaxane showed approximately two orders of magnitude enhancement in anion binding.

van 't Hoff analysis revealed that iodide binding in the halogen-bonding [2]rotaxane was exclusively driven by favourable enthalpic contributions owing to the formation of I···I$^-$ halogen bonds, whereas the hydrophobic effect played a dominant role in iodide anion binding in the hydrogen-bonding [2]rotaxanes which were entropically driven.

Future Work

The work presented in this chapter could be expanded by preparing interlocked anion host structural frameworks which contain both the 3,5-bis-iodotriazole pyridinium motif as well as a suitable reporter group for anion sensing. Furthermore, the synthesis of an all-halogen-bonding [2]rotaxane containing halogen-bond donor groups in both the axle and macrocycle components, to bind anions exclusively through halogen bonds, may potentially facilitate even greater binding affinities in pure water.

In the following chapters, the incorporation of the 3,5-bis-iodotriazole pyridinium motif into [2]rotaxane host systems for nitrate recognition is investigated. Furthermore, the neutral 3,5-bis-iodotriazole pyridine-*N*-oxide group is presented and its integration into interlocked structural frameworks is studied.

Chapter 3

Halogen-bonding [2]rotaxanes for nitrate recognition

3.1 Introduction

Nitrate and phosphate anions are of great environmental, biological and medical importance. The anthropogenic overuse of these oxoanions in fertilisers in arable farming in the UK for the past 60–70 years has led to eutrophication of natural aquatic systems. Worthy of particular notice is nitrate, which has been implicated in the formation of carcinogenic nitrosamines, and as a cause of methemoglobinemia, also known as blue-baby syndrome, in infants.

The design of suitable receptors for nitrate is challenging due to a combination of key factors:[186]

- high hydration energy of $\Delta G_{hyd} = -314$ kJ mol^{-1},[464]
- low basicity of the anion—where the conjugate acid p$K_a = -1.4$, implying a low affinity for hydrogen bonds, and
- the molecular anion adopts a trigonal planar geometry which must be taken into consideration.

Several tripodal, macrocyclic and cage-like host systems have been designed to exploit the trigonal planar geometry of the nitrate anion by directing hydrogen-bond donors in a complementary arrangement.[86,465–471] In particular, tripodal C_3 symmetric receptors have been designed: Singh has reported a receptor containing three fluorescent dansyl-appended amide groups, which binds nitrate ($K_a = 550$ M^{-1}) over chloride, bromide and hydrogen sulfate in DMSO-d_6 solution, resulting in the quenching of the dansyl fluorophore emission (Figure 3.1.1a).[466] Johnson and Haley employed a tripodal urea motif that binds nitrate anions *via* six hydrogen bonds in 9:1 $CDCl_3$/DMSO-d_6 ($K_a = 24000$ M^{-1}), with an additional contribution from anion–π interactions proposed (Figure 3.1.1b).[468] A tridentate macrocycle containing amide groups in which the hydrogen-bond donors are directed within the macrocyclic cavity was reported by Hamilton[465], and recognises NO_3^- in 98:2 $CDCl_3$/DMSO-d_6 ($K_a = 4.6\times 10^5$ M^{-1}) (Figure 3.1.1c). More complex structures have been described such as a bicyclic cyclophane receptor by Anslyn with six converging amide hydrogen bonds, binding nitrate selectively over halide anions in 3:1 CD_3CN/CD_2Cl_2 ($K_a = 300$ M^{-1}) (Figure 3.1.1d).[86] However, the more basic acetate anion was found to bind more strongly ($K_a = 770$ M^{-1}) than nitrate in this receptor. In addition, a macrotricyclic heteroditopic receptor by Romański and Piatek (Figure 3.1.1e) bound nitrate selectively *via* three convergent hydrogen bonds in DMSO-d_6 solution ($K_a = 280$ M^{-1}).[467] The binding of nitrate was significantly enhanced in the presence of an ammonium cation complexed in the aza-crown ether motif due to strong ion-pairing ($K_a = 1050$ M^{-1}).

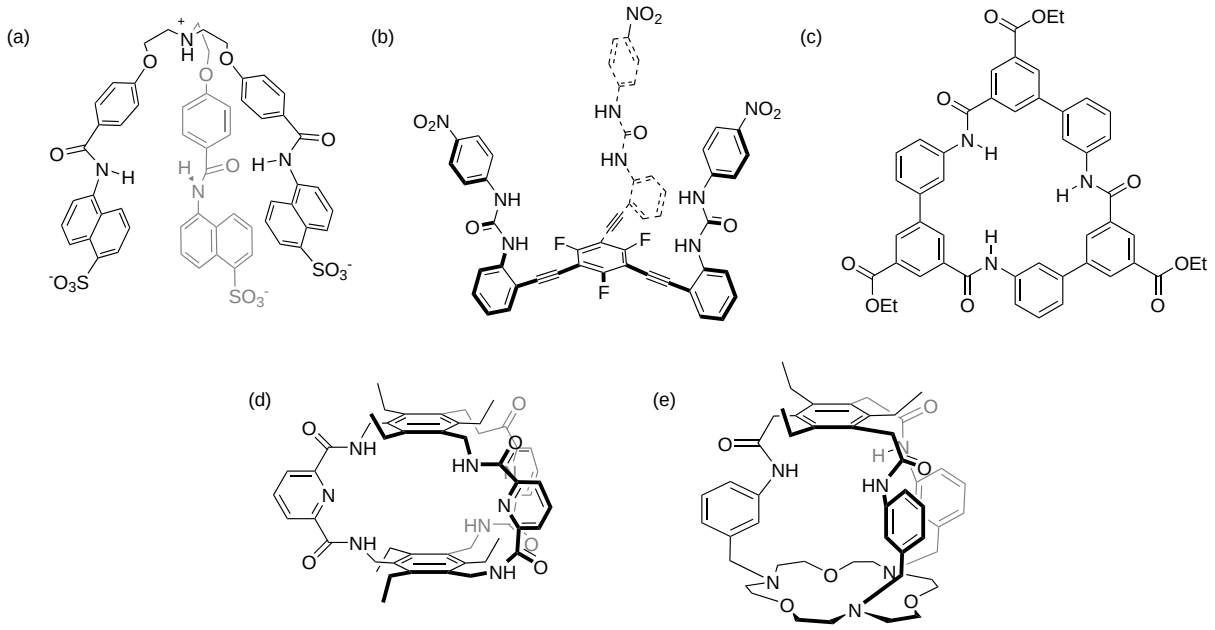


Figure 3.1.1: Examples of hydrogen-bonding nitrate receptors: (a) Singh's fluorescent nitrate sensor,[466] (b) Johnson and Haley's tripodal urea receptor[468] (c) Hamilton's tri-amide macrocycle,[465] (d) Anslyn's bicyclic cyclophane,[86] and (e) Romański's heteroditopic receptor.[467]

Recently, Beer and co-workers synthesised a [2]rotaxane *via* nitrate anion templation in which the axle component contains two bis-amide hydrogen-bonding donor sites to coordinate to two of the nitrate oxygen atoms, with the third oxygen coordinated by the 5-*tert*-butyl-isophthalamide macrocyclic component (Figure 3.1.2).[398] Strong binding of nitrate was observed in competitive 45:45:10 $CDCl_3$:CD_3OD:D_2O aqueous solvent mixture ($K_a = 430$ M^{-1}), showing selectivity over more basic oxoanions such as HCO_3^-, $H_2PO_4^-$ and OAc^-. Chloride was bound slightly stronger ($K_a = 490$ M^{-1}) than nitrate due to its similar size.

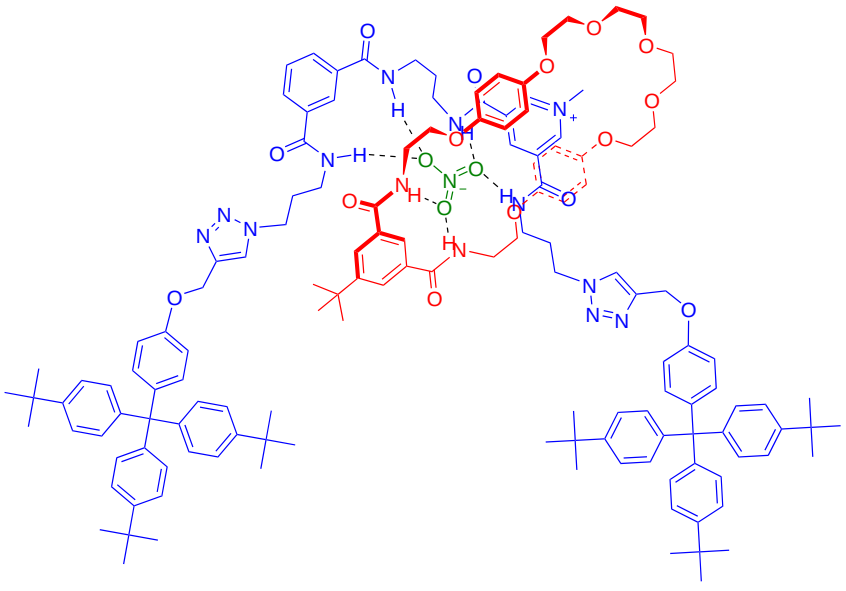


Figure 3.1.2: Figure showing the hydrogen-bonding nitrate-binding [2]rotaxane.

This work was extended *via* an analogous nitrate anion templation synthetic strategy in the preparation of a [2]catenane which exhibited nitrate selectivity in competitive 45:45:10 $CDCl_3$:CD_3OD:D_2O aqueous solvent mixture (Figure 3.1.3).[175]

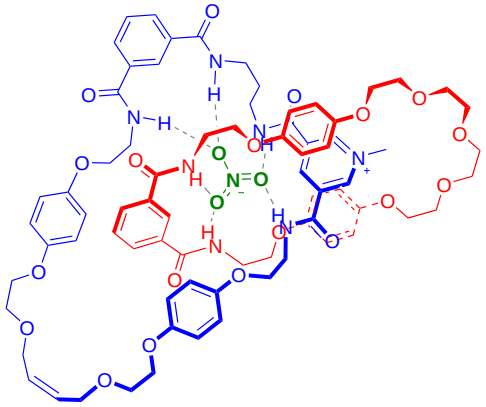


Figure 3.1.3: Figure showing the hydrogen-bonding nitrate-binding [2]catenane.

Considering the impressive anion recognition properties of the halogen-bonding 3,5-bis-iodotriazole pyridinium motif discussed in the previous chapter, the design and synthesis of novel halogen-bonding rotaxane hosts for the aqueous recognition of nitrate was undertaken.

3.1.1 Halogen bonding receptor design

Whilst it was shown in Chapter 2 that the 3,5-bis-iodotriazole pyridinium motif is capable of binding oxoanions such as acetate when incorporated into an acyclic host structure, its integration into interlocked structures resulted in the complete preclusion of oxoanions in favour of spherical halides. This is attributed to a conformationally restrained three-dimensional anion binding cavity that is too small and of unsuitable geometry to accommodate the larger molecular oxoanions. Consequently, the trigonal planar geometry of nitrate must be considered in the design of interlocked host molecules. In simplistic terms, this would require three complementary donor sites in order to coordinate each of the nitrate oxygen atoms. Furthermore, considering the remarkable enhancement of anion binding by halogen bonding over hydrogen bonding, it was envisaged that a halogen-bonding analogue to the [2]rotaxane shown in Figure 3.1.2 may allow for unprecedented nitrate recognition in pure water. Consequently, the target [2]rotaxane would comprise an axle containing two 3,5-bis-iodotriazole pyridine or pyridinium halogen-bond donor sites with a macrocyclic component bearing an isophthalamide hydrogen-bond donor site to fulfill the tridentate coordination of nitrate (Figure 3.1.4).

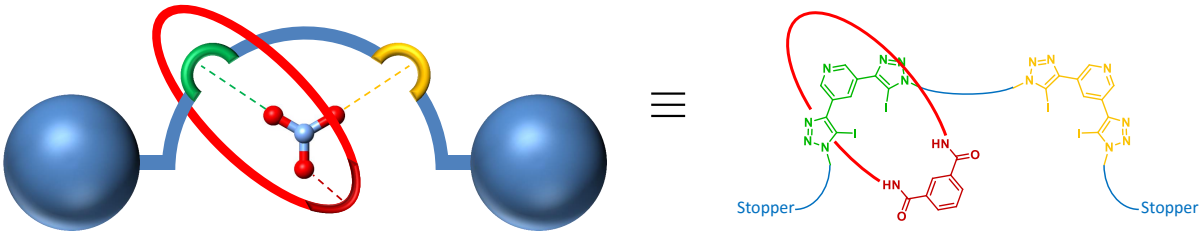


Figure 3.1.4: Cartoon representation of the design of the target halogen-bonding [2]rotaxane for nitrate binding.

3.1.2 Chapter aims

This chapter discusses attempts to construct target halogen-bonding [2]rotaxane host structural frameworks for nitrate recognition. Specifically, these interlocked hosts comprise an axle component bearing two 3,5-bis-iodotriazole pyridine or pyridinium groups and an isophthalamide-containing macrocyclic component. Initially, asymmetric methods towards the synthesis of the axle are detailed, and the anion recognition properties of the resulting [2]rotaxanes are investigated.

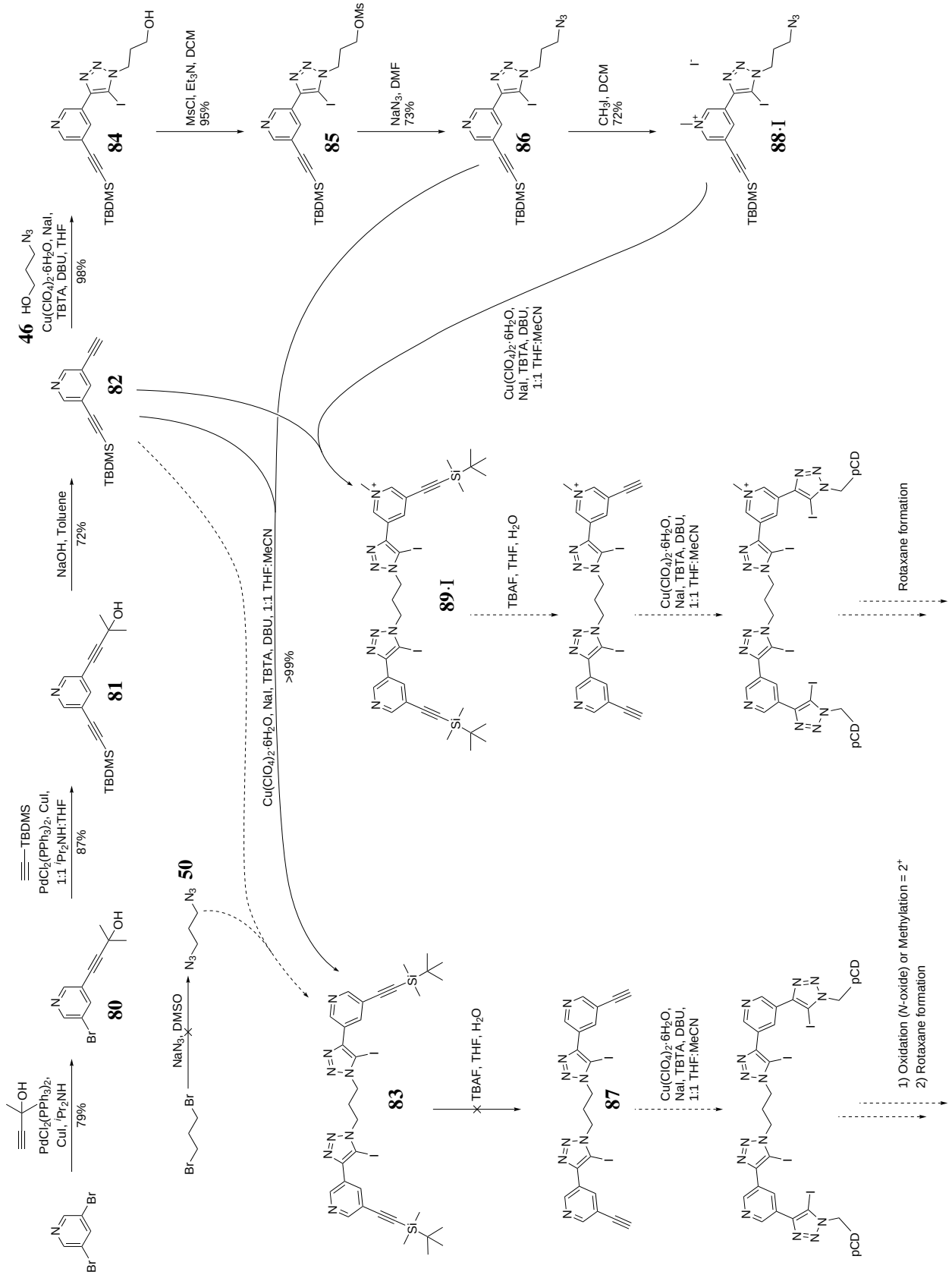
3.2 Axle synthesis *via* asymmetric methods

The initial approach to the synthesis of the axle component made use of an asymmetrically protected diethynylpyridine derivative: selective deprotection of each of the alkynes would allow for chemical modification, leading to an axle containing two 3,5-bis-iodotriazole pyridinium motifs.

3.2.1 Initial synthetic attempts

The proposed synthetic strategy is shown in Scheme 3.2.1. Asymmetric functionalisation of commercial 3,5-dibromopyridine *via* Sonogashira[436] reaction followed a modified protocol by Inouye.[472] Coupling of 2-methyl-3-butyn-2-ol with 3,5-dibromopyridine proceeded efficiently to afford mono-functionalised alkynyl pyridine **80** in 79% yield. Subsequent coupling with *tert*-butyl-dimethylsilyl (TBDMS) acetylene gave the asymmetrically protected diyne **81** in 87% yield. Deprotection of **81** was undertaken *via* reaction with NaOH in toluene, affording **82** in 72% yield.[472]

At this stage, the synthetic strategy diverged to allow for the synthesis of the symmetric and asymmetric axles. The reaction to form the symmetric axle **83** required the preparation of propane 1,3-diazide **50** and subsequent CuAAC click reaction with **82**. However, the reaction did not produce the desired bis-protected alkyne. Instead, **82** was reacted with 3-azido-propan-1-ol[473] **46** using the one-pot CuAAC click reaction in the presence of NaI, $Cu(ClO_4)_2 \cdot 6\,H_2O$, TBTA and DBU in THF, affording **84** in 98% yield after silica gel column chromatography. Subsequent reaction with MsCl and Et_3N in DCM gave

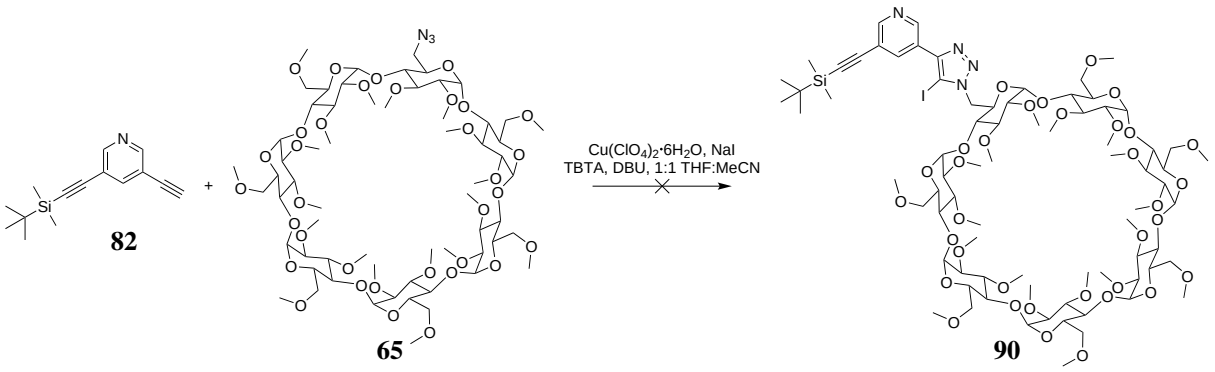


Scheme 3.2.1: Synthetic scheme to prepare an asymmetric halogen-bonding axle.

the mesylate **85** in 95% yield, and substitution using NaN_3 in DMF afforded the azide **86** in 73% yield. The synthesis of **83** was attempted again *via* the one-pot click reaction of **82** and **86** in THF, however, the product could not be isolated, despite mass spectrometric and ^{1}H NMR spectroscopic evidence of its formation, due to a low yield. The reaction was repeated using 1:1 THF:MeCN as the solvent which, after purification by preparative thin layer chromatography (3% MeOH/DCM), resulted in quantitative formation of **83** in the first instance and 76% yield upon doubling the scale. Deprotection was undertaken using TBAF in THF, however, this resulted in decomposition of one of the iodotriazole moieties in addition to the desired diyne **87** which could not be isolated thereafter from the prototriazole decomposition product. Replacing the commercial TBAF solution (1 M in THF) with 'dry' commercial TBAF (manually dissolved in THF for addition) was also unsuccessful in removing the TBDMS protecting groups. As a result, subsequent steps employing this strategy were not undertaken and an alternative route was sought.

In terms of the asymmetric axle, **86** was methylated using CH_3I in DCM, affording **88**·I in 72% yield after purification by preparative thin layer chromatography (Scheme 3.2.1). The one-pot CuAAC click reaction between **82** and **88**·I (used as the iodide salt to minimise anion interference) was undertaken in 1:1 THF:MeCN, affording the desired monocationic asymmetric axle intermediate **89**·I. However, purification proved challenging: the product could not be obtained cleanly even after preparative thin layer chromatography. Deprotection of **89**·I was not attempted after TBAF was shown to decompose the neutral axle intermediate.

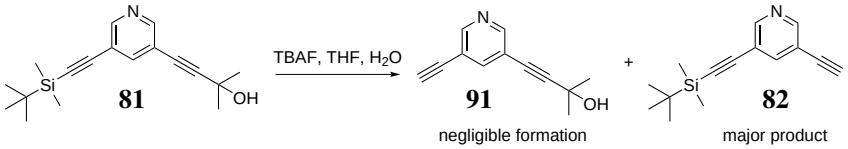
The one-pot click reaction between permethyl-β-cyclodextrin azide **65** and **82** to afford **90** was considered as a method to prepare the axle from an initial stoppering approach (Scheme 3.2.2). Further, it was hoped that the large cyclodextrin stoppers would protect the iodotriazole from degradation by TBAF during the reaction to deprotect the TBDMS-alkyne, allowing for subsequent axle synthesis. However, the click reaction to form **90** was unsuccessful: while the desired product was evident in the ESI mass spectrum, TLC and ^{1}H NMR analysis showed the formation of an inclusion complex between **65** and **82**, or an inclusion complex between **65** and **90** which were inseparable using conventional chromatographic purification techniques.



Scheme 3.2.2: Scheme for the attempted synthesis of **90**.

3.2.2 Alternative synthetic strategies

Since the iodotriazole moieties decomposed in the presence of TBAF, attention was turned towards an alternative deprotection of the asymmetrically protected diyne **81** earlier in the synthetic route: removal of the TBDMS-protecting group on **81** (instead of the hydroxy-propyl protecting group which was discussed in the previous section) was attempted using TBAF (Scheme 3.2.3) to afford **91**. However, mass spectrometric analysis of the reaction with TBAF in THF at 0 °C revealed the deprotection of the hydroxy-propyl protecting group to form **82** and not the desired alkyne **91**, and repetition at room temperature offered the same result. Substitution of the old commercial TBAF (1 M in THF) for new commercial 'dry' TBAF·xH_2O (dissolved in THF) at 0 °C resulted in the same deprotection of the hydroxy-propyl protecting group to form **82** (Table 3.2.1).



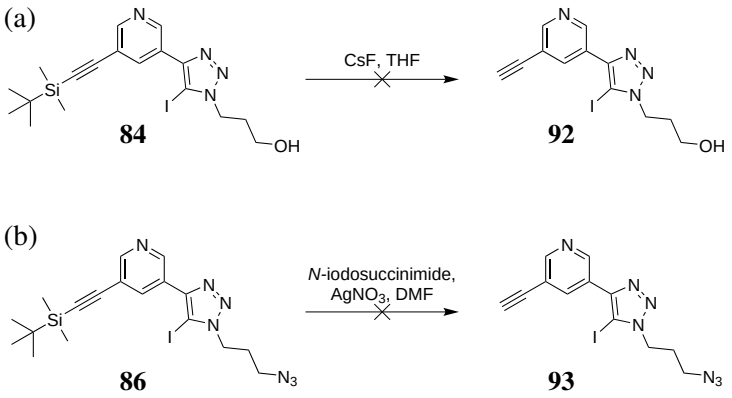
Scheme 3.2.3: Synthetic scheme to deprotect **81** with TBAF to facilitate asymmetric synthesis *via* a different route.

Table 3.2.1: Synthetic conditions for the deprotection of **81**.

TBAF source	Temperature (°C)	Product
TBAF (1 M in THF)	0	**82**
TBAF (1 M in THF)	rt	**82**
TBAF·xH_2O	0	**82**

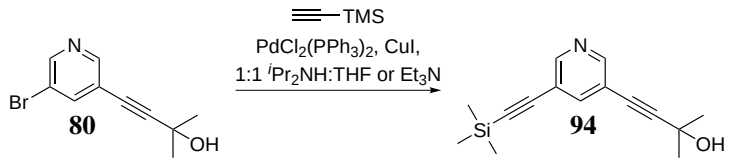
To determine whether deprotection of the TBDMS-alkyne was possible using alternative reagents at an intermediary stage in the synthetic route, and in the presence of iodotriazoles, **84** was stirred in the presence of CsF. This did not afford the desired alkyne **92** (Scheme 3.2.4); instead, the iodotriazole was

degraded to the prototriazole. Furthermore, no reaction was observed when **86** was stirred in the presence of $AgNO_3$ and *N*-iodosuccinimide in the hope of forming **93** (Scheme 3.2.4).

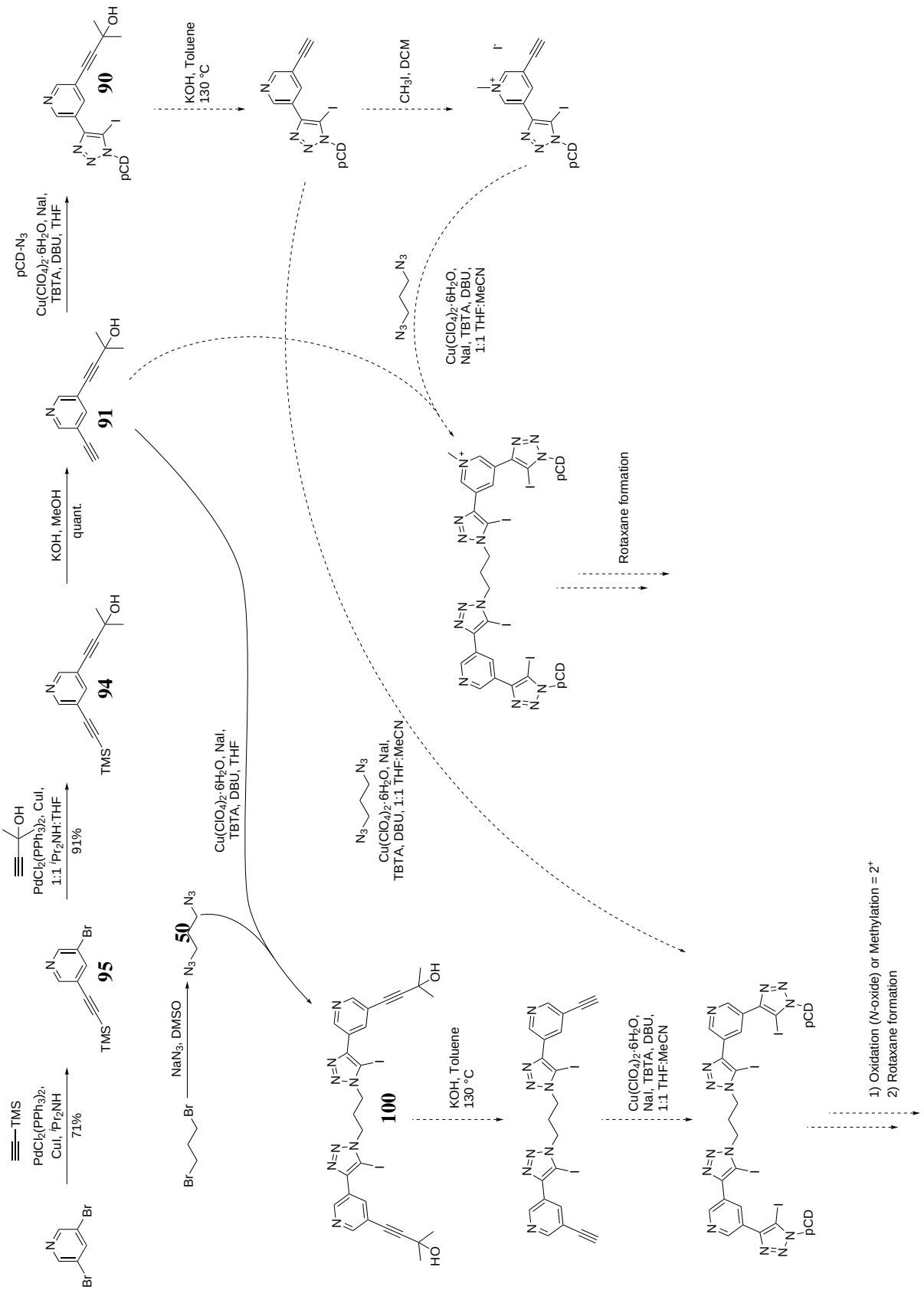


Scheme 3.2.4: Alternative attempts at TBDMS-alkyne deprotection using intermediates in the synthetic route and different deprotection agents.

Consequently, the possibility of synthesising an asymmetrically protected diyne with a more labile silyl protecting group, such as trimethylsilyl (TMS) was investigated with the key intermediate **94** shown in the modified Scheme 3.2.5. The initial synthetic attempts to form **94** are summarised in Table 3.2.2. An initial reaction using the same conditions as the synthesis of **81** was attempted with **80** but using TMS-acetylene instead (Scheme 3.2.6). However, after 4 h, the reaction had not run to completion. The reaction was repeated for 18 h at room temperature to the same result. Increasing the amount of TMS-acetylene to 2.5 equivalents and reacting for 18 h was also unsuccessful in improving the yield of **94**. Varying the base to Et_3N was investigated with 18 h reaction time at both room temperature and 70 °C; however, both cases resulted in incomplete reactions and inseparable products. In all cases the catalyst loading ($PdCl_2(PPh_3)_2$ and CuI) was kept constant.



Scheme 3.2.6: Synthetic scheme to prepare TMS-protected asymmetric diyne **94**.

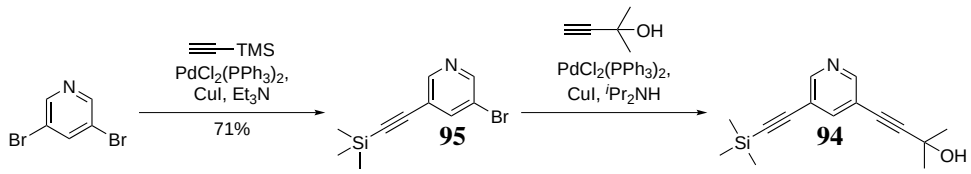


Scheme 3.2.5: Synthetic scheme to prepare an asymmetric halogen-bonding axle.

Table 3.2.2: Synthetic conditions for the preparation of **94**.

80	TMS-acetylene	Pd		Cu^I		Base	Temp.	Yield
		Source	%	Source	%		(°C)	(%)
1 eq.	1.48	$PdCl_2(PPh_3)_2$	5	CuI	10	$^iPr_2NH$	0	0
1 eq.	1.48	$PdCl_2(PPh_3)_2$	5	CuI	10	$^iPr_2NH$	rt	0
1 eq.	2.5	$PdCl_2(PPh_3)_2$	5	CuI	10	$^iPr_2NH$	rt	0
1 eq.	2	$PdCl_2(PPh_3)_2$	5	CuI	10	Et_3N	rt	0
1 eq.	2	$PdCl_2(PPh_3)_2$	5	CuI	10	Et_3N	70	0
1 eq.	1.5	$Pd(PPh_3)_4$	1	$[Cu(MeCN)_4][PF_6]$	2	Et_3N	50	0
1 eq.	1.5	$Pd_2(dba)_3$	3	CuI	15	Et_3N	75	0

Since these Sonogashira[436] reactions to produce **94** proved fruitless, the order of alkyne substitution was varied (Scheme 3.2.7). Employing a literature procedure,[474] 3,5-dibromopyridine was reacted with 1.1 eq. of TMS-acetylene to afford the mono-substituted alkynylpyridine **95** in 71% yield after optimisation of the reaction conditions. Subsequent Sonogashira[436] reaction to form **94** from the reaction between **95** and 2-methylbut-3-yn-2-ol was attempted but did not afford **94** when $PdCl_2(PPh_3)_2$ was used as the catalyst.



Scheme 3.2.7: Alternative synthetic scheme to prepare TMS-protected asymmetric diyne **94**.

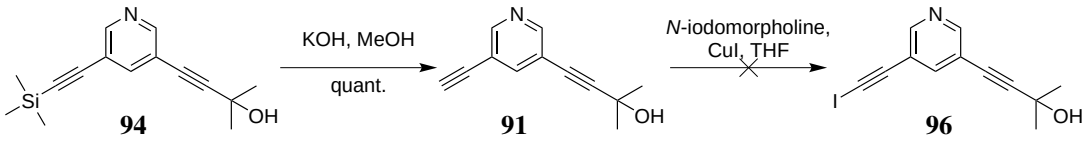
Various alternative Sonogashira reaction conditions were investigated, summarised in Table 3.2.3. Ultimately, the conditions that reproducibly afforded **94** in yields up to 91% employed $Pd_2(dba)_3$ as catalyst, with CuI co-catalyst, in the presence of PPh_3 and Et_3N at 75 °C.

Table 3.2.3: Attempted reaction conditions for the synthesis of **94**.

95	Alkyne	Pd	Additives	Solvent	Temp. (°C)	Yield (%)
1 eq.	1	$PdCl_2(PPh_3)_2$	CuI	$^iPr_2NH$	rt	0
1 eq.	1.5	$PdCl_2(PPh_3)_2$	CuI	1:1 $^iPr_2NH$:THF	rt	0
1 eq.	1.5	$Pd_2(dba)_3$	CuI, PPh_3	Et_3N	75	91

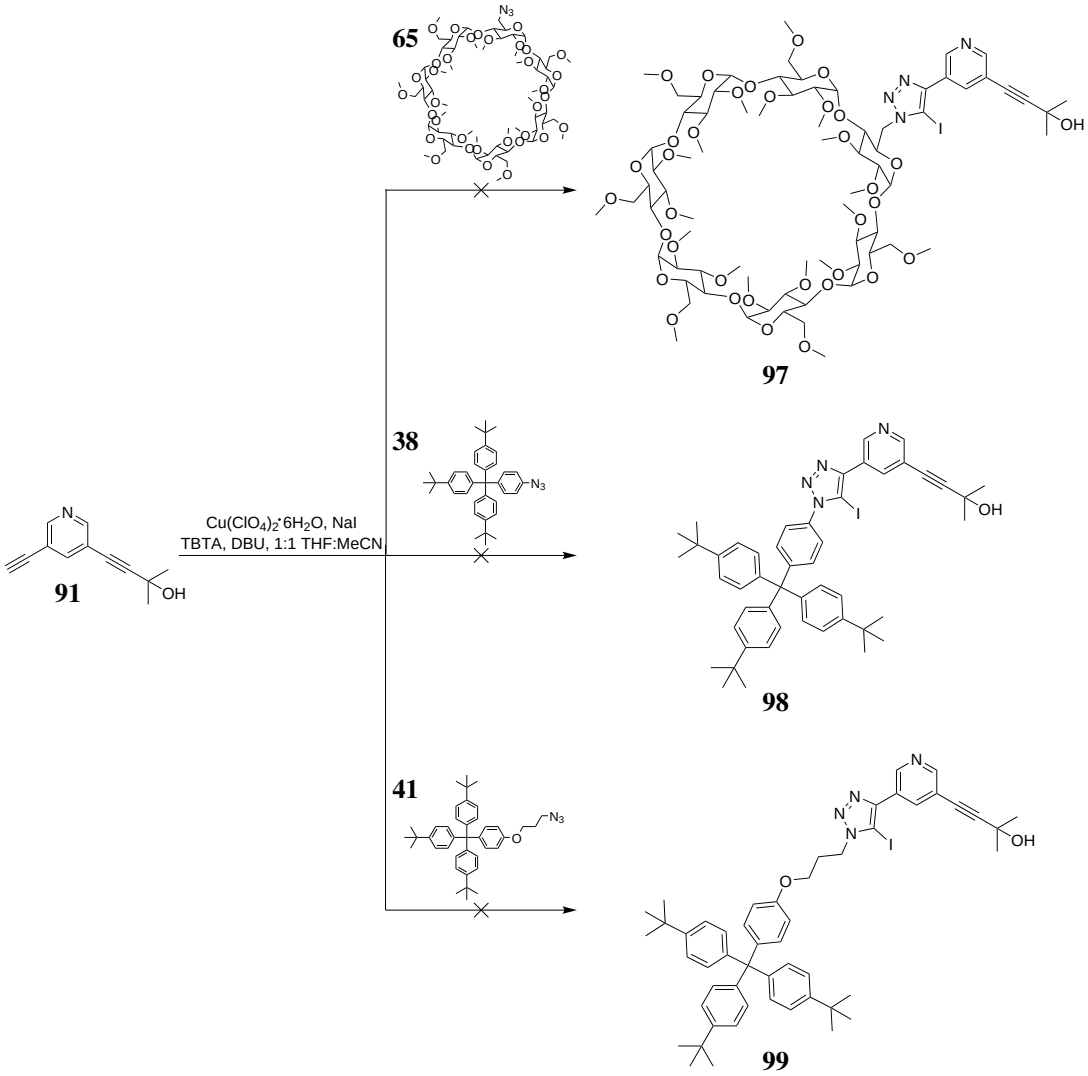
Removal of the trimethylsilyl-protecting group from **94** was achieved with KOH in methanol to afford **91** quantitatively (Scheme 3.2.8). This synthon presented the possibility of building up the axle component from the outside (*i.e.* stoppering, deprotection of the alkyne and joining the two halves together) or from the inside out (*i.e.* joining two pyridyl units together, deprotection of the alkynes and stoppering). Deprotection of the hydroxy-propyl-protected alkyne could then be accomplished using

NaOH in refluxing toluene (*vide supra*). While iodination of **91** to form the iodoalkyne for use in two-pot click reactions was attempted, the desired product **96** could not be isolated (Scheme 3.2.8).



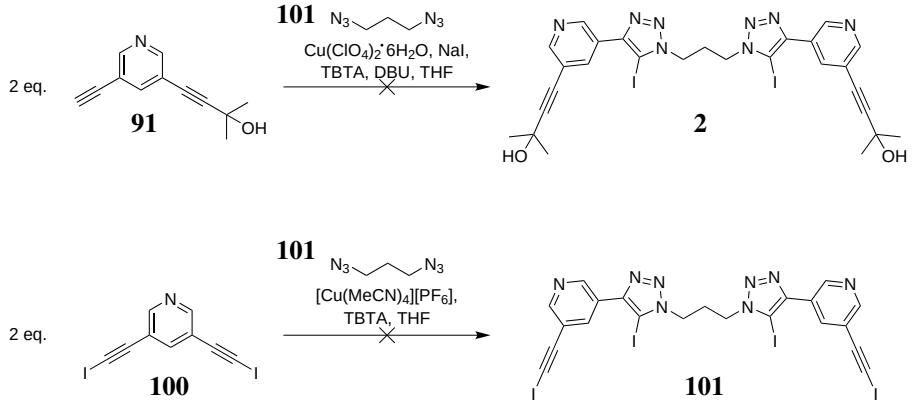
Scheme 3.2.8: Synthetic scheme for the deprotection of **94** to form **91** and the subsequent attempt at iodination of the alkyne to form **96**.

The one-pot click methodology was employed to append suitable stopper units to **91** (Scheme 3.2.9). An initial reaction with permethyl-β-cyclodextrin azide **65** was unsuccessful despite attempts at optimising the reaction: while ESI-MS showed the formation of the desired product **97**, TLC and ^{1}H NMR spectroscopy revealed the formation of an inclusion complex of **91** inside **65** rather than the click product. Consequently, terphenyl stopper units were investigated: terphenyl azide **38** and terphenyl propyl-azide **41**, however, one-pot click reactions to afford **98** and **99**, respectively, were unsuccessful, and only starting materials were recovered after purification.



Scheme 3.2.9: Attempted syntheses to append suitable stopper units to **91** *via* the one-pot click methodology with azides **65**, **38** and **41**.

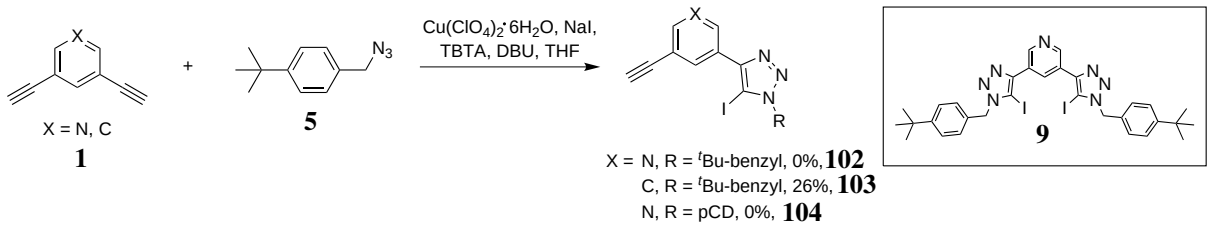
Construction of the axle component from the inside out was investigated *via* reaction of two equivalents of precursor alkyne **91** with bis-azide **50** *via* the one-pot click method to form **100** (Scheme 3.2.10). However, only starting materials were obtained after purification. Moreover, the two-pot click reaction between **2** and **50** to form **101** was similarly unsuccessful.



Scheme 3.2.10: Attempted syntheses to form the axle component from the inside out by joining two equivalents of precursor alkynes with bis-azide **50**.

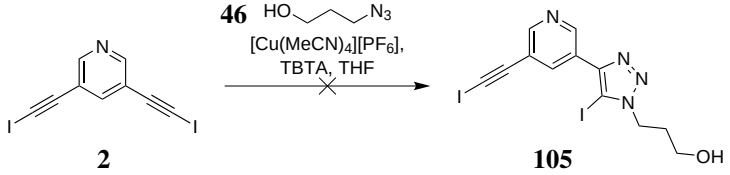
3.3 Axle synthesis *via* statistical methods

Since the route to form the axle components *via* asymmetric alkyne protection–deprotection procedures proved to be problematic, statistical synthetic methodologies were undertaken to prepare key intermediates. A test one-pot click reaction of one equivalent of *tert*-butylbenzyl azide **5** with diethynylpyridine **1** did not produce the desired mono-clicked synthon **102**, rather the disubstituted product **9** and starting material **1** were repeatedly isolated (Scheme 3.3.1). Analogous reaction of **5** and commercially available diethynylbenzene did afford the monosubstituted product **103** in 26% yield, however, repeating the one-pot reaction using permethyl-β-cyclodextrin azide **65** to obtain **104** was unsuccessful affording only the inclusion complex between the alkyne and the azide-appended cyclodextrin.



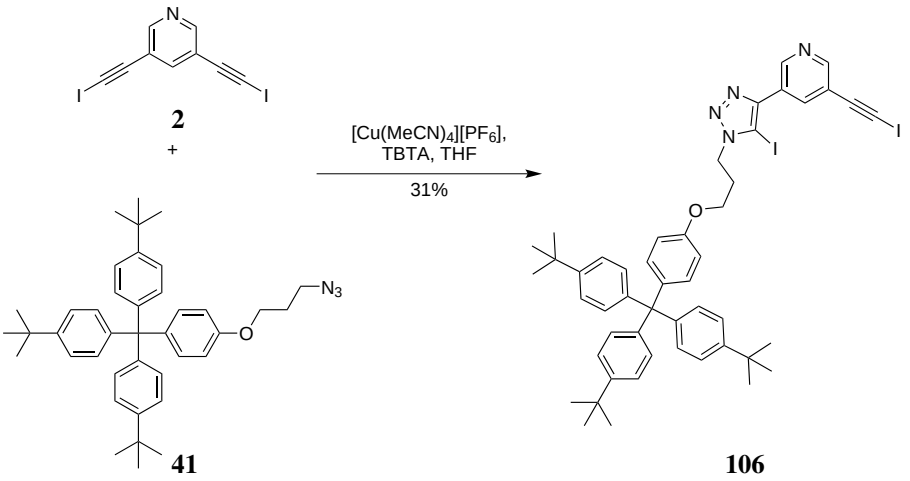
Scheme 3.3.1: Initial test reactions of the one-pot click methodology for the formation of mono-substituted alkynes.

Alternatively, the two-pot method was considered: di-iodoethynyl pyridine **2** was reacted with one equivalent of azido propanol **46** in THF, but no product **105** (Scheme 3.3.2) was isolated.



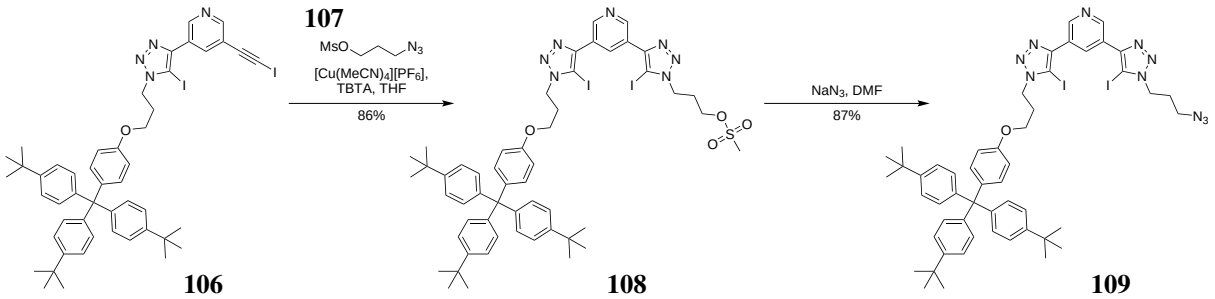
Scheme 3.3.2: Attempted mono-click of di-iodoethynyl pyridine **2** and azido propanol **46** to form monosubstituted pyridine **105**.

The reaction of one equivalent of terphenyl-stopper propyl-azide **41** with **2** did successfully afford **106** in yields of up to 31% (Scheme 3.3.3). This presented the key precursor to the synthesis of an asymmetric axle component.



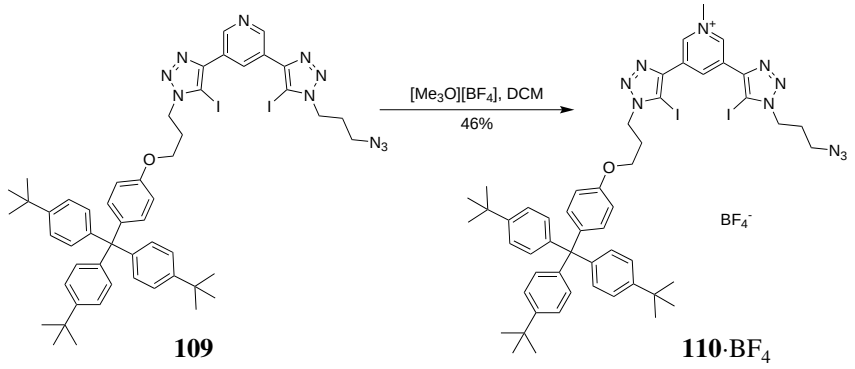
Scheme 3.3.3: Synthesis of the key intermediate in the preparation of an asymmetric axle component: mono-stoppered iodoalkyne pyridine **106**.

Thereafter, **106** was reacted with a large excess of azido-propyl mesylate **107** *via* the two-pot click method to form **108** in yields of up to 86% (Scheme 3.3.4). Subsequent substitution of the mesylate with NaN_3 in DMF at 85 °C produced the corresponding azide **109** in 87% yield.



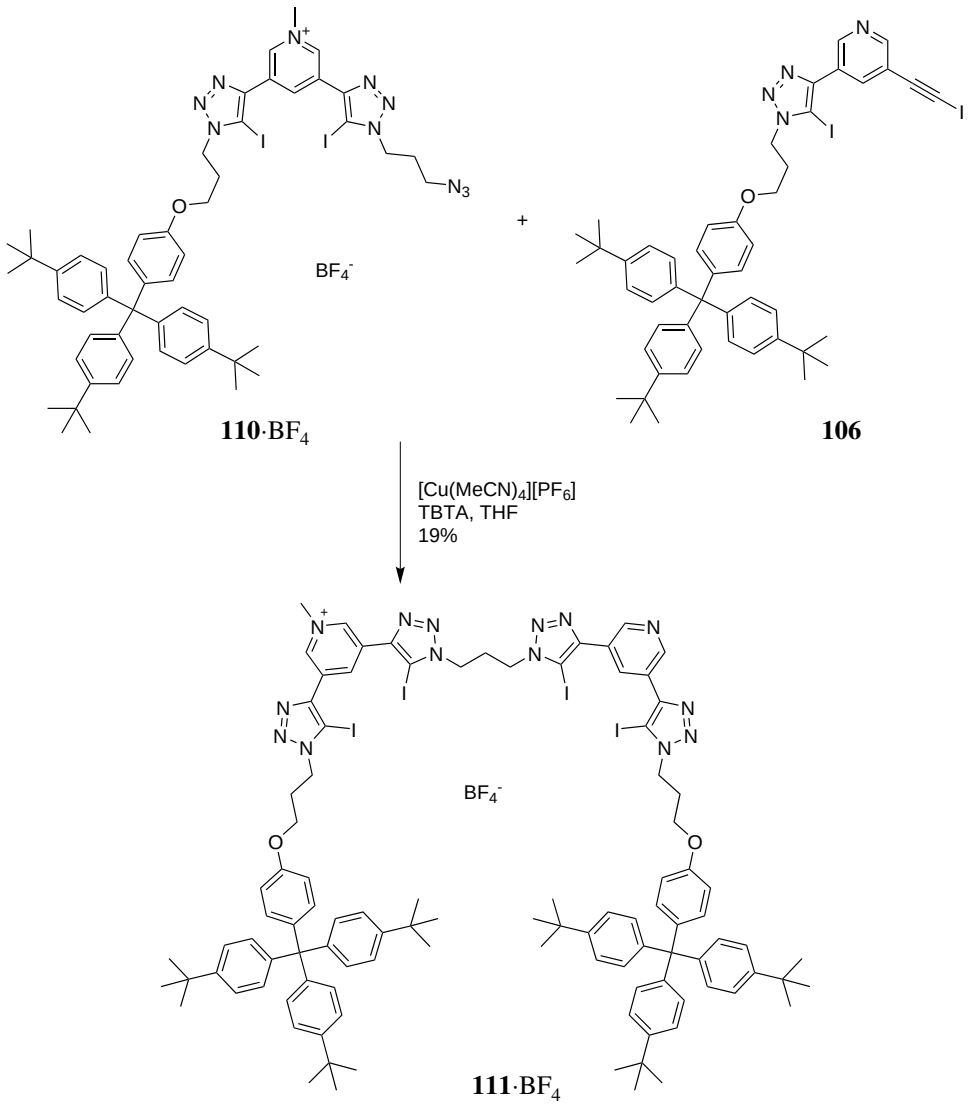
Scheme 3.3.4: Synthesis of asymmetric stoppered 3,5-bis-iodotriazole mesylate **108** and subsequent stoppered 3,5-bis-iodotriazole azide **109**.

Methylation of **109** to form **110**·A was attempted initially using CH_3I, however, this formed a poorly soluble product that degraded upon anion exchange to the chloride salt. Subsequent methylation reactions were conducted using the stronger methylating agent $[Me_3O][BF_4]$ to afford the soluble tetrafluoroborate salt **110**·BF_4 (Scheme 3.3.5). Unfortunately, due to the stronger methylating power of $[Me_3O][BF_4]$, some evidence of methylation of the iodotriazole moieties was observed, resulting in a lower yield of the desired product $\sim$ 46%.



Scheme 3.3.5: Synthesis of cationic asymmetric axle precursor **110**·BF_4.

Synthesis of the asymmetric axle component was attempted using **110**·BF_4 and **106** in THF using catalytic $[Cu(MeCN)_4][PF_6]$ and TBTA, affording the long-awaited axle **111**·BF_4 in low 19% yield (Scheme 3.3.6).



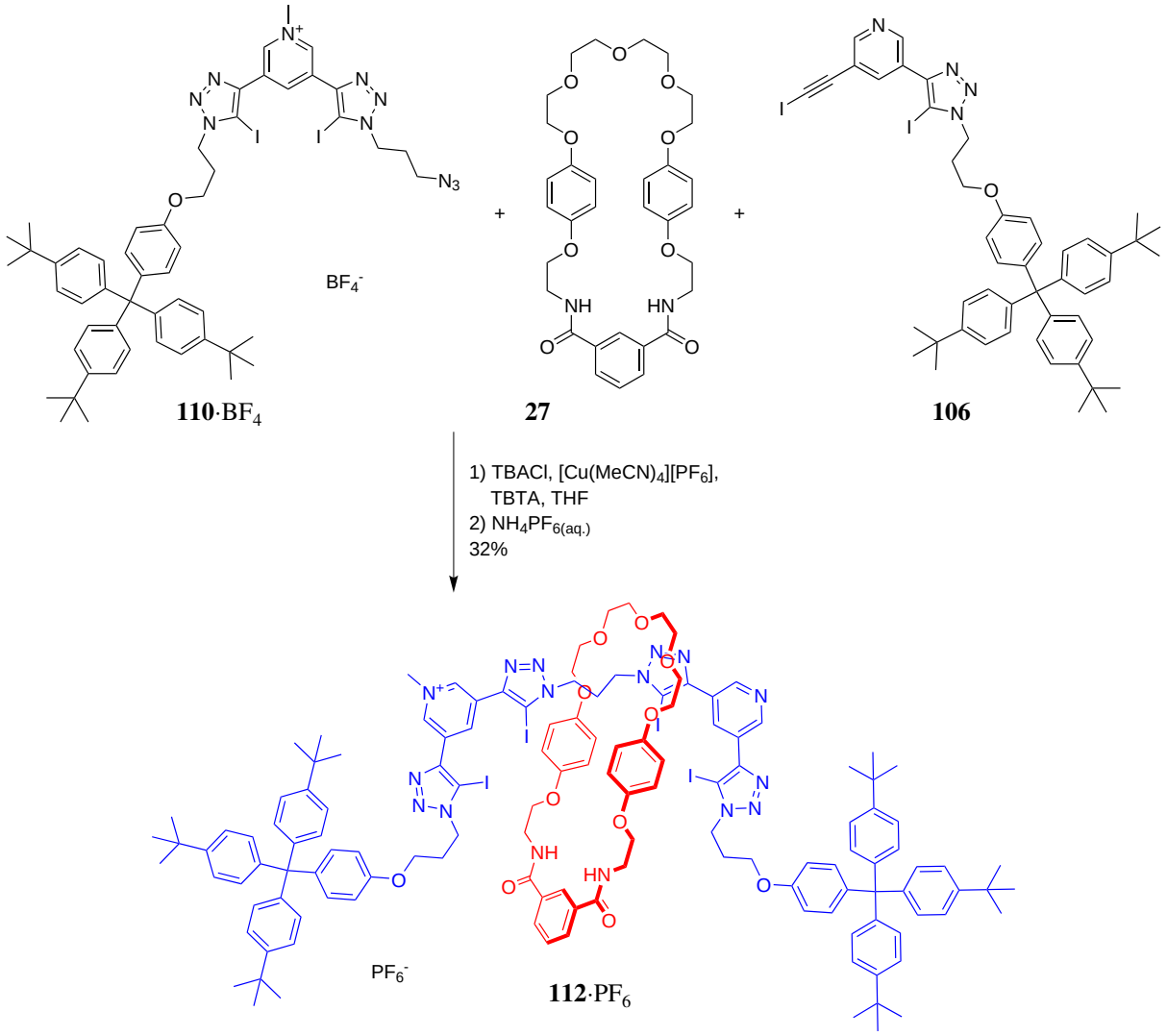
Scheme 3.3.6: Synthesis of the asymmetric axle *via* a two-pot click reaction between **110**·BF_4 and **106**.

3.4 Monocationic and dicationic halogen-bonding [2]rotaxanes

The successful implementation of the two-pot click reaction to form **111**·A suggested that it could be used to form [2]rotaxane structural frameworks *via* a 'stoppering' methodology.

3.4.1 Synthesis

To an equimolar solution of stopper-azide **110**·BF_4, isophthalamide macrocycle **27** and template TBA·Cl in THF were added catalytic $[Cu(MeCN)_4][PF_6]$ and TBTA, followed by the stopper iodoalkyne pyridine **106** (Scheme 3.4.1), and the reaction stirred overnight at room temperature. Purification by preparative thin layer chromatography and anion exchange to the non-coordinating hexafluorophosphate salt, afforded the desired rotaxane **112**·PF_6 in 32% yield.



Scheme 3.4.1: Synthetic scheme for the two-pot click reaction to form the monocationic asymmetric [2]rotaxane **112**·PF_6.

High-resolution ESI mass spectrometry and ^{1}H NMR spectroscopy confirmed the formation of the [2]rotaxane, and further evidence for the interlocked nature of the [2]rotaxane was obtained by 2D ROESY NMR analysis (Figure 3.4.1).

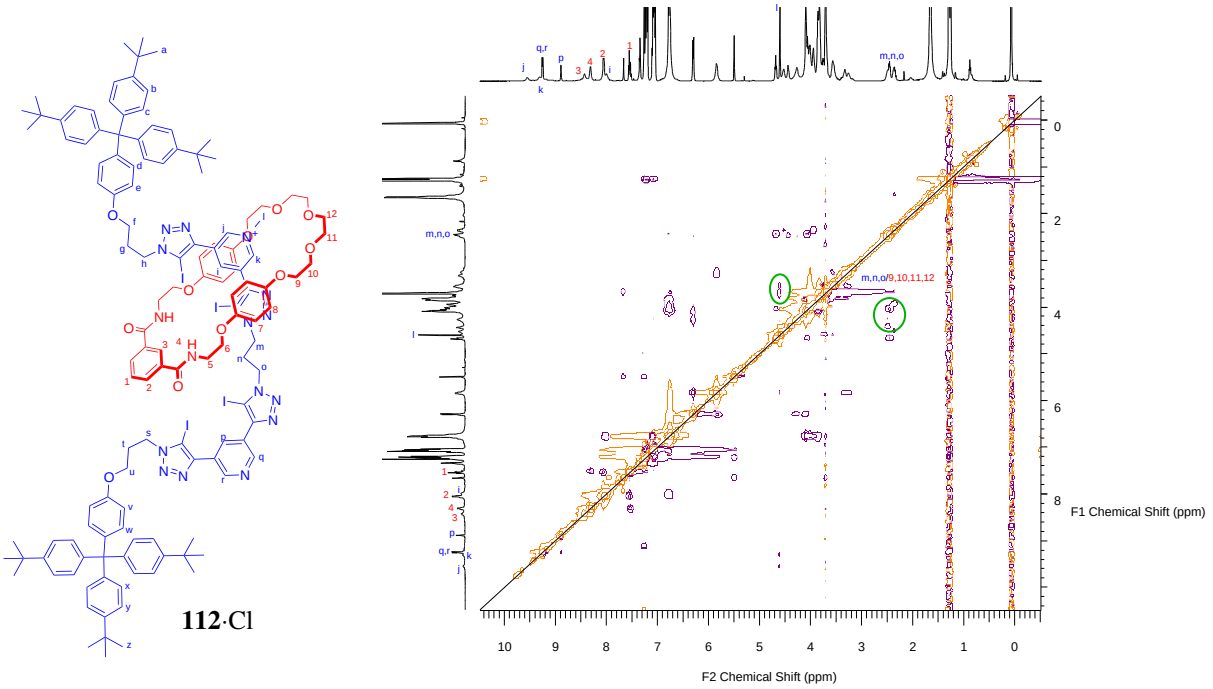
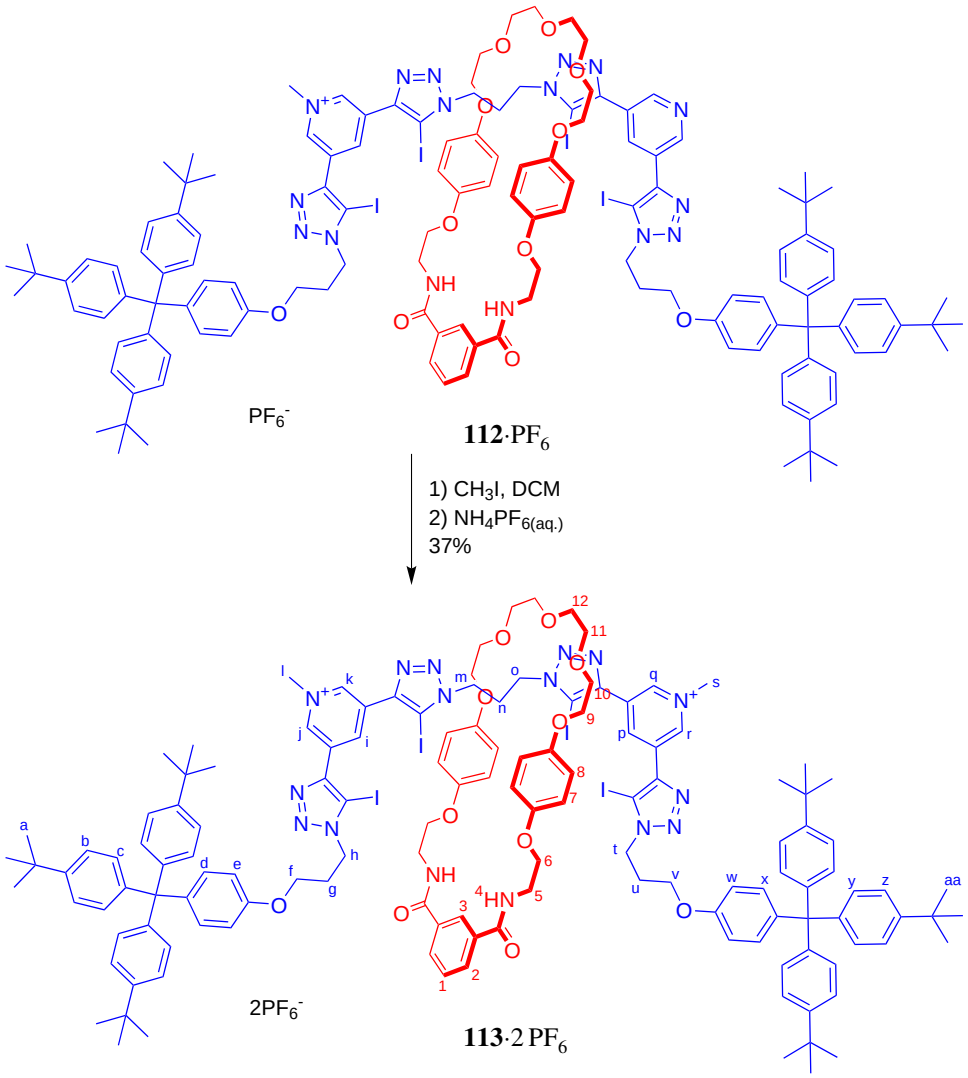


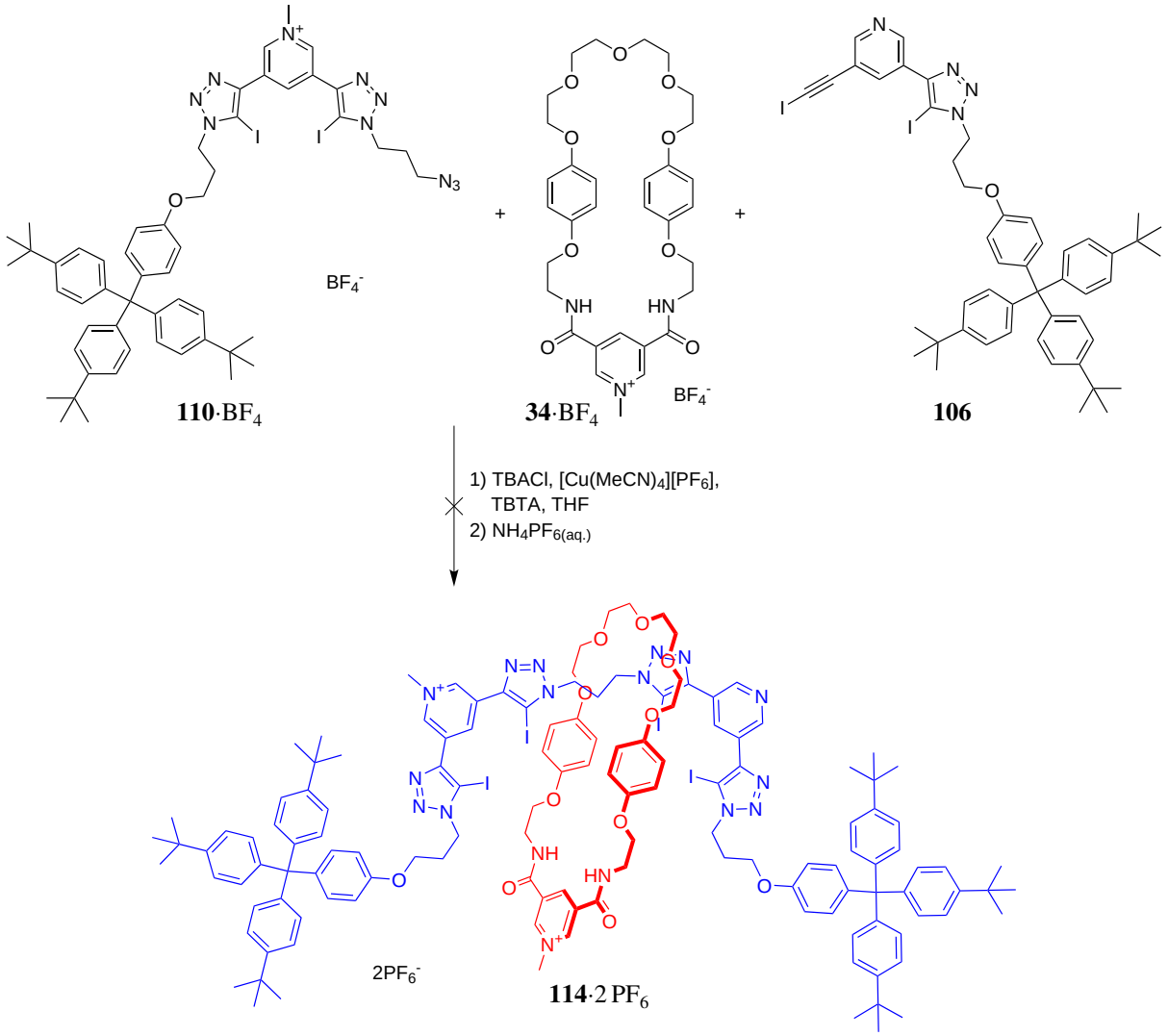
Figure 3.4.1: 2D ROESY NMR spectrum of **112**·Cl showing selected through-space ^{1}H–^{1}H correlations indicative of an interlocked assembly.

Methylation of the monocationic analogue **112**·PF_6 was undertaken using CH_3I to produce a symmetric dicationic [2]rotaxane **113**·2 PF_6 (37%) after anion exchange to the non-coordinating hexafluorophosphate salt (Scheme 3.4.2). The symmetric dicationic [2]rotaxane **113**·2 PF_6 was characterised by ^{1}H NMR spectroscopy and high resolution ESI mass spectrometry.



Scheme 3.4.2: Methylation of monocationic asymmetric [2]rotaxane **112**·PF_6 to form the dicationic symmetric [2]rotaxane **113**·2 PF_6.

The synthesis of an asymmetric dicationic [2]rotaxane was attempted using an analogous chloride-anion templated stoppering methodology: equimolar quantities of azide **110**·BF_4, the pyridinium bis-amide macrocycle **34**·BF_4 and TBA·Cl were mixed in THF (Scheme 3.4.3). Thereafter, catalytic amounts of $[Cu(MeCN)_4][PF_6]$ and TBTA were added, followed by the stopper iodoalkyne pyridine **106**, and the reaction stirred overnight at room temperature. Purification was undertaken by preparative thin layer chromatography but did not afford **114**·2 A; rather, the axle and macrocycle components were isolated.



Scheme 3.4.3: Synthetic scheme for the two-pot click reaction to form the dicationic asymmetric [2]rotaxane **114**·2 PF_6.

3.4.2 ^{1}H NMR anion binding studies

As a consequence of limited quantities of the mono- and di-cationic [2]rotaxanes **112**·PF_6 and **113**·2 PF_6, respectively, anion binding studies were restricted to chloride and nitrate ^{1}H NMR titration experiments. In the case of the monocationic [2]rotaxane **112**·PF_6, a preliminary titration with TBA·NO_3 in 45:45:10 $CDCl_3$:CD_3OD:D_2O showed no binding for nitrate. Consequently, titrations were repeated in 1:1 $CDCl_3$:CD_3OD, and chemical shifts were monitored for the protons *i* and *3*, incumbent on the anion binding cavity of the rotaxane, as well as protons *j* and *k* (Figure 3.4.2a). Analogous titrations for the dicationic [2]rotaxane host **113**·2 PF_6 were conducted in 45:45:10 $CDCl_3$:CD_3OD:D_2O. Upfield chemical shifts were observed for the pyridinium internal (*i* and *p*) and external (*j,k* and *q,r*) protons, whilst a downfield shift was observed for the isophthalamide proton *3*. Figure 3.4.2b shows the downfield shift for proton *j,k* of **113**·2 PF_6 upon addition of anions. WinEQNMR2[437] analysis and Job plot approxima-

tions of the titration data for both [2]rotaxanes **112**·PF_6 and **113**·2 PF_6 determined the 1:1 stoichiometric association constants for Cl^- and NO_3^- (Table 3.4.1), which were determined to be independent of the proton monitored for a given anion.

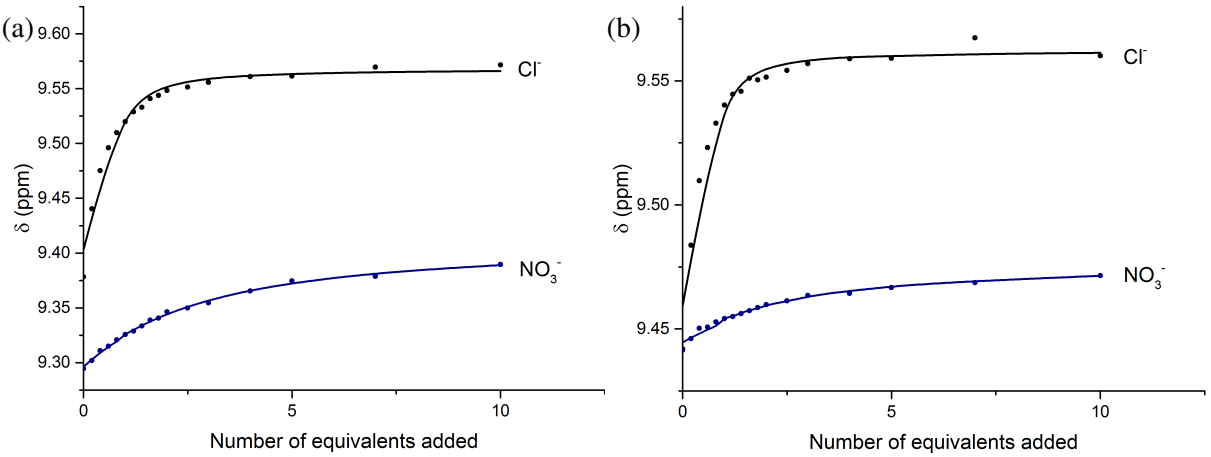


Figure 3.4.2: Anion binding titrations: (a) **112**·PF_6 following pyridinium proton *j* (1:1 $CDCl_3$:CD_3OD), and (b) **113**·2 PF_6 following the external pyridinium protons *j,k* in the aqueous solvent mixture 45:45:10 $CDCl_3$:CD_3OD:D_2O. Experimental titration data (circles) with WinEQNMR2[437] fitted binding isotherms indicated as lines (298 K).

Table 3.4.1: Association constants (K_a)[a] determined for **112**·PF_6 and **113**·2 PF_6 with various TBA·anions.

Anion	K_a (M^{-1})	
	112·PF_6[b]	**113**·2 PF_6[c]
Cl^-	7970(1890)	$> 10^4$
NO_3^-	374(31)	364(38)

[a] Estimated standard errors are given in parentheses. Association constants calculated using WINEQNMR2,[437] [b] 1:1 $CDCl_3$:CD_3OD, [c] 45:45:10 $CDCl_3$:CD_3OD:D_2O (298 K).

The [2]rotaxane **112**·PF_6 shows remarkably strong binding for chloride in 1:1 $CDCl_3$:CD_3OD. Although binding for nitrate is much weaker than chloride by an order of magnitude, indicating chloride selectivity, the [2]rotaxane host displays notable binding for the oxoanion in this competitive solvent mixture. Moreover, this represents the first example of nitrate binding by an interlocked halogen-bonding receptor.

In the highly competitive aqueous mixture, the dicationic [2]rotaxane binds chloride so strongly ($K_a > 10^4$ M^{-1}) that it was not possible to determine an accurate K_a value. The binding for nitrate is approximately two orders of magnitude weaker ($K_a = 360$ M^{-1}), however, considering the challenge that nitrate recognition represents with its low basicity, the relative strength of association in this aqueous mixture is noteworthy. Interestingly, the halogen-bonding [2]rotaxane **113**·2 PF_6 bound nitrate with comparable strength to the previously reported hydrogen-bonding analogue (Figure 3.1.2).[398] Con-

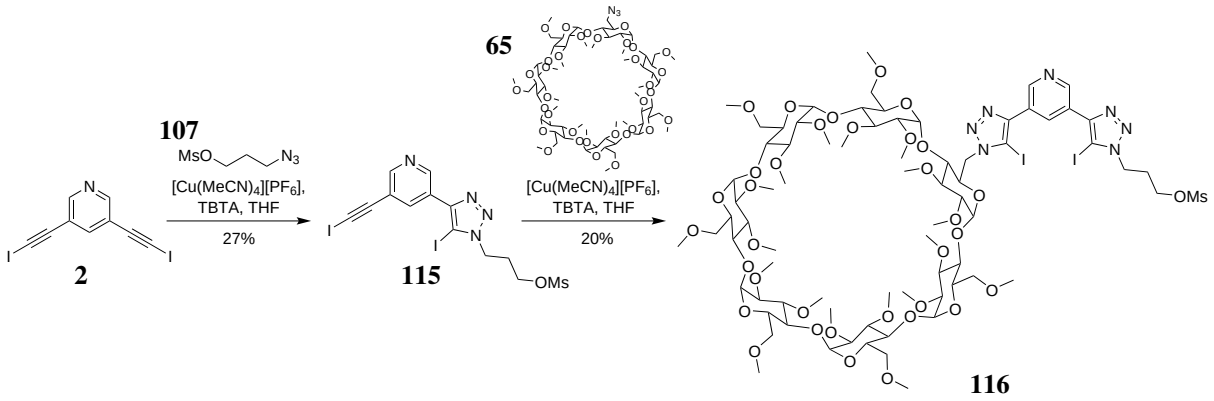
trasting the modest nitrate selectivity of the hydrogen-bonding rotaxane receptor, both halogen-bonding [2]rotaxanes **112**·PF_6 and **113**·2 PF_6 display much stronger binding for chloride than nitrate.

3.5 A water-soluble rotaxane

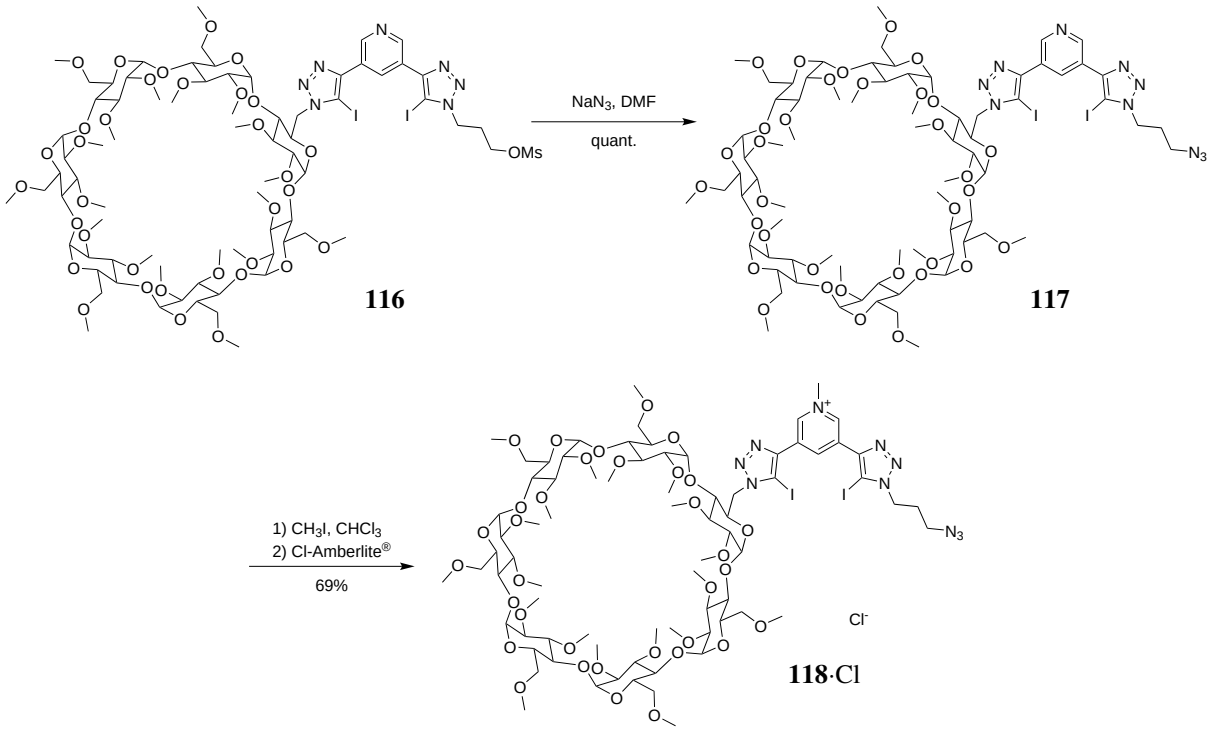
Encouraged by the strong binding of chloride and nitrate by the dicationic [2]rotaxane **113**·2 PF_6, the synthesis of a water-soluble halogen-bonding analogue was undertaken using permethyl-β-cyclodextrin stoppers.

3.5.1 Synthesis

Considering the challenges experienced in the synthesis of monosubstituted β-cyclodextrin-pyridine derivatives (*vide supra*), the statistical reaction to form a monosubstituted pyridine precursor was initially undertaken by the reaction of one equivalent of azido-propyl mesylate **107** with di-iodoethynyl pyridine **2** to afford **115** in 27% (Scheme 3.5.1). The CuAAC click reaction of permethyl-β-cyclodextrin azide **65** with **115** gave the cyclodextrin-appended 3,5-bis-iodotriazole pyridine propyl mesylate **116**, which was converted to the azide with NaN_3 by heating in DMF to afford **117** quantitatively (Scheme 3.5.2). Methylation with CH_3I afforded **118**·I and anion-exchange to the chloride salt **118**·Cl was achieved using a chloride-loaded Amberlite® column (Scheme 3.5.2).

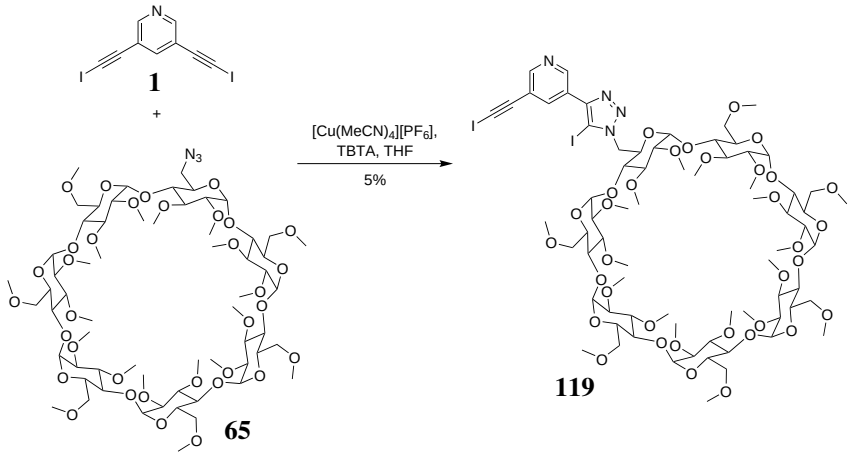


Scheme 3.5.1: Synthetic route towards the preparation of a cyclodextrin-appended asymmetric axle precursor *via* the monosubstituted pyridine-iodoalkyne **115** and the permethyl-β-cyclodextrin-appended bis-iodotriazole pyridine mesylate **116**.



Scheme 3.5.2: Synthesis of the asymmetric cyclodextrin-appended bis-iodotriazole azide **117**, and subsequent methylation and anion exchange to **118**·Cl.

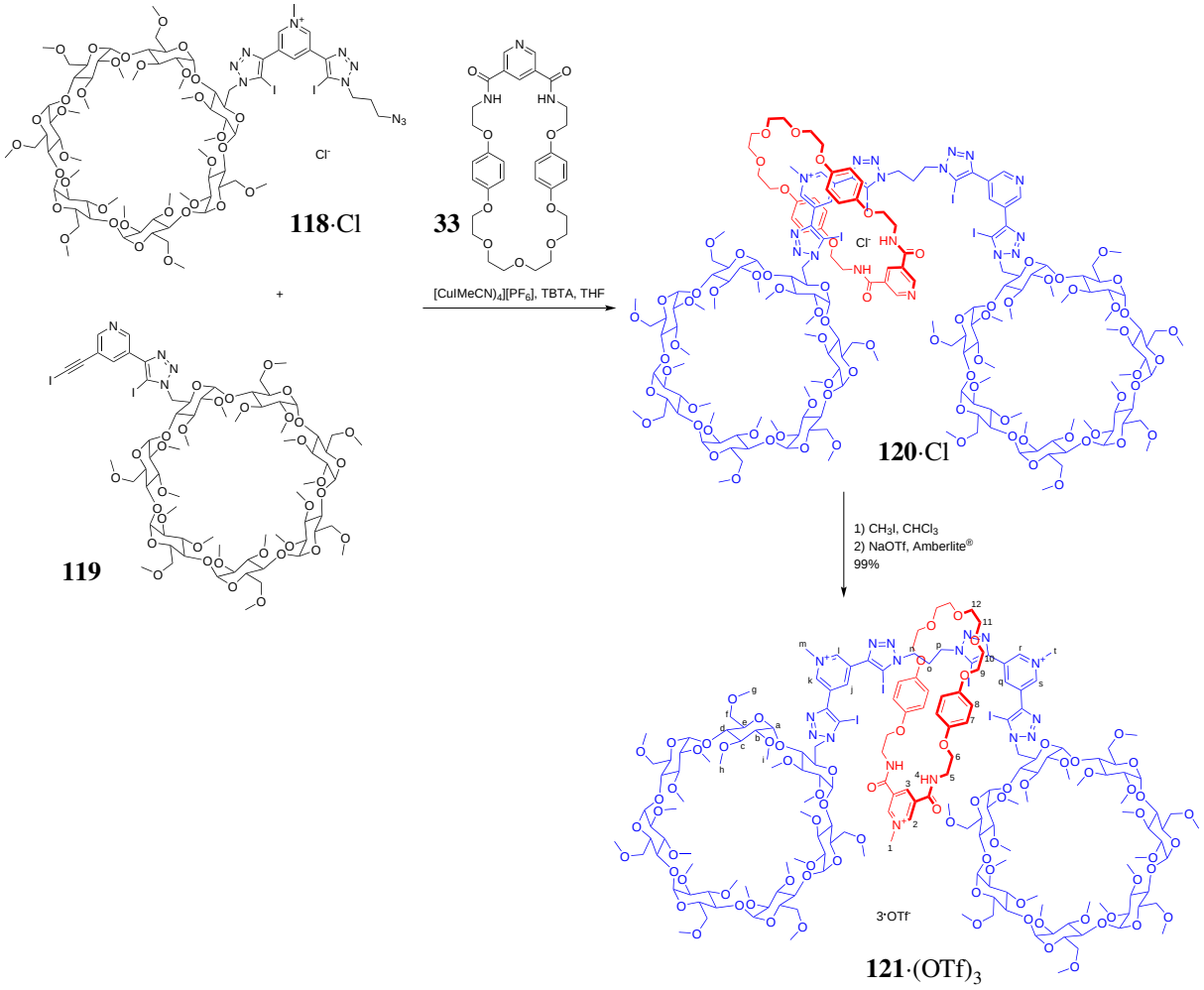
After many attempts at the statistical two-pot click reaction between one equivalent of permethyl-β-cyclodextrin azide **65** and di-iodoethynyl pyridine **2**, a 5% yield of the monosubstituted cyclodextrin-appended iodoethynyl pyridine **119** was obtained, allowing an attempt at the synthesis of a cyclodextrin-appended [2]rotaxane (Scheme 3.5.3).



Scheme 3.5.3: Two-pot synthetic scheme to prepare the monosubstituted cyclodextrin-appended iodo-ethynyl pyridine **119**.

The water-soluble cyclodextrin-appended [2]rotaxane **120**·Cl was prepared by mixing an equimolar solution of the cyclodextrin-appended bis-iodotriazole pyridinium azide **118**·Cl with macrocycle **33** in THF for 30 minutes to form the interpenetrated pseudorotaxane intermediate (Scheme 3.5.4). Cat-

alytic $[Cu(MeCN)_4][PF_6]$ and TBTA were added thereafter, followed by **119**. The [2]rotaxane **120**·Cl was obtained after preparative thin layer chromatography. Methylation with excess CH_3I and anion-exchange to the non-coordinating triflate salt was achieved by passing a solution of **120**·Cl through a triflate-loaded Amberlite® column, affording the tricationic [2]rotaxane **121**·$(OTf)_3$ in 9% yield over three steps. Triflate was chosen as the counteranion since it would aid the solubility of the rotaxane in water without competing for the anion binding site due to its incompatible geometry and high hydration enthalpy ($\Delta H_{hyd} > 460$ kJ mol^{-1}).[475] The [2]rotaxane was characterised by ^{1}H and ^{13}C NMR spectroscopy and high resolution mass spectrometry.



Scheme 3.5.4: Synthesis of the permethyl-β-cyclodextrin-appended asymmetric monocationic and symmetric dicationic [2]rotaxanes, **120**·Cl and **121**·$(OTf)_3$, respectively.

3.5.2 ^{1}H NMR anion binding studies

^{1}H NMR titration experiments were restricted to chloride and nitrate anions as their sodium salts as a result of limited quantities of the tricationic [2]rotaxane **121**·$(OTf)_3$. Since the receptor was only partially soluble in pure water, the anion binding studies were conducted in 9:1 D_2O:acetone-d_6. Upon

addition of chloride, noteworthy downfield shifts were observed for the various pyridinium protons (*j, k , l, 2* and *4*), whilst proton *3* shifted upfield (Figure 3.5.1). In contrast, modest upfield shifts were detected for all pyridinium protons upon addition of nitrate to the interlocked host **121**·$(OTf)_3$. Job plot approximations and WinEQNMR2[437] analysis of the titration data determined the 1:1 stoichiometric association constants for Cl^- and NO_3^- (Table 3.5.1).

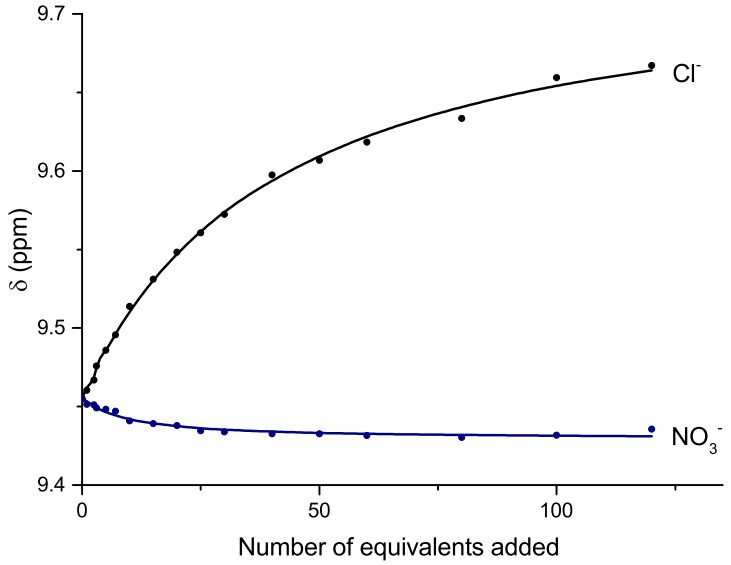


Figure 3.5.1: Anion binding titration data for **121**·$(OTf)_3$ following pyridinium proton *j*. Experimental titration data (circles) with WinEQNMR2[437] fitted binding isotherms indicated as lines (9:1 D_2O:acetone-d_6, 298 K).

Table 3.5.1: Association constants $(K_a)^{[a]}$ determined for **121**·$(OTf)_3$ with various Na·anions.

Anion	K_a (M^{-1})
Cl^-	112(16)
NO_3^-	114(4)

[a] Estimated standard errors are given in parentheses. Association constants calculated using WINEQNMR2,[437] (9:1 D_2O:acetone-d_6, 298 K).

The tricationic [2]rotaxane **121**·$(OTf)_3$ binds both chloride and nitrate in competitive aqueous 9:1 D_2O:acetone-d_6 with equal strength: $K_a(Cl^-) = 112(16)$ and $K_a(NO_3^-) = 114(4)$ M^{-1}. The incorporation of additional positive charge makes the [2]rotaxane capable of recognising both anions in 90% water, and results in enhanced anion binding ability when compared to the [2]rotaxanes discussed earlier in this Chapter. Although the anion binding cavity is evidently complementary towards the trigonal geometry of nitrate, it does not preclude the binding of the spherical halide anion. Presumably, a more rigid axle component joining the two bis-iodotriazole pyridinium groups would preorganise the host more and improve the selectivity for nitrate over chloride (and other halide anions). Nonetheless, whilst the receptor shows no selectivity between chloride and nitrate, increasing the percentage of water from 10%

to 90% appears to have a much greater influence upon chloride anion binding than the nitrate oxoanion, which reflects the higher hydration enthalpy of chloride ($\Delta H_{hyd}(\text{Cl}^-) = -381$ kJ mol^{-1} vs $\Delta H_{hyd}(\text{NO}_3^-) = -314$ kJ mol^{-1}).[464,476] Indeed, the relatively strong binding of nitrate in this aqueous mixture presents an important step towards nitrate recognition in pure water.

3.6 Conclusion and future work

Conclusion

This chapter aimed to produce a [2]rotaxane comprised of an isophthalamide macrocycle and an axle component containing two 3,5-bis-iodotriazole pyridine or pyridinium units for nitrate recognition. While asymmetric synthetic methods were initially investigated to prepare the axle component, these were unsuccessful owing to sensitivity of the iodotriazole group in the presence of fluoride. The use of statistical synthetic methods ultimately led to the successful preparation of a monocationic asymmetric [2]rotaxane **112**·PF_6 which showed high affinity for chloride ($K_a = 7970$ M^{-1}) in 1:1 $CDCl_3$:CD_3OD. As hoped, the [2]rotaxane also binds nitrate ($K_a = 374$ M^{-1}), although the association is much weaker than chloride.

Increasing the positive electrostatic charge by methylating the monocationic [2]rotaxane to form the dicationic [2]rotaxane **113**·2 PF_6 allowed for anion recognition in the aqueous solvent mixture 45:45:10 $CDCl_3$:CD_3OD:D_2O. Similarly, it was found to bind chloride very strongly ($K_a > 10^4$ M^{-1}) in this solvent mixture with weaker binding observed for nitrate ($K_a = 364$ M^{-1}).

Finally, a tricationic water-soluble halogen-bonding [2]rotaxane **121**·$(OTf)_3$ was synthesised using similar statistical synthetic methods with permethyl-β-cyclodextrin stopper units. Titration experiments conducted in 9:1 D_2O:acetone-d_6 revealed that chloride and nitrate are bound with equal strength ($\sim$ 110 M^{-1}). The [2]rotaxane **121**·$(OTf)_3$ displays improved anion binding strength over the mono- and di-cationic [2]rotaxanes **112**·PF_6 and **113**·2 PF_6, respectively, owing to the incorporation of additional positive charge. Furthermore, increasing the solvent water percentage from 10% to 90% has a greater effect upon the binding of chloride than the oxoanion, and correlates with their relative energies of hydration. Whilst the trigonal design of the anion binding site complements the geometry of nitrate, it is still able to accommodate the spherical chloride anion owing to flexibility in the axle component.

The [2]rotaxanes discussed in this Chapter represent the first examples of halogen bonding receptors capable of nitrate binding. Furthermore, the tricationic [2]rotaxane **121**·$(OTf)_3$ illustrates the potential anion binding ability of halogen-bonding receptors for anion recognition in pure water.

Future work

The work in this chapter could be expanded by synthesising an asymmetric mixed hydrogen- and halogen-bonding axle component to determine the influence that would have on the binding of nitrate in aqueous media. The use of more rigid spacer units between the two 3,5-bis-iodotriazole pyridinium groups may preorganise the host and reverse the selectivity of spherical halides in favour of the trigonal nitrate anion, and the synthesis of such axle components could be investigated.

Recent developments in the Beer group have shown that active-metal templation can advantageously assist in the synthesis of mechanically interlocked host structural frameworks that otherwise present significant synthetic challenges. To that end, the asymmetric-stoppered azide half-axle components present very interesting synthons which could lead to the preparation of previously unattainable interlocked target structures.

Chapter 4

The 3,5-bis-iodotriazole pyridine-*N*-oxide motif

4.1 Introduction

The use of electrostatic enhancement for anion binding and recognition has been widely exploited in the design of receptors. The obvious choice is the incorporation of positive charge into the host receptor, however, these receptors then become associated with counter-anions that may compete for the anion binding site. The use of non-coordinating anions is prevalent in these systems in order to minimise competition. Schmidtchen showed that substitution of the ammonium methyl-substituents with aryl-carboxylates or borates, to produce zwitterionic host systems (Figure 4.1.1), resulted in a large increase in halide binding strength in aqueous media.[477–479]

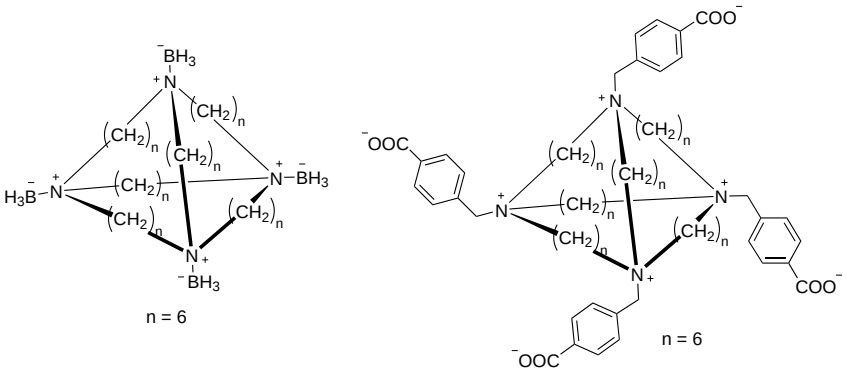


Figure 4.1.1: Figure showing Schmidtchen's zwitterionic anion host systems.[139,477–479]

Recently, the pyridine-*N*-oxide zwitterionic motif has been exploited in the assembly of pseudorotaxanes and rotaxanes. Ballester has used the combination of anion templation and pyrrole–pyridine-*N*-oxide hydrogen bonding in the formation of a [2]pseudorotaxane between a ditopic bis-calix[4]pyrrole-functionalised macrocycle and a pyridine-*N*-oxide threading component in the presence of polyatomic anions (cyanate, azide) in chloroform.[480] The most effective anion templates for pseudorotaxane assembly were found to be the linear thiocyanate and azide anions (Figure 4.1.2).

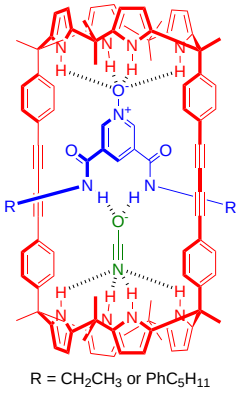


Figure 4.1.2: Figure showing Ballester's pyridine-*N*-oxide-containing [2]pseudorotaxane templated by cyanate.[480]

Similarly, the threading of a pyridine-*N*-oxide component with an isophthalamide-containing macrocycle in chloroform results in [2]pseudorotaxane formation (Figure 4.1.3). Manipulation of the pH affords reversible control of the interpenetration process: acidification with TFA results in the protonation of the *N*-oxide moiety and the disassembly of the [2]pseudorotaxane, whilst subsequent addition of base (triethylamine) reverses the process.

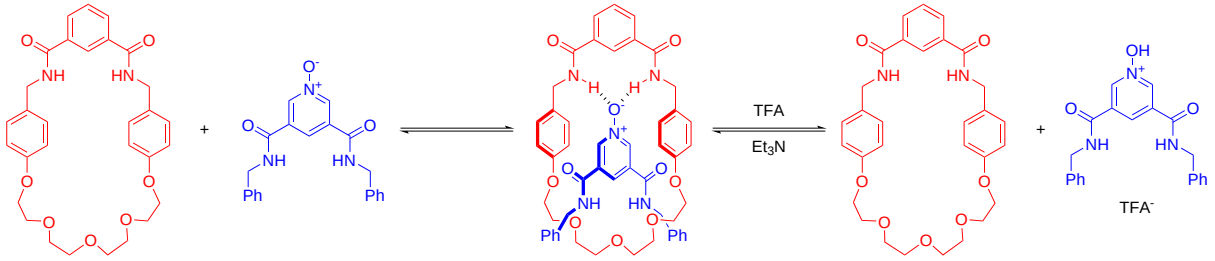


Figure 4.1.3: Jiang's pseudorotaxane assembly with pH-switchable threading capability between a pyridine-*N*-oxide threading species and an isophthalamide macrocycle.[372]

The assembly and disassembly of a pyridine-*N*-oxide–isophthalamide macrocycle [2]pseudorotaxane can also be manipulated *via* the addition of anions (Figure 4.1.4).[481] The interpenetrated structure is stabilised by amide N–H···pyridine-*N*-oxide hydrogen bonds and aromatic donor–acceptor interactions. However, upon addition of chloride a conformational change in the pyridine-*N*-oxide-imidazolium threading component was induced, causing the [2]pseudorotaxane to disassemble.

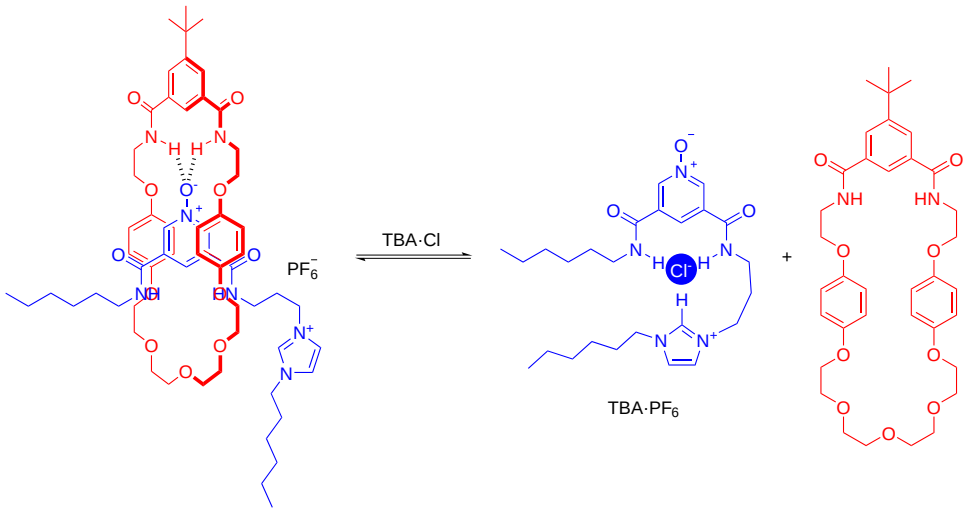


Figure 4.1.4: The formation of an interpenetrated assembly with a pyridine-*N*-oxide thread and an isophthalamide macrocycle, with dethreading induced by chloride.[481]

Sodium and barium cation templation has been used to construct a pyridine-*N*-oxide axle-containing rotaxane which displays cation-induced pirouetting molecular motion in chloroform solution (Figure 4.1.5a).[482] Lanthanide metal cations template the formation of a [2]rotaxane *via* coordination of the pyridine-*N*-oxide to the vacant coordination site of a cyclen-complexed lanthanide (Figure 4.1.5b).[483]

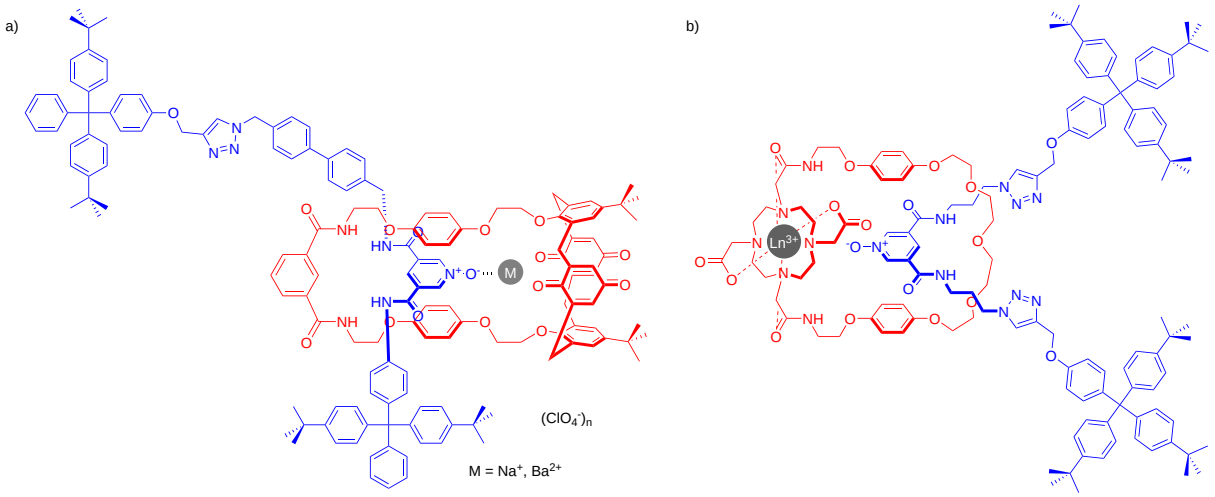


Figure 4.1.5: Figure showing *N*-oxide-containing [2]rotaxanes: a) alkali metal-templated [2]rotaxane displaying cation-induced pirouetting molecular motion,[482] and b) lanthanide-containing [2]rotaxane.[483]

Beer and co-workers prepared ditopic bis-isophthalamide-containing macrocycles capable of the simultaneous recognition of an anion and pyridine-*N*-oxide motif where an anion may template [2]rotaxane formation *via* stoppering a pyridine-*N*-oxide-containing thread. This led to the preparation of a series of [2]rotaxanes (Figure 4.1.6) which showed considerable anion binding strength for halides in competitive aqueous 10:45:45 D_2O:$CDCl_3$:CD_3OD solution. Moreover, the incorporation of positive charge *via* a pyridinium group further enhanced the anion binding properties of the [2]rotaxane.[484,485]

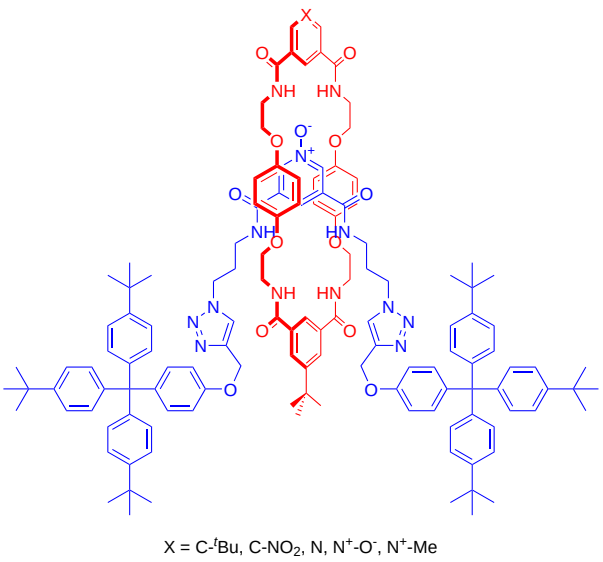


Figure 4.1.6: Figure showing *N*-oxide-containing neutral[484] and cationic [2]rotaxanes for anion recognition.[485]

4.1.1 Chapter aims

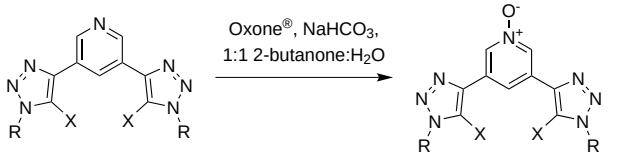
This chapter will focus on the synthesis of halogen-bonding 3,5-bis-iodotriazole pyridine-*N*-oxide derivatives; specifically, acyclic receptors and their anion recognition properties, followed by the incorporation of this motif into [2]rotaxane host frameworks.

4.2 Acyclic receptors

Based on the strong anion binding properties of the halogen-bonding 3,5-bis-iodotriazole pyridinium motif, the synthesis of a neutral analogue capable of similar anion binding affinity was desirable, since neutral zwitterionic derivatives have shown improved anion binding properties in pure water (Figure 4.1.1). In the case of the 3,5-bis-iodotriazole pyridinium motif, the simplest neutral counterpart is the 3,5-bis-iodotriazole pyridine-*N*-oxide motif. Consequently, the investigation into this synthon began with the synthesis of acyclic host systems and studying their anion binding properties before integrating the motif into interlocked structural frameworks.

4.2.1 Synthesis

The synthesis of acyclic receptors containing the 3,5-bis-iodotriazole pyridine-*N*-oxide motif simply involved oxidation of various hydrogen- and halogen-bonding precursor molecules described previously in this thesis (Section 2.2). For example, quantitative formation of bis-octyl-appended bis-iodotriazole pyridine-*N*-oxide **124** was achieved *via* oxidation of **8** with Oxone® (Scheme 4.2.1). The bis-*tert*-butylbenzyl-appended analogue **125** was similarly prepared by oxidation of **9**. For comparison, hydrogen-bonding pyridine-*N*-oxide derivative **123** was also prepared.



X = H, R = hexyl **122**
X = I, R = octyl **8**
X = I, R = ^{t}Bu-benzyl **9**

X = H, R = hexyl **123**
X = I, R = octyl **124**
X = I, R = ^{t}Bu-benzyl **125**

Scheme 4.2.1: Synthesis of acyclic bis-proto- and iodo-triazole pyridine-*N*-oxide receptors.

4.2.2 ^{1}H NMR anion binding studies

The anion recognition properties of neutral *N*-oxide receptor **124** were studied by ^{1}H NMR titration experiments. The halogen-bonding receptor **124** was initially titrated with chloride in competitive 1:1

$CDCl_3$:CD_3OD, however, no binding was observed. The solvent mixture 9:1 $CDCl_3$:CD_3OD gave a 1:1 stoichiometric association constant of $K_a(Cl^-) = 111$ M^{-1}. Subsequent titrations were conducted in this solvent mixture affording the binding isotherms shown in Figure 4.2.1, and approximate Job plots combined with WinEQNMR2[437] analysis determined the 1:1 stoichiometric association constants shown in Table 4.2.1.

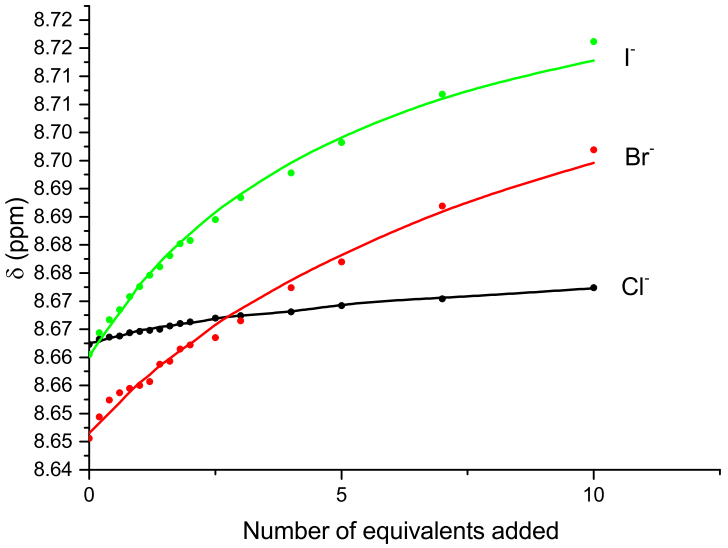


Figure 4.2.1: Anion binding titrations with **124** following the internal pyridine-*N*-oxide proton *i* in the solvent mixture 9:1 $CDCl_3$:CD_3OD: experimental titration data (circles) with WinEQNMR2[437] fitted binding isotherms indicated as lines (298 K).

Table 4.2.1: Association constants (K_a)[a] determined for various TBA·anions with acyclic 3,5-bis-iodotriazole pyridine-*N*-oxide receptor **124**.

Anion	K_a (M^{-1})	
	124[b]	**123**[c]
Cl^-	111(55)	90(6)
Br^-	81(3)	–[e]
I^-	215(22)	–[e]
NO_3^-	–[d]	–[e]
OAc^-	–[d]	–[e]
$H_2PO_4^-$	–[d]	–[e]
SO_4^{2-}	–[d]	–[e]

[a]Estimated standard errors are given in parentheses. Association constants calculated using WINEQNMR2,[437] [b]9:1 $CDCl_3$:CD_3OD, 298 K, [c]Acetone-d_6, 298 K, [d]No binding, [e]Anion not titrated.

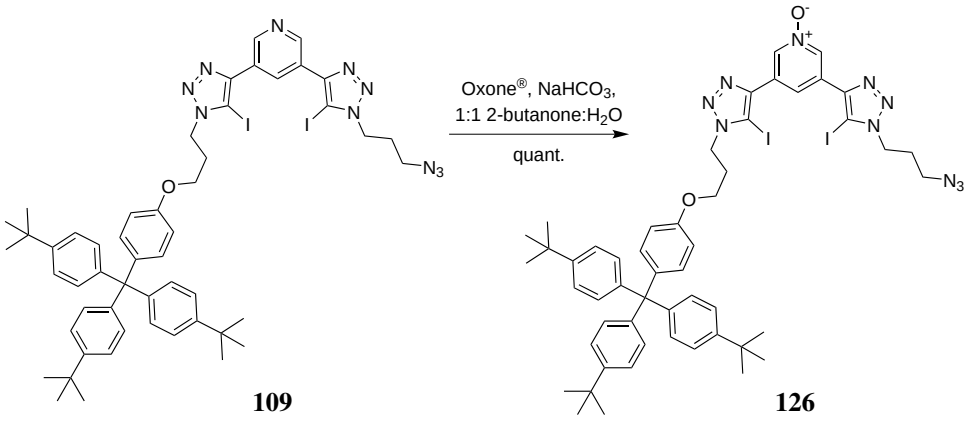
The neutral halogen-bonding pyridine-*N*-oxide receptor **124** shows selectivity for halides over the oxoanions which are not bound. There is modest selectivity between the halides with the strongest binding for iodide ($K_a = 215$ M^{-1}). In contrast, the hydrogen-bonding analogue bound chloride much more weakly in acetone-d_6 ($K_a = 90$ M^{-1}). Notably, the neutral halogen-bonding host **124** binds anions more weakly than the pyridinium analogue **13**·PF_6, discussed in Section 2.2.

4.3 [2]Rotaxane host systems

Following the successful binding of nitrate by the positively-charged asymmetric and symmetric halogen-bonding [2]rotaxanes described in Chapter 3, the synthesis of an analogous neutral halogen-bonding pyridine-*N*-oxide [2]rotaxane was undertaken.

4.3.1 Synthesis of axle precursors

Since the design of the target neutral [2]rotaxane was analogous to the asymmetric monocationic [2]rotaxane **112**·PF_6, the synthesis of precursors for the neutral host system conveniently drew on previously prepared organic synthons. The terphenyl stopper-appended bis-iodotriazole pyridine azide **109**, upon oxidation with Oxone®, gave pyridine-*N*-oxide axle precursor **126** quantitatively (Scheme 4.3.1).



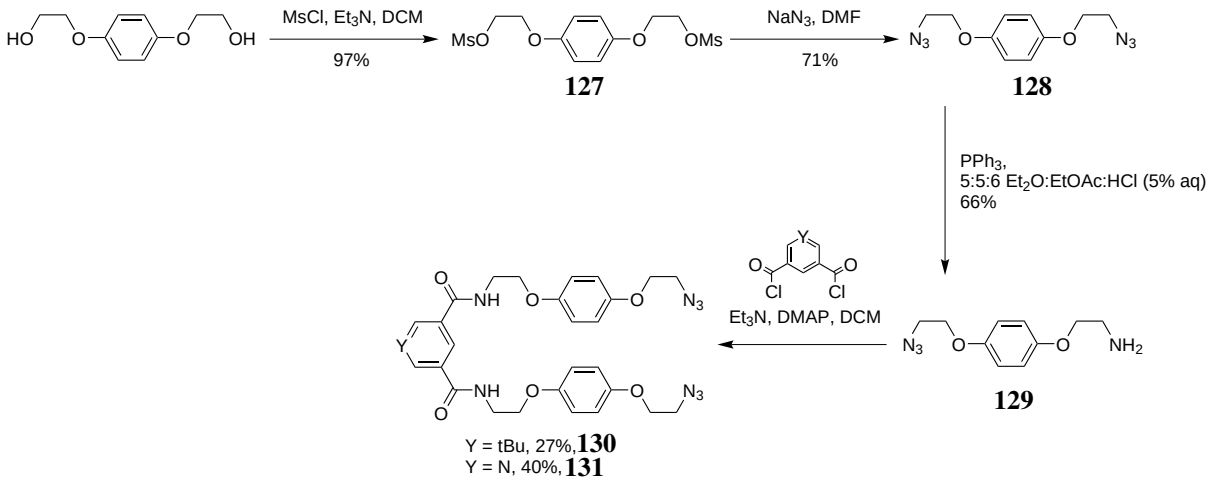
109 **126**

Scheme 4.3.1: Synthesis of the 3,5-bis-iodotriazole pyridine-*N*-oxide half-axle **126**.

4.3.2 Synthesis of macrocyclic components

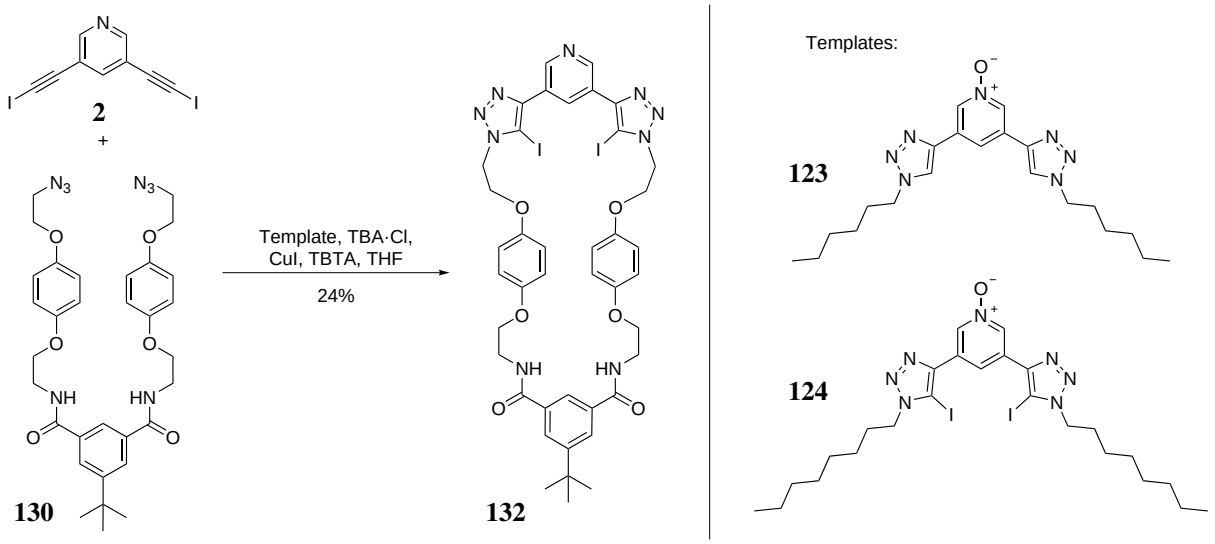
Ditopic macrocycles were prepared that contained both an anion binding site and a recognition site containing complementary interactions to accommodate the pyridine-*N*-oxide moiety, affording greater stability and preorganisation to the interlocked host structure.

The macrocycle components were prepared by mesylation of hydroquinone bis-(2-hydroxyethyl)-ether to form the bis-mesylate **127** in 91% yield (Scheme 4.3.2).[484,485] The mesylate groups were substituted *via* a S_N2 reaction with NaN_3 in DMF to afford the bis-azide **128** in 71% yield. Thereafter, selective mono-reduction of the azide groups *via* a Staudinger reaction afforded the primary amine **129** in 66% yield. Bis-azide appended macrocycle precursors **130** and **131** were obtained from the amide condensation reaction of two equivalents of the mono-amine **129** with either freshly prepared 5-*tert*-butylisophthalyl dichloride or pyridine-3,5-diacid chloride in reasonable yields.



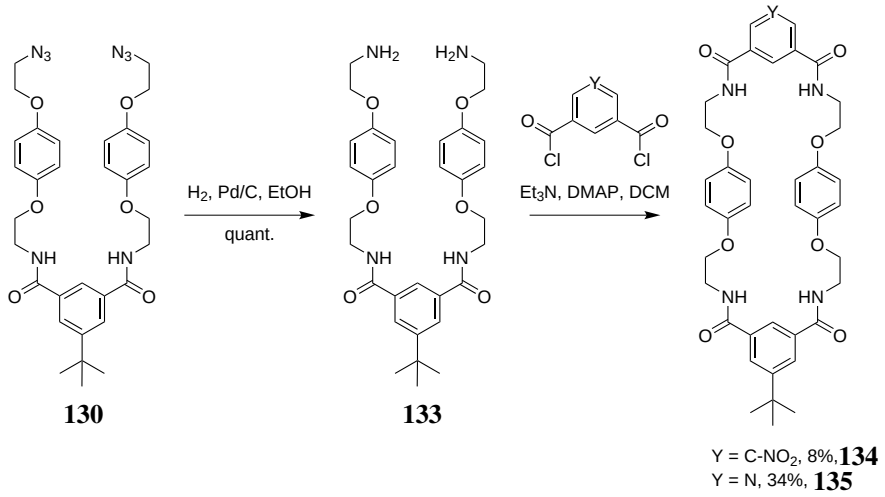
Scheme 4.3.2: Synthetic scheme to prepare the bis-azide ditopic macrocycle precursor **130**.

A halogen-bonding macrocycle was prepared *via* a chloride-templated cyclisation reaction between di-iodoethynyl pyridine **2** and the bis-azide appended macrocycle precursor **130** in the presence of the octyl-appended bis-iodotriazole pyridine-*N*-oxide and TBA·Cl templates, affording the novel ditopic hydrogen- and halogen-bonding macrocycle **132** in 24% yield. (Scheme 4.3.3). It is noteworthy that the macrocycle was not formed in the absence of the templates or when the hexyl-appended C–H hydrogen-bonding analogue **123** was used.



Scheme 4.3.3: Synthesis of the halogen-bonding ditopic macrocycle, **132**.

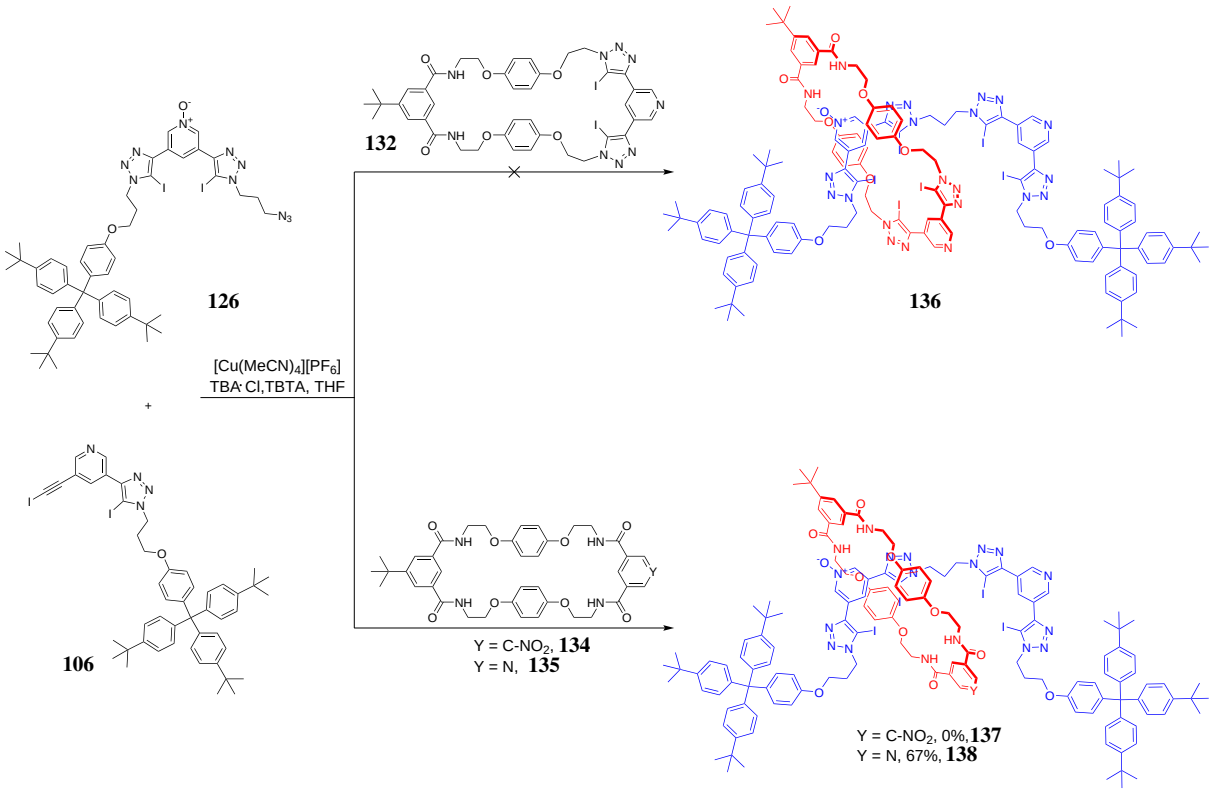
Previously reported hydrogen-bonding ditopic macrocycles were also prepared by hydrogenation of the bis-azide appended macrocycle precursor **130** to afford the bis-amine macrocycle precursor **133**, followed by condensation with the appropriate bis-acid chloride (Scheme 4.3.4).[484] The nitro-isophthalamide macrocycle **134** was formed in very low 8% yield, whereas the pyridine-bis-amide macrocycle was obtained in slightly higher 24% yield.



Scheme 4.3.4: Synthesis of hydrogen-bonding ditopic macrocycles **134** and **135**.

4.3.3 [2]Rotaxane synthesis

The synthesis of neutral asymmetric [2]rotaxanes was undertaken *via* a chloride-templated mono-stoppering procedure. An equimolar amount of the terphenyl-stoppered bis-iodotriazole pyridine-*N*-oxide azide axle precursor **126** was stirred with either the halogen-bonding macrocycle **132**, or the hydrogen-bonding ditopic macrocycles (**134** and **135**, respectively) in dry THF with 1 equivalent of TBA·Cl for 30 mins (Scheme 4.3.5). Thereafter, catalytic $[Cu(MeCN)_4][PF_6]$ and TBTA were added, as well as the terphenyl-stoppered iodoethynyl pyridine half axle **106**. In the case of the reaction with the halogen-bonding macrocycle, the desired [2]rotaxane **136** was not detected by mass spectrometry after purification: starting materials and the axle component were isolated. It is assumed that the annulus of the macrocycle is too small to accommodate the bis-iodotriazole pyridine-*N*-oxide motif, thus hindering the formation of the pseudorotaxane intermediate and the resultant [2]rotaxane. A similar result was obtained with the hydrogen-bonding nitro/*tert*-butyl-isophthalamide ditopic macrocycle **134**: the desired [2]rotaxane **137** was not detected by mass spectroscopy. However, for the pyridine/*tert*-butyl-isophthalamide ditopic macrocycle **135**, the neutral asymmetric [2]rotaxane **138** was obtained in 67% yield after purification by preparative thin layer chromatography (Scheme 4.3.5), and was characterised by ^{1}H and ^{13}C NMR spectroscopy, and high resolution mass spectrometry.



Scheme 4.3.5: Synthesis of the neutral asymmetric [2]rotaxane **138**, and the attempted synthesis of **136** and **137**.

Evidence for the interlocked nature of the axle and macrocyclic components of [2]rotaxane **138** was obtained by 2D ROESY NMR which revealed significant through-space interactions including those between the hydroquinone groups of the macrocycle and the pyridine protons of the axle (Figure 4.3.1a). An enlargement of the aromatic region (Figure 4.3.1b) suggests that the pyridine-*N*-oxide preferentially occupies the *tert*-butyl-isophthalamide site of the macrocycle by the presence of cross-couplings between *11*↔*k* and *3*↔*i*. Some minor interactions are observed between *2*↔*j,k* and *10*↔*i*, however, these are considered to be negligible, and are attributed to pirouetting motion of the pyridine-*N*-oxide within the macrocycle.

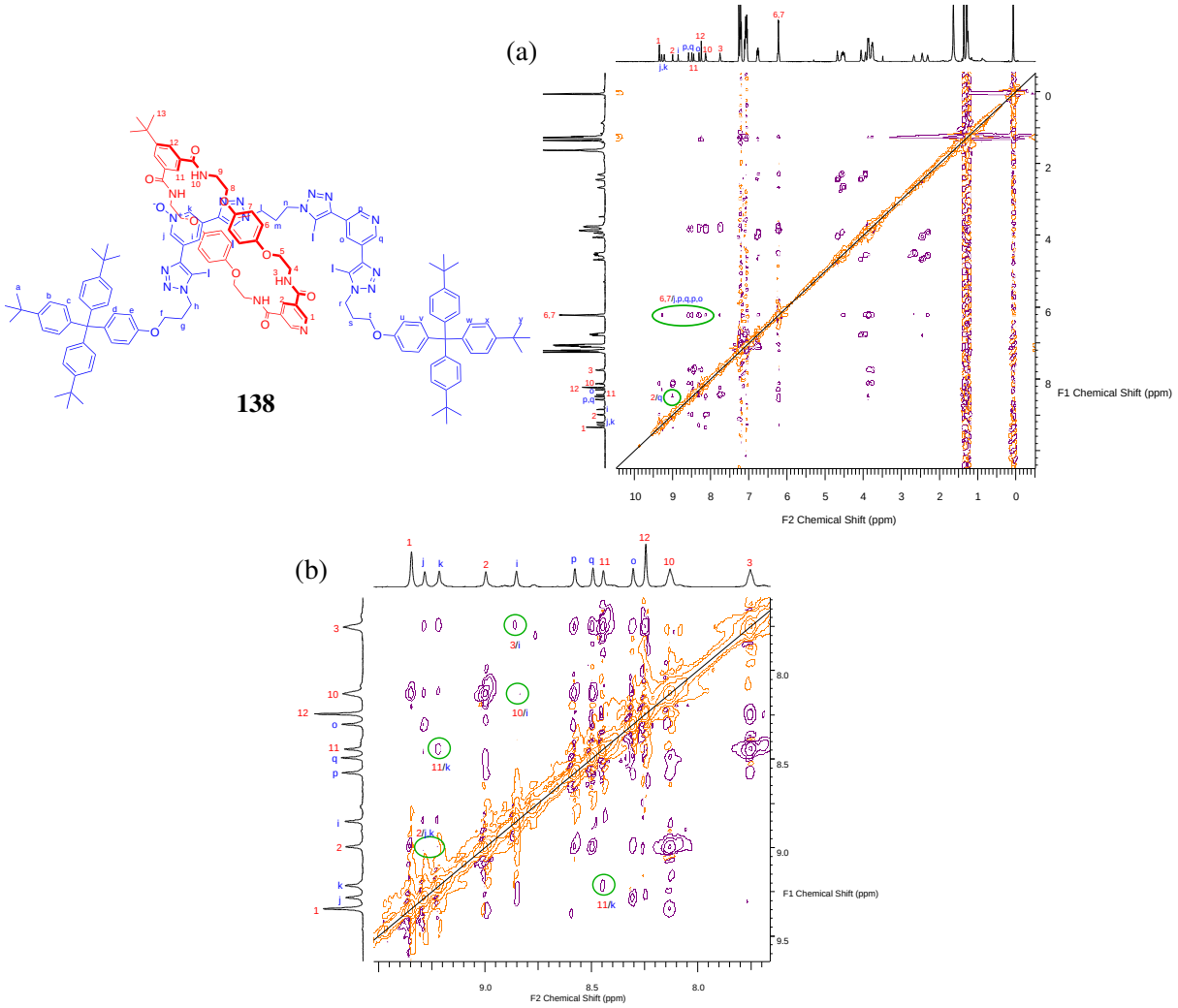
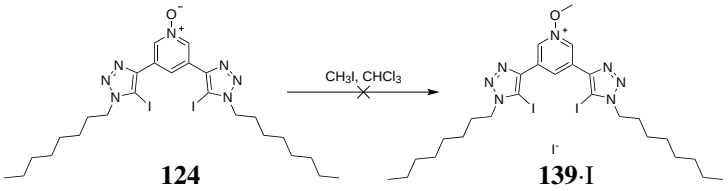


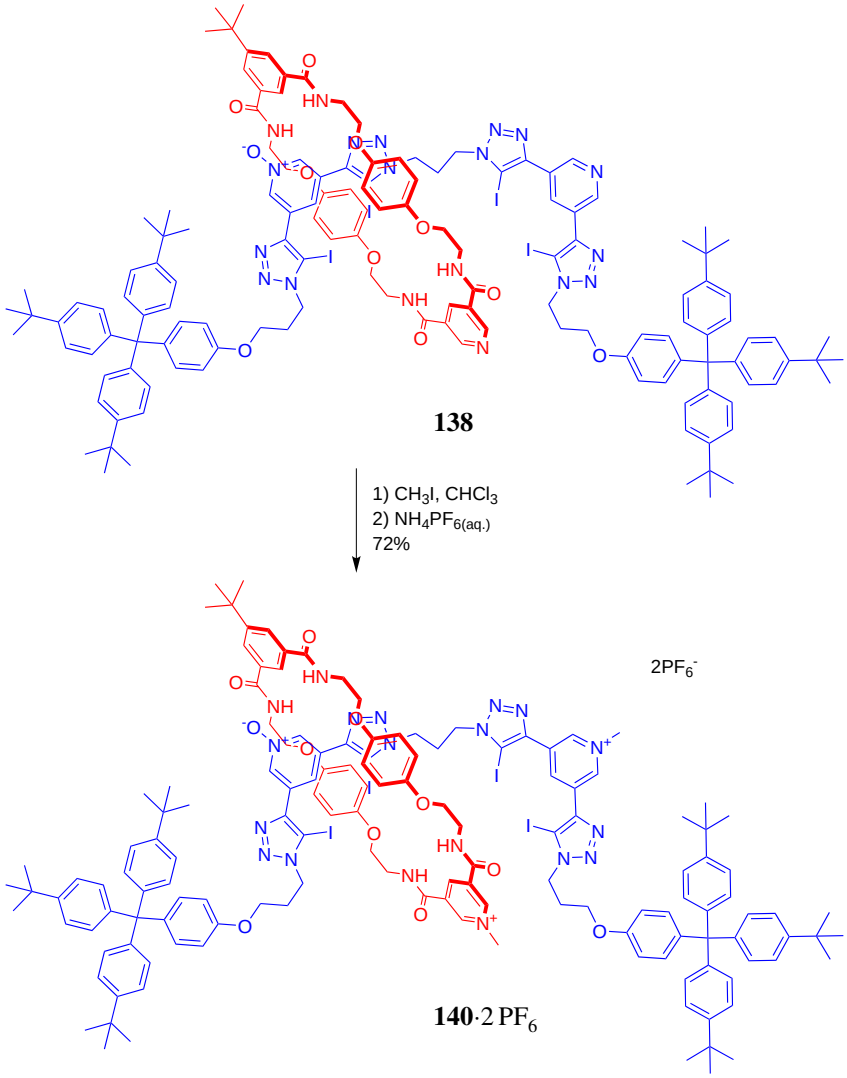
Figure 4.3.1: 2D ROESY NMR spectrum of **138** showing (a) selected through-space ^{1}H–^{1}H correlations indicative of an interlocked assembly, and (b) an enlargement of the aromatic region of the spectrum showing selected cross-couplings which reveal the preferred co-conformation of the axle and macrocycle components.

Methylation of [2]rotaxane **138** was undertaken using CH_3I; however, considering the pyridine-*N*-oxide moiety might also be susceptible to methylation, a preliminary test reaction was conducted. The simple acyclic pyridine-*N*-oxide receptor **124** was stirred with a large excess of CH_3I overnight. However, the methylated product **139**·I was not detected by mass spectrometry, and only the starting material **124** was isolated after the reaction.



Scheme 4.3.6: Test reaction to determine whether CH_3I could methylate the pyridine-*N*-oxide using **124** as the test compound.

Therefore, the neutral asymmetric [2]rotaxane **138** was stirred in $CHCl_3$ adding aliquots of CH_3I over three days until the reaction reached completion. Subsequent anion exchange to the hexafluorophosphate salt by washing with $NH_4PF_{6(aq.)}$ led to the isolation of **140**·2 PF_6 in 72% yield (Scheme 4.3.7).



Scheme 4.3.7: Synthesis of the dicationic asymmetric *N*-oxide [2]rotaxane **140**·2 PF_6.

4.3.4 ^{1}H NMR anion binding studies

The anion recognition properties of the neutral asymmetric [2]rotaxane **138** and the dicationic asymmetric [2]rotaxane **140**·2 PF_6 were investigated using ^{1}H NMR anion titrations. Titrations for **138** and **140**·2 PF_6 were conducted in 1:1 $CDCl_3$:CD_3OD and 45:45:10 $CDCl_3$:CD_3OD:D_2O, respectively, monitoring shifts in the protons incumbent upon the anion binding cavity which generated the binding isotherms shown in Figure 4.3.2. WinEQNMR2[437] analysis and Job plot approximations of the titration data determined the 1:1 stoichiometric association constants shown in Table 4.3.1.

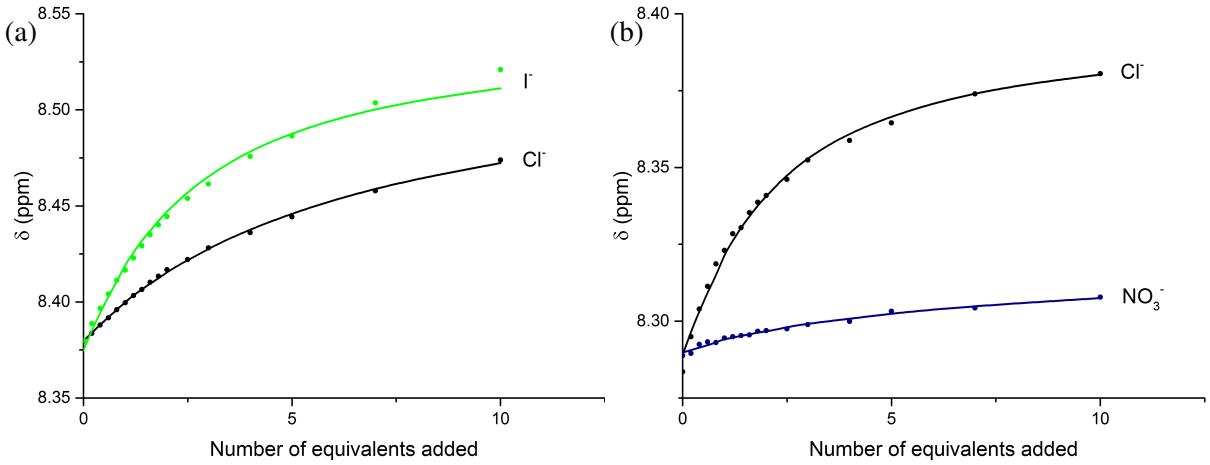


Figure 4.3.2: Anion binding titrations: (a) **138** following the internal pyridine proton *o* (1:1 $CDCl_3$:CD_3OD), and (b) **140**·2 PF_6 following the internal pyridine-*N*-oxide proton *i* (45:45:10 $CDCl_3$:CD_3OD:D_2O): experimental titration data (circles) with WinEQNMR2[437] fitted binding isotherms indicated as lines (298 K).

Table 4.3.1: Association constants (K_a)[a] determined for various TBA·anions with neutral asymmetric [2]rotaxane **138** and dicationic asymmetric [2]rotaxane **140**·2 PF_6.

Anion	K_a (M^{-1})	
	138[b]	**140**·2 PF_6[c]
Cl^-	180(5)	670(28)
I^-	330(10)	–[e]
NO_3^-	–[d]	180(41)
OAc^-	–[d]	–[e]

[a] Estimated standard errors are given in parentheses. Association constants calculated using WINEQNMR2 (298 K),[437] [b] 1:1 $CDCl_3$:CD_3OD, [c] 45:45:10 $CDCl_3$:CD_3OD:D_2O, [d] No binding, [e] Anion not titrated.

Reasonably strong binding for the halides is observed for the neutral host **138**, where binding follows anion hydrophobicity trends: iodide is bound stronger than chloride. No binding of the trigonal NO_3^- anion is observed, and neither for the congruent and more basic acetate anion. The neutral rotaxane **138** binds chloride much more weakly than the monocationic [2]rotaxane **112**·PF_6, where the incorporated positive charge enhances the binding strength in this solvent mixture (Section 3.4.2). It is possible that the formation of intramolecular hydrogen or halogen bonds and pirouetting motion of the axle component within the macrocycle contribute towards the diminished anion binding ability of the neutral [2]rotaxane. Indeed, the 2D ROESY spectrum of the rotaxane **138** in $CDCl_3$ shows ^1H–^1H cross-couplings between the macrocycle amide protons, *3* and *10* and both the pyridine/pyridine-*N*-oxide protons, *j,k* and *p,q* (Figure 4.3.1), indicating that the axle pyridine and pyridine-*N*-oxide groups may form hydrogen bonds with both bis-amide groups of the macrocycle.

The [2]rotaxane **140**·2 PF_6 displays enhanced anion binding strength over the neutral host **138**. Chloride and nitrate (K_a = 670 and 180 M^{-1}, respectively) are bound strongly in the competitive aqueous

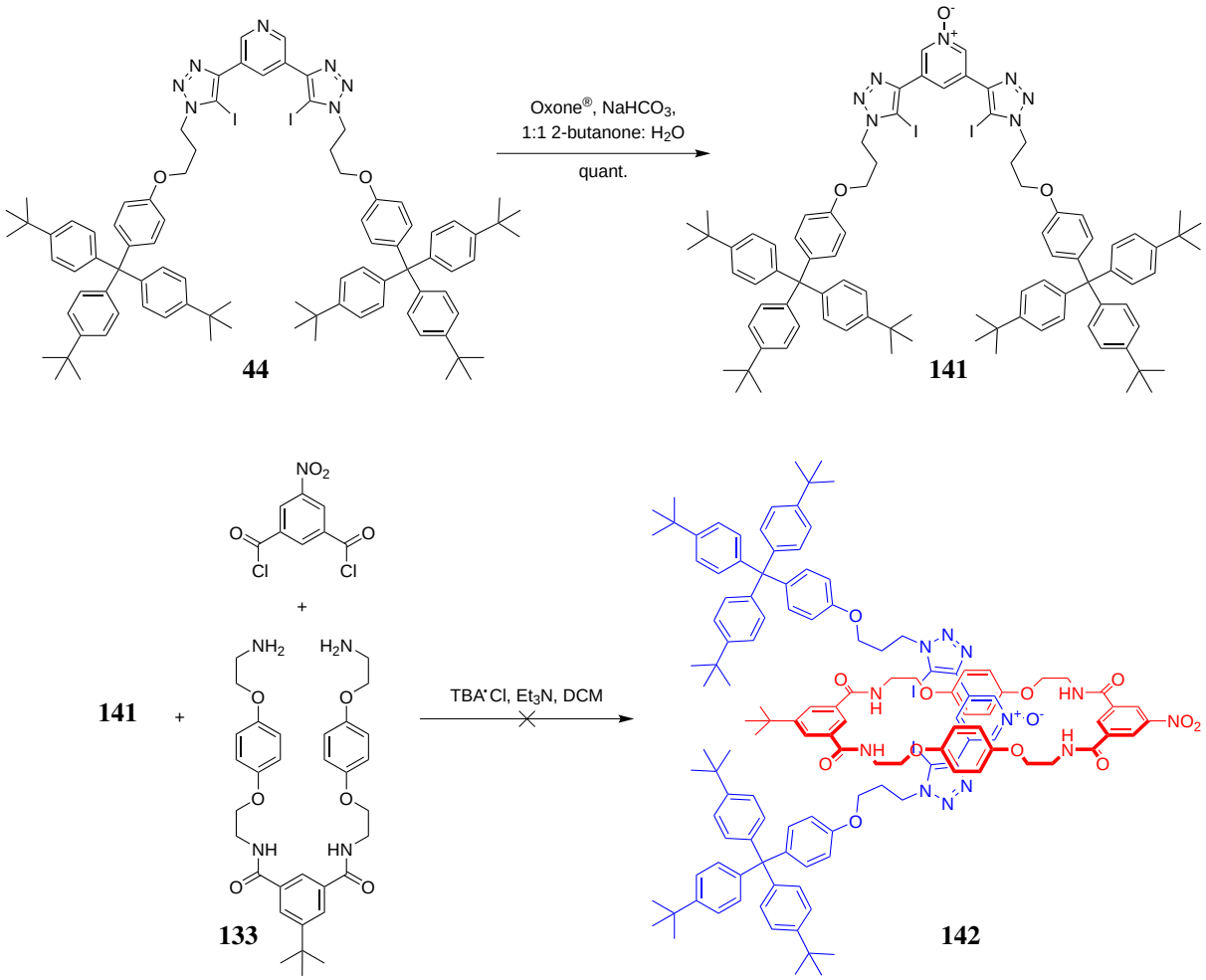
45:45:10 $CDCl_3$:CD_3OD:D_2O solvent mixture, however, both anions are bound less strongly than the dicationic [2]rotaxane **113**·2 PF_6 discussed in Chapter 3. This may also be attributed to the potential formation of intramolecular N^+–O^-···I–C halogen bonds and pirouetting of the axle in the macrocycle. Interestingly, the [2]rotaxane **140**·2 PF_6 binds chloride approximately four times more strongly than nitrate, showing a reduction in selectivity when compared to the [2]rotaxane **113**·2 PF_6 (Section 3.4), which binds chloride at least two orders of magnitude more strongly than the oxoanion.

4.4 Attempted syntheses towards water-soluble neutral [2]rotaxanes

The incorporation of the 3,5-bis-iodotriazole pyridine-*N*-oxide motif into other neutral interlocked [2]rotaxane host structural frameworks was further investigated with a view towards water-soluble anion receptors.

4.4.1 Terphenyl-stoppered axle

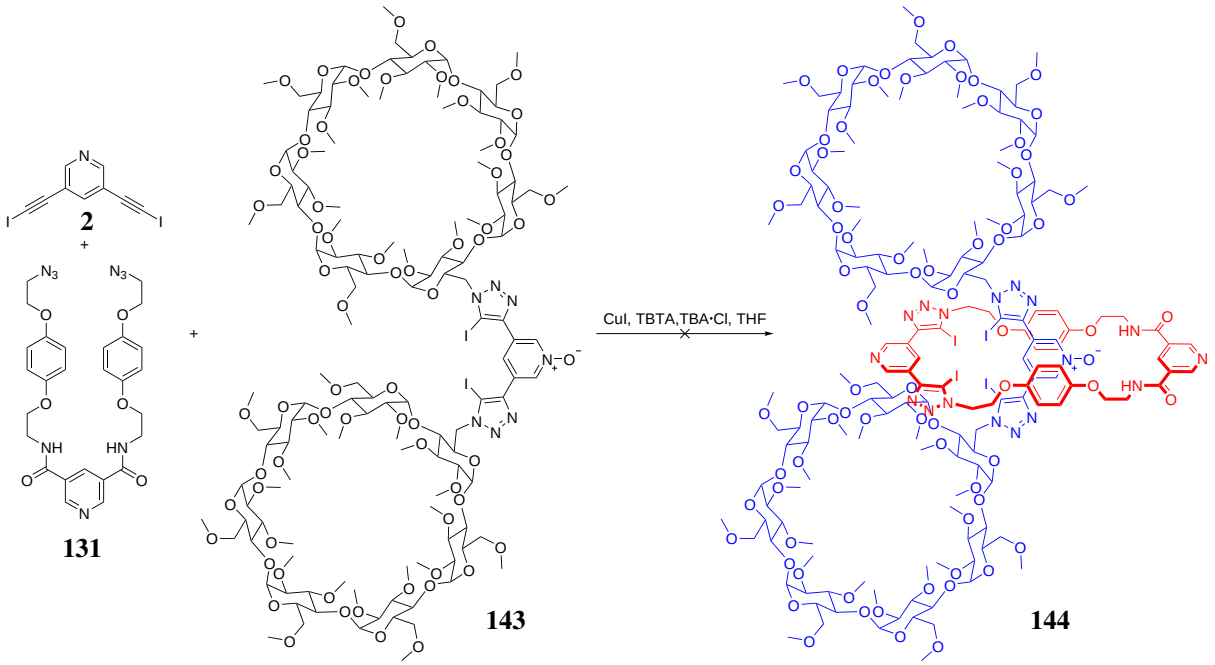
A terphenyl-stoppered bis-iodotriazole pyridine-*N*-oxide axle **141** was synthesised by oxidation of the axle-precursor **44** using Oxone® (Scheme 4.4.1). Thereafter, the preparation of a [2]rotaxane with this axle was attempted using chloride-anion templated clipping of **133** with 5-nitroisophthaloyl dichloride in dichloromethane. However, no evidence for the formation of the target [2]rotaxane **142** was observed; rather, the free axle and macrocycle components were detected by ESI mass spectrometry.



Scheme 4.4.1: Attempted synthesis of a neutral terphenyl-stoppered [2]rotaxane **142**.

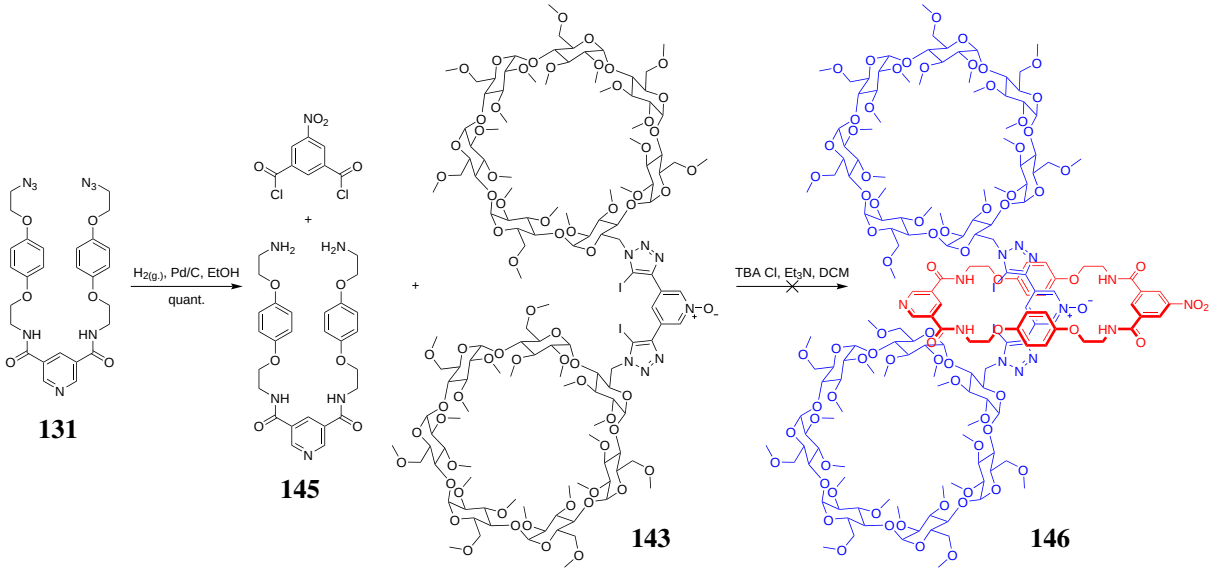
4.4.2 Permethyl-β-cyclodextrin-stoppered axle

In a similar fashion, the permethyl-β-cyclodextrin-stoppered bis-iodotriazole pyridine axle precursor **67** (Section 2.6) was oxidised with Oxone® to give the pyridine-*N*-oxide axle **143** in 46% yield. The preparation of an all-halogen-bonding neutral [2]rotaxane **144** was attempted *via* chloride-templated double CuAAC click reaction between equimolar quantities of the bis-azide-appended pyridine bis-amide macrocycle precursor **131** and di-iodoethynyl pyridine **2** around the axle **143** (Scheme 4.4.2). However, only starting materials were isolated after the reaction and the desired [2]rotaxane **144** was not detected by mass spectrometry. Presumably, this may be due to steric considerations and slower CuAAC click reaction kinetics.



Scheme 4.4.2: Attempted synthesis of a neutral water-soluble permethyl-β-cyclodextrin-appended all-halogen-bonding [2]rotaxane **144** *via* chloride-templated double CuAAC click reaction.

An alternative method was investigated to prepare a neutral water-soluble permethyl-β-cyclodextrin-appended [2]rotaxane: the bis-azide macrocycle precursor **131** was hydrogenated to the bis-amine **145**, which was stirred with stoichiometric amounts of the pyridine-*N*-oxide axle **143** and 5-nitroisophthaloyl dichloride in dichloromethane to form the target [2]rotaxane **146** *via* chloride-templated amide condensation (Scheme 4.4.3). However, the [2]rotaxane **146** was not detected by ESI mass spectrometry, which revealed the presence of the axle and macrocycle components.



Scheme 4.4.3: Attempted synthesis of a neutral water-soluble permethyl-β-cyclodextrin-appended [2]rotaxane **146** *via* chloride-templated amide condensation.

4.5 Conclusion and future work

Conclusion

This chapter has demonstrated that the 3,5-bis-iodotriazole pyridine-*N*-oxide group is a strong anion-binding motif, although it is somewhat weaker in comparison to the pyridinium analogue (Chapter 2). An asymmetric neutral [2]rotaxane was prepared, which bound halides in 1:1 $CDCl_3$:CD_3OD, with iodide bound more strongly than chloride ($K_a = 330$ and 180 M^{-1}, respectively). The neutral [2]rotaxane **138** showed no binding for the trigonal nitrate anion nor the more basic acetate anion.

Methylation of [2]rotaxane **138** gave the dicationic asymmetric [2]rotaxane **140**·2 PF_6, which is capable of binding chloride and nitrate in the aqueous solvent mixture 45:45:10 $CDCl_3$:CD_3OD:D_2O.

Interestingly, the halogen-bonding pyridine-*N*-oxide-containing [2]rotaxanes are relatively weaker anion host systems in comparison to the previously reported neutral hydrogen-bonding pyridine-*N*-oxide [2]rotaxanes,[484] which bind chloride selectively ($K_a \sim 500$ M^{-1}) in 45:45:10 $CDCl_3$:CD_3OD:D_2O. Presumably, reduced preorganisation in the halogen-bonding axle component and the possible formation of intramolecular pyridine-*N*-oxide–iodotriazole halogen bonds contributes towards the attenuated binding strength of the rotaxanes.

Attempts to prepare water-soluble [2]rotaxane analogues containing permethyl-β-cyclodextrin-stoppered axles were unsuccessful.

Future work

In order to improve the nitrate selectivity of the 3,5-bis-iodotriazole pyridine-*N*-oxide rotaxanes, future work should investigate the use of a more rigid spacer, such as aryl groups, between the two 3,5-bis-iodotriazole pyridine groups. Additionally, utilising a macrocyclic component that would reduce pirouetting of the axle within the macrocycle could lead to improved anion binding properties of the rotaxanes; for example, the rotaxane shown in Figure 4.5.1, in which the macrocycle is preferentially located at the pyridinium group on the axle.

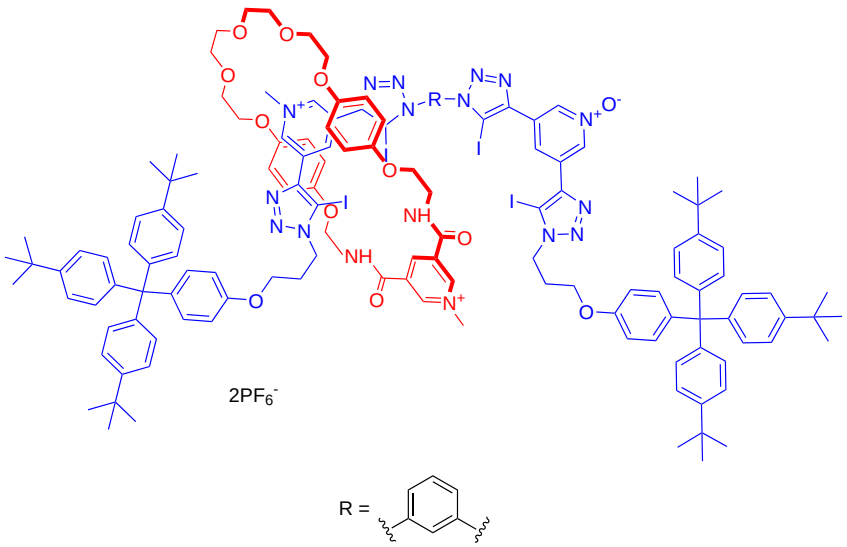


Figure 4.5.1: Proposed structure of a terphenyl-stoppered 3,5-bis-iodotriazole pyridine-*N*-oxide-containing [2]rotaxane.

Chapter 5

Conclusions

Conclusions

The *leitmotif* of this thesis was the incorporation of halogen-bond donor groups into acyclic and interlocked host systems for anion recognition. Specifically, this was achieved using two particular motifs: the 3,5-bis-iodotriazole pyridinium and pyridine-*N*-oxide groups.

Chapter 2 introduced the 3,5-bis-iodotriazole pyridinium motif and illustrated the remarkable enhancement in anion binding strength of halogen bonding in comparison to the hydrogen bonding prototriazole analogue through the use of acyclic and interlocked [2]catenane and [2]rotaxane host systems. X-ray structural analysis confirmed the anion binding data obtained by ^{1}H NMR titration experiments, and X-ray absorption spectroscopy gave the first quantitative measurement of the covalent character of the halogen-bond–chloride anion interaction. These pioneering results show that the degree of covalency for a monodentate charge-assisted halogen bond is comparable to transition metal coordinate bonds ($\sim 6\%$). Furthermore, the covalency of halogen bonds in a similar bidentate system are found to be independent and additive when chelating a chloride anion, but is reduced in the presence of competing electrostatic hydrogen bonds as shown in the [2]catenane **28**·PF_6. Indeed, these results provide concrete evidence for the superior anion binding ability of charge-assisted halogen bonding, arising from these significant covalent contributions, over hydrogen bonding, which is widely-known to be a purely electrostatic interaction. Further investigation into the covalent nature of halogen bonds is necessary between acyclic and interlocked host systems with a variety of neutral and anionic guest species.

Employing permethyl-β-cyclodextrin stopper units to imbue [2]rotaxane hosts with aqueous solubility led to the first examples of interlocked receptors for anion recognition in pure water, where the incorporation of halogen bonding resulted in a remarkable two orders of magnitude enhancement in iodide binding affinity when compared to hydrogen-bonding analogues. Studying the thermodynamics of these systems by van 't Hoff analysis revealed this enhancement was driven by enthalpy, whereas entropy governed anion binding in the hydrogen-bonding [2]rotaxanes. These data show the remarkable robustness of halogen bonding in aqueous media, and support Perutz, Brammer and Hunter's report detailing the protic/apolar organic solvent-resistant nature of halogen bonding, which was published during the course of this work.[486] Future endeavours should exploit isothermal calorimetry (ITC) experiments to determine the thermodynamic contributions to anion binding in novel halogen bonding receptor systems.

Considering the notable enhancement in anion binding affinity of the 3,5-bis-iodotriazole pyridinium motif, Chapter 3 aimed to incorporate two of these groups into a rotaxane axle component for nitrate recognition. Statistical synthetic methodologies ultimately led to the preparation of interlocked [2]rotax-

ane host systems containing terphenyl- and permethyl-β-cyclodextrin-stoppered axle components. Due to limited quantities of the mono- and di-cationic rotaxanes, ^{1}H NMR titration experiments were restricted to chloride and nitrate; however, the use of active-metal templation synthetic techniques may, in the future, allow for improved yields of these intricate host systems. In both cases, selectivity for chloride was observed in organic-aqueous media, presumably due to flexibility in the axle component. Extension of this work to a tricationic water-soluble permethyl-β-cyclodextrin-stoppered [2]rotaxane resulted in comparable binding for chloride and nitrate in 90% D_2O:acetone-d_6. Interestingly, increasing the percentage of D_2O in the solvent mixture appears to have a much greater effect on chloride binding than it does for nitrate, corresponding to their differing hydration enthalpies. ITC studies to determine the thermodynamic contributions to anion binding in this system should be undertaken. Nonetheless, these results, in turn, show the potency of the halogen-bonding 3,5-bis-iodotriazole pyridinium motif for anion recognition in competitive aqueous media.

The neutral 3,5-bis-iodotriazole pyridine-*N*-oxide motif was presented in Chapter 4 through acyclic and interlocked [2]rotaxane structural frameworks. In comparison to their pyridinium analogues which are positively charged, these hosts display diminished anion binding affinity owing to their neutrality and the potential to form *N*-oxide halogen bonds. Indeed, charge-assisted halogen-bonding receptors exhibit enhanced anion binding properties when compared with their neutral *N*-oxide zwitterionic counterparts. Future work should explore the use of a more rigid aryl spacer in the axle between the two 3,5-bis-iodotriazole pyridine groups, and the incorporation of different macrocycle components.

In general, the results in this thesis clearly show the remarkable enhancement in anion binding affinity of halogen bonding over hydrogen bonding in both acyclic and interlocked host systems, particularly in cases where the 3,5-bis-iodotriazole pyridinium motif has been used. This may be attributed to the strong covalent character of halogen bonds, which has allowed for the recognition of halide anions in pure water.

Finally, the 3,5-bis-iodotriazole pyridinium and pyridine-*N*-oxide motifs should in the future be integrated into the design of anion sensing host systems which contain optical or electrochemical reporter groups. Moreover, combining these groups with other hydrogen- and halogen-bonding anion binding functionalities in interlocked host systems could allow for highly selective receptors with high affinity for anions in aqueous media.

Chapter 6

Experimental

6.1 General considerations

6.1.1 Chemicals and solvents

All solvents and reagents were purchased from commercial suppliers and used as received unless otherwise stated. Dry solvents were obtained by purging with nitrogen and then passing through an MBraun MPSP-800 column. H_2O was de-ionised and micro filtered using a Milli-Q® Millipore machine. TBA salts, Grubbs' II catalyst, $Pd_2(dba)_3$, $[Cu(MeCN)_4][PF_6]$, imidazoliumsulfonyl azide·HSO_4[487] and TBTA[488] were stored in a vacuum desiccator containing phosphorus pentoxide prior to use. Where mixtures of solvents were used, ratios are reported by volume. Triethylamine was distilled from and stored over potassium hydroxide. Brine refers to a saturated aqueous solution of NaCl, $NH_4OH_{(aq.)}$ refers to a 28–30% solution of NH_3 in water. Petrol refers to the fraction of petroleum ether boiling between 40 and 60 °C. Column chromatography was carried out on Merck® silica gel 60 under a positive pressure of nitrogen, preparative TLC was performed on 20 × 20 cm plates, with a silica layer of thickness 1 mm. Amberlite® was "loaded" by washing the resin with $NaOH_{(aq.)}$ (10%), water, and either $NH_4Cl_{(aq.)}$ (1 M), $NaOTf_{(aq.)}$ (1 M) or $NH_4PF_{6(aq.)}$ (0.1 M), followed by further water, and the solvent to be used in the anion exchange.

Safety note

CAUTION: Low molecular weight organic azides, sodium azide and 1,2,3-triazole and triazolium groups are potentially explosive. While no problems were encountered in the course of this work, they should be handled in small quantities and with appropriate care.

In an addendum to the communication reporting its preparation,[487] the authors reported that the hydrochloride salt of imidazolylsulfonyl azide is hygroscopic, and potentially explosive when wet.

6.1.2 Instrumentation

NMR Spectra

Routine NMR spectra were recorded on either a Varian Mercury 300, a Bruker AVIII 400 or a Bruker AVIII 500 spectrometer with ^{1}H NMR titrations recorded on a Bruker AVIII 500 spectrometer. Chemical shifts are quoted in parts per million relative to the residual solvent peak.

Mass Spectra

Mass spectra were recorded on a Bruker μTOF spectrometer. Low resolution ESI mass spectra were recorded on a Waters LCT premier spectrometer.

6.1.3 Titration protocols

Organic and aqueous–organic solvents

Spectra for ^{1}H NMR titrations were recorded at 293 K on a Varian Unity Plus 500 spectrometer with ^{1}H operating at 500 MHz. Initial sample volumes were 0.50 mL and concentrations were either 1.0 or 2.0 mM of host. Solutions (50 or 100 mM) of anions as their tetrabutylammonium salts were added in aliquots, the samples thoroughly shaken and spectra recorded. Spectra were recorded at 0, 0.2, 0.4, 0.6, 0.8, 1.0, 1.2, 1.4, 1.6, 1.8, 2.0, 2.5, 3.0, 4.0, 5.0, 7.0 and 10 equivalents of anion. In all cases where association constants were calculated, bound and unbound species were found to be in fast exchange on the NMR timescale.

Aqueous titrations

For the permethyl-β-cyclodextrin-appended [2]rotaxanes in Chapter 2, aliquots of the anion guest, as the sodium salt (0.75 M in D_2O), were added to 0.5 mL of a 1.5 mM solution of the host in D_2O at 298 K. Similarly, a solution of the tricationic [2]rotaxane (1 mM) in Chapter 3 was titrated with anions as the sodium salts (0.5 M) in 9:1 D_2O:acetone-d_6 at 298 K. The chemical shift of protons *b*, *2* and *3*, as appropriate, were monitored. A trace amount of acetone was added as an internal reference, such that it made up less than 0.05% of the total volume, and all spectra referenced to its resonance at 2.10 ppm. Spectra were recorded at 0, 1, 2, 3, 5, 7, 10, 15, 20, 25, 30, 40, 50, 60, 80, 100 and 120 equivalents of anion. van 't Hoff analysis titrations were conducted using the same procedure, at 303 K, 308 K, 313 K and 318 K. The temperature of NMR sample was allowed to equilibrate for 15 minutes prior to the titration, and then for a further 2 minutes after each anion addition.

Data fitting

Stability constants were obtained by analysis of the resulting data using the WinEQNMR2[437] computer program. Binding stoichiometries were investigated by visual analysis of the titration data, and using approximations of Job plots. A graph of $\Delta\delta.\chi_{\mathrm{H}}$ against χ_{H} was plotted, with a 1:1 binding sto-

ichiometry corresponding to a maximum $\delta.\chi_{\mathrm{H}} \sim 0.5$ (χ_{H} = mole fraction of host, $\Delta\delta$ = change in chemical shift relative to free host).

Estimates for the association constant and the limiting chemical shifts were added to the program's input file. The parameters were refined by non-linear least-squares analysis using WINEQNMR2[437] to achieve the best fit between observed and calculated chemical shifts. The input parameters for the final chemical shift and association constant were adjusted based on the program output until convergence was reached. Comparison of the calculated and experimental binding isotherms demonstrated that an appropriate model with an appropriate stoichiometry was being used.

WinEQNMR2[437] also provides an estimate of the standard error of the measurement, which is included with all data. It should also be noted that these estimated errors only account for the fitting of a binding isotherm to the titration data, they do not consider systematic error behind such data, for example an incorrect concentration of the titrant solution. While the relative concentrations of solutions were checked by integration of the ^{1}H NMR spectra, the magnitude of the errors provided by WINEQNMR2 are probably underestimated.

6.1.4 X-ray Crystallography

Single crystal X-ray diffraction data for **11**·Cl were collected using graphite monochromated Mo Kα radiation ($\lambda = 0.71073$ Å) on a Nonius Kappa CCD diffractometer equipped with a Cryostream N2 open-flow cooling device,[489] at 150 K. Raw frame data (including data reduction, inter-frame scaling, unit cell refinement and absorption corrections) were processed using the DENZO-SMN package.[490] Single crystal X-ray diffraction data for the acyclic receptor **12**·I and the catenane **28**$^{+}$ with chloride, bromide, iodide, sulfate and dihydrogen phosphate were collected using synchrotron radiation on Beamline I19 at Diamond Lightsource.[491] The diffractometer was equipped with a Cryostream N2 open-flow cooling device,[489] and the data were collected at 100(2) K. Cell parameters and intensity data (including inter-frame scaling) were processed using CrysAlis Pro.[492]

All structures were solved by charge-flipping methods using SUPERFLIP.[493] All structures were refined using full-matrix least-squares on F^2 within the CRYSTALS suite.[494,495] All non-hydrogen atoms were refined with anisotropic displacement parameters. Hydrogen atoms were generally visible in the difference map and their positions and displacement parameters were refined using restraints prior to inclusion into the model using riding constraints.[496]

Crystallographic data for the structures (except **12**·I) in CIF format have been deposited with the Cambridge Crystallographic Data Centre, CCDC: 1033644–1033649. These CIFs are also supplied as an electronic appendix.

6.1.5 X-ray Absorption Spectroscopy

6.1.5.1 Sample Preparation

Samples for Cl K-edge and Br K-edge XAS were mounted as a finely ground powder diluted (1:1) with boron nitride (BN) dusted on sulfur-free Kapton tape across the window of an Al plate. All XAS samples were finely ground. The resultant homogeneous, finely dispersed powders were pressed into a 0.5 mm thick Al spacer, sealed on both sides with Kapton tape.

6.1.5.2 XAS Data Collection

Cl K-edge XAS data were collected at beamline 4-3 the Stanford Synchrotron Radiation Laboratory (SSRL) using a modified low Z setup allowing for low temperature data acquisition under ring conditions of 3 GeV and 60–100 mA. The setup is a 54-pole wiggler beamline operating in high field (10 kG) mode with a Ni coated harmonic rejection mirror and a fully tuned Si (111) double crystal monochromator. Calibration scans were performed before and after every data set to ensure stable monochromator readings. Signal was detected with a N_2 fluorescence (Lytle) detector at ambient temperature and pressure (1 atm, 298 K). Br K-edge XAS data were collected at SSRL on beamline 7-3 under ring conditions 80–100 mA at 3.0 GeV. This beamline has a 20-pole, 2 T wigglers, 0.8 mrad beam, and a Si (220) double crystal monochromator that was detuned by 50% intensity to attain harmonic rejection. The incident X-ray intensity (I0), sample absorption (I1), and Br reference absorption (I2) were measured as transmittance using argon-filled ionisation chambers. Six to eight sweeps were taken for each sample, and all data were measured at 19 ± 7 K within an Oxford Instruments CF1208 continuous-flow liquid helium cryostat.

6.1.5.3 XAS data analysis

SixPack was used to calibrate and average all acceptable spectra.[497] KBr ($E_0 = 13474$ eV) and NaCl ($E_0 = 2820.2$ eV) spectra acquired at the same time as sample data were used as a calibrant for Cl K-edge and Br K-edge spectra, respectively. BlueprintXAS version 2.7 was then used for background subtraction and normalisation. To minimise the user bias introduced during data work-up, BlueprintXAS fits the spline, peaks and background concurrently.[445,446] While the parameters for each variable are user

defined, the fits were run in AUTO mode, as in this mode, a Monte Carlo methodology is used to choose the starting point of each fit to further remove user bias. Each fit contained the following components: piecewise spline + Edge; peak for the edge peak; normalised peak for the pre-edge peak.

Fits were filtered (removed from final set) (a) if any error occurred during calculations (b) if fit significantly deviated from spectra, i.e. sum of square errors (SSE) was too large (c) if fit is a significant outlier for peak height, peak energy or E_0. The 'time average' option (used for all fits except **30**·Cl and **32**·Cl) calculates the average time taken to calculate each fit and filters any fits above this value. This setting was used to remove failed fits as the user recognised that the fits with the longest calculation times usually corresponded with the fits that failed.

Although fits were calculated for the Br spectra, the resulting fits were not considered viable for the following reasons. Fits for all Br K-edge spectra were discarded due to multiple inconsistencies within each fit. Examples include three distinct solution sets for the intensities of the pre-edge and edge features for **28**·Br indicating that there are at least 3 distinct viable solutions for the fits calculated. Additionally, there also exists a very good 1:1 correlation between the intensities of the pre-edge and edge features for **32**·Br. This correlation indicates that the values for these variables are interdependent and therefore unreliable.

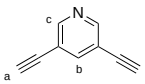
6.1.5.4 Computational Details

All calculations were performed using ORCA 2.9 on either a local computing cluster or using WestGrid computing facilities (lattice and/or grex).[448] All structures were fully geometry optimised using the B3LYP functional, the def2-TZVP basis set, and included relativistic corrections (ZORA). All optimisations were verified using frequency calculations to confirm that all vibrational frequencies were positive. Cl K-edge and Br K-edge XAS TDDFT simulations were performed using the same level of theory as in the optimisations.

6.2 Synthesis

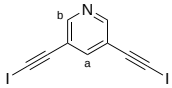
6.2.1 Compounds from Chapter 2

3,5-Diethynylpyridine, 1



3,5-Dibromopyridine (1.426 g, 6.02 mmol), CuI (0.068 g, 0.35 mmol), PPh_3 (0.268 g, 1.02 mmol) and $Pd_2(dba)_3$ (0.095 g, 0.10 mmol) were added to a round-bottomed flask. Et_3N (30 mL) was added and deoxygenated. Thereafter, trimethylsilylacetylene (2.2 mL, 1.529 g, 15.6 mmol) was added. The flask was then sealed and heated to 75 °C for 18 h. The mixture was then cooled to room temperature and filtered through a cotton wool plug. The dark green residue was washed with Et_2O (5 × 40 mL). The resulting yellow solution was dried under reduced pressure and the residual yellow oil was taken up in MeOH (40 mL). KOH (1.13 g, 20.0 mmol) in H_2O (4 mL) was added to the solution and was stirred for 30 mins. The product, **1**, was then extracted with pentane (7 × 40 mL). The fractions were combined and filtered through a cotton wool plug. The pentane was allowed to evaporate at standard temperature and pressure to yield a yellow solid. The product was purified by sublimation (130 °C at standard pressure) to yield **1** as feathery white crystals. Yield: 0.418 g (55%). ^{1}**H NMR** (300 MHz; $CDCl_3$) δ (ppm): 8.68 (2H, br. s., H_c), 7.86 (1H, t, $^4J_{b|c} = 2$ Hz, H_b), 3.25 (2H, s, H_a). ^{13}**C**$\{^1$**H**$\}$ **NMR** (75 MHz; $CDCl_3$) δ (ppm): 151.8, 141.9, 81.5, 79.3.

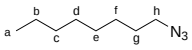
3,5-Bis-iodoethynylpyridine, 2



1 (0.128 g, 1.00 mmol) was dissolved in THF (10 mL). CuI (0.034 g, 0.18 mmol) and *N*-iodomorpholine (0.751 g, 2.20 mmol) were added to this solution and stirred at room temperature for 2 h after which a white precipitate had formed. The suspension was poured onto a pad of neutral alumina. The filtrate was collected under vacuum and the solid phase washed with DCM (4 × 20 mL). The combined organic fractions were washed with saturated $Na_2S_2O_3$ (40 mL), dried over $MgSO_4$ and the solvent removed under reduced pressure. The residue was taken up in 10% EtOAc in hexane and the solution poured onto a pad of silica. The filtrate was collected under vacuum and the solid phase washed with 10%

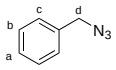
EtOAc in hexane (4 × 20 mL). The organic fractions were combined and the solvent removed *in vacuo*. Purification by recrystallisation from hexane yielded **2** as shiny, feathery white crystals. Yield: 0.254 g (65%). ^{1}**H NMR** (300 MHz; $CDCl_3$) δ (ppm): 8.59 (2H, d, $^{4}J_{a|b} = 2$ Hz, H_b), 7.75 (1H, t, $^{4}J_{a|b} = 2$ Hz, H_a). ^{13}**C**$\{^{1}$**H**$\}$ **NMR** (75 MHz; $CDCl_3$) δ (ppm): 151.9, 142.3, 120.2, 89.8. **HRESI-MS** (pos.): 379.8421, calc. for $[C_9H_3I_2N \cdot H]^+ = 379.8428$.

Octylazide, 3



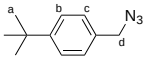
Octylbromide (1.80 mL, 10.4 mmol) and NaN_3 (0.793 g, 12.2 mmol) were dissolved in dimethylsulfoxide (40 mL) and stirred overnight under an atmosphere of N_2. The mixture was diluted with H_2O (50 mL) and extracted with Et_2O (3 × 60 mL). The combined Et_2O extracts were washed with H_2O (2 × 60 mL) and brine (60 mL) and dried over $MgSO_4$. The solvent was removed *in vacuo* without heating to give the product, **3**. Yield: 1.481 g (96%). ^{1}**H NMR** (300 MHz; $CDCl_3$) δ (ppm): 3.26 (2H, t, $J_{g|h} = 7$ Hz, H_h), 1.52–1.67 (2H, m, H_g), 1.19–1.43 (10H, m, $H_{b,c,d,e,f}$), 0.88 (3H, t, $J_{a|b} = 7$ Hz, H_a).

Benzyl azide, 4



Benzyl bromide (1.2 mL, 10 mmol) and NaN_3 (0.785 g, 12 mmol) were dissolved in DMSO and stirred under N_2 overnight. The mixture was diluted with H_2O (50 mL) and extracted with EtOAc (3 × 80 mL). The combined organics were washed with H_2O (2 × 80 mL) and brine (2 × 80 mL) and dried over $MgSO_4$. The solvent was removed *in vacuo* without heating to yield the product as a pale yellow oil (1.128 g, 85%). ^{1}**H NMR** (300 MHz; $CDCl_3$) δ (ppm): 7.28–7.48 (5H, m, $H_{a,b,c}$), 4.35 (2H, s, H_d).

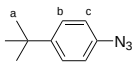
4-*tert*-Butylbenzyl azide, 5



4-*tert*-Butylbenzyl bromide and NaN_3 were dissolved in DMSO and stirred for 16 h under N_2. The mixture was diluted with H_2O (50 mL) and extracted with Et_2O (3 × 80 mL). The combined organics were washed with H_2O (2 × 80 mL), brine (80 mL) and dried over $MgSO_4$. The solvent was removed

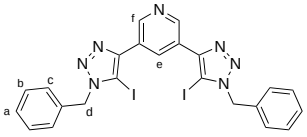
in vacuo to yield **5** as a pale yellow oil (1.86 g, 98%). ^{1}**H NMR** (300 MHz; $CDCl_3$) δ (ppm): 7.15–7.48 (4H, m, $H_{b,c}$), 4.31 (2H, s, H_d), 1.33 (9H, s, H_a).

4-*tert*-Butylphenyl azide, 6



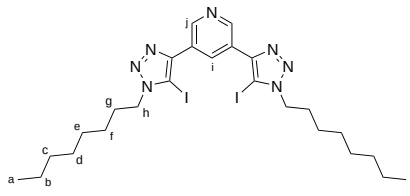
4-*tert*-Butylaniline was added to HCl (17% aq., 20 mL). EtOH (5 mL) was added to the mixture which was heated gently to dissolve the solid residue. The solution was cooled to 0 °C and $NaNO_2$ (0.36 g, 5.0 mmol) added portionwise and stirred for 15 mins. NaN_3 (0.33 g, 5.0 mmol) was added portionwise while stirring at 0 °C. The mixture was allowed to warm to room temperature and stirred for 16 h. The solution was transferred to a separating funnel, diluted with H_2O (20 mL) and the aqueous phase extracted into Et_2O (3 × 20 mL). The combined organics were washed with saturated aqueous $NaHCO_3$ (3 × 20 mL) and brine (20 mL) and dried over $MgSO_4$. The solvent was removed *in vacuo* to yield **6** as a red oil (0.407 g, 69%). ^{1}**H NMR** (300 MHz; $CDCl_3$) δ (ppm): 7.33–7.41 (2H, m, H_c), 6.93–7.01 (2H, m, H_b), 1.29–1.33 (9H, m, H_a).

Bis-benzyl(iodotriazolyl)-pyridine, 7



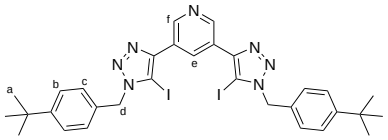
CuI (0.007 g, 0.04 mmol) and TBTA (0.015 g, 0.03 mmol) were dissolved in dry, degassed THF (1.6 mL). The mixture was allowed to stir for 1 h at room temperature after which it was added to a solution of **2** (0.076 g, 0.2 mmol) in THF (0.4 mL). A solution of benzylazide (0.061 g, 0.46 mmol) in THF (0.4 mL) was added to the above mixture over 1–2 mins. The mixture was stirred for 18 h at room temperature in the dark. The solvent was removed *in vacuo* and the residue taken up in DCM (3 mL). The solution was washed with NH_4OH/EDTA (1 mL), H_2O (1 mL), brine (1 mL), dried over $MgSO_4$ and the solvent removed *in vacuo*. Purification by silica gel column chromatography (1% MeOH in DCM) yielded **7** as a cream-coloured powder (0.074 g, 57%). ^{1}**H NMR** (300 MHz; $CDCl_3$) δ (ppm): 9.25 (2H, d, $^4J_{e|f} = 2$ Hz, H_f), 8.87 (1H, t, $^4J_{e|f} = 2$ Hz, H_e), 7.29–7.44 (10H, m, $H_{a,b,c}$), 5.71 (4H, s, H_d). ^{13}**C**$\{^1$**H**$\}$ **NMR** (75 MHz; $CDCl_3$) δ (ppm): 152.59, 147.56, 147.32, 137.80, 134.08, 133.36, 129.15, 128.82, 128.00, 54.72. **HRESI-MS** (pos.): 645.9699, calc. for $[C_{23}H_{17}I_2N_7 \cdot H]^+ = 645.9708$.

Bis-octyl(iodotriazolyl)-pyridine, 8



CuI (0.007 g, 0.04 mmol) and TBTA (0.013 g, 0.03 mmol) were dissolved in dry, degassed THF (1.6 mL). The mixture was allowed to stir for 1 h at room temperature after which it was added to a solution of **2** (0.083 g, 0.22 mmol) in THF (0.4 mL). A solution of **3** (0.068 g, 0.44 mmol) in THF (0.4 mL) was added to the above mixture over 1–2 mins. The mixture was stirred for 18 h at room temperature in the dark. The solvent was removed *in vacuo* and the residue taken up in DCM (3 mL). The solution was washed with NH_4OH/EDTA (1 mL), H_2O (1 mL), brine (1 mL), dried over $MgSO_4$ and the solvent removed *in vacuo*. Purification by silica gel column chromatography (1% MeOH in DCM) yielded **8** as a cream-coloured powder. Yield: 0.067 g (49%). ^{1}**H NMR** (300 MHz; $CDCl_3$) δ (ppm): 9.27 (2H, br. s., H_j), 8.95 (1H, s, H_i), 4.49 (4H, t, $J_{g|h} = 7$ Hz, H_h), 1.98 (4H, t, $J_{g|h} = 7$ Hz, H_g), 1.18–1.52 (20H, m, $H_{b,c,d,e,f}$), 0.81–0.96 (6H, m, H_a). ^{13}**C**$\{^1$**H**$\}$ **NMR** (75 MHz; $CDCl_3$) δ (ppm): 147.6, 146.7, 132.8, 130.8, 128.7, 51.0, 31.6, 29.8, 28.9, 26.3, 22.5, 14.0. **HRESI-MS** (pos.): 712.1086, calc. for $[C_{25}H_{37}I_2N_7 \cdot Na]^+ = 712.1092$.

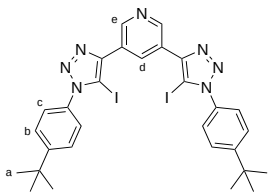
Bis-(*tert*-butylbenzyl-iodotriazolyl) pyridine, 9



5 (0.209 g, 1.1 mmol) was dissolved in dry degassed THF (2 mL) and the reaction vessel was covered in foil. NaI (0.60 g, 4.0 mmol) and $Cu(ClO_4)_2 \cdot 6\,H_2O$ (0.748 g, 2.0 mmol) were added and stirred under N_2 for 5 mins. TBTA (0.005 g, 0.01 mmol), DBU (0.153 g, 1.0 mmol) and **1** (0.064 g, 0.5 mmol) were added in order. The mixture was stirred for 16 h, diluted and transferred to a separating funnel with DCM (100 mL). The organics were washed with NH_4OH (2 $\times$ 40 mL), brine (2 $\times$ 40 mL) and dried over $MgSO_4$. The solvent was removed *in vacuo*. Purification by silica gel column chromatography (1% MeOH in DCM) yielded **9** as a white powder (0.289 g, 76%). ^{1}**H NMR** (500 MHz; $CDCl_3$) δ (ppm): 9.23 (2H, d, $^4J_{f|e} = 1.7$ Hz, H_f), 8.84 (1H, t, $^4J_{e|f} = 1.7$ Hz, H_e), 7.27–7.42 (8H, m, $H_{b,c}$), 5.65 (4H, s, H_d), 1.30 (18H, s, H_a). ^{13}**C**$\{^1$**H**$\}$ **NMR** (126 MHz; $CDCl_3$) δ (ppm): 150.7, 146.9, 146.2, 131.9, 130.0,

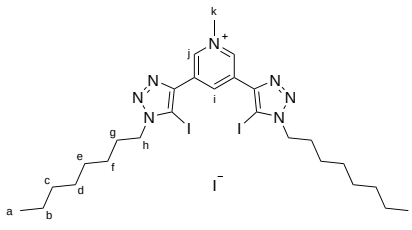
126.7, 125.3, 124.9, 53.2, 33.6, 30.2. **HRESI-MS** (pos.): 758.09443, calc. for $[C_{31}H_{33}I_2N_7 \cdot H]^+ =$ 758.09596.

Bis-(*tert*-butylphenyl-iodotriazole) pyridine, 10



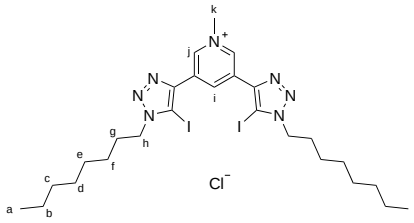
6 (0.20 g, 1.1 mmol) was dissolved in deoxygenated THF (2 mL) and the reaction vessel covered in foil. NaI (0.601 g, 4 mmol) and $Cu(ClO_4)_2 \cdot 6\,H_2O$ (0.746 g, 2 mmol) were added and the mixture stirred for 5 mins under N_2. TBTA (0.006 g, 0.01 mmol), DBU (0.151 g, 1 mmol) (syringe/pipette washed with deoxygenated THF (2 mL) to ensure quantitative transfer) and **1** (0.064 g, 0.5 mmol) were added to the mixture which was then stirred for 16 h. The mixture was diluted and transferred to a separating funnel with DCM (100 mL) and washed with NH_4OH (2 $\times$ 40 mL) and brine (2 $\times$ 40 mL). The organics were dried over $MgSO_4$ and the solvent removed *in vacuo*. Purification by silica gel column chromatography (1% MeOH in DCM) as the eluent to yield **10** as an off-white powder (0.311 g, 85%). ^{1}**H NMR** (300 MHz; $CDCl_3$) δ (ppm): 9.37 (2H, br. s., H_e), 9.07 (1H, s, H_d), 7.57–7.68 (4H, m, H_c), 7.45–7.55 (4H, m, H_b), 1.41 (9H, s, H_a). ^{13}**C**$\{^1$**H**$\}$ **NMR** (101 MHz; $CDCl_3$) δ (ppm): 153.8, 147.4, 134.0, 133.1, 129.0, 128.7, 127.9, 126.4, 125.9, 35.0, 31.3. **HRESI-MS** (pos.): 752.0444, calc. for $[C_{29}H_{29}I_2N_7 \cdot Na]^+ =$ 752.0466.

Bis-octyl(iodotriazolyl)-*N*-methyl-pyridinium iodide, 11·I



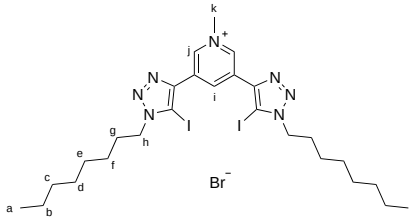
8 (0.20 g, 0.29 mmol) was dissolved in dry DCM (25 mL). CH_3I (0.50 mL, 8.0 mmol) was added and the solution was stirred under an atmosphere of N_2 for 7 days. The solvent was removed *in vacuo*. Purification by preparative thin layer chromatography (5% MeOH in DCM) yielded **11** as a white solid. Yield: 0.23 g (94%). Due to poor solubility, **11**·I was used in subsequent anion exchanges without further characterisation. **HRESI-MS** (pos.): 704.1428, calc. for $[C_{26}H_{40}I_2N_7]^+ = 704.1429$.

Bis-octyl(iodotriazolyl)-*N*-methyl-pyridinium chloride, 11·Cl



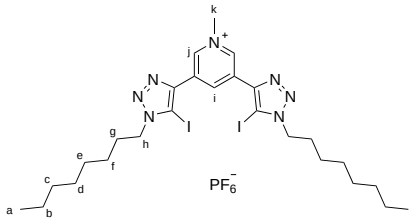
11·I (0.050 g, 60 μmol) was suspended in $CHCl_3$ (50 mL) and washed with 1 M $NH_4Cl_{(aq.)}$ (8 × 10 mL) and H_2O (2 × 10 mL). The solvent was removed *in vacuo* to yield **11**·Cl (0.030 g, 67%). ^{1}**H NMR** (500 MHz; 1 :1 $CDCl_3$:MeOD) δ (ppm): 9.98 (1H, br. s., H_i), 9.37 (2H, br. s., H_j), 4.59 (3H, br. s., H_k), 4.37 (4H, t, $J_{h|g} = 6.6$ Hz, H_h), 1.88 (4H, br. s., H_g), 1.15–1.42 (20H, m, $H_{b,c,d,e,f}$), 0.83 (6H, br. s., H_a). ^{13}**C**$\{^1$**H**$\}$ **NMR** (126 MHz; 1 :1 $CDCl_3$:MeOD) δ (ppm): 141.9, 140.7, 133.7, 133.3, 92.0, 51.6, 32.0, 30.1, 29.3, 29.2, 26.7, 22.8, 14.2. **HRESI-MS** (pos.): 704.1427, calc. for $[C_{26}H_{40}I_2N_7]^+ =$ 704.1429.

Bis-octyl(iodotriazolyl)-*N*-methyl-pyridinium bromide, 11·Br



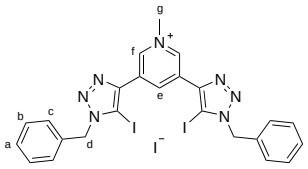
11·I (0.050 g, 60 μmol) was suspended in $CHCl_3$ (50 mL) and washed with 1 M $NH_4Br_{(aq.)}$ (8 × 10 mL) and H_2O (2 × 10 mL). The solvent was removed *in vacuo* to yield **11**·Br (0.031 g, 66%). ^{1}**H NMR** (400 MHz; 1 :1 $CDCl_3$:MeOD) δ (ppm): 9.94 (1H, s, H_i), 9.41 (2H, s, H_j), 4.63 (3H, s, H_k), 4.33 (4H, t, $J_{h|g} = 7.4$ Hz, H_h), 1.86 (4H, quin, $J_{g|h,f} = 6.5$ Hz, H_g), 1.09–1.45 (20H, m, $H_{b,c,d,e,f}$), 0.84 (6H, t, $J_{a|b} = 6.3$ Hz, H_a). ^{13}**C**$\{^1$**H**$\}$ **NMR** (101 MHz; 1 :1 $CDCl_3$:MeOD) δ (ppm): 142.1, 141.0, 133.4, 133.1, 89.7, 51.6, 50.3, 32.0, 30.1, 29.4, 29.3, 26.7, 22.9, 14.2. **HRESI-MS** (pos.): 704.1428, calc. for $[C_{26}H_{40}I_2N_7]^+ = 704.1429$.

Bis-octyl(iodotriazolyl)-*N*-methyl-pyridinium hexafluorophosphate, 11·PF_6



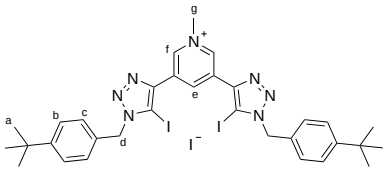
11·I (0.050 g, 60 μmol) was suspended in $CHCl_3$ (50 mL) and washed with 0.1 M $NH_4PF_{6(aq.)}$ (8 × 10 mL) and H_2O (2 × 10 mL). The solvent was removed *in vacuo* to yield **11**·PF_6 (0.032 g, 63%). ^{1}**H NMR** (400 MHz; $CDCl_3$) δ (ppm): 9.68 (1H, s, H_i), 9.29 (2H, s, H_j), 4.62 (3H, s, H_k), 4.45 (4H, t, $J_{h|g} = 7.3$ Hz, H_h), 1.94 (4H, q, $J_{g|h,i} = 6.6$ Hz, H_g), 1.18–1.45 (20H, m, $H_{b,c,d,e,f}$), 0.87 (6H, t, $J_{a|b} =$ 6.4 Hz, H_a). ^{13}**C**$\{^1$**H**$\}$ **NMR** (101 MHz; $CDCl_3$) δ (ppm): 142.5, 141.0, 137.1, 132.1, 79.7, 51.5, 50.0, 31.7, 29.7, 29.0, 28.9, 26.4, 22.6, 14.0. ^{31}**P NMR** (162 MHz; $CDCl_3$) δ (ppm): -144.63 (spt, $J = 714.0$ Hz, PF_6). ^{19}**F NMR** (376 MHz; $CDCl_3$) δ (ppm): -72.18 (d, $J = 714.0$ Hz, PF_6). **HRESI-MS** (pos.): 704.1428, calc. for $[C_{26}H_{40}I_2N_7]^+ = 704.1429$.

Bis-benzyl(iodotriazolyl)-*N*-methyl-pyridinium iodide, 12·I



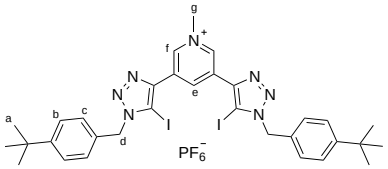
7 (0.068 g, 0.11 mmol) was dissolved in dry DCM (10 mL). CH_3I (0.20 mL, 0.46 g, 3.2 mmol) was added and the solution was stirred under an atmosphere of N_2 for 72 h after which a shiny white precipitate had formed. The solvent was removed under reduced pressure. The mixture was cooled to 0 °C in an ice bath, filtered through a frit, washed with DCM and dried *in vacuo* to give **12**·I as an off-white powder. Yield: 0.070 g (85%). ^{1}**H NMR** (300 MHz; DMSO$-d_6$) δ (ppm): 9.45–9.68 (3H, m, $H_{e,f}$), 7.16– 7.52 (10H, m, $H_{a,b,c}$), 5.83 (4H, s, H_d), 4.53 (3H, s, H_g). ^{13}**C**$\{^1$**H**$\}$ **NMR** (75 MHz; DMSO$-d_6$) δ (ppm): 143.3, 142.5, 136.3, 135.0, 130.4, 128.9, 128.4, 127.5, 53.7, 48.7. **HRESI-MS** (pos.): 659.9860 calc. for $[C_{24}H_{20}I_2N_7]^+ = 659.9564$.

Bis-(*tert*-butyliodotriazolyl)-*N*-methyl pyridinium iodide, 13·I



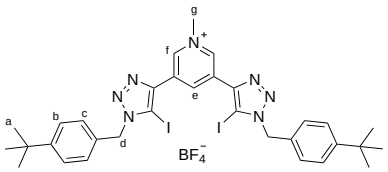
9 (0.14 g, 0.18 mmol) was dissolved in dry DCM (10 mL). CH_3I (0.40 mL, 6.2 mmol) was added and the mixture stirred under N_2 for 7 days. The mixture was cooled to 0 °C, filtered through a glass frit and washed with cold DCM. The precipitate was collected and dried *in vacuo*. Due to poor solubility, **13**·I was used in subsequent anion exchanges without characterisation.

Bis-(*tert*-butyliodotriazolyl)-*N*-methyl pyridinium PF_6, 13·PF_6



13·I (0.093 g, 0.1 mmol) was taken up in DCM (50 mL) and was washed with $NH_4PF_{6(aq.)}$ (8 × 20 mL) and H_2O (2 × 20 mL). The solvent was removed *in vacuo* to afford **13**·PF_6 (0.086 g, 91%). ^{1}**H NMR** (500 MHz; $CDCl_3$) δ (ppm): 9.62 (1H, s, H_e), 9.25 (2H, s, H_f), 7.14–7.43 (8H, m, $H_{b,c}$), 5.61 (4H, s, H_d), 4.56 (3H, s, H_g), 1.28 (18H, s, H_a). ^{13}**C**$\{^1$**H**$\}$ **NMR** (126 MHz; $CDCl_3$) δ (ppm): 152.0, 142.9, 141.1, 137.0, 132.0, 130.4, 127.8, 126.0, 80.2, 54.5, 50.0, 34.6, 31.2. ^{31}**P NMR** (202 MHz; $CDCl_3$) δ (ppm): -144.6 (spt, $J = 714$ Hz, PF_6). ^{19}**F NMR** (283 MHz; $CDCl_3$) δ (ppm): -72.5 (d, $J = 714$ Hz, PF_6). **HRESI-MS** (pos.): 772.10947, calc. for $[C_{32}H_{36}I_2N_7]^+ = 772.11161$.

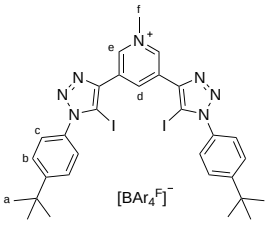
Bis-(*tert*-butyliodotriazolyl)-*N*-methyl pyridinium BF_4, 13·BF_4



9 (76 mg, 0.10 mmol) was dissolved in dry DCM (10 mL) under N_2. $[Me_3O][BF_4]$ (15 mg, 0.10 mmol) was dissolved in dry DCM (6 mL) and added dropwise to the above solution over 3 mins. The reaction mixture was stirred for 16 h. The remaining $[Me_3O][BF_4]$ was quenched with MeOH (2mL) and

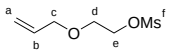
the solvent was removed *in vacuo*. Purification by preparative thin layer chromatography (4% MeOH in DCM) yielded **13**·BF_4 (0.093 g, 57%). ^{1}**H NMR** (300 MHz; $CDCl_3$) δ (ppm): 9.66 (1H, br. s., H_e), 9.31 (2H, br. s., H_f), 7.16–7.46 (8H, m, $H_{b,c}$), 5.57 (4H, s., H_d), 4.60 (3H, s., H_g), 1.10–1.39 (18H, m, H_a). ^{19}**F NMR** (283 MHz; $CDCl_3$) δ (ppm): -150.73 (s, BF_4).

Bis-(*tert*-butylphenyliodotriazolyl)-*N*-methyl pyridinium BAr^F_4, 14·BAr^F_4



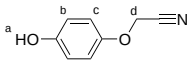
10 (0.15 g, 0.2 mmol) was dissolved in dry DCM (10 mL). CH_3I (0.40 mL, 6.2 mmol) was added and the mixture stirred under N_2 for 7 days. The mixture was cooled to 0 °C, filtered through a glass frit and washed with cold DCM. The precipitate was collected and dried *in vacuo*. The solid was suspended in $CHCl_3$ (60 mL). $NaBAr^F_4$ (0.16 g, 0.2 mmol) was added and the mixture stirred for 16 h. H_2O (20 mL) was added. The organic layer was separated and dried over $MgSO_4$. The solvent was removed *in vacuo* to yield **14**·BAr^F_4 as a pale brown powder (0.26 g, 81%). ^{1}**H NMR** (300 MHz; $CDCl_3$) δ (ppm): 10.09 (1H, s, H_d), 9.29 (2H, d, $^4J_{e|d} = 1.2$ Hz, H_e), 7.36–7.73 (20H, m, $H_{b,c,g,h}$), 4.43 (3H, s, H_f), 1.33–1.48 (18H, m, H_a). ^{19}**F NMR** (283 MHz; $CDCl_3$) δ (ppm): -62.31 (s, BAr^F_4). **HRESI-MS** (pos.): 744.08059, calc. for $[C_{30}H_{32}I_2N_7]^+ = 744.08031$.

Allyloxyethyl mesylate, 15



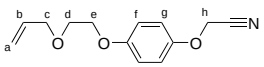
2-Allyloxyethanol (7.5 mL, 70.1 mmol) and Et_3N (20.5 mL, 147 mmol) were dissolved in dry DCM (100 mL) and stirred at 0 °C under N_2. MsCl (6.5 mL, 83 mmol) in dry DCM (50 mL) was then added dropwise and the resultant mixture was left to warm to room temperature and stirred for 1 h. The mixture was washed with H_2O (2 × 75 mL), HCl (1 M aq., 3 × 75 mL) and brine (3 × 75 mL) and dried over $MgSO_4$. The solvent was removed *in vacuo* to yield **15** as an orange oil (12.3 g, 98%). ^{1}**H NMR** (300 MHz; $CDCl_3$) δ (ppm): 5.78–5.97 (1H, m, H_b), 5.14– 5.34 (2H, m, H_a), 4.30–4.41 (4H, m, H_e), 4.02 (4H, dt, $J_{b|c} = 5.6$ Hz, $^4J_{a|c} = 1.4$ Hz, H_c), 3.65–3.73 (4H, m, H_d), 3.00–3.09 (3H, m, H_f). **LRESI-MS** (pos.): 181.1, calc. for $[C_6H_{12}O_4S \cdot H]^+ = 181.1$.

Monosubstituted hydroquinone, 16



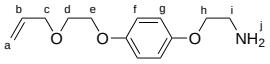
A 1:1 mixture of dioxane:H_2O (400 mL) was thoroughly degassed and stirred under an atmosphere of N_2. NaOH (8.43 g, 211 mmol) and hydroquinone (11.6 g, 105 mmol) were added and dissolved. Thereafter, a solution of bromoacetonitrile in degassed dioxane (50 mL) was added. The reaction mixture was stirred for 1 h with continuous degassing. Once the reaction had run to completion, it was acidified with 1 M $HCl_{(aq.)}$ (250 mL) and extracted with DCM (3 $\times$ 200 mL). The organic fractions were combined, washed with brine (200 mL), dried over $MgSO_4$ and dried under reduced pressure. Purification by silica gel column chromatography (2% MeOH in DCM) gave the product, **16**, as an off-white solid. Yield: 10.5 g (67%). ^{1}**H NMR** (300 MHz; $CDCl_3$) δ (ppm): 6.76–6.96 (4H, m, $H_{b,c}$), 5.15 (1H, br. s., H_a), 4.71 (2H, s, H_d). ^{13}**C**$\{^1$**H**$\}$ **NMR** (75 MHz; $CDCl_3$) δ (ppm): 151.6, 150.6, 116.9, 116.4, 115.4, 55.0. **LRESI-MS** (neg.): 148.0, calc. for $[C_8H_8NO_2]^- = 148.0$.

Vinyl- and MeCN-appended hydroquinone, 17



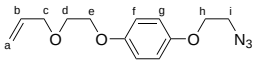
16 (3.30 g, 22.0 mmol), **15** (3.98 g, 22.0 mmol) and K_2CO_3 (3.35 g, 24.0 mmol) were dissolved in dry MeCN (150 mL) and the solution stirred and heated at reflux under N_2 for 3 days. The mixture was allowed to cool to room temperature, filtered and the solvent removed *in vacuo*. The resulting residue was dissolved in DCM (75 mL) and washed with 1 M $HCl_{(aq.)}$ (2 $\times$ 50 mL), H_2O (2 $\times$ 50 mL) and brine (2 $\times$ 50 mL) and dried over $MgSO_4$. The solvent was removed *in vacuo*. Purification by silica gel column chromatography (7:3 hexane:EtOAc) yielded **17** as a brown oil (3.60 g, 70%). ^{1}**H NMR** (300 MHz; $CDCl_3$) δ (ppm): 6.82–7.00 (4H, m, $H_{f,g}$), 5.82–6.04 (1H, m, H_b), 5.14–5.37 (2H, m, H_a), 4.69 (2H, s, H_h), 4.02–4.14 (4H, m, $H_{c,e}$), 3.74–3.84 (2H, m, H_d). **LRESI-MS** (pos.): 256.1, calc. for $[C_{13}H_{15}NO_3 \cdot Na]^+ = 256.1$.

Vinyl-appended amine, 18



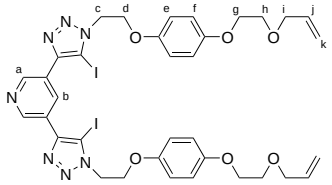
17 (1.5 g, 6.4 mmol) dissolved in dry Et_2O (30 mL) was added dropwise to a suspension of $LiAlH_4$ (0.422 g, 11.1 mmol) in dry Et_2O (30 mL) under N_2. The mixture was stirred at reflux for 3 h and cooled to room temperature thereafter. H_2O (0.5 mL) and NaOH (10% aq., 0.5 mL) were added dropwise to begin quenching the reaction followed by the dropwise addition of H_2O (4.5 mL), NaOH (10% aq., 4.5 mL) and additional H_2O (10 mL). The aluminium salts were removed by filtration and washed with Et_2O (3×50 mL). The combined organics were dried over $MgSO_4$ and the solvent removed *in vacuo* to yield **18** as an orange oil (1.26 g, 83%). ^{1}**H NMR** (300 MHz; $CDCl_3$) δ (ppm): 6.70–6.98 (4H, m, $H_{f,g}$), 5.80–6.05 (1H, m, H_b), 5.10–5.39 (2H, m, H_a), 4.00–4.12 (4H, m, $H_{c,h}$), 3.91 (2H, t, $J_{e|d} = 5.0$ Hz, H_e), 3.70–3.80 (2H, t, $J_{d|e} = 5.0$ Hz, H_d), 3.03 (2H, t, $J_{i|h} = 5.0$ Hz, H_i), 1.58 (2H, br. s, H_j). **LRESI-MS** (pos.): 238.1, calc. for $[C_{13}H_{19}NO_3 \cdot H]^+ = 238.1$.

Vinyl-appended azide, 19



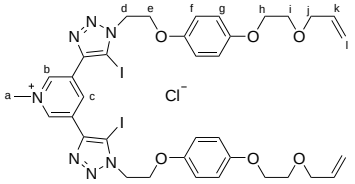
Vinyl-appended hydroquinone-ethylamine (0.912 g, 3.8 mmol) was dissolved in MeOH (60mL). Imidazolylsulfonyl azide·H_2SO_4 (1.26 g, 4.6 mmol), K_2CO_3 (1.334 g, 9.6 mmol) and $CuSO_4 \cdot 5\,H_2O$ (0.010 g, 0.04 mmol) were added and the white suspension stirred at room temperature under N_2 for 16 h. The mixture was cautiously concentrated to $\sim$ 5 mL under reduced pressure. The mixture was then diluted with HCl (10% aq., 100 mL) and extracted with EtOAc (3×100 mL). The combined organics were washed with brine (100 mL), dried over $MgSO_4$ and the solvent removed *in vacuo*. Purification by silica gel column chromatography (2:1 Petroleum ether:EtOAc) yielded **19** as a colourless oil (0.747 g, 75%). ^{1}**H NMR** (400 MHz; $CDCl_3$) δ (ppm): 6.78–6.93 (21H, m, $H_{f,g}$), 5.94 (1H, ddt, $J_{b|a_{trans}} = 17.2$ Hz, $J_{b|a_{cis}} = 10.4$ Hz, $J_{b|c} = 5.7$ Hz, H_b), 5.12–5.40 (2H, m, H_a), 4.00–4.19 (6H, m, $H_{c,h,i}$), 3.78 (2H, t, $J_{e|d} = 5.1$ Hz, H_e), 3.56 (2H, t, $J_{d|e} = 5.1$ Hz, H_d). **LRESI-MS** (pos.): 286.1, calc. for $[C_{13}H_{17}N_3O_3 \cdot Na]^+ = 286.1$.

Bis-vinyl appended iodotriazolyl pyridine, 20



19 (0.29 g, 1.1 mmol) was dissolved in dry degassed THF (2 mL) and the reaction vessel was covered in foil. NaI (0.61 g, 4.0 mmol) and $Cu(ClO_4)_2 \cdot 6\,H_2O$ (0.748 g, 2.0 mmol) were added and stirred under N_2 for 5 mins. TBTA (0.008 g, 0.02 mmol), DBU (0.152 g, 1.0 mmol) and **1** (0.065 g, 0.5 mmol) were added in order. The mixture was stirred for 16 h, diluted and transferred to a separating funnel with DCM (100 mL). The organics were washed with NH_4OH (2 $\times$ 40 mL), brine (2 $\times$ 40 mL) and dried over $MgSO_4$. The solvent was removed *in vacuo*. Purification by silica gel column chromatography (2% MeOH in DCM) as the eluent to yield **20** as a white powder (0.374 g, 83%). ^{1}**H NMR** (500 MHz; $CDCl_3$) δ (ppm): 9.24 (2H, d, $^4J_{a|b} = 1.8$ Hz, H_a), 8.83 (1H, t, $^4J_{b|a} = 2.0$ Hz, H_b), 6.75–6.90 (8H, m, $H_{e,f}$), 5.86–5.98 (2H, m, H_j), 5.14–5.35 (4H, m, H_k), 4.85 (4H, t, $J_{c|d} = 5.6$ Hz, H_c), 4.45 (4H, t, $J_{d|c} = 5.6$ Hz, H_d), 4.01–4.15 (8H, m, $H_{g,i}$), 3.72–3.80 (4H, m, H_h). ^{13}**C**$\{^1$**H**$\}$ **NMR** (126 MHz; $CDCl_3$) δ (ppm): 153.6, 152.1, 148.1, 147.0, 134.5, 133.1, 126.2, 117.4, 115.7, 115.6, 78.6, 72.4, 68.5, 68.1, 66.7, 50.1. **HRESI-MS** (pos.): 906.09576, calc. for $[C_{35}H_{37}I_2N_7O_6 \cdot H]^+ = 906.09674$.

Bis-vinyl appended iodotriazolyl *N*-methyl pyridinium chloride, 21·Cl

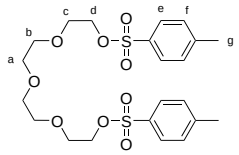


20 (92 mg, 0.10 mmol) was dissolved in dry DCM (5 mL) under N_2. $[Me_3O][BF_4]$ (15 mg, 0.10 mmol) was dissolved in dry DCM (10 mL) and added dropwise to the above solution over 3 mins. The reaction mixture was stirred for 16 h. The remaining $[Me_3O][BF_4]$ was quenched with MeOH (2mL) and the solvent was removed *in vacuo*. Purification was undertaken by Preparative TLC using 4% MeOH/DCM as the eluent to yield **21**·BF_4 (0.083 g, 82%) after extraction from the silica with 10% MeOH/DCM and subsequent *in vacuo* solvent removal.

Alternate method: 20 (0.37 g, 0.41 mmol) was dissolved in dry DCM (20 mL). CH_3I (0.19 mL, 9.6 mmol) was added and the mixture stirred under N_2 for 7 days. The solvent and CH_3I were removed *in*

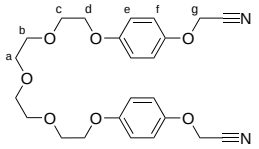
vacuo. The residue was taken up in $CHCl_3$ (20 mL) and washed with NH_4Cl (1 M aq., 8 × 10 mL) and H_2O (2 × 10 mL) and dried over $MgSO_4$. The solvent was removed *in vacuo* to yield **21**·Cl as a white powder (0.22 g, 57%). ^{1}**H NMR** (500 MHz; $CDCl_3$) δ (ppm): 9.94 (1H, br. s., H_c), 9.38 (2H, br. s., H_b), 6.78 (8H, s, $H_{f,g}$), 5.78–6.02 (2H, m, H_k), 5.10–5.39 (2H, m, H_l), 4.76 (3H, br. s., H_a), 4.60 (4H, br. s., H_d), 4.27 (4H, br. s., H_j), 3.94–4.13 (8H, m, $H_{e,h}$), 3.74 (4H, t, $J_{i|h} = 4.2$ Hz, H_i). ^{13}**C**$\{^1$**H**$\}$ **NMR** (126 MHz; $CDCl_3$) δ (ppm): 153.6, 152.1, 141.1, 140.3, 134.5, 132.7, 117.4, 115.7, 115.6, 72.3, 68.6, 68.0, 66.2, 51.0, 50.3, 29.7. **HRESI-MS** (pos.): 920.11064, calc. for $[C_{36}H_{40}I_2N_7O_6]^+ = 920.11239$.

Bis-tosylate polyether, 22



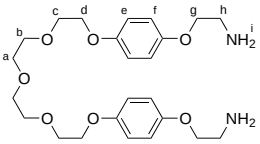
Tetraethylene glycol (10.4 mL, 60 mmol) was dissolved in dry DCM (100 mL). To this solution was added *p*-toluenesulfonyl chloride (23.4 g, 123 mmol) and the resulting mixture cooled in an ice bath. Thereafter, freshly ground KOH was added in small portions maintaining a temperature below 5 °C. The mixture was stirred under an atmosphere of N_2 for 3 h. The resulting mixture was poured onto ice water and DCM (100 mL) was added. The organic layer was then separated and the aqueous layer washed with DCM (3 × 100 mL). The organic fractions were combined, dried over $MgSO_4$ and the solvent removed under reduced pressure. The resulting colourless oil was dissolved with hot ethanol (350 mL) which was cooled in the freezer overnight to give a waxy white solid. The supernatant was decanted and the solid warmed to room temperature to give **22** as a colourless oil which was dried *in vacuo* at less than 7 mbar for 2 days. Yield: 2.835 g (99%). ^{1}**H NMR** (300 MHz; $CDCl_3$) δ (ppm): 7.80 (4H, dt, $J_{e|f} = 8$, H_e), 7.34 (4H, d, $J_{e|f} = 8$ Hz, H_f), 4.16 (4H, t, $J_{c|d} = 5$ Hz, H_d), 3.50–3.73 (12H, m, $H_{a,b,c}$), 2.45 (6H, s, H_g). ^{13}**C**$\{^1$**H**$\}$ **NMR** (75 MHz; $CDCl_3$) δ (ppm): 144.8, 132.9, 129.8, 127.9, 70.7, 70.5, 69.2, 68.6, 21.6. **LRESI-MS** (pos.): 503.1, calc. for $[C_{22}H_{30}O_9S_2 \cdot H]^+ = 503.1$.

Bis-nitrile polyether, 23



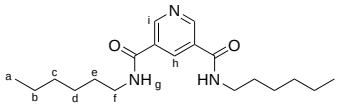
16 (1.68 g, 11.2 mmol) and **22** (2.6 g, 5.1 mmol) were dissolved in dry MeCN (100 mL). K_2CO_3 (6.91 g, 50.0 mmol) was added to the solution which was heated to reflux under an atmosphere of N_2 for 72 h. The mixture was cooled to room temperature and filtered through a cotton wool plug to remove the excess base. The MeCN was removed *in vacuo* and the residue taken up in $CHCl_3$ (75 mL) and filtered through a cotton wool plug. The $CHCl_3$ was removed *in vacuo* to yield **23** as a white oily solid. Yield: 0.935 g (41%). ^{1}**H NMR** (300 MHz; $CDCl_3$) δ (ppm): 6.83–6.99 (8H, m, $H_{e,f}$), 4.71 (4H, s, H_g), 4.04–4.16 (4H, m, H_d), 3.79–3.91 (4H, m, H_c), 3.63–3.78 (8H, m, $H_{a,b}$). **LRESI-MS** (pos.): 479.2, calc. for $[C_{24}H_{28}N_2O_7 \cdot Na]^+ = 479.2$.

Bis-amine polyether, 24



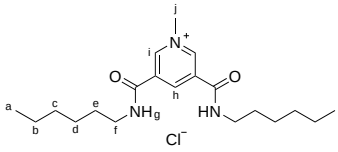
23 (0.935 g, 2.05 mmol) was dissolved in dry THF (100 mL) and added dropwise to 1 M $BH_3 \cdot$ THF (14 mL, 14 mmol) that had been preheated to 70 °C. The solution was heated at reflux under an atmosphere of N_2 for 4 h and then cooled to 0 °C in an ice bath. The reducing agent was quenched by the dropwise addition of MeOH (35 mL). 6 M $HCl_{(aq.)}$ (35 mL) was added until the precipitate that was formed by addition of acid had redissolved. The organic solvents were removed *in vacuo*. The aqueous solution was basified by the addition of NaOH (10% aq., 60 mL) resulting in the formation of a white precipitate. The mixture was cooled to 5 °C, filtered and washed with H_2O (3 $\times$ 20 mL). The white powder, **24**, was dried *in vacuo*. Yield: 0.81 g (85%). ^{1}**H NMR** (300 MHz; $CDCl_3$) δ (ppm): 6.84 (8H, s, $H_{e,f}$), 4.08 (4H, t, $J_{g|h} = 5$ Hz, H_g), 3.93 (4H, t, $J_{c|d} = 5$ Hz, H_d), 3.84 (4H, t, $J_{g|h} = 5$ Hz, H_h), 3.66–3.77 (8H, m, $H_{a,b}$), 3.06 (4H, br. s., H_c). **LRESI-MS** (pos.): 465.3 calc. for $C_{24}H_{36}N_2O_7 \cdot H]^+ = 465.3$.

Bis-hexylamide pyridine, 25



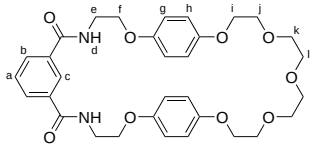
Pyridine-3,5-dicarboxylic acid (1.72 g, 9.00 mmol) was suspended in $SOCl_2$ (5 mL) and a catalytic drop of DMF was added to start the reaction. The mixture was refluxed for 16 h. Excess $SOCl_2$ was removed *in vacuo* and collected in a dry ice–acetone bath. The bis-acid chloride was reacted on immediately assuming quantitative conversion. The bis-acid chloride was dissolved in DCM (20 mL) and added dropwise to a solution of *n*-hexylamine (2.4 mL, 18 mmol) and Et_3N (5 mL) in dry DCM (80 mL) at 0 °C. The mixture was stirred for 2 h at room temperature under N_2. The mixture was washed with citric acid (10% aq., 4 × 120 mL) and H_2O (2 × 120 mL) and dried over $MgSO_4$. The solvent was removed *in vacuo* to yield **25** as an off-white solid (2.94 g, 98%). **^{1}H NMR** (300 MHz; $CDCl_3$) δ (ppm): 9.09 (2H, d, $^4J_{i|h} = 1.8$ Hz, H_i), 8.45 (1H, t, $^4J_{h|i} = 2.3$ Hz, H_h), 6.45 (2H, br. s., H_g), 3.39–3.56 (4H, m, H_f), 1.64 (4H, quin, $J_{e|f,d} = 7.2$ Hz, H_e), 1.28–1.46 (12H, m, $H_{b,c,d}$), 0.85–0.94 (6H, m, H_a). **LRESI-MS** (pos.): 334.2, calc. for $[C_{19}H_{31}N_3O_2 \cdot H]^+ = 334.2$.

Bis-hexylamide *N*-methyl pyridinium, 26·Cl



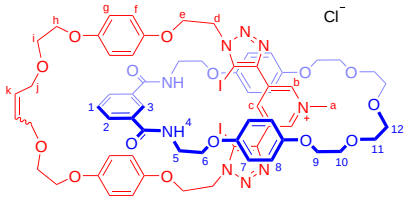
25 (1.5 g, 4.5 mmol) and CH_3I (2.3 mL, 36 mmol) were dissolved in $CHCl_3$ (50 mL) and the solution refluxed for 3 days under N_2. The mixture was cooled to room temperature and the solvent and CH_3I were removed *in vacuo*. The residue was redissolved in $CHCl_3$ and washed with NH_4Cl (8 × 100 mL) and H_2O (2 × 100 mL). The organics were dried over $MgSO_4$ and The solvent was removed *in vacuo* to yield **26**·Cl as a yellow solid (1.51 g, 88%). **^{1}H NMR** (300 MHz; $CDCl_3$) δ (ppm): 10.58 (1H, s, H_h), 9.49 (2H, t, $J_{g|h} = 5.3$ Hz, H_g), 9.35 (2H, s, H_i), 4.56 (3H, s, H_j), 3.44 (4H, dt, $J_{f|e} = 7.3$ Hz, $J_{f|g} = 5.9$ Hz, H_f), 1.64–1.78 (4H, m, H_e), 1.22–1.45 (12H, m, $H_{b,c,d}$), 0.82–0.98 (6H, m, H_a). **LRESI-MS** (pos.): 348.3, calc. for $[C_{20}H_{34}N_3O_2]^+ = 348.3$.

Isophthalamide macrocycle, 27



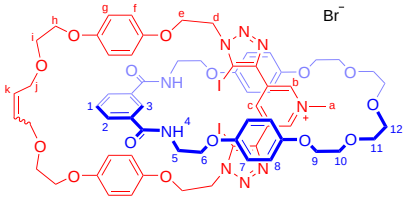
24 (0.47 g, 1.0 mmol), **26**·Cl (0.38 g, 1.0 mmol) and Et_3N (3.4 mL, 23 mmol) were dissolved in dry DCM (50 mL) and stirred until all solid had dissolved. Isophthalyl dichloride (0.21 g, 1.0 mmol) in dry DCM (20 mL) was added dropwise and the mixture was stirred for 1 h. Thereafter, the organics were washed with HCl (10% aq, 2 × 50 mL) and H_2O (2 × 50 mL), and dried over $MgSO_4$. The solvent was removed *in vacuo*. Purification by silica gel column chromatography (5% MeOH in DCM) afforded **27** as a white solid (0.213 g, 36%). ^{1}**H NMR** (300 MHz; $CDCl_3$) δ (ppm): 8.04 (2H, dd, $J_{b|a} = 7.6$ Hz, $^4J_{b|c} = 1.5$ Hz, H_b), 7.96 (1H, s, H_c), 7.55 (1H, t, $J_{a|b} = 7.6$ Hz, H_a), 6.78 (8H, s, $H_{g,h}$), 6.71 (2H, s, H_d), 3.98–4.13 (8H, m, $H_{e,f}$), 3.80–3.89 (8H, m, $H_{i,j}$), 3.66–3.72 (9H, m, $H_{k,l}$). **LRESI-MS** (pos.): 595.31, calc. for $[C_{32}H_{38}N_2O_9 \cdot H]^+ = 595.27$.

Isophthalamide–bis-iodotriazole pyridinium catenane chloride, 28·Cl



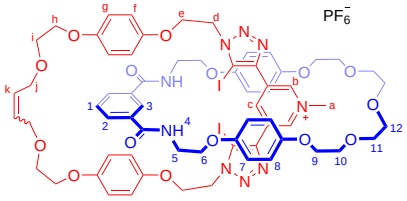
21·Cl (0.031 g, 50 μmol) and **27** (0.018 g, 50 μmol) were dissolved in dry DCM (6 mL) and stirred for 30 mins. Grubbs' II catalyst (4 mg, 10% by weight) was added and the mixture was stirred at room temperature under N_2 for 7 days. The solvent was removed *in vacuo*. Purification by preparative thin layer chromatography (5% MeOH in DCM) afforded **28**·Cl (0.020 g, 41%). ^{1}**H NMR** (500 MHz; $CDCl_3$) δ (ppm): 9.56 (2H, br. s., H_b), 9.27 (1H, br. s., H_3), 8.57 (1H, br. s., H_4), 8.39 (3H, m, $H_{2,4}$), 7.61 (1H, s, H_c), 7.51 (1H, t, $J_{1|2} = 7.6$ Hz, H_1), 6.62–6.88 (8H, m, $H_{f,g}$), 6.35 (2H, d, $J_{7|8} = 7.8$ Hz, $H_{7,8}$), 5.95 (2H, d, $J_{7|8} = 7.3$ Hz, $H_{7,8}$), 5.69 (2H, br. s., H_k), 5.42 (2H, d, $J_{7|8} = 7.2$ Hz, $H_{7,8}$), 5.21 (2H, d, $J_{7|8} = 7.9$ Hz, $H_{7,8}$), 4.76 (3H, br. s., H_a), 3.35–4.40 (44H, m, $H_{d,e,h,i,j,5,6,9,10,11,12}$). **HRESI-MS** (pos.): 1486.3396, calc. for $[C_{66}H_{74}I_2N_9O_{15}]^+ = 1486.3388$.

Isophthalamide–bis-iodotriazole pyridinium catenane bromide, 28·Br



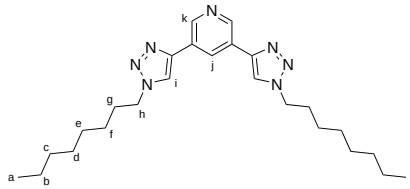
28·Cl (0.016 g, 11 μmol) was taken up in $CHCl_3$ (40 mL) and washed with 1 M $NH_4Br_{(aq.)}$ (8 × 25 mL) and H_2O (2 × 25 mL). The solvent was removed *in vacuo* to afford **28**·Br (9.6 mg, 57%). **^{1}H NMR** (500 MHz; $CDCl_3$) δ (ppm): 9.56 (2H, br. s., H_b), 9.19 (1H, br. s., H_3), 8.31–8.49 (2H, m, H_4), 8.24 (2H, br. s., H_2), 7.61 (1H, s, H_c), 7.54 (1H, t, $J_{1|2} = 7.9$ Hz, H_1), 6.63–6.87 (8H, m, $H_{f,g}$), 6.36 (2H, d, $J_{7|8} = 8.2$ Hz, $H_{7,8}$), 5.98 (2H, d, $J_{7|8} = 8.2$ Hz, $H_{7,8}$), 5.68 (2H, br. s., H_k), 5.44 (2H, d, $J_{7|8} = 8.4$ Hz, $H_{7,8}$), 5.21 (2H, d, $J_{7|8} = 8.4$ Hz, $H_{7,8}$), 4.73 (3H, s, H_a), 3.37–4.42 (44H, m, $H_{d,e,h,i,j,5,6,9,10,11,12}$). **^{13}C{^{1}H} NMR** (126 MHz; $CDCl_3$) δ (ppm): 165.3, 164.8, 152.4, 151.3, 151.0, 133.5, 132.4, 131.2, 129.3, 127.9, 123.8, 114.4, 114.3, 113.1, 112.3, 87.8, 69.9, 69.0, 67.8, 66.8, 65.7, 49.5, 47.0, 39.0, 28.7. **HRESI-MS** (pos.): 1486.3393, calc. for $[C_{66}H_{74}I_2N_9O_{15}]^+ = 1486.3388$.

Isophthalamide–bis-iodotriazole pyridinium catenane hexafluorophosphate, 28·PF$_6$



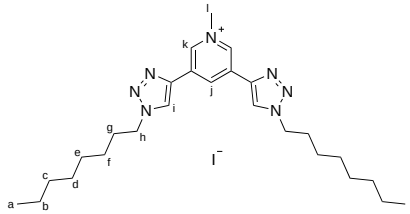
28·Cl (0.020 g, 13 μmol) was taken up in $CHCl_3$ (40 mL) and washed with 0.1 M $NH_4PF_{6(aq.)}$ (8 × 25 mL) and H_2O (2 × 25 mL). The solvent was removed *in vacuo* to afford **28**·PF_6 (0.019 g, 89%). **^{1}H NMR** (500 MHz; $CDCl_3$) δ (ppm): 9.62 (2H, br. s., H_b), 9.03 (1H, br. s., H_3), 8.66 (3H, m, $H_{2,c}$), 8.13 (1H, m, H_1), 7.72–7.87 (2H, m, H_4), 7.10–7.24 (8H, m, $H_{f,g}$), 6.40 (8H, br. s., $H_{7,8}$), 6.17 (2H, br. s., H_k), 5.08 (3H, br. s., H_a), 3.85–4.45 (44H, m, $H_{d,e,h,i,j,5,6,9,10,11,12}$). **^{13}C{^{1}H} NMR** (126 MHz; $CDCl_3$) δ (ppm): 165.3, 152.4, 151.0, 150.5, 141.9, 133.6, 132.8, 130.9, 129.9, 128.0, 127.3, 114.5, 114.3, 113.6, 113.0, 70.0, 70.0, 69.9, 69.1, 67.8, 66.9, 65.0, 49.5, 28.7 **^{31}P NMR** (202 MHz; $CDCl_3$) δ (ppm): -140.33 (spt, $J = 714.0$ Hz, PF_6) **^{19}F NMR** (470 MHz; $CDCl_3$) δ (ppm): -71.16 (d, $J = 714.0$ Hz, PF_6). **HRESI-MS** (pos.): 1486.3392, calc. for $[C_{66}H_{74}I_2N_9O_{15}]^+ = 1486.3388$.

Bis-octyltriazolyl pyridine, 29



Na_2CO_3 (0.054 g, 0.5 mmol), ascorbic acid (0.089 g, 0.5 mmol) and $CuSO_4 \cdot 5\,H_2O$ (0.009 g, 30 μmol) were added to a solution of **1** (0.064 g, 0.5 mmol) in 4:1 DMF:H_2O (7.5 mL). **3** (0.17 g, 1.1 mmol) was added and the solution was heated to 80 °C under N_2 for 3 days. The mixture was cooled to room temperature and partitioned between EtOAc (25 mL) and NH_4OH (25 mL). The aqueous layer was washed with a further portion of EtOAc (25 mL). The combined organics were washed with H_2O (15 mL) and brine (15 mL) and dried over $MgSO_4$. The solvent was removed *in vacuo*. Purification by silica gel column chromatography (3% MeOH in DCM) afforded **29** (0.133 g, 61%). ^{1}**H NMR** (500 MHz; $CDCl_3$) δ (ppm): 9.02 (2H, br. s., H_k), 8.60 (1H, t, $^4J_{j|k} = 1.8$ Hz, H_j), 7.91 (2H, s, H_i), 4.43 (4H, t, $J_{h|g} = 7.2$ Hz, H_h), 1.96 (4H, quin, $J_{g|h,f} = 7.0$ Hz, H_g), 1.17–1.45 (20H, m, $H_{b,c,d,e,f}$), 0.86 (6H, t, $J_{a|b} = 6.9$ Hz, H_a). ^{13}**C**$\{^1$**H**$\}$ **NMR** (126 MHz; $CDCl_3$) δ (ppm): 146.2, 144.4, 129.6, 126.9, 120.1, 50.6, 31.7, 30.3, 29.0, 28.9, 26.5, 22.6, 14.0. **HRESI-MS** (pos.): 438.33290, calc. for $[C_{25}H_{39}N_7 \cdot H]^+ = 438.33397$.

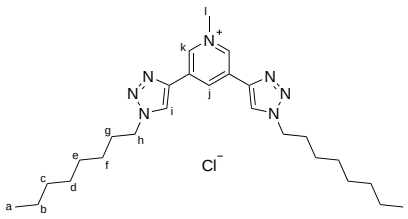
Bis-octyltriazolyl-pyridinium iodide, 30·I



29 (0.10 g, 0.22 mmol) was dissolved in dry DCM (20 mL). CH_3I (0.37 mL, 5.7 mmol) was added and the mixture was stirred under N_2 for 7 days. The solvent was removed *in vacuo*. Purification by preparative thin layer chromatography (5% MeOH in DCM) yielded **30**·I (0.12 g, 91%). ^{1}**H NMR** (500 MHz; $CDCl_3$) δ (ppm): 9.57 (1H, s, H_k), 9.55 (2H, s, H_j), 9.32 (2H, s, H_i), 4.66 (3H, s, H_l), 4.44 (4H, t, $J_{h|g} = 7.3$ Hz, H_h), 2.01 (4H, quin, $J_{g|h,f} = 7.3$ Hz, H_g), 1.20–1.42 (20H, m, $H_{b,c,d,e,f}$), 0.87 (6H, t, $J_{a|b} = 6.9$ Hz, H_a). ^{13}**C**$\{^1$**H**$\}$ **NMR** (126 MHz; $CDCl_3$) δ (ppm): 139.9, 138.7, 136.4, 133.1, 125.9, 51.1,

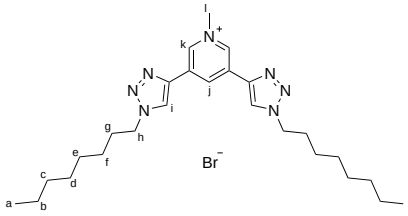
49.3, 31.7, 30.1, 29.1, 28.9, 26.4, 22.6, 14.1. **HRESI-MS** (pos.): 452.34748, calc. for $[C_{26}H_{42}N_7]^+ =$ 452.34962.

Bis-octyltriazolyl-pyridinium chloride, 30·Cl



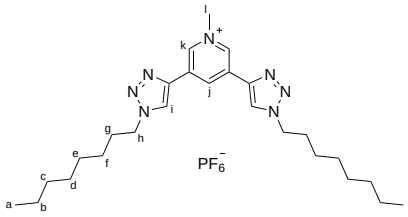
30·I (0.030 g, 52 μmol) was suspended in $CHCl_3$ (50 mL) and washed with 1 M $NH_4Cl_{(aq.)}$ (8 × 10 mL) and H_2O (2 × 10 mL). The solvent was removed *in vacuo* to yield **30**·Cl (0.025 g, quant.). ^{1}**H NMR** (500 MHz; $CDCl_3$) δ (ppm): 9.68 (1H, s, H_j), 9.61 (2H, s, H_k), 9.26 (2H, s, H_i), 4.66 (3H, s, H_l), 4.36 (4H, t, $J_{h|g} = 7.4$ Hz, H_h), 1.93 (4H, quin, $J_{g|h,i} = 6.7$ Hz, H_g), 1.16–1.36 (20H, m, $H_{b,c,d,e,f}$), 0.84 (6H, t, $J_{a|b} = 6.8$ Hz, H_a). ^{13}**C**$\{^1$**H**$\}$ **NMR** (126 MHz; $CDCl_3$) δ (ppm): 140.1, 139.0, 136.4, 132.7, 125.5, 50.9, 49.1, 31.6, 30.1, 29.0, 28.9, 26.4, 22.5, 14.0. **HRESI-MS** (pos.): 452.3501, calc. for $[C_{26}H_{42}N_7]^+$ = 452.3496.

Bis-octyltriazolyl-pyridinium bromide, 30·Br



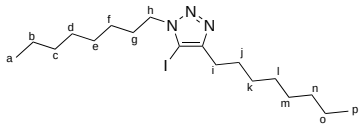
30·I (0.030 g, 52 μmol) was suspended in $CHCl_3$ (50 mL) and washed with 1 M $NH_4Br_{(aq.)}$ (8 × 10 mL) and H_2O (2 × 10 mL). The solvent was removed *in vacuo* to yield **30**·Br (0.026 g, 94%). ^{1}**H NMR** (500 MHz; $CDCl_3$) δ (ppm): 9.58 (1H, s, H_j), 9.53 (2H, s, H_k), 9.26 (2H, s, H_i), 4.66 (3H, s, H_l), 4.35 (4H, t, $J_{h|g} = 7.4$ Hz, H_h), 1.93 (4H, t, $J_{g|h,f} = 6.8$ Hz, H_g), 1.17–1.37 (20H, m, $H_{b,c,d,e,f}$), 0.84 (6H, t, $J_{a|b} = 6.9$ Hz, H_a). ^{13}**C**$\{^1$**H**$\}$ **NMR** (126 MHz; $CDCl_3$) δ (ppm): 140.0, 138.9, 136.2, 132.7, 125.6, 50.9, 49.3, 31.6, 30.0, 29.0, 28.9, 26.4, 22.5, 14.0. **HRESI-MS** (pos.): 452.3498, calc. for $[C_{26}H_{42}N_7]^+$ = 452.3496.

Bis-octyltriazolyl-pyridinium hexafluorophosphate, 30·PF_6



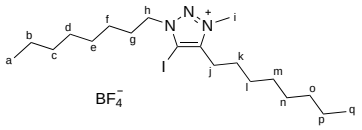
30·I (0.020 g, 36 μmol) was suspended in $CHCl_3$ (50 mL) and washed with 0.1 M $NH_4PF_{6(aq.)}$ (8 × 10 mL) and H_2O (2 × 10 mL). The solvent was removed *in vacuo* to yield **30**·PF_6 (0.019 g, 92%). ^{1}**H NMR** (500 MHz; $CDCl_3$) δ (ppm): 9.06 (2H, s, H_k), 8.96 (1H, s, H_j), 8.35 (2H, s, H_i), 4.49 (3H, s, H_l), 4.34 (4H, t, $J_{h|g} = 7.4$ Hz, H_h), 1.91 (4H, t, $J_{g|h,f} = 6.9$ Hz, H_g), 1.15–1.38 (20H, m, $H_{b,c,d,e,f}$), 0.86 (6H, t, $J_{a|b} = 6.9$ Hz, H_a). ^{13}**C**$\{^1$**H**$\}$ **NMR** (126 MHz; $CDCl_3$) δ (ppm): 139.8, 138.9, 135.6, 133.0, 123.8, 51.0, 49.3, 31.7, 29.8, 29.0, 28.8, 26.4, 22.6, 14.0. ^{31}**P NMR** (202 MHz; $CDCl_3$) δ (ppm): -144.16 (spt, $J = 714.0$ Hz, PF_6). ^{19}**F NMR** (376 MHz; $CDCl_3$) δ (ppm): -71.50 (d, $J = 714.0$ Hz, PF_6). **HRESI-MS** (pos.): 452.3494, calc. for $[C_{26}H_{42}N_7]^+ = 452.3496$.

Bis-octyliodotriazole thread, 31



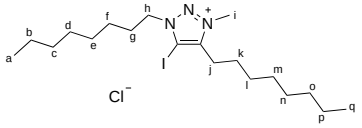
3 (0.17 g, 1.1 mmol) was dissolved in THF (2 mL) and covered in foil. NaI (0.60 g, 4.0 mmol) and $Cu(ClO_4)_2 \cdot 6\,H_2O$ (0.74 g, 2.0 mmol) were added and the mixture was stirred for 5 mins under N_2. TBTA (0.008 g, 10 μmol), DBU (0.15 g, 1 mmol, 2 × 0.5 mL THF) and decyne (0.14 g, 1.0 mmol, 2 × 0.5 mL THF) were added and the mixture was stirred under N_2 for 16 h. The reaction was diluted with DCM (80 mL) and washed with NH_4OH (2 × 40 mL) and brine (2 × 40 mL) and dried over $MgSO_4$. The solvent was removed *in vacuo*. Purification by silica gel column chromatography (1% MeOH in DCM) afforded **31** (0.384 g, 92%). ^{1}**H NMR** (500 MHz; $CDCl_3$) δ (ppm): 4.32 (2H, t, $J_{h|g} = 7.4$ Hz, H_h), 2.63 (2H, t, $J_{i|j} = 7.7$ Hz, H_i), 1.88 (2H, quin, $J_{g|h,f} = 7.4$ Hz, H_g), 1.68 (2H, quin, $J_{j|i,k} = 7.4$ Hz, H_j), 1.17–1.43 (20H, m, $H_{b,c,d,e,f,k,l,m,n,o}$), 0.87 (6H, t, $J_{a-b|o-p} = 6.8$ Hz, $H_{a,p}$). ^{13}**C**$\{^1$**H**$\}$ **NMR** (126 MHz; $CDCl_3$) δ (ppm): 150.9, 76.7, 49.7, 30.8, 30.8, 30.7, 28.9, 28.3, 28.2, 28.0, 28.0, 27.9, 25.4, 25.1, 21.7, 21.6, 13.1, 13.1. **HRESI-MS** (pos.): 420.18602, calc. for $[C_{18}H_{34}IN_3 \cdot H]^+ = 420.18702$.

Bis-octyliodotriazolium tetrafluoroborate thread, 32·BF_4



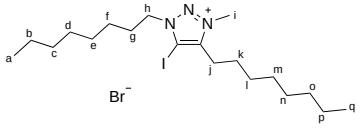
31 (0.41 g, 0.97 mmol) was dissolved in dry DCM (100 mL). $[Me_3O][BF_4]$ (0.17 g, 1.2 mmol) was added and the mixture was stirred under N_2 at room temperature for 4 days. The reaction was quenched with MeOH (10 mL). The solvent was removed *in vacuo*. Purification by preparative thin layer chromatography (5% MeOH in DCM) afforded **32**·BF_4 (0.40 g, 80%). ^{1}**H NMR** (400 MHz; $CDCl_3$) δ (ppm): 4.49 (2H, t, $J_{h|g} = 7.4$ Hz, H_h), 4.29 (3H, s, H_i), 2.90 (2H, t, $J_{j|k} = 7.9$ Hz, H_j), 2.00 (2H, quin, $J_{g|h,f} = 7.3$ Hz, H_g), 1.63 (2H, quin, $J_{k|j,l} = 7.6$ Hz, H_k), 1.17–1.46 (20H, m, $H_{b,c,d,e,f,l,m,n,o,p}$), 0.88 (6H, t, $J_{a-b|p-q} = 6.4$ Hz, $H_{a,q}$). ^{13}**C**$\{^1$**H**$\}$ **NMR** (126 MHz; $CDCl_3$) δ (ppm): 148.6, 85.2, 54.8, 38.6, 31.7, 31.6, 29.2, 29.0, 29.0, 28.9, 28.8, 28.6, 27.2, 26.2, 24.5, 22.6, 22.6, 14.1, 14.0. ^{19}**F NMR** (376 MHz; $CDCl_3$) δ (ppm): -154.64 (s, BF_4). **HRESI-MS** (pos.): 434.20070, calc. for $[C_{19}H_{37}IN_3]^+ =$ 434.20267.

Bis-octyliodotriazolium chloride thread, 32·Cl



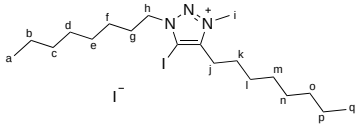
32·BF_4 (0.050 g, 96 μmol) was suspended in $CHCl_3$ (50 mL) and washed with 1 M $NH_4Cl_{(aq.)}$ ($8 \times$ 10 mL) and H_2O (2×10 mL). The solvent was removed *in vacuo* to yield **30**·Cl (0.045 g, quant.). ^{1}**H NMR** (500 MHz; $CDCl_3$) δ (ppm): 4.46 (2H, t, $J_{h|g} = 7.5$ Hz, H_h), 4.32 (3H, s, H_i), 3.02 (2H, t, $J_{j|k}$ $= 7.9$ Hz, H_j), 1.94 (2H, quin, $J_{g|h,f} = 7.4$ Hz, H_g), 1.60 (2H, quin, $J_{k|j,l} = 7.7$ Hz, H_k), 1.17–1.42 (20H, m, $H_{b,c,d,e,f,l,m,n,o,p}$), 0.86 (6H, t, $J_{a-b|p-q} = 6.6$ Hz, $H_{a,q}$). ^{13}**C**$\{^1$**H**$\}$ **NMR** (126 MHz; $CDCl_3$) δ (ppm): 146.8, 100.2, 53.3, 37.5, 30.7, 30.7, 28.4, 28.3, 28.3, 28.1, 28.0, 27.9, 26.9, 25.2, 24.1, 21.6, 21.6, 13.1, 13.1. **HRESI-MS** (pos.): 434.2029, calc. for $[C_{19}H_{37}IN_3]^+ = 434.2027$.

Bis-octyliodotriazolium bromide thread, 32·Br



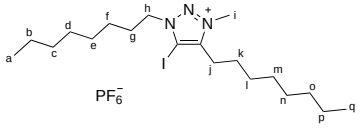
30·BF_4 (0.050 g, 96 μmol) was suspended in $CHCl_3$ (50 mL) and washed with 1 M $NH_4Br_{(aq.)}$ (8 × 10 mL) and H_2O (2 × 10 mL). The solvent was removed *in vacuo* to yield **30**·Br (0.050 g, quant.). ^{1}**H NMR** (500 MHz; $CDCl_3$) δ (ppm): 4.46 (2H, t, $J_{h|g} = 7.6$ Hz, H_h), 4.32 (3H, s, H_i), 3.02 (2H, t, $J_{j|k} = 7.9$ Hz, H_j), 1.95 (2H, quin, $J_{g|h,f} = 7.6$ Hz, H_g), 1.61 (2H, quin, $J_{k|j,l} = 7.7$ Hz, H_k), 1.15–1.41 (20H, m, $H_{b,c,d,e,f,l,m,n,o,p}$), 0.86 (6H, t, $J_{a-b|p-q} = 6.7$ Hz, $H_{a,q}$). ^{13}**C**$\{^1$**H**$\}$ **NMR** (126 MHz; $CDCl_3$) δ (ppm): 147.5, 101.6, 101.6, 54.3, 38.7, 31.7, 31.6, 29.6, 29.3, 29.2, 29.0, 28.9, 28.8, 27.8, 26.1, 25.1, 22.5, 22.5, 14.0. **HRESI-MS** (pos.): 434.2028, calc. for $[C_{19}H_{37}IN_3]^+ = 434.2027$.

Bis-octyliodotriazolium iodide thread, 32·I



30·BF_4 (0.050 g, 96 μmol) was suspended in $CHCl_3$ (50 mL) and washed with 1 M $NH_4I_{(aq.)}$ (8 × 10 mL) and H_2O (2 × 10 mL). The solvent was removed *in vacuo* to yield **30**·I (0.054 g, quant.). However, this sample was not required for study and was therefore, not characterised.

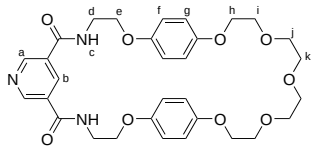
Bis-octyliodotriazolium hexafluorophosphate thread, 32·PF_6



30·BF_4 (0.20 g, 0.39 mmol) was suspended in $CHCl_3$ (50 mL) and washed with 0.1 M $NH_4PF_{6(aq.)}$ (8 × 10 mL) and H_2O (2 × 10 mL). The solvent was removed *in vacuo* to yield **30**·PF_6 (0.20 g, 92%). ^{1}**H NMR** (500 MHz; $CDCl_3$) δ (ppm): 4.46 (2H, t, $J_{h|g} = 7.6$ Hz, H_h), 4.24 (3H, s, H_i), 2.85 (2H, t, $J_{j|k} = 7.9$ Hz, H_j), 1.99 (2H, quin, $J_{g|h,f} = 7.4$ Hz, H_g), 1.63 (2H, quin, $J_{k|j,l} = 7.6$ Hz, H_k), 1.19–1.44 (20H, m, $H_{b,c,d,e,f,l,m,n,o,p}$), 0.88 (6H, t, $J_{a-b|p-q} = 6.7$ Hz, $H_{a,q}$). ^{13}**C**$\{^1$**H**$\}$ **NMR** (126 MHz; $CDCl_3$) δ (ppm): 148.3, 84.9, 54.8, 38.4, 31.7, 31.6, 29.1, 29.0, 28.9, 28.9, 28.7, 28.6, 27.0, 26.1, 24.4, 22.6,

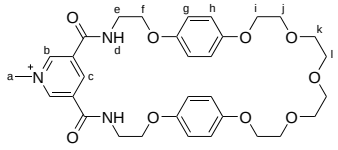
22.5, 14.0, 14.0. ^{31}**P NMR** (202 MHz; $CDCl_3$) δ (ppm): -144.94 (spt, $J = 714.0$ Hz, PF_6). ^{19}**F NMR** (376 MHz; $CDCl_3$) δ (ppm): -74.15 (d, $J = 714.0$ Hz, PF_6). **HRESI-MS** (pos.): 434.2031, calc. for $[C_{19}H_{37}IN_3]^+ = 434.2027$.

Pyridine-bis-amide 5-oxygen-polyether macrocycle, 33



Pyridine-3,5-dicarboxylic acid (0.19 g, 1.0 mmol) was suspended in DCM (4 mL), and $(COCl)_2$ (0.4 mL) was added. The mixture was refluxed overnight under N_2. The solvent was removed *in vacuo*, and the residue was redissolved in dry DCM (20 mL). This was added dropwise to a solution of **24** (0.54 g, 1.0 mmol), **26**·Cl (0.38 g, 1.0 mmol) and Et_3N (3.3 mL, 23 mmol) dissolved in dry DCM (50 mL). The mixture was stirred at room temperature for 1 h under N_2. Thereafter, the mixture was washed with HCl (10% aq., 2 $\times$ 50 mL) and H_2O (2 $\times$ 50 mL). The organics were dried over $MgSO_4$. The solvent was removed *in vacuo*. Purification by silica gel column chromatography (3% MeOH in $CHCl_3$) afforded **33** (0.25 g, 43%) as a white powder. ^{1}**H NMR** (400 MHz; CD_3OD) δ (ppm): 9.08 (2H, d, $^4J_{a|b} = 2.2$ Hz, H_a), 8.39–8.51 (1H, m, H_b), 6.77 (8H, s, $H_{f,g}$), 4.07 (4H, t, $J_{d|e} = 4.9$ Hz, H_d), 3.97–4.03 (4H, m, H_e), 3.75–3.82 (8H, m, $H_{h,i}$), 3.62–3.70 (8H, m, $H_{j,k}$). **HRESI-MS** (pos.): 596.28, calc. for $[C_{31}H_{37}N_3O_9 \cdot H]^+ = 596.26$.

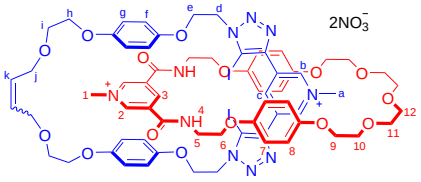
Pyridinium-bis-amide 5-oxygen-polyether macrocycle, 34·BF_4



33 (0.15 g, 0.25 mmol) was dissolved in dry DCM (25 mL). $[Me_3O][BF_4]$ (47 mg, 0.30 mmol) was added, and the mixture was stirred at room temperature, overnight under N_2. Thereafter, MeOH (1 mL) was added and the solvent was removed *in vacuo*. Purification by preparative thin layer chromatography (3% MeOH in DCM) to afford **34**·BF_4 (84 mg, 48%) as a white powder. ^{1}**H NMR** (400 MHz; CD_3CN) δ (ppm): 9.16 (2H, d, $^4J_{b|c} = 1.0$ Hz, H_b), 8.97 (1H, s, H_c), 7.70 (2H, br. s., H_d), 6.68–6.96 (8H, m, $H_{g,h}$), 4.40 (3H, s, H_a), 4.11 (4H, t, $J_{e|f} = 4.9$ Hz, H_e), 3.96–4.03 (4H, m, H_f), 3.80 (4H, q, $J_{i|j} = 5.3$ Hz, H_i), 3.71–3.77 (4H, m, H_j), 3.54–3.66 (8H, m, $H_{k,l}$). ^{13}**C**$\{^1$**H**$\}$ **NMR** (101 MHz; CD_3CN) δ

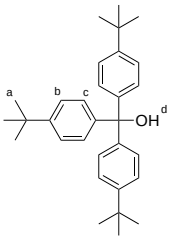
(ppm): 161.9, 154.3, 153.8, 148.2, 141.0, 135.1, 116.5, 116.3, 71.4, 71.4 (*sic.*), 70.5, 69.0, 67.5, 50.1, 41.1. ^{19}**F NMR** (377 MHz; CD_3CN) δ (ppm): -151.81 (s, BF_4). **HRESI-MS** (pos.): 610.28, calc. for $[C_{32}H_{40}N_3O_9]^+ = 610.28$.

Pyridinium bis-amide–3,5-bis-iodotriazole pyridinium catenane nitrate, 35·$(NO_3)_2$



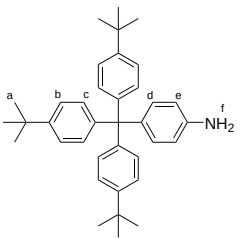
The bis-iodotriazole pyridinium precursor **21**·Cl (0.050 g, 0.052 mmol) and the pyridinium bis-amide macrocycle **34**·PF_6 (0.040 g, 0.052 mmol) were dissolved in dry DCM (10 mL) and stirred under N_2 for 30 mins. Grubbs' II catalyst (0.005 g, 10% by wt.) was added and the mixture stirred at room temperature under N_2 for 7 days. The solvent was then removed in vacuo, and the crude material purified by preparative TLC (silica, 14:2:1 $CH_3OH/CH_2Cl_2/KNO_{3(aq.)}$), before dissolving in 1:1 CH_3OH/H_2O and passing the solution down a nitrate-loaded Amberlite® anion exchange column. The solvent was removed *in vacuo* to afford **35**·$(NO_3)_2$ as a yellow solid (8.8 mg, 10%). ^{1}**H NMR** (500 MHz; 1 :1 CD_3OD:D_2O) δ (ppm): 9.69 (1H, s, H_3), 9.43 (2H, s, H_2), 9.25 (2H, s, H_b), 8.20 (1H, s, H_c), 6.77–6.84 (8H, m, $H_{f,g}$), 5.90–6.10 (8H, m, $H_{7,8}$), 5.64 (2H, s, H_k), 4.94 (4H, t, H_d), 4.65 (3H, s, H_a), 4.59 (3H, s, H_1), 4.46 (4H, t, $J_{e|d} = 4.27$ Hz, H_e), 3.93–3.99 (4H, m, H_h), 3.88 (4H, s, H_j), 3.82 (4H, t, $J_{11|12} = 3.51$ Hz, H_{11}), 3.78 (4H, s, H_{12}), 3.71 (4H, d, $J_{9|10} = 4.12$ Hz, H_9), 3.68 (4H, d, $J_{5|6} = 4.88$ Hz, H_5), 3.603.65 (8H, m, $H_{i,10}$), 3.53 (4H, d, $J_{6|5} = 4.73$ Hz, H_6). ^{13}**C**$\{^1$**H**$\}$ **NMR** (125 MHz; 1 :1 CD_3OD:D_2O) δ (ppm): 162.7, 153.2, 153.0, 152.8, 152.5, 152.4, 152.1, 147.1, 142.5, 134.4, 130.1, 129.0, 115.9, 115.4, 114.6, 114.4, 90.6, 83.7, 77.7, 70.4, 70.3, 69.4, 68.2, 68.0, 67.7, 66.9, 66.2, 55.9, 50.9, 49.1, 40.0. **HRESI-MS** (pos.): 751.1785, calc. for $[C_{66}H_{76}I_2N_{10}O_{15}]^{2+} = 751.1785$.

***tris-tert*-Butylphenyl MeOH, 36**



Mg turnings (1.56 g, 63.5 mmol) were loaded into a 100 mL 3-neck round-bottomed flask and washed with petroleum ether (2 × 20 mL), decanted and dried *in vacuo* while heating with a heat gun. The flask was fitted with a condenser and a dropping funnel. Dry degassed THF (10 mL) was added to cover the Mg turnings followed by 5 I_2 beads. *p-tert*-Butylbromobenzene (10.0 mL, 57.7 mmol) was dissolved in dry degassed THF (30 mL) and an initial 5 mL of this solution was added to the Mg turnings initiate the formation of the Grignard reagent. Thereafter, it was added at such a rate as to maintain a gentle reaction. The mixture was then refluxed for 1 h. Diethyl carbonate (2.40 mL, 19.2 mmol) in dry degassed THF (10 mL) was added dropwise and the mixture refluxed for 1 h. The mixture was cooled to room temperature and poured onto a mixture of ice (60 mL) and H_2SO_4 (conc., 10 mL). The THF was removed *in vacuo*. The aqueous phase was washed with DCM (3 × 50 mL). The combined organics were concentrated to ∼ 60 mL and washed with $NaHCO_3$ (5% aq., 30 mL) and H_2O (30 mL) and dried over $MgSO_4$. The solvent was removed *in vacuo*. The residue was repeatedly recrystallised from boiling cyclohexane to yield **36** as a white powder (6.27 g, 76%). ^{1}**H NMR** (300 MHz; $CDCl_3$) δ (ppm): 7.27–7.36 (6H, m, H_c), 7.14–7.23 (6H, m, H_b), 1.28–1.33 (27H, m, H_a). **LRESI-MS** (pos.): 451.3, calc. for $[C_{31}H_{40}O \cdot Na]^+ =$ 451.3.

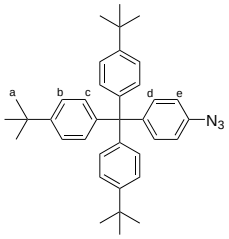
Aniline stopper, 37



Trityl alcohol (1.97 g, 4.6 mmol) was suspended in acetyl chloride (10 mL, 115 mmol) and heated at 60 °C under N_2 for 16 h. The solvent was removed *in vacuo* and the residue dissolved immediately in aniline (14 mL, 147 mmol). The mixture was heated to 130 °C for 16 h under N_2. The mixture

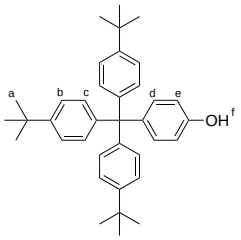
was allowed to cool to room temperature and poured onto HCl (10% aq., 25 mL) resulting in a purple precipitate. The mixture was stirred for 20 mins. The residue was extracted into DCM (3 × 20 mL). The combined organics were washed with HCl (10% aq., 25 mL), Na_2CO_3 (saturated aq., 2 × 25 mL), H_2O (2 × 25 mL) and dried over $MgSO_4$. The solvent was removed *in vacuo*. Purification by silica gel column chromatography (DCM) yielded **37** as yellow powder (1.30 g, 56%). ^{1}**H NMR** (300 MHz; $CDCl_3$) δ (ppm): 7.19–7.25 (6H, m, H_c), 7.06–7.12 (6H, m, H_b), 6.94 (2H, s, H_e), 6.57 (2H, d, $J_{d|e} = 8.8$ Hz, H_d), 3.36–3.77 (2H, m, H_f), 1.30 (27H, s, H_a). **LRESI-MS** (pos.): 504.4, calc. for $[C_{37}H_{45}N \cdot H]^+ = 504.36$.

Stopper phenyl azide, 38



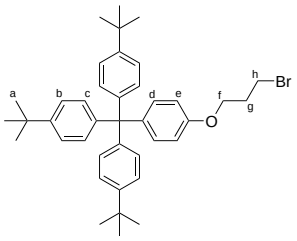
37 (1.0 g, 2.0 mmol) was suspended in 9:1 EtOH:HCl (concentrated, aq.) (800 mL). Mixture was warmed to dissolve all aniline stopper. Further conc. HCl (aq., 25 mL) was added and the colourless solution was cooled to 0 °C. $NaNO_2$ (0.316 g, 4.5 mmol) was added followed by NaN_3 (0.310 g, 4.5 mmol). The mixture was stirred under N_2 for 1 h in an ice bath. The mixture was allowed to warm to room temperature and stirred for 16 h. EtOH was removed under reduced pressure. The resulting aqueous suspension was diluted with H_2O (200 mL) and extracted with Et_2O (2 × 200 mL). The combined organics were washed with Na_2CO_3 (saturated aq., 2x 150 mL), brine (150 mL) and dried over $MgSO_4$. The solvent was removed *in vacuo*. The resulting yellow powder was taken up in 1:1 petroleum ether:DCM and filtered through a short pad of silica using 1:1 petroleum ether:DCM as the eluent. The solvent was removed *in vacuo* to yield **38** as a yellow powder (1.02 g, 96%). ^{1}**H NMR** (300 MHz; Toluene$-d_8$) δ (ppm): 7.22 (6H, s, H_c), 7.18 (2H, d, $J_{e|d} = 8.8$ Hz, H_e), 7.07 (6H, d, $J_{b|c} = 8.2$ Hz, H_b), 6.92 (2H, s, H_d), 1.30 (27H, s, H_a).

***tris*-*tert*-Butylphenylmethyl phenol, 39**



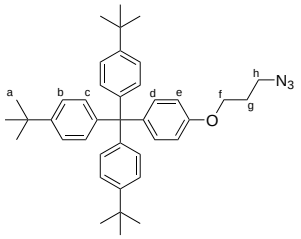
36 (2.50 g, 5.83 mmol) was dissolved in molten phenol (20.6 g, 210 mmol). HCl (6 M aq., 0.2 mL) was added and the mixture was stirred and heated to 120 °C under N_2 for 16 h. The orange mixture was cooled to room temperature and KOH (120 g) in H_2O (300 mL) was added forming a white suspension. This mixture was stirred until the orange particulates had disappeared. The suspension was filtered and the residue washed with further KOH (120 g) in H_2O (300 mL). The white solid was washed with H_2O (100 mL), acetic acid (20% aq., 100 mL) and further H_2O (100 mL). The white solid was dissolved in DCM (200 mL) and dried over $MgSO_4$. The solvent was removed *in vacuo* to yield **39** as a white powder (2.291 g, 78%). ^{1}**H NMR** (300 MHz; $CDCl_3$) δ (ppm): 7.20–7.25 (6H, m, H_c), 7.02–7.11 (8H, m, $H_{b,e}$), 6.69 (2H, d, $J_{d|e} = 8.8$ Hz, H_d), 2.10 (1H, s, H_f), 1.30 (27H, s, H_a).

Stopper propyl bromide, 40



39 (1.2 g, 2.4 mmol), 3-bromopropan-1-ol (0.45 mL, 5.0 mmol) and PPh_3 (1.25 g, 4.8 mmol) were dissolved in dry degassed THF at 0 °C. DEAD (0.75 mL, 4.8 mmol) was added dropwise and the reaction mixture was allowed to warm to room temperature and stirred for 48 h. The solvent was removed *in vacuo* and the residue redissolved in DCM (25 mL) and precipitated with MeOH (75 mL). The precipitate was filtered and washed with further MeOH (3 × 75 mL) and redissolved in DCM (20 mL). The solution was passed through a plug of silica using DCM as the eluent. The solvent was removed *in vacuo* to yield **40** as a white solid. (0.950 g, 64%). ^{1}**H NMR** (300 MHz; $CDCl_3$) δ (ppm): 7.19–7.27 (6H, m, H_c), 7.04–7.12 (8H, m, $H_{b,e}$), 6.76 (4H, d, $J_{d|e} = 8.8$ Hz, H_d), 4.07 (2H, s, H_h), 3.60 (2H, s, H_f), 2.17–2.37 (2H, m, H_g), 1.29 (27H, s, H_a).

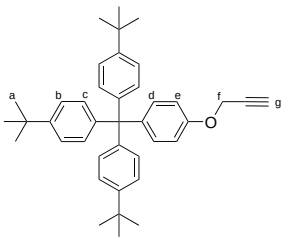
Stopper propyl azide, 41



Method 1: 40 (0.75 g, 1.2 mmol) and NaN_3 (0.316 g, 4.8 mmol) were dissolved in DMF (18 mL). The mixture was heated at 80 °C for 16 h. Thereafter, the mixture was partitioned between EtOAc (125 mL) and H_2O (125 mL). The organic phase was washed with H_2O (2 × 100 mL) and dried over $MgSO_4$. The solvent was removed *in vacuo*. Purification by silica gel column chromatography (2:1 petroleum ether:DCM) afforded **41** as a white solid (0.598 g, 85%).

Method 2: 39 (5.15 g, 10.1 mmol) and **107** (2.0 g, 11 mmol) were dissolved in 2-butanone (130 mL). K_2CO_3 (7.1 g, 51 mmol) was added and the mixture was refluxed at 80 °C under N_2 overnight. Thereafter, the mixture was cooled to room temperature and filtered. The solvent was removed *in vacuo*. Purification by silica gel column chromatography (7:3 hexane/DCM) afforded the stopper propyl azide **41** (4.6 g, 76%) as a white solid. ^{1}**H NMR** (300 MHz; $CDCl_3$) δ (ppm): 7.20–7.25 (7H, m, H_c), 7.04–7.12 (9H, m, $H_{b,e}$), 6.76 (2H, d, $J_{d|e} = 8.8$ Hz, H_d), 3.98–4.06 (2H, m, H_h), 3.51 (2H, s, H_f), 2.04 (2H, s, H_g), 1.30 (31H, s, H_a). **LRESI-MS** (pos.): 610.15 calc. for $[C_{40}H_{49}N_3O \cdot Na]^+ = 610.38$.

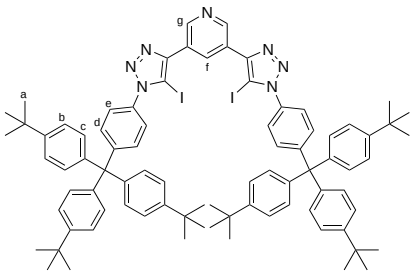
Stopper alkyne, 42



39 (1.1 g, 2.1 mmol) and propargyl bromide (0.48 mL, 3.2 mmol) were dissolved in dry DMF (30 mL). K_2CO_3 (0.22 g, 1.6 mmol) was added and the mixture was heated at 80 °C under N_2 for 16 h. After cooling to room temperature, the mixture was concentrated *in vacuo* and diluted with H_2O (30 mL). The product was extracted with EtOAc (3 × 20 mL). The combined organics were washed with brine (30 mL) and the solvent was removed *in vacuo*. Purification by recrystallisation from 5% $CHCl_3$ in MeCN afforded **42** (0.985 g, 85%). ^{1}**H NMR** (400 MHz; $CDCl_3$) δ (ppm): 7.19–7.24 (6H, m, H_b), 7.01–7.13

(8H, m, $H_{c,d}$), 6.85 (2H, s, H_e), 4.66 (2H, d, $J_{f|g} = 2.3$ Hz, H_f), 2.51 (1H, s, H_g), 1.30 (27H, s, H_a). **HRESI-MS** (pos.): calc. for $[C_{40}H_{46}O \cdot H]^+ = 543.36$.

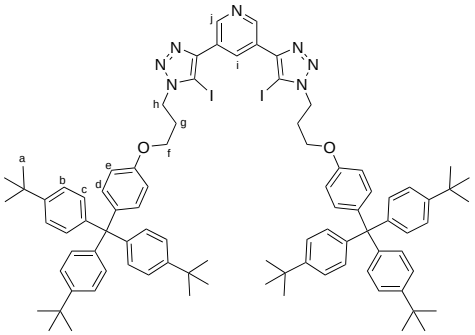
Bis-stopper phenyliodotriazole pyridine, 43



One Pot Method: **38** (0.23 g, 0.44 mmol) was dissolved in dry degassed THF (1.4 mL) and the reaction vessel was covered in foil. NaI (0.24 g, 1.6 mmol) and $Cu(ClO_4)_2 \cdot 6\,H_2O$ (0.30 g, 0.8 mmol) were added and the solution was stirred under N_2 for 5 mins. TBTA (0.003 g, 0.004 mmol), DBU (0.061 g, 0.4 mmol), washed from the syringe/pipette using dry degassed THF (0.2 mL) and **1** (0.026 g, 0.2 mmol) were added and the reaction was stirred for 16 h in the dark at room temperature. The mixture was diluted and transferred to a separating funnel using DCM (40 mL) and washed with NH_4OH (2 $\times$ 16 mL) and brine (2 $\times$ 16 mL). The organics were dried over $MgSO_4$ and the solvent removed *in vacuo*. Purification was undertaken using silica gel column chromatography using 1% MeOH/DCM as the eluent. However, **43** was not isolated.

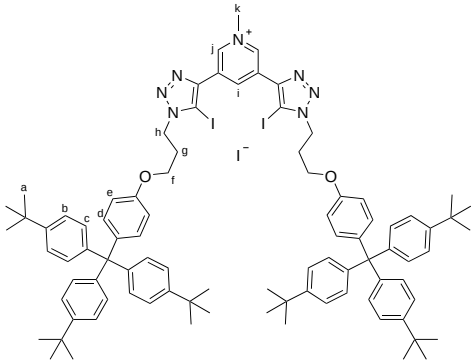
Iodoalkyne method: $CuI \cdot P(OEt)_3$ (0.005 g, 0.01 mmol) and TBTA (0.006 g, 0.01 mmol) were dissolved in dry degassed THF (0.4 mL). **2** (0.039 g, 0.1 mmol) was added followed by **38** (0.12 g, 0.22 mmol) dissolved in dry degassed THF (0.8 mL). The mixture was stirred in the dark at room temperature for 16 h. The solvent was removed *in vacuo* and the residue was taken up in DCM (5 mL). The solution was washed with NH_4OH (2 $\times$ 1 mL), H_2O (2 $\times$ 1 mL) and brine (2 $\times$ 1 mL) and the organics dried over $MgSO_4$. The solvent was removed *in vacuo*. Purification by silica gel column chromatography (1% MeOH in DCM) as the eluent however **43** was not isolated.

Bis-stopper propyl iodotriazolyl pyridine, 44



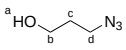
41 (0.13 g, 0.22 mmol) was dissolved in dry deoxygenated THF (0.6 mL) and the reaction vessel was covered in foil. NaI (0.12 g, 0.8 mmol) and $Cu(ClO_4)_2 \cdot 6\,H_2O$ (0.15 g, 0.4 mol) were added and the solution was stirred for 5 mins. TBTA (0.005 g, 0.01 mmol), DBU (0.030 g, 0.2 mmol, washing the syringe/pipette with dry deoxygenated THF (0.2 mL)) and **1** (0.013 g, 0.1 mmol) were added and the mixture stirred under N_2 at room temperature for 16 h. The mixture was diluted and transferred to a separating funnel with DCM (20 mL) and washed with NH_4OH (2 $\times$ 8 mL) and brine (2 $\times$ 8 mL) and dried over $MgSO_4$. The solvent was removed *in vacuo*. Purification by silica gel column chromatography (2% MeOH in DCM) and thereafter preparative TLC using 2% MeOH/DCM by running the plate twice to yield **44** as a white powder (0.259 g, 81%). ^{1}**H NMR** (300 MHz; $CDCl_3$) δ (ppm): 9.23–9.25 (2H, m, H_j), 8.83 (1H, s, H_i), 7.16–7.26 (12H, m, H_c), 7.04–7.16 (16H, m, $H_{b,e}$), 6.78 (4H, d, $J_{d|e} = 8.8$ Hz, H_d), 4.70 (4H, t, $J_{h|g} = 7.0$ Hz, H_h), 4.06 (4H, t, $J_{f|g} = 5.6$ Hz, H_f), 2.43–2.50 (4H, m, H_g), 1.29 (54H, s, H_a). ^{13}**C**$\{^1$**H**$\}$ **NMR** (101 MHz; $CDCl_3$) δ (ppm): 156.2, 148.3, 148.0, 146.9, 144.1, 140.1, 132.3, 130.7, 126.3, 124.1, 113.1, 63.9, 63.1, 48.2, 34.3, 31.4, 29.7. **LRESI-MS** (pos.): 1554.61710 calc. for $[C_{89}H_{101}I_2N_7O_2 \cdot H]^+ = 1554.61789$.

Pyridinium-bis-iodotriazole iodide axle, 45·I



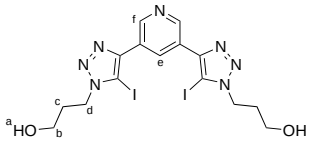
44 (0.028 g, 0.02 mmol) was dissolved in dry DCM (1.5 mL). CH_3I (0.05 mL, 0.5 mmol) was added and the mixture stirred under N_2 for 7 days. The solvent was removed *in vacuo*. Purification by preparative thin layer chromatography (10% MeOH in DCM); however **45**·I could not be isolated.

Azidohydroxy propane, 46



3-Bromopropan-1-ol (1.25 mL, 13.8 mmol) and NaN_3 (3.62 g, 56 mmol) were suspended in H_2O (40 mL). The mixture was heated at 80 °C under N_2 for 16 h. The product was extracted with EtOAc (5 × 40 mL). The combined organics were washed with brine (30 mL) and dried over $MgSO_4$. The solvent was removed carefully *in vacuo* to afford **46** (1.34 g, 96%). ^{1}**H NMR** (300 MHz; $CDCl_3$) δ (ppm): 3.75 (2H, t, $J_{d|c} = 6.3$ Hz, H_d), 3.45 (2H, t, $J_{b|c} = 6.6$ Hz, H_b), 1.83 (2H, quin, $J_{c|d,e} = 6.5$ Hz, H_c), 1.78 (1H, s, H_a).

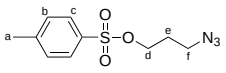
Bis-hydroxypropyl-iodotriazolyl pyridine, 47



46 (0.11 g, 1.1 mmol) was dissolved in dry, degassed THF (2 mL) and covered in foil. NaI (0.60 g, 4.0 mmol) and $Cu(ClO_4)_2 \cdot 6\,H_2O$ (0.74 g, 2.0 mmol) were added and the mixture was stirred at room temperature for 5 mins under N_2. TBTA (0.01 g, 0.02 mmol), DBU (0.15 g, 1.0 mmol, 2 × 1 mL THF) and **1** (0.064 g, 0.5 mmol) were added. The mixture was stirred at room temperature for 16 h under N_2. Thereafter, the mixture was diluted with DCM (80 mL) and washed with NH_4OH (2 × 40 mL) and brine

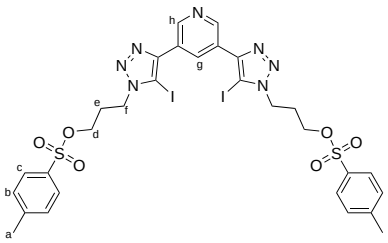
(2 × 40 mL). The organics were dried over $MgSO_4$ and the solvent was removed *in vacuo*. Purification by silica gel column chromatography (3% MeOH in DCM) afforded **47**; however it could not be isolated.

Azidotosylpropane, 48



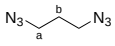
46 (1.20 g, 11.9 mmol) and Et_3N (3.4 mL, 24 mmol) were dissolved in dry DCM (100 mL) and cooled to 0 °C. TsCl (2.50 g, 13.1 mmol) was added portionwise over 30 mins and the mixture was stirred at room temperature under N_2 for 16 h. The organics were washed with 0.1 M $HCl_{(aq.)}$ (3 × 40 mL), H_2O (2 × 40 mL) and brine (40 mL) and dried over $MgSO_4$. The solvent was removed *in vacuo*. Purification by silica gel column chromatography (7:3 hexane:DCM) afforded **48** as a colourless oil (2.51 g, 83%). ^{1}**H NMR** (300 MHz; $CDCl_3$) δ (ppm): 7.79 (2H, d, $J_{c|b} = 8.0$ Hz, H_c), 7.36 (2H, d, $J_{b|c} = 7.6$ Hz, H_b), 4.10 (2H, t, $J_{f|e} = 5.9$ Hz, H_f), 3.37 (2H, t, $J_{d|e} = 6.6$ Hz, H_d), 2.45 (3H, s, H_a), 1.88 (2H, quin, $J_{e|d,f} = 6.3$ Hz, H_e). **HRESI-MS** (pos.): 278.1, calc. for $[C_{10}H_{13}N_3O_3S \cdot Na]^+ = 278.1$.

Bis-(tosyl-propyl-iodotriazolyl) pyridine, 49



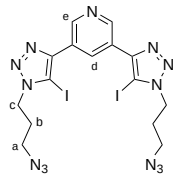
48 (0.28 g, 1.1 mmol) was dissolved in THF (2 mL) and covered in foil. NaI (0.60 g, 4.0 mmol) and $Cu(ClO_4)_2 \cdot 6\,H_2O$ (0.75 g, 2.0 mmol) were added and the mixture stirred for 3–5 mins. TBTA (0.005 g, 0.01 mmol), DBU (0.15 g, 1.0 mmol) in THF (2 mL) and **1** (0.064 g, 0.5 mmol) were added, and the mixture was stirred at room temperature, overnight under N_2. The mixture was diluted with DCM (80 mL) and washed with NH_4OH (2 × 40 mL) and brine (2 × 40 mL). The organics were dried over $MgSO_4$. The solvent was removed *in vacuo*. However, this resulted in the formation of an inseparable mixture of the desired bis-tosylate product, as well as the mono- and di-iodo-substituted products.

Diazidopropane, 50



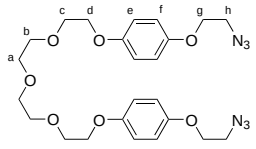
NaN_3 (1.34 g, 20.6 mmol) was dissolved in DMSO (38 mL) and stirred until no solid remained. The solution was sparged with N_2 and 1,3-dibromopropane (0.51 mL, 5.0 mmol) was added *via* syringe. The mixture was stirred for 16 h at room temperature. H_2O (5 $\times$ 2 mL) was added portionwise allowing the mixture to cool between portions. The product was extracted with Et_2O (3 $\times$ 5 mL). The combined organics were washed with H_2O (2 $\times$ 10 mL) and brine (5 mL) and dried over $MgSO_4$. The solvent was removed *in vacuo* without heating to give **50** as a colourless oil (0.59 g, 93%). ^{1}**H NMR** (400 MHz; $CDCl_3$) δ (ppm): 3.42 (4H, t, $J_{a|b} = 6.5$ Hz, H_a), 1.83 (2H, quin, $J_{b|a} = 6.5$ Hz, H_b).

3,5-Bis-(azidopropyl-iodotriazolyl)pyridine, 51



50 (0.14 g, 1.1 mmol) was dissolved in THF (2 mL) and covered in foil. NaI (0.60 g, 4.0 mmol) and $Cu(ClO_4)_2 \cdot 6\,H_2O$ (0.74 g, 2.0 mmol) were added, and stirred for 3–5 mins. TBTA (0.005 g, 0.01 mmol), DBU (0.153 g, 1 mmol) in THF (2 mL) and **1** (0.064 g, 0.5 mmol) were added, and the mixture was stirred at room temperature, overnight under N_2. The mixture was diluted with DCM (80 mL) and washed with NH_4OH (2 $\times$ 40 mL) and brine (2 $\times$ 40 mL). The organics were dried over $MgSO_4$. The solvent was removed *in vacuo* but did not afford **51**.

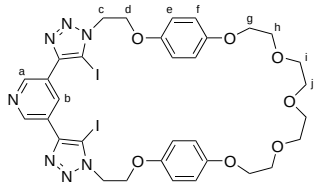
Bis-azido polyether, 52



24 (1.50 g, 3.2 mmol), K_2CO_3 (2.27 g, 16.4 mmol), $CuSO_4 \cdot 5\,H_2O$ (0.018 g, 0.08 mmol) and imidazolylsulfonyl azide (2.1 g, 7.6 mmol) were dissolved in MeOH (40 mL). The cloudy blue solution mixture was stirred under N_2 for 48 h after which it was concentrated to +/- 4 mL. The mixture was diluted with H_2O (30 mL), acidified with conc. $HCl_{(aq.)}$ (6.4 mL) and extracted with EtOAc (3 $\times$ 30

mL). The organic layer was dried over $MgSO_4$ and dried *in vacuo*. It was filtered through a short pad of silica gel and eluted with 4% MeOH in DCM and dried *in vacuo* to give a yellow oil. This was triturated with ice cold Et_2O (8 mL). The resulting white powder was isolated by filtration, washed with cold Et_2O (2×2 mL) and dried *in vacuo*. Yield: 1.22 g (73%). ^{1}**H NMR** (300 MHz; $CDCl_3$) δ (ppm): 6.79–6.91 (8H, m, $H_{e,f}$), 4.01–4.16 (8H, m, $H_{d,h}$), 3.83 (4H, t, $J_{g|h} = 4.6$ Hz, H_g), 3.65–3.75 (8H, m, $H_{a,b}$), 3.56 (4H, t, $J_{c|d} = 5.0$ Hz, H_c).

Bis-iodotriazole pyridine polyether macrocycle, 53



Without template: CuI (0.012 g, 0.06 mmol) and TBTA (0.019 g, 0.04 mmol) were dissolved in dry THF (50 mL) and stirred for 2 h at room temperature in a foil covered round-bottomed flask. A solution of **2** (0.079 g, 0.2 mmol) in dry THF (25 mL) was added to the above solution. Thereafter, a solution of **52** (0.11 g, 0.2 mmol) in dry THF (25 mL) was added and the mixture was stirred for 10 days in the dark. The solvent was removed *in vacuo* and the residue dissolved in DCM (4 mL). The organics were washed with an NH_4OH/EDTA solution (1 mL), H_2O (1 mL) and brine (1 mL) and dried over $MgSO_4$. The solvent was removed *in vacuo*. The residue was purified by Preparative TLC using 1% MeOH/DCM as the eluent. Product **53** was not isolated.

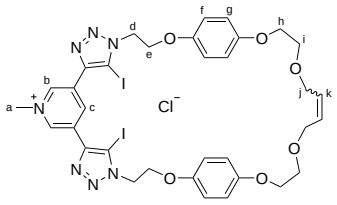
With Pyridinium-bis-amide chloride template: CuI (3.8 mg, 20 μmol) and TBTA (3.5 mg, 6.6 μmol) were dissolved in dry THF (10 mL) and covered in foil. **52** (0.042 g, 66 μmol) and **26**·Cl (0.025 g, 66 μmol) were added and the mixture was stirred for 30 mins under N_2. **2** (0.025 g, 66 μmol) was added and the reaction was stirred under N_2 for 7 days. The solvent was removed *in vacuo*. The residue was taken up in DCM (10 mL) and washed with NH_4OH (2×5 mL) and brine (2×5 mL) and dried over $MgSO_4$. The solvent was removed *in vacuo*. However, the macrocycle **53** was not obtained.

With Pyridinium-bis-iodotriazole chloride template: CuI (6.6 mg, 35 μmol) and TBTA (4.8 mg, 9.0 μmol) were dissolved in dry THF (10 mL) and covered in foil. **52** (0.043 g, 66 μmol) and **11**·Cl (0.050 g, 66 μmol) were added and the mixture was stirred for 30 mins under N_2. **2** (0.026 g, 66 μmol) was added and the reaction was stirred under N_2 for 7 days. The solvent was removed *in vacuo*. The residue was taken up in DCM (10 mL) and washed with NH_4OH (2×5 mL) and brine (2×5 mL) and dried

over $MgSO_4$. The solvent was removed *in vacuo*. Purification by preparative thin layer chromatography (3%, extracted, then 5% MeOH in DCM) afforded macrocycle **53** (17.1 mg, 28%).

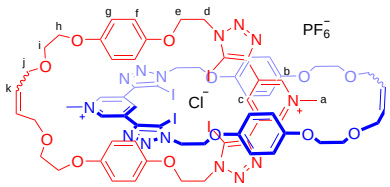
^{1}**H NMR** (400 MHz; $CDCl_3$) δ (ppm): 9.20 (2H, d, $^4J_{a|b} = 2.1$ Hz, H_a), 8.69 (1H, t, $^4J_{b|a} = 2.1$ Hz, H_b), 6.68–6.82 (8H, m, $H_{e,f}$), 4.87 (4H, t, $J_{c|d} = 4.8$ Hz, H_c), 4.44 (4H, t, $J_{d|c} = 4.8$ Hz, H_d), 3.98–4.04 (4H, m, H_g), 3.74–3.79 (4H, m, H_h), 3.62–3.68 (8H, m, $H_{i,j}$). ^{13}**C**$\{^1$**H**$\}$ **NMR** (101 MHz; $CDCl_3$) δ (ppm): 153.4, 152.0, 148.2, 147.0, 144.2, 133.3, 126.1, 115.6, 115.4, 79.6, 70.7, 70.6, 69.6, 68.0, 67.2, 29.6. **HRESI-MS** (pos.): 896.07634, calc. for $[C_{33}H_{35}I_2N_7O_7 \cdot H]^+ = 896.07601$.

Grubbs' II ring closed bis-iodotriazolyl *N*-methyl pyridinium chloride macrocycle, 54



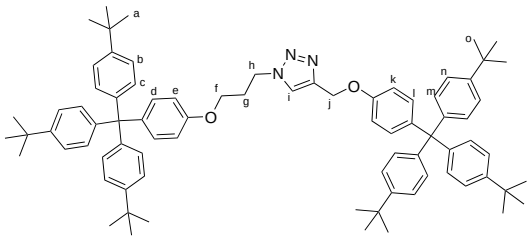
21 (0.026 g, 0.03 mL) was dissolved in DCM (10 mL). TBACl (0.009 g, 0.03 mmol) was added and the resulting solution was stirred for 30 mins. Grubb's II (cat., 0.003 g, 10% by weight) was added and the mixture stirred at room temperature under N_2 for 5 days. The solvent was removed *in vacuo* and the residue was taken up in DCM (5 mL). The solution was washed with NH_4PF_6 (0.1 M aq., 5 $\times$ 10 mL) and H_2O (2 $\times$ 10 mL). The organics were dried over $MgSO_4$ and the solvent removed *in vacuo*. Purification by preparative thin layer chromatography (10% MeOH in DCM) as the eluent. However, **54** was not isolated.

Bis-vinyl-appended iodotriazolyl *N*-methyl pyridinium homocatenane, 55



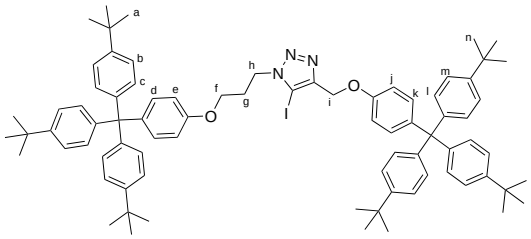
21 (0.03 g, 0.03 mmol) was dissolved in DCM (5 mL). TBACl (0.0040 g, 0.015 mmol) was added and the resulting solution stirred for 30 mins at room temperature under N_2. Grubbs' II (cat., 0.003 g, 10% by weight) was added and the mixture stirred at room temperature under N_2 for 14 days. The solvent was removed *in vacuo*. Purification by preparative thin layer chromatography (10% MeOH in DCM) as the eluent. However, the homocatenane **55** was not isolated.

Mono-triazole axle precursor, 56



41 (0.10 g, 0.17 mmol), [Cu(MeCN)$_4$][PF$_6$] (14 mg, 0.03 mmol) and TBTA (cat.) were dissolved in dry degassed THF (2 mL). **42** (0.092 g, 0.17 mmol) and DIPEA (45 μL, 0.26 mmol) were added. The mixture was stirred at room temperature, overnight under N_2. The mixture was diluted with DCM (40 mL) and washed with NH_4OH (2 $\times$ 10 mL) and brine (2 $\times$ 10 mL). The solvent was removed *in vacuo*. Purification by preparative thin layer chromatography (1:5 hexane:DCM) to afford **56** (61 mg, 32%) as a white powder. ^{1}**H NMR** (400 MHz; $CDCl_3$) δ (ppm): 7.62 (1H, s, H_i), 7.22 (12H, d, $J_{b,n|c,m} = 8.4$ Hz, $H_{b,n}$), 7.02–7.11 (16H, m, $H_{c,d,l,m}$), 6.82 (2H, d, $J_{k|l} = 8.9$ Hz, H_k), 6.72 (2H, d, $J_{e|d} = 8.9$ Hz, H_e), 5.18 (2H, s, H_h), 4.59 (2H, br. s., H_j), 3.94 (2H, t, $J_{f|g} = 5.6$ Hz, H_f), 2.39 (2H, quin, $J_{g|f,h} = 5.6$ Hz, H_g), 1.29 (54H, s, $H_{a,o}$). **LRESI-MS** (pos.): 1130.87, calc. for $[C_{80}H_{95}N_3O_2 \cdot H]^+ = 1130.66$.

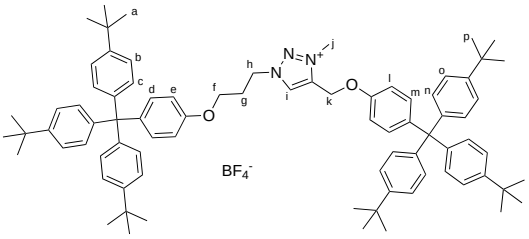
Mono-iodotriazole axle precursor, 57



41 (0.10 g, 0.17 mmol) was dissolved in dry degassed THF (1 mL) and the flask was covered in tin foil. NaI (0.11 g, 0.70 mmol) and $Cu(ClO_4)_2 \cdot 6\,H_2O$ (0.13 g, 0.34 mmol) were added and the mixture was stirred for 3–5 mins. Thereafter, TBTA (cat.), DBU (23 μL, 0.15 mmol) and **42** (0.085 g, 0.15 mmol) were added. The mixture was stirred at room temperature, overnight under N_2. The mixture was diluted with DCM (40 mL) and washed with NH_4OH (2 $\times$ 10 mL) and brine (2 $\times$ 10 mL). The organics were dried over $MgSO_4$. The solvent was removed *in vacuo*. Purification by preparative thin layer chromatography (2% MeOH in DCM) afforded **57** as a white solid (0.19 g, 96%). ^{1}**H NMR** (400 MHz; $CDCl_3$) δ (ppm): 7.23 (12H, d, $J_{b,m|c,l} = 6.8$ Hz, $H_{b,m}$), 7.03–7.13 (16H, m, $H_{c,d,k,l}$), 6.86–6.91 (2H, m, H_j), 6.75 (2H, d, $J_{e|d} = 8.9$ Hz, H_e), 4.59 (2H, t, $J_{h|g} = 6.3$ Hz, H_h), 3.96–4.05 (2H, m, H_i),

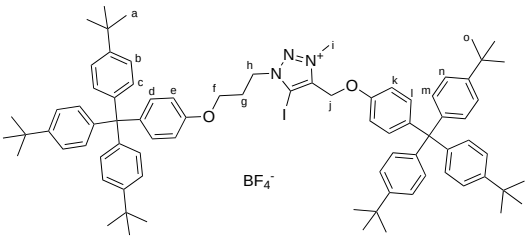
3.51 (2H, t, $J_{f|g} = 6.3$ Hz, H_f), 2.40 (2H, quin, $J_{g|f,h} = 6.3$ Hz, H_g), 1.30 (54H, s, $H_{a,n}$). **LRESI-MS** (pos.): 1256.78, calc. for $[C_{80}H_{94}IN_3O_2 \cdot H]^+ = 1256.65$.

Mono-triazolium axle·BF_4, 58·BF_4



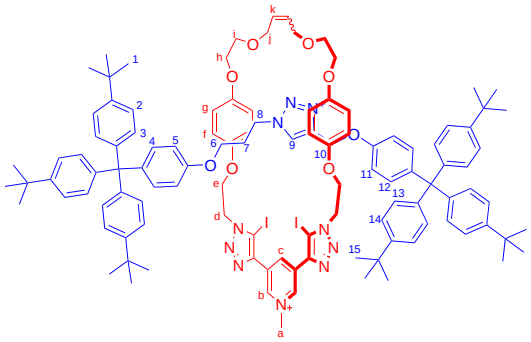
56 (0.13 g, 0.11 mmol) was suspended in dry DCM (2.5 mL). $[Me_3O][BF_4]$ (23 mg, 160 μmol) was added and the solution was stirred at room temperature, under N_2 for 2 days. Thereafter, the mixture was quenched with MeOH (1 mL) and the solvent was removed *in vacuo*. Purification by preparative thin layer chromatography (3% MeOH in DCM) afforded **58**·BF_4 (0.084 g, 60%) as a white solid. ^{1}**H NMR** (500 MHz; $CDCl_3$) δ (ppm): 7.61 (1H, s, H_i), 7.22 (12H, d, $J_{b,o|c,n} = 8.4$ Hz, $H_{b,o}$), 7.00–7.12 (16H, m, $H_{c,d,m,n}$), 6.78–6.87 (2H, m, H_l), 6.66–6.77 (2H, m, H_e), 5.17 (2H, s, H_k), 4.59 (2H, t, $J_{h|g} = 6.4$ Hz, H_h), 4,17 (3H, s, H_j), 3.94 (2H, t, $J_{f|g} = 6.2$ Hz, H_f), 2.39 (1H, quin, $J_{g|f,h} = 6.3$ Hz, H_g), 1.19–1.36 (54H, m, $H_{a,p}$). **HRESI-MS** (pos.): 1144.74, calc. for $[C_{81}H_{98}N_3O_2]^+ = 1144.77$.

Mono-iodotriazolium axle·BF_4, 59·BF_4



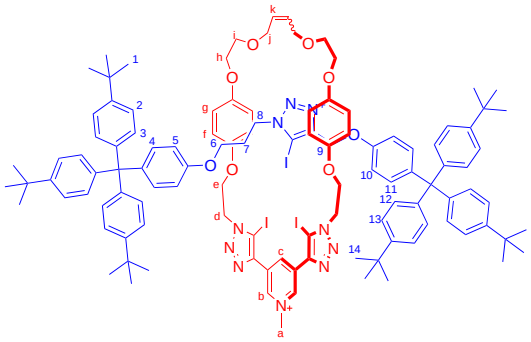
57 (0.10 g, 80 μmol) was dissolved in dry DCM (5 mL). $[Me_3O][BF_4]$ (26 mg, 160 μmol) was added and the solution was stirred at room temperature, under N_2 for 2 days. Thereafter, the mixture was quenched with MeOH (1 mL) and the solvent was removed *in vacuo*. Purification by preparative thin layer chromatography (3% MeOH in DCM) afforded **59**·BF_4 (0.054 g, 50%) as a white solid. ^{1}**H NMR** (500 MHz; CD_3OD) δ (ppm): 7.10–7.23 (14H, m, $H_{b,n,l}$), 6.97–7.08 (14H, m, $H_{c,d,m}$), 6.76 (2H, d, $J_{k|l} = 8.7$ Hz, H_k), 6.55 (2H, d, $J_{e|d} = 8.5$ Hz, H_e), 4.80 (2H, s, H_h), 4,28 (3H, s, H_i), 3.77 (4H, br. s., $H_{f,j}$), 2.36–2.56 (2H, m, H_g), 1.24 (54H, app. s, $H_{a,o}$). **LRESI-MS** (pos.): 1270.68 calc. for $[C_{81}H_{97}IN_3O_2]^+ = 1270.66$.

[2]Rotaxane: mono-triazolium axle/3,5-bis-iodotriazole pyridinium, 60·Cl · BF_4



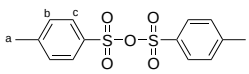
21·Cl (26 mg, 24 μmol) and **58**·BF_4 (36 mg, 24 μmol) were dissolved in dry DCM (8 mL), or 2% MeOH in $CHCl_3$, and stirred for 30 mins under N_2. Grubbs' II catalyst (10 wt%, 3.9 mg) was added and the mixture was stirred at room temperature, for 5 days under N_2. The solvent was removed *in vacuo* but did not afford **60**·Cl · BF_4.

All-XB [2]rotaxane: mono-iodotriazolium axle/3,5-bis-iodotriazole pyridinium, 61·Cl · BF_4



21·Cl (36 mg, 37 μmol) and **59**·BF_4 (54 mg, 37 μmol) were dissolved in dry DCM (8 mL), or 2% MeOH in $CHCl_3$, and stirred for 30 mins under N_2. Grubbs' II catalyst (10 wt%, 4.1 mg) was added and the mixture was stirred at room temperature, for 5 days under N_2. The solvent was removed *in vacuo* but did not afford **61**·Cl · BF_4.

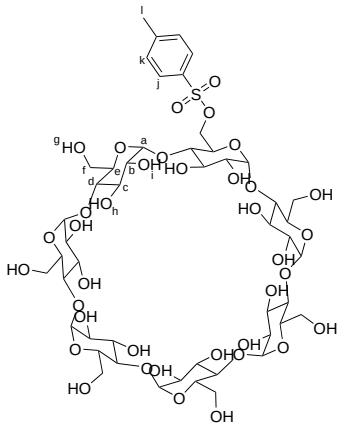
Tosyl anhydride, 62



TsCl (16.0 g 84 mmol) and TsOH·H_2O (4.0 g, 21 mmol) were suspended in DCM (100 mL). The mixture was stirred for 16 h at room temperature under N_2. Thereafter, the mixture was filtered through

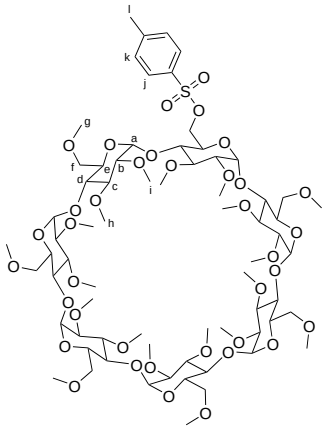
a silica plug. Purification by recrystallisation from hexane for 16 h at 4 °C to afford **62** (10.1 g, 50%). ^{1}**H NMR** (400 MHz; $CDCl_3$) δ (ppm): 7.90–7.95 (4H, m, H_b), 7.38–7.44 (4H, m, H_c), 2.49 (6H, s, H_a).

Monotosyl-cyclodextrin, 63



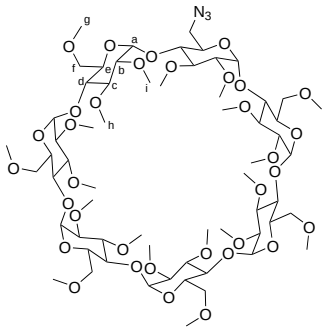
β-Cyclodextrin (11.4 g, 10.0 mmol) and **62** (4.90 g, 15.0 mmol) were suspended in H_2O (250 mL) and stirred at room temperature for 2 h. A solution of NaOH (5.1 g, 13 mmol) in H_2O (5 mL) was added and the mixture was stirred for no longer than 10 mins and then filtered. The mixture was acidified to pH $\sim$ 8 with 10% $HCl_{(aq.)}$. The mixture was stored at 4 °C for 16 h and the precipitate was collected. Purification by recrystallisation from 1:1 MeOH:H_2O (128 mL) afforded **63** (4.1 g, 32%). ^{1}**H NMR** (400 MHz; 1 :1 CD_3OD:D_2O) δ (ppm): 7.75 (2H, d, $J_{j|k} = 8.2$ Hz, H_j), 7.49 (2H, d, $J_{k|j} = 8.2$ Hz, H_k), 4.26–5.13 (34H, m, $H_{f,g,h,i}$), 3.35–4.10 (35H, m, $H_{a,b,c,d,e}$), 2.60 (3H, s, H_l). **LRESI-MS** (pos.): 1289.40, calc. for $[C_{49}H_{76}O_{37}S \cdot H]^+ = 1289.39$.

Monotosyl-permethylcyclodextrin, 64



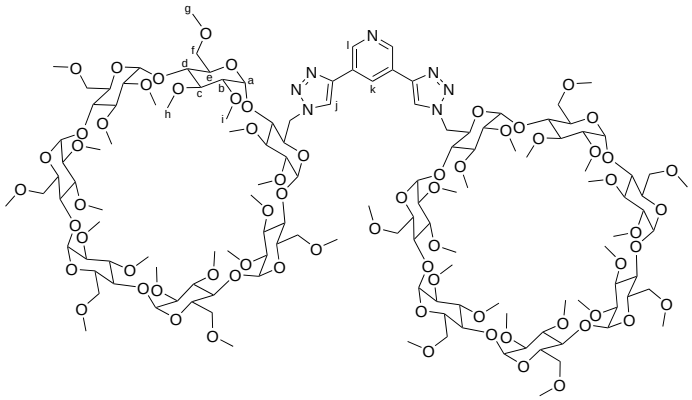
63 (2.0 g, 1.6 mmol) was dissolved in dry, degassed DMF (204 mL) and the mixture was cooled to 0 °C. NaH (60% dispersion in mineral oil) (4.28 g, 107 mmol) was added carefully and the mixture was stirred for 1 h at 0 °C. After stirring for a further 1 h at room temperature, the mixture was again cooled to 0 °C. CH_3I (14 mL, 225 mmol) was added dropwise and the mixture was stirred for 1 h at 0 °C. The reaction was stirred for 24 h at room temperature under N_2. Thereafter, the reaction was again cooled to 0 °C and H_2O (20 mL) was added and the mixture was poured onto ice water (200 mL). The product was extracted with $CHCl_3$ (5 × 50 mL). The combined organics were washed with 3% $Na_2S_2O_{3(aq.)}$ (25 mL) and H_2O (25 mL) and dried over $MgSO_4$. The solvent was removed *in vacuo*. Purification by silica gel column chromatography (gradient: 0.1–0.5% MeOH in EtOAc) afforded **64** (1.52 g, 62%). ^{1}**H NMR** (500 MHz; $CDCl_3$) δ (ppm): 7.78 (2H, d, $J_{j|k} = 8.1$ Hz, H_j), 7.38 (2H, d, $J_{k|j} = 8.1$ Hz, H_k), 4.97–5.24 (7H, m, H_a), 2.99–4.21 (102H, m, $H_{b,c,d,e,f,g,h,i}$), 2.46 (3H, s, H_l). ^{13}**C**$\{^1$**H**$\}$ **NMR** (126 MHz; $CDCl_3$) δ (ppm): 144.8, 133.3, 129.9, 127.9, 100.0, 99.1, 98.9, 82.1, 81.9, 81.9, 81.8, 81.7, 81.6, 80.8, 80.3, 79.6, 71.3, 71.1, 70.9, 70.7, 69.4, 61.7, 61.6, 61.6, 61.4, 61.3, 61.2, 59.1, 59.1, 59.1, 59.0, 59.0, 58.9, 58.8, 58.6, 58.5, 58.4, 58.3, 58.1, 21.7. **HRESI-MS** (pos.): 1591.68081, calc. for $[C_{69}H_{116}O_{37}S \cdot Na]^+$ = 1591.68084.

Monoazide-permethylcyclodextrin, 65



64 (0.50 g, 0.32 mmol) and NaN_3 (0.083 g, 1.3 mmol) were dissolved in dry, degassed DMF (5.5 mL). The mixture was refluxed at 100 °C for 16 h under N_2. Thereafter, the reaction was cooled to room temperature and partitioned between H_2O (50 mL) and $CHCl_3$ (50 mL). The aqueous layer was washed with further $CHCl_3$ (2 × 50 mL). The combined organics were dried over $MgSO_4$. The solvent was removed *in vacuo* to yield **65** (0.46 g, quant.). ^{1}**H NMR** (400 MHz; $CDCl_3$) δ (ppm): 4.99–5.24 (7H, m, H_a), 3.29–4.03 (101H, m, $H_{b,c,d,e,f,g,h,i}$). **LRESI-MS** (pos.): 1440.73, calc. for $[C_{62}H_{109}N_3O_{34} \cdot H]^+ =$ 1440.70.

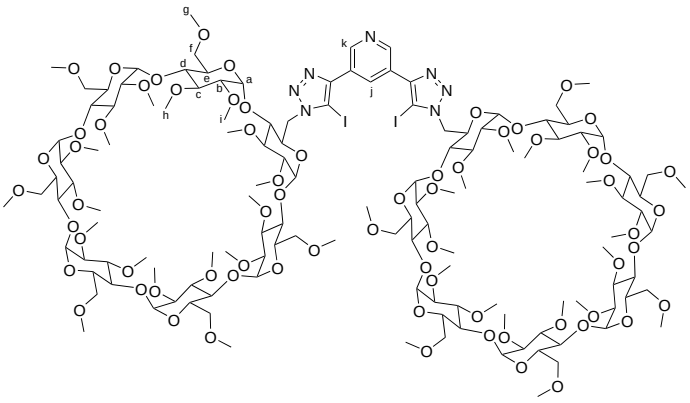
Bis-cyclodextrin-appended-triazole pyridine, 66



Method 1: Na_2CO_3 (1.1 mg, 10 μmol), ascorbic acid (1.6 mg, 9.1 μmol) and $CuSO_4 \cdot 5\,H_2O$ (0.2 mg, 1 μmol) were added to a solution of **1** (1.0 mg, 8.2 μmol) in 4:1 DMF:H_2O (0.125 mL). **65** (0.026 g, 18 μmol) was added and the solution was heated to 80 °C under N_2 for 3 days. After cooling to room temperature, the reaction was partitioned between EtOAc (10 mL) and NH_4OH (10 mL). The aqueous layer was washed with a further portion of EtOAc (10 mL). The combined organics were washed with H_2O (10 mL) and brine (10 mL) and dried over $MgSO_4$. The solvent was removed *in vacuo*. Purification by preparative thin layer chromatography (5% MeOH in EtOAc) afforded **66** (9.0 mg, 38%).

Method 2: To a solution of **65** (100 mg, 0.071 mmol) and **1** (4.0 mg, 0.032 mmol) in dry DCM (10 mL) was added $[Cu(MeCN)_4][PF_6]$ (5.0 mg, 0.016 mmol), TBTA (9.0 mg, 0.016 mmol) and diisopropylethylamine (DIPEA) (2.0 mg, 0.016 mmol) and the mixture was stirred under N_2 for 2 days. The reaction mixture was washed with NH_4OH (1 mL), brine (2 × 1 mL) and dried over $MgSO_4$. Purification by preparative thin layer chromatography (9:1 EtOAc/CH_3OH) afforded the axle precursor **66** (50 mg, 52 %). ^{1}**H NMR** (400 MHz; $CDCl_3$) δ (ppm): 9.01 (2H, s, H_l), 8.63 (1H, s, H_k), 8.06 (2H, s, H_j), 4.78–5.47 (14H, m, H_a), 2.61–4.31 (204H, m, $H_{b,c,d,e,f,g,h,i}$). ^{13}**C**$\{^1$**H**$\}$ **NMR** (125 MHz; $CDCl_3$) δ (ppm): 144.6, 142.6, 126.2, 121.9, 98.2–97.2, 81.5–77.8, 70.6–69.1, 60.8–60.4, 60.0–57.5, 50.6. **HRESI-MS** (pos.): 1526.2020, calc. for $[C_{133}H_{223}N_7O_{68} \cdot 2\,Na]^{2+} = 1526.1996$.

Bis-cyclodextrin-appended iodotriazolyl pyridine, 67

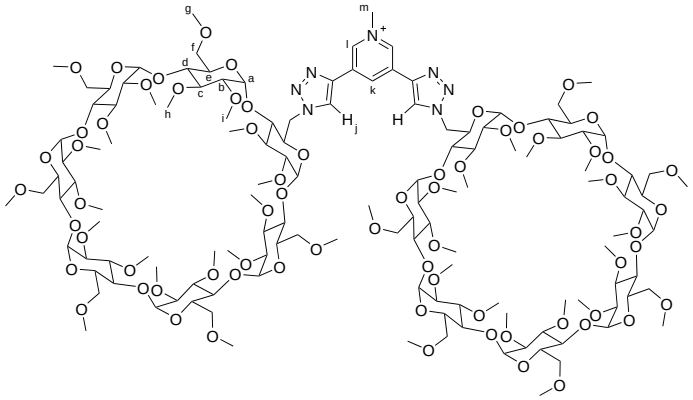


Method 1: 65 (0.050 g, 35 μmol) was dissolved in dry, degassed 1:1 THF:MeCN (0.125 mL) and covered in foil. NaI (0.022 g, 126 μmol) and $Cu(ClO_4)_2 \cdot 6\,H_2O$ (0.025 g, 63 μmol) were added and the solution was stirred for 5 mins. TBTA (0.8 mg, 0.3 μmol), DBU (4.7 μL, 32μmol, 0.125 mL 1:1 THF:MeCN) and **1** (0.002 g, 16 μmol) were added and the mixture was stirred over 3 days at room temperature under N_2. The mixture was diluted with DCM (15 mL) and washed with NH_4OH (2 × 5 mL) and brine (2 × 5 mL) and dried over $MgSO_4$. The solvent was removed *in vacuo*. Purification by preparative thin layer chromatography (5% MeOH in EtOAc) afforded **67** (0.034 g, 65%).

Method 2: $[Cu(MeCN)_4][PF_6]$ (11 mg, 30 μmol) and TBTA (8.9 mg, 17 μmol) were dissolved in dry, degassed THF (5 mL) and covered in foil. permethyl-β-cyclodextrinazide **65** (0.20 g, 0.14 mmol) and di-iodoethynyl pyridine **2** (24 mg, 64 μmol) were added, and the mixture was stirred overnight under N_2 at room temperature. Thereafter, the mixture was diluted with $CHCl_3$ (50 mL) and washed with NH_4OH (2 × 15 mL) and brine (2 × 15 mL). The organics were dried over $MgSO_4$, and the solvent was removed *in vacuo*. Purification by preparative thin layer chromatography (5% MeOH/EtOAc) afforded

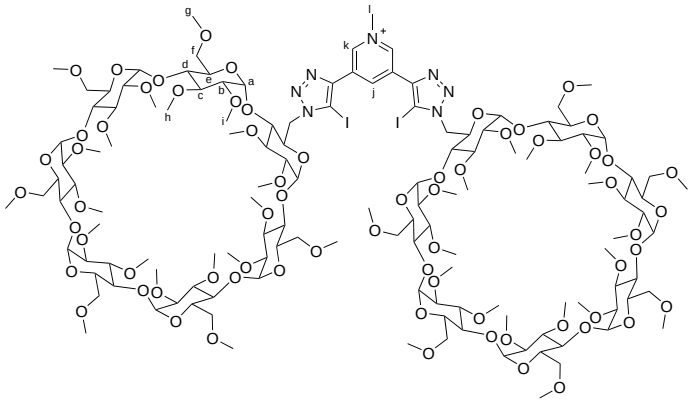
67 (0.17 g, 82%) as an off-white solid. ^{1}**H NMR** (400 MHz; $CDCl_3$) δ (ppm): 9.25 (2H, d, $^{4}J_{k|j} = 2.1$ Hz, H_k), 8.85–8.94 (1H, m, H_j), 4.94–5.46 (14H, m, H_a), 2.94–3.98 (204H, m, $H_{b,c,d,e,f,g,h,i}$). ^{13}**C**$\{^{1}$**H**$\}$ **NMR** (125 MHz; $CDCl_3$) δ (ppm): 146.4, 144.9, 125.9, 98.7–97.2, 83.0–78.4, 70.4–69.5, 60.9–60.4, 58.0–57.5, 50.6. **HRESI-MS** (pos.): 1652.5981 calc. for $[C_{133}H_{221}I_2N_7O_{68} \cdot 2\,Na]^{2+} = 1652.5979$.

Bis-cyclodextrin-appended triazolyl pyridinium chloride, 68·Cl



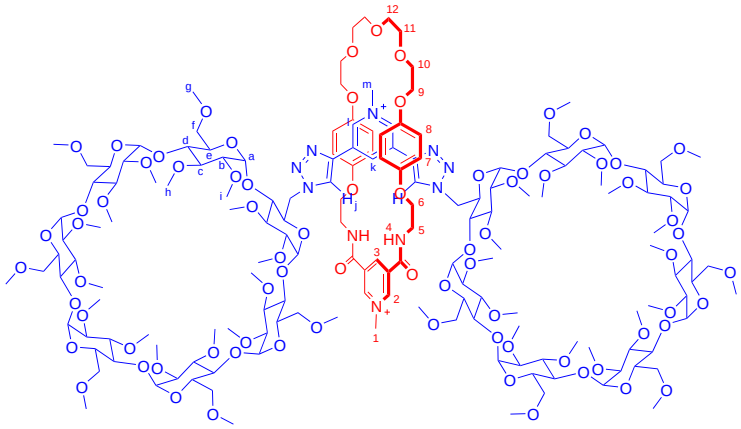
66 (50 mg, 0.017 mmol) was dissolved in 2 mL of CH_3I and stirred at 35 °C for 4 h. The CH_3I was removed under vacuum and the residue re-dissolved in 1:1 acetone/H_2O, and passed through a chloride-loaded Amberlite® column. The solvent was removed *in vacuo* and the product dried under high vacuum to yield **68**·Cl (50 mg, 99%). Anion exchange to the nitrate salt: **68**·Cl was passed down a nitrate-loaded Amberlite® column (1:1 acetone/H_2O) and the solvent was removed *in vacuo* to afford **68**·NO_3 quantitatively. ^{1}**H NMR** (500 MHz; $CDCl_3$) δ (ppm): 9.75 (2H, s, H_l), 9.36 (1H, s, H_k), 8.96 (2H, s, H_j), 5.45–5.11 (14H, m, H_a), 4.75 (3H, s, H_m), 4.13–3.02 (204H, $H_{b,c,d,e,f,g,h,i}$). ^{13}**C**$\{^{1}$**H**$\}$ **NMR** (125 MHz; $CDCl_3$) δ (ppm): 138.7, 135.0, 131.8, 126.1, 124.1, 98.2–97.1, 81.0–77.5, 70.7–69.8, 68.6, 60.7–57.3. **HRESI-MS** (pos.): 1522.2143 calc. for $[C_{134}H_{226}N_7O_{68} \cdot Na]^{2+} = 1522.2164$.

Bis-cyclodextrin-appended iodotriazolyl pyridinium chloride, 69·Cl



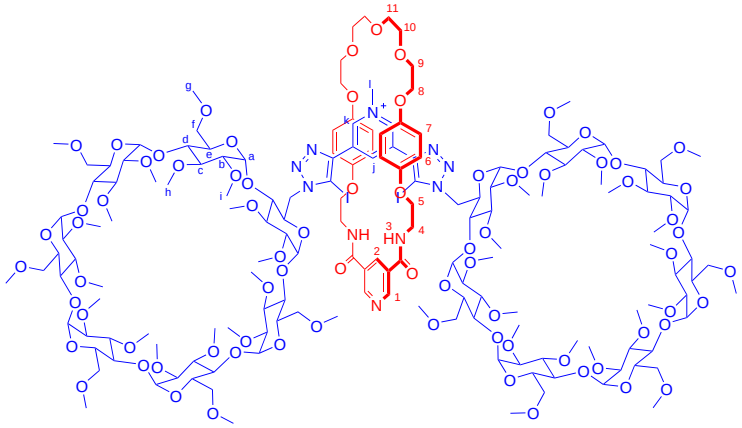
67 (35 mg, 0.012 mmol) was dissolved in CH_3I (2 mL) and stirred at 35 °C for 16 h. The CH_3I was removed under vacuum and the residue re-dissolved in 1:1 acetone/H_2O, and passed through a chloride-loaded Amberlite® column. The solvent was removed *in vacuo* and the product dried under high vacuum to yield **69**·Cl (38 mg, 98%). Anion exchange to the nitrate salt: **69**·Cl was passed down a nitrate-loaded Amberlite® column, three times, and the solvent was removed *in vacuo* to afford **69**·NO_3 quantitatively. ^{1}**H NMR** (500 MHz; $CDCl_3$) δ (ppm): 10.11 (1H, s, H_j), 9.32 (2H, s, H_k), 5.48 (2H, app s, H_a), 5.27 (2H, app s, H_a), 5.14–4.96 (10H, m, H_a), 4.53 (3H, s, H_l), 4.37-3.10 (202H, m, $H_{b,c,d,e,f,g,h,i}$). ^{13}**C**$\{^1$**H**$\}$ **NMR** (125 MHz; $CDCl_3$) δ (ppm): 140.6, 139.1, 134.4, 133.9, 98.4–97.9, 82.9.0–79.4, 71.0–70.8, 70.5, 62.0–61.1, 59.9–58.1. **HRESI-MS** (pos.): 1648.6129, calc. for $[C_{134}H_{224}I_2N_7O_{68} \cdot Na]^{2+} = 1648.6147$.

Monocationic HB [2]rotaxane precursor 70·Cl and dicationic HB [2]rotaxane: pCD-appended prototriazolyl pyridinium axle–pyridinium bis-amide macrocycle nitrate, 72·$(NO_3)_2$



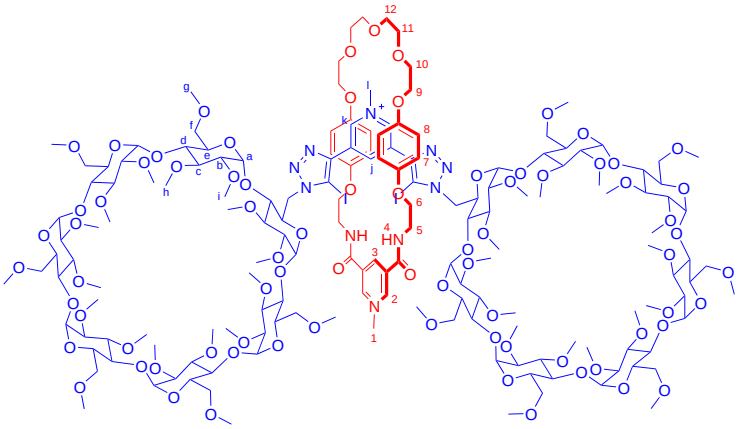
68·Cl (22 mg, 0.007 mmol) and **24** (51 mg, 0.110 mmol) were dissolved in dry DCM (20 mL) and stirred for 30 mins at 0 °C under N_2. Et_3N (0.025 mL, 0.20 mmol) was then added followed immediately by the dropwise addition of 3,5-bis-chlorocarbonyl pyridine (18 mg, 0.109 mmol) dissolved in dry DCM (2 mL). The reaction was allowed to reach room temperature and was stirred for 3 h. The solvent was removed *in vacuo*, and initially purified by preparative silica gel thin-layer chromatography (9:1 EtOAc/CH_3OH), to yield a mixture of the mono-cationic rotaxane (**70**) and macrocycle by-product which could not be separated at this stage. The mixture was then subjected to methylation conditions: CH_3I (2 mL) and stirred at 35 °C for 4 h, after which the solvent was removed *in vacuo*. Anion exchange to the nitrate salt: **72**·2 X was passed through a nitrate-loaded Amberlite® column. The solvent was removed *in vacuo* and the product dried under high vacuum to yield rotaxane **72**·$(NO_3)_2$ (7 mg, 25%). **^{1}H NMR** (500 MHz; D_2O) δ (ppm): 9.59 (1H, s, H_3), 9.44 (2H, s, H_2), 8.79 (2H, s, H_l), 8.57 (2H, s, H_j), 8.43 (1H, s, H_k), 6.30 (4H, d, $J_{8|7} = 8.3$ Hz, H_8), 6.17 (4H, d, $J_{7|8} = 8.3$ Hz, H_7), 5.37 (4H, m, H_a), 5.21 (6H, m, H_a), 4.99 (4H, m, H_a), 4.56 (3H, s, H_m), 4.33 (3H, s, H_1), 4.16 (2H, m, H_f), 4.00 (2H, m, H_f), 3.80–2.93 (226H, m, H_f, $H_{b,c,d,e,g,h,i,5,6,9,10,11,12}$). **^{13}C{^{1}H} NMR** (125 MHz; D_2O) δ (ppm): 163.1, 152.3, 152.0, 147.5, 140.2, 140.1, 134.6, 130.4, 114.9, 114.5, 97.4–96.2, 82.2–79.7, 78.7–76.7, 70.9–69.4, 67.7, 66.4, 60.4–59.6, 58.8–57.7. **HRESI-MS** (pos.): 1815.8610, calc. for $[C_{166}H_{266}N_{10}O_{77}]^{2+}$ = 1815.8598.

Monocationic XB [2]rotaxane: pCD-appended iodotriazole pyridinium axle–pyridine bis-amide macrocycle nitrate, 71·Cl



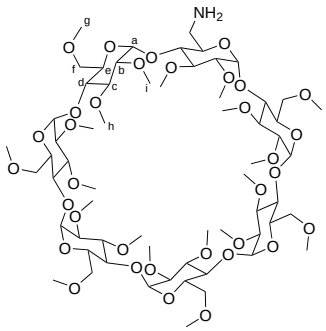
69·Cl (46 mg, 0.014 mmol) and **24** (66 mg, 0.139 mmol) were dissolved in dry DCM (40 mL) and stirred for 30 mins at 0 °C under N_2. Et_3N (0.05 mL, 0.410 mmol) was then added followed immediately by the dropwise addition of 3,5-bis-chlorocarbonyl pyridine (28 mg, 0.139 mmol) dissolved in dry DCM (5 mL). The reaction was allowed to reach room temperature and was then stirred for 3 h. The solvent was removed *in vacuo*, and purified by preparative silica gel thin-layer chromatography (9:1 $CHCl_3$/CH_3OH), to yield the mono-cationic rotaxane **71**·Cl (20 mg, 37%). ^{1}**H NMR** (500 MHz; D_2O) δ (ppm): 9.41 (1H, s, H_2), 9.13 (2H, s, H_1), 9.10 (2H, s, H_k), 8.26 (1H, s, H_j), 6.34 (4H, d, $J_{7|6} = 7.9$ Hz, H_7), 6.06 (4H, br app s, H_6), 5.34–4.90 (14H, m, H_a), 4.56 (3H, s, H_l), 4.28 (2H, app s, H_f), 4.04 (2H, app s, H_f), 3.88–3.07 (224H, m, H_f, $H_{b,c,d,e,g,h,i,4,5,8,9,10,11}$). ^{13}**C**$\{^1$**H**$\}$ **NMR** (125 MHz; D_2O) δ (ppm): 166.6, 157.0, 156.8, 152.4, 151.8, 151.6, 142.1, 141.6, 115.2, 114.4, 97.3–97.0, 81.9–81.0, 79.8, 71.4–67.5, 60.1–57.8. **HRESI-MS** (pos.): 1945.7426, calc. for $[C_{165}H_{261}I_2N_{10}O_{77} \cdot Na]^{2+} = 1945.7396$.

Dicationic XB [2]rotaxane: pCD-appended iodotriazolyl pyridinium axle–pyridinium bis-amide macrocycle nitrate, 73·$(NO_3)_2$



71·Cl (20 mg, 0.005 mmol) was dissolved in neat CH_3I (2 mL), and stirred at 35 °C for 4 h, after which the solvent was removed *in vacuo*. Anion exchange to the nitrate salt: **73**·2 X was passed through a nitrate-loaded Amberlite® column. The solvent was removed *in vacuo* and the product dried under high vacuum to yield rotaxane **73**·$(NO_3)_2$ (20 mg, 96%). **^{1}H NMR** (500 MHz; D_2O) δ (ppm): 9.70 (1H, s, H_3), 9.45 (2H, s, H_2), 9.24 (2H, s, H_k), 8.47 (1H, s, H_j), 6.33 (4H, d, $J_{8|7} = 8.2$ Hz, H_8), 6.21 (4H, d, $J_{7|8} = 8.2$ Hz, H_7), 5.44–4.87 (14H, m, H_a), 4.56 (3H, s, H_l), 4.53 (3H, s, H_1), 4.30 (2H, m, H_f), 4.01 (2H, m, H_f), 3.86–3.09 (224H, m, H_f, $H_{b,c,d,e,g,h,i,5,6,9,10,11,12}$). **^{13}C{^{1}H} NMR** (125 MHz; D_2O) δ (ppm): 163.0, 152.3, 152.0, 146.9, 142.4, 141.6, 141.6, 134.6, 130.4, 114.9, 97.8–96.6, 81.6–76.6, 70.7–69.4, 67.5, 66.6, 60.5–59.9, 58.8–57.8. **HRESI-MS** (pos.): 1941.7617, calc. for $[C_{166}H_{264}I_2N_{10}O_{77}]^{2+}$ = 1941.7617.

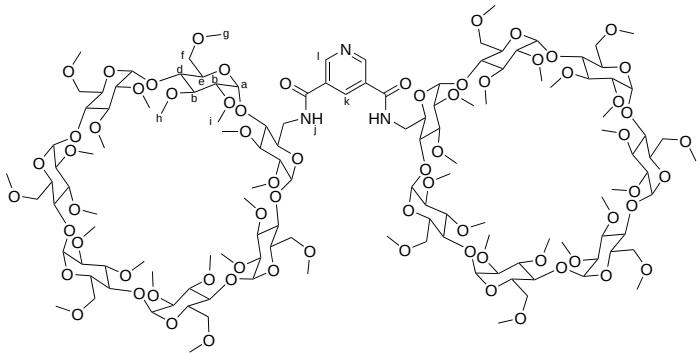
Monoamine-permethylcyclodextrin, 74



This literature compound[456] was prepared through a novel reduction procedure: To a solution of monoazide-permethylcyclodextrin **65** (120 mg, 0.083 mmol) in CH_3OH (2 mL) was added a suspension

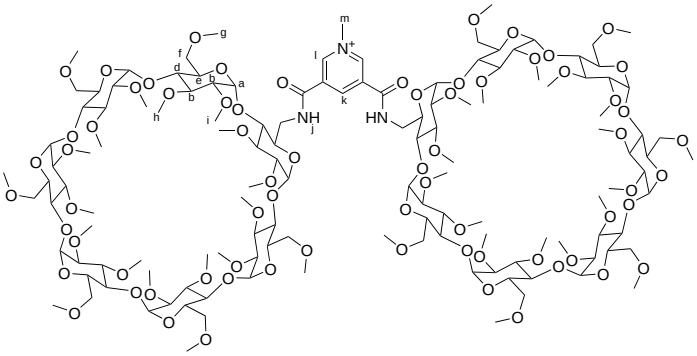
of Pd/C (10 wt%, 20 mg) in H_2O (1 mL), followed by hydrazine monohydrate (25 μL, 0.42 mmol). The reaction mixture was refluxed for 1 h, before cooling to room temperature. The catalysts were filtered off by passing through Celite® and the solvent was removed *in vacuo*. The residue was dissolved in DCM (10 mL) and washed with H_2O (2 × 2 mL), dried over $MgSO_4$, filtered and the solvent was removed *in vacuo* to afford the product **74** as a white solid (118 mg, 97%). ^{1}**H NMR** (300 MHz; $CDCl_3$) δ (ppm): 5.15 (7H, m, H_a), 4.00–3.70 (14H, m, H_f), 3.65–3.10 (88H, m, $H_{b,c,d,e,g,h,i}$). **LRESI-MS** (pos.): 1414.6, calc. for $[C_{62}H_{111}O_{34} \cdot H]^+ = 1414.5$.

Permethyl-β-cyclodextrin-appended pyridine bis-amide axle precursor, 75



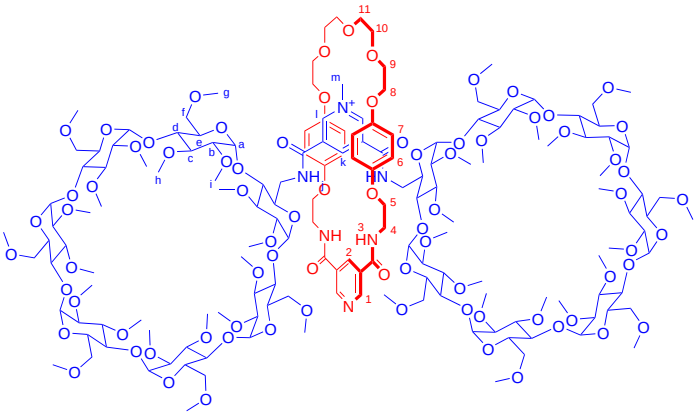
To a solution of 3,5-pyridine dicarboxylic acid (30 mg, 0.18 mmol), EDC·HCl (67 mg, 0.59 mmol), DMAP (cat.) and 1-hydroxy-benzotriazole (60 mg, 0.36 mmol) in DCM (30 mL) was added a solution of monoamine-permethylcyclodextrin **74** (510 mg, 0.36 mmol) and Et_3N (0.1 mL) and stirred at room temperature for 72 h. Purification by silica gel column chromatography (3% MeOH in $CHCl_3$) gave **75** as a white solid (385 mg, 70%). ^{1}**H NMR** (500 MHz; CD_3OD) δ (ppm): 9.16 (2H, d, $^4J_{l|k} = 2.1$ Hz, H_l), 8.68 (1H, t, $^4J_{k|l} = 2.1$ Hz, H_k), 5.36–5.15 (14H, m, H_a), 4.05–3.11 (206H, m, $H_{b,c,d,e,f,g,h,i}$). ^{13}**C**$\{^1$**H**$\}$ **NMR** (125 MHz; CD_3OD) δ (ppm): 167.0, 151.6, 136.0, 131.9, 99.7–99.2, 83.7–82.7, 81.1–79.4, 72.9–72.2, 61.9–61.5, 59.8–58.9. **HRESI-MS** (pos.): 1502.6870, calc. for $[C_{131}H_{223}N_3O_{70} \cdot 2\,Na]^{2+}$ = 1502.6900).

Permethyl-β-cyclodextrin-appended pyridinium bis-amide chloride axle, 76·Cl



75 (135 mg, 0.046 mmol) was dissolved in CH_3I (5 mL) and stirred at 35 °C for 4 h, after which the solvent was removed *in vacuo*. Anion exchange to the chloride salt was achieved by passing through a chloride-loaded Amberlite® column. The solvent was removed *in vacuo* and the product dried under high vacuum to yield **76**·Cl as the chloride salt (117 mg, 90%). To exchange to the nitrate salt, **76**·Cl (20 mg, 0.007 mmol) was passed down a nitrate-loaded Amberlite® column, and the solvent was removed *in vacuo*, quantitatively yielding **76**·NO_3. **^{1}H NMR** (500 MHz; CD_3OD) δ (ppm): 9.52 (2H, d, $^4J_{l|k} = 1.3$ Hz, H_l), 9.32 (1H, t, $^4J_{k|l} = 1.3$ Hz, H_k), 7.97 (2H, s, H_j), 5.45–5.10 (14H, m, H_a), 4.58 (3H, s, H_m), 4.05–3.10 (206H, m, $H_{b,c,d,e,f,g,h,i}$). **^{13}C{^{1}H} NMR** (125 MHz; CD_3OD) δ (ppm): 163.2, 148.2, 143.0, 135.8, 99.7–98.7, 84.0–82.0, 81.1–78.9, 73.2–72.0, 71.4, 61.9–61.6, 60.0–58.7. **HRESI-MS** (pos.): 1498.7098 calc. for $[C_{132}H_{226}N_3O_{70} \cdot 2\,Na]^{2+} = 1498.7069$.

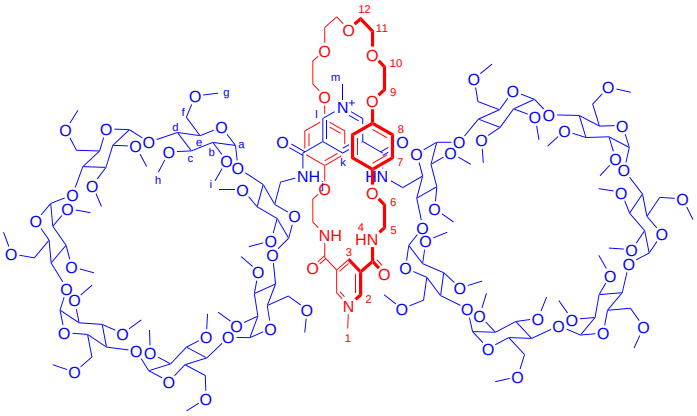
Monocationic HB amide [2]rotaxane: pCD-appended pyridinium bis-amide axle–pyridine bis-amide macrocycle chloride, 77·Cl



76·Cl (90 mg, 0.029 mmol) and bis-amine **24** (138 mg, 0.290 mmol) were dissolved in dry DCM (70 mL) and stirred for 30 mins at 0 °C under N_2. Et_3N (0.1 mL, 0.82 mmol) was then added, followed

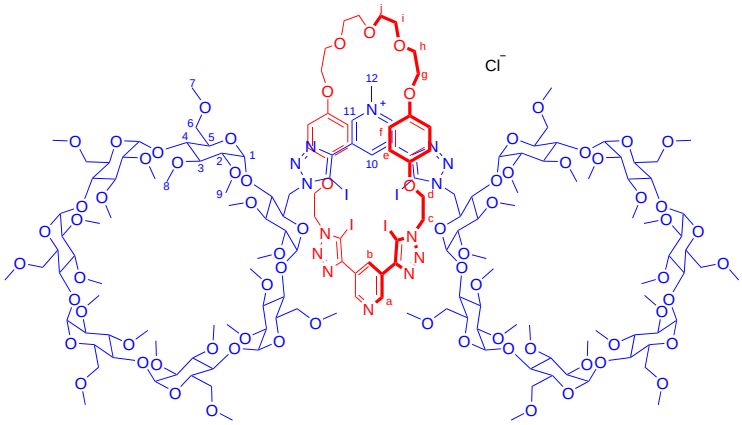
immediately by the dropwise addition of 3,5-bis-chlorocarbonyl pyridine (59 mg, 0.290 mmol) dissolved in dry DCM (5 mL). The reaction was allowed to reach room temperature and was then stirred for 3 h. The solvent was removed *in vacuo*, and purified first by silica gel preparative thin layer chromatography (10% MeOH in DCM), and then size-exclusion chromatography to remove the free macrocycle by-product, to yield the mono-cationic rotaxane **77**·Cl (28 mg, 33%). ^{1}**H NMR** (500 MHz; CD_3OD) δ (ppm): 9.58 (2H, s, $H_{k,2}$), 9.32 (2H, d, $^{4}J_{1|2} = 1.9$ Hz, H_1), 9.11 (2H, app. s, H_l), 6.64 (4H, d, $J_{7|6} = 8.9$ Hz, H_7), 6.34 (4H, d, $J_{6|7} = 8.9$ Hz, H_6), 5.40–5.03 (14H, m, H_a), 4.53 (3H, s, H_m), 4.27–2.83 (228H, m, $H_{b,c,d,e,f,g,h,i,4,5,8,9,10,11}$). ^{13}**C**$\{^{1}$**H**$\}$ **NMR** (125 MHz; CD_3OD) δ (ppm): 166.5, 162.3, 154.5, 153.7, 152.4, 147.3, 136.3, 134.6, 132.4, 131.0, 129.9, 116.3, 116.0, 99.7–98.4, 84.079.3, 77.8, 73.4–67.3, 62.2–58.5. **HRESI-MS** (pos.): 1796.3348 calc. for $[C_{163}H_{263}N_6O_{79} \cdot 2\,Na]^{2+} = 1796.3333$.

Dicationic HB amide [2]rotaxane: pCD-appended pyridinium bis-amide axle–pyridinium bis-amide macrocycle nitrate, 78·$(NO_3)_2$



Dicationic rotaxane **78**·$(NO_3)_2$ was prepared by dissolving rotaxane **77**·Cl (28 mg, 0.008 mmol) in neat CH_3I (2 mL), and stirring at 35 °C for 4 h, after which the solvent was removed *in vacuo*. Anion exchange to the nitrate salt was achieved by passing through a nitrate-loaded Amberlite® column. The solvent was removed *in vacuo* and the product dried under high vacuum to yield rotaxane **78**·$(NO_3)_2$ (27 mg, 95%). ^{1}**H NMR** (500 MHz; CD_3OD) δ (ppm): 9.79 (1H, s, H_3), 9.61 (2H, s, H_2), 9.17 (1H, s, H_k), 9.01 (2H, s, H_l), 6.69 (4H, d, $J_{8|7} = 8.5$ Hz, H_8), 6.41 (4H, d, $J_{7|8} = 8.5$ Hz, H_7), 5.49–5.09 (14H, m, H_a), 4.64 (6H, s, H_m), 4.25–3.06 (228H, m, $H_{b,c,d,e,f,g,h,i,5,6,9,10,11,12}$). ^{13}**C**$\{^{1}$**H**$\}$ **NMR** (125 MHz; CD_3OD) δ (ppm): 163.0, 162.7, 154.4, 153.6, 148.8, 147.5, 135.7, 134.8, 132.4, 129.9, 116.4, 116.1, 100.0–98.2, 84.6–79.1, 77.0, 73.5–67.3, 62.2–58.4. **HRESI-MS** (pos.): 1803.8410, calc. for $[C_{163}H_{265}N_6O_{79} \cdot 2\,Na]^{2+} = 1803.8428$.

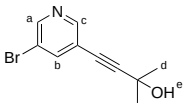
XB pyridinium cyclodextrin rotaxane, 79



[Cu(MeCN)$_4$][BF$_4$] (cat.) and TBTA (cat.) were dissolved in dry degassed THF (10 mL) and covered in foil. Bis-azide macrocycle precursor **52** (31 mg, 60 μmol) and permethyl-β-cyclodextrinaxle **69**·Cl (20 mg, 6 μmol) were added, and the mixture was stirred for 30 mins. Thereafter, di-iodoethynyl pyridine **2** (24 mg, 60 μmol) was added, and the mixture was stirred under N_2 at room temperature for 4 days. The mixture was diluted with $CHCl_3$ (30 mL) and washed with NH_4OH (2 $\times$ 15 mL) and brine (2 $\times$ 15 mL). The organics were dried over $MgSO_4$. The solvent was removed *in vacuo*, however no evidence for the formation of the [2]rotaxane was obtained after attempted purification by preparative thin layer chromatography.

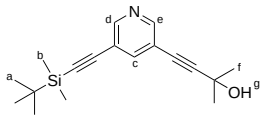
6.2.2 Compounds from Chapter 3

3-Bromo-5-(3-hydroxy-3-methyl-1-butynyl)pyridine, 80



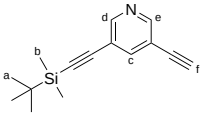
3,5-Dibromopyridine (0.24 g, 1.0 mmol), $PdCl_2(PPh_3)_2$ (0.028 g, 40 μmol) and CuI (4.6 mg, 24 μmol) were suspended in *i*-Pr_2NH (5.95 mL) and degassed with argon. 3-Hydroxy-3-methyl-but-1-yne (0.097 mL, 1 mmol) was added dropwise over 35 mins at 0 °C. The reaction was allowed to warm to room temperature and was stirred for 23 h. The solvent was removed *in vacuo*. Purification by silica gel column chromatography (0.5% MeOH in DCM) afforded **80** (0.19 g, 79%). **^{1}H NMR** (400 MHz; $CDCl_3$) δ (ppm): 8.57 (2H, dd, J = 9.7 Hz, $^4J_{a,b|c}$ = 1.9 Hz, $H_{a,b}$), 7.86 (1H, t, $^4J_{c|a,b}$ = 2.0 Hz, H_c), 2.37 (1H, s, H_e), 1.53–1.68 (6H, m, H_d). **LRESI-MS** (pos.): 240.0, calc. for $[C_{10}H_{10}BrNO \cdot H]^+$ = 240.0.

3-(*tert*-Butyldimethylsilylethynyl)-5-(3-hydroxy-3-methyl-1-butynyl)pyridine, 81



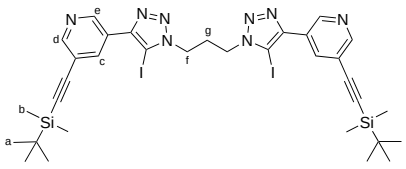
80 (0.93 g, 3.9 mmol) was dissolved in 1:1 *i*-Pr_2NH:THF (32 mL) and degassed with argon. Thereafter, $PdCl_2(PPh_3)$ (0.11 g, 0.16 mmol), CuI (0.017 g, 90 μmol) and TBDMS-acetylene (0.81 g, 5.7 mmol) were added and the mixture was stirred at room temperature for 4 h. Thereafter, the reaction was filtered through a Florisil® bed and washed with THF ($\sim$ 100 mL). The solvent was removed *in vacuo*. Purification by silica gel column chromatography (1% MeOH in DCM) afforded **81** (1.01 g, 87%). ^{1}**H NMR** (400 MHz; $CDCl_3$) δ (ppm): 8.56 (2H, s, $H_{d,e}$), 7.77 (1H, t, $^4J_{c|d,e} = 2.0$ Hz, H_c), 2.54 (1H, s, H_g), 1.61 (6H, s, H_f), 0.99 (9H, s, H_a), 0.19 (6H, s, H_b). **LRESI-MS** (pos.): 300.2, calc. for $[C_{18}H_{25}NOSi \cdot H]^+ = 300.2$.

3-(*tert*-Butyldimethylsilylethynyl)-5-ethynylpyridine, 82



81 (1.76 g, 5.9 mmol) was dissolved in toluene. Freshly ground NaOH (0.295 g, 7.4 mmol) was added and the mixture was stirred for 30 h at 110 °C. After cooling to room temperature, the mixture was filtered. The solvent was removed *in vacuo*. Purification by silica gel column chromatography (DCM) yielded **82** (1.02 g, 72%). ^{1}**H NMR** (500 MHz; $CDCl_3$) δ (ppm): 8.58–8.67 (2H, m, $H_{d,e}$), 7.83 (1H, t, $^4J_{c|d,e} = 1.9$ Hz, H_c), 3.23 (1H, s, H_f), 1.00 (9H, s, H_a), 0.20 (6H, s, H_b). **LRESI-MS** (pos.): 242.1, calc. for $[C_{15}H_{19}NSi \cdot H]^+ = 242.1$.

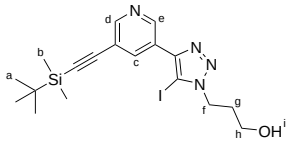
Bis-TBDMS-ethynyl-pyridyl-iodotriazolyl propane, 83



86 (0.10 g, 0.2 mmol) was dissolved in dry, degassed 1:1 THF:MeCN (0.72 mL) and covered in foil. NaI (0.11 g, 0.74 mmol) and $Cu(ClO_4)_2 \cdot 6\,H_2O$ (0.14 g, 0.37 mmol) were added and the mixture was

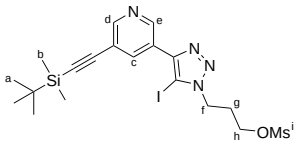
stirred for 5 mins under N_2. TBTA (cat.), DBU (28 μL, 0.18 mmol, 0.35 mL 1:1 THF:MeCN) and **82** (0.045 g, 0.18 mmol, 0.35 mL 1:1 THF:MeCN) were added and the mixture was stirred under N_2 for 16 h. The reaction was diluted with DCM (40 mL) and washed with NH_4OH (2 $\times$ 10 mL) and brine (2 $\times$ 10 mL) and dried over $MgSO_4$. The solvent was removed *in vacuo*. Purification by preparative thin layer chromatography (3% MeOH in DCM) yielded **83** (0.16 g, quant.). ^{1}**H NMR** (400 MHz; $CDCl_3$) δ (ppm): 9.11 (2H, d, $^4J_{e|c} = 2.1$ Hz, H_e), 8.71 (2H, d, $^4J_{d|c} = 2.0$ Hz, H_d), 8.31 (2H, t, $^4J_{c|d,e} = 2.0$ Hz, H_c), 4.60 (4H, t, $J_{f|g} = 6.8$ Hz, H_f), 2.76 (2H, quin, $J_{g|f} = 6.7$ Hz, H_g), 1.01 (18H, s, H_a), 0.21 (12H, s, H_b). ^{13}**C**$\{^1$**H**$\}$ **NMR** (101 MHz; $CDCl_3$) δ (ppm): 152.4, 146.9, 137.4, 125.7, 120.4, 101.6, 97.7, 47.9, 26.1, 16.7, 1.0, -4.7. **HRESI-MS** (pos.): 861.12152, calc. for $[C_{33}H_{42}I_2N_8Si_2 \cdot H]^+ = 861.12331$.

TBDMS-ethynyl-hydroxypropyl-iodotriazole pyridine, 84



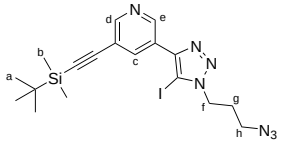
46 (0.10 g, 1.0 mmol) was dissolved in dry, degassed THF (1.0 mL) and covered in foil. NaI (0.50 g, 3.3 mmol) and $Cu(ClO_4)_2 \cdot 6\,H_2O$ (0.62 g, 1.7 mmol) were added and the mixture was stirred for 5 mins under N_2. TBTA (0.006 g, 11 μmol), DBU (0.13 g, 0.83 mmol, 0.5 mL THF) and **82** (0.20 g, 0.84 mmol, 0.5 mL THF) were added and the mixture was stirred under N_2 for 16 h. The reaction was diluted with DCM (80 mL) and washed with NH_4OH (2 $\times$ 40 mL) and brine (2 $\times$ 40 mL) and dried over $MgSO_4$. The solvent was removed *in vacuo*. Purification by silica gel column chromatography (5% MeOH in DCM) afforded **84** (0.375 g, 96%). ^{1}**H NMR** (400 MHz; $CDCl_3$) δ (ppm): 9.12 (1H, d, $^4J_{c|e} = 2.1$ Hz, H_e), 8.70 (1H, d, $^4J_{c|d} = 1.8$ Hz, H_d), 8.31 (1H, t, $^4J_{c|e} = 2.1$ Hz, H_c), 4.64 (2H, t, $J_{f|g} = 6.8$ Hz, H_f), 3.73 (2H, q, $J_{g|h,i} = 5.6$ Hz, H_h), 2.21 (2H, quin, $J_{f|g,h} = 6.4$ Hz, H_g), 1.79 (1H, t, $J_{h|i} = 5.3$ Hz, H_i), 1.01 (9H, s, H_a), 0.21 (6H, s, H_b). ^{13}**C**$\{^1$**H**$\}$ **NMR** (126 MHz; $CDCl_3$) δ (ppm): 152.2, 150.5, 146.9, 146.6, 146.1, 137.5, 137.1, 125.9, 120.4, 101.6, 97.5, 58.9, 47.9, 32.1, 26.1, 16.7, 1.0, -4.7. **HRESI-MS** (pos.): 469.09090, calc. for $[C_{18}H_{25}IN_4OSi \cdot H]^+ = 469.09151$.

TBDMS-ethynyl-mesylpropyl-iodotriazole pyridine, 85



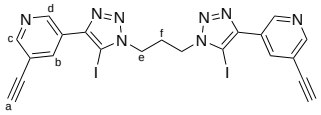
84 (0.16 g, 0.34 mmol) and Et_3N (0.10 mL, 0.72 mmol) were dissolved in dry DCM (0.45 mL) and stirred at 0 °C under N_2. MsCl (0.040 mL, 0.41 mmol) in dry DCM (0.23 mL) was added dropwise. The mixture was allowed to warm to room temperature and stirred for 1 h. The reaction was then diluted with DCM (10 mL) and washed with H_2O (2 × 5 mL), 1 M $HCl_{(aq.)}$ (3 × 5 mL) and brine (3 × 5 mL) and dried over $MgSO_4$. The solvent was removed *in vacuo* to yield **85** (0.174 g, 94%). ^{1}**H NMR** (400 MHz; $CDCl_3$) δ (ppm): 9.11 (1H, br. s., H_e), 8.71 (1H, br. s., H_d), 8.30 (1H, t, $^4J_{c|d,e} = 2.0$ Hz, H_c), 4.63 (2H, t, $J_{f|g} = 6.7$ Hz, H_f), 4.32 (2H, t, $J_{h|g} = 5.7$ Hz, H_h), 3.08 (3H, s, H_i), 2.45 (2H, quin, $J_{g|f,h}$ = 6.0 Hz, H_g), 1.01 (9H, s, H_a), 0.21 (6H, s, H_b). ^{13}**C**$\{^1$**H**$\}$ **NMR** (126 MHz; $CDCl_3$) δ (ppm): 149.4, 146.1, 129.2, 128.9, 128.2, 123.1, 102.6, 98.5, 65.8, 53.4, 47.4, 37.6, 29.1, 26.0, 16.6, -4.9. **HRESI-MS** (pos.): 547.06813, calc. for $[C_{19}H_{27}IN_4O_3SSi \cdot H]^+ = 547.06906$.

TBDMS-ethynyl-azidopropyl-iodotriazolyl pyridine, 86



85 (0.45 g, 0.82 mmol) and NaN_3 (0.30 g, 3.4 mmol) were dissolved in dry, degassed DMF (15.5 mL). The mixture was refluxed at 85 °C for 16 h under N_2. After cooling to room temperature, the reaction was partitioned between H_2O (10 mL) and Et_2O (10 mL). The aqueous layer was washed with Et_2O (2 × 10 mL) and the combined organics were washed with brine (3 × 5 mL) and dried over $MgSO_4$. The solvent was removed *in vacuo* to afford **86** (0.298 g, 73%). ^{1}**H NMR** (500 MHz; $CDCl_3$) δ (ppm): 9.11 (1H, d, $^4J_{e|c} = 2.1$ Hz, H_e), 8.70 (1H, d, $^4J_{d|c} = 1.8$ Hz, H_d), 8.31 (1H, t, $^4J_{c|d,e} = 2.1$ Hz, H_c), 4.57 (2H, t, $J_{h|g} = 6.9$ Hz, H_h), 3.43–3.49 (2H, m, H_f), 2.24 (2H, quin, $J_{g|f,h} = 6.6$ Hz, H_g), 1.00 (9H, s, H_a), 0.20 (6H, s, H_b). ^{13}**C**$\{^1$**H**$\}$ **NMR** (126 MHz; $CDCl_3$) δ (ppm): 151.2, 149.6, 145.9, 145.7, 145.1, 136.5, 136.1, 124.9, 119.4, 100.6, 96.6, 64.8, 47.0, 28.1, 25.1, 15.7, 14.3, −5.7. **HRESI-MS** (pos.): 494.09724, calc. for $[C_{18}H_{24}IN_7Si \cdot H]^+ = 494.09799$.

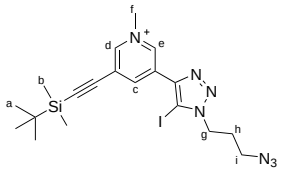
Bis-ethynyl-pyridyl-iodotriazolyl propane, 87



Method 1: 83 (0.10 g, 0.12 mmol) was dissolved in THF (3.2 mL) and 1 drop of H_2O was added. TBAF (1 M in THF, 0.3 mL, 0.3 mmol) was added dropwise at 0 °C and the reaction was stirred for 1 h at 0 °C. Further TBAF (1 M in THF, 0.3 mL, 0.3 mmol) was added dropwise at 0 °C and stirred for 16 h. A final portion of TBAF (1 M in THF, 0.15 mL, 0.15 mmol) was added dropwise at 0 °C. The solvent was removed *in vacuo*. The residue was taken up in DCM (50 mL) and washed with H_2O (20 mL) and brine (20 mL) and dried over $MgSO_4$. The solvent was removed *in vacuo*. However, this resulted in the degradation of one of the iodotriazole moieties to the prototriazole.

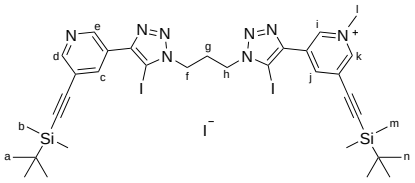
Method 2: 83 (0.05 g, 0.06 mmol) was dissolved in THF (1.2 mL). TBAF·$x$$H_2O$ (0.015 g, 0.06 mmol), dissolved in THF (0.4 mL), was added dropwise at 0 °C and stirred for 1 h at 0 °C. The solvent was removed *in vacuo*. The residue was taken up in DCM (20 mL) and washed with H_2O (10 mL) and brine (10 mL). The organics were dried over $MgSO_4$. The solvent was removed *in vacuo*. However, this resulted in the degradation of one of the iodotriazole moieties to the prototriazole.

TBDMS-ethynyl-azidopropyl-iodotriazolyl pyridinium iodide, 88·I



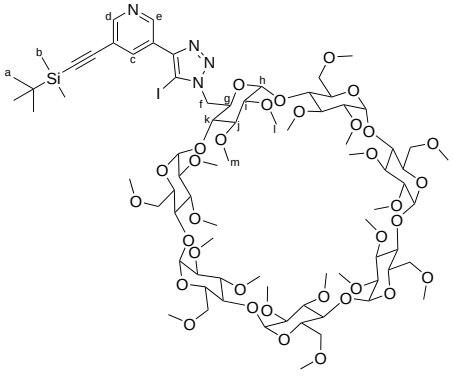
86 (0.10 g, 0.20 mmol) was dissolved in dry DCM (20 mL). CH_3I (0.35 mL, 5.0 mmol) was added and the mixture was stirred at room temperature under N_2 for 7 days. Extra portions of CH_3I (2 × 0.35 mL) were added during this time while monitoring the reaction *via* TLC. The solvent was removed *in vacuo*. Purification by preparative thin layer chromatography (3% MeOH in DCM) yielded **88**·I (0.093 g, 72%). ^{1}**H NMR** (400 MHz; $CDCl_3$) δ (ppm): 9.55 (1H, s, H_e), 9.01 (1H, s, H_d), 8.77 (1H, s, H_c), 4.77 (3H, s, H_f), 4.51 (2H, t, $J_{i|h} = 6.8$ Hz, H_i), 3.43 (2H, t, $J_{g|h} = 6.4$ Hz, H_g), 2.19 (2H, quin, $J_{h|g,i} = 6.5$ Hz, H_h), 1.01 (9H, s, H_a), 0.24 (6H, s, H_b). ^{13}**C**$\{^1$**H**$\}$ **NMR** (101 MHz; $CDCl_3$) δ (ppm): 145.0, 143.8, 141.4, 140.4, 132.5, 125.2, 106.5, 96.5, 89.4, 51.2, 48.4, 48.1, 29.0, 26.1, 16.7, 1.0, −5.0. **HRESI-MS** (pos.): 508.11227, calc. for $[C_{19}H_{27}IN_7Si]^+ = 508.11364$.

Bis-TBDMS-ethynyl-pyridine/pyridinium-iodotriazolyl propane iodide, 89·I



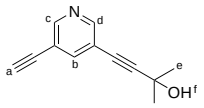
88·I (0.080 g, 0.16 mmol) was dissolved in dry, degassed 1:1 THF:MeCN (0.55 mL) and covered in foil. NaI (0.088 g, 0.57 mmol) and $Cu(ClO_4)_2 \cdot 6\,H_2O$ (0.11 g, 0.29 mmol) were added and the mixture was stirred for 5 mins under N_2. TBTA (1.0 mg, 1.6 μmol), DBU (21.5 μL, 0.14 mmol, 2 $\times$ 25 μL 1:1 THF:MeCN) and **82** (0.036 g, 0.14 mmol, 2 $\times$ 0.20 mL 1:1 THF:MeCN) were added and the mixture was stirred under N_2 for 16 h. The reaction was diluted with DCM (40 mL) and washed with NH_4OH (2 $\times$ 10 mL) and brine (2 $\times$ 10 mL) and dried over $MgSO_4$. The solvent was removed *in vacuo*. Purification by preparative thin layer chromatography (3% MeOH in DCM) yielded **89**. However, since this compound could not be used in subsequent steps due the degradation of iodotriazole moieties with TBAF, no further characterisation was undertaken. **LRESI-MS** (pos.): 875.12, calc. for $[C_{34}H_{45}I_2N_8Si_2]^+ = 875.14$.

3-(β-Cyclodextrin-appended iodotriazole)-5-(TBDMS-ethynyl)-pyridine, 90



65 (0.10 g, 69 μmol) was dissolved in 1:1 THF:MeCN (0.125 mL) and covered in foil. NaI (0.038 g, 252 μmol) and $Cu(ClO_4)_2 \cdot 6\,H_2O$ (0.048 g, 130 μmol) were added and allowed to stir for 3–5 mins. TBTA (cat.), DBU (9.4 μL, 63 μmol) in 1:1 THF:MeCN (0.125 mL) and **82** (0.015 g, 63 μmol) were added, and the mixture was stirred at room temperature, overnight under N_2. The mixture was diluted with DCM (10 mL) and washed with NH_4OH (2 $\times$ 5 mL) and brine (2 $\times$ 5 mL), and dried over $MgSO_4$. The solvent was removed *in vacuo*. Purification by preparative thin layer chromatography (3% MeOH in EtOAc) revealed the formation of an inclusion complex between **65** and **82**, and the desired product **90** was not isolated.

4-(5-Ethynylpyridin-3-yl)-2-methylbut-3-yn-2-ol, 91



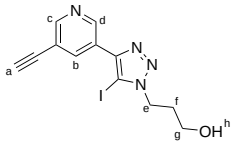
Method 1: 81 (0.30 g, 1.0 mmol) was dissolved in THF (25 mL) and one drop of H_2O was added. TBAF (1 M in THF, 1.25 mL, 1.25 mmol) was added dropwise at 0 °C and the mixture was stirred for 1 h at 0 °C. The solvent was removed *in vacuo*. The residue was taken up in DCM (50 mL) and washed with H_2O (20 mL) and brine (20 mL). The organics were dried over $MgSO_4$. The solvent was removed *in vacuo*. However, this did not afford the desired product—**82** was obtained instead.

Method 2: 81 (0.05 g, 0.17 mmol) was dissolved in THF (4.5 mL) and one drop of H_2O was added. TBAF (1 M in THF, 0.22 mL, 0.22 mmol) was added dropwise at room temperature and the mixture was stirred for 1 h. The solvent was removed *in vacuo*. The residue was taken up in DCM (20 mL) and washed with H_2O (10 mL) and brine (10 mL). The organics were dried over $MgSO_4$. The solvent was removed *in vacuo*. However, this did not afford the desired product—**82** was obtained instead.

Method 3: 81 (0.050 g, 0.17 mmol) was dissolved in THF (4 mL). TBAF·$x$$H_2O$ (0.050 g, 0.17 mmol) dissolved in THF (0.4 mL) was added dropwise at 0 °C and the mixture was stirred for 1 h at 0 °C. The residue was taken up in DCM (20 mL) and washed with H_2O (10 mL) and brine (10 mL). The organics were dried over $MgSO_4$. The solvent was removed *in vacuo*. However, this did not afford the desired product—**82** was obtained instead.

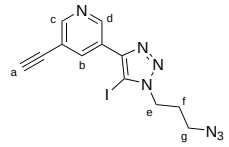
Method 4: 94 (0.48 g, 1.9 mmol) was dissolved in MeOH (2.3 mL) and KOH (0.11 g, 1.9 mmol) was added. The mixture was stirred at room temperature, overnight under N_2. Thereafter, H_2O (10 mL) and HCl (1 M aq., 5 mL) was added and the mixture was extracted with DCM (4 x 20 mL). The combined organics were dried over $MgSO_4$. The solvent was removed *in vacuo* to afford **91** (0.344 g, quant.). ^{1}**H NMR** (400 MHz; $CDCl_3$) δ (ppm): 8.60 (2H, d, $^4J_{c,d|b} = 3.4$ Hz, $H_{c,d}$), 7.80 (1H, t, $^4J_{b|c,d} = 2.0$ Hz, H_b), 3.23 (1H, s, H_a), 1.62 (6H, s, H_e). ^{13}**C**$\{^1$**H**$\}$ **NMR** (101 MHz; $CDCl_3$) δ (ppm): 151.3, 141.5, 132.0, 128.5, 119.7, 119.0, 98.5, 81.4, 79.4, 77.7, 65.3, 31.3. **HRESI-MS** (pos.): 186.09116 calc. for $[C_{12}H_{11}NO \cdot H]^+ = 186.09134$.

3-(Hydroxy-propyl-iodotriazolyl)-5-ethynyl-pyridine, 92



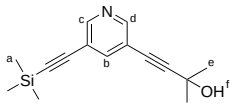
84 (0.020 g, 43 μmol) was dissolved in THF (2 mL). CsF (0.010 g, 60 μmol) was added and the mixture was stirred at room temperature, overnight under N_2. The solvent was removed *in vacuo*. However, this did not afford the desired product and resulted in the degradation of the iodotriazole moiety to the prototriazole.

3-Ethynyl-5-(azidopropyl-iodotriazolyl)-pyridine, 93



86 (223 mg, 40 μmol), $AgNO_3$ (8 mg, 5 μmol) and *N*-iodosuccinimide (21 mg, 85 μmol) were dissolved in DMF (2 mL). The flask was covered in tin foil. The mixture was stirred at room temperature, under N_2 for 3 h. Thereafter, cold water was added and the precipitate was collected. The residue was taken up in Et_2O and washed with H_2O. The organics were dried over $MgSO_4$. The solvent was removed *in vacuo* but did not afford the product.

2-Methyl-4-(5-((trimethylsilyl)ethynyl)pyridin-3-yl)but-3-yn-2-ol, 94



Method 1: 80 (0.10 g, 0.40 mmol) was dissolved in 1:1 diisopropylamine:THF (3.4 mL) and degassed with argon. $PdCl_2(PPh_3)_2$ (0.012 g, 0.020 mmol), CuI (0.003 g, 0.01 mmol) and trimethylsilylacetylene (0.09 mL, 0.6 mmol) were added and the mixture was stirred at room temperature for 4 h under N_2. The mixture was filtered through a Florisil® bed and washed through with THF (50 mL). The solvent was removed *in vacuo*. However, this did not afford the desired product.

Method 2: 80 (0.10 g, 0.40 mmol) was dissolved in 1:1 diisopropylamine:THF (3.4 mL) and degassed with argon. $PdCl_2(PPh_3)_2$ (0.012 g, 0.020 mmol), CuI (0.003 g, 0.01 mmol) and trimethylsilylacetylene (0.09 mL, 0.6 mmol) were added and the mixture was stirred at room temperature for overnight

under N_2. The mixture was filtered through a Florisil® bed and washed through with THF (50 mL). The solvent was removed *in vacuo*. However, this did not afford the desired product.

Method 3: 80 (0.02 g, 0.08 mmol) was dissolved in 1:1 diisopropylamine:THF (3.4 mL) and degassed with argon. $PdCl_2(PPh_3)_2$ (0.002 g, 0.003 mmol), CuI (0.001 g, 0.006 mmol) and trimethylsilylacetylene (30 μL, 0.2 mmol) were added and the mixture was stirred at room temperature for overnight under N_2. The mixture was filtered through a Florisil® bed and washed through with THF (50 mL). The solvent was removed *in vacuo*. However, this did not afford the desired product.

Method 4: 80 (0.02 g, 0.08 mmol) was dissolved in Et_3N (0.7 mL) and the mixture was degassed with argon. $PdCl_2(PPh_3)_2$ (0.003 g, 0.003 mmol), CuI (0.001 g, 0.006 mmol) and trimethylsilylacetylene (25 μL, 0.16 mmol) were added and the mixture was stirred at room temperature for overnight under N_2. The mixture was filtered through a Florisil® bed and washed through with THF (50 mL). The solvent was removed *in vacuo*. However, this did not afford the desired product.

Method 5: 80 (0.02 g, 0.08 mmol) was dissolved in Et_3N (0.7 mL) and the mixture was degassed with argon. $PdCl_2(PPh_3)_2$ (0.003 g, 0.003 mmol), CuI (0.001 g, 0.006 mmol) and trimethylsilylacetylene (25 μL, 0.16 mmol) were added and the mixture was stirred at 70 °C for overnight under N_2. The mixture was filtered through a Florisil® bed and washed through with THF (50 mL). The solvent was removed *in vacuo*. However, this did not afford the desired product.

Method 6: 95 (0.02 g, 0.08 mmol), $PdCl_2(PPh_3)_2$ (0.004 g, 0.005 mmol) and CuI (0.003 g, 0.02 mmol) were suspended in diisopropylamine (0.5 mL) and degassed with argon. 2-Methylbut-3-yn-2-ol (8 μL, 0.08 mmol) was added dropwise and the mixture was stirred overnight at room temperature under N_2. The solvent was removed *in vacuo*. However, this did not afford the desired product.

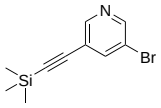
Method 7:[498] **80** (0.05 g, 0.2 mmol), $[Cu(MeCN)_4][PF_6]$ (0.002 g, 0.004 mmol) and $Pd(PPh_3)_4$ (2.6 mg, 2.0 μmol) were suspended in THF (1 mL) in a dry flask and degassed with argon. Trimethylsilylacetylene (46 μL, 0.3 mmol) and Et_3N (0.2 mL) were added, and the mixture was stirred at 50 °C for 24 h under N_2. The mixture was filtered through Celite® and washed with EtOAc (3 × 10 mL). The solvent was removed *in vacuo*. However, this did not afford the desired product.

Method 8: 95 (0.025 g, 0.10 mmol) was dissolved in 1:1 diisopropylamine:THF (0.8 mL) and degassed with argon. $PdCl_2(PPh_3)_2$ (0.007 g, 0.008 mmol), CuI (0.004 g, 0.02 mmol) and 2-methylbut-3-yn-2-ol (15 μL, 0.15 mmol) were added, and the mixture was stirred at room temperature for 4 h under N_2. The mixture was filtered through a Florisil® bed and washed through with THF (20 mL). The solvent was removed *in vacuo*. However, this did not afford the desired product.

Method 9: 80 (0.025 g, 0.10 mmol), CuI (0.003 g, 0.01 mmol), PPh_3 (0.006 g, 0.02 mmol) and $Pd_2(dba)_3$ (0.003 g, 0.003 mmol) were suspended in Et_3N (0.5 mL) and deoxygenated with N_2. Trimethylsilylacetylene (21 μL, 0.15 mmol) was added, and the mixture was stirred at 75 °C under N_2 overnight. Thereafter, the mixture was cooled to room temperature and filtered through Celite® and washed with EtOAc (3 × 10 mL). The solvent was removed *in vacuo*. However, this did not afford the desired product.

Method 10: 95 (0.10 g, 0.40 mmol), CuI (0.02 g, 0.09 mmol), PPh_3 (0.02 g, 0.09 mmol) and $Pd_2(dba)_3$ (0.02 g, 0.02 mmol) were suspended in Et_3N and deoxygenated with N_2. 2-Methylbut-3-yn-2-ol (62 μL, 0.64 mmol) was added and the mixture was stirred overnight at 75 °C under N_2. The mixture was cooled to room temperature and filtered through Celite® and washed with EtOAc (3 × 10 mL). The solvent was removed *in vacuo*. Purification by preparative thin layer chromatography (3% MeOH in DCM) afforded **94** (0.093 g, 91%). ^{1}**H NMR** (400 MHz; $CDCl_3$) δ (ppm): 8.58 (2H, br. s., $H_{c,d}$), 7.80 (1H, s, H_b), 1.62 (6H, s, H_e), 0.26 (9H, s, H_a). ^{13}**C**$\{^1$**H**$\}$ **NMR** (101 MHz; $CDCl_3$) δ (ppm): 151.1, 150.9, 141.3, 119.9, 119.5, 100.4, 99.2, 98.1, 78.0, 65.4, 31.3, 1.0. **HRESI-MS** (pos.): 258.13110, calc. for $[C_{15}H_{19}NOSi \cdot H]^+ = 258.13087$.

3-Bromo-5-((trimethylsilyl)ethynyl)pyridine, 95

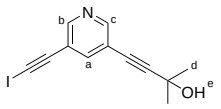


Method 1: 3,5-Dibromopyridine (0.24 g, 1.0 mmol), $PdCl_2(PPh_3)_2$ (0.03 g, 0.04 mmol) and CuI (0.006 g, 0.03 mmol) were suspended in diisopropylamine (5.95 mL), and degassed with argon. Trimethylsilylacetylene (0.15 mL, 1.0 mmol) was added dropwise over 35 mins at 0 °C. The mixture was allowed to warm to room temperature and stirred for 23 h. The solvent was removed *in vacuo*. However, this did not afford the desired product.

Method 2:[474] 3,5-Dibromopyridine (0.96 g, 4.0 mmol), $PdCl_2(PPh_3)_2$ (0.3 g, 0.4 mmol) and CuI (0.08 g, 0.4 mmol) were dissolved in Et_3N (2.8 mL). Trimethylsilylacetylene (0.60 mL, 4.4 mmol) was added dropwise, and the mixture was stirred at room temperature under N_2 for 16 h. H_2O (20 mL) was added and extracted with Et_2O (3 × 15 mL). The combined organics were dried over $MgSO_4$. The solvent was removed *in vacuo*. Purification by silica gel column chromatography (3:2 petroleum ether:DCM) afforded the **95** (0.734 g, 71%). ^{1}**H NMR** (400 MHz; $CDCl_3$) δ (ppm): 8.49–8.64 (2H, m,

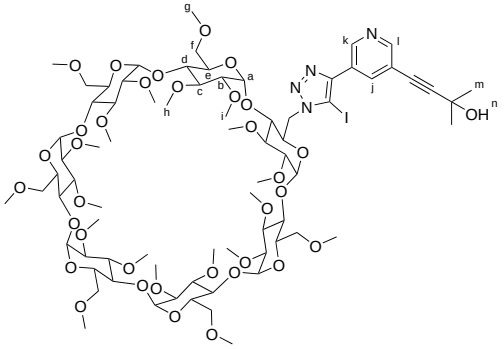
$H_{c,d}$), 7.91 (1H, t, $^4J_{b|c,d} = 2.0$ Hz, H_b), 0.18–0.31 (9H, m, H_a). **LRESI-MS** (pos.): 254.0, calc. for $[C_{10}H_{12}BrNSi \cdot H]^+ = 254.0$.

4-(5-(Iodoethynyl)pyridin-3-yl)-2-methylbut-3-yn-2-ol, 96



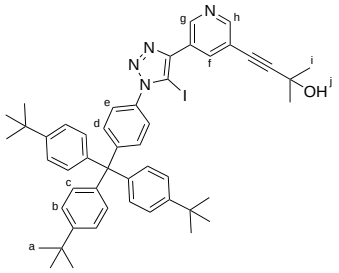
91 (0.051 g, 0.27 mmol) was dissolved in THF (2.7 mL), and CuI (0.009 g, 0.05 mmol) and *N*-iodomorpholine (0.10 g, 0.30 mmol) were added. The mixture was stirred at room temperature, under N_2 for 2 h. Thereafter, it was poured onto a pad of alumina, and washed through with DCM (4 × 10 mL). The combined organics were washed with saturated $Na_2S_2O_{3(aq.)}$ (20 mL). The organics were dried over $MgSO_4$. The solvent was removed *in vacuo*. The residue was taken up in 10% EtOAc/hexane and passed through a silica plug. The solvent was removed *in vacuo* but did not afford **96**.

3-(Cyclodextrin-appended iodotriazolyl)-5-(hydroxypropyl-ethynyl)-pyridine, 97



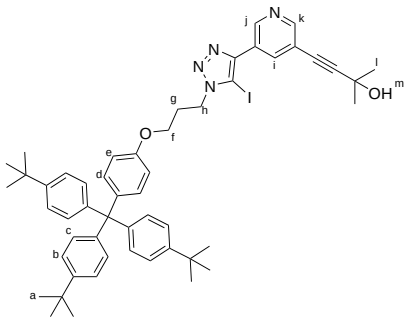
65 (0.10 g, 69 μmol) was dissolved in 1:1 THF:MeCN (0.14 mL) and covered in foil. NaI (0.040 g, 250 μmol) and $Cu(ClO_4)_2 \cdot 6\,H_2O$ (0.048 g, 130 μmol) were added and stirred for 3–5 mins. TBTA (cat.), DBU (9.4 μL, 63 μmol) in 1:1 THF:MeCN (0.14 mL) and **91** (0.012 g, 63 μmol) were added, and the mixture was stirred at room temperature, overnight under N_2. The mixture was diluted with DCM (20 mL) and washed with NH_4OH (2 × 10 mL) and brine (2 × 10 mL). The organics were dried over $MgSO_4$. The solvent was removed *in vacuo* but did not afford **97**.

3-(Stopper-aryl-iodotriazolyl)-5-(hydroxypropyl-ethynyl)-pyridine, 98



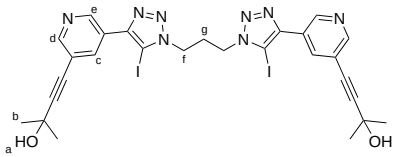
38 (59 mg, 0.11 mmol) was dissolved in dry degassed 1:1 THF: MeCN (0.2 mL) and the flask was covered in tin foil. NaI (60 mg, 0.4 mmol) and $Cu(ClO_4)_2 \cdot 6\,H_2O$ (75 mg, 0.20 mmol) were added and the mixture was stirred for 3–5 mins. TBTA (cat.), DBU (15 mg, 0.10 mmol) and **91** (19 mg, 0.10 mmol) were added. The mixture was stirred overnight, at room temperature under N_2. The mixture was diluted with DCM (40 mL) and washed with NH_4OH (2 $\times$ 10 mL) and brine (2 $\times$ 10 mL). The organics were dried over $MgSO_4$. The solvent was removed *in vacuo* but did not afford **98**.

3-(Stopper-propyl-iodotriazolyl)-5-(hydroxypropyl-ethynyl)-pyridine, 99



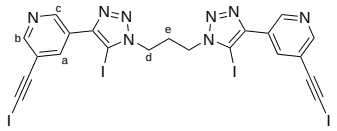
41 (66 mg, 0.11 mmol) was dissolved in dry degassed 1:1 THF: MeCN (0.2 mL) and the flask was covered in tin foil. NaI (61 mg, 0.4 mmol) and $Cu(ClO_4)_2 \cdot 6\,H_2O$ (76 mg, 0.20 mmol) were added and the mixture was stirred for 3–5 mins. TBTA (cat.), DBU (15 mg, 0.10 mmol) and **91** (19 mg, 0.10 mmol) were added. The mixture was stirred overnight, at room temperature under N_2. The mixture was diluted with DCM (40 mL) and washed with NH_4OH (2 $\times$ 10 mL) and brine (2 $\times$ 10 mL). The organics were dried over $MgSO_4$. The solvent was removed *in vacuo* but did not afford **99**.

Bis-(3-(hydroxypropyl-ethynyl)-5-iodotriazolyl-pyridine)-propane, 100



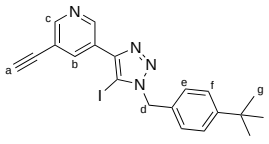
50 (18 mg, 0.13 μmol) was dissolved in dry degassed THF (0.5 mL) and the flask was covered in tin foil. NaI (0.162 g, 1.1 μmol) and $Cu(ClO_4)_2 \cdot 6\,H_2O$ (0.20 g, 0.54 μmol) were added and the mixture was stirred for 3–5 mins. TBTA (cat.), DBU (40 mg, 0.27 μmol) and **91** (50 mg, 0.27 μmol) were added. The mixture was stirred overnight, at room temperature under N_2. The mixture was diluted with DCM (40 mL) and washed with NH_4OH (2 $\times$ 10 mL) and brine (2 $\times$ 10 mL). The organics were dried over $MgSO_4$. The solvent was removed *in vacuo* but did not afford **100**.

Bis-(3-(iodoethynyl)-5-iodotriazolyl-pyridine)-propane, 101



$[Cu(MeCN)_4][PF_6]$ (10 mg, 27 μmol) and TBTA (cat.) were dissolved in dry degassed THF (3 mL). **50** (0.013 g, 0.10 mmol) and **2** (76 mg, 0.20 mmol) were added. The mixture was stirred overnight, at room temperature under N_2. The solvent was removed *in vacuo*. The residue was redissolved in DCM (40 mL) and washed with NH_4OH (2 $\times$ 10 mL) and brine (2 $\times$ 10 mL). The organics were dried over $MgSO_4$. The solvent was removed *in vacuo* but did not afford **119**.

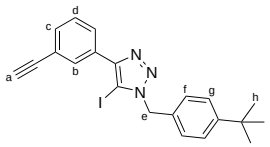
Ethynyl-*tert*-butylbenzyl-iodotriazolyl-pyridine, 102



5 (0.19 g, 1.0 mmol) was dissolved in dry, degassed THF (2 mL) and covered in foil. NaI (0.30 g, 2.0 μmol) and $Cu(ClO_4)_2 \cdot 6\,H_2O$ (0.37 g, 1.0 μmol) were added and the solution was stirred for 5 mins. TBTA (0.003 mg, 5 μmol), DBU (0.075 g, 0.50 mmol, 2 $\times$ 1 mL THF) and **1** (0.064 g, 0.50 mmol) were added and the mixture was stirred for 16 h at room temperature under N_2. The mixture was diluted with DCM (80 mL) and washed with NH_4OH (2 $\times$ 40 mL) and brine (2 $\times$ 40 mL) and dried over $MgSO_4$.

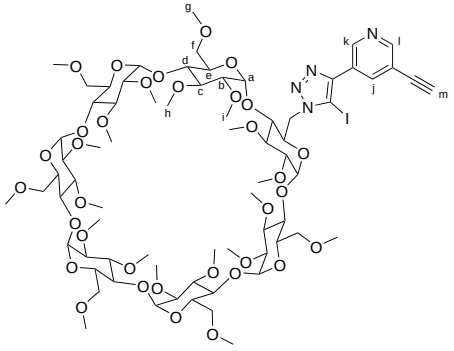
The solvent was removed *in vacuo*. Purification by preparative thin layer chromatography (1% MeOH in DCM) did not afford **102**.

Ethynyl-*tert*-butylbenzyl-iodotriazolyl-benzene, 103



5 (0.21 g, 1.1 mmol) was dissolved in dry THF (1.5 mL) and covered in foil. NaI (0.31 g, 2.0 mmol) and $Cu(ClO_4)_2 \cdot 6\,H_2O$ (0.37 g, 1.0 mmol) were added and the mixture was stirred for 5 mins under N_2. TBTA (0.004 g, 8 μmol), DBU (0.011 g, 0.50 mmol, 2 $\times$ 0.25 mL THF) and 1,3-diethynylbenzene (0.63 g, 0.50 mmol, 2 mL MeCN) were added and the mixture was stirred under N_2 for 16 h. The reaction was diluted with DCM (80 mL) and washed with NH_4OH (2 $\times$ 40 mL) and brine (2 $\times$ 40 mL) and dried over $MgSO_4$. The solvent was removed *in vacuo*. Purification by silica gel column chromatography (1:1 petroleum ether: DCM) afforded **103** (0.058 g, 26%). Since this compound was not used in subsequent reactions, it was not fully characterised. ^{1}**H NMR** (400 MHz; $CDCl_3$) δ (ppm): 8.09 (1H, s, H_b), 7.93 (1H, d, $J_{e|d} = 7.8$ Hz, H_e), 7.51 (1H, d, $J_{c|d} = 7.7$ Hz, H_c), 7.41 (1H, t, $J_{d|c,e} = 7.4$ Hz, H_d), 7.35–7.40 (2H, m, H_g), 7.24–7.30 (2H, m, H_h), 5.63 (2H, s, H_f), 3.10 (1H, s, H_a), 1.30 (9H, s, H_i). ^{13}**C**$\{^1$**H**$\}$ **NMR** (101 MHz; $CDCl_3$) δ (ppm): 151.6, 149.1, 132.1, 131.1, 130.9, 130.5, 128.6, 127.8, 127.7, 125.8, 122.4, 83.2, 77.6, 54.1, 34.6, 31.2. **LRESI-MS** (pos.): 442.1, calc. for $[C_{21}H_{20}IN_3 \cdot H]^+ = 442.1$.

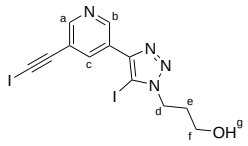
3-(Cyclodextrin-appended iodotriazolyl)-5-ethynyl-pyridine, 104



65 (0.10 g, 69 μmol) was dissolved in 1:1 THF:MeCN (0.125 mL) and covered in foil. NaI (0.038 g, 252 μmol) and $Cu(ClO_4)_2 \cdot 6\,H_2O$ (0.050 g, 130 μmol) were added and allowed to stir for 3–5 mins. TBTA (cat.), DBU (9.5 μL, 63 μmol) in 1:1 THF:MeCN (0.125 mL) and **1** (0.008 g, 60 μmol) were

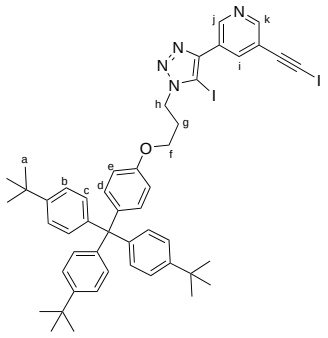
added, and the mixture was stirred at room temperature, overnight under N_2. The mixture was diluted with DCM (10 mL) and washed with NH_4OH (2 $\times$ 5 mL) and brine (2 $\times$ 5 mL), and dried over $MgSO_4$. The solvent was removed *in vacuo*. Purification by preparative thin layer chromatography (3% MeOH in DCM) afforded separation of the inclusion complex between **65** and **1**, and the desired **104** was not isolated.

3-Iodoethynyl-5-(hydroxypropyl-iodotriazolyl) pyridine, 105



CuI (0.01 g, 0.05 mmol) and Et_3N (28 μL, 0.20 mmol) were dissolved in THF (1 mL) and the flask was covered in foil. The mixture was stirred for 30 mins. Thereafter, **46** (0.010 g, 0.10 mmol) in THF (1 mL) and **2** (0.038 g, 0.10 mmol) were added, and the mixture was stirred at room temperature, under N_2 overnight. The mixture was diluted with DCM (30 mL) and washed with NH_4OH (2 $\times$ 10 mL), H_2O (10 mL) and brine (10 mL) and dried over $MgSO_4$. The solvent was removed *in vacuo*. However, this did not afford the desired product.

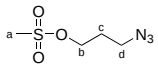
3-(Stopper-propyl-iodotriazolyl)-5-iodoethynyl-pyridine, 106



$[Cu(MeCN)_4][PF_6]$ (15 mg, 40 μmol) and TBTA (cat.) were dissolved in dry degassed THF (3 mL). **41** (0.13 g, 0.20 mmol) and **2** (82 mg, 0.20 mmol) were added. The mixture was stirred overnight, at room temperature under N_2. The solvent was removed *in vacuo*. The residue was redissolved in DCM (40 mL) and washed with NH_4OH (2 $\times$ 10 mL) and brine (2 $\times$ 10 mL). The organics were dried over $MgSO_4$. The solvent was removed *in vacuo*. Purification by preparative thin layer chromatography (0.5% MeOD/DCM) afforded **106** (66 mg, 34%). ^{1}**H NMR** (400 MHz; $CDCl_3$) δ (ppm): 9.16 (1H, s,

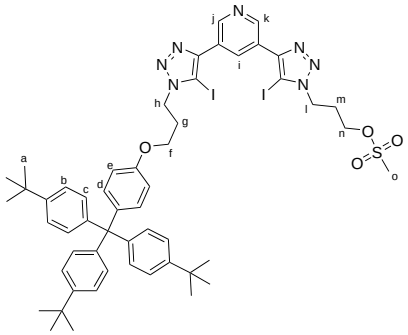
H_j), 8.68 (1H, s, H_k), 8.36 (1H, s, H_i), 7.17–7.25 (6H, m, H_b), 7.03–7.17 (8H, m, $H_{c,d}$), 6.77 (2H, d, $J_{e|d} = 8.8$ Hz, H_e), 4.68 (2H, t, $J_{h|g} = 7.0$ Hz, H_h), 4.05 (2H, t, $J_{f|g} = 5.6$ Hz, H_f), 2.46 (2H, quin, $J_{g|f,h} = 6.5$ Hz, H_g), 1.30 (27H, s, H_a). $^{13}\mathbf{C}\{^1\mathbf{H}\}$ **NMR** (101 MHz; $CDCl_3$) δ (ppm): 156.1, 152.5, 148.3, 147.4, 146.3, 144.0, 140.1, 137.6, 132.3, 130.7, 126.0, 124.0, 120.4, 113.0, 90.4, 63.8, 63.0, 53.4, 48.1, 34.3, 31.4, 29.6, 11.9. **HRESI-MS** (pos.): 989.21199 calc. for $[C_{49}H_{52}ON_4I_2 \cdot Na]^+ = 989.21227$.

1-Mesyl-3-azidopropane, 107



46 (1.4 g, 14 mmol) and Et_3N (4.0 mL, 29 mmol) were dissolved in dry degassed THF (150 mL). The solution was cooled to 0 °C. MsCl (1.5 mL, 19 mmol) was added and the mixture was stirred at room temperature, overnight under N_2. The solvent was removed *in vacuo*. The residue was taken up in DCM (100 mL) and washed with H_2O (3 × 100 mL) and $NaHCO_3$ (5% aq., 3 × 100 mL). The organics were dried over $MgSO_4$. The solvent was removed *in vacuo* to afford **107** (2.1 g, 87%). $^1\mathbf{H}$ **NMR** (400 MHz; $CDCl_3$) δ (ppm): 4.32 (2H, t, $J_{d|c} = 6.0$ Hz, H_d), 3.49 (2H, t, $J_{b|c} = 6.4$ Hz, H_b), 3.03 (3H, s, H_a), 2.01 (2H, quin, $J_{c|b,d} = 6.2$ Hz, H_c).

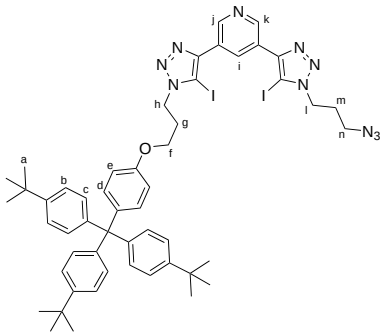
3-(Stopper-propyl-iodotriazolyl)-5-(mesylpropyl-iodotriazolyl)-pyridine, 108



$[Cu(MeCN)_4][PF_6]$ (14 mg, 40 μmol) and TBTA (cat.) were dissolved in dry degassed THF (6 mL), and the flask was covered in tin foil. **107** (0.22 g, 1.3 mmol) and **106** (0.16 g, 0.16 mmol) were added. The mixture was stirred at room temperature, overnight under N_2. The mixture was diluted with $CHCl_3$ (60 mL) and washed with NH_4OH (2 × 10 mL) and brine (2 × 10 mL). The organics were dried over $MgSO_4$. The solvent was removed *in vacuo*. Purification by silica gel column chromatography (0–0.5% MeOH in DCM) afforded **108** (0.165 g, 86%) as a brown solid. $^1\mathbf{H}$ **NMR** (500 MHz; $CDCl_3$) δ (ppm): 9.33 (2H, s, $H_{j,k}$), 9.23 (1H, s, H_i), 7.23 (6H, d, $J_{b|c} = 8.5$ Hz, H_b), 7.02–7.14 (8H, m, $H_{c,d}$), 6.77 (2H,

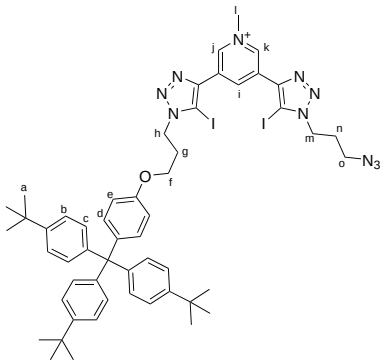
d, $J_{e|d} = 8.7$ Hz, H_e), 4.71 (2H, t, $J_{l|m} = 6.4$ Hz, H_l), 4.65 (2H, t, $J_{h|g} = 6.4$ Hz, H_h), 4.33 (2H, t, $J_{n|m} = 5.6$ Hz, H_n), 4.06 (2H, t, $J_{f|g} = 5.6$ Hz, H_f), 3.08 (3H, s, H_o), 2.47 (4H, quin, $J_{f,h,l,n|g,m} = 6.3$ Hz, $H_{g,m}$), 1.29 (27H, s, H_a). $^{13}\mathbf{C}\{^1\mathbf{H}\}$ **NMR** (101 MHz; $CDCl_3$) δ (ppm): 156.2, 148.3, 148.0, 147.9, 147.1, 146.8, 144.0, 140.1, 132.8, 132.3, 130.6, 126.3, 126.1, 124.0, 113.0, 66.0, 63.9, 63.0, 53.4, 48.1, 47.2, 37.5, 34.2, 31.3, 29.6, 29.2. **HRESI-MS** (pos.): 1168.2486, calc. for $[C_{53}H_{61}I_2N_7O_4S \cdot Na]^+ = 1168.2487$.

3-(Stopper-propyl-iodotriazolyl)-5-(azidopropyl-iodotriazolyl)-pyridine, 109



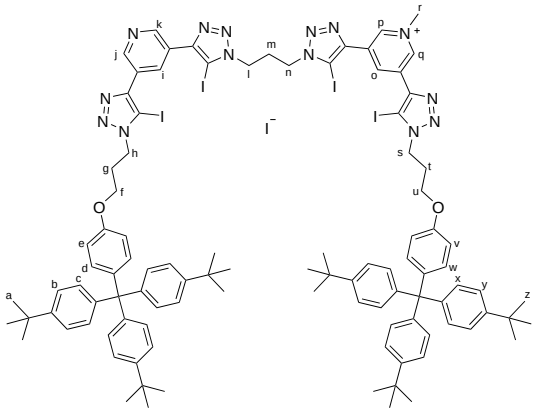
108 (0.16 g, 0.14 mmol) and NaN_3 (39 mg, 0.59 mmol) were dissolved in dry degassed DMF (6 mL) and stirred at 85 °C overnight under N_2. Thereafter, the mixture was cooled to room temperature, and partitioned between H_2O (20 mL) and EtOAc (20 mL). The aqueous layer was washed with further EtOAc (2 × 20 mL). The combined organics were washed with brine (3 × 10 mL) and dried over $MgSO_4$. The solvent was removed *in vacuo* afforded **109** (0.137 g, 87%) as a brown solid. $^1\mathbf{H}$ **NMR** (400 MHz; $CDCl_3$) δ (ppm): 9.26 (2H, s, $H_{j,k}$), 8.87 (1H, s, H_i), 7.23 (6H, d, $J_{b|c} = 8.0$ Hz, H_b), 7.05–7.14 (8H, m, $H_{c,d}$), 6.78 (2H, d, $J_{e|d} = 8.7$ Hz, H_e), 4.70 (2H, t, $J_{l|m} = 6.8$ Hz, H_l), 4.58 (2H, t, $J_{h|g} = 6.8$ Hz, H_h), 4.06 (2H, t, $J_{n|m} = 5.6$ Hz, H_n), 3.47 (2H, t, $J_{f|g} = 6.4$ Hz, H_f), 2.47 (2H, quin, $J_{m|l,n} = 6.4$ Hz, H_m), 2.25 (2H, quin, $J_{g|f,h} = 6.4$ Hz, H_g), 1.30 (27H, s, H_a). $^{13}\mathbf{C}\{^1\mathbf{H}\}$ **NMR** (101 MHz; $CDCl_3$) δ (ppm): 156.1, 148.3, 148.2, 147.9, 147.8, 147.0, 146.8, 144.0, 140.1, 133.0, 132.4, 132.3, 130.7, 129.0, 128.9, 128.5, 128.2, 126.4, 126.2, 125.3, 124.0, 124.0, 113.0, 63.9, 63.0, 48.2, 48.1, 48.0, 34.3, 31.3, 29.6, 29.0, 21.4. **HRESI-MS** (pos.): 1115.27745, calc. for $[C_{52}H_{58}I_2N_{10}O \cdot Na]^+ = 1115.27766$.

Axle precursor: 3-(stopper-propyl-iodotriazolyl)-5-(azidopropyl-iodotriazolyl)-pyridinium tetrafluoroborate, 110·BF_4



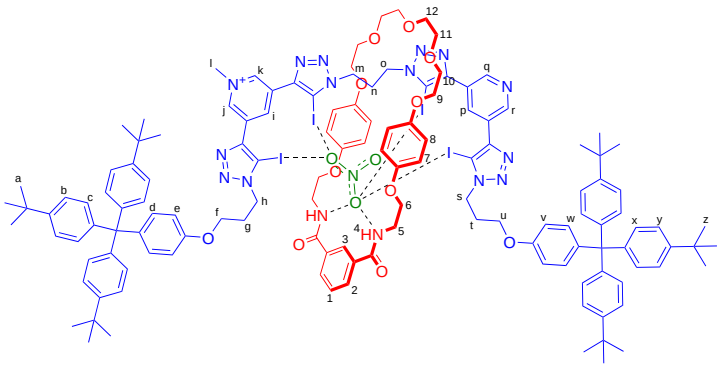
Initially, **109** (38 mg, 35 μmol) was dissolved in CH_3I (2 mL) and stirred at 35 °C overnight under N_2. The solvent was removed *in vacuo* but afforded an insoluble powder that could not be anion exchanged to a more soluble anion. Consequently, in a second method, **109** (60 mg, 55 μmol) was dissolved in dry DCM (5 mL). [Me_3O][BF_4] (8.8 mg, 60 μmol) was added and the mixture was stirred at room temperature overnight under N_2. Thereafter, the reaction was quenched with MeOH (1 mL) and the solvent was removed *in vacuo*. Purification by preparative thin layer chromatography (3% MeOH in DCM) afforded **110**·BF_4 (30.0 mg, 46%) as a white powder. ^{1}**H NMR** (400 MHz; CD_3OD) δ (ppm): 9.75 (1H, s, H_i), 9.30–9.51 (2H, m, $H_{j,k}$), 7.15–7.25 (6H, m, H_b), 6.99–7.10 (8H, m, $H_{c,d}$), 6.74 (2H, d, $J_{e|d} = 8.9$ Hz, H_e), 4.73 (2H, t, $J_{o|n} = 6.9$ Hz, H_o), 4.61 (2H, t, $J_{h|g} = 6.6$ Hz, H_h), 4.58 (3H, s, H_l), 4.04 (2H, t, $J_{m|n} = 5.6$ Hz, H_m), 3.45 (2H, t, $J_{f|g} = 6.3$ Hz, H_f), 2.46 (2H, quin, $J_{n|m,o} = 6.1$ Hz, H_n), 2.23 (2H, quin, $J_{g|f,h} = 6.4$ Hz, H_g), 1.26 (27H, s, H_a). ^{13}**C**$\{^1$**H**$\}$ **NMR** (101 MHz; CD_3OD) δ (ppm): 148.4, 144.1, 140.2, 132.3, 130.6, 124.0, 113.0, 63.9, 63.0, 42.2, 34.2, 31.1, 28.8. ^{19}**F NMR** (377 MHz; CD_3OD) δ (ppm): -153.84 (s, BF_4). **HRESI-MS** (pos.): 1107.31149, calc. for $[C_{53}H_{61}I_2N_{10}O]^+$ = 1107.31137.

Asymmetric pyridine/pyridinium bis-iodotriazole terphenyl-stoppered axle, 111·I



$[Cu(MeCN)_4][PF_6]$ (14 mg, 40 μmol) and TBTA (cat.) were dissolved in dry degassed THF (2 mL), and the flask was covered in tin foil. **110**·I (40 mg, 32 μmol) and **106** (31 mg, 32 μmol) were added. The mixture was stirred at room temperature, overnight under N_2. The mixture was diluted with $CHCl_3$ (20 mL) and washed with NH_4OH (2 $\times$ 10 mL) and brine (2 $\times$ 10 mL). The organics were dried over $MgSO_4$. The solvent was removed *in vacuo*. Purification by preparative thin layer chromatography (7% MeOH in DCM) afforded **111**·I (1.5 mg, 19%) as a brown solid. ^{1}**H NMR** (400 MHz; $CDCl_3$) δ (ppm): 9.82 (1H, s, H_q), 9.75 (1H, br. s., H_p), 9.38 (1H, br. s., H_j), 9.25 (1H, br. s., H_k), 8.83 (1H, br. s., H_o), 7.69 (1H, br. s., H_i), 7.17–7.22 (12H, m, $H_{b,y}$), 7.01–7.11 (16H, m, $H_{c,d,w,x}$), 6.73 (4H, d, $H_{e,v}$), 4.05 (8H, m, $H_{h,l,n,s}$), 3.80–3.89 (7H, m, $H_{f,r,u}$), 1.98–2.12 (6H, m, $H_{g,m,t}$), 1.26–1.30 (54H, m, $H_{a,z}$). **HRESI-MS** (pos.): 2074.53876, calc. for $[C_{102}H_{113}I_4N_{14}O_2]^+ = 2074.53777$.

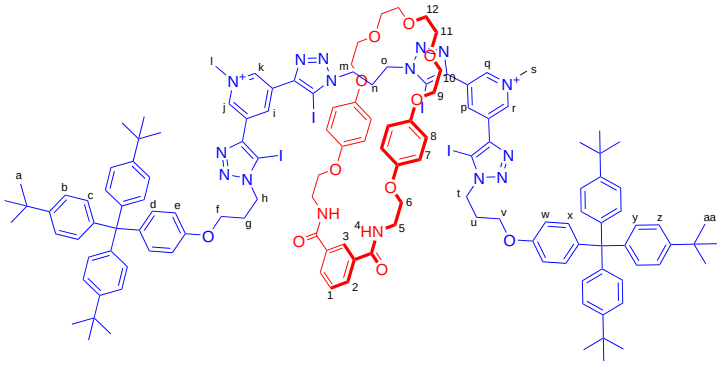
Asymmetric rotaxane: pyridinium/pyridine bis-iodotriazole axle–isophthalamide 5-*O*-polyether macrocycle, 112·A



27 (13 mg, 20 μmol), **110**·BF_4 (12 mg, 10 μmol) and TBA · Cl (2.5 mg, 10 μmol) were dissolved in dry, degassed THF (1 mL), and the flask was covered in tin foil. The mixture was stirred for 30 mins,

and thereafter, $[Cu(MeCN)_4][PF_6]$ (cat.), TBTA (cat.) and **106** (10.5 mg, 10 μmol) were added. The mixture was stirred at room temperature, overnight under N_2. The mixture was diluted with $CHCl_3$ (20 mL), and washed with NH_4OH (2 × 10 mL) and brine (2 × 10 mL). The solvent was removed *in vacuo*. Purification by preparative thin layer chromatography (3% MeOH in DCM) afforded **112**·Cl which was anion exchanged to the hexafluorophosphate salt by washing with NH_4PF_6 (0.1 M aq., 8 × 10 mL) and H_2O (2 × 10 mL). The solvent was removed *in vacuo* to afford **112**·PF_6 (9.0 mg, 32%). **^{1}H NMR** (400 MHz; $CDCl_3$) δ (ppm): 9.57 (1H, br. s., H_j), 9.33 (1H, br. s., H_k), 9.27 (3H, br. s., $H_{p,q,r}$), 8.91 (1H, s, H_3), 8.48 (2H, br. s., H_4), 8.40 (1H, s, H_i), 8.35 (2H, d, $J_{2|1} = 7.8$ Hz, H_2), 7.53 (1H, t, $J_{1|2} = 7.8$ Hz, H_1), 7.17–7.24 (12H, m, $H_{b,y}$), 7.02–7.12 (16H, m, $H_{c,d,w,x}$), 6.78 (4H, d, $J_{e,v|d,w} = 7.5$ Hz, $H_{e,v}$), 6.31 (4H, d, $J_{8|7} = 9.0$ Hz, H_8), 5.79 (4H, d, J = 8.9 Hz, H_7), 4.69 (2H, t, J = 6.9 Hz, H_h), 4.59 (3H, s, H_l), 3.46–4.56 (36H, m, $H_{f,m,o,s,u,5,6,9,10,11,12}$), 2.30–2.53 (6H, m, $H_{g,n,t}$), 1.29 (54H, s, $H_{a,z}$). **^{13}C{^{1}H} NMR** (101 MHz; $CDCl_3$) δ (ppm): 148.4, 132.3, 130.7, 129.1, 128.2, 124.1, 113.1, 69.5, 34.3, 31.4 (several peaks were too weak to be detected). **^{31}P NMR** (162 MHz MHz; $CDCl_3$) δ (ppm): −144.20 (spt, $J = 714.0$ Hz, PF_6). **^{19}F NMR** (377 MHz; $CDCl_3$) δ (ppm): −71.08 (d, $J = 714.0$ Hz, PF_6). **HRESI-MS** (pos.): 2669.80135, calc. for $[C_{134}H_{151}I_4N_{16}O_{11}]^+ = 2669.80333$.

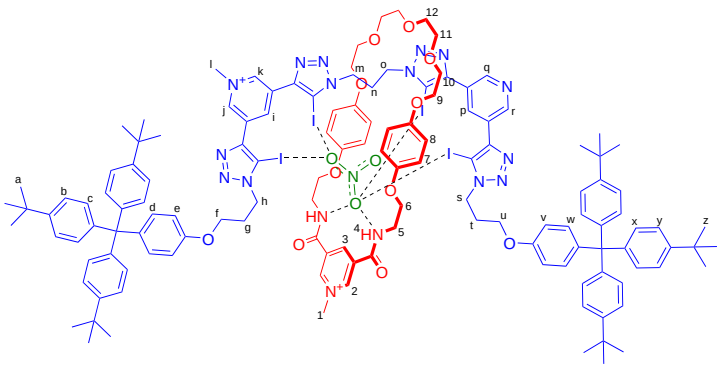
Dicationic rotaxane: bis-(3,5-bis-iodotriazole pyridinium) axle–isophthalamide 5-*O*-polyether macrocycle, 113·2 PF_6



112·PF_6 (7.6 mg, 2.7 μmol) was dissolved in dry $CHCl_3$ (1 mL) and CH_3I (10 μL) was added. The mixture was stirred overnight at room temperature under N_2. However, no evidence of product formation was observed by mass spectrometric analysis. A further portion of CH_3I (0.1 mL) was added and the mixture was stirred for 3 days. Thereafter, the solvent was removed *in vacuo* and rotaxane was anion exchanged to the hexafluorophosphate salt by washing a $CHCl_3$ solution (25 mL) of the crude mixture with NH_4PF_6 (0.1 M, 8 × 10 mL) and H_2O (2 × 10 mL). The solvent was removed *in vacuo* to afford the target rotaxane **140**·2 PF_6 (2.9 mg, 36%). **^{1}H NMR** (500 MHz; 45 :45 :10 $CDCl_3$:CD_3OD:D_2O) δ

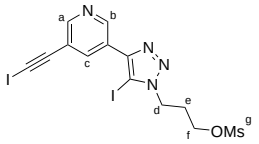
(ppm): 9.44 (2H, s, $H_{j,k}$), 9.38 (2H, s, $H_{q,r}$), 9.19 (1H, br. s., H_3), 8.66 (1H, br. s., H_i), 8.26 (2H, br. s., $H_{p,1}$), 8.05 (2H, d, H_4), 8.01 (2H, d, H_2), 7.15–7.26 (12H, m, $H_{b,z}$), 6.98–7.14 (16H, m, $H_{c,d,x,y}$), 6.74–6.86 (12H, m, $H_{e,w,7,8}$), 3.56–4.16 (42H, m, $H_{f,h,l,m,o,s,t,v,5,6,9,10,11,12}$), 2.54 (2H, br. s., H_n), 2.44 (4H, br. s., $H_{g,u}$), 1.18–1.36 (54H, m, $H_{a,aa}$). **^{13}C{^{1}H} NMR** (101 MHz; $CDCl_3$) δ (ppm): 155.64, 148.51, 130.85, 129.59, 124.20, 115.82, 115.57, 95.87, 70.88, 69.88, 60.03, 39.85, 34.44, 31.53, 29.22, 18.32, 1.18 (several resonances were too weak to detect). **^{31}P NMR** (162 MHz; $CDCl_3$) δ (ppm): -144.36 (spt, J = 714.0 Hz, PF_6). **^{19}F NMR** (377 MHz; $CDCl_3$) δ (ppm): -70.82 (d, J = 714.0 Hz, PF_6). **HRESI-MS** (pos.): 1341.90639, calc. for $[C_{135}H_{154}I_4N_{16}O_{112}]^+ = 1341.90922$.

Asymmetric rotaxane: pyridinium/pyridine bis-iodotriazole axle–pyridinium-bis-amide macrocycle, 114·A



34·PF_6 (15 mg, 20 μmol), **110**·BF_4 (12 mg, 10 μmol) and TBA · Cl (2.7 mg, 10 μmol) was dissolved in dry, degassed THF (1 mL), and the flask was covered in tin foil. The mixture was stirred for 30 mins, and thereafter, [Cu(MeCN)$_4$][PF$_6$] (cat.), TBTA (cat.) and **106** (11 mg, 10 μmol) were added. The mixture was stirred at room temperature, overnight under N_2. The mixture was diluted with $CHCl_3$ (20 mL), and washed with NH_4OH (2 × 10 mL) and brine (2 × 10 mL). The solvent was removed *in vacuo*. Purification by preparative thin layer chromatography (3% MeOH in DCM) did not afford **114**·Cl.

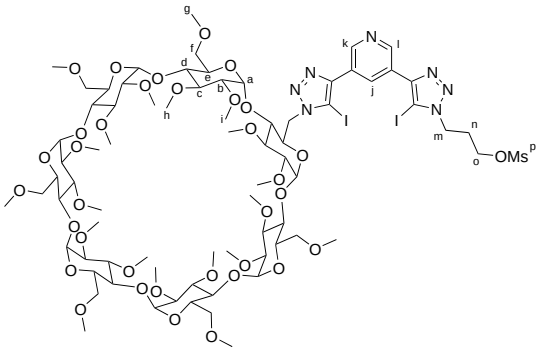
3-(Iodoethynyl)-5-(mesylpropyl iodotriazolyl)-pyridine, 115



[Cu(MeCN)$_4$][PF$_6$] (23 mg, 62 μmol) and TBTA (cat.) were dissolved in dry, degassed THF, and the flask was covered in foil. **107** (56 mg, 0.30 mmol) and **2** (0.12 g, 0.30 mmol) were added, and the

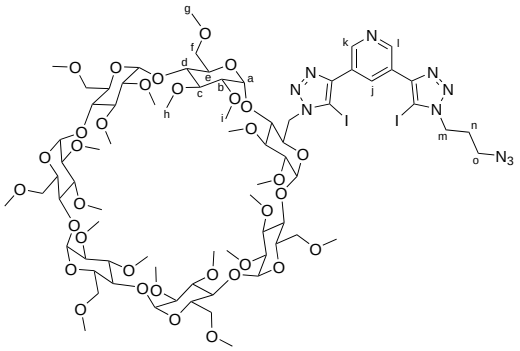
mixture was stirred at room temperature, overnight under N_2. Thereafter, the mixture was diluted with $CDCl_3$ (50 mL), and washed with NH_4OH (2 × 10 mL) and brine (2 × 10 mL). The organics were dried over $MgSO_4$. The solvent was removed *in vacuo*. Purification by silica gel column chromatography (0.75% MeOH in DCM) afforded **115** (47 mg, 27%). ^{1}**H NMR** (400 MHz; $CDCl_3$) δ (ppm): 9.13 (1H, s, H_b), 8.69 (1H, s, H_a), 8.28 (1H, t, $^4J_{c|a,b} = 2.0$ Hz, H_c), 4.63 (2H, t, $J_{d|e} = 6.7$ Hz, H_d), 4.32 (2H, t, $J_{f|e} = 5.7$ Hz, H_f), 3.07 (3H, s, H_g), 2.45 (2H, quin, $J_{e|d,f} = 6.1$ Hz, H_e). ^{13}**C**$\{^1$**H**$\}$ **NMR** (101 MHz; 5 :1 $CDCl_3$:CD_3OD) δ (ppm): 152.4, 151.2, 147.1, 146.8, 138.5, 126.7, 66.7, 47.8, 37.6, 29.6. **HRESI-MS** (pos.): 558.87936, calc. for $[C_{13}H_{12}I_2N_4O_3S \cdot H]^+ = 558.87922$.

3-(pCD-stoppered iodotriazolyl)-5-(mesylpropyl iodotriazolyl)-pyridine, 116



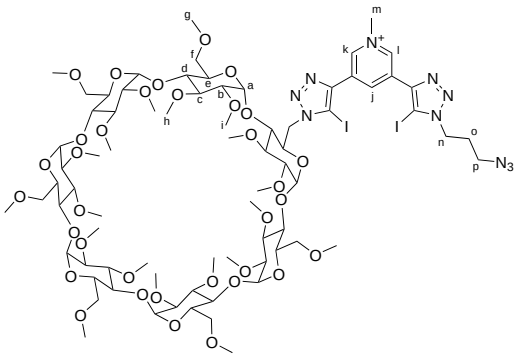
115 (14 mg, 26 μmol), **65** (43 mg, 29 μmol), $[Cu(MeCN)_4][PF_6]$ (cat.) and TBTA (cat.) were dissolved in dry, degassed THF (1.5 mL), and the flask was covered in foil. The mixture was stirred at room temperature, overnight under N_2. The mixture was diluted with $CHCl_3$ (20 mL) and washed with NH_4OH (2 × 10 mL) and brine (2 × 10 mL). The organics were dried over $MgSO_4$. The solvent was removed *in vacuo*. Purification by preparative thin layer chromatography (3% MeOH in DCM) afforded **116** (10.2 mg, 20%). ^{1}**H NMR** (400 MHz; $CDCl_3$) δ (ppm): 9.24 (2H, d, $^4J_{k,l|j} = 2.0$ Hz, $H_{k,l}$), 8.85 (1H, t, $^4J_{j|k,l} = 2.0$ Hz, H_j), 4.94–5.26 (7H, m, H_a), 4.62 (2H, t, $J_{m|n} = 6.7$ Hz, H_m), 4.32 (2H, t, $J_{o|n} = 5.7$ Hz, H_o), 3.06 (3H, s, H_p), 2.84–4.12 (102H, m, $H_{b,c,d,e,f,g,h,i}$), 2.45 (2H, quin, $J_{n|m,o} = 6.1$ Hz, H_n). ^{13}**C**$\{^1$**H**$\}$ **NMR** (126 MHz; $CDCl_3$) δ (ppm): 148.0, 147.1, 146.2, 132.8, 126.5, 126.2, 124.8, 99.8–98.2, 84.2, 82.3–79.8, 71.4–70.3, 65.9, 61.9–58.4, 51.8, 47.2, 37.6, 29.7, 29.2. **HRESI-MS** (pos.): 1998.56222, calc. for $[C_{75}H_{121}O_{37}N_7I_2S \cdot H]^+ = 1998.56847$.

3-(Permethyl-cyclodextrin-iodotriazolyl)-5-(azidopropyl-iodotriazolyl)-pyridine, 117



116 (64 mg, 32 μmol) and NaN_3 (11 mg, 0.16 mmol) were dissolved in dry, degassed DMF (2 mL), and the mixture was stirred at 85 °C, overnight under N_2. The mixture was cooled to room temperature and partitioned between H_2O (10 mL) and EtOAc (10 mL). The aqueous layer was washed with EtOAc (2×10 mL). The combined organics were washed with brine (3×10 mL), and dried over $MgSO_4$. The solvent was removed *in vacuo* to afford **117** (62 mg, quant.). ^{1}**H NMR** (400 MHz; $CDCl_3$) δ (ppm): 9.22 (2H, s, $H_{k,l}$), 8.85 (1H, s, H_j), 4.90–5.36 (7H, m, H_a), 4.55 (2H, t, $J_{m|n} = 6.8$ Hz, H_m), 3.01–3.97 (104H, m, $H_{b,c,d,e,f,g,h,i,o}$), 2.22 (1H, quin, $J_{n|m,o} = 6.5$ Hz, H_n). ^{13}**C**$\{^1$**H**$\}$ **NMR** (101 MHz; $CDCl_3$) δ (ppm): 147.8, 147.7, 146.8, 146.1, 132.8, 130.8, 128.7, 126.4, 126.3, 99.7–98.7, 84.1, 82.2, 81.9–79.7, 71.3–70.1, 61.7–61.1, 59.1–58.3, 51.8, 48.0, 48.0, 29.6, 29.0. **HRESI-MS** (pos.): 1945.59012, calc. for $[C_{74}H_{118}O_{34}N_{10}I_2 \cdot H]^+ = 1945.59850$.

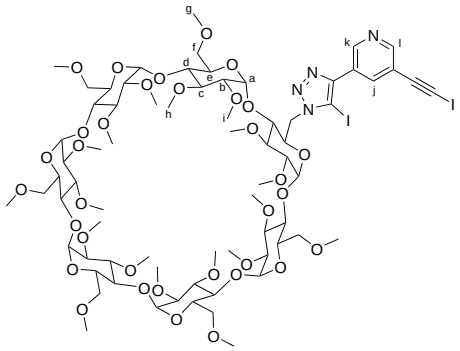
3-(pCD-iodotriazolyl)-5-(azidopropyl-iodotriazolyl)-pyridinium chloride, 118·Cl



117 (80 mg, 41 μmol) was dissolved in $CHCl_3$ (0.2 mL) and CH_3I (0.1 mL 1.0 mmol) was added. The mixture was stirred overnight at 40 °C under N_2. The solvent was removed *in vacuo*. The residue was taken up in $CHCl_3$ (1.5 mL) and passed through a chloride-loaded Amberlite® column to afford the desired product **118**·Cl (56.6 mg, 69%). ^{1}**H NMR** (400 MHz; $CDCl_3$) δ (ppm): 10.17 (1H, s, H_j), 9.40

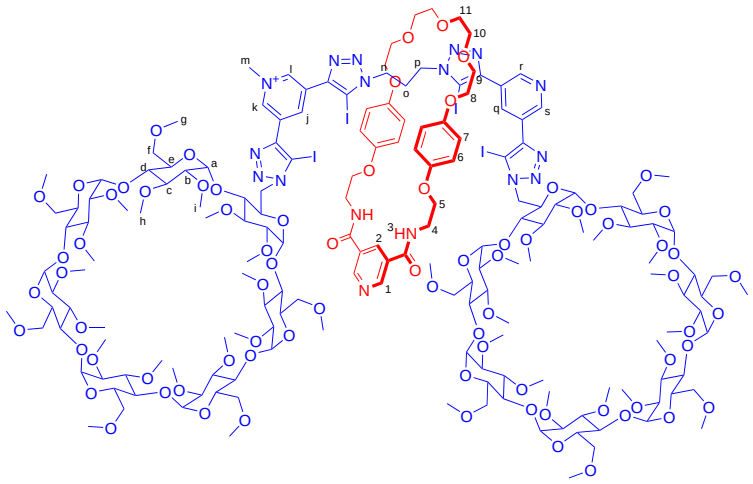
(2H, s, $H_{k,l}$), 4.88–5.29 (7H, m, H_a), 4.67 (3H, s, H_m), 2.88–4.49 (106H, m, $H_{b,c,d,e,f,g,h,i,n,p}$), 2.05 (2H, quin, $J_{o|n,p} = 6.8$ Hz, H_o).^{13}**C**$\{^1$**H**$\}$ **NMR** (101 MHz; $CDCl_3$) δ (ppm): 141.7, 141.1, 140.2, 140.1, 133.3, 133.0, 132.2, 131.9, 130.9, 128.8, 99.1–97.7, 83.0–81.1, 80.5–78.7, 71.3–69.5, 61.9–57.9, 53.7, 50.4, 48.2, 48.1, 31.7, 29.6, 29.2, 28.9. **HRESI-MS** (pos.): 1959.60753, calc. for $[C_{75}H_{121}O_{34}N_{10}I_2]^+ = 1959.61305$.

3-(Iodoethynyl)-5-(permethyl-cyclodextrin-appended iodotriazolyl)-pyridine, 119



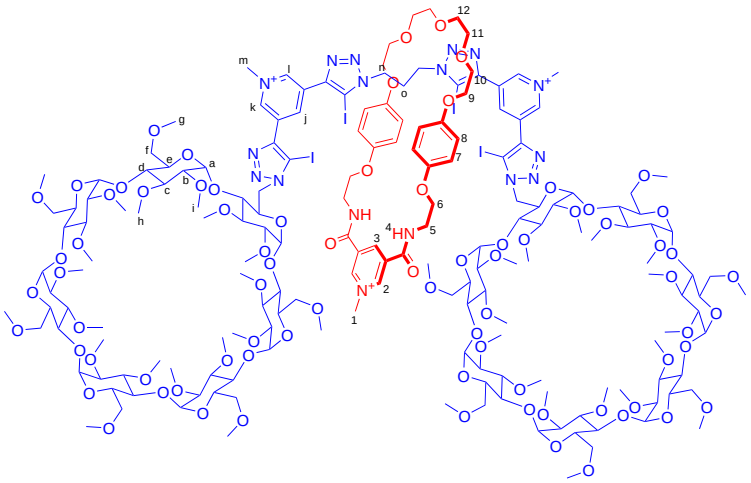
$[Cu(MeCN)_4][PF_6]$ (10 mg, 27 μmol) and TBTA (cat.) were dissolved in dry degassed THF (1 mL). **65** (0.10 g, 69 μmol) and **2** (26 mg, 69 μmol) were added. The mixture was stirred overnight, at room temperature under N_2. The solvent was removed *in vacuo*. The residue was redissolved in DCM (40 mL) and washed with NH_4OH (2 $\times$ 10 mL) and brine (2 $\times$ 10 mL). The organics were dried over $MgSO_4$. The solvent was removed *in vacuo*. Purification by preparative thin layer chromatography (3% MeOH in DCM) afforded **119** (6.4 mg, 5%). ^{1}**H NMR** (400 MHz; $CDCl_3$) δ (ppm): 9.17 (1H, d, $^4J_{k|j} = 1.6$ Hz, H_k), 8.68 (1H, s, H_l), 8.30 (1H, s, H_j), 4.96–5.29 (7H, m, H_a), 2.80–4.16 (102H, m, $H_{b,c,d,e,f,g,h,i}$). ^{13}**C**$\{^1$**H**$\}$ **NMR** (126 MHz; $CDCl_3$) δ (ppm): 147.1, 145.6, 137.6, 137.4, 126.4, 126.1, 104.4, 99.8–98.2, 84.1–79.9, 71.5–70.5, 61.8–58.4, 51.9, 29.7. **HRESI-MS** (pos.): 1819.52786, calc. for $[C_{71}H_{112}O_{34}N_4I_2 \cdot H]^+ = 1819.53201$.

Water-soluble asymmetric monocationic [2]rotaxane: permethyl-β-cyclodextrin-stoppered pyridinium/pyridine bis-iodotriazole axle with pyridine bis-amide 5-*O*-polyether macrocycle, 120·Cl



33 (8.0 mg, 13 μmol), **118**·Cl (7.3 mg, 3.5 μmol) and **119** (6.4 mg, 3.5 μmol) were dissolved in dry, degassed THF (0.1 mL). The flask was covered in foil and the mixture was stirred for 30 mins. Thereafter, a solution of $[Cu(MeCN)_4][PF_6]$ (cat.) and TBTA (cat.) in dry, degassed THF (0.1 mL) was added, and the mixture was stirred overnight at room temperature under N_2. The mixture was then diluted with $CHCl_3$ (20 mL) and washed with NH_4OH (10 mL) and brine (10 mL). The solvent was removed *in vacuo* and the organics were dried over $MgSO_4$. Purification by preparative thin layer chromatography (8% MeOH in DCM) afforded the [2]rotaxane **120**·Cl (1.7 mg, 9%). **^{1}H NMR** (400 MHz; $CDCl_3$) δ (ppm): 9.81 (1H, br. s., H_k), 9.73 (1H, br. s., H_l), 9.50 (2H, d, $H_{r,s}$), 9.28 (2H, d, H_1), 9.10 (1H, br. s., H_j), 8.94 (1H, br. s., H_2), 8.62 (2H, br. s., H_3), 8.26 (1H, br. s., H_q), 6.27–6.44 (8H, m, $H_{6,7}$), 4.98–5.33 (14H, m, H_a), 2.79–4.83 (235H, m, $H_{b,c,d,e,f,g,h,i,m,n,p,4,5,8,9,10,11}$), 2.21–2.47 (2H, m, H_o). **HRESI-MS** (pos.): 2188.20672, calc. for $[C_{177}H_{270}O_{77}N_{17}I_4 \cdot H]^+ = 2188.20236$.

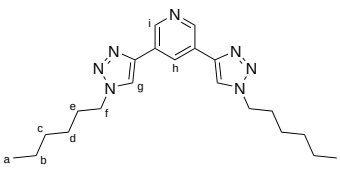
Water-soluble symmetric tricationic [2]rotaxane: permethyl-β-cyclodextrin-stoppered bis-(3,5-bis-iodotriazole pyridinium) axle with pyridinium bis-amide 5-*O*-polyether macrocycle 121·(OTf)$_3$



The [2]rotaxane **120**·Cl (4.0 mg, 0.9 μmol) was dissolved in $CHCl_3$ (1.5 mL) and CH_3I (0.5 mL) was added. The solution was stirred at room temperature overnight, under N_2. The solvent was removed *in vacuo*. Anion exchange to the triflate (OTf^-) salt was achieved by passing a solution of the [2]rotaxane through a triflate-loaded Amberlite® column to afford **121**·(OTf)$_3$ (4.0 mg, 99%). **^{1}H NMR** (500 MHz; $CDCl_3$) δ (ppm): 9.74–10.33 (6H, m, $H_{j,k,l}$), 9.24 (2H, br. s., H_2), 8.46 (1H, br. s., H_3), 6.14 (8H, br. s., $H_{7,8}$), 5.00–5.25 (14H, m, H_a), 2.78–4.99 (241H, m, $H_{b,c,d,e,f,g,h,i,m,n,1,5,6,9,10,11,12}$), 2.25–2.43 (2H, m, H_o). **^{13}C{^{1}H} NMR** (126 MHz; $CDCl_3$) δ (ppm): 167.8, 159.7, 152.0, 137.2, 132.4, 130.9, 130.0, 129.9, 129.7, 128.8, 99.2–98.5, 90.8, 82.0–80.0, 71.2–68.0, 61.6–58.2, 45.9, 38.7–35.9, 32.7, 32.2, 31.9, 31.4, 30.3, 30.3, 30.0, 29.7, 29.7, 29.5, 29.4, 29.2, 28.9, 27.2, 27.1, 26.4, 25.6, 24.8, 24.3, 23.7, 23.4, 23.0, 22.7, 14.1, 14.0, 10.9. **^{19}F NMR** (377 MHz; $CDCl_3$) δ (ppm): -78.28 (s, $CF_3SO_3^-$). **HRESI-MS** (pos.): 1468.47832, calc. for $[C_{179}H_{276}I_4N_{17}O_{77}]_3^+ = 1468.48110$.

6.2.3 Compounds from Chapter 4

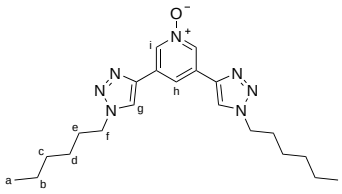
Bis-hexyltriazolyl-pyridine, 122



NaN_3 (0.16 g, 2.4 mmol), Na_2CO_3 (0.106 g, 1.00 mmol), ascorbic acid (0.176 g, 1.00 mmol) and $CuSO_4$·5 H_2O (20 mg, 0.08 mmol) were added to a solution of **1** in 4:1 DMF:H_2O (15 mL). Bromohexane

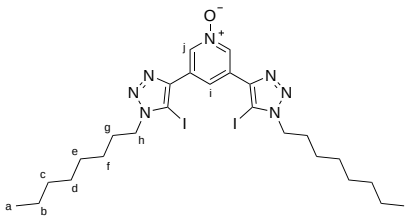
(0.35 mL, 0.41 g, 2.5 mmol) was added and the yellow solution heated to 80 °C under an atmosphere of N_2 and stirred for 72 h. The reaction was cooled to room temperature and partitioned between EtOAc (50 mL) and $NH_4OH/EDTA_{(aq.)}$ (50 mL). The aqueous layer was washed with a further portion of EtOAc (50 mL). The organic fractions were combined and washed with H_2O (50 mL), brine (50 mL) and dried over $MgSO_4$. The solvent was removed *in vacuo*. Purification by silica gel column chromatography (3% MeOH in DCM) to give **122** as a white powder. Yield: 0.222 g (58%). **^{1}H NMR** (300 MHz; $CDCl_3$) δ (ppm): 9.05 (2H, br. s., H_i), 8.66 (1H, s, H_h), 7.95 (2H, t, $^4J_{f|g} = 4$ Hz, H_g), 4.45 (4H, t, $J_{e|f} = 7$ Hz, H_f), 1.98 (4H, quin, $J_{e|f} = 7$ Hz, H_e), 1.23–1.48 (12H, m, $H_{b,c,d}$), 0.90 (6H, t, $J_{a|b} = 7$ Hz, H_a). **LRESI-MS** (pos.): 382.24, calc. for $[C_{21}H_{31}N_7 \cdot H]^+ = 382.27$.

Bis-hexyltriazolyl-pyridine *N*-oxide, 123



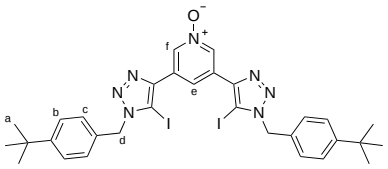
122 (0.11 g, 0.30 mmol) and $NaHCO_3$ (0.76 g, 9.0 mmol) were dissolved in a 1:1 mixture of 2-butanone:H_2O (50 mL). A saturated solution of Oxone® (0.28 g, 0.90 mmol) in H_2O (2 mL) was added dropwise. The solution was stirred vigorously for 2 h. Thereafter, NaCl (1.75 g, 30 mmol) was added. The product was extracted with $CHCl_3$ (3 × 50 mL); the organic layers were combined, dried over $MgSO_4$ and the solvent removed *in vacuo* to yield **123** as a white powder. Yield: 0.085 g (71%). **^{1}H NMR** (300 MHz; $CDCl_3$) δ (ppm): 8.74 (2H, s, H_i), 8.32 (1H, s, H_h), 7.99 (2H, s, H_g), 4.45 (4H, t, $J_{e|f} = 7$ Hz, H_f), 1.84–2.07 (4H, m, H_e), 1.27–1.47 (12H, m, $H_{b,c,d}$), 0.84–0.97 (6H, m, H_a). **^{13}C{^{1}H} NMR** (75 MHz; 1 :1 $CDCl_3$:MeOD) δ (ppm): 142.5, 135.4, 131.8, 123.4, 122.8, 51.5, 31.8, 30.8, 26.8, 23.1, 14.3. **HRESI-MS** (pos.): 420.2480, calc. for $[C_{12}H_{31}N_7O \cdot Na]^+ = 420.2482$.

Bis-octyliodotriazole pyridinium *N*-oxide, 124



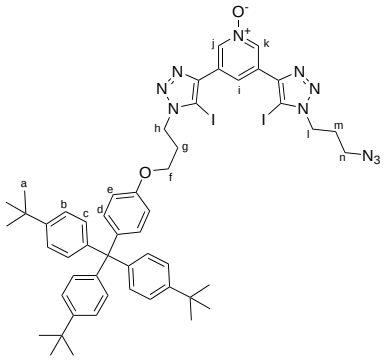
8 (0.050 g, 0.070 mmol) and $NaHCO_3$ (0.19 g, 2.2 mmol) were dissolved in a 1:1 mixture of 2-butanone:H_2O (15 mL). A saturated solution of Oxone® (0.070 g, 0.22 mmol) in H_2O (0.5 mL) was added dropwise. The solution was stirred vigorously for 2 h under N_2. NaCl (0.42 g, 7.3 mmol) was added. The product was extracted with $CHCl_3$ (3 × 15 mL). The combined organics were dried over $MgSO_4$ and the solvent removed *in vacuo* to yield **124** as a white powder (0.047 g, 95%). ^{1}**H NMR** (300 MHz; $CDCl_3$) δ (ppm): 9.02 (2H, s, H_j), 8.77 (1H, s, H_i), 4.47 (4H, t, $J_{g|h} = 7.3$ Hz, H_h), 1.97 (4H, br. s., H_g), 1.17–1.45 (20H, m, $H_{b,c,d,e,f}$), 0.82–0.95 (6H, m, H_a). ^{13}**C**$\{^1$**H**$\}$ **NMR** (101 MHz; $CDCl_3$) δ (ppm): 250.34, 135.45, 128.99, 121.56, 102.90, 50.24, 30.70, 28.83, 28.03, 27.93, 25.39, 21.59, 13.05. **HRESI-MS** (pos.): 728.1042, calc. for $[C_{25}H_{37}I_2N_7O \cdot Na]^+ = 728.1041$.

Bis-*tert*-butylbenzyl-iodotriazolyl pyridinium *N*-oxide, 125



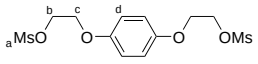
9 (0.076 g, 0.10 mmol) and $NaHCO_3$ (0.26 g, 3.0 mmol) were dissolved in a 1:1 mixture of 2-butanone:H_2O (20 mL). A saturated solution of Oxone® (0.095 g, 0.30 mmol) in H_2O (0.5 mL) was added dropwise. The solution was stirred vigorously for 2 h. NaCl (0.63 g, 10.0 mmol) was added and the product was extracted with $CHCl_3$ (3 × 20 mL). The combined organics were dried over $MgSO_4$ and the solvent removed *in vacuo* to yield **125** as a white powder (0.077 g, 100%). ^{1}**H NMR** (300 MHz; $CDCl_3$) δ (ppm): 8.90 (1H, d, $^4J_{f|e} = 1.5$ Hz, H_f), 8.57 (1H, t, $^4J_{e|f} = 1.5$ Hz, H_e), 7.39 (4H, d, $J_{c|b} = 8.2$ Hz, H_c), 7.28 (4H, d, $J_{b|c} = 8.2$ Hz, H_b), 5.65 (4H, s, H_d), 1.25–1.35 (18H, m, H_a). **LRESI-MS** (pos.): 774.14, calc. for $[C_{31}H_{34}I_2N_7O]^+ = 774.09$.

Bis-stopper propyl iodotriazolyl pyridine-*N*-oxide, 126



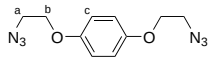
109 (53 mg, 49 μmol) and $NaHCO_3$ (0.13 g, 1.5 mmol) were dissolved in 1:1 2-butanone:H_2O (11 mL). Oxone® (46 mg, 0.15 mmol) in H_2O (sat. 0.4 mL) was added dropwise. The mixture was stirred vigorously for 2 h, and thereafter, NaCl (0.28 g, 4.8 mmol) was added. The product was extracted in $CHCl_3$ (3 × 30 mL). The organics were dried over $MgSO_4$. The solvent was removed *in vacuo* to afford **126** (55 mg, 100%) as an off-white powder. ^{1}**H NMR** (400 MHz; $CDCl_3$) δ (ppm): 8.88–8.96 (2H, m, $H_{j,k}$), 8.58 (1H, t, $^4J_{i|j,k} = 1.5$ Hz, H_i), 7.23 (6H, d, $J_{b|c} = 8.6$ Hz, H_b), 7.04–7.13 (8H, m, $H_{c,d}$), 6.77 (2H, d, $J_{e|d} = 8.8$ Hz, H_e), 4.70 (2H, t, $J_{l|m} = 7.0$ Hz, H_l), 4.58 (2H, t, $J_{h|g} = 7.0$ Hz, H_h), 4.05 (2H, t, $J_{n|m} = 5.6$ Hz, H_n), 3.47 (2H, t, $J_{f|g} = 6.2$ Hz, H_f), 2.47 (2H, quin, $J_{m|l,n} = 6.5$ Hz, H_m), 2.25 (2H, quin, $J_{g|f,h} = 6.5$ Hz, H_g), 1.30 (27H, s, H_a). ^{13}**C**$\{^1$**H**$\}$ **NMR** (101 MHz; $CDCl_3$) δ (ppm): 147.4, 143.0, 135.6, 131.3, 129.7, 123.1, 121.5, 112.0, 88.8, 62.8, 62.1, 47.0, 33.3, 30.4, 28.6, 28.0. **HRESI-MS** (pos.): 1109.28883, calc. for $[C_{52}H_{58}I_2N_{10}O_2 \cdot H]^+ = 1109.29063$.

Bis-mesylethyl-hydroquinone, 127



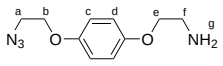
Hydroquinone bis-(2-hydroxyethyl)ether (10.0 g, 50.4 mmol) and Et_3N (18 mL, 130 mmol) were dissolved in dry DCM (250 mL) at 0 °C. MsCl (15 mL, 190 mmol) in dry DCM (100 mL) was added dropwise over 10 mins. The resulting mixture was stirred for 15 mins. The organics were washed with 1 *m* $HCl_{(aq.)}$ (3 × 50 mL), saturated $NaHCO_{3(aq.)}$ (3 × 50 mL) and brine (2 × 50 mL) and dried over $MgSO_4$. The solvent was removed *in vacuo* to afford **127** (17.4 g, 97%). ^{1}**H NMR** (300 MHz; $CDCl_3$) δ (ppm): 6.76–6.94 (4H, m, H_d), 4.48–4.63 (4H, m, H_b), 4.12–4.28 (4H, m, H_c), 3.09 (6H, s, H_a). **HRESI-MS** (pos.): 377.0, calc. for $[C_{12}H_{18}O_8S_2 \cdot Na]^+ = 377.0$.

Bis-azidoethyl-hydroquinone, 128



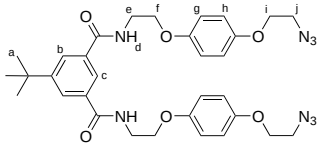
127 (5.00 g, 14.1 mmol) and NaN_3 (3.00 g, 46.1 mmol) were dissolved in dry, degassed DMF (200 mL). The mixture was refluxed at 85 °C for 16 h under N_2. After cooling to room temperature, the mixture was partitioned between H_2O (300 mL) and Et_2O (100 mL). The aqueous layer was washed with Et_2O (2 × 100 mL). The combined organics were washed with brine (3 × 200 mL) and dried over $MgSO_4$ and the solvent was removed *in vacuo* to afford **128** (2.48 g, 71%). ^{1}**H NMR** (300 MHz; $CDCl_3$) δ (ppm): 6.87 (4H, s, H_c), 4.11 (4H, t, $J_{a|b} = 5.0$ Hz, H_a), 3.57 (4H, t, $J_{b|a} = 5.0$ Hz, H_b).

Azidoethyl-aminoethyl-hydroquinone, 129



128 (2.88 g, 11.6 mmol) was dissolved in 1:1:2 Et_2O:EtOAc:5% $HCl_{(aq.)}$ (240 mL) at 0 °C and stirred vigorously. PPh_3 in 1:1 Et_2O:EtOAc (40 mL) was added dropwise. Thereafter, the solution was allowed to warm to room temperature and stirred for 16 h. The organic layer was separated and discarded. The aqueous phase was washed with 1:1 Et_2O:EtOAc (3 × 50 mL) and basified with 10% $NaOH_{(aq.)}$ to pH 9. The product was extracted with DCM (3 × 80 mL) and dried over $MgSO_4$. The solvent was removed *in vacuo* afforded **129** (1.71 g, 66%). ^{1}**H NMR** (300 MHz; $CDCl_3$) δ (ppm): 6.85 (4H, s, $H_{c,d}$), 4.09 (2H, t, $J_{a|b} = 5.0$ Hz, H_a), 3.93 (2H, t, $J_{f|e} = 5.1$ Hz, H_f), 3.55 (2H, t, $J_{b|a} = 5.0$ Hz, H_b), 3.05 (2H, t, $J_{e|f} = 5.1$ Hz, H_e). **HRESI-MS** (pos.): 223.1, calc. for $[C_{10}H_{14}N_4O_2 \cdot H]^+ = 223.1$.

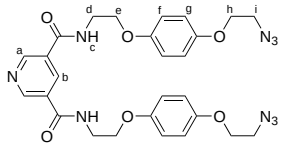
Bis-azide-appended-*tert*-butylisophthalamide macrocycle precursor, 130



5-*tert*-Butylisophthalic acid (0.33 g, 1.5 mmol) was suspended in excess $SOCl_2$ (2 mL) and 1 drop of DMF was added. The mixture was heated at 75 °C for 16 h or until all solid had dissolved. The excess $SOCl_2$ was removed *in vacuo* and the bis-acid chloride was used immediately assuming a quantitative yield of formation. To a solution of **129** (0.68 g, 3.0 mmol), DMAP (cat.) and Et_3N in dry DCM (20 mL)

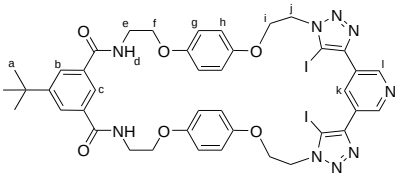
at 0 °C was added dropwise the 5-*tert*-butylisophthalyl dichloride in dry DCM (15 mL). The reaction was left to stir for 2 h at room temperature. The organics were washed with 10% $HCl_{(aq.)}$ (10 mL) and H_2O (2 × 10 mL) and dried over $MgSO_4$. The solvent was removed *in vacuo*. Purification by silica gel column chromatography (6:4 EtOAc:hexane) afforded **130** (0.367 g, 39%). **^{1}H NMR** (500 MHz; $CDCl_3$) δ (ppm): 7.95 (2H, s, H_b), 7.93 (1H, s, H_c), 6.86 (8H, s, $H_{g,h}$), 6.67 (2H, t, $J_{d|e} = 5.3$ Hz, H_d), 4.11 (8H, m, $H_{e,j}$), 3.86 (4H, m, H_f), 3.56 (4H, t, $J_{i|j} = 5.0$ Hz, H_i), 1.36 (9H, s, H_a). **LRESI-MS** (pos.): 631.4, calc. for $[C_{32}H_{38}N_8O_6 \cdot H]^+ = 631.3$.

Bis-azide-appended-pyridine-bis-amide macrocycle precursor, 131



Pyridine-3,5-dicarboxylic acid (0.30 g, 1.6 mmol) was suspended in $SOCl_2$ and 1 drop of DMF was added. The mixture was heated at reflux for 16 h under N_2. Excess $SOCl_2$ was removed *in vacuo* and the bis-acid chloride was used immediately assuming quantitative yield of formation. To a solution of **129** (0.77 g, 3.5 mmol), DMAP (cat.) and Et_3N (1.1 mL, 7.9 mmol) in dry DCM (30 mL) at 0 °C was added dropwise pyridine-bis-acid chloride in dry DCM (15 mL). The mixture was stirred at room temperature for 16 h under N_2. The mixture was washed with 10% $HCl_{(aq.)}$ (50 mL) and H_2O (2 × 50 mL) and dried over $MgSO_4$. The solvent was removed *in vacuo*. Purification by silica gel column chromatography (3% MeOH in $CHCl_3$) afforded **131** (0.37 g, 40%). **^{1}H NMR** (500 MHz; 1 :1 $CDCl_3$:CD_3OD) δ (ppm): 9.07 (2H, d, $^4J_{a|b} = 2.1$ Hz, H_a), 8.58 (1H, t, $^4J_{b|a} = 2.1$ Hz, H_b), 6.79–6.89 (8H, m, $H_{f,g}$), 4.11 (4H, t, $J_{i|h} = 5.4$ Hz, H_i), 4.08 (4H, t, $J_{d|e} = 4.9$ Hz, H_d), 3.78 (4H, t, $J_{h|i} = 5.4$ Hz, H_h), 3.54 (4H, t, $J_{e|d} = 4.9$ Hz, H_e). **^{13}C{^{1}H} NMR** (126 MHz; 1 :1 $CDCl_3$:CD_3OD) δ (ppm): 166.7, 154.1, 153.6, 151.1, 135.3, 131.0, 116.5, 116.3, 68.5, 67.6, 50.9, 40.6. **HRESI-MS** (pos.): 598.21292, calc. for $[C_{27}H_{29}N_9O_6 \cdot Na]^+ = 598.21330$.

Pyridine-bis-iodotriazole-*tert*-butylisophthalamide macrocycle, 132

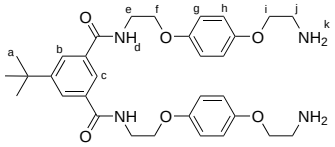


Without template: CuI (0.006 g, 32 μmol), TBTA (0.005 g, 10 μmol), **130** (0.043 g, 68 μmol) and **2** (0.026 g, 67 μmol) were dissolved in THF (10 mL) and covered in foil. The mixture was stirred at room temperature for 7 days under N_2. The solvent was removed *in vacuo*. The residue was taken up in DCM (10 mL) and washed with NH_4OH (2 $\times$ 5 mL) and brine (2 $\times$ 5 mL) and dried over $MgSO_4$. The solvent was removed *in vacuo*. Purification by preparative thin layer chromatography (5% MeOH in DCM) did not afford **132**.

With pyridinium-bis-prototriazole template: CuI (0.004 g, 22μmol) and TBTA (0.003 g, 10 μmol) were dissolved in THF (10 mL) and covered in foil. **130** (0.042 g, 66 μmol), **123** (0.026 g, 66 μmol) and TBA·Cl (0.025 g, 89 μmol) were added and the mixture was stirred for 30 mins. **2** (0.025 g, 66 μmol) was added and the mixture was stirred under N_2 at room temperature for 7 days. The solvent was removed *in vacuo*. The residue was taken up in DCM (10 mL) and washed with NH_4OH (2 $\times$ 5 mL) and brine (2 $\times$ 5 mL) and dried over $MgSO_4$. The solvent was removed *in vacuo*. Purification by preparative thin layer chromatography (5% MeOH in DCM) did not afford **132**.

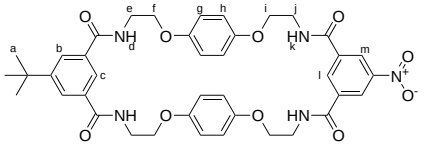
With pyridinium-bis-iodotriazole template: CuI (0.004 g, 22μmol) and TBTA (0.004 g, 10 μmol) were dissolved in THF (10 mL) and covered in foil. **130** (0.042 g, 66 μmol), **124** (0.030 g, 42 μmol) and TBA·Cl (0.021 g, 76 μmol) were added and the mixture was stirred for 30 mins. **2** (0.025 g, 66 μmol) was added and the mixture was stirred under N_2 at room temperature for 7 days. The solvent was removed *in vacuo*. The residue was taken up in DCM (10 mL) and washed with NH_4OH (2 $\times$ 5 mL) and brine (2 $\times$ 5 mL) and dried over $MgSO_4$. The solvent was removed *in vacuo*. Purification by preparative thin layer chromatography (5% MeOH in DCM) afforded **132** (16.1 mg, 24%). ^{1}**H NMR** (500 MHz; 1 :1 $CDCl_3$:CD_3OD) δ (ppm): 9.07 (2H, d, $^4J_{l|k} = 1.7$ Hz, H_l), 8.78 (1H, t, $^4J_{k|l} = 1.7$ Hz, H_k), 8.03 (2H, d, $^4J_{b|c} = 1.5$ Hz, H_b), 7.99 (1H, t, $^4J_{c|b} = 1.5$ Hz, H_c), 6.68–6.85 (8H, m, $H_{g,h}$), 4.90 (4H, t, $J_{j|i} = 4.9$ Hz, H_j), 4.41 (4H, t, $J_{e|f} = 4.9$ Hz, H_e), 4.04 (4H, t, $J_{i|j} = 5.3$ Hz, H_i), 3.74 (5H, t, $J_{f|e} = 5.2$ Hz, H_f), 1.34 (9H, s, H_a). ^{13}**C**$\{^1$**H**$\}$ **NMR** (126 MHz; 1 :1 $CDCl_3$:CD_3OD) δ (ppm): 169.3, 154.2, 153.2, 148.3, 147.5, 134.9, 134.8, 128.6, 123.3, 116.3, 116.2, 81.9, 67.9, 67.8, 51.1, 40.5, 35.7, 31.5. **HRESI-MS** (pos.): 1010.13368, calc. for $[C_{41}H_{41}I_2N_9O_6 \cdot H]^+ = 1010.13419$.

Bis-amine-appended 5-*tert*-butylisophthalamide macrocycle precursor, 133



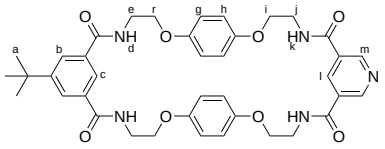
130 (0.28 g, 0.44 mmol) was dissolved in EtOH (25 mL). Pd/C was carefully added and the mixture was placed under H_{2g} (5 atm). The mixture was stirred overnight and filtered through Celite®. The solvent was removed *in vacuo* to afford **133**, which, assuming quantitative yield, was used immediately in the subsequent step without further purification or characterisation.

Ditopic macrocycle: 5-*tert*-butylisophthalamide–nitro-isophthalamide, 134



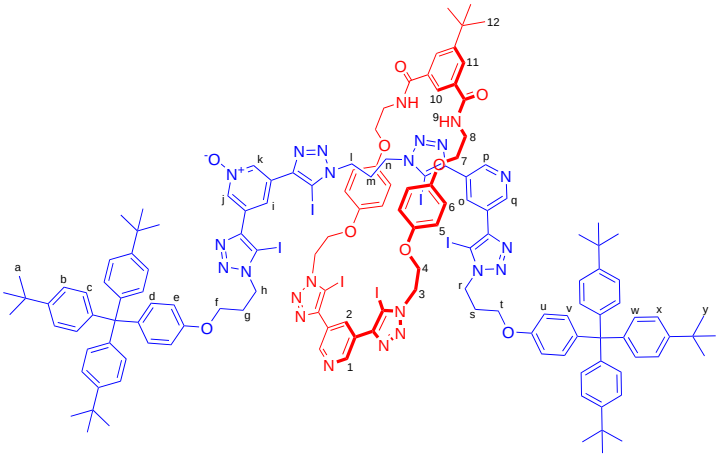
5-Nitroisophthalic acid (0.11 g, 0.44 mmol) was dissolved in dry DCM (3 mL) and $(COCl)_2$ (0.25 mL) was added. The mixture was refluxed under N_2 overnight. Thereafter, the solvent was removed *in vacuo*, and the residue was taken up in dry DCM (20 mL). In a separate flask, **133** (0.25 g, 0.44 mmol), Et_3N (0.25 mL) and DMAP (cat.) were dissolved in DCM (20 mL). The two solutions were added dropwise to a flask of dry DCM (750 mL) over 6 h. The mixture was stirred at room temperature, overnight under N_2. The volume was reduced *in vacuo* (150 mL) and washed with citric acid (10% aq., 3 × 75 mL), water (3 × 75 mL) and brine (3 × 75 mL). The organics were dried over $MgSO_4$. The solvent was removed *in vacuo*. Purification by silica gel column chromatography (2–5% MeOH in DCM) afforded **134** (61 mg, 34%). ^{1}**H NMR** (400 MHz; CD_3OD) δ (ppm): 8.82 (2H, d, $^4J_{m|l} = 1.5$ Hz, H_m), 8.57 (1H, s, H_l), 8.11 (2H, br. s., H_k), 8.04 (2H, d, $^4J_{b|c} = 1.3$ Hz, H_b), 7.97 (1H, s, H_c), 7.41–7.54 (2H, m, H_d), 6.78 (8H, s, $H_{g,h}$), 4.06 (8H, q, $J_{e,j|f,i} = 5.1$ Hz, $H_{e,j}$), 3.68–3.84 (8H, m, $H_{f,i}$), 1.34 (9H, s, H_a). **HRESI-MS** (pos.): 754.41 calc. for $[C_{40}H_{43}N_5O_{10} \cdot H]^+ = 754.31$.

Ditopic macrocycle: 5-*tert*-butylisophthalamide–pyridine-bis-amide, 135



Pyridine-3,5-dicarboxylic acid (86 mg, 0.44 mmol) was dissolved in dry DCM (3 mL) and $(COCl)_2$ (0.25 mL) was added. The mixture was refluxed under N_2 overnight. Thereafter, the solvent was removed *in vacuo*, and the residue was taken up in dry DCM (20 mL). In a separate flask, **133** (0.25 g, 0.44 mmol), Et_3N (0.25 mL) and DMAP (cat.) were dissolved in DCM (20 mL). The two solutions were added dropwise to a flask of dry DCM (600 mL) over 6 h. The mixture was stirred at room temperature, overnight under N_2. The volume was reduced *in vacuo* (150 mL) and washed with citric acid (10% aq., 3 × 75 mL), water (3 × 75 mL) and brine (3 × 75 mL). The organics were dried over $MgSO_4$. The solvent was removed *in vacuo*. Purification by silica gel column chromatography (2–5% MeOH in DCM) afforded **135** (25 mg, 7.7%). ^{1}**H NMR** (400 MHz; CD_3OD) δ (ppm): 9.06 (2H, s, H_m), 8.46 (1H, s, H_l), 8.01 (2H, s, H_b), 7.91 (1H, s, H_c), 6.75 (8H, s, $H_{g,h}$), 3.99–4.08 (8H, m, $H_{e,j}$), 3.69–3.79 (8H, m, $H_{f,i}$), 1.32 (9H, s, H_a). **HRESI-MS** (pos.): 710.40, calc. for $[C_{39}H_{43}N_5O_8 \cdot H]^+ = 710.32$.

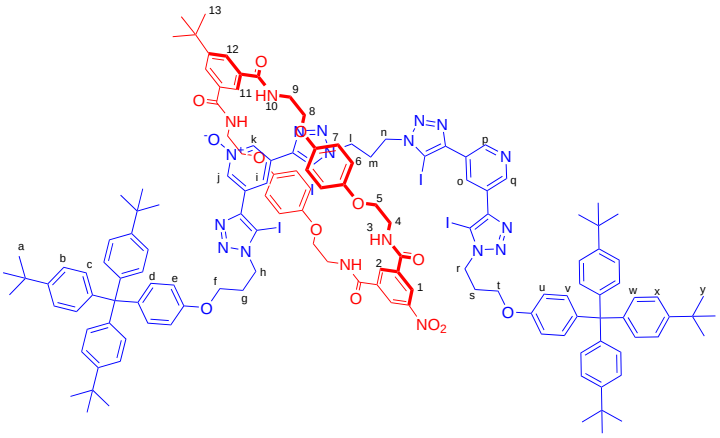
Neutral rotaxane: pyridine-*N*-oxide/pyridine bis-iodotriazole axle–ditopic XB macrocycle, 136



132 (13 mg, 13 μmol), **126** (7.6 mg, 6.8 μmol) and TBA · Cl (2.3 mg, 8.3 μmol) were dissolved in dry, degassed THF (1 mL), and the flask was covered in tin foil. The mixture was stirred for 30 mins, and thereafter, $[Cu(MeCN)_4][PF_6]$ (cat.), TBTA (cat.) and **106** (6.0 mg, 6.2 μmol) were added. The mixture was stirred at room temperature, overnight under N_2. The mixture was diluted with $CHCl_3$ (20

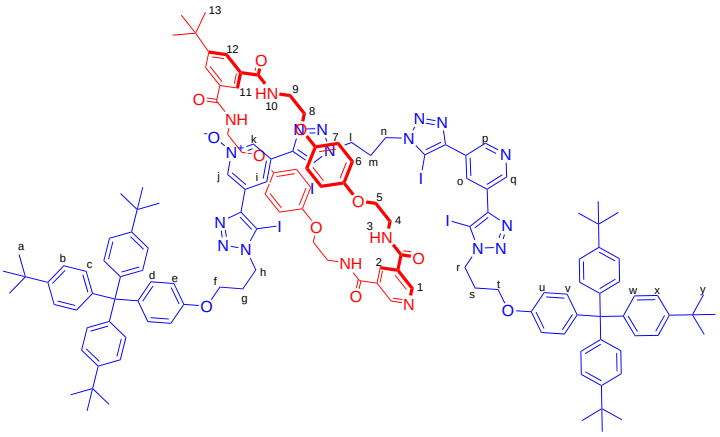
mL), and washed with NH_4OH (2 × 10 mL) and brine (2 × 10 mL). The solvent was removed *in vacuo*. Purification by preparative thin layer chromatography (5% MeOH in DCM) did not afford **136**.

Neutral asymmetric rotaxane: *N*-oxide/pyridine axle with nitro/*tert*-butyl isophthalamide ditopic macrocycle, 137



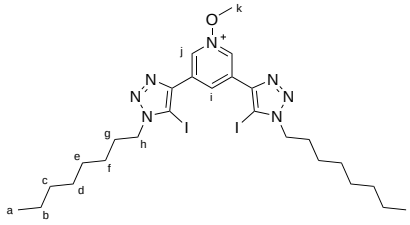
134 (30 mg, 40 μmol), **126** (22 mg, 20 μmol) and TBA · Cl (5.2 mg, 20 μmol) were dissolved in dry, degassed THF (0.8 mL) The flask was covered in foil and the mixture was stirred for 30 mins. Thereafter, a solution of $[Cu(MeCN)_4][PF_6]$ (1.3 mg, 4.0 μmol) and TBTA (cat.) dissolved in THF (0.2 mL) was added. **106** (19 mg, 20 μmol) was then added and the mixture was stirred for 3 days at room temperature under N_2. The mixture was then diluted with $CHCl_3$ (20 mL) and washed with NH_4OH (2 × 10 mL) and brine (2 × 10 mL). The solvent was removed *in vacuo*, and the organics were dried over $MgSO_4$. Unfortunately, the reaction did not afford the target rotaxane **137**.

Neutral asymmetric rotaxane: *N*-oxide/pyridine axle with pyridine/*tert*-butyl isophthalamide ditopic macrocycle, 138



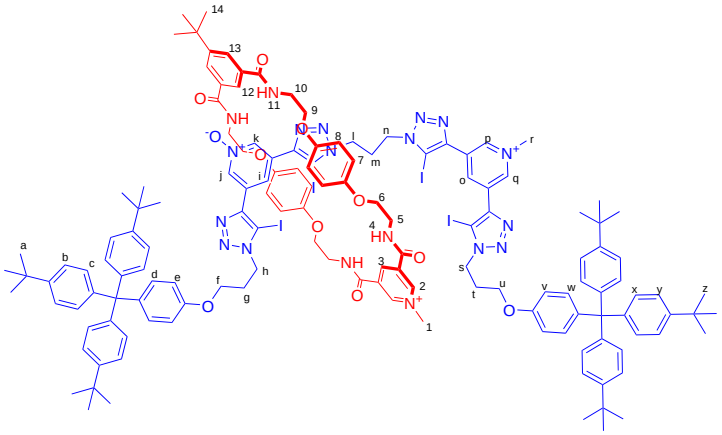
135 (30 mg, 42 μmol), **126** (23 mg, 21 μmol) and TBA · Cl (5.8 mg, 21 μmol) were dissolved in dry, degassed THF (0.8 mL) The flask was covered in foil and the mixture was stirred for 30 mins. Thereafter, a solution of $[Cu(MeCN)_4][PF_6]$ (1.7 mg, 4 μmol) and TBTA (cat.) dissolved in THF (0.2 mL) was added. **106** (20 mg, 21 μmol) was then added and the mixture was stirred for 3 days at room temperature under N_2. The mixture was then diluted with $CHCl_3$ (20 mL) and washed with NH_4OH (2 × 10 mL) and brine (2 × 10 mL). The solvent was removed *in vacuo*, and the organics were dried over $MgSO_4$. Purification by preparative thin layer chromatography (5% MeOH in DCM) afforded the target rotaxane **138** as a white solid (13.5 mg, 67%). ^{1}**H NMR** (500 MHz; $CDCl_3$) δ (ppm): 9.35 (2H, s, H_1), 9.28 (1H, s, H_k), 9.22 (1H, s, H_j), 9.00 (1H, s, H_2), 8.85 (1H, s, H_i), 8.58 (1H, s, H_p), 8.49 (1H, s, H_q), 8.44 (1H, s, H_{11}), 8.30 (1H, s, H_o), 8.24 (2H, s, H_{12}), 8.13 (2H, br. s., H_{10}), 7.75 (2H, br. s., H_3), 7.21 (12H, t, $J_{b,x|c,w} = 9.2$ Hz, $H_{b,x}$), 6.99–7.14 (16H, m, $H_{c,d,v,w}$), 6.76 (4H, d, $J_{e,u|d,v} = 8.5$ Hz, $H_{e,u}$), 6.13–6.28 (8H, m, $H_{6,7}$), 4.44–4.75 (8H, m, $H_{h,l,n,r}$), 3.67–4.13 (20H, m, $H_{f,t,4,5,8,9}$), 2.67 (2H, quin, $J_{m|l,n} = 6.4$ Hz, H_m), 2.45 (2H, quin, $J_{g|f,h} = 6.4$ Hz, H_g), 2.31 (2H, quin, $J_{s|r,t} = 6.4$ Hz, H_s), 1.36 (9H, s, H_{13}), 1.19–1.32 (54H, m, $H_{a,y}$). ^{13}**C**$\{^1$**H**$\}$ **NMR** (126 MHz; $CDCl_3$) δ (ppm): 167.6, 165.7, 160.5, 156.2, 155.9, 152.9, 152.7, 152.6, 152.5, 148.4, 148.3, 148.0, 147.3, 146.7, 144.0, 144.0, 143.7, 142.8, 140.4, 140.1, 134.4, 134.0, 132.9, 132.4, 132.3, 130.7, 130.7, 129.0, 128.9, 128.7, 126.5, 126.0, 124.1, 121.9, 115.0, 114.9, 113.0, 113.0, 67.2, 67.1, 63.9, 63.5, 63.0, 48.3, 48.1, 47.8, 40.3, 35.2, 34.3, 31.4, 31.3, 29.7, 29.4, 28.7. **HRESI-MS** (pos.): 1392.91602, calc. for $[C_{140}H_{153}I_4N_{19}O_{11} \cdot 2\,H]^+$ = 1392.91606.

3,5-Bis-iodotriazole *N*-methoxy-pyridinium iodide, 139·I



This was a test reaction to determine whether CH_3I would be able to methylate a pyridine-*N*-oxide. **124** (0.020 g, 28 μmol) was dissolved in $CHCl_3$ (3 mL) and CH_3I (3 mL) was added. The mixture was stirred for 3 days at room temperature under N_2. Thereafter, the solvent was removed *in vacuo*, however, mass spectrometric analysis did not indicate the formation of the methylate product **139**.

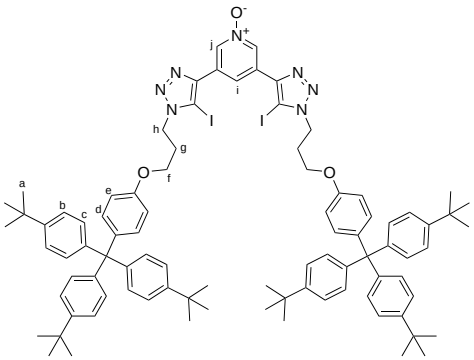
Asymmetric dicationic pyridine-*N*-oxide/pyridinium rotaxane, 140·2 PF_6



138 (5.0 mg, 1.8 μmol) was dissolved in dry $CHCl_3$ (1 mL) and CH_3I (2 μL) was added. The mixture was stirred overnight at room temperature under N_2 and thereafter a further portion of CH_3I (5 μL) was added, stirring overnight again. However, no evidence of product formation was observed by mass spectrometric analysis. Further CH_3I (0.1 mL) was added and the mixture was stirred for 3 days. Thereafter, the solvent was removed *in vacuo* and rotaxane was anion exchanged to the hexafluorophosphate salt by washing a $CHCl_3$ solution (25 mL) of the crude mixture with NH_4PF_6 (0.1 M, 8 × 10 mL) and H_2O (2 × 10 mL). The solvent was removed *in vacuo* to afford the target rotaxane **140**·2 PF_6 (4.0 mg, 72%). **^{1}H NMR** (400 MHz; $CDCl_3$) δ (ppm): 9.56 (1H, br. s., H_q), 9.28 (1H, br. s., H_2), 9.15 (1H, br. s., H_p), 8.62 (1H, br. s., H_j), 8.48–8.58 (1H, m, H_k), 8.32 (1H, br. s., $H_{i,3}$), 8.17 (1H, br. s., H_{12}), 7.70 (1H, br. s., H_o), 7.58 (2H, s, H_{13}), 7.20 (12H, d, $J_{b,y|c,x} = 8.3$ Hz, $H_{b,y}$), 7.02–7.14 (18H, m, $H_{c,d,v,w,x}$), 6.98 (2H, d, $J_{e|d} = 8.7$ Hz, H_e), 6.73 (4H, d, $J_{8|7} = 7.0$ Hz, H_8), 6.18 (4H, br. s., H_7), 3.46–4.76 (34H, m,

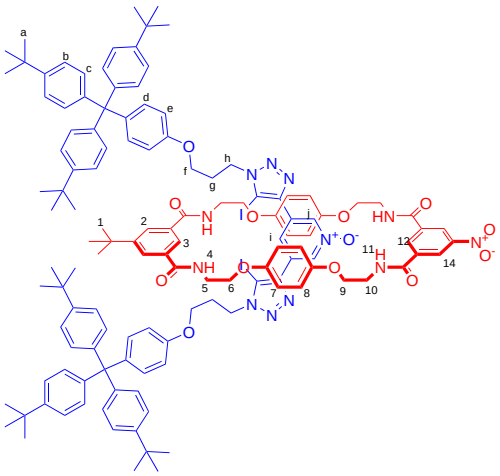
$H_{f,h,l,n,r,s,u,1,5,6,9,10}$), 2.35 (6H, br. s., $H_{g,m,t}$), 1.14–1.40 (63H, m, $H_{a,14}$). ^{13}**C**$\{^{1}$**H**$\}$ **NMR** (101 MHz; $CDCl_3$) δ (ppm): 148.3, 134.0, 132.3, 130.7, 124.1, 117.6, 115.3, 92.8, 77.2, 72.4, 68.1, 34.3, 31.4, 29.7, 15.8 (several peaks were too weak to be detected). ^{31}**P NMR** (162 MHz; $CDCl_3$) δ (ppm):: -144.66 (spt, $J = 714.0$ Hz, PF$_6$). ^{19}**F NMR** (377 MHz; $CDCl_3$) δ (ppm):: -71.63 (d, $J = 714.0$ Hz, PF_6). **HRESI-MS** (pos.): 1407.43347, calc. for $[C_{142}H_{159}I_4N_{19}O_{11}]_2^+ = 1407.43339$.

Bis-stopper propyl iodotriazolyl pyridine-*N*-oxide, 141



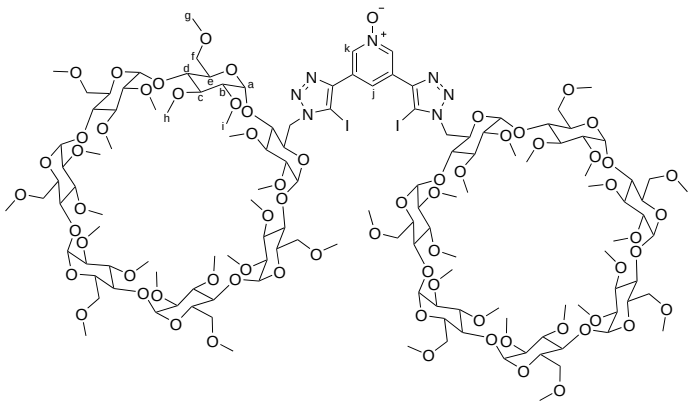
44 (0.10 g, 64 μmol) and $NaHCO_3$ (0.16 g, 1.9 mmol) were dissolved in 1:1 2-butanone:H_2O (13.6 mL). Oxone® (61 mg, 0.19 mmol) in H_2O (sat., 0.5 mL) was added dropwise. The mixture was stirred vigorously for 2 h, and thereafter, NaCl (0.37 g, 6.4 mmol) was added. The product was extracted with $CHCl_3$ (3 $\times$ 40 mL) and the combined organics were dried over $MgSO_4$. The solvent was removed *in vacuo* to afford **141** (0.10 g, quant.) as an off-white powder. ^{1}**H NMR** (400 MHz; $CDCl_3$) δ (ppm): 8.91 (2H, d, $^{4}J_{j|i} = 1.4$ Hz, H_j), 8.57 (1H, s, H_i), 7.23 (12H, d, $J_{b|c} = 8.6$ Hz, H_b), 7.03–7.14 (16H, m, $H_{c,d}$), 6.72–6.83 (4H, m, H_e), 4.69 (4H, t, $J_{h|g} = 7.0$ Hz, H_h), 4.05 (4H, t, $J_{f|g} = 5.6$ Hz, H_f), 2.46 (4H, quin, $J_{g|f,h} = 6.4$ Hz, H_g), 1.29 (54H, s, H_a). ^{13}**C**$\{^{1}$**H**$\}$ **NMR** (101 MHz; $CDCl_3$) δ (ppm): 156.1, 148.4, 144.5, 144.0, 140.2, 136.5, 132.3, 130.7, 129.9, 124.1, 113.0, 63.8, 63.1, 48.3, 36.9, 34.3, 31.4, 29.7, 29.6, 29.5, 7.8. **HRESI-MS** (pos.): 1570.61458, calc. for $[C_{89}H_{101}I_2N_7O_3 \cdot H]^+ = 1570.61280$.

Neutral rotaxane: 3,5-bis-iodotriazole pyridine-*N*-oxide axle with nitro/*tert*-butyl ditopic macrocycle, 142



5-Nitroisophthalic acid (94 mg, 0.44 mmol) was suspended in DCM (3 mL). $(COCl)_2$ (0.25 mL) and DMF (1 drop, cat.) were added and the mixture was refluxed overnight under N_2. The solvent was removed *in vacuo*, and the bis-acid chloride was used immediately assuming quantitative conversion. **141** (50 mg, 32 μmol), **133** (0.25 g, 0.44 mmol) and TBA · Cl (12 mg, 44 μmol) were dissolved in dry DCM (100 mL), and the mixture was stirred for 30 mins at 0 °C under N_2. Et_3N (0.31 mL) was added, followed immediately by the dropwise addition of a solution of 5-nitroisophthalyl dichloride in DCM (2 mL). The mixture was warmed to room temperature and stirred for 3 h. The solvent was removed *in vacuo*, however, the reaction did not afford the desired rotaxane, **142**.

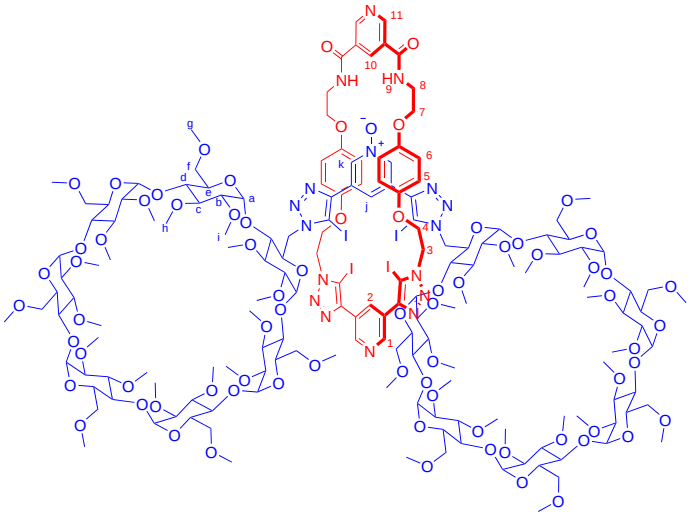
Bis-cyclodextrin-appended-iodotriazole pyridine-*N*-oxide, 143



67 (0.012 g, 3.7 μmol) and $NaHCO_3$ (0.01 g, 110 μmol) were dissolved in 1:1 2-butanone:H_2O (0.8 mL). A saturated solution of Oxone® in H_2O (26 μL) was added dropwise. The solution was stirred vigorously for 2 h. NaCl (0.025 g) was added. The mixture was diluted with H_2O (10 mL) the product

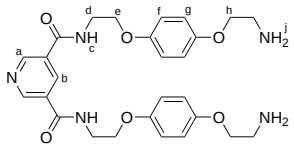
was extracted with $CHCl_3$ (3 × 5 mL). The organics were dried over $MgSO_4$. The solvent was removed *in vacuo* to yield **143** (5.6 mg, 46%). **^{1}H NMR** (500 MHz; $CDCl_3$) δ (ppm): 8.92 (2H, d, $^4J_{k|j} = 0.9$ Hz, H_k), 8.63 (1H, s, H_j), 4.90–5.47 (14H, m, H_a), 2.91–4.08 (204H, m, $H_{b,c,d,e,f,g,h,i}$). **^{13}C{^{1}H} NMR** (126 MHz; $CDCl_3$) δ (ppm): 143.5, 136.3, 130.1, 99.3–98.2, 83.8–79.3, 71.4–70.4, 61.8–58.3, 51.4, 50.7, 29.6. **HRESI-MS** (pos.): 1660.59729, calc. for $[C_{133}H_{221}I_2N_7O_{69} \cdot 2\,Na]^{2+} = 1660.59535$.

N-oxide XB cyclodextrin appended rotaxane, 144



CuI (cat.) and TBTA (cat.) were dissolved in THF (0.27 mL) and covered in foil. **131** (1.0 mg, 1.8 μmol), **143** (5.6 g, 1.8 μmol) and TBA·Cl (cat.) were added and the mixture was stirred for 30 mins. **2** (0.7 mg, 1.8 μmol) was added and the mixture was stirred under N_2 at room temperature for 7 days. The solvent was removed *in vacuo* and the residue was taken up in DCM (10 mL) and washed with NH_4OH (2 × 5 mL) and brine (2 × 5 mL) and dried over $MgSO_4$. The solvent was removed *in vacuo*. However, the reaction did not yield the desired [2]rotaxane **144**.

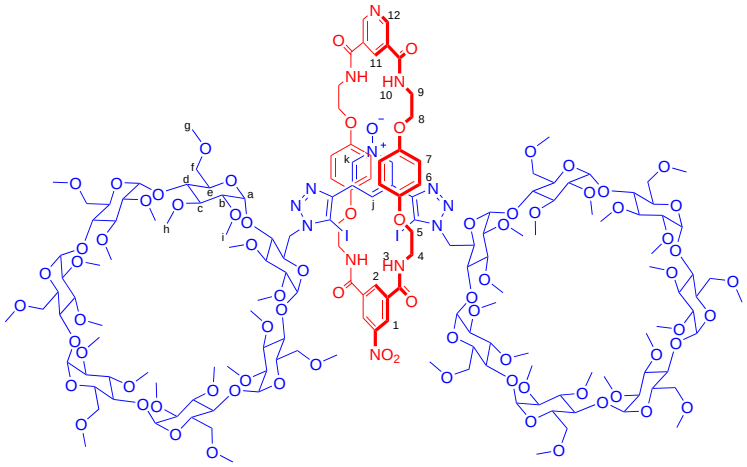
Bis-amine-appended pyridine-bis-amide macrocycle precursor, 145



131 (0.12 g, 0.20 mmol) was dissolved in EtOH (25 mL). Pd/C (10 wt %, 47 mg) was added to the solution and placed under H_2 (5 atm) in a bomb. The mixture was stirred overnight. Thereafter, it was

filtered through Celite®, and the solvent was removed *in vacuo*. The product was used in subsequent reactions without further purification, assuming quantitative yield.

Cyclodextrin-stoppered rotaxane: 3,5-bis-iodotriazole pyridine-*N*-oxide axle with ditopic pyridine bis-amide/nitro-isophthalyl macrocycle, 146



5-Nitroisophthalic acid (12 mg, 52 μmol) was suspended in $SOCl_2$ (2 mL) and a catalytic drop of DMF was added. The mixture was refluxed for 16 h. Thereafter, the excess $SOCl_2$ was removed *in vacuo* and the bis-acid chloride was used immediately in the subsequent step. **143** (17 mg, 5.2 μmol), **145** (27 mg, 52 μmol) and TBACl (1.4 mg, 5.2 μmol) were dissolved in dry DCM (15 mL). The mixture was stirred for 30 mins at 0 °C under N_2. Thereafter, Et_3N (25 μL, 0.18 mmol) was added, followed immediately by 5-nitroisophthalyl dichloride (from the previous step) dissolved in DCM (1 mL) dropwise. The mixture was allowed to warm to room temperature and stirred for 3 h. The solvent was removed *in vacuo* but did not afford **146**.

Chapter 7

References

[1] G. R. Desiraju, *Angew. Chem. Int. Ed. Engl.*, 1995, **34**, 2311–2327.
[2] E. J. Corey, *Pure Appl. Chem.*, 1967, **14**, 19–38.
[3] J.-M. Lehn, *Angew. Chem. Int. Ed. Engl.*, 1988, **27**, 89–112.
[4] C. J. Pedersen, *J. Am. Chem. Soc.*, 1967, **89**, 7017–7036.
[5] J. M. Lehn, *Acc. Chem. Res.*, 1978, **11**, 49–57.
[6] D. J. Cram, *Angew. Chem. Int. Ed. Engl.*, 1986, **25**, 1039–1057.
[7] D. J. Cram, T. Kaneda, R. C. Helgeson and G. M. Lein, *J. Am. Chem. Soc.*, 1979, **101**, 6752–6754.
[8] D. J. Cram, *Angew. Chem. Int. Ed. Engl.*, 1988, **27**, 1009–1020.
[9] C. J. Pedersen, *Angew. Chem. Int. Ed. Engl.*, 1988, **27**, 1021–1027.
[10] C. H. Park and H. E. Simmons, *J. Am. Chem. Soc.*, 1968, **90**, 2431–2432.
[11] J. L. Sessler, P. Gale and W.-S. Cho, *Anion Receptor Chemistry*, The Royal Society of Chemistry, 2006, pp. i–414.
[12] K. S. Chichak, S. J. Cantrill, A. R. Pease, S.-H. Chiu, G. W. V. Cave, J. L. Atwood and J. F. Stoddart, *Science*, 2004, **304**, 1308–1312.
[13] J.-F. Ayme, J. E. Beves, D. A. Leigh, R. T. McBurney, K. Rissanen and D. Schultz, *J. Am. Chem. Soc.*, 2012, **134**, 9488–9497.
[14] J.-F. Ayme, J. E. Beves, D. A. Leigh, R. T. McBurney, K. Rissanen and D. Schultz, *Nat Chem*, 2012, **4**, 15–20.
[15] E. Fischer, *Ber. Dtsch. Chem. Ges.*, 1894, **27**, 2985–2993.
[16] D. E. Koshland, *Proc. Natl. Acad. Sci. U. S. A.*, 1958, **44**, 98–104.
[17] D. E. Koshland, *Angew. Chem. Int. Ed. Engl.*, 1995, **33**, 2375–2378.
[18] C. A. Hunter and H. L. Anderson, *Angew. Chem. Int. Ed. Engl.*, 2009, **48**, 7488–7499.
[19] J. D. Badjić, A. Nelson, S. J. Cantrill, W. B. Turnbull and J. F. Stoddart, *Acc. Chem. Res.*, 2005, **38**, 723–732.
[20] A. Martell, R. Hancock and R. Motekaitis, *Coord. Chem. Rev.*, 1994, **133**, 39–65.
[21] Y. Li and A. H. Flood, *Angew. Chem. Int. Ed. Engl.*, 2008, **47**, 2649–2652.
[22] D. K. Cabbiness and D. W. Margerum, *J. Am. Chem. Soc.*, 1969, **91**, 6540–6541.
[23] P. Atkins and J. de Paula, *Atkins' Physical Chemistry*, OUP Oxford, 2010.
[24] H.-J. Schneider, *Angew. Chem. Int. Ed. Engl.*, 2009, **48**, 3924–3977.
[25] J. W. Steed and J. L. Atwood, *Supramolecular chemistry*, New York : John Wiley, New York, 2000, pp. 223–284.
[26] E. Arunan, G. R. Desiraju, R. A. Klein, J. Sadlej, S. Scheiner, I. Alkorta, D. C. Clary, R. H. Crabtree, J. J. Dannenberg, P. Hobza, H. G. Kjaergaard, A. C. Legon, B. Mennucci and D. J. Nesbitt, *Pure Appl. Chem.*, 2011, **83**, 1637–1641.
[27] G. A. Jeffrey, *An introduction to hydrogen bonding*, Oxford : Oxford University Press, Oxford, 1997, pp. 1–303.
[28] G. R. Desiraju, P. S. Ho, L. Kloo, A. C. Legon, R. Marquardt, P. Metrangolo, P. Politzer, G. Resnati and K. Rissanen, *Pure Appl. Chem.*, 2013, **85**, 1711–1713.
[29] T. Clark, M. Hennemann, J. S. Murray and P. Politzer, *J Mol Model*, 2007, **13**, 291–296.
[30] P. Metrangolo, H. Neukirch, T. Pilati and G. Resnati, *Acc. Chem. Res.*, 2005, **38**, 386–395.
[31] P. Metrangolo, F. Meyer, T. Pilati, G. Resnati and G. Terraneo, *Angew. Chem. Int. Ed. Engl.*, 2008, **47**, 6114–6127.
[32] C. A. Hunter and J. K. M. Sanders, *J. Am. Chem. Soc.*, 1990, **112**, 5525–5534.
[33] S. Burley and G. Petsko, *Science*, 1985, **229**, 23–28.
[34] S. Grimme, *Angew. Chem. Int. Ed. Engl.*, 2008, **47**, 3430–3434.
[35] C. R. Martinez and B. L. Iverson, *Chem. Sci.*, 2012, **3**, 2191–2201.
[36] J. W. G. Bloom and S. E. Wheeler, *Angew. Chem. Int. Ed.*, 2011, **50**, 7847–7849.
[37] S. E. Wheeler and K. N. Houk, *J. Am. Chem. Soc.*, 2008, **130**, 10854–10855.
[38] S. E. Wheeler, *J. Am. Chem. Soc.*, 2011, **133**, 10262–10274.
[39] M. S. Cubberley and B. L. Iverson, *J. Am. Chem. Soc.*, 2001, **123**, 7560–7563.
[40] W. R. Carroll, P. Pellechia and K. D. Shimizu, *Org. Lett.*, 2008, **10**, 3547–3550.
[41] W. Blokzijl and J. B. F. N. Engberts, *Angew. Chem. Int. Ed. Engl.*, 1993, **32**, 1545–1579.
[42] Y. S. Djikaev and E. Ruckenstein, *J. Phys. Chem. B*, 2012, **116**, 2820–2830.
[43] I. A. Sedov, M. A. Stolov and B. N. Solomonov, *J. Phys. Org. Chem.*, 2011, **24**, 1088–1094.
[44] F. Biedermann, W. M. Nau and H.-J. Schneider, *Angew. Chem. Int. Ed.*, 2014, **53**, 11158–11171.
[45] M. J. Langton, C. J. Serpell and P. D. Beer, *Angew. Chem. Int. Ed.*, 2016, **55**, 1974–1987.
[46] J. C. Ma and D. A. Dougherty, *Chem. Rev.*, 1997, **97**, 1303–1324.
[47] G. W. Gokel, L. J. Barbour, R. Ferdani and J. Hu, *Acc. Chem. Res.*, 2002, **35**, 878–886.
[48] L. M. Salonen, C. Bucher, D. W. Banner, W. Haap, J.-L. Mary, J. Benz, O. Kuster, P. Seiler, W. B. Schweizer and F. Diederich, *Angew. Chem. Int. Ed. Engl.*, 2009, **48**, 811–814.
[49] L. M. Salonen, M. Ellermann and F. Diederich, *Angew. Chem. Int. Ed.*, 2011, **50**, 4808–4842.
[50] B. L. Schottel, H. T. Chifotides and K. R. Dunbar, *Chem. Soc. Rev.*, 2008, **37**, 68–83.
[51] T. J. Mooibroek, C. A. Black, P. Gamez and J. Reedijk, *Cryst. Growth Des.*, 2008, **8**, 1082–1093.
[52] D. Quiñonero, C. Garau, C. Rotger, A. Frontera, P. Ballester, A. Costa and P. M. Deyà, *Angew. Chem. Int. Ed. Engl.*, 2002, **41**, 3389–3392.
[53] Y. S. Rosokha, S. V. Lindeman, S. V. Rosokha and J. K. Kochi, *Angew. Chem. Int. Ed. Engl.*, 2004, **43**, 4650–4652.
[54] G. Gil-Ramírez, E. C. Escudero-Adán, J. Benet-Buchholz and P. Ballester, *Angew. Chem. Int. Ed. Engl.*, 2008, **47**, 4114–4118.
[55] D.-X. Wang, Q.-Y. Zheng, Q.-Q. Wang and M.-X. Wang, *Angew. Chem. Int. Ed. Engl.*, 2008, **47**, 7485–7488.

[56] O. B. Berryman and D. W. Johnson, *Chem. Commun.*, 2009, 3143–3153.
[57] H. T. Chifotides, B. L. Schottel and K. R. Dunbar, *Angew. Chem. Int. Ed. Engl.*, 2010, **49**, 7202–7207.
[58] J. Mareda and S. Matile, *Chem. Eur. J.*, 2009, **15**, 28–37.
[59] F. Inokuchi, Y. Miyahara, T. Inazu and S. Shinkai, *Angew. Chem. Int. Ed. Engl.*, 1995, **34**, 1364–1366.
[60] Q.-F. Sun, J. Iwasa, D. Ogawa, Y. Ishido, S. Sato, T. Ozeki, Y. Sei, K. Yamaguchi and M. Fujita, *Science*, 2010, **328**, 1144–1147.
[61] K. Harris, D. Fujita and M. Fujita, *Chem. Commun.*, 2013, **49**, 6703–6712.
[62] J. M. Berg, J. L. Tymoczko, G. J. Gatto and L. Stryer, *Biochemistry*, New York : W. H. Freeman & Company, 2015, pp. 1–1056.
[63] P. Chakrabarti, *J. Mol. Biol.*, 1993, **234**, 463–482.
[64] V. L. Katch, W. D. McArdle and F. I. Katch, *Essentials of exercise physiology*, London : Lippincott Williams & Wilkins, London, 2011, pp. 1–699.
[65] S. Ebihara, K. Shirato, N. Harata and N. Akaike, *J. Physiol.*, 1995, **484**, 77–86.
[66] M. Anderson, R. Gregory, S. Thompson, D. Souza, S. Paul, R. Mulligan, A. Smith and M. Welsh, *Science*, 1991, **253**, 202–205.
[67] C. Hartzell, I. Putzier and J. Arreola, *Annu. Rev. Physiol.*, 2005, **67**, 719–758.
[68] O. Devuyst, P. T. Christie, P. J. Courtoy, R. Beauwens and R. V. Thakker, *Hum. Mol. Genet.*, 1999, **8**, 247–257.
[69] R. Shannon, *Acta Crystallogr. Sect. A*, 1976, **32**, 751–767.
[70] P. Beer, P. Gale and D. Smith, *Supramolecular Chemistry*, Oxford University Press, 1999.
[71] C. Caltagirone, G. W. Bates, P. A. Gale and M. E. Light, *Chem. Commun.*, 2008, 61–63.
[72] A. Albert, R. Goldacre and J. Phillips, *J. Chem. Soc.*, 1948, 2240–2249.
[73] S. Goldman and R. G. Bates, *J. Am. Chem. Soc.*, 1972, **94**, 1476–1484.
[74] F. Hofmeister, *Arch. Exp. Pathol. Pharmacol.*, 1888, **24**, 247–260.
[75] J. L. Cook, C. A. Hunter, C. M. Low, A. Perez-Velasco and J. G. Vinter, *Angew. Chem. Int. Ed. Engl.*, 2008, **47**, 6275–6277.
[76] S. Kubik, *Chem. Soc. Rev.*, 2010, **39**, 3648–3663.
[77] H. Luecke and F. A. Quiocho, *Nature*, 1990, **347**, 402–406.
[78] J. W. Pflugrath and F. A. Quiocho, *Nature*, 1985, **314**, 257–260.
[79] A. Fürstner, *Angew. Chem. Int. Ed. Engl.*, 2003, **42**, 3582–3603.
[80] J. L. Seganish and J. T. Davis, *Chem. Commun.*, 2005, 5781–5783.
[81] J. T. Davis, O. Okunola and R. Quesada, *Chem. Soc. Rev.*, 2010, **39**, 3843–3862.
[82] R. A. Pascal Jr., J. Spergel and D. Van Engen, *Tetrahedron Lett.*, 1986, **27**, 4099–4102.
[83] K. Kavallieratos, S. R. de Gala, D. J. Austin and R. H. Crabtree, *J. Am. Chem. Soc.*, 1997, **119**, 2325–2326.
[84] M. J. Chmielewski and J. Jurczak, *Chem. Eur. J.*, 2005, **11**, 6080–6094.
[85] M. J. J. Chmielewski and J. Jurczak, *Chem. Eur. J.*, 2006, **12**, 7652–7667.
[86] A. P. Bisson, V. M. Lynch, M.-K. C. Monahan and E. V. Anslyn, *Angew. Chem. Int. Ed. Engl.*, 1997, **36**, 2340–2342.
[87] S. O. Kang, J. M. Llinares, D. Powell, D. VanderVelde and K. Bowman-James, *J. Am. Chem. Soc.*, 2003, **125**, 10152–10153.
[88] S. O. Kang, D. VanderVelde, D. Powell and K. Bowman-James, *J. Am. Chem. Soc.*, 2004, **126**, 12272–12273.
[89] S. O. Kang, V. W. Day and K. Bowman-James, *Org. Lett.*, 2009, **11**, 3654–3657.
[90] S. Kubik, R. Kirchner, D. Nolting and J. Seidel, *J. Am. Chem. Soc.*, 2002, **124**, 12752–12760.
[91] V. Amendola, D. Esteban-Gmez, L. Fabbrizzi and M. Licchelli, *Acc. Chem. Res.*, 2006, **39**, 343–353.
[92] T. Zieliński and J. Jurczak, *Tetrahedron*, 2005, **61**, 4081–4089.
[93] M. P. Hughes and B. D. Smith, *J. Org. Chem.*, 1997, **62**, 4492–4499.
[94] S. Valiyaveettil, J. F. J. Engbersen, W. Verboom and D. N. Reinhoudt, *Angew. Chem. Int. Ed. Engl.*, 1993, **32**, 900–901.
[95] K. Kavallieratos, C. M. Bertao and R. H. Crabtree, *J. Org. Chem.*, 1999, **64**, 1675–1683.
[96] K. Kavallieratos, A. Danby, G. J. Van Berkel, M. A. Kelly, R. A. Sachleben, B. A. Moyer and K. Bowman-James, *Anal. Chem.*, 2000, **72**, 5258–5264.
[97] J. M. Boon and B. D. Smith, *J. Am. Chem. Soc.*, 1999, **121**, 11924–11925.
[98] J. M. Boon and B. D. Smith, *J. Am. Chem. Soc.*, 2001, **123**, 6221–6226.
[99] J. M. Boon, T. N. Lambert, B. D. Smith, A. M. Beatty, V. Ugrinova and S. N. Brown, *J. Org. Chem.*, 2002, **67**, 2168–2174.
[100] J. M. Boon, R. Shukla, B. D. Smith, G. Licini and P. Scrimin, *Chem. Commun.*, 2002, 260–261.
[101] B. D. Smith and T. N. Lambert, *Chem. Commun.*, 2003, 2261–2268.
[102] P. J. Smith, M. V. Reddington and C. S. Wilcox, *Tetrahedron Lett.*, 1992, **33**, 6085–6088.
[103] M. Boiocchi, L. Del Boca, D. E. Gómez, L. Fabbrizzi, M. Licchelli and E. Monzani, *J. Am. Chem. Soc.*, 2004, **126**, 16507–16514.
[104] S. J. Brooks, P. A. Gale and M. E. Light, *Chem. Commun.*, 2005, 4696–4698.
[105] I. Ravikumar, P. S. Lakshminarayanan, M. Arunachalam, E. Suresh and P. Ghosh, *Dalton Trans.*, 2009, 4160–4168.
[106] D. A. Jose, D. K. Kumar, B. Ganguly and A. Das, *Inorg. Chem.*, 2007, **46**, 5817–5819.
[107] D. Meshcheryakov, F. Arnaud-Neu, V. Böhmer, M. Bolte, J. Cavaleri, V. Hubscher-Bruder, I. Thondorf and S. Werner, *Org. Biomol. Chem.*, 2008, **6**, 3244–3255.
[108] G. V. Oshovsky, W. Verboom, R. H. Fokkens and D. N. Reinhoudt, *Chem. Eur. J.*, 2004, **10**, 2739–2748.

[109] Y. Zhang, R. Zhang, Y. Zhao, L. Ji, C. Jia and B. Wu, *New J. Chem.*, 2013, **37**, 2266–2270.
[110] C. Jia, B. Wu, S. Li, Z. Yang, Q. Zhao, J. Liang, Q.-S. Li and X.-J. Yang, *Chem. Commun.*, 2010, **46**, 5376–5378.
[111] P. A. Gale, J. L. Sessler, V. Král and V. Lynch, *J. Am. Chem. Soc.*, 1996, **118**, 5140–5141.
[112] P. A. Gale, *Chem. Commun.*, 2008, 4525–4540.
[113] D.-W. Yoon, D. Gross, V. Lynch, J. Sessler, B. Hay and C.-H. Lee, *Angew. Chem. Int. Ed. Engl.*, 2008, **47**, 5038–5042.
[114] B. Turner, M. Botoshansky and Y. Eichen, *Angew. Chem. Int. Ed. Engl.*, 1998, **37**, 2475–2478.
[115] I. E. D. Vega, S. Camiolo, P. A. Gale, M. B. Hursthouse and M. E. Light, *Chem. Commun.*, 2003, 1686–1687.
[116] J. L. Sessler, D.-G. Cho and V. Lynch, *J. Am. Chem. Soc.*, 2006, **128**, 16518–16519.
[117] M. Yu, H. Lin and H. Lin, *Supramol. Chem.*, 2008, **20**, 357–361.
[118] K.-J. Chang, B.-N. Kang, M.-H. Lee and K.-S. Jeong, *J. Am. Chem. Soc.*, 2005, **127**, 12214–12215.
[119] J.-m. Suk and K.-S. Jeong, *J. Am. Chem. Soc.*, 2008, **130**, 11868–11869.
[120] K.-J. Chang, D. Moon, M. S. Lah and K.-S. Jeong, *Angew. Chem. Int. Ed. Engl.*, 2005, **44**, 7926–7929.
[121] N.-K. Kim, K.-J. Chang, D. Moon, M. S. Lah and K.-S. Jeong, *Chem. Commun.*, 2007, 3401–3403.
[122] W. B. Farnham, D. C. Roe, D. A. Dixon, J. C. Calabrese and R. L. Harlow, *J. Am. Chem. Soc.*, 1990, **112**, 7707–7718.
[123] S. S. Zhu, H. Staats, K. Brandhorst, J. Grunenberg, F. Gruppi, E. Dalcanale, A. Lützen, K. Rissanen and C. A. Schalley, *Angew. Chem. Int. Ed. Engl.*, 2008, **47**, 788–792.
[124] J. Svec, M. Necas and V. Sindelar, *Angew. Chem. Int. Ed.*, 2010, **49**, 2378–2381.
[125] M. A. Yawer, V. Havel and V. Sindelar, *Angew. Chem. Int. Ed.*, 2015, **54**, 276–279.
[126] R. Meudtner and S. Hecht, *Angew. Chem. Int. Ed. Engl.*, 2008, **47**, 4926–4930.
[127] H. Juwarker, J. Lenhardt, D. Pham and S. Craig, *Angew. Chem. Int. Ed. Engl.*, 2008, **47**, 3740–3743.
[128] Y. Li and A. H. Flood, *J. Am. Chem. Soc.*, 2008, **130**, 12111–12122.
[129] S. Lee, C.-H. Chen and A. H. Flood, *Nat Chem*, 2013, **5**, 704–710.
[130] E. Graf and J. M. Lehn, *J. Am. Chem. Soc.*, 1975, **97**, 5022–5024.
[131] E. Graf and J. M. Lehn, *J. Am. Chem. Soc.*, 1976, **98**, 6403–6405.
[132] J. P. Kintzinger, J. M. Lehn, E. Kauffmann, J. L. Dye and A. I. Popov, *J. Am. Chem. Soc.*, 1983, **105**, 7549–7553.
[133] B. Dietrich, J. Guilhem, J.-M. Lehn, C. Pascard and E. Sonveaux, *Helv. Chim. Acta*, 1984, **67**, 91–104.
[134] J. M. Lehn, E. Sonveaux and A. K. Willard, *J. Am. Chem. Soc.*, 1978, **100**, 4914–4916.
[135] B. Dietrich, J.-M. Lehn, J. Guilhem and C. Pascard, *Tetrahedron Lett.*, 1989, **30**, 4125–4128.
[136] B. Dietrich, B. Dilworth, J.-M. Lehn, J.-P. Souchez, M. Cesario, J. Guilhem and C. Pascard, *Helv. Chim. Acta*, 1996, **79**, 569–587.
[137] S. D. Reilly, G. R. K. Khalsa, D. K. Ford, J. R. Brainard, B. P. Hay and P. H. Smith, *Inorg. Chem.*, 1995, **34**, 569–575.
[138] M. W. Hosseini and J. M. Lehn, *J. Am. Chem. Soc.*, 1982, **104**, 3525–3527.
[139] F. P. Schmidtchen, *Angew. Chem. Int. Ed. Engl.*, 1977, **16**, 720–721.
[140] W. J. Belcher, M. Fabre, T. Farhan and J. W. Steed, *Org. Biomol. Chem.*, 2006, **4**, 781–786.
[141] S. Shinoda, M. Tadokoro, H. Tsukube, S. Shinoda and R. Arakawa, *Chem. Commun.*, 1998, 181–182.
[142] P. A. Gale, *Coord. Chem. Rev.*, 2000, **199**, 181–233.
[143] D. W. Christianson and W. N. Lipscomb, *Acc. Chem. Res.*, 1989, **22**, 62–69.
[144] T. H. Wirth and N. Davidson, *J. Am. Chem. Soc.*, 1964, **86**, 4325–4329.
[145] B. Dietrich, T. M. Fyles, J.-M. Lehn, L. G. Pease and D. L. Fyles, *J. Chem. Soc., Chem. Commun.*, 1978, 934–936.
[146] B. Dietrich, D. L. Fyles, T. M. Fyles and J.-M. Lehn, *Helv. Chim. Acta*, 1979, **62**, 2763–2787.
[147] E. Fan, S. A. Van Arman, S. Kincaid and A. D. Hamilton, *J. Am. Chem. Soc.*, 1993, **115**, 369–370.
[148] A. Metzger, V. M. Lynch and E. V. Anslyn, *Angew. Chem. Int. Ed. Engl.*, 1997, **36**, 862–865.
[149] G. Müller, J. Riede and F. P. Schmidtchen, *Angew. Chem. Int. Ed. Engl.*, 1988, **27**, 1516–1518.
[150] M. Berger and F. P. Schmidtchen, *J. Am. Chem. Soc.*, 1999, **121**, 9986–9993.
[151] S. Camiolo, P. A. Gale, M. I. Ogden, B. W. Skelton and A. H. White, *J. Chem. Soc., Perkin Trans. 2*, 2001, 1294–1298.
[152] K. Sato, S. Arai and T. Yamagishi, *Tetrahedron Lett.*, 1999, **40**, 5219–5222.
[153] E. Alcalde, N. Mesquida, L. Perez-Garcia, C. Alvarez-Rua, S. Garcia-Granda and E. Garcia-Rodriguez, *Chem. Commun.*, 1999, 295–296.
[154] H.-Y. Gong, B. M. Rambo, E. Karnas, V. M. Lynch and J. L. Sessler, *Nat Chem*, 2010, **2**, 406–409.
[155] H. Kim, S. In and J. Kang, *Supramol. Chem.*, 2006, **18**, 141–145.
[156] A. Kumar and P. S. Pandey, *Org. Lett.*, 2008, **10**, 165–168.
[157] B. Schulze, C. Friebe, M. D. Hager, W. Günther, U. Köhn, B. O. Jahn, H. Görls and U. S. Schubert, *Org. Lett.*, 2010, **12**, 2710–2713.
[158] N. G. White, S. Carvalho, V. Felix and P. D. Beer, *Org. Biomol. Chem.*, 2012, **10**, 6951–6959.
[159] T. W. Hudnall, C.-W. Chiu and F. P. Gabbaï, *Acc. Chem. Res.*, 2009, **42**, 388–397.
[160] M. Newcomb, J. H. Horner and M. T. Blanda, *J. Am. Chem. Soc.*, 1987, **109**, 7878–7879.
[161] T. J. Wedge and M. Hawthorne, *Coord. Chem. Rev.*, 2003, **240**, 111–128.
[162] E. J. O'Neil and B. D. Smith, *Coord. Chem. Rev.*, 2006, **250**, 3068–3080.
[163] R. Vilar, *Eur. J. Inorg. Chem.*, 2008, **2008**, 357–367.
[164] M. Melaimi and F. P. Gabbaï, *J. Am. Chem. Soc.*, 2005, **127**, 9680–9681.
[165] J. V. Carolan, S. J. Butler and K. A. Jolliffe, *J. Org. Chem.*, 2009, **74**, 2992–2996.
[166] L. Fabbrizzi, A. Leone and A. Taglietti, *Angew. Chem. Int. Ed.*, 2001, **40**, 3066–3069.
[167] S. L. Wiskur, H. Ait-Haddou, J. J. Lavigne and E. V. Anslyn, *Acc. Chem. Res.*, 2001, **34**, 963–972.

[168] X. Lou, D. Ou, Q. Li and Z. Li, *Chem. Commun.*, 2012, **48**, 8462–8477.
[169] J. Du, M. Hu, J. Fan and X. Peng, *Chem. Soc. Rev.*, 2012, **41**, 4511–4535.
[170] D.-G. Cho, J. H. Kim and J. L. Sessler, *J. Am. Chem. Soc.*, 2008, **130**, 12163–12167.
[171] Y. Willener, K. M. Joly, C. J. Moody and J. H. R. Tucker, *J. Org. Chem.*, 2008, **73**, 1225–1233.
[172] P. D. Beer and A. D. Keefe, *J. Organomet. Chem.*, 1989, **375**, C40–C42.
[173] P. D. Beer, D. Hesek, J. Hodacova and S. E. Stokes, *J. Chem. Soc., Chem. Commun.*, 1992, 270–272.
[174] P. D. Beer and E. J. Hayes, *Coord. Chem. Rev.*, 2003, **240**, 167–189.
[175] M. J. Langton and P. D. Beer, *Acc. Chem. Res.*, 2014, **47**, 1935–1949.
[176] C. Bejger, J. S. Park, E. S. Silver and J. L. Sessler, *Chem. Commun.*, 2010, **46**, 7745–7747.
[177] K. A. Nielsen, J. O. Jeppesen, E. Levillain and J. Becher, *Angew. Chem. Int. Ed. Engl.*, 2003, **42**, 187–191.
[178] M. E. Huston, E. U. Akkaya and A. W. Czarnik, *J. Am. Chem. Soc.*, 1989, **111**, 8735–8737.
[179] H. Miyaji, W. Sato and J. L. Sessler, *Angew. Chem. Int. Ed. Engl.*, 2000, **39**, 1777–1780.
[180] J. K. Day, C. Bresner, N. D. Coombs, I. A. Fallis, L.-L. Ooi and S. Aldridge, *Inorg. Chem.*, 2008, **47**, 793–804.
[181] A. E. Broomsgrove, D. Addy, C. Bresner, I. Fallis, A. Thompson and S. Aldridge, *Chem. Eur. J.*, 2008, **14**, 7525–7529.
[182] N. Busschaert, P. A. Gale, C. J. E. Haynes, M. E. Light, S. J. Moore, C. C. Tong, J. T. Davis and W. A. Harrell, Jr., *Chem. Commun.*, 2010, **46**, 6252–6254.
[183] N. Busschaert, M. Wenzel, M. E. Light, P. Iglesias-Hernández, R. Pérez-Tomás and P. A. Gale, *J. Am. Chem. Soc.*, 2011, **133**, 14136–14148.
[184] A. Hennig, L. Fischer, G. Guichard and S. Matile, *J. Am. Chem. Soc.*, 2009, **131**, 16889–16895.
[185] M. W. Hosseini, J. M. Lehn, K. C. Jones, K. E. Plute, K. B. Mertes and M. P. Mertes, *J. Am. Chem. Soc.*, 1989, **111**, 6330–6335.
[186] J. W. Steed, *Chem. Soc. Rev.*, 2010, **39**, 3686–3699.
[187] J. A. Foster, P.-O. M., G. O. Lloyd, N. Clarke, H. A. K. and J. W. Steed, *Nat Chem*, 2010, **2**, 1037–1043.
[188] L. C. Gilday, S. W. Robinson, T. A. Barendt, M. J. Langton, B. R. Mullaney and P. D. Beer, *Chem. Rev.*, 2015, **115**, 7118–7195.
[189] M. Colin, *Ann. Chim.*, 1814, **91**, 252–272.
[190] F. Guthrie, *J. Chem. Soc.*, 1863, **16**, 239–244.
[191] J.-M. Dumas, M. Gomel and M. Guerin, in *Molecular interactions involving organic halides*, John Wiley & Sons, Ltd., 1983, pp. 985–1020.
[192] P. Groth, O. Hassel, T. Terho, U.-M. Kantonen and L. Nilsson, *Acta Chem. Scand.*, 1964, **18**, 402–408.
[193] O. Hassel, *Science*, 1970, **170**, 497–502.
[194] H. A. Benesi and J. H. Hildebrand, *J. Am. Chem. Soc.*, 1949, **71**, 2703–2707.
[195] R. S. Mulliken, *J. Am. Chem. Soc.*, 1950, **72**, 600–608.
[196] C. Laurence, M. Queignec-Cabanetos, T. Dziembowska, R. Queignec and B. Wojtkowiak, *J. Am. Chem. Soc.*, 1981, **103**, 2567–2573.
[197] A. C. Legon, *Angew. Chem. Int. Ed. Engl.*, 1999, **38**, 2686–2714.
[198] P. Metrangolo, G. Resnati, T. Pilati and S. Biella, in *Structure and Bonding*, ed. P. Metrangolo and G. Resnati, Springer Berlin Heidelberg, 2008, vol. 126, pp. 105–136.
[199] P. Metrangolo and G. Resnati, *Chem. Eur. J.*, 2001, **7**, 2511–2519.
[200] P. Metrangolo, G. Resnati, T. Pilati, R. Liantonio and F. Meyer, *J. Polym. Sci. A Polym. Chem.*, 2007, **45**, 1–15.
[201] F. Meyer and P. Dubois, *CrystEngComm*, 2013, **15**, 3058–3071.
[202] A. Priimagi, G. Cavallo, P. Metrangolo and G. Resnati, *Acc. Chem. Res.*, 2013, **46**, 2686–2695.
[203] R. Bertani, P. Metrangolo, A. Moiana, E. Perez, T. Pilati, G. Resnati, I. Rico-Lattes and A. Sassi, *Adv. Mater.*, 2002, **14**, 1197–1201.
[204] D. W. Bruce, P. Metrangolo, F. Meyer, C. Präsang, G. Resnati, G. Terraneo and A. C. Whitwood, *New J. Chem.*, 2008, **32**, 477–482.
[205] P. Metrangolo, C. Präsang, G. Resnati, R. Liantonio, A. C. Whitwood and D. W. Bruce, *Chem. Commun.*, 2006, 3290–3292.
[206] H. L. Nguyen, P. N. Horton, M. B. Hursthouse, A. C. Legon and D. W. Bruce, *J. Am. Chem. Soc.*, 2004, **126**, 16–17.
[207] C. Präsang, H. L. Nguyen, P. N. Horton, A. C. Whitwood and D. W. Bruce, *Chem. Commun.*, 2008, 6164–6166.
[208] C. Präsang, A. C. Whitwood and D. W. Bruce, *Cryst. Growth Des.*, 2009, **9**, 5319–5326.
[209] L. C. Roper, C. Präsang, V. N. Kozhevnikov, A. C. Whitwood, P. B. Karadakov and D. W. Bruce, *Cryst. Growth Des.*, 2010, **10**, 3710–3720.
[210] J. Xu, X. Liu, T. Lin, J. Huang and C. He, *Macromolecules*, 2005, **38**, 3554–3557.
[211] J. Xu, X. Liu, J. K.-P. Ng, T. Lin and C. He, *J. Mater. Chem.*, 2006, **16**, 3540–3545.
[212] F. F. Awwadi, S. F. Haddad, M. M. Turnbull, C. P. Landee and R. D. Willett, *CrystEngComm*, 2013, **15**, 3111–3118.
[213] J. M. Clemente-Juan, E. Coronado, G. Minguez Espallargas, H. Adams and L. Brammer, *CrystEngComm*, 2010, **12**, 2339–2342.
[214] G. M. Espallargas, A. Recuenco, F. M. Romero, L. Brammer and S. Libri, *CrystEngComm*, 2012, **14**, 6381–6383.
[215] M. Fourmigué, in *Structure and Bonding*, ed. P. Metrangolo and G. Resnati, Springer Berlin Heidelberg, 2008, vol. 126, pp. 181–207.
[216] M. Fourmigué and P. Batail, *Chem. Rev.*, 2004, **104**, 5379–5418.
[217] P. Metrangolo and G. Resnati, *Science*, 2008, **321**, 918–919.

[218] K.-S. Shin, M. Brezgunova, O. Jeannin, T. Roisnel, F. Camerel, P. Auban-Senzier and M. Fourmigué, *Cryst. Growth Des.*, 2011, **11**, 5337–5345.
[219] J. A. R. P. Sarma, F. H. Allen, V. J. Hoy, J. A. K. Howard, R. Thaimattam, K. Biradha and G. R. Desiraju, *Chem. Commun.*, 1997, 101–102.
[220] E. Cariati, G. Cavallo, A. Forni, G. Leem, P. Metrangolo, F. Meyer, T. Pilati, G. Resnati, S. Righetto, G. Terraneo and E. Tordin, *Cryst. Growth Des.*, 2011, **11**, 5642–5648.
[221] E. Cariati, A. Forni, S. Biella, P. Metrangolo, F. Meyer, G. Resnati, S. Righetto, E. Tordin and R. Ugo, *Chem. Commun.*, 2007, 2590–2592.
[222] J. Hulliger and P. J. Langley, *Chem. Commun.*, 1998, 2557–2558.
[223] P. K. Thallapally, G. R. Desiraju, M. Bagieu-Beucher, R. Masse, C. Bourgogne and J.-F. Nicoud, *Chem. Commun.*, 2002, 1052–1053.
[224] P. Metrangolo, F. Meyer, T. Pilati, G. Resnati and G. Terraneo, *Chem. Commun.*, 2008, 1635–1637.
[225] K. Rissanen, *CrystEngComm*, 2008, **10**, 1107–1113.
[226] L. Meazza, J. A. Foster, K. Fucke, P. Metrangolo, G. Resnati and J. W. Steed, *Nat Chem*, 2013, **5**, 42–47.
[227] A. Priimagi, G. Cavallo, A. Forni, M. Gorynsztejn-Leben, M. Kaivola, P. Metrangolo, R. Milani, A. Shishido, T. Pilati, G. Resnati and G. Terraneo, *Adv. Funct. Mater.*, 2012, **22**, 2572–2579.
[228] A. Priimagi, M. Saccone, G. Cavallo, A. Shishido, T. Pilati, P. Metrangolo and G. Resnati, *Adv. Mater.*, 2012, **24**, OP345–OP352.
[229] T. Caronna, R. Liantonio, T. A. Logothetis, P. Metrangolo, T. Pilati and G. Resnati, *J. Am. Chem. Soc.*, 2004, **126**, 4500–4501.
[230] G. Marras, P. Metrangolo, F. Meyer, T. Pilati, G. Resnati and A. Vij, *New J. Chem.*, 2006, **30**, 1397–1402.
[231] J. Martí-Rujas, L. Meazza, G. K. Lim, G. Terraneo, T. Pilati, K. D. M. Harris, P. Metrangolo and G. Resnati, *Angew. Chem. Int. Ed.*, 2013, **52**, 13444–13448.
[232] L. Meazza, J. Marti-Rujas, G. Terraneo, C. Castiglioni, A. Milani, T. Pilati, P. Metrangolo and G. Resnati, *CrystEng-Comm*, 2011, **13**, 4427–4435.
[233] A. Sun, J. W. Lauher and N. S. Goroff, *Science*, 2006, **312**, 1030–1034.
[234] S. P. Bew, S. A. Fairhurst, D. L. Hughes, L. Legentil, J. Liddle, P. Pesce, S. Nigudkar and M. A. Wilson, *Org. Lett.*, 2009, **11**, 4552–4555.
[235] A. Bruckmann, M. A. Pena and C. Bolm, *Synlett*, 2008, **2008**, 900–902.
[236] O. Coulembier, F. Meyer and P. Dubois, *Polym. Chem.*, 2010, **1**, 434–437.
[237] R. N. Haszeldine and J. Jander, *J. Chem. Soc.*, 1953, 4172–4173.
[238] S. Dordonne, B. Crousse, D. Bonnet-Delpon and J. Legros, *Chem. Commun.*, 2011, **47**, 5855–5857.
[239] A. P. Dove, R. C. Pratt, B. G. G. Lohmeijer, R. M. Waymouth and J. L. Hedrick, *J. Am. Chem. Soc.*, 2005, **127**, 13798–13799.
[240] S. H. Jungbauer, S. Schindler, F. Kniep, S. M. Walter, L. Rout and S. M. Huber, *Synlett*, 2013, **24**, 2624–2628.
[241] S. H. Jungbauer, S. M. Walter, S. Schindler, L. Rout, F. Kniep and S. M. Huber, *Chem. Commun.*, 2014, **50**, 6281–6284.
[242] F. Kniep, S. H. Jungbauer, Q. Zhang, S. M. Walter, S. Schindler, I. Schnapperelle, E. Herdtweck and S. M. Huber, *Angew. Chem. Int. Ed.*, 2013, **52**, 7028–7032.
[243] F. Kniep, L. Rout, S. M. Walter, H. K. V. Bensch, S. H. Jungbauer, E. Herdtweck and S. M. Huber, *Chem. Commun.*, 2012, **48**, 9299–9301.
[244] F. Kniep, S. M. Walter, E. Herdtweck and S. M. Huber, *Chem. Eur. J.*, 2012, **18**, 1306–1310.
[245] V. N. G. Lindsay, C. Nicolas and A. B. Charette, *J. Am. Chem. Soc.*, 2011, **133**, 8972–8981.
[246] S. M. Walter, F. Kniep, E. Herdtweck and S. M. Huber, *Angew. Chem. Int. Ed.*, 2011, **50**, 7187–7191.
[247] T. M. Beale, M. G. Chudzinski, M. G. Sarwar and M. S. Taylor, *Chem. Soc. Rev.*, 2013, **42**, 1667–1680.
[248] G. Mínguez Espallargas, L. Brammer, J. van de Streek, K. Shankland, A. J. Florence and H. Adams, *J. Am. Chem. Soc.*, 2006, **128**, 9584–9585.
[249] A. Mele, P. Metrangolo, H. Neukirch, T. Pilati and G. Resnati, *J. Am. Chem. Soc.*, 2005, **127**, 14972–14973.
[250] T. Beweries, L. Brammer, N. A. Jasim, J. E. McGrady, R. N. Perutz and A. C. Whitwood, *J. Am. Chem. Soc.*, 2011, **133**, 14338–14348.
[251] L. Brammer, G. Minguez Espallargas and S. Libri, *CrystEngComm*, 2008, **10**, 1712–1727.
[252] S. Libri, N. A. Jasim, R. N. Perutz and L. Brammer, *J. Am. Chem. Soc.*, 2008, **130**, 7842–7844.
[253] G. Mínguez Espallargas, F. Zordan, L. Arroyo Marín, H. Adams, K. Shankland, J. van de Streek and L. Brammer, *Chem. Eur. J.*, 2009, **15**, 7554–7568.
[254] M. Adler, M. J. Kochanny, B. Ye, G. Rumennik, D. R. Light, S. Biancalana and M. Whitlow, *Biochemistry (Mosc.)*, 2002, **41**, 15514–15523.
[255] P. Auffinger, F. A. Hays, E. Westhof and P. S. Ho, *Proc. Natl. Acad. Sci. U. S. A.*, 2004, **101**, 16789–16794.
[256] M. Carter and P. S. Ho, *Cryst. Growth Des.*, 2011, **11**, 5087–5095.
[257] E. Howard, R. Sanishvili, R. Cachau, A. Mitschler, B. Chevrier, P. Barth, V. Lamour, M. Van Zandt, E. Sibley, C. Bon, D. Moras, T. Schneider, A. Joachimiak and A. Podjarny, *Proteins*, 2004, **55**, 792–804.
[258] Y. Jiang, A. A. Alcaraz, J.-M. Chen, H. Kobayashi, Y. J. Lu and J. P. Snyder, *J. Med. Chem.*, 2006, **49**, 1891–1899.
[259] Y. Lu, Y. Wang and W. Zhu, *Phys. Chem. Chem. Phys.*, 2010, **12**, 4543–4551.
[260] A. R. Voth, F. A. Hays and P. S. Ho, *Proc. Natl. Acad. Sci. U. S. A.*, 2007, **104**, 6188–6193.

[261] H. Matter, M. Nazaré, S. Güssregen, D. W. Will, H. Schreuder, A. Bauer, M. Urmann, K. Ritter, M. Wagner and V. Wehner, *Angew. Chem. Int. Ed. Engl.*, 2009, **48**, 2911–2916.
[262] P. Metrangolo, T. Pilati, G. Terraneo, S. Biella and G. Resnati, *CrystEngComm*, 2009, **11**, 1187–1196.
[263] G. Cavallo, P. Metrangolo, T. Pilati, G. Resnati, M. Sansotera and G. Terraneo, *Chem. Soc. Rev.*, 2010, **39**, 3772–3783.
[264] M. G. Sarwar, B. Dragisic, S. Sagoo and M. S. Taylor, *Angew. Chem. Int. Ed. Engl.*, 2010, **49**, 1674–1677.
[265] M. G. Chudzinski, C. A. McClary and M. S. Taylor, *J. Am. Chem. Soc.*, 2011, **133**, 10559–10567.
[266] S. M. Walter, F. Kniep, L. Rout, F. P. Schmidtchen, E. Herdtweck and S. M. Huber, *J. Am. Chem. Soc.*, 2012, **134**, 8507–8512.
[267] M. Cametti, K. Raatikainen, P. Metrangolo, T. Pilati, G. Terraneo and G. Resnati, *Org. Biomol. Chem.*, 2012, **10**, 1329–1333.
[268] N. L. Kilah, M. D. Wise, C. J. Serpell, A. L. Thompson, N. G. White, K. E. Christensen and P. D. Beer, *J. Am. Chem. Soc.*, 2010, **132**, 11893–11895.
[269] A. Caballero, F. Zapata, N. G. White, P. J. Costa, V. Flix and P. D. Beer, *Angew. Chem. Int. Ed.*, 2012, **51**, 1876–1880.
[270] F. Zapata, A. Caballero, N. G. White, T. D. W. Claridge, P. J. Costa, V. Flix and P. D. Beer, *J. Am. Chem. Soc.*, 2012, **134**, 11533–11541.
[271] A. Caballero, N. G. White and P. D. Beer, *Angew. Chem. Int. Ed.*, 2011, **50**, 1845–1848.
[272] R. Tepper, B. Schulze, M. Jger, C. Friebe, D. H. Scharf, H. Grls and U. S. Schubert, *J. Org. Chem.*, 2015, **80**, 3139–3150.
[273] M. F. Perutz, M. G. Rossmann, A. F. Cullis, H. Muirhead, G. Will and A. C. T. North, *Nature*, 1960, **185**, 416–422.
[274] H. G. L. Coster, *Aust. J. Phys.*, 1999/01/01, **52**, 117–140.
[275] T. J. Hubin and D. H. Busch, *Coord. Chem. Rev.*, 2000, **200202**, 5–52.
[276] S. Anderson, H. L. Anderson and J. K. M. Sanders, *Acc. Chem. Res.*, 1993, **26**, 469–475.
[277] Benjah-bmm27, *https://commons.wikimedia.org/wiki/File:Haemoglobin-3D-ribbons.png*, 2007.
[278] D. Munnur, E. Mitchell, V. Forsyth, S. Teixeira and S. Neidle, *http://dx.doi.org/10.2210/pdb4ah0/pdb*, 2013, PDB: 4AH0.
[279] M. C. Thompson and D. H. Busch, *J. Am. Chem. Soc.*, 1964, **86**, 3651–3656.
[280] M. C. Thompson and D. H. Busch, *J. Am. Chem. Soc.*, 1964, **86**, 213–217.
[281] M. C. Thompson and D. H. Busch, *J. Am. Chem. Soc.*, 1962, **84**, 1762–1763.
[282] N. Curtis, *Coord. Chem. Rev.*, 1968, **3**, 3–47.
[283] M.-T. Youinou, N. Rahmouni, J. Fischer and J. A. Osborn, *Angew. Chem. Int. Ed. Engl.*, 1992, **31**, 733–735.
[284] K. Ladomenou, V. Nikolaou, G. Charalambidis and A. G. Coutsolelos, *Coord. Chem. Rev.*, 2016, **306, Part 1**, 1–42.
[285] P. Kumar, A. Deep and K.-H. Kim, *Trends Anal. Chem.*, 2015, **73**, 39–53.
[286] P. Mal, B. Breiner, K. Rissanen and J. R. Nitschke, *Science*, 2009, **324**, 1697–1699.
[287] P. Mal, D. Schultz, K. Beyeh, K. Rissanen and J. Nitschke, *Angew. Chem. Int. Ed. Engl.*, 2008, **47**, 8297–8301.
[288] M. Hoffmann, C. Wilson, B. Odell and H. Anderson, *Angew. Chem. Int. Ed. Engl.*, 2007, **46**, 3122–3125.
[289] D. V. Kondratuk, J. K. Sprafke, M. C. O'Sullivan, L. M. A. Perdigao, A. Saywell, M. Malfois, J. N. O'Shea, P. H. Beton, A. L. Thompson and H. L. Anderson, *Chem. Eur. J.*, 2014, **20**, 12826–12834.
[290] L. Favereau, A. Cnossen, J. B. Kelber, J. Q. Gong, R. M. Oetterli, J. Cremers, L. M. Herz and H. L. Anderson, *J. Am. Chem. Soc.*, 2015, **137**, 14256–14259.
[291] M. C. O'Sullivan, J. K. Sprafke, D. V. Kondratuk, C. Rinfray, T. D. W. Claridge, A. Saywell, M. O. Blunt, J. N. O'Shea, P. H. Beton, M. Malfois and H. L. Anderson, *Nature*, 2011, **469**, 72–75.
[292] B. Hasenknopf, J.-M. Lehn, N. Boumediene, A. Dupont-Gervais, A. Van Dorsselaer, B. Kneisel and D. Fenske, *J. Am. Chem. Soc.*, 1997, **119**, 10956–10962.
[293] B. Hasenknopf, J.-M. Lehn, B. O. Kneisel, G. Baum and D. Fenske, *Angew. Chem. Int. Ed. Engl.*, 1996, **35**, 1838–1840.
[294] C. S. Campos-Fernández, B. L. Schottel, H. T. Chifotides, J. K. Bera, J. Bacsa, J. M. Koomen, D. H. Russell and K. R. Dunbar, *J. Am. Chem. Soc.*, 2005, **127**, 12909–12923.
[295] D. Meshcheryakov, V. Böhmer, M. Bolte, V. Hubscher-Bruder, F. Arnaud-Neu, H. Herschbach, A. Van Dorsselaer, I. Thondorf and W. Mögelin, *Angew. Chem. Int. Ed. Engl.*, 2006, **45**, 1648–1652.
[296] E. A. Katayev, G. D. Pantos, M. D. Reshetova, V. N. Khrustalev, V. M. Lynch, Y. A. Ustynyuk and J. L. Sessler, *Angew. Chem. Int. Ed. Engl.*, 2005, **44**, 7386–7390.
[297] J. L. Sessler, T. D. Mody and V. Lynch, *Inorg. Chem.*, 1992, **31**, 529–531.
[298] M. Bru, I. Alfonso, M. I. Burguete and S. V. Luis, *Angew. Chem. Int. Ed. Engl.*, 2006, **45**, 6155–6159.
[299] H. Amouri, L. Mimassi, M. N. Rager, B. E. Mann, C. Guyard-Duhayon and L. Raehm, *Angew. Chem. Int. Ed. Engl.*, 2005, **44**, 4543–4546.
[300] J. S. Fleming, K. L. V. Mann, C.-A. Carraz, E. Psillakis, J. C. Jeffery, J. A. McCleverty and M. D. Ward, *Angew. Chem. Int. Ed. Engl.*, 1998, **37**, 1279–1281.
[301] Y. Kubota, S. Sakamoto, K. Yamaguchi and M. Fujita, *Proc. Natl. Acad. Sci. U. S. A.*, 2002, **99**, 4854–4856.
[302] R. Wang, H. D. Selby, H. Liu, M. D. Carducci, T. Jin, Z. Zheng, J. W. Anthis and R. J. Staples, *Inorg. Chem.*, 2002, **41**, 278–286.
[303] M. Aoyagi, K. Biradha and M. Fujita, *J. Am. Chem. Soc.*, 1999, **121**, 7457–7458.
[304] J. F. Stoddart, *Chem. Soc. Rev.*, 2009, **38**, 1802–1820.
[305] P. L. Anelli, P. R. Ashton, R. Ballardini, V. Balzani, M. Delgado, M. T. Gandolfi, T. T. Goodnow, A. E. Kaifer and D. Philp, *J. Am. Chem. Soc.*, 1992, **114**, 193–218.
[306] P. R. Ashton, M. Belohradsky, D. Philp and J. F. Stoddart, *J. Chem. Soc., Chem. Commun.*, 1993, 1269–1274.

[307] K. D. Hanni and D. A. Leigh, *Chem. Soc. Rev.*, 2010, **39**, 1240–1251.
[308] C.-W. Chiu, C.-C. Lai and S.-H. Chiu, *J. Am. Chem. Soc.*, 2007, **129**, 3500–3501.
[309] S.-Y. Hsueh, J.-L. Ko, C.-C. Lai, Y.-H. Liu, S.-M. Peng and S.-H. Chiu, *Angew. Chem. Int. Ed.*, 2011, **50**, 6643–6646.
[310] I. Yoon, M. Narita, T. Shimizu and M. Asakawa, *J. Am. Chem. Soc.*, 2004, **126**, 16740–16741.
[311] A. F. M. Kilbinger, S. J. Cantrill, A. W. Waltman, M. W. Day and R. H. Grubbs, *Angew. Chem. Int. Ed.*, 2003, **42**, 3281–3285.
[312] J. S. Hannam, T. J. Kidd, D. A. Leigh and A. J. Wilson, *Org. Lett.*, 2003, **5**, 1907–1910.
[313] C. O. Dietrich-Buchecker and J. P. Sauvage, *Chem. Rev.*, 1987, **87**, 795–810.
[314] E. N. Guidry, S. J. Cantrill, J. F. Stoddart and R. H. Grubbs, *Org. Lett.*, 2005, **7**, 2129–2132.
[315] G. Agam, D. Graiver and A. Zilkha, *J. Am. Chem. Soc.*, 1976, **98**, 5206–5214.
[316] G. Agam and A. Zilkha, *J. Am. Chem. Soc.*, 1976, **98**, 5214–5216.
[317] I. T. Harrison and S. Harrison, *J. Am. Chem. Soc.*, 1967, **89**, 5723–5724.
[318] E. Wasserman, *J. Am. Chem. Soc.*, 1960, **82**, 4433–4434.
[319] J. D. Crowley, S. M. Goldup, A.-L. Lee, D. A. Leigh and R. T. McBurney, *Chem. Soc. Rev.*, 2009, **38**, 1530–1541.
[320] J. P. Sauvage, *Acc. Chem. Res.*, 1990, **23**, 319–327.
[321] G. Brancato, F. Coutrot, D. A. Leigh, A. Murphy, J. K. Y. Wong and F. Zerbetto, *Proc. Natl. Acad. Sci. U. S. A.*, 2002, **99**, 4967–4971.
[322] D. G. Hamilton, N. Feeder, L. Prodi, S. J. Teat, W. Clegg and J. K. M. Sanders, *J. Am. Chem. Soc.*, 1998, **120**, 1096–1097.
[323] C. A. Hunter, *J. Am. Chem. Soc.*, 1992, **114**, 5303–5311.
[324] G. Wenz, B.-H. Han and A. Müller, *Chem. Rev.*, 2006, **106**, 782–817.
[325] N. H. Evans and P. D. Beer, *Angew. Chem. Int. Ed.*, 2014, **53**, 11716–11754.
[326] C. Dietrich-Buchecker, J. Sauvage and J. Kintzinger, *Tetrahedron Lett.*, 1983, **24**, 5095–5098.
[327] C. O. Dietrich-Buchecker, J. P. Sauvage and J. M. Kern, *J. Am. Chem. Soc.*, 1984, **106**, 3043–3045.
[328] C. O. Dietrich-Buchecker, A. Khemiss and J. P. Sauvage, *J. Chem. Soc., Chem. Commun.*, 1986, 1376–1378.
[329] J. P. Sauvage and J. Weiss, *J. Am. Chem. Soc.*, 1985, **107**, 6108–6110.
[330] A. Joosten, Y. Trolez, J.-P. Collin, V. Heitz and J.-P. Sauvage, *J. Am. Chem. Soc.*, 2012, **134**, 1802–1809.
[331] C. O. Dietrich-Buchecker and J.-P. Sauvage, *Angew. Chem. Int. Ed. Engl.*, 1989, **28**, 189–192.
[332] J.-P. Collin, F. Durola, J. Frey, V. Heitz, F. Reviriego, J.-P. Sauvage, Y. Trolez and K. Rissanen, *J. Am. Chem. Soc.*, 2010, **132**, 6840–6850.
[333] S. Goldup, D. Leigh, P. Lusby, R. McBurney and A. Slawin, *Angew. Chem. Int. Ed.*, 2008, **47**, 6999–7003.
[334] A.-M. Fuller, D. A. Leigh, P. J. Lusby, I. D. H. Oswald, S. Parsons and D. B. Walker, *Angew. Chem. Int. Ed.*, 2004, **43**, 3914–3918.
[335] A. I. Prikhod'ko, F. Durola and J.-P. Sauvage, *J. Am. Chem. Soc.*, 2008, **130**, 448–449.
[336] A. I. Prikhod'ko and J.-P. Sauvage, *J. Am. Chem. Soc.*, 2009, **131**, 6794–6807.
[337] J. P. Sauvage and M. Ward, *Inorg. Chem.*, 1991, **30**, 3869–3874.
[338] C. Hamann, J.-M. Kern and J.-P. Sauvage, *Inorg. Chem.*, 2003, **42**, 1877–1883.
[339] H. C. Kolb, M. G. Finn and K. B. Sharpless, *Angew. Chem. Int. Ed.*, 2001, **40**, 2004–2021.
[340] V. Aucagne, K. D. Hänni, D. A. Leigh, P. J. Lusby and D. B. Walker, *J. Am. Chem. Soc.*, 2006, **128**, 2186–2187.
[341] J. Berná, J. D. Crowley, S. M. Goldup, K. D. Hänni, A.-L. Lee and D. A. Leigh, *Angew. Chem. Int. Ed.*, 2007, **46**, 5709–5713.
[342] J. Berná, S. M. Goldup, A.-L. Lee, D. A. Leigh, M. D. Symes, G. Teobaldi and F. Zerbetto, *Angew. Chem. Int. Ed.*, 2008, **47**, 4392–4396.
[343] S. M. Goldup, D. A. Leigh, P. R. McGonigal, V. E. Ronaldson and A. M. Z. Slawin, *J. Am. Chem. Soc.*, 2010, **132**, 315–320.
[344] S. Saito, E. Takahashi and K. Nakazono, *Org. Lett.*, 2006, **8**, 5133–5136.
[345] Y. Sato, R. Yamasaki and S. Saito, *Angew. Chem. Int. Ed.*, 2009, **48**, 504–507.
[346] J. D. Crowley, K. D. Hánni, A.-L. Lee and D. A. Leigh, *J. Am. Chem. Soc.*, 2007, **129**, 12092–12093.
[347] S. Goldup, D. Leigh, P. Lusby, R. McBurney and A. Slawin, *Angew. Chem. Int. Ed.*, 2008, **47**, 3381–3384.
[348] H. M. Cheng, D. A. Leigh, F. Maffei, P. R. McGonigal, A. M. Z. Slawin and J. Wu, *J. Am. Chem. Soc.*, 2011, **133**, 12298–12303.
[349] S. M. Goldup, D. A. Leigh, R. T. McBurney, P. R. McGonigal and A. Plant, *Chem. Sci.*, 2010, **1**, 383–386.
[350] W. Jiang, D. Sattler, K. Rissanen and C. A. Schalley, *Org. Lett.*, 2011, **13**, 4502–4505.
[351] S.-Y. Hsueh, K.-W. Cheng, C.-C. Lai and S.-H. Chiu, *Angew. Chem. Int. Ed.*, 2008, **47**, 4436–4439.
[352] M.-V. Martínez-Díaz, N. Spencer and J. F. Stoddart, *Angew. Chem. Int. Ed. Engl.*, 1997, **36**, 1904–1907.
[353] P. R. Ashton, P. J. Campbell, P. T. Glink, D. Philp, N. Spencer, J. F. Stoddart, E. J. T. Chrystal, S. Menzer, D. J. Williams and P. A. Tasker, *Angew. Chem. Int. Ed. Engl.*, 1995, **34**, 1865–1869.
[354] M. C. T. Fyfe and J. F. Stoddart, *Acc. Chem. Res.*, 1997, **30**, 393–401.
[355] M. E. Belowich, C. Valente, R. A. Smaldone, D. C. Friedman, J. Thiel, L. Cronin and J. F. Stoddart, *J. Am. Chem. Soc.*, 2012, **134**, 5243–5261.
[356] A. R. Williams, B. H. Northrop, T. Chang, J. F. Stoddart, A. J. P. White and D. J. Williams, *Angew. Chem. Int. Ed.*, 2006, **45**, 6665–6669.
[357] B. H. Northrop, F. Aricó, N. Tangchiavang, J. D. Badjić and J. F. Stoddart, *Org. Lett.*, 2006, **8**, 3899–3902.
[358] S. Suzuki, K. Nakazono and T. Takata, *Org. Lett.*, 2010, **12**, 712–715.

[359] K. Nakazono, S. Kuwata and T. Takata, *Tetrahedron Lett.*, 2008, **49**, 2397–2401.
[360] A. Mirzoian and A. E. Kaifer, *J. Org. Chem.*, 1995, **60**, 8093–8095.
[361] P. L. Anelli, N. Spencer and J. F. Stoddart, *J. Am. Chem. Soc.*, 1991, **113**, 5131–5133.
[362] D. Philp, A. M. Z. Slawin, N. Spencer, J. F. Stoddart and D. J. Williams, *J. Chem. Soc., Chem. Commun.*, 1991, 1584–1586.
[363] P. R. Ashton, T. T. Goodnow, A. E. Kaifer, M. V. Reddington, A. M. Z. Slawin, N. Spencer, J. F. Stoddart, C. Vicent and D. J. Williams, *Angew. Chem. Int. Ed. Engl.*, 1989, **28**, 1396–1399.
[364] M. Asakawa, P. R. Ashton, V. Balzani, A. Credi, C. Hamers, G. Mattersteig, M. Montalti, A. N. Shipway, N. Spencer, J. F. Stoddart, M. S. Tolley, M. Venturi, A. J. P. White and D. J. Williams, *Angew. Chem. Int. Ed.*, 1998, **37**, 333–337.
[365] W. Devonport, M. A. Blower, M. R. Bryce and L. M. Goldenberg, *J. Org. Chem.*, 1997, **62**, 885–887.
[366] Z.-T. Li, P. C. Stein, J. Becher, D. Jensen, P. Mørk and N. Svenstrup, *Chem. Eur. J.*, 1996, **2**, 624–633.
[367] M. Asakawa, W. Dehaen, G. L'abbé, S. Menzer, J. Nouwen, F. M. Raymo, J. F. Stoddart and D. J. Williams, *J. Org. Chem.*, 1996, **61**, 9591–9595.
[368] F. Vögtle, S. Meier and R. Hoss, *Angew. Chem. Int. Ed. Engl.*, 1992, **31**, 1619–1622.
[369] F. G. Gatti, D. A. Leigh, S. A. Nepogodiev, A. M. Z. Slawin, S. J. Teat and J. K. Y. Wong, *J. Am. Chem. Soc.*, 2001, **123**, 5983–5989.
[370] D. A. Leigh, A. Murphy, J. P. Smart and A. M. Z. Slawin, *Angew. Chem. Int. Ed. Engl.*, 1997, **36**, 728–732.
[371] D. A. Leigh, A. Venturini, A. J. Wilson, J. K. Y. Wong and F. Zerbetto, *Chem. Eur. J.*, 2004, **10**, 4960–4969.
[372] M. Chen, S. Han, L. Jiang, S. Zhou, F. Jiang, Z. Xu, J. Liang and S. Zhang, *Chem. Commun. (Cambridge, U. K.)*, 2010, **46**, 3932–3934.
[373] E. Arunkumar, C. C. Forbes, B. C. Noll and B. D. Smith, *J. Am. Chem. Soc.*, 2005, **127**, 3288–3289.
[374] F. B. L. Cougnon, H. Y. Au-Yeung, G. D. Pantoş and J. K. M. Sanders, *J. Am. Chem. Soc.*, 2011, **133**, 3198–3207.
[375] S. P. Black, J. K. M. Sanders and A. R. Stefankiewicz, *Chem. Soc. Rev.*, 2014, **43**, 1861–1872.
[376] N. Ponnuswamy, F. B. L. Cougnon, J. M. Clough, G. D. Pantoş and J. K. M. Sanders, *Science*, 2012, **338**, 783–785.
[377] S. Anderson, T. D. W. Claridge and H. L. Anderson, *Angew. Chem. Int. Ed. Engl.*, 1997, **36**, 1310–1313.
[378] E. J. F. Klotz, T. D. W. Claridge and H. L. Anderson, *J. Am. Chem. Soc.*, 2006, **128**, 15374–15375.
[379] A. Harada, J. Li and M. Kamachi, *Chem. Commun.*, 1997, 1413–1414.
[380] A. Harada, J. Li and M. Kamachi, *Nature*, 1992, **356**, 325–327.
[381] G. M. Hübner, J. Gläser, C. Seel and F. Vögtle, *Angew. Chem. Int. Ed.*, 1999, **38**, 383–386.
[382] P. Ghosh, O. Mermagen and C. A. Schalley, *Chem. Commun.*, 2002, 2628–2629.
[383] J. A. Wisner, P. D. Beer and M. G. B. Drew, *Angew. Chem. Int. Ed.*, 2001, **40**, 3606–3609.
[384] M. D. Lankshear and P. D. Beer, *Acc. Chem. Res.*, 2007, **40**, 657–668.
[385] M. R. Sambrook, P. D. Beer, J. A. Wisner, R. L. Paul and A. R. Cowley, *J. Am. Chem. Soc.*, 2004, **126**, 15364–15365.
[386] J. A. Wisner, P. D. Beer, M. G. B. Drew and M. R. Sambrook, *J. Am. Chem. Soc.*, 2002, **124**, 12469–12476.
[387] P. D. Beer, M. R. Sambrook and D. Curiel, *Chem. Commun.*, 2006, 2105–2117.
[388] M. D. Lankshear and P. D. Beer, *Coord. Chem. Rev.*, 2006, **250**, 3142–3160.
[389] A. Brown, K. M. Mullen, J. Ryu, M. J. Chmielewski, S. M. Santos, V. Felix, A. L. Thompson, J. E. Warren, S. I. Pascu and P. D. Beer, *J. Am. Chem. Soc.*, 2009, **131**, 4937–4952.
[390] M. J. Chmielewski, L. Zhao, A. Brown, D. Curiel, M. R. Sambrook, A. L. Thompson, S. M. Santos, V. Felix, J. J. Davis and P. D. Beer, *Chem. Commun.*, 2008, 3154–3156.
[391] G. T. Spence, C. J. Serpell, J. Sardinha, P. J. Costa, V. Félix and P. D. Beer, *Chem. Eur. J.*, 2011, **17**, 12955–12966.
[392] K. Mullen, J. Mercurio, C. Serpell and P. Beer, *Angew. Chem. Int. Ed.*, 2009, **48**, 4781–4784.
[393] Y. Li, K. M. Mullen, T. D. W. Claridge, P. J. Costa, V. Felix and P. D. Beer, *Chem. Commun.*, 2009, 7134–7136.
[394] N. H. Evans, C. J. Serpell and P. D. Beer, *Angew. Chem. Int. Ed.*, 2011, **50**, 2507–2510.
[395] N. H. Evans, C. J. Serpell and P. D. Beer, *Chem. Commun.*, 2011, **47**, 8775–8777.
[396] M. J. Langton and P. D. Beer, *Chem. Eur. J.*, 2012, **18**, 14406–14412.
[397] N. H. Evans and P. D. Beer, *Chem. Eur. J.*, 2011, **17**, 10542–10546.
[398] M. J. Langton, L. C. Duckworth and P. D. Beer, *Chem. Commun.*, 2013, **49**, 8608–8610.
[399] M. J. Langton, O. A. Blackburn, T. Lang, S. Faulkner and P. D. Beer, *Angew. Chem. Int. Ed.*, 2014, **53**, 11463–11466.
[400] N. Hirokawa, *Science*, 1998, **279**, 519–526.
[401] J. E. Walker, *Angew. Chem. Int. Ed.*, 1998, **37**, 2308–2319.
[402] S. F. M. van Dongen, S. Cantekin, J. A. A. W. Elemans, A. E. Rowan and R. J. M. Nolte, *Chem. Soc. Rev.*, 2014, **43**, 99–122.
[403] V. Balzani, A. Credi, S. Silvi and M. Venturi, *Chem. Soc. Rev.*, 2006, **35**, 1135–1149.
[404] E. R. Kay, D. A. Leigh and F. Zerbetto, *Angew. Chem. Int. Ed.*, 2007, **46**, 72–191.
[405] P. R. Ashton, R. Ballardini, V. Balzani, I. Baxter, A. Credi, M. C. T. Fyfe, M. T. Gandolfi, M. Gömez-Löpez, M.-V. Martínez-Díaz, A. Piersanti, N. Spencer, J. F. Stoddart, M. Venturi, A. J. P. White and D. J. Williams, *J. Am. Chem. Soc.*, 1998, **120**, 11932–11942.
[406] H.-R. Tseng, S. A. Vignon and J. F. Stoddart, *Angew. Chem. Int. Ed.*, 2003, **42**, 1491–1495.
[407] J. D. Badjić, V. Balzani, A. Credi, S. Silvi and J. F. Stoddart, *Science*, 2004, **303**, 1845–1849.
[408] A. Livoreil, C. O. Dietrich-Buchecker and J.-P. Sauvage, *J. Am. Chem. Soc.*, 1994, **116**, 9399–9400.
[409] M. C. Jiménez, C. Dietrich-Buchecker and J.-P. Sauvage, *Angew. Chem. Int. Ed.*, 2000, **39**, 3284–3287.
[410] D. A. Leigh, J. K. Y. Wong, F. Dehez and F. Zerbetto, *Nature*, 2003, **424**, 174–179.

[411] J. Berná, D. A. Leigh, M. Lubomska, S. M. Mendoza, E. M. Perez, P. Rudolf, G. Teobaldi and F. Zerbetto, *Nat. Mater.*, 2005, **4**, 704–710.
[412] V. Blanco, A. Carlone, K. D. Hnni, D. A. Leigh and B. Lewandowski, *Angew. Chem. Int. Ed.*, 2012, **51**, 5166–5169.
[413] B. Lewandowski, G. De Bo, J. W. Ward, M. Papmeyer, S. Kuschel, M. J. Aldegunde, P. M. E. Gramlich, D. Heckmann, S. M. Goldup, D. M. D'Souza, A. E. Fernandes and D. A. Leigh, *Science*, 2013, **339**, 189–193.
[414] G. T. Spence and P. D. Beer, *Acc. Chem. Res.*, 2013, **46**, 571–586.
[415] A. Caballero, F. Zapata and P. D. Beer, *Coord. Chem. Rev.*, 2013, **257**, 2434–2455.
[416] Y. Nagawa, J.-i. Suga, K. Hiratani, E. Koyama and M. Kanesato, *Chem. Commun.*, 2005, 749–751.
[417] W. Zhou, J. Li, X. He, C. Li, J. Lv, Y. Li, S. Wang, H. Liu and D. Zhu, *Chem. Eur. J.*, 2008, **14**, 754–763.
[418] N. H. Evans, H. Rahman, A. V. Leontiev, N. D. Greenham, G. A. Orlowski, Q. Zeng, R. M. J. Jacobs, C. J. Serpell, N. L. Kilah, J. J. Davis and P. D. Beer, *Chem. Sci.*, 2012, **3**, 1080–1089.
[419] A. Fernandes, A. Viterisi, F. Coutrot, S. Potok, D. Leigh, V. Aucagne and S. Papot, *Angew. Chem. Int. Ed.*, 2009, **48**, 6443–6447.
[420] W. Brotherton, R. Clark and L. Zhu, *J. Org. Chem.*, 2012, **77**, 6443–6455.
[421] J. E. Hein and V. V. Fokin, *Chem. Soc. Rev.*, 2010, **39**, 1302–1315.
[422] B. T. Worrell, J. A. Malik and V. V. Fokin, *Science*, 2013, **340**, 457–60.
[423] Y. Hua and A. Flood, *J. Am. Chem. Soc.*, 2010, **132**, 12838–12840.
[424] Y. Hua and A. Flood, *Chem. Soc. Rev.*, 2010, **39**, 1262–1271.
[425] Y. Hua, R. Ramabhadran, J. Karty, K. Raghavachari and A. Flood, *Chem. Commun. (Cambridge, U. K.)*, 2011, **47**, 5979–5981.
[426] J. L. Sessler, J. Cai, H.-Y. Gong, X. Yang, J. F. Arambula and B. P. Hay, *J. Am. Chem. Soc.*, 2010, **132**, 14058–14060.
[427] N. G. White, A. R. Colaço, I. Marques, V. Félix and P. D. Beer, *Org. Biomol. Chem.*, 2014, **12**, 4924–4931.
[428] N. G. White, *Ph.D. thesis*, University of Oxford, 2012.
[429] N. G. White, C. J. Serpell and P. D. Beer, *Cryst. Growth Des.*, 2014, **14**, 3472–3479.
[430] N. G. White and P. D. Beer, *Chem. Commun. (Cambridge, U. K.)*, 2012, **48**, 8499–501.
[431] B. R. Mullaney, B. E. Partridge and P. D. Beer, *Chem. Eur. J.*, 2014, **21**, 1660–1665.
[432] B. R. Mullaney, B. E. Partridge, P. D. Beer, B. R. Mullaney, A. L. Thompson and P. D. Beer, *Angew. Chem. Int. Ed. Engl.*, 2014, **53**, 11458–11562.
[433] J. Hein, J. Tripp, L. Krasnova, K. Sharpless and V. Fokin, *Angew. Chem. Int. Ed. Engl.*, 2009, **48**, 8018–8021.
[434] H. Goto, J. Heemstra, D. Hill and J. Moore, *Org. Lett.*, 2004, **6**, 889–892.
[435] T. X. Neenan and G. M. Whitesides, *J. Org. Chem.*, 1988, **53**, 2489–2496.
[436] K. Sonogashira, Y. Tohda and N. Hagihara, *Tetrahedron Lett.*, 1975, **16**, 4467–4470.
[437] M. J. Hynes, *Journal of the Chemical Society, Dalton Transactions*, 1993, 311–312.
[438] L. M. Hancock and P. D. Beer, *Chem. Eur. J.*, 2009, **15**, 42–4.
[439] A. Bondi, *J. Phys. Chem.*, 1964, **68**, 441–451.
[440] F. Jalilehvand, *http://www.chem.ucalgary.ca/research/groups/faridehj/xas.pdf*, 2002.
[441] T. Glaser, B. Hedman, K. O. Hodgson, E. I. Solomon, S. E. Shadle, B. Hedman, K. O. Hodgson and E. I. Solomon, *Inorg. Chem.*, 1994, **33**, 4235–4244.
[442] S. E. Shadle, B. Hedman, K. O. Hodgson and E. I. Solomon, *Inorg. Chem.*, 1994, **33**, 4235–4244.
[443] E. I. Solomon, B. Hedman, K. O. Hodgson, A. Dey and R. K. Szilagyi, *Coord. Chem. Rev.*, 2005, **249**, 97–129.
[444] M. U. Delgado-Jaime, J. C. Conrad, D. E. Fogg and P. Kennepohl, *Inorg. Chim. Acta*, 2006, **359**, 3042–3047.
[445] M. U. Delgado-Jaime, C. P. Mewis and P. Kennepohl, *J. Synchrotron Rad.*, 2010, **17**, 132–137.
[446] M. U. Delgado-Jaime, J. C. Conrad, D. E. Fogg, P. Kennepohl, M. U. Delgado-Jaime and P. Kennepohl, *J. Synchrotron Rad.*, 2010, **17**, 119–128.
[447] S. V. Rosokha, C. L. Stern and J. T. Ritzert, *Chem. Eur. J.*, 2013, **19**, 8774–8788.
[448] F. Neese, *WIREs Computational Molecular Science*, 2012, **2**, 73–78.
[449] S. DeBeer George, T. Petrenko and F. Neese, *Inorg. Chim. Acta*, 2008, **361**, 965–972.
[450] C. J. Serpell, R. Chall, A. L. Thompson and P. D. Beer, *Dalton Trans.*, 2011, **40**, 12052–12055.
[451] G. Wenz, *Angew. Chem. Int. Ed. Engl.*, 1994, **33**, 803–822.
[452] M. V. Rekharsky and Y. Inoue, *Chem. Rev.*, 1998, **98**, 1875–1918.
[453] T. Aree, B. Schulz and G. Reck, *J. Inclusion Phenom. Macrocyclic Chem.*, 2003, **47**, 39–45.
[454] J. Szejtli, *Chem. Rev.*, 1998, **98**, 1743–1754.
[455] T. Loftsson and M. E. Brewster, *J. Pharm. Sci.*, 1996, **85**, 1017–1025.
[456] P. J. Skinner, A. Beeby, R. S. Dickins, D. Parker, S. Aime and M. Botta, *J. Chem. Soc., Perkin Trans. 2*, 2000, 1329–1338.
[457] Z. Chen, J. S. Bradshaw and M. L. Lee, *Tetrahedron Lett.*, 1996, **37**, 6831–6834.
[458] B. du Roizel, J.-P. Baltaze and P. Sinaÿ, *Tetrahedron Lett.*, 2002, **43**, 2371–2373.
[459] N. Zhong, H. S. Byun and R. Bittman, *Tetrahedron Lett.*, 1998, **39**, 2919–2920.
[460] J. A. Faiz, N. Spencer and Z. Pikramenou, *Org. Biomol. Chem.*, 2005, **3**, 4239–4245.
[461] M. G. Sarwar, B. Dragisić, E. Dimitrijević and M. S. Taylor, *Chem. Eur. J.*, 2013, **19**, 2050–2058.
[462] D. A. Smith, L. Brammer, C. A. Hunter and R. N. Perutz, *J. Am. Chem. Soc.*, 2014, **136**, 1288–1291.
[463] C. L. D. Gibb and B. C. Gibb, *Supramolecular chemistry : from molecules to nanomaterials*, Hoboken, NJ : Wiley, Hoboken, NJ, 2012, vol. 1, pp. 45–66.
[464] R. Dutta and P. Ghosh, *Chem. Commun.*, 2015, **51**, 9070–9084.

[465] K. Choi and A. Hamilton, *J. Am. Chem. Soc.*, 2001, **123**, 2456–2457.
[466] A. S. Singh and S.-S. Sun, *J. Org. Chem.*, 2012, **77**, 1880–1890.
[467] J. Romański and P. Piatek, *J. Org. Chem.*, 2013, **78**, 4341–4347.
[468] M. M. Watt, L. N. Zakharov, M. M. Haley and D. W. Johnson, *Angew. Chem. Int. Ed.*, 2013, **52**, 10275–10280.
[469] R. Herges, A. Dikmans, U. Jana, F. Khler, P. Jones, I. Dix, T. Fricke and B. Knig, *Eur. J. Org. Chem.*, 2002, **2002**, 3004–3014.
[470] P. Blondeau, J. Benet-Buchholz and J. de Mendoza, *New J. Chem.*, 2007, **31**, 736–740.
[471] M. Arunachalam, I. Ravikumar and P. Ghosh, *J. Org. Chem.*, 2008, **73**, 9144–9147.
[472] H. Abe, K. Ohtani, D. Suzuki, Y. Chida, Y. Shimada, S. Matsumoto and M. Inouye, *Org. Lett.*, 2014, **16**, 828–831.
[473] M. D. LoCoco, X. Zhang and R. F. Jordan, *J. Am. Chem. Soc.*, 2004, **126**, 15231–15244.
[474] G. Barker, J. L. McGrath, A. Klapars, D. Stead, G. Zhou, K. R. Campos and P. O'Brien, *J. Org. Chem.*, 2011, **76**, 5936–5953.
[475] D. Kurniawan, S. Morita and K. Kitagawa, *Comp. Theor. Chem.*, 2012, **982**, 30–33.
[476] D. W. Smith, *J. Chem. Educ.*, 1977, **54**, 540–542.
[477] F. P. Schmidtchen and G. Muller, *J. Chem. Soc., Chem. Commun.*, 1984, 1115–1116.
[478] K. Worm, F. P. Schmidtchen, A. Schier, A. Schäfer and M. Hesse, *Angew. Chem. Int. Ed. Engl.*, 1994, **33**, 327–329.
[479] K. Worm and F. P. Schmidtchen, *Angew. Chem. Int. Ed. Engl.*, 1995, **34**, 65–66.
[480] V. Valderrey, E. Escudero-Adán and P. Ballester, *J. Am. Chem. Soc.*, 2012, **134**, 10733–10736.
[481] G. T. Spence, C. Chan, F. Szemes and P. D. Beer, *Dalton Trans.*, 2012, **41**, 13474–13485.
[482] L. Hancock and P. Beer, *Chem. Commun. (Cambridge, U. K.)*, 2011, **47**, 6012–6014.
[483] F. Zapata, O. A. Blackburn, M. J. Langton, S. Faulkner and P. D. Beer, *Chem. Commun.*, 2013, **49**, 8157–8159.
[484] J. M. Mercurio, F. Tyrrell, J. Cookson and P. D. Beer, *Chem. Commun.*, 2013, **49**, 10793–10795.
[485] J. M. Mercurio, *Ph.D. thesis*, University of Oxford, 2014.
[486] C. Robertson, R. Perutz, L. Brammer and C. Hunter, *Chem. Sci.*, 2014, **5**, 4179–4183.
[487] E. D. Goddard-Borger and R. V. Stick, *Org. Lett.*, 2007, **9**, 3797–3800.
[488] B.-Y. Lee, S. R. Park, H. B. Jeon and K. S. Kim, *Tetrahedron Lett.*, 2006, **47**, 5105–5109.
[489] J. Cosier and A. M. Glazer, *J. Appl. Crystallogr.*, 1986, **19**, 105–107.
[490] Z. Otwinowski and W. Minor, *Methods Enzymol.*, 1997, **276**, 307–326.
[491] H. Nowell, S. A. Barnett, K. E. Christensen, S. J. Teat and D. R. Allan, *J. Synchrotron Rad.*, 2012, **19**, 435–441.
[492] Agilent Technologies, *CrysAlis Pro*, 2010.
[493] L. Palatinus and G. Chapuis, *J. Appl. Crystallogr.*, 2007, **40**, 786–790.
[494] P. W. Betteridge, J. R. Carruthers, R. I. Cooper, K. Prout, D. J. Watkin, R. I. Cooper, A. L. Thompson and D. J. Watkin, *J. Appl. Crystallogr.*, 2010, **43**, 1100–1107.
[495] P. Parois, R. I. Cooper and A. L. Thompson, *Chem. Cent. J.*, 2015, **9**, 30–44.
[496] R. I. Cooper, A. L. Thompson and D. J. Watkin, *J. Appl. Crystallogr.*, 2010, **43**, 1100–1107.
[497] S. M. Webb, *Phys. Scr.*, 2005, **2005**, 1011–1014.
[498] M. Zurro, S. Asmus, S. Beckendorf, C. Mück-Lichtenfeld and O. G. Mancheño, *J. Am. Chem. Soc.*, 2014, **136**, 13999–14002.

Chapter 8

Appendix

8.1 Crystallographic Data Tables

Acyclic Receptor 11·Cl

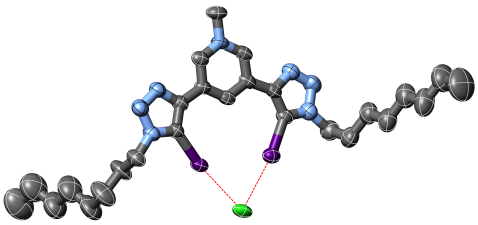


Figure 8.1.1: Thermal ellipsoid plot showing the asymmetric unit for the single-crystal structure of compound **11**·Cl. Atomic displacement ellipsoids drawn at the 50% probability level. Hydrogen atoms have been omitted.

Table 8.1.1: Crystal data and structure refinement for **11**·Cl

Empirical formula	$C_{26}H_{40}I_2N_7 \cdot Cl$	
Formula weight	739.91	
Temperature	150 K	
Wavelength	0.71073 Å	
Crystal system	Triclinic	
Space group	$P\bar{1}$	
Unit cell dimensions	a = 7.1984(3) Å	$\alpha = 86.3176(15)^\circ$
	b = 11.0786(4) Å	$\beta = 86.4171(14)^\circ$
	c = 20.0022(8) Å	$\gamma = 89.6638(19)^\circ$
Volume	1588.73(11) $Å^3$	
Z	2	
Density (calculated)	1.547 Mg/m^3	
Absorption coefficient	2.090 mm^{-1}	
F(000)	736	
Crystal size	0.14 × 0.02 × 0.01 mm^3	
Theta range for data collection	5.112 to 27.418°	
Index ranges	$-9 \leqslant h \leqslant 9, -12 \leqslant k \leqslant 14, -25 \leqslant l \leqslant 25$	
Reflections collected	18945	
Independent reflections	6896 [$R_{(int)} = 0.065$]	
Completeness to theta = 25.225°	96.5%	
Absorption correction	Semi-empirical from equivalents	
Max. and min. transmission	1.00 and 0.94	
Refinement method	Full-matrix least-squares on F^2	
Data / restraints / parameters	5461 / 162 / 325	
Goodness-of-fit on F^2	0.9549	
Final R indices [I>2sigma(I)]	R1 = 0.0471, wR2 = 0.1114	
R indices (all data)	R1 = 0.0732, wR2 = 0.1360	
Largest diff. peak and hole	1.55 and −0.93 $e.Å^{-3}$	

Acyclic Receptor 12·I

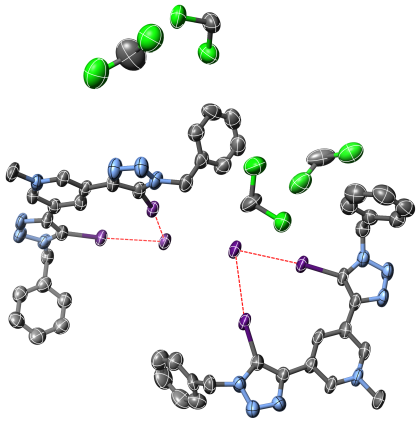


Figure 8.1.2: Thermal ellipsoid plot showing the asymmetric unit for the single-crystal structure of compound **12**·I. Atomic displacement ellipsoids drawn at the 90% probability level. Hydrogen atoms have been omitted.

Table 8.1.2: Crystal data and structure refinement for **12**·I

Empirical formula	$C_{24}H_{20}I_2N_7 \cdot I \cdot (CH_2Cl_2)_2$	
Formula weight	957.05	
Temperature	100 K	
Wavelength	0.68890 Å	
Crystal system	Triclinic	
Space group	$P\bar{1}$	
Unit cell dimensions	a = 8.59853(16) Å	$\alpha = 79.806(2)^\circ$
	b = 17.2143(4) Å	$\beta = 89.6072(17)^\circ$
	c = 21.7900(5) Å	$\gamma = 83.3089(18)^\circ$
Volume	3152.45(7) $Å^3$	
Z	4	
Density (calculated)	2.016 Mg/m^3	
Absorption coefficient	3.344 mm^{-1}	
F(000)	1824	
Crystal size	0.040 × 0.100 × 0.020 mm^3	
Theta range for data collection	1.614 to 32.105°	
Index ranges	$-11 \leqslant h \leqslant 13, -24 \leqslant k \leqslant 25, -33 \leqslant l \leqslant 33$	
Reflections collected	42069	
Independent reflections	20094 [$R_{(int)} = 0.036$]	
Completeness to theta = 25.042°	93.3%	
Absorption correction	Semi-empirical from equivalents	
Max. and min. transmission	1.00 and 0.63	
Refinement method	Full-matrix least-squares on F^2	
Data / restraints / parameters	17432 / 698 / 721	
Goodness-of-fit on F^2	0.9822	
Final R indices [I>2sigma(I)]	R1 = 0.0609, wR2 = 0.1670	
R indices (all data)	R1 = 0.0678, wR2 = 0.1716	
Largest diff. peak and hole	5.53 and −2.25 e.$Å^{-3}$	

[2]Catenane 28·Cl

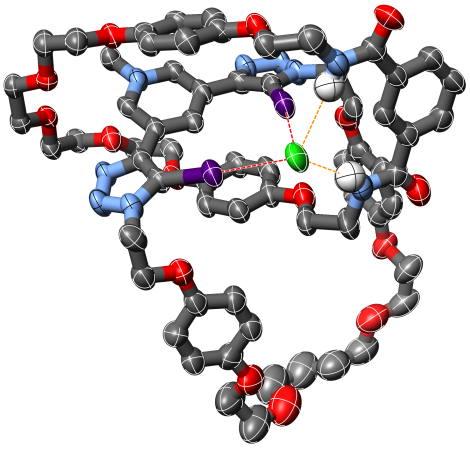


Figure 8.1.3: Thermal ellipsoid plot showing the asymmetric unit for the single-crystal structure of compound **28**·Cl. Atomic displacement ellipsoids drawn at the 50% probability level. Hydrogen atoms have been omitted.

Table 8.1.3: Crystal data and structure refinement for **28**·Cl

Empirical formula	$C_{66}H_{74}I_2N_9O_{15} \cdot Cl$	
Formula weight	1522.62	
Temperature	100 K	
Wavelength	0.68890 Å	
Crystal system	Triclinic	
Space group	$P\bar{1}$	
Unit cell dimensions	a = 13.8599(6) Å	$\alpha = 75.334(4)^\circ$
	b = 15.3852(8) Å	$\beta = 70.075(4)^\circ$
	c = 17.8614(7) Å	$\gamma = 86.233(4)^\circ$
Volume	3463.2(3) $Å^3$	
Z	2	
Density (calculated)	1.460 Mg/m^3	
Absorption coefficient	1.017 mm^{-1}	
F(000)	1552	
Crystal size	0.025 × 0.006 × 0.005 mm^3	
Theta range for data collection	1.515 to 26.693°	
Index ranges	$-16 \leqslant h \leqslant 17, -19 \leqslant k \leqslant 19, 0 \leqslant l \leqslant 22$	
Reflections collected	42842	
Independent reflections	13714 [$R_{(int)} = 0.055$]	
Completeness to theta = 25.091°	89.2%	
Absorption correction	Semi-empirical from equivalents	
Max. and min. transmission	1.00 and 0.63	
Refinement method	Full-matrix least-squares on F^2	
Data / restraints / parameters	10603 / 200 / 838	
Goodness-of-fit on F^2	1.0532	
Final R indices [I>2sigma(I)]	R1 = 0.0722, wR2 = 0.1827	
R indices (all data)	R1 = 0.0967, wR2 = 0.2079	
Largest diff. peak and hole	1.98 and −1.31 e.$Å^{-3}$	

[2]Catenane 28·Br

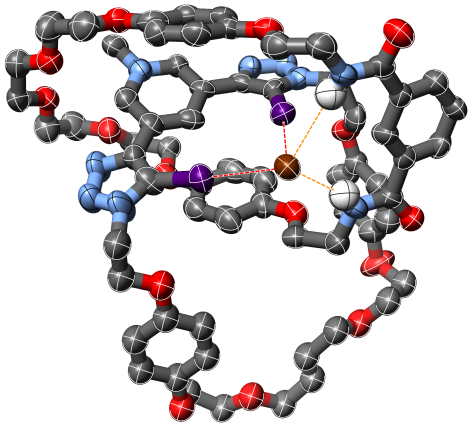


Figure 8.1.4: Thermal ellipsoid plot showing the asymmetric unit for the single-crystal structure of compound **28**·Br. Atomic displacement ellipsoids drawn at the 50% probability level. Hydrogen atoms have been omitted.

Table 8.1.4: Crystal data and structure refinement for **28**·Br

Empirical formula	$C_{66}H_{74}I_2N_9O_{15} \cdot Br$	
Formula weight	1567.08	
Temperature	100 K	
Wavelength	0.68890 Å	
Crystal system	Triclinic	
Space group	$P\bar{1}$	
Unit cell dimensions	a = 13.9754(16) Å	$\alpha = 73.074(9)^\circ$
	b = 15.0529(19) Å	$\beta = 69.278(9)^\circ$
	c = 17.8496(9) Å	$\gamma = 84.858(10)^\circ$
Volume	3359.6(7) $Å^3$	
Z	2	
Density (calculated)	1.549 Mg/m^3	
Absorption coefficient	1.603 mm^{-1}	
F(000)	1587.999	
Crystal size	0.023 × 0.016 × 0.004 mm^3	
Theta range for data collection	1.510 to 26.360°	
Index ranges	$-15 \leqslant h \leqslant 18, -17 \leqslant k \leqslant 19, 0 \leqslant l \leqslant 21$	
Reflections collected	32498	
Independent reflections	12496 [$R_{(int)} = 0.116$]	
Completeness to theta = 25.042°	85.9%	
Absorption correction	Semi-empirical from equivalents	
Max. and min. transmission	1.00 and 0.72	
Refinement method	Full-matrix least-squares on F^2	
Data / restraints / parameters	9186 / 544 / 1019	
Goodness-of-fit on F^2	1.0047	
Final R indices [I>2sigma(I)]	R1 = 0.1009, wR2 = 0.2635	
R indices (all data)	R1 = 0.1480, wR2 = 0.3519	
Largest diff. peak and hole	1.97 and −2.33 e.$Å^{-3}$	

[2]Catenane 28·I

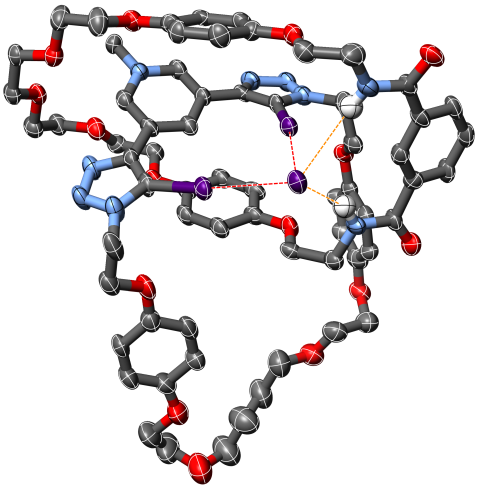


Figure 8.1.5: Thermal ellipsoid plot showing the asymmetric unit for the single-crystal structure of compound **28**·I. Atomic displacement ellipsoids drawn at the 50% probability level. Hydrogen atoms have been omitted.

Table 8.1.5: Crystal data and structure refinement for **28**·I

Empirical formula	$C_{66}H_{74}I_2N_9O_{15} \cdot I$	
Formula weight	1614.08	
Temperature	100 K	
Wavelength	0.68890 Å	
Crystal system	Triclinic	
Space group	$P\bar{1}$	
Unit cell dimensions	a = 13.8570(4) Å	$\alpha = 72.227(3)^\circ$
	b = 15.5217(7) Å	$\beta = 68.038(3)^\circ$
	c = 17.8913(6) Å	$\gamma = 83.956(3)^\circ$
Volume	3398.4(2) $Å^3$	
Z	2	
Density (calculated)	1.577 Mg/m^3	
Absorption coefficient	1.451 mm^{-1}	
F(000)	1624	
Crystal size	0.024 × 0.007 × 0.004 mm^3	
Theta range for data collection	1.536 to 26.240°	
Index ranges	$-15 \leqslant h \leqslant 17, -17 \leqslant k \leqslant 19, 0 \leqslant l \leqslant 22$	
Reflections collected	40577	
Independent reflections	12756 [$R_{(int)} = 0.077$]	
Completeness to theta = 25.191°	86.0%	
Absorption correction	Semi-empirical from equivalents	
Max. and min. transmission	1.00 and 0.63	
Refinement method	Full-matrix least-squares on F^2	
Data / restraints / parameters	9564 / 314 / 838	
Goodness-of-fit on F^2	0.9820	
Final R indices [I>2sigma(I)]	R1 = 0.0615, wR2 = 0.1331	
R indices (all data)	R1 = 0.0881, wR2 = 0.1519	
Largest diff. peak and hole	2.36 and −1.79 $e.Å^{-3}$	

[2]Catenane $\mathbf{28}_2 \cdot SO_4$

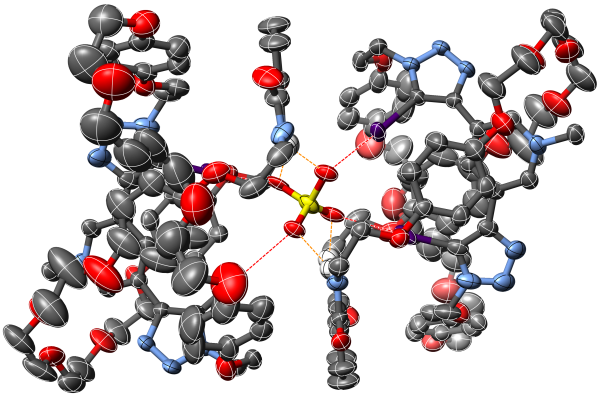


Figure 8.1.6: Thermal ellipsoid plot showing the asymmetric unit for the single-crystal structure of compound $\mathbf{28}_2 \cdot SO_4$. Atomic displacement ellipsoids drawn at the 50% probability level. Hydrogen atoms have been omitted.

Table 8.1.6: Crystal data and structure refinement for $\mathbf{28}_2 \cdot SO_4$

Empirical formula	$C_{66}H_{74}I_2N_9O_{15} \cdot (SO_4)_{0.5}$	
Formula weight	1535.20	
Temperature	100 K	
Wavelength	0.68890 Å	
Crystal system	Triclinic	
Space group	$P\bar{1}$	
Unit cell dimensions	a = 13.3432(3) Å	$\alpha = 78.747(2)^\circ$
	b = 16.0601(4) Å	$\beta = 89.835(2)^\circ$
	c = 19.3748(5) Å	$\gamma = 67.026(2)^\circ$
Volume	3736.71(17) $Å^3$	
Z	2	
Density (calculated)	1.364 Mg/m^3	
Absorption coefficient	0.924 mm^{-1}	
F(000)	1566	
Crystal size	0.070 × 0.020 × 0.010 mm^3	
Theta range for data collection	1.612 to 31.879°	
Index ranges	$-20 \leqslant h \leqslant 20, -23 \leqslant k \leqslant 24, 0 \leqslant l \leqslant 29$	
Reflections collected	81677	
Independent reflections	25126 [$R_{(int)} = 0.045$]	
Completeness to theta = 25.185°	97.1%	
Absorption correction	Semi-empirical from equivalents	
Max. and min. transmission	1.00 and 0.66	
Refinement method	Full-matrix least-squares on F^2	
Data / restraints / parameters	16347 / 1093 / 871	
Goodness-of-fit on F^2	0.9839	
Final R indices [I>2sigma(I)]	R1 = 0.0871, wR2 = 0.1908	
R indices (all data)	R1 = 0.1007, wR2 = 0.2049	
Largest diff. peak and hole	3.5 and −3.51 $e.Å^{-3}$	

[2]Catenane 28·H_2PO_4

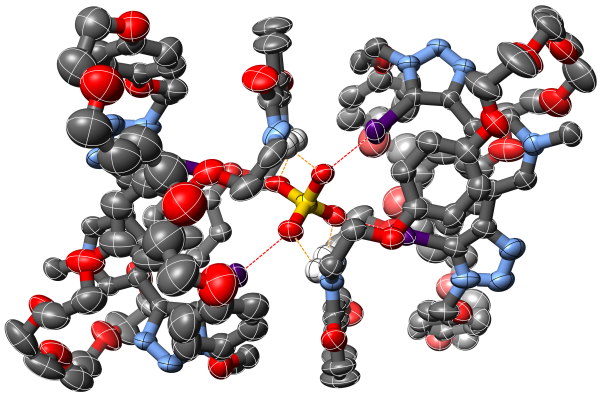


Figure 8.1.7: Thermal ellipsoid plot showing the asymmetric unit for the single-crystal structure of compound **28**·H_2PO_4. Atomic displacement ellipsoids drawn at the 50% probability level. Hydrogen atoms have been omitted.

Table 8.1.7: Crystal data and structure refinement for **28**·H_2PO_4

Empirical formula	$C_{66}H_{74}I_2N_9O_{15} \cdot (H_2PO_4)_{0.5}$	
Formula weight	1534.66	
Temperature	100 K	
Wavelength	0.68890 Å	
Crystal system	Triclinic	
Space group	$P\bar{1}$	
Unit cell dimensions	a = 13.3757(4) Å	$\alpha = 78.599(3)^\circ$
	b = 16.0589(6) Å	$\beta = 89.672(3)^\circ$
	c = 19.4107(7) Å	$\gamma = 66.939(3)^\circ$
Volume	3748.6(2) $Å^3$	
Z	2	
Density (calculated)	1.360 Mg/m^3	
Absorption coefficient	0.918 mm^{-1}	
F(000)	1565	
Crystal size	0.050 × 0.030 × 0.030 mm^3	
Theta range for data collection	1.532 to 26.376°	
Index ranges	$-16 \leqslant h \leqslant 16, -19 \leqslant k \leqslant 20, 0 \leqslant l \leqslant 24$	
Reflections collected	45435	
Independent reflections	14253 [$R_{(int)} = 0.098$]	
Completeness to theta = 25.057°	87.9%	
Absorption correction	Semi-empirical from equivalents	
Max. and min. transmission	1.00 and 0.59	
Refinement method	Full-matrix least-squares on F^2	
Data / restraints / parameters	11532 / 1063 / 871	
Goodness-of-fit on F^2	0.8627	
Final R indices [I>2sigma(I)]	R1 = 0.0785, wR2 = 0.2329	
R indices (all data)	R1 = 0.1033, wR2 = 0.3024	
Largest diff. peak and hole	1.51 and −1.84 e.$Å^{-3}$	